Springer Proceedings in Complexity

Douw Steyn
Rohit Mathur *Editors*

# Air Pollution Modeling and its Application XXIII

Springer

# Springer Proceedings in Complexity

For further volumes:
http://www.springer.com/series/11637

# Springer Complexity

Springer Complexity is an interdisciplinary program publishing the best research and academic-level teaching on both fundamental and applied aspects of complex systems – cutting across all traditional disciplines of the natural and life sciences, engineering, economics, medicine, neuroscience, social and computer science.

Complex Systems are systems that comprise many interacting parts with the ability to generate a new quality of macroscopic collective behavior the manifestations of which are the spontaneous formation of distinctive temporal, spatial or functional structures. Models of such systems can be successfully mapped onto quite diverse "real-life" situations like the climate, the coherent emission of light from lasers, chemical reaction-diffusion systems, biological cellular networks, the dynamics of stock markets and of the internet, earthquake statistics and prediction, freeway traffic, the human brain, or the formation of opinions in social systems, to name just some of the popular applications.

Although their scope and methodologies overlap somewhat, one can distinguish the following main concepts and tools: self-organization, nonlinear dynamics, synergetics, turbulence, dynamical systems, catastrophes, instabilities, stochastic processes, chaos, graphs and networks, cellular automata, adaptive systems, genetic algorithms and computational intelligence.

The three major book publication platforms of the Springer Complexity program are the monograph series "Understanding Complex Systems" focusing on the various applications of complexity, the "Springer Series in Synergetics", which is devoted to the quantitative theoretical and methodological foundations, and the "SpringerBriefs in Complexity" which are concise and topical working reports, case-studies, surveys, essays and lecture notes of relevance to the field. In addition to the books in these two core series, the program also incorporates individual titles ranging from textbooks to major reference works.

Douw Steyn • Rohit Mathur
Editors

# Air Pollution Modeling and its Application XXIII

Springer

*Editors*
Douw Steyn
Department of Earth, Ocean
and Atmospheric Sciences
The University of British Columbia
Vancouver, BC, Canada

Rohit Mathur
Atmospheric Modeling
and Analysis Division
United States Environmental
Protection Agency
Research Triangle Park, NC, USA

ISSN 2213-8684 ISSN 2213-8692 (electronic)
ISBN 978-3-319-04378-4 ISBN 978-3-319-04379-1 (eBook)
DOI 10.1007/978-3-319-04379-1
Springer Cham Heidelberg New York Dordrecht London

Library of Congress Control Number: 2014939005



Printed on acid-free paper

Springer is part of Springer Science+Business Media (www.springer.com)

# Preface

In 1969, the North Atlantic Treaty Organization (NATO) established the Committee on the Challenges of Modern Society (CCMS). From its inception, the committee supported studies of air pollution as one of its priorities. An important NATO/CCMS activity relating to air pollution was the periodic organization of a conference series called the **International Technical Meeting** (ITM) **on Air Pollution Modelling and Its Application**. This activity continued until 2013, under the successor of NATO/CCMS, the NATO Committee on Science for Peace and Security (NATO/SPS). NATO Pilot Countries organizing these meetings have been the USA, Federal Republic of Germany, Belgium, the Netherlands, Denmark, Portugal, and Canada. In 2013, the ITM continued its meeting series independently of NATO/SPS.

This volume contains the abstracts of papers and posters presented at the 33rd ITM, held in Miami, USA, from August 27 to 31, 2013. This ITM was organized by the US EPA (Host Country) and the University of British Columbia (Pilot Country). Key topics presented at this ITM were: local and urban scale modelling, regional and intercontinental modelling, data assimilation and air quality forecasting, model assessment and verification, aerosols in the atmosphere, interactions between climate change and air quality, and air quality and human health.

The ITM was attended by 92 participants representing 22 countries. Invited papers were presented by Lise Frohn, Denmark (Air Quality and Human Health); Armistead Russell, USA (Regional and Intercontinental Modelling); and Steve Hanna, USA (Local and Urban Scale Modelling).

On behalf of the ITM Scientific Committee and as organizers and editors, we would like to thank all the participants who contributed to the success of the meeting. We especially recognize the organizational and support efforts of the chairpersons and rapporteurs, and staff at AMEC. Finally, special thanks go to the sponsoring institutions: Environmental Protection Agency, USA, Environment Canada,

and the University of British Columbia (Canada). The European Association for the Science of Air Pollution (EURASAP) gave a special grant to award prizes to Early Career Researchers for the best paper or poster presentations.

The next meeting will be held in May 2014 in Montpellier, France.

Douw Steyn
(Scientific Committee Chair)
Rohit Mathur
(Local Conference Organizer)

# Members of the Scientific Committee for the 33rd International Technical Meeting (ITM) on Air Pollution Modelling and Its Application

| | |
|---|---|
| Clemens Mensink | Belgium |
| Ekaterina Batchvarova | Bulgaria |
| Douw Steyn | Canada (chair) |
| Wanmin Gong | Canada |
| Sven-Erik Gryning | Denmark |
| Nadine Chaumerliac | France |
| Heinke Schlünzen | Germany |
| George Kallos | Greece |
| Silvia Trini Castelli | Italy |
| Hilde Fagerli | Norway |
| Ana Isabel Miranda | Portugal |
| Oriol Jorba | Spain |
| Renske Timmermans | The Netherlands |
| Selahattin Incecik | Turkey |
| Tony Dore | UK |
| Rohit Mathur | USA |
| Werner Klug | Germany (honorary life member) |
| Han van Dop | The Netherlands (honorary life member) |
| Frank Schiermeier | USA (honorary life member) |

# History of International Technical Meeting on Air Pollution Modelling and Its Application

## Pilot Studies

| | |
|---|---|
| 1969–1974 | Air Pollution Pilot Study (*Pilot Country: USA*) |
| 1975–1979 | Air Pollution Assessment Methodology and Modelling (*Pilot Country: Germany*) |
| 1980–1944 | Air Pollution Control Strategies and Impact Modelling (*Pilot Country: Germany*) |

## Pilot Follow-Up Meetings

| *Pilot Country – USA (R. A. McCormick, L. E. Niemeyer)* | | |
|---|---|---|
| Feb. 1971 | Eindhoven, the Netherlands | First Conference on Low Pollution Power Systems Development |
| July 1971 | Paris, France | Second Meeting of the Expert Panel on Air Pollution Modelling |

## NATO/CCMS International Technical Meeting (ITM) on Air Pollution Modelling and Its Application

Subsequent meetings were supported by the NATO Committee on the Challenges of Modern Society and were designated NATO/CCMS International Technical Meeting (ITM) on Air Pollution Modelling and Its Application.

| | |
|---|---|
| 3rd Oct. 1972 | ITM, Paris, France |
| 4th May 1973 | ITM, Oberursel, Federal Republic of Germany |
| 5th Jun. 1974 | ITM, Roskilde, Denmark |
| *Pilot Country – Germany (Erich Weber)* | |
| 6th Sept. 1975 | ITM, Frankfurt, Federal Republic of Germany |
| 7th Sept. 1976 | ITM, Airlie House, USA |
| 8th Sept. 1977 | ITM, Louvain-la-Neuve, Belgium |
| 9th Aug. 1978 | ITM, Toronto, Canada |
| 10th Oct. 1979 | ITM, Rome, Italy |
| *Pilot Country – Belgium (C. De Wispelaere)* | |
| 11th Nov. 1980 | ITM, Amsterdam, the Netherlands |
| 12th Sept. 1981 | ITM, Menlo Park, California, USA |
| 13th Sept. 1982 | ITM, Ile des Embiez, France |
| 14th Sept. 1983 | ITM, Copenhagen, Denmark |
| 15th Apr. 1985 | ITM, St. Louis, Missouri, USA |
| *Pilot Country – The Netherlands (H. van Dop)* | |
| 16th Apr. 1987 | ITM, Lindau, Federal Republic of Germany |
| 17th Sept. 1988 | ITM, Cambridge, UK |
| 18th May 1990 | ITM, Vancouver, BC, Canada |
| 19th Sept. 1991 | ITM, Ierapetra, Greece |
| *Pilot Country – Denmark (Sven-Erik Gryning)* | |
| 20th Nov. 1993 | ITM, Valencia, Spain |
| 21st Nov. 1995 | ITM, Baltimore, Maryland, USA |
| 22nd May 1997 | ITM, Clermont-Ferrand, France |
| 23rd Sept. 1998 | ITM, Varna, Bulgaria |
| 24th May 2000 | ITM, Boulder, Colorado, USA |
| *Pilot Country – Portugal (Carlos Borrego)* | |
| 25th Sept. 2001 | ITM, Louvain-la-Neuve, Belgium |
| 26th May 2003 | ITM, Istanbul, Turkey |
| 27th Oct. 2004 | ITM, Banff, Canada |
| 28th May 2006 | ITM, Leipzig, Germany |

## NATO/SPS International Technical Meeting (ITM) on Air Pollution Modelling and Its Application

In 2007, the NATO Committee on the Challenges of Modern Society was disbanded and replaced by the NATO Committee on Science for Peace and Security (NATO/SPS), which continued support for the ITM.

| | |
|---|---|
| 29th Sept. 2007 | ITM, Aveiro, Portugal |
| *Pilot Country – Canada (Douw Steyn)* | |
| 30th May 2009 | ITM, San Francisco, California, USA |
| 31st Sept. 2010 | ITM, Torino, Italy |
| 32nd May 2012 | ITM, Utrecht, the Netherlands |

## International Technical Meeting (ITM) on Air Pollution Modelling and Its Application

In 2012, the NATO Committee on Science for Peace and Security refocused its mandate, and the ITM became independent of NATO/SPS support.

| | |
|---|---|
| 33rd Sept. 2013 | ITM, Miami, USA |

# List of Participants

## Barbados

**Gill, Andrew**
andygillbarbados@gmail.com
Larco Investment Inc
No. 3 Prior Park Close
St. James bb23017

## Belgium

**Delcloo, Andy**
andy.delcloo@meteo.be
Royal Meteorological Institute of Belgium
Ringlaan 3 9000
Ukkel 9000

**Mensink, Clemens**
clemens.mensink@vito.be
VITO
Boeretang 200
B-2400 Mol

## Canada

**Chen, Jack**
jack.chen@ec.gc.ca
21 Taunton Pl
Ottawa, ON
K1J7J7

**Chtcherbakov, Andrei**
125 Resources Road
Toronto, ON
M9P 3 V6

**Hakami, Amir**
amir_hakami@carleton.ca
Carleton University
1125 Colonel by Drive Civil and Environmental Engineering
Ottawa, ON
K1S 5B6

**Makar, Paul**
paul.maker@ec.gc.ca
Environment Canada
146 Indian Road Crescent
Toronto, ON
M6P ZG3

**Menard, Sylvain**
sylvain.menard@ec.gc.ca
2121 TransCanada North
Dorval, QC
H9P1J3

**Steyn, Douw**
dsteyn@eos.ubc.ca
2207 Main Mall
Vancouver, BC
V6T 1Z4

## Czech Republic

**Fuka, Vladimir**
vladimir.fuka@mff.cuni.cz
V Holesovickach 2
18000 Prague

**Huszar, Peter**
huszarpet@gmail.com
Charles University in Prague
KMOP V Holesovickach 2
18000 Prague

## Denmark

**Batchvarova, Ekaterina**
ekba@dtu.dk
DTU Wind Energy
Technical University of Denmark
Frederiksborgvej 399
DK-4000 Roskilde

**Gryning, Sven-Erik**
sveg@dtu.dk
DTU Wind Energy
Technical University of Denmark
DK-4000 Roskilde

**Silver, Jeremy**
jds@dmu.dk
Department of Environmental Science, Aarhus University
Frederiksborgvej 399 4000
4000 Roskilde

## Estonia

**Kaasik, Marco**
marko.kaasik@ut.ee
University of Tartu
Ulikooli St.
50090 Tartu

## Finland

**Soares, Joana**
joana.soares@fmi.fi
Erik Palmenin Aukio 1
00560 Helsinki

## France

**Bessagnet, Bertrand**
fabienne.carette@ineris.fr
INERIS
Parc Technologique Alata BP 7
60550 Verneuil-en-Halatte

**Chaumerliac, Nadine**
N.Chaumerliac@opgc.univ-bpclermont.fr
24 Avenue Des Landais
63177 Aubiere

**Courcot, Dominique**
Dominique.Courcot@univ-littoral.fr
UCEIV
145 Avenue Maurice Schumann
59140 Dunkerque

**Deguillaume, Laurent**
L.Deguillaume@opgc.univ-bpclermont.fr
24 Avenue Des Landais
63177 Aubiere

**Kfoury, Adib**
adibkfoury@hotmail.com
UCEIV
145 Avenue Maurice Schumann
59140 Dunkerque

**Patryl, Luc**
luc.patryl@cea.fr
Commissariat à l'Energie Atomique
Centre DAM-Ile de France
91297 Arpajon Cedex Bruyères-le-Chatel

**Tedeschi, Gilles**
tedeschi@univ-tln.fr
Mediterranean Institute of Oceanography – University of Toulon-Var
ISITV BP 56 Av. G. Pompidou
83162 La Valette Du Var

## Germany

**Aulinger, Armin**
armin.aulinger@hzg.de
Helmholtz-Zentrum Geesthacht
Max-Planck-Strasse 1
21502 Hamburg

**Banzhaf, Sabine**
sabine.banzhaf@met-fu-berlin.de
Freie Universität Berlin
Carl-Heinrich-Becker-Weg 6–10
12165 Berlin

**Bieser, Johannes**
johannes.bieser@hzg.de
Helmholtz Zentrum Geesthacht
Max-Planck Strasse 1
20099 Geesthacht

**Fallmann, Joachim**
joachim.fallmann@kit.edu
Karlsruhe Institute of Technology
Kreuzeckbahnstr. 19
82467 Garmisch-Partenkirchen

**Schlünzen, K. Heinke**
heinke.schluenzen@uni-hamburg.de
Univ. Hamburg. Met. Inst.
Bundesstr. 55
20146 Hamburg

**Uphoff, Malte**
malte.uphoff@zmaw.de
Meteorological Institute University of Hamburg
Bundesstr. 55
D20146 Hamburg

**Wolke, Ralf**
wolke@tropos.de
Leibniz Institute for Tropospheric Research
Permoserstr. 15
4318 Leipzig

## Greece

**Kallos, George**
kallos@mg.uoa.gr
University of Athens
University Campus Bldg Phys-5
15784 Athens

**Moussiopoulos, Nicolas**
moussio@eng.auth.gr
Aristotle University Thessaloniki
University Campus
GR54124 Thessaloniki

**Poupkou, Anastasia**
poupkou@auth.gr
Filellinon 11
54645 Thessaloniki

## Hungary

**Ferenczi, Zita**
ferenczi.z@met.hu
Hungarian Meteorological Service
Budapest Kitaibel Pal Utca 1
1024 Budapest

## Israel

**Kishcha, Pavel**
pavel@cyclone.tau.ac.il
Tel-Aviv University
69978 Tel-Aviv

## Italy

**Balzarini, Alessandra**
Alessandra.Balzarini@rse-web.it
Via Rubattino 54
20134 Milan

**Curci, Gabriele**
gabriele.curci@aquila.infn.it
University of L'Aquila
Universita Dell'Aquila CETEMPS
67100 L'Aquila

**Galmarini, Stefano**
stefano.galmarini@jrc.ec.europa.eu
Tp441 Jrc
21027 Ispra

**Gariazzo, Claudio**
c.gariazzo@inail.it
INAIL
Via Fontana Candida 1
00040 Monte Porzio Catone (RM)

**Thunis, Philippe**
philippe.thunis@jrc.ec.europa.eu
Via Fermi
21020 Ispra

**Trini Castelli, Silvia**
s.trinicastelli@isac.cnr.it
CNR-ISAC
I-10133 Torino

## The Netherlands

**Gromke, Christof**
c.b.gromke@tue.nl
Eindhoven University of Technology
P.O. Box 513
5600 MB Eindhoven

**Timmermans, Renske**
renske.timmermans@tno.nl
TNO
Princetonlaan 6
3584 CB Utrecht

## Poland

**Kryza, Maclej**
maciel.kryza@uni.wroc.pl
University of Wroclaw
pl. Uniwersytecki 1
51–621 Wroclaw

**Werner, Malgorzata**
malgorzata.werner@uni.wroc.pl
University of Wroclaw
Kosiby 8
51–621 Wroclaw

## Portugal

**Borrego, Carlos**
borrego@ua.pt
University of Aveiro
Department of Environment and Planning
3810–193 Aveiro

**Miranda, Ana**
miranda@ua.pt
University of Aveiro
Department of Environment and Planning
3810–193 Aveiro

## Saudi Arabia

**Alqahtani, Jumaan**
jqahtani@yahoo.com
EPD/Saudi Aramco
P. O. Box 18036
31311 Dhahran

## South Africa

**Abiodun, Babatunde**
babiodun@csag.uct.ac.za
University of Cape Town
34 Dartmouth Road
Muizenberg

## Spain

**Jorba, Oriol**
oriol.jorba@bsc.es
Jordi Girona 31
8034 Barcelona

**Saez De Camara, Estibaliz**
estibaliz.saezdecamara@ehu.es
University of the Basque Country UPV/EHU
Alameda Urquijo S/n
48013 Bilbao

**San Jose, Roberto**
roberto@fi.upm.es
Technical University of Madrid (UPM)
Campus De Montegancedo
28223 Boadilla Del Monte

**Valdenebro, Veronica**
veronica.valdenebro@ehu.es
School of Engineering
University of the Basque Country UPV/EHU ESQ4818001B
Alameda De Urquijo S/n
48013 Bilbao

## Switzerland

**Aksoyoglu, Sebnem**
sebnem.aksoyoglu@psi.ch
Paul Scherrer Institute
5232 Villigen

**Brunner, Dominik**
dominik.brunner@empa.ch
Empa Swiss Federal Laboratories for Materials Science and Technology
Ueberlandstrasse 129
8600 Empa Duebendorf

## United Kingdom

**Chemel, Charles**
c.chemel@herts.ac.uk
University of Hertfordshire
University of Hertfordshire Centre for Atmos. and Instrum. Research College Lane
AL10 9AB Hatfield

**Davis, Lucy**
lucy.davis@metoffice.gov.uk
Met Office
Fitzroy Road
EX1 3 PB Exeter

**Dore, Anthony**
todo@ceh.ac.uk
Centre for Ecology and Hydrology
Bush Estate Penicuik Midlothian
EH26 OQB Midlothian

**Fraser, Andrea**
andrea.fraser@ricardo-aea.com
Ricardo-AEA
Gemini Building Fermi Avenue Harwell
OX11 0QR Didcot

**Ots, Riinu**
riis78@ceh.ac.uk
Bush Estate
EH26 0QB Penicuik Midlothian

**Timmis, Roger**
roger.timmis@environment-agency.gov.uk
Environment Agency
C/o Lancaster Environment Centre
LA1 4YQ Lancaster

## USA

**Arunachalam, Saravanan**
sarav@email.unc.edu
UNC Institute for the Environment
137 E. Franklin St. Bank of America Plaza
CB #6116
Chapel Hill, NC
27599–6116

**Bondehagen, Diane**
dbondeha@fgcu.edu
Florida Gulf Coast University
10501 FGCU Blvd South Whitaker College Of Engineering
Fort Myers FL 33965

**Chai, Tianfeng**
tianfeng.chai@noaa.gov
NOAA Center for Weather and Climate Pred
5830 University Research Court
College Park MD 20740

**Cooter, Ellen**
cooter.ellen@epa.gov
USEPA/ORD/NERL
E243-02
Research Triangle Park NC 27711

**Delle Monache, Luca**
lucadm@ucar.edu
NCAR/RAL
3450 Mitchell Lane
Boulder CO 80301

**Foley, Kristen**
foley.kristen@epa.gov
US EPA
109 TW Alexander Dr
Research Triangle Park NC 27711

**Hanna, Steve**
hannaconsult@roadrunner.com
Hanna Consultants
7 Crescent Ave
Kennebunkport ME 04046–7235

**Hogrefe, Christian**
hogrefe.christian@epa.gov
U.S. EPA
Atmospheric Modeling and Analysis Div. U.S. EPA
Mail Drop E243-04
Research Triangle Park NC 27711

**Holmes, Heather**
heather.holmes@ce.gatech.edu
Georgia Tech
311 Ferst Drive EST Bldg Environmental Engineering
Atlanta GA 30306

**Isakov, Vlad**
isakov.vlad@epa.gov
US EPA Atmospheric Modeling Division
Mail Drop E243-02
109 T.W. Alexander Drive
Research Triangle Park NC 27711

**Knote, Christoph**
knote@ucar.edu
NCAR
3450 Mitchell Lane
Boulder CO 80301

**Lee, Pius**
pius.lee@noaa.gov
Ncwcp 5830 University Research Ct
College Park MD 20740

**Loughner, Chris**
Christopher.p.loughner@nasa.gov
UMD ESSIC/NASA GSFC
309 11th St SE Washington DC 20003
Washington DC 20003

**Mathur, Rohit**
mathur.rohit@epa.gov
USEPA/ORD/NERL
109 TW Alexander Dr
Research Triangle Park NC 27703

**Minoura, Hiroaki**
hiroaki.minoura@tema.toyota.com
Toyota Motor E&M North America
1555 Woodridge Ave
Ann Arbor MI 48105

**Nolte, Chris**
nolte.chris@epa.gov
US EPA
Mail Drop E243-03
Durham NC 27703

**Pagowski, Mariusz**
Mariusz.Pagowski@noaa.gov
325 Broadway R/GSD
Boulder CO 80305

**Pappin, Amanda**
mailto:ajpappin@gmail.com
Carleton University
827 Woodward Ave Apt 2
New Haven CT 6512

**Pleim, Jonathan**
plein.jon@epa.gov
US EPA
Mail Drop E243-04
Durham NC 27703

**Pouliot, George**
pouliot.george@epa.gov
US EPA
Mail Drop E243-04
Durham NC 27703

**Rogers, Chris**
chris.rogers@amec.com
AMEC
3901 Carmichael Avenue
Jacksonville FL 32207

**Russell, Ted**
ted.russell@gatech.edu
Georgia Institute of Technology
School of Civil and Env Engineering
311 Ferst Drive
Atlanta GA 30332

**Sarwar, Golam**
sarwar.golam@epa.gov
US EPA Office of Research and Development
MD-E243-03 109 T.W. Alexander Drive
Research Triangle Park NC 27711

**Vennam, Lakshmi Pradeepa**
lakshmi@email.unc.edu
UNC Chapel Hill
601 Jones Ferry Road #L15
Carrboro NC 27510

**Yarwood, Greg**
gyarwood@environcorp.com
ENVIRON
773 San Marin Drive Ste. 2115
Novato CA 94998

**Zhang, Yang**
yang_zhang@ncsu.edu
North Carolina State University
1125 Jordan Hall Department of MEAS
Campus Box 8208
Raleigh NC 27695

## Venezuela

**Sena, Arcangelo**
senaa@pdvsa.com
Urb. Santa Rosa Sector El Tambor
PDVSA Intevep Gerencia de Ambiente
Norte 4 Piso 3
Los Teques Edo. Miranda

# Contents

# Chapter 1
# Use of Air Quality Modeling Results in Health Effects Research

**Armistead Russell, Heather Holmes, Mariel Friberg, Cesunica Ivey, Yongtao Hu, Siv Balachandran, James Mulholland, Paige Tolbert, Jeremy Sarnat, Stefanie Sarnat, Matt Strickland, Howard Chang, and Yang Liu**

**Abstract** The most recent Global Burden of Disease study (Lim SS et al, Lancet 380(9859):2224–2260, 2012), for example, finds that combined exposure to ambient and indoor air pollution is one of the top five risks worldwide. Of particular concern is particulate matter (PM). Health researchers are now trying to assess how this mixture of air pollutants links to various health outcomes and how to tie the mixture components and health outcomes back to sources. This process involves the use of air quality models. As part of an EPA Clean Air Research Center, the Southeastern Center for Air Pollution and Epidemiology (SCAPE), a variety of air quality models are being developed and applied to provide enhanced temporal and spatial resolution of pollutant concentrations for use in epidemiologic analysis. Air quality models that are being further developed and used as part of the center include Bayesian-based ensemble methods and hybrid chemical transport-chemical mass balance modeling. The hybrid method uses knowledge of the emissions, modeling and measurement uncertainties, and can provide spatially and temporally complete pollutant fields.

## 1.1 Introduction

Evidence continues to grow that exposure to ambient air pollutants impacts health. The most recent Global Burden of Disease study [11], for example, finds that combined exposure to ambient and indoor air pollution is one of the top five risks worldwide. This study, as well as similar ones conducted for more limited

A. Russell (✉) • H. Holmes • M. Friberg • C. Ivey • Y. Hu • S. Balachandran • J. Mulholland
School of Civil and Environmental Engineering, Georgia Institute of Technology, Atlanta, GA 30332, USA
e-mail: ted.russell@ce.gatech.edu; heather.holmes@ce.gatech.edu

P. Tolbert • J. Sarnat • S. Sarnat • M. Strickland • H. Chang • Y. Liu
Rollins School of Public Health, Emory University, Atlanta, GA 30322, USA

D. Steyn and R. Mathur (eds.), *Air Pollution Modeling and its Application XXIII*, Springer Proceedings in Complexity, DOI 10.1007/978-3-319-04379-1_1,

domains (e.g., by country), relies on results from epidemiologic studies that quantify exposure-health effect relationships (e.g., by calculating concentration-response functions). Traditionally, epidemiologic studies associate observed pollutant concentrations with observed health endpoints (e.g., hospital admissions or deaths). However, air pollutant observations are limited spatially, temporally, and chemically, and do not directly identify source contributions to pollution and, thus, health. Air quality models, both receptor-based and chemical transport models, are now being used to address the limitations of using observations alone. However, air quality models also have limitations, in particular uncertainties and biases that arise from errors in the inputs (e.g., emissions timing, speciation and magnitude and meteorological) and model parameters and structure (e.g., grid resolution).

## 1.2 Methods and Results

Air pollution is a mixture of a variety of pollutants. Historically, the related health effects have been tied to individual pollutants, though a question of current interest is how the "mixture" of pollutants plays a role. Past studies have found that particulate matter (PM) is the primary air pollutant of concern when considering premature death or disability adjusted life-years [11], while ozone is of concern for respiratory diseases, such as asthma [15]. Identifying the sources of those two pollutants is challenging. Ozone is a secondary pollutant, and is formed by a series of non-linear chemical reactions involving emissions from a variety of sources. PM formation and morphology is more complicated, being composed of thousands of different compounds which can be both secondary and primary in origin on differently sized particles. Health researchers are now trying to assess how this mixture of air pollutants links to various health outcomes and how to tie the mixture components and health outcomes back to sources. This process involves the use of air quality models. Various methods of identifying sources of ozone using chemical transport air quality models have been used, including both "brute force" and direct sensitivity (e.g., DDM and adjoint) approaches [4, 5, 7, 16]. Identifying source impacts on PM (e.g. PM2.5, PM with aerodynamic diameters less than 2.5 $\mu$m) have utilized both receptor models (e.g., [13]) and chemical transport models (e.g. [3, 6, 10]). Marmur et al. [12] examined the use of various types of air quality models for use in epidemiologic research and found that source apportionment models based on chemical transport models tend to reduce day-to-day variability in source impact estimates (e.g., due to reducing variability in temporal and spatial source emissions and missing sub-synoptic scale meteorological variability), while receptor models can increase variability. More recently, Balachandran et al. [1] applied a number of source apportionment models to assess model differences and uncertainties and also found increased variability in receptor model results, and that the various air quality models, including receptor and chemical transport models, had similar uncertainties in their results. As part of an EPA Clean Air Research Center, the Southeastern Center for Air Pollution and Epidemiology (SCAPE), a variety of air quality models are being developed and applied to provide enhanced temporal and

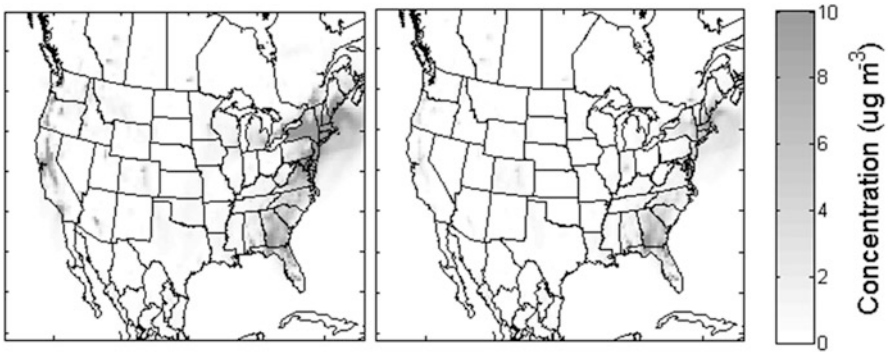


**Fig. 1.1** Spatial fields of biomass burning impacts on January 4, 2004, as simulated by CMAQ (original, *left*) and a hybrid CTM-RM model (refined, *right*). Spatial fields are generated for a 36-km resolution grid. Biomass burning fields include impacts from agricultural burning, lawn waste burning, open fires, prescribed burning, wildfires, wood fuel burning, and woodstoves

spatial resolution of pollutant concentrations for use in epidemiologic analysis. The Center is also assessing how pollutant mixtures and the sources of these mixtures are linked to various health endpoints. In particular, two hybrid approaches that use both observations and air quality models address many of the limitations identified in the direct use of measured or modeled concentrations. One method, the Bayesian Ensemble approach [2], uses results of multiple models to develop an ensemble simulated source impact and then used with observed air quality to develop an improved estimate of the composition of source emissions. With the updated source compositions, a Bayesian approach is used to get improved estimates of air quality impacts and uncertainties.

A second set of methods use results of a chemical transport model (CMAQ) to provide simulated species concentrations and source impacts based on estimated emissions and modeled meteorology. In one approach, simulated species concentrations are fused with observations to develop spatial pollutant fields that are coherent with observations but use the air quality model to provide spatial gradients [8, 14]. This does not link the pollutant fields to individual sources, but does provide a spatially and temporally complete data set of pollutant fields for use in health assessments. In a more involved approach used to link the pollutants to sources, observed concentrations of individual pollutant species (e.g., single elements and gaseous compounds) are used to adjust source impacts to better match observations. This is done in a manner similar to the Chemical Mass Balance Method. However, the method involves using knowledge of the emission uncertainties and can be used to quantify many more source impacts. These results are then used to develop spatially and temporally complete fields for epidemiologic analysis using kriging [9] (Fig. 1.1).

Chemical transport model pollutant fields can also be used with satellite and ground-based observations and land-use information to develop finer scale (e.g., sub-grid scale) pollutant concentration estimates.

**Acknowledgments** This work was made possible in part by USEPA STAR grants R833626, R833866 and R834799 and by NASA project SV6-76007 under grant NNG04GE15G. Its contents are solely the responsibility of the grantee and do not necessarily represent the official views of the USEPA and NASA. Further, neither USEPA nor NASA endorses the purchase of any commercial products or services mentioned in the publication. We also acknowledge the Southern Company for their support and thank Eric Edgerton of ARA, Inc. for access to the SEARCH data.

## References

1. Balachandran S, Pachon JE, Hu Y, Lee D, Mulholland JA, Russell AG (2012) Ensemble-trained source apportionment of fine particulate matter and method uncertainty analysis. Atmos Environ 61:387–394
2. Balachandran S, Chang HH, Pachon JE, Holmes HA, Mulholland JA, Russell AG (2013) A Bayesian–based ensemble technique for source apportionment of PM2.5. Environ Sci Technol 47(23):13511–13518
3. Boylan JW, Odman MT, Wilkinson JG, Russell AG, Doty KG, Norris WB, McNider RT (2002) Development of a comprehensive, multiscale "one-atmosphere" modeling system: application to the Southern Appalachian Mountains. Atmos Environ 36(23):3721–3734
4. Dunker AM (1981) Efficient calculation of sensitivity coefficients for complex atmospheric models. Atmos Environ 15(7):1155–1161
5. Hakami A, Odman MT, Russell AG (2003) High-order, direct sensitivity analysis of multidimensional air quality models. Environ Sci Technol 37(11):2442–2452
6. Held T, Ying Q, Kleeman MJ, Schauer JJ, Fraser MP (2005) A comparison of the UCD/CIT air quality model and the CMB source-receptor model for primary airborne particulate matter. Atmos Environ 39(12):2281–2297
7. Henze DK, Hakami A, Seinfeld JH (2007) Development of the adjoint of GEOS-Chem. Atmos Chem Phys 7(9):2413–2433
8. Holmes H et al (2013) Improved spatiotemporal air pollutant mixtures characterization for health studies. In: NATO/SPS international technical meeting on air pollution modelling and its application, Miami
9. Ivey C, Holmes H, Hu Y, Russell A, Mulholland J (2013) Spatial and temporal extension of a novel hybrid source apportionment model. Paper presented at NATO/SPS international technical meeting on air pollution modelling and its application, Miami
10. Koo B, Dunker AM, Yarwood G (2007) Implementing the decoupled direct method for sensitivity analysis in a particulate matter air quality model. Environ Sci Technol 41(8):2847–2854
11. Lim SS et al (2012) A comparative risk assessment of burden of disease and injury attributable to 67 risk factors and risk factor clusters in 21 regions, 1990–2010: a systematic analysis for the Global Burden of Disease Study 2010. Lancet 380(9859):2224–2260
12. Marmur A, Park SK, Mulholland JA, Tolbert PE, Russell AG (2006) Source apportionment of PM2.5 in the southeastern United States using receptor and emissions-based models: conceptual differences and implications for time-series health studies. Atmos Environ 40(14):2533–2551
13. Seigneur C (2001) Current status of air quality models for particulate matter. J Air Waste Manage Assoc 51(11):1508–1521
14. Sororian S, Holmes H, Friberg M, Ivey C, Hu Y, Mulholland J, Russell A, Strickland M, Chang H (2013) Temporally and spatially resolved air pollution in Georgia using fused ambient monitoring data and chemical transport model results. In: NATO/SPS international technical meeting on air pollution modelling and its application, Miami
15. US EPA (2011) The benefits and costs of the Clean Air Act from 1990 to 2020. US EPA, Washington, DC
16. Yang YJ, Wilkinson JG, Russell AG (1997) Fast, direct sensitivity analysis of multidimensional photochemical models. Environ Sci Technol 31(10):2859–2868

## Questions and Answers

**Questioner Name:** Heinke Schlunzen

**Q:** Is the outdoor air quality really relevant for epidemiology and human health since most people spend most of their time indoors?

**A:** While much of the time is spent indoors, the air indoors is strongly impacted by outdoor air. Epidemiologic studies continue to find associations between outdoor air quality and health. The Global Burden of Disease study finds ambient PM exposure to be one of the top ten contributors to premature death. Exposure to outdoor air continues to be a serious, and apparently growing, contributor to adverse health outcomes.

**Questioner Name:** Clemens Mensink

**Q:** You focus on source impacts on health. The fact is that it's difficult to obtain statistical significant results. Does that say something about the relevance of background conditions.?

**A:** Background concentrations are relevant, but multiple epidemiological, animal and mechanistic studies strongly support that air pollution, above the background, has a significant impact on health. It is true that any one study may not (many are) be statistically significant, but that is due not only to the influence of background concentrations, but other confounders and small sample sizes. Using models to isolate source impacts can help identify which sources and components of the air pollution mixture are of greatest concern and then help direct control efforts.

**Questioner Name:** Stefano Galmarini

**Q:** Did you consider the non-independence of your modeling tools and that the results cluster about the truth may be accidental?

**A:** First, the ensembled methods have a variety of different inputs, and while some are less independent than others (e.g., PMF and CMB-LGO that use similar, but not the same inputs), others use rather different inputs, e.g., CMB-molecular markers is driven by detailed organic chemical speciation that is not used in PMF or CMB-LGO, and CMAQ does not use observations at all, except for initialization, which has little impact on the simulated values during the modeled period. Still, we were concerned about demonstrating that the ensemble results are an improvement over any one method because you can not measure source impacts directly. To provide further support, we took independent data for water soluble organic compounds (WSOC) that can be used as a marker for SOA, and levoglucosan (though for a period not used in the ensemble development), and compared the ensemble results to those, and found better agreement than any one method.

# Chapter 2
# Air Quality Effects on Human Health

**J. Brandt, J.D. Silver, J.H. Christensen, M.S. Andersen, J.H. Bønløkke, T. Sigsgaard, C. Geels, K.M. Hansen, E. Kaas, and L.M. Frohn**

**Abstract** An integrated model system based on the impact-pathway chain, EVA (Economic Valuation of Air pollution), has been developed, to assess the health-related economic externalities of air pollution resulting from specific emission sources or sectors. In this study, we apply the EVA system to Europe, and perform a detailed assessment of past, present, and future health-cost externalities of the total air pollution levels in Europe, represented by the years 2000, 2007, 2011, and 2020. Furthermore we perform a detailed analysis of health-related external costs from the ten major emission sectors and their relative contributions.

The paper contains a short description of the EVA system and the results from the assessment of the main contributors. The overall conclusion from the analysis of the ten major emission sectors in Europe is that the main contributors to health-related external costs are major power production, agriculture, road traffic, and non-industrial domestic combustion, including wood combustion. We conclude that when regulating the emissions of ammonia from the agricultural sector, both the

J. Brandt (✉) • J.D. Silver • J.H. Christensen • M.S. Andersen • C. Geels • K.M. Hansen
Department of Environmental Science, Aarhus University, Frederiksborgvej 399, 4000 Roskilde, Denmark
e-mail: jbr@dmu.dk; jds@dmu.dk; jc@dmu.dk; msa@dmu.dk; cag@dmu.dk; kmh@dmu.dk

J.H. Bønløkke • T. Sigsgaard
Section of Environment, Occupation, and Health, Institute of Public Health, Aarhus University, Bartholins Allé 2, Building 1260, 8000 Aarhus C, Denmark
e-mail: jb@mil.au.dk; ts@mil.au.dk

E. Kaas
Planet and Geophysics, Niels Bohr Institute, University of Copenhagen, Juliane Maries Vej 30, 2100 København Ø, Denmark
e-mail: kaas@nbi.ku.dk

L.M. Frohn
AU Knowledge, Aarhus University, Tuborgvej 164, 2400 København NV, Denmark
e-mail: lmf@adm.au.dk

D. Steyn and R. Mathur (eds.), *Air Pollution Modeling and its Application XXIII*, Springer Proceedings in Complexity, DOI 10.1007/978-3-319-04379-1_2,

impacts on nature and on human health should be taken into account. This study confirms that air pollution constitutes a serious problem to human health and that the related external costs are considerable.

## 2.1 Introduction

Air pollution has significant negative impacts on human health and well-being, entailing substantial economic consequences. In order to carry out regulatory actions, knowledge about the magnitude of the problem, both with respect to the number of incidents of different health impacts and to the estimates of the related external costs, is required. An assessment of the health-related external costs from air pollution, based on the best available methodologies, is a powerful tool for decision making, since the external costs can be compared to other socio-economic costs.

We have developed an integrated model system, EVA (Economic Valuation of Air pollution; [7, 8]), to assess health-related economic externalities of air pollution. The EVA system integrates a regional-scale atmospheric chemistry transport model, gridded population data, exposure-response functions, and monetary valuation.

The main goal of the present work is to assess and analyse the contribution from the ten major emission sectors in Europe and quantify their relative importance in terms of impacts on human health and related external costs. Using the EVA system, we also assessed the impacts on human health and related external costs due to total air pollution levels in Europe. Furthermore, we estimated the impacts and external costs of air pollution stemming from emissions from international ship traffic, since this sector is an important contributor. Both for international ship traffic and for the total air pollution levels, results are presented for past, present, and future conditions, represented by the emission years 2000, 2007, 2011, and 2020. For the first 3 years, emissions are based on the EMEP emission database. For the year 2020, emissions are based on the NEC-II emission directive for Europe in order to assess the impacts of the future general emission reductions.

## 2.2 The Integrated Model System EVA

The concept of the EVA system [2–5, 7, 8, 15, 16] is based on the impact pathway chain (e.g., [12, 17]) and illustrated in Fig. 2.1. The EVA system consists of a regional-scale chemistry transport model, address-level or gridded population data, exposure-response functions for health impacts and economic valuations of the impacts from air pollution. The essential idea behind the EVA system is that the best available and most accurate, yet computationally demanding methods are used in each part of the impact-pathway chain. The applied chemistry transport model

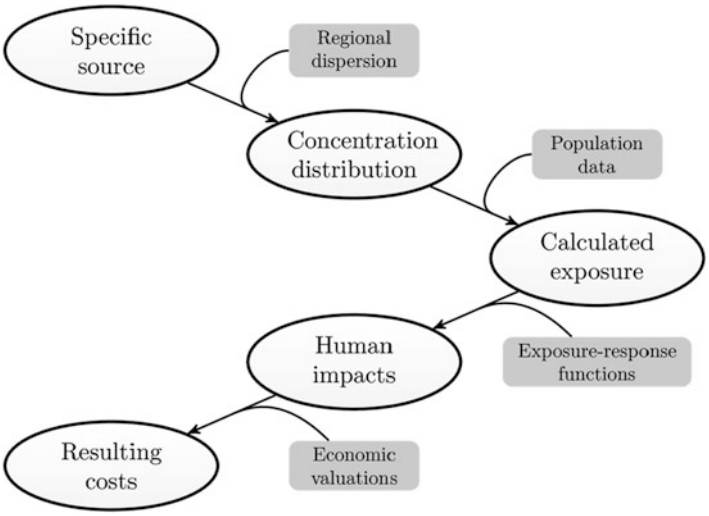


**Fig. 2.1** A schematic diagram of the impact-pathway methodology. The site-specific emissions result (via atmospheric transport and chemistry) in a concentration distribution, which together with detailed population data, is used to estimate the population-level exposure. Using exposure-response functions and economic valuations, the exposure is transformed into impacts on human health and related external costs

(DEHM) covers the Northern Hemisphere, and includes higher resolution nesting over Europe, thereby describing the intercontinental atmospheric transport.

Estimates of changes in concentrations due to a specific source are calculated by a special "tagging" scheme, which accounts for nonlinear effects from chemical transformations [7], which are combined with gridded population data for Europe, to calculate the exposure. Population-level health impacts are estimated by combining the exposure with published exposure-response functions. External costs for the entire population are estimated using cost functions customised for European conditions.

### *2.2.1 The Danish Eulerian Hemispheric Model*

The Danish Eulerian Hemispheric Model (DEHM) is a three-dimensional, offline, large-scale, Eulerian, atmospheric chemistry transport model [6, 9, 10, 13, 14] developed to study long-range transport of air pollution in the Northern Hemisphere and Europe. The model setup used in this study includes three two-way nested domains. The mother domain covers most of the Northern Hemisphere, the second domain covers Europe and the third domain covers Northern Europe with a resolution of 16.67 km $\times$ 16.67 km. The model describes concentration fields of 58 chemical compounds and 8 classes of particulate matter, including a total of

122 chemical reactions. The model has been validated extensively, including a comparison with measurements from the entire Europe (see e.g. [6]). For a more detailed description of the DEHM model, see Brandt et al. [6].

### 2.2.2 Population Data

A gridded data set was obtained from the EUROSTAT 2000 database (http://epp.eurostat.ec.europa.eu/), covering Europe. The health cost assessment part of the EVA system is not applied outside of Europe in this work and therefore population data for the rest of the world are not included.

### 2.2.3 Exposure-Response Functions and Monetary Values

To calculate the impacts of emissions from a specific source or sector, δ-concentrations (i.e., the additional concentration resulting from emissions of a particular emission source) and population data are combined to estimate human exposure, and then the response is calculated using an exposure-response function (ERF) on the form:

$$R = \alpha \cdot \delta c \cdot P$$

where $R$ is the response (e.g., in cases, days, or episodes), $\delta c$ is the δ-concentration, $P$ is the affected share of the population, and $\alpha$ is an empirically-determined constant for the particular health outcome, typically obtained from published cohort studies. In this study, we model the exposure-response relationship as a linear function. Pope [18] showed that this is a reasonable approximation, based on a cohort study of 500,000 individuals and this is also supported by the joint World Health Organization/UNECE Task Force on Health [11, 19]. The exposure-response relations and valuations used in the EVA system are applicable for European conditions [7].

All relevant chemical compounds (i.e., those endorsed by the WHO and the EU Commission) are included in the study. For compounds in aerosol phase, the impacts are assumed to be proportional to their contribution to the particle mass, as opposed to the number of particles. Presently, the compounds related to human health impacts included in the EVA system are: $O_3$, CO, $SO_2$, $SO_4^{2-}$, $NO_3^-$, and the primary emitted part of $PM_{2.5}$. In the present study it is assumed that all components of the PM are equally harmful. This assumption is also assumed valid in the Clean Air for Europe (CAFE) calculation presented in Watkiss et al. [19] and Amann et al. [1].

## 2.3 Health Impacts and External Cost in Europe

The overall EVA model results for human health impacts in Europe are presented in the Table 2.1 showing the number of incidents in Europe, due to the total air pollution concentrations for four different years. As an example of these results, Fig. 2.2 shows the geographical distribution of premature deaths in Europe, calculated from the chronic YOLL (Years Of Life Lost) for the year 2000 divided by a factor of 10.6 as given in Watkiss et al. [19].

Table 2.2 shows the total health-related externalities for Europe related to international ship traffic and to the total air pollution levels due to all sources for the same 4 years. The total health-related external costs for the whole of Europe is estimated at 803 billion Euro/year for the year 2000, decreasing to 537 billion Euro/year in the year 2020. The decrease is due to the general emission reductions in Europe provided that the NEC-II directive is implemented and given emission control regulation of international ship traffic in the North Sea and the Baltic Sea. We estimate the total number of premature deaths in Europe in the year 2000 due to air pollution to be around 680,000/year, decreasing to approximately 450,000 in the year 2020.

**Table 2.1** Total number of incidents in Europe of the impacts related to the air pollution levels stemming from all the emissions in the Northern Hemisphere for the four different years

| Health impact | Number of incidents (cases, days or years) in Europe | | | |
|---|---|---|---|---|
| Year | 2000 | 2007 | 2011 | 2020 |
| Chronic bronchitis | 633, 000 | 535, 000 | 532, 000 | 418,000 |
| Restricted activity days | 647, 000, 000 | 547, 000, 000 | 544, 000, 000 | 427,000,000 |
| Respiratory hospital admissions | 37, 800 | 31, 400 | 31, 200 | 23,800 |
| Cerebrovascular hospital admissions | 81, 200 | 68, 600 | 68, 200 | 53,600 |
| Congestive heart failure | 50, 200 | 42, 700 | 42, 500 | 35,200 |
| Lung cancer | 96, 900 | 81, 900 | 81, 400 | 64,000 |
| Bronchodilator use children | 18, 900, 000 | 16, 000, 000 | 15, 900, 000 | 12,500,000 |
| Bronchodilator use adults | 124, 000, 000 | 105, 000, 000 | 104, 000, 000 | 81,800,000 |
| Cough children | 65, 300, 000 | 55, 200, 000 | 54, 900, 000 | 43,100,000 |
| Cough adults | 128, 000, 000 | 108, 000, 000 | 107, 000, 000 | 84,200,000 |
| Lower respiratory symptoms children | 25, 200, 000 | 21, 300, 000 | 21, 200, 000 | 16,600,000 |
| Lower respiratory symptoms adults | 46, 000, 000 | 38, 800, 000 | 38, 600, 000 | 30,400,000 |
| Acute mortality | 49, 800 | 43, 900 | 43, 700 | 36,200 |
| Chronic mortality (YOLL) | 7, 220, 000 | 6, 100, 000 | 6, 070, 000 | 4,770,000 |
| Infant mortality | 710 | 599 | 596 | 468 |

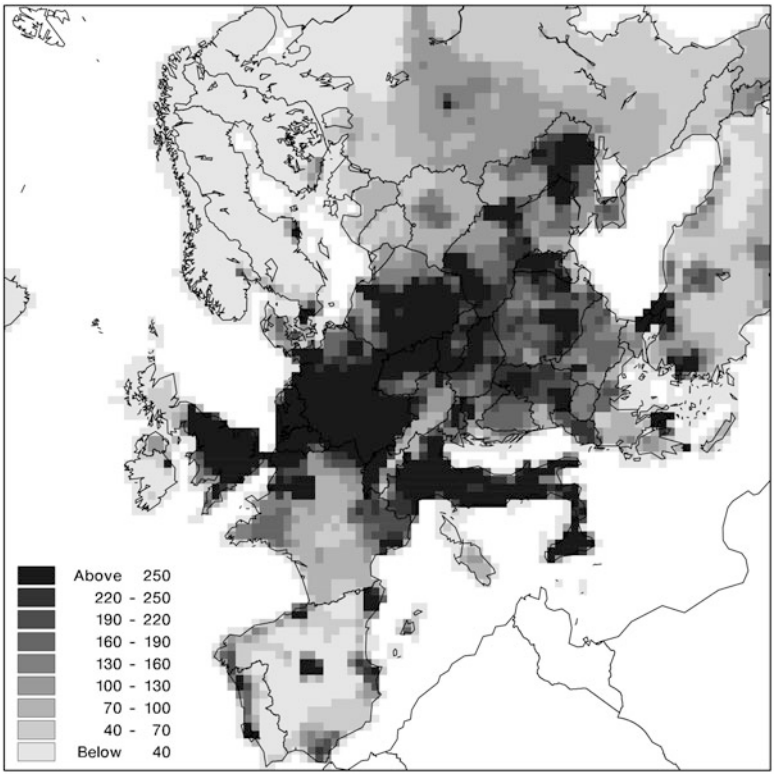


**Fig. 2.2** Number of premature deaths per grid cell in Europe (DEHM European model domain) calculated with the EVA model system for the year 2000 for the total air pollution levels. The area of the grid cells are 50 km × 50 km, so the *shading* refers to the number of premature deaths per 2,500 km$^2$. Note that high numbers of premature deaths require both high annual particle concentrations and high population density

**Table 2.2** Total health-related externalities for Europe related to international ship traffic and to the total air pollution levels for four different emission years

| Year | 2000 | 2007 | 2011 | 2020 |
|---|---|---|---|---|
| Total external cost in Europe due to international ship traffic | 58.4 | 56.9 | 54.3 | 64.1 |
| Total external cost in Europe due to total air pollution levels | 803 | 682 | 678 | 537 |

All costs are in 2006 prices and given in billion Euros

International ship traffic constitutes a major problem in relation to impacts on human health. We estimate that the total external costs in Europe will increase from 58.4 billion Euro/year in the year 2000 to 64.1 billion Euro/year in the year 2020, due to an expected general increase in the ship traffic worldwide (see Table 2.2). If we examine the relative external costs from all international ship traffic, it is responsible for an estimated 7 % of the total health effects in Europe due to air

**Table 2.3** Total health-related external costs for Europe (billion Euros) from the ten major individual emission categories in Europe (DEHM domain 2) for the emission year 2000 as well as their contributions in % to the total external cost in Europe

| European emission sector | Billion Euros | % of cost in Europe |
|---|---|---|
| 1. Combustion in energy and transf. industries | 185 | 24.1 |
| 2. Non-indus. combustion plants/wood | 73 | 9.5 |
| 3. Combustion in manufacturing industry | 60 | 7.9 |
| 4. Production processes | 50 | 6.5 |
| 5. Extr. and distr. of fossil fuels/geoth. energy | 10 | 1.3 |
| 6. Solvents and other product use | 13 | 1.7 |
| 7. Road transport | 138 | 18.0 |
| 8. Other mobile sources and machinery | 50 | 6.5 |
| 9. Waste treatment and disposal | 7.8 | 1.0 |
| 10. Agriculture | 180 | 23.5 |

All costs are in 2006 prices

pollution in the year 2000, increasing to 12 % in the year 2020. In contrast, the contribution from international ship traffic in the Baltic Sea and the North Sea decreases by 36 % due to the regulatory efforts of reducing sulphur emissions from ship traffic. Introducing this regulatory instrument for all international ship traffic in the Northern Hemisphere, or at least in areas close to Europe, would have a significant positive impact on human health in Europe.

In Table 2.3, the total health-related externalities for Europe are shown for the ten major individual emission SNAP categories as well as their contribution in % to the total external cost. Based on the latter it is possible to assess which emission sectors are most important with respect to impacts on human health. The dominating contributors are: (1) the major power plants, which contribute with 24.1 % of the external health costs in Europe, (2) the agricultural sector with around 23.5 %, and (3) the road transport sector, which contributes with 18 % for Europe. Following these sectors are non-industrial combustion plants, which in Northern Europe is dominated by domestic heating and wood burning with around 10 %. The remaining sectors contribute with 8 % or less.

## 2.4 Discussions and Overall Conclusions

In this paper we have presented results from the integrated model system, EVA, which is based on the impact pathway approach and customised for European conditions. The EVA system has been run for different scenarios, assessing the human health impacts and associated external costs from international ship traffic as well as the total concentration levels for four different years (2000, 2007, 2011, and 2020).

The results in this study show that air pollution constitutes a serious problem to human health and that the related external costs are considerable. The main objective of this work was to find the primary activities and emission sources in Europe that give the largest contribution to human health impacts and related external costs taking into account non-linear atmospheric chemistry. The related external costs found in this work can be used to directly compare the contributions from the different emission sectors, potentially as a basis for decision making on regulation and emission reduction.

A key conclusions from this work is that the major contributors from European emissions to the total health-related external costs in the whole of Europe (in order of impact) are power production, agriculture, road traffic and non-industrial (domestic) combustion (including wood combustion). An important assumption here is that the different secondary inorganic aerosols and the primary emitted particles are equally harmful to human health. This is worth noting because particulate matter typically dominates the health impacts, and thus the external costs. The results suggest that the agricultural sector contributes significantly to health impacts and related external costs. The agricultural sector already contributes significantly to impacts on the environment in terms of eutrophication effects in terrestrial and marine eco-systems. From the results in this study, we conclude that not only the impacts on nature should be taken into account when regulating the emissions of ammonia. Impacts on human health should also be considered.

This study shows that the major visible and already highly regulated emission sources (e.g., power plants and road traffic) do not always constitute the most significant problems related to human health. Other less obvious sources can have significant impacts on nature and human health. It is therefore important to make an overall screening of all emission sectors or emission sources in order to create a scientific basis for sound political decisions.

The economic valuation in this study only includes some of the known harmful chemical compounds. In these calculations, we did not include compounds such as polycyclic-aromatic hydrocarbons, persistent organic pollutants, metals, heavy metals, dioxins, and secondary organic aerosols. However, these compounds commonly share the same sources as the compounds included in this study, and the health effects are likely to be included in our calculations due to their correlations with the included compounds, since the exposure-response functions used correlates the $PM_{2.5}$ concentrations with the total health impacts. The system does not presently include impacts and external costs in relation to the natural environment or climate. Furthermore, taking into account that we only included health impacts where the ERF are well-documented and accepted by the WHO and EU Commission, and that the economic valuation of the health impacts has been conservative, the overall results in this work can also be considered conservative.

The absolute external costs in this work should be interpreted carefully. The external costs are, of course, associated with uncertainties, which are very difficult to quantify in such a complex model system and arise at each link of the impact pathway chain. The main uncertainties in the integrated model system are associated with the emissions (which have an uncertainty of $\pm 30$ % on annual basis) and

with the health impacts from the individual chemical compounds associated to air pollution (i.e. the ERFs). Sub-grid scale variability in pollutant concentrations and population density can also have large effects on exposure. With our present knowledge we are not able to distinguish between the impacts from different particle types, and this constitutes a major shortcoming of such a study. However, there are many studies linking the total mass of $PM_{2.5}$ with health effects, showing strong and significant correlations.

Air pollution still constitutes a serious problem to human health and the related external costs are considerable. The results in this work show that the integrated EVA model system can be used to answer relevant health-related socio-economic questions. The results depend highly on geography, emission sector and the nature and extent of emission reductions. Therefore, we recommend that health impacts and related external costs should be calculated for specific emission reduction scenarios, if precise estimates of the outcome of specific regulation initiatives are required.

**Acknowledgments** The present study is a part of the research of the 'Center for Energy, Environment and Health (CEEH)', financed by The Danish Strategic Research Program on Sustainable Energy under contract no 2104-06-0027. Homepage: www.ceeh.dk.

## References

1. Amann M, Bertok I, Cabala R, Cofala J, Heyes C, Gyarfas F, Klimont Z, Schöpp W, Wagner F (2005) A final set of scenarios for the Clean Air For Europe (CAFE) programme. International Institute for Applied Systems Analysis (IIASA, Austria) CAFE Scenario Analysis Report Nr. 6. http://www.iiasa.ac.at/rains/CAFE_files/CAFE-D3.pdf
2. Andersen MS, Frohn LM, Nielsen JS, Nielsen M, Jensen JB, Jensen SS, Christensen J, Brandt J (2006) EVA – a non-linear, Eulerian approach for assessment of health-cost externalities of air pollution. In: Biennial conference of the International Society for Ecological Economics, New Delhi, December 2006
3. Andersen MS, Frohn LM, Brandt J, Jensen SS (2007) External effects from power production and the treatment of wind energy (and other renewables) in the Danish energy taxation system. In: Deketelaere K, Milne JE, Kreiser LA, Ashiabor H (eds) Critical issues in environmental taxation: international and comparative perspectives: vol IV. Oxford University Press, Oxford, pp 319–336
4. Andersen MS, Frohn LM, Nielsen JS, Nielsen M, Jensen SS, Christensen JH, Brandt J (2008) A non-linear Eulerian approach for assessment of health-cost externalities of air pollution. In: Proceedings of the European association of environmental and resource economists 16th annual conference, Gothenburg, Sweden, 28 June 2008, p 23
5. Brandt J, Silver JD, Christensen JH, Andersen MS, Geels C, Gross A, Hansen AB, Hansen KM, Hedegaard GB, Skjøth CA (2010) Assessment of health-cost externalities of air pollution at the national level using the EVA model system. In: Proceedings from the international conference on energy, environment and health – optimisation of future energy systems, Carlsberg Academy, Valby, Denmark, 31 May–02 June 2010, p 5
6. Brandt J, Silver JD, Frohn LM, Geels C, Gross A, Hansen AB, Hansen KM, Hedegaard GB, Skjøth CA, Villadsen H, Zare A, Christensen JH (2012) An integrated model study for Europe and North America using the Danish Eulerian Hemispheric Model with focus on intercontinental transport. Atmos Environ 53:156–176. doi:10.1016/j.atmosenv.2012.01.011

7. Brandt J, Silver JD, Christensen JH, Andersen MS, Bønløkke J, Sigsgaard T, Geels C, Gross A, Hansen AB, Hansen KM, Hedegaard GB, Kaas E, Frohn LM (2013) Contribution from the ten major emission sectors in Europe to the health-cost externalities of air pollution using the EVA model system – an integrated modelling approach. Atmos Chem Phys 13:7725–7746. www.atmos-chem-phys.net/13/7725/2013/. doi:10.5194/acp-13-7725-2013
8. Brandt J, Silver JD, Christensen JH, Andersen MS, Bønløkke J, Sigsgaard T, Geels C, Gross A, Hansen AB, Hansen KM, Hedegaard GB, Kaas E, Frohn LM (2013) Assessment of past, present and future health-cost externalities of air pollution in Europe and the contribution from international ship traffic using the EVA model system. Atmos Chem Phys 13:7747–7764. www.atmos-chem-phys.net/13/7747/2013/. doi:10.5194/acp-13-7747-2013
9. Christensen JH (1997) The Danish Eulerian Hemispheric Model – a three-dimensional air pollution model used for the Arctic. Atmos Environ 31:4169–4191
10. Christensen JH, Brandt J, Frohn LM, Skov H (2004) Modelling of mercury in the Arctic with the Danish Eulerian Hemispheric Model. Atmos Chem Phys 4:2251–2257
11. EU (2004) Modelling and assessment of the health impact of particulate matter and ozone. Economic commission for Europe. Executive body for the convention on long-range transboundary air pollution, Working group on effects. Twenty-third session, Geneva, 1–3 Sept 2004
12. Friedrich R, Bickel P (2001) Environmental external costs of transport. Springer, München
13. Frohn LM, Christensen JH, Brandt J, Hertel O (2001) Development of a high resolution nested air pollution model for studying air pollution in Denmark. Phys Chem Earth 26:769–774
14. Frohn LM, Christensen JH, Brandt J (2002) Development of a high resolution nested air pollution model – the numerical approach. J Comput Phys 179:68–94
15. Frohn LM, Brandt J, Hertel O, Christensen JH, Geels C, Andersen MS, Nielsen JS, Frydendall J, Hvidberg M, Jensen SS, Petersen J, Madsen PV (2006) Assessment of air pollution related damages on human health – and the subsequent costs. In: Proceedings from the 3rd GLOREAM/EURASAP workshop on modern developments in modelling and chemical data analysis, Apeldoorn, The Netherlands, September 2005, p 8
16. Frohn LM, Andersen MS, Geels C, Brandt J, Christensen JH, Hansen KM, Nielsen JS, Hertel O, Skjøth CA, Madsen PV (2007) EVA – an integrated model system for assessing external costs related to air pollution emissions. A contribution to ACCENT T&TP. In: Proceedings from the 2nd ACCENT symposium, p 10. http://www.accent-network.org/
17. Krewitt W, Mayerhofer P, Trukenmüller A, Friedrich R (1998) Application of the impact pathway analysis in the context of LCA. Int J Life Cycle Assess 3(2):86–94
18. Pope CA (2000) Particulate matter-mortality exposure-response relations and threshold. Am J Epidemiol 152(5):407–412
19. Watkiss P, Pye S, Holland M (2005) CAFE CBA: baseline analysis 2000 to 2020. Service contract for carrying out cost-benefit analysis of air quality related issues, in particular in the Clean Air for Europe (CAFE) Programme, AEA Technology Environment, Oxon, UK. http://www.cafe-cba.org/assets/baseline_analysis_2000-2020_05-05.pdf

## Questions and Answers

**Questioner Name:** Nicolas Moussiopoulos

**Q:** Does you system take into account synergies between various pollutants and/or between air pollution and meteorological parameters?

**A:** The system does not presently take into account synergetic effects between air pollution and meteorological parameters, which is a very interesting research field. Concerning synergies between various pollutants, the health impacts research field is not presently at a stage, where we can take this into account.

**Questioner Name:** Joana Soares

**Q:** Do you use indoor/outdoor rations and activity data in your exposure computations?

**A:** No, all exposure calculations are based on the outdoor delta concentrations at residence level. Activity data for the population are not included either.

**Questioner Name:** Tony Dore

**Q:** Your presentation focused on the importance of agricultural emissions in impacting human health. However European emissions have shown only small recent decreases in $NH_3$ compared to other pollutants and policy makers are reluctant to commit to future ammonia reductions. Can you comment on this issue?

**A:** This is a difficult issue, since the connection between ammonia emissions and health impacts is not very commonly acknowledged. I think the only way to create awareness of the complexity of the air quality and human health relation is to perform and publish studies with this focus.

**Questioner Name:** K. Heinke Schlünzen

**Q:** Would acute death and chronic death not have need for different concentration values (peak versus average)?

**A:** Acute death is related to $SO_2$ and $O_3$ only in the calculations. For $SO_2$ it is the yearly average concentration that is used (and this should probably be evaluated), however for $O_3$ it is the daily 8 h maximum concentration. In order to change the calculation procedure, however, new concentration-response functions are needed for $SO_2$.

**Questioner Name:** S. Hanna

**Q:** In your list of components of the comprehensive model system from emissions to health and economic effects, which component is the most uncertain?

**A:** We have chosen to apply only very well documented exposure-response relations, and furthermore to apply a rather conservative estimate for the economic effects in the calculations. I therefore believe that it is the emissions and the proxy for exposure (home address) which are the most uncertain components.

**Questioner Name:** Douw Steyn

**Q:** How do you get politicians and policy makers to use the results of your research?

**A:** We have published the results not only as peer-reviewed literature, but also as more popular scientific reports, suitable for policy making. This has resulted in an extensive use of the results in Denmark recently both at the governmental level as well as for the city of Copenhagen.

# Chapter 3
# Development of Model-Based Air Pollution Exposure Metrics for Use in Epidemiologic Studies

**V. Isakov, M. Snyder, D. Heist, S. Perry, J. Burke, S. Bereznicki, Saravanan Arunachalam, S. Batterman, and CAAA**

**Abstract** Population-based epidemiological studies of air pollution have traditionally relied upon imperfect surrogates of personal exposures, such as area-wide ambient air pollution levels based on readily available concentrations from central monitoring sites. U.S. EPA in collaboration with University of Michigan is developing and evaluating several types or tiers of exposure metrics for traffic-related and regional pollutants that differ in their modeling approaches for addressing the spatial and temporal heterogeneity of pollutant concentrations. We hypothesize that using more refined exposure estimates will provide greater power to detect associations with health outcomes, particularly for traffic-related pollutants that can vary considerably over short distances and time scales. The Near-road Exposures to Urban air pollutant Study (NEXUS) design is focused on determining if children in Detroit, MI with asthma living in close proximity to major roadways have greater health impacts associated with air pollutants than those living

V. Isakov (✉) • M. Snyder • D. Heist • S. Perry
Atmospheric Modeling and Analysis Division, National Exposure Research Laboratory, Office of Research and Development, U.S. EPA, Research Triangle Park, NC 27711, USA
e-mail: isakov.vlad@epa.gov

J. Burke • S. Bereznicki
Human Exposure and Atmospheric Sciences Division, National Exposure Research Laboratory, Office of Research and Development, U.S. EPA, Research Triangle Park, NC 27711, USA

S. Arunachalam
Institute for the Environment, The University of North Carolina, Chapel Hill, NC, USA
e-mail: sarav@email.unc.edu

S. Batterman
Environmental Health Sciences, School of Public Health, University of Michigan, Ann Arbor, MI, USA

CAAA
Community Action Against Asthma (CAAA) is a community-based participatory research partnership and also an affiliated project of the Detroit Community-Academic Urban Research Center, Ann Arbor, MI, USA

D. Steyn and R. Mathur (eds.), *Air Pollution Modeling and its Application XXIII*, Springer Proceedings in Complexity, DOI 10.1007/978-3-319-04379-1_3,

farther away, particularly for children living near roadways with high diesel traffic. One tier for estimating exposures to traffic-generated pollutants uses local-scale dispersion modeling. Temporally and spatially-resolved pollutant concentrations, associated with local variations of emissions and meteorology, were estimated using a combination of the AERMOD and RLINE dispersion models, local emission source information from the National Emissions Inventory, detailed road network locations and traffic activity, and meteorological data from the Detroit City Airport. Hourly pollutant concentrations for CO, $NO_x$, $PM_{2.5}$ and its components (EC and OC) were predicted at each study participant location ($n = 160$). The exposure metrics were evaluated in their ability to characterize the spatial and temporal variations of multiple ambient air pollutants across the study area. This research will be used for improving exposure assessments in future air pollution epidemiology studies, and for informing future multipollutant exposure analyses.

## 3.1 Introduction

Through the Clean Air Act (CAA), the U.S. Environmental Protection Agency (EPA) develops air quality standards to protect the public from the health effects of criteria air pollutants (ozone, carbon monoxide, oxides of nitrogen, particulate matter, lead and oxides of sulfur) and hazardous air pollutants (HAPs). These Congressional mandates have led to a systematic risk assessment approach that encompasses hazard identification, dose-response assessment, exposure assessment, and risk characterization. As this field of risk assessment has evolved, so has the reliance on epidemiologic studies for identifying hazards to air pollutants, quantifying the relationship between dose, exposure, or concentration and the response, and determining and assessing mitigation strategies. In the absence of personal exposure measurements, epidemiologic studies have traditionally relied upon alternate indicators of exposure, such as area-wide ambient air pollution concentrations from central monitoring sites. For the criteria air pollutants, epidemiologic studies typically use ambient monitoring data collected for regulatory purposes or study-specific monitors for short duration (e.g., 2 week time periods) for selected research studies. These studies assume that concentrations at a single monitor, or average concentrations over a few monitors, are representative of the complex spatial and temporal patterns of air quality within a study area. However, there is increasing evidence that the monitoring network is not capturing the sharp gradients in exposure due to locally high concentrations (e.g., near major roadways, factories, ports). For many of the HAPs, ambient monitoring data are often nonexistent or very sparse. In order to reduce uncertainty that may be introduced via exposure misclassification and/or prediction error, these epidemiologic studies (especially time-series studies) require an accurate assessment of the complex temporal and spatial variations in ambient concentrations. Improving characterization of air pollution exposures involves novel approaches to estimating ambient concentrations, a better understanding of the personal-ambient relationships, and personal exposure modeling.

## 3.2 Air Quality Modeling Approach for Estimating Exposures

U.S. EPA in collaboration with University of Michigan is developing and evaluating several types or tiers of exposure metrics for traffic-related and regional pollutants that differ in their modeling approaches for addressing the spatial and temporal heterogeneity of pollutant concentrations [1]. We hypothesize that using more refined exposure estimates will provide greater power to detect associations with health outcomes, particularly for traffic-related pollutants that can vary considerably over short distances and time scales. We use air quality modeling to estimate exposures to traffic-generated pollutants in support of the Near-road Exposures to Urban air pollutant Study (NEXUS) study assessing the impact of near-roadway pollution on children's exposures and resulting respiratory effects. Three traffic exposure groups were identified in order to test for differences between the low diesel (LD), high diesel (HD) and low traffic (LT) areas (Fig. 3.1). Children in the LD and HD groups live within 150 m of a major roadway while those in the LT group live greater than 300 m for a major roadway.

In this study, we use a combination of local-scale dispersion models, region-scale models and observations to provide spatially-resolved pollutant concentrations for the epidemiologic analysis. Temporally and spatially-resolved pollutant

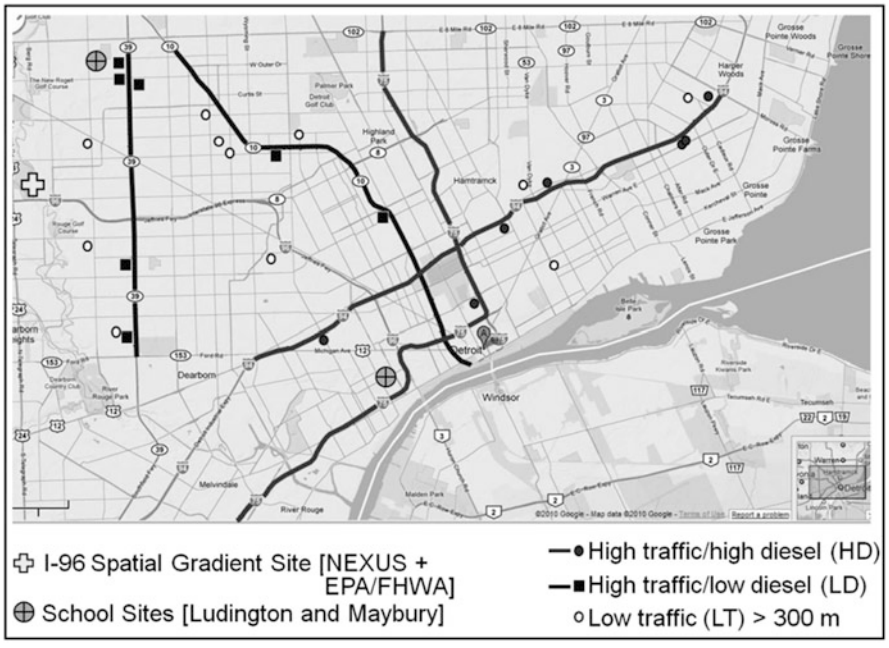


**Fig. 3.1** Modeling domain for the NEXUS study

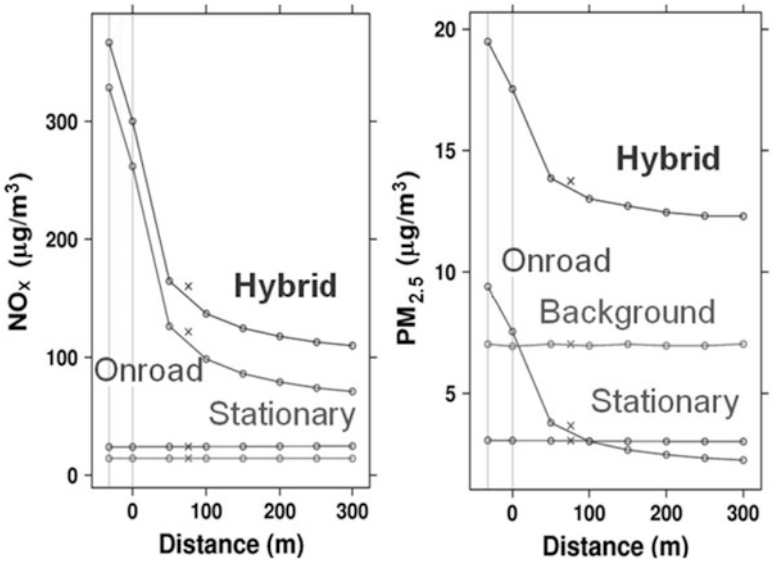


**Fig. 3.2** Near road gradients of modeled concentrations for $NO_X$ (*left panel*) and $PM_{2.5}$ (*right panel*)

concentrations, associated with local variations of emissions and meteorology, were estimated using a combination of AERMOD [2] and RLINE [3] dispersion models. RLINE is a research-level, line-source dispersion model being developed by EPA's Office of Research and Development as a part of the ongoing effort to develop tools for a comprehensive evaluation of air quality impacts in the near-road environment. This model is being used in conjunction with traffic activity and primary mobile source emission estimates to model hourly exposure from roadway emissions for study participants' home and school locations. AERMOD is used to estimate additional exposures from stationery sources. For the background estimates, we used a space/time ordinary kriging (STOK) method that combines air quality system (AQS) measurements and results from two CMAQ simulations: (1) using all emissions in a broad region and (2) all anthropogenic emissions in the Detroit study domain removed. The ratios of concentrations from two CMAQ simulations along with AQS data from background sites in the region were used to estimate the background concentrations. An example of modelled $PM_{2.5}$ and $NO_x$ concentrations as a function of distance from a roadway is shown in Fig. 3.2.

Figure 3.2 represents average hourly pollutant concentration gradients for one major roadway in Detroit, MI. These panels show the homogeneity in the background pollutant levels. For this particular location, the stationary source pollutant levels also seem homogeneous as a function of distance from the roadway suggesting there is no large nearby source of these pollutants. Thus in this case, the pollutant gradients are completely due to the dispersion of primary emissions from traffic on this roadway. The interesting thing to note is that NOx concentrations

from traffic remain above background levels even 300 m from the roadway, however $PM_{2.5}$ concentrations are slightly elevated above background levels from primary traffic emissions within ~50 m from the roadway then fall below background levels. This behavior shows the mostly regional behavior of PM2.5, but source specific behavior of NOx in the absence of a large nearby stationary source. This reemphasizes the need to have highly resolved emissions and modeling to adequately resolve concentration differences in the near-road environment that impact personal exposures.

## 3.3 Model-Based Exposure Metrics for Use in the Epidemiologic Study NEXUS

The modeling provided hourly pollutant concentrations for CO, $NO_x$, $PM_{2.5}$ and its components (EC and OC) at each study participant location. From the hourly concentration, exposure metrics were calculated for the following time periods: daily: 24 h period; a.m. off-peak: 1–6; a.m. peak: 7–8; mid-day: 9–14; p.m. peak: 15–17; and p.m. off-peak: 18–24. These daily exposure metrics capturing spatial and temporal variability across health study domain (Fall 2010–Spring 2012) were used in the epidemiologic analyses. Preliminary results (not shown here) using simple proximity-based exposure metrics in epidemiologic models with health outcomes were mixed (i.e. expected effect but not statistically significant), so may not be adequate for this study. However, advanced model-based exposure metrics may help to discern the relationships between air quality and health outcomes. Table 3.1 below compares the Asthma Control Test (ACT) scores using two different exposure metrics as inputs – primary $PM_{2.5}$ from mobile sources and urban background $PM_{2.5}$. ACT scores have a maximum of 25 (good asthma control); scores below 19 suggest poor asthma control.

The results indicate that for primary traffic-related $PM_{2.5}$, each 1 $\mu g/m^3$ increase in $PM_{2.5}$ concentration is associated with a 0.5 decrease in ACT which obtained statistical significance. Thus, 3–5 $\mu g/m^3$ level of primary $PM_{2.5}$ concentrations typically observed near roads would lead to a 1.5–2.5 change in ACT score which is very significant. The elevated $PM_{2.5}$ levels near roadways are dependent on the dispersion conditions, traffic volume, and fleet mix (diesel percentage). From the results presented in Table 3.1, a positive association begins to emerge between roadways with large traffic volumes (especially those with large diesel percentages) and a decrease in ACT scores, suggesting worsening asthmatic symptoms.

**Table 3.1** Asthma Control Test (*ACT*) scores using GEE models

| Modeled exposure metric | ACT score | Standard error | p value |
|---|---|---|---|
| Primary $PM_{2.5}$ (from mobile sources) | **−0.51** | **0.26** | **0.05** |
| Urban background $PM_{2.5}$ | 0.22 | 0.22 | 0.30 |

**Acknowledgment** This paper has been subjected to Agency review and approved for publication. Approval does not signify that the contents reflect the views of the Agency nor does mention of trade names or commercial products constitute endorsement or recommendation for use. The authors would like to acknowledge contributions by Toby Lewis, Tom Robins, Graciela Mentz of University of Michigan.

## References

1. Vette A, Burke J, Norris G, Landis M, Batterman S, Breen M, Isakov V, Lewis T, Gilmour M, Kamal A, Hammond D, Vedantham R, Bereznicki S, Tian N, Croghan C, CAAA (2013) The Near-Road Exposures and Effects of Urban Air Pollutants Study (NEXUS): study design and methods. Sci Total Environ 448:38–47
2. Cimorelli A, Perry S, Venkatram A, Weil J, Paine R, Wilson R, Lee R, Peters W, Brode R (2005) AERMOD: a dispersion model for industrial source applications. Part I: General model formulation and boundary layer characterization. Appl Meteorol 44:682–693
3. Snyder M, Venkatram A, Heist D, Perry SG, Petersen W, Isakov V (2013) RLINE: a line source dispersion model for near-surface releases. Atmos Environ 77:748–756

## Questions and Answer

**Questioner Name:** Pius Lee

Q: As high diesel emission is tracked well by $PM_{2.5}$. That seemed to be the primary species triggering asthma attack. Also is one of your listing of possible species of air pollutants contributing to ACT score: e.g. one slide showed $PM_{2.5}$, EC, $NO_x$ ... Are these ranked in their contribution to ACT score?

A: We showed only preliminary results from the epidemiologic analysis using exposure metrics for primary $PM_{2.5}$ as an input. The analysis is still ongoing and we expect to have the risk coefficients for other pollutants when the epidemiologic study is completed so we would be able to compare relative risks coefficients for diesel PM and other pollutants such as CO and $NO_x$.

# Chapter 4
# Improved Spatiotemporal Source-Based Air Pollutant Mixture Characterization for Health Studies

**Heather A. Holmes, Xinxin Zhai, Jeremiah Redman, Kyle Digby, Cesunica Ivey, Sivaraman Balachandran, Sheila A. Sororian, Mariel Friberg, Wenxian Zhang, Marissa L. Maier, Yongtao Hu, Armistead G. Russell, James A. Mulholland, and Howard H. Chang**

**Abstract** The growing availability of spatially resolved health data sets (i.e., resident and county level patient records) requires spatially resolved exposure or air quality metrics to investigate the impact of air pollution on health outcomes. While daily air quality data are essential in time-series epidemiologic analysis, the spatial distribution of the observations is limited. Air pollution modeling (i.e., chemical transport modeling (CTM)) addresses this by producing spatially resolved air quality predictions using terrain, emissions and meteorology inputs. However, predicted concentrations may be biased. This work incorporates unique data fusion approaches to combine air quality observations from regulatory monitoring networks (OBS) with the output from a CTM (CMAQ) to generate spatially and temporally resolved gaseous and PM species concentrations. Species concentrations alone cannot directly identify emission sources or characterize pollutant mixtures, therefore source apportionment (SA) models are required to estimate source impacts. The focus of this work is a comparison of SA results for three U.S. regions with differing air pollution sources, St. Louis, Missouri; Atlanta, Georgia; and Dallas-Fort Worth, Texas.

H.A. Holmes (✉) • X. Zhai • J. Redman • K. Digby • C. Ivey • S. Balachandran • S.A. Sororian • M. Friberg • W. Zhang • M.L. Maier • Y. Hu • A.G. Russell • J.A. Mulholland
School of Civil and Environmental Engineering, Georgia Institute of Technology, Atlanta, GA 30332, USA
e-mail: heather.holmes@ce.gatech.edu

H.H. Chang
Department of Biostatistics and Bioinformatics, Emory University, Atlanta, GA 30322, USA

D. Steyn and R. Mathur (eds.), *Air Pollution Modeling and its Application XXIII*, Springer Proceedings in Complexity, DOI 10.1007/978-3-319-04379-1_4,

## 4.1 Introduction

Air pollution concentrations measured from regulatory monitoring networks are commonly used as air quality metrics in time-series epidemiologic analysis to investigate air quality and human health associations. While these data provide useful indicators for air pollution impacts in a region, the data are limited temporally, spatially and chemically. The growing availability of spatially resolved health data sets (i.e., resident and county level patient records) requires spatially resolved exposure or air quality metrics to investigate the impact of air pollution on health outcomes [3]. The species concentration data in combination with chemical transport models (CTM) and source apportionment (SA) techniques can be used to characterize sources and species impacting both individual locations and wider areas. As part of the Southeastern Center for Air Pollution and Epidemiology (SCAPE), a Mixtures Characterization (MC) Toolkit is being developed to effectively analyze air pollution and air quality modeling data to better understand how sources are combining to impact air quality for use in health assessments.

## 4.2 Methods

Statistical data analysis is done using the daily observations of species concentrations to calculate a time-series of spatial air pollution metrics based on both area and population weighted averages [6]. While daily air quality data are essential in time-series epidemiological analysis, the spatial distribution of the observations is limited. Air pollution modeling (i.e., chemical transport modeling (CTM)) addresses this by producing spatially resolved air quality predictions. The CTM used is CMAQ (U.S. EPA), which uses meteorology outputs from a numerical weather prediction model and emissions modeling to generate a spatial and temporal allocation of the source emissions. The CMAQ model incorporates emissions, meteorological and chemical processes but the model output is not nudged or calibrated to observations therefore predicted concentrations may be biased. Thus, a data fusion approach is utilized to combine air quality observations from regulatory monitoring networks (OBS) with the output from CMAQ to improve the spatially and temporally resolved gaseous and PM species concentrations [13].

Species concentrations alone cannot directly be used to identify emission sources or characterize pollutant mixtures [12, 14]. Hence, the fused OBS-CMAQ data is incorporated into an Emissions Based Integrated Mobile Source Indicator ($IMSI_{EB}$) to obtain spatiotemporal mobile source impact estimates [9]. The method developed by Pachon et al. [9] is for ambient monitor data, this work extends that method and applies it to each grid cell in the OBS-CMAQ modeling domain. Where, concentrations of EC, CO and $NO_x$ are used as tracers to estimate the impact of mobile sources on $PM_{2.5}$. The ratio of the mobile emissions to total emissions for each species (i.e., EC, CO and $NO_x$) is used with the species concentrations to

weight the mobile source contributions in each grid. The estimated mobile source impact is scaled using the relationship between the annual EC concentration and annual mobile source impact estimated by receptor modeling.

Source impacts are also estimated using traditional receptor oriented SA methods, Chemical Mass Balance (CMB) and Positive Matrix Factorization (PMF), and source oriented modeling from CMAQ [4, 7, 10, 15]. As part of the MC Toolkit, two novel SA techniques are being developed to improve the characterization of exposure estimates by source emissions. First, an ensemble method that generates new source profiles for CMB based on an ensemble-trained approach utilizing results from CMB, PMF and CMAQ [1, 2, 8]. The second is a hybrid source-receptor model approach that adjusts the original CMAQ source impact estimates based on scaling factors obtained using simulations and observations in a CMB-fashion optimization [5, 11].

## 4.3 Results

Results from the methods described above are presented for three regions with differing air pollution sources, St. Louis, Missouri; Atlanta, Georgia; and Dallas-Fort Worth, Texas. There is a significant impact of point source emissions, e.g., chemicals manufacturing and metals processing, on the air pollution in St. Louis. While in Atlanta large biogenic emissions interact with emissions from mobile sources and power plants which lead to a large amount of secondary organic aerosol formation. The primary sources impacting air pollution in Dallas-Fort Worth are mobile sources. Spatially resolved species concentrations and source impact estimates are shown for the state of Georgia because air quality modeling is utilized to provide air quality metrics for a spatially resolved health study in Georgia.

Spatially resolved health studies require more information about the spatial distribution of pollutant concentrations. The OBS-CMAQ method provides the spatial distribution of air quality metrics by combining the monitor data and CMAQ results. Figure 4.1, shows the 8-h ozone concentration from the monitors and the original CMAQ results (left) and the fused OBS-CMAQ predictions are also shown (right). The ratio of the observation and CMAQ results are spatially interpolated to each grid cell in the domain using ordinary kriging which is then multiplied by the original CMAQ field to adjust the concentrations predicted by CMAQ. The result is an unbiased species concentration at a 4-km resolution for the state of Georgia. While 8-h ozone is shown here this is being done for additional pollutant gases (CO, $NO_2$, $NO_x$, $SO_2$) and particulate matter species ($PM_{10}$, $PM_{2.5}$, $SO_4^{2-}$, $NO_3^-$, $NH_4^+$, EC, OC).

The OBS-CMAQ species concentrations can be used in combination with the emissions inventory to calculate mobile source impacts in Georgia (Fig. 4.2). An emissions model is used to generate spatially and temporally resolved emissions estimates for each grid in the modeling domain. Then, the emissions information and OBS-CMAQ species concentrations for EC, CO and $NO_x$ are used to generate

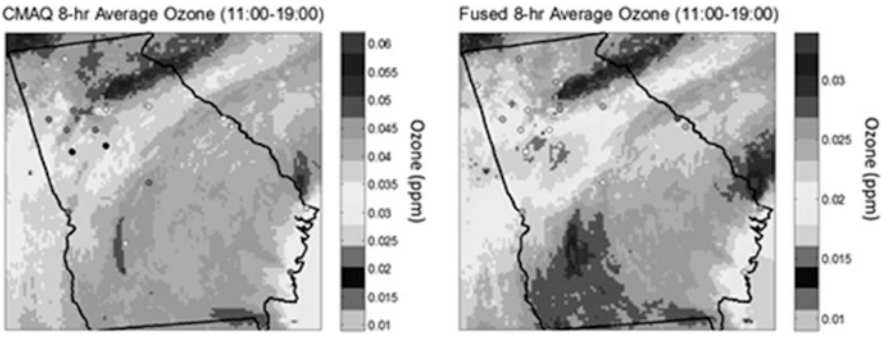


**Fig. 4.1** Improved spatial concentration estimates: Georgia 4-km resolution CMAQ simulated 8-h ozone 18 July 2010 (*left*) CMAQ and observations (*right*) Fused OBS-CMAQ, spatially interpolated ratio of observation to CMAQ concentration using ordinary kriging (*Note scale difference on color axis*)

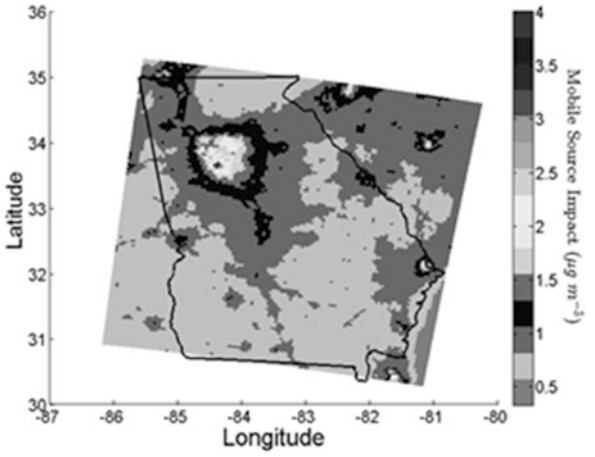


**Fig. 4.2** Spatial mobile source impact estimates: 2010 annual average Georgia 4-km resolution using CMAQ-OBS EC, CO and $NO_x$ concentrations and emissions inventory data

daily mobile source impacts at a 4-km resolution for Georgia. The 2010 annual average mobile source impact is shown in Fig. 4.2. The major urban areas can be seen in the figure with the highest mobile source impacts and the structure of the major freeways north and south of Atlanta is also evident.

For time-series health studies, results from multiple SA receptor models are ensemble averaged to generate updated source profiles that are used as inputs to CMB. The ensemble method is an improvement over using a single SA model because there are less zero impact days which is physically unrealistic and the source profiles are more indicative of the sources impacting the location.

The difference in source profiles can be seen by comparing the ensemble based source profiles (EBSP) and measurement based source profiles (MBSP) for multiple receptor locations, shown in Fig. 4.3 for gasoline and diesel vehicles. The ensemble method assumes that there is a seasonality in source impacts and therefore the data is split into summer and winter seasons when generating the EBSPs.

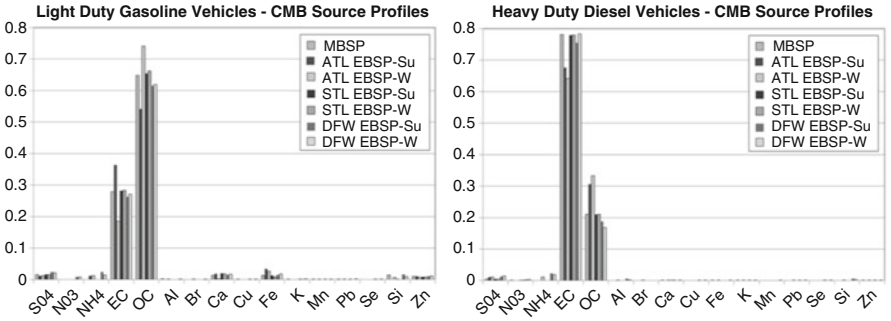


**Fig. 4.3** Ensemble source apportionment: Comparison of measurement based (*MBSP*) and ensemble based (*EBSP*) summer and winter source profiles used in CMB for Atlanta (*ATL*), St. Louis (*STL*) and Dallas-Fort Worth (*DFW*)

Future work will incorporate the source impact estimates in each region into epidemiologic studies to investigate the city-to-city variability in pollutant mixtures and associations with health outcomes.

**Acknowledgments** This research was supported, in part, by USEPA grant R834799. Its contents are solely the responsibility of the grantee and do not necessarily represent the official views of the USEPA. Further, USEPA does not endorse the purchase of any commercial products or services mentioned in the publication. Additional support was made possible by grants from Georgia Power and the Southern Company.

## References

1. Balachandran S, Chang HH, Pachon JE, Holmes HA, Mulholland JA, Russell AG (2013) A Bayesian-based ensemble technique for source apportionment of $PM_{2.5}$. Environ Sci Technol 47:13511–13518
2. Balachandran S, Pachon JE, Hu Y, Lee D, Mulholland JA, Russell AG (2012) Ensemble trained source apportionment of fine particulate matter and method uncertainty analysis. Atmos Environ 61:387–394
3. Bell ML (2006) The use of ambient air quality modeling to estimate individual and population exposure for human health research: a case study of ozone in the northern Georgia region of the United States. Environ Int 32(5):586
4. Cohan DS, Hakami A, Hu Y, Russell AG (2005) Nonlinear response of ozone to emissions: source apportionment and sensitivity analysis. Environ Sci Technol 39(17):6739–6748
5. Ivey C, Holmes H, Hu Y, Russell A, Mulholland J (2013) Spatial and temporal extension of a novel hybrid source apportionment model. In: International technical meeting on air pollution modelling and its application, Miami, FL
6. Ivy D, Mulholland JA, Russell AG (2008) Development of ambient air quality population-weighted metrics for use in time-series health studies. J Air Waste Manage Assoc 58(5):711–720
7. Koo B, Dunker AM, Yarwood G (2007) Implementing the decoupled direct method for sensitivity analysis in a particulate matter air quality model. Environ Sci Technol 41(8):2847–2854

8. Maier ML, Balachandran S, Mulholland JA, Russell AG, Ebelt S, Turner JR (2013) Application of an ensemble-trained source apportionment approach at a site impacted by multiple point sources. Environ Sci Technol 47:3743–3751
9. Pachon JE, Balachandran S, Hu Y, Mulholland JA, Darrow LA, Sarnat JA, Tolbert PE, Russell AG (2012) Development of outcome-based, multipollutant mobile source indicators. J Air Waste Manage Assoc 62(4):431–442
10. Reff A, Eberly SI, Bhave PV (2007) Receptor modeling of ambient particulate matter data using positive matrix factorization: review of existing methods. J Air Waste Manage Assoc 57(2):146–154
11. Russell A, Holmes H, Friberg M, Ivey C, Hu Y, Balachandran S, Mulholland J, Tolbert P, Sarnat J, Sarnat S, Strickland M, Chang H, Liu Y (2013) Use of air quality modeling results in health effects research. In: International technical meeting on air pollution modelling and its application, Miami, FL
12. Sarnat JA, Marmur A, Klein M, Kim E, Russell AG, Sarnat SE, Mulholland JA, Hopke PK, Tolbert PE (2008) Fine particle sources and cardiorespiratory morbidity: an application of chemical mass balance and factor analytical source-apportionment methods. Environ Health Perspect 116(4):459
13. Sororian S, Holmes H, Friberg M, Ivey C, Hu Y, Mulholland J, Russell A, Strickland M, Chang H (2013) Temporally and spatially resolved air pollution in Georgia using fused ambient monitoring data and chemical transport model results. In: International technical meeting on air pollution modelling and its application, Miami, FL
14. Stanek LW, Sacks JD, Dutton SJ, Dubois JJB (2011) Attributing health effects to apportioned components and sources of particulate matter: an evaluation of collective results. Atmos Environ 45(32):5655–5663
15. Watson JG, Zhu T, Chow JC, Engelbrecht J, Fujita EM, Wilson WE (2002) Receptor modeling application framework for particle source apportionment. Chemosphere 49(9):1093–1136

## Questions and Answer

**Questioner Name:** Clemens Mensink

**Q:** How far do we have to go in increasing the model resolution and improving temporal aspects (e.g., on traffic emissions) in order to make sure that there is a scientific sound and well understood association with health?

**A:** The air quality (AQ) data needed to support the epidemiologic analysis depends on the health association being investigated, e.g. if location of residents is being used spatially resolved AQ metrics are necessary and for daily emergency department visits daily AQ metrics are required. The purpose of this work is to provide surrogates of exposure for a spatially resolved health analysis (i.e., 250 m) therefore improving the AQ model resolution to match the health study resolution is desired.

# Chapter 5
# Advances in Linked Air Quality, Farm Management and Biogeochemistry Models to Address Bidirectional Ammonia Flux in CMAQ

**Ellen J. Cooter, Jesse O. Bash, Verel Benson, and Limei Ran**

**Abstract** Recent increases in anthropogenic inputs of nitrogen to air, land and water media pose a growing threat to human health and ecosystems. Modeling of air-surface N flux is one area in need of improvement. Implementation of a linked air quality and cropland management system is described, and a tool to facilitate estimation of fertilizer input information required by the air quality model is presented. Preliminary evaluation of the coupled system against observations indicates improved wet deposition estimates.

## 5.1 Introduction

Recent increases in regional-to-global air, land and water nitrogen (N) inputs pose a growing threat to human health and ecosystem. Policy actions that address this threat demand improved characterization of all aspects of the N-cycle, including air quality. Areas in which improvements are needed include: (1) modeling of N species that exhibit bi-directional surface exchange (e.g., ammonia ($NH_3$)), (2) integration of agricultural practices and meteorologically-driven emissions to reduce $NH_3$ and inorganic fine particulate ($PM_{2.5}$) concentration and deposition uncertainty, and (3) modeling systems that support joint air, land and water environmental options to protect human health and ecosystems. This chapter describes the implementation

E.J. Cooter (✉) • J.O. Bash
U.S. Environmental Protection Agency/ORD/NERL/AMAD, Research Triangle Park, NC, USA
e-mail: Cooter.Ellen@epa.gov

V. Benson
Benson Consulting, Columbia, MO, USA

L. Ran
Institute for the Environment, University of North Carolina, Chapel Hill, NC, USA

D. Steyn and R. Mathur (eds.), *Air Pollution Modeling and its Application XXIII*,
Springer Proceedings in Complexity, DOI 10.1007/978-3-319-04379-1_5,

of linked bi-directional air quality and cropland agricultural management models to improve estimates of $NH_3$ soil flux, total reduced N deposition and ambient $PM_{2.5}$ concentrations.

## 5.2 Methodology

The first step towards these improvements is to implement a bi-directional flux approach into the Community Multi-scale Air Quality (CMAQ) model [2]. Figure 5.1 illustrates this implementation. The primary changes to the standard CMAQ approach include the separate treatment of agricultural cropland from other sources of $NH_3$, input of the rate and depth of fertilizer applications as a driver of cropland emissions, and dynamic tracking of the soil ammonium ($NH_4^+$) pool. Details of the bidirectional flux model in CMAQ (BIDI) is provided in Bash et al. [1]. In BIDI, the emissions inventory for cropland $NH_3$ emissions is replaced by a compensation point approach described in Nemitz et al. [5] to allow for bi-directional exchange. The compensation point is a function of temperature and emission potential ($\Gamma$). Sensitivity analyses suggest that soil emission potential ($\Gamma_s$) can be a significant contributor to flux uncertainty [4] and so its credible estimation is important.

The U.S. Department of Agriculture Environmental Policy Impact Climate (EPIC) model is used to calculate soil nitrogen biogeochemistry leading to $\Gamma_s$ (http://www.epicapex.brc.tamus.edu). The initial implementation for CMAQ is

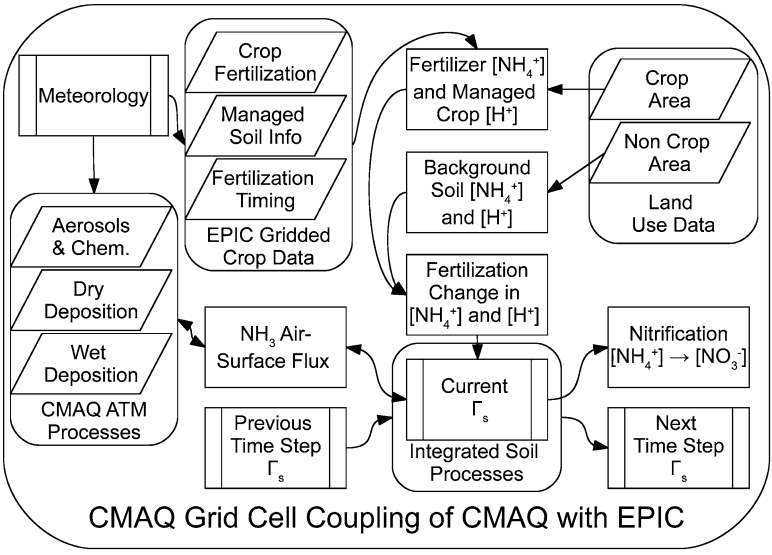


**Fig. 5.1** Implementation in bi-directional CMAQ (After Cooter et al. [3])

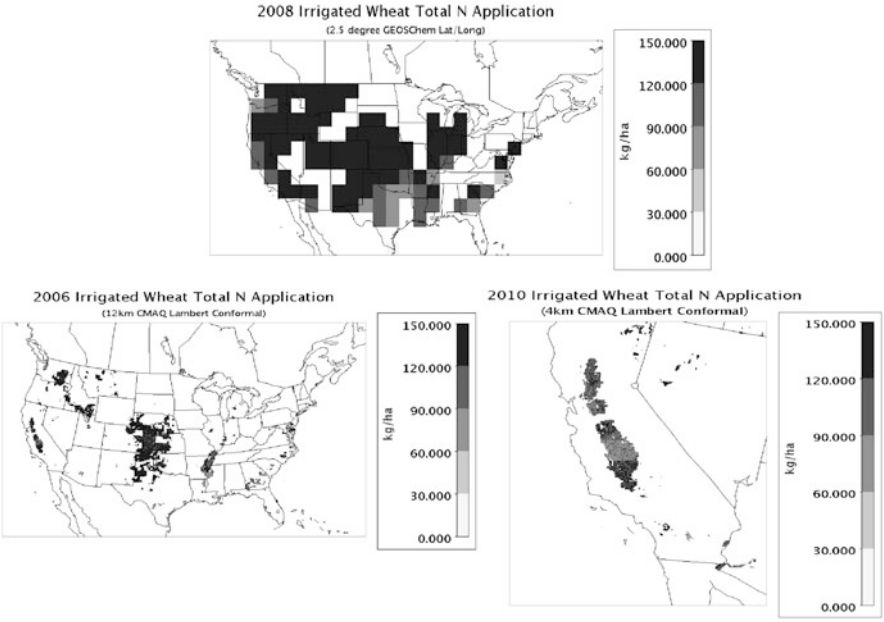


**Fig. 5.2** The FEST-C interface supports generation of model-ready daily fertilizer rate and depth for multiple gridded U.S. domains and resolutions (*Top*, GEOschem 2.5° CONUS; *Lower left*, CMAQ 12 km CONUS; *Lower right*, CMAQ 4 km CalNex)

described in Cooter et al. [3]. The system now also includes year-specific gridded modeled hourly meteorology and daily deposition. A user interface, the Fertilizer Emissions Scenario Tool for CMAQ (FEST-C) has been developed to produce EPIC-based, BIDI-ready input files containing initial soil pH and soil $NH_4^+$ in the upper 1 cm and underlying soil layers. This is followed by daily simulated fertilizer application rate in each layer. BIDI then uses this information to track the ammonium-N in each layer and to compute $\Gamma_s$, and to determine whether $NH_3$ is emitted or deposited. FEST-C produces this information on any projected or latitude/longitude grid, for any U.S. domain and grid resolution for which gridded meteorology is available (Fig. 5.2).

## 5.3 Results and Discussion

Evaluation of BIDI system results shows improved CMAQ estimates of annual NHx wet deposition. The bias is reduced from −20 to −4 %. Estimates of ambient nitrate aerosol and inorganic $PM_{2.5}$ concentrations improve during the spring and fall seasons [1].

Applications that make use of this linked system include: simulating the air quality response to increased corn production in support of the U.S. Renewable Fuels Standard (RFS); improving our understanding of the seasonal and regional signature of nitrous oxide emissions from intensive agricultural areas; linkage of this system to water quality models to explore the impact of alternative management practices on nutrient loading to estuaries, especially the hypoxic zone in the U.S. Gulf of Mexico; and the exploration of the response of various ecosystem services to future alternative climate and land use futures.

A linked air quality and farm management system has been implemented to reduce uncertainty in our estimates of $NH_3$ flux from agricultural soils. Support tools have been developed to facilitate use of this linked system by the air quality modeling community. Preliminary evaluations indicate that the system does indeed improve our estimates of regional wet deposition and inorganic $PM_{2.5}$. This flexible system is being used to address a number of questions related to joint air, land and water issues in order to better protect human health and to sustain ecosystems.

**Acknowledgments and Disclaimer** Although this work has been reviewed and approved for publication by the U.S. Environmental Protection Agency, it does not reflect the views and policies of the agency. FEST-C tool developed was performed by the UNC Institute for the Environment under Contracts EP-D-12-044 and EP-W-09-023.

## References

1. Bash JO, Cooter EJ, Dennis RL, Walker JT, Pleim JE (2013) Evaluation of a regional air quality model with bidirectional $NH_3$ exchange coupled to an agro-ecosystem model. Biogeosciences 10:1635–1645
2. Byun EW, Schere KL (2006) Review of the governing equations, computational algorithms, and other components of the models-3 Community Multiscale Air Quality (CMAQ) modeling system. Appl Mech Rev 59:51–77
3. Cooter E, Bash J, Benson V, Ran L (2012) Linking agricultural crop management and air quality models for regional to national-scale nitrogen assessments. Biogeosciences 9:4023–4035
4. Dennis RL, Schwede DB, Bash JO, Pleim JE, Walter JT, Foley KM (2013) Sensitivity of continental United States atmospheric budgets of oxidized and reduced nitrogen to dry deposition parameterizations. Philos Trans R Soc B 368:1621, 20130124
5. Nemitz E, Milford C, Sutton MA (2001) A two-layer canopy compensation point model for describing bi-directional biosphere-atmosphere exchange of ammonia. Q J R Meteorol Soc 127:815–833

## Questions and Answers

**Questioner Name:** Clemens Mensink

**Q:** In the bi-directional ammonia flux model, what are the most sensitive input parameters?

**A:** Dennis et al. [4] address the sensitivity of bi-directional flux estimates in detail. The authors conclude that at the continental scale, $NH_3$ emissions change by 40 % with a 50 % change in $\Gamma_s$ and by 30 % with a 50 % change in fertilizer application rate. Continental deposition changes are much smaller because of the dominance of livestock emissions.

**Questioner Name:** Pius Lee

**Q:** Since bi-directional flux of $NH_3$ is very sensitive to soil moisture (e.g. WRF soil moisture nudging), one of the studies in CalNex domain attempted 12 and 4 km CMAQ measurements coupled with EPIC. How is the soil moisture (precipitation) accuracy handled across those two horizontal scales?

**A:** Each example case employs, WRF results simulated at the desired air quality model scale, so two different WRF simulations are used. EPIC is run at the native scale of the WRF data, e.g., either 12 km or 4 km. No additional downscaling is performed. EPIC has its own dynamic soil temperature and soil moisture process models that are driven on a daily time scale by the same WRF information that drives CMAQ. In CMAQ, soil layer 2 (the entire soil profile less the topmost 1 cm) temperature and soil moisture are nudged. The soil nitrifiction process (a function of soil moisture and soil temperature) have been added to CMAQ so that the hourly $NH_4^+$ transformation and volatilization processes within CMAQ are driven by consistent meteorology, soil moisture and soil temperature. There are potential differences between CMAQ and EPIC soil moisture and soil temperature estimates that could impact estimates of daily fertilizer demand. A formal evaluation has yet to be completed, but differences appear to be small enough that we do not anticipate this to be a significant source of additional uncertainty.

# Chapter 6
# A Temporal $NO_x$ Emissions Trading System: Case Study of US Power Plants

**S. Morteza Mesbah, Amir Hakami, and Stephan Schott**

**Abstract** Despite the significant $NO_x$ reduction in the past decade, ozone concentrations in the eastern US are in violation of the National Ambient Air Quality Standard (NAAQS). This is because the location- and time-specific effects of $NO_x$ emissions on ozone formation have not been taken into consideration under cap-and-trade programs where polluters trade their emission quotas on a one-to-one basis. To account for such effects, a cap-and-trade program can be reformed by inclusion of exchange rates set by the regulator on an hourly basis. We examine the performance of such a reformed cap-and-trade program using a case study of US power plants. Our results indicate that shifting emissions from high-damage hours to low-damage hours can significantly improve the performance of the system.

## 6.1 Introduction

Surface ozone can harm humans' respiratory system and has been indirectly controlled through $NO_x$ emissions reduction by cap-and-trade programs in the US. Under these programs, emissions quotas are defined as the right to emit 1 ton of $NO_x$ in the ozone season (May to September) which can be exchanged between polluters on a one-to-one basis. In a reformed cap-and-trade system with exchange rates, polluters exchange their quotas based on rates set by the regulator. These exchange rates represent how many units of emissions a polluter can increase its emissions by when it buys one quota from another polluter. In this paper, exchange rates are defined as the ratios of polluters' marginal contribution to damage on

S.M. Mesbah (✉) • A. Hakami
Department of Civil and Environmental Engineering, Carleton University, Ottawa, ON, Canada
e-mail: smesbah@connect.carleton.ca

S. Schott
School of Public Policy and Administration, Carleton University, Ottawa, ON, Canada

D. Steyn and R. Mathur (eds.), *Air Pollution Modeling and its Application XXIII*,
Springer Proceedings in Complexity, DOI 10.1007/978-3-319-04379-1_6,

human health, known as marginal damage (MD), and are calculated on an hourly basis. We utilize a backward (adjoint) sensitivity analysis to calculate exchange rates, and use an optimization framework to predict emissions behavior under the reformed cap-and-trade system. We examine the performance of a temporal exchange rate cap-and-trade system via a case study of 218 coal-fired electric-utility units participating in the US cap-and-trade program in 2007.

## 6.2 Methodology

Under a cap-and-trade system, the number of quotas sold by emitter $i$ to emitter $j$ ($T_{ij}$), and the post-trade emissions ($e_i$) can be estimated by solving an optimization problem that minimizes the summation of abatement costs of $n$ emitters [2]:

$$Minimize: \sum_{i=1}^{n} c_i \left(e_i^0 - e_i\right) \tag{6.1a}$$

$$Subject\ to: e_i \leq e_i^0 - \sum_{\forall i \neq j} T_{ij} + \sum_{\forall i \neq j} T_{ji} \quad i\&j = 1, 2, .. n \tag{6.1b}$$

$$e_i \in \left[0, e_i^{\max}\right]; T_{ij}, T_{ji} \geq 0 \tag{6.1c}$$

where $c_i$ is the abatement cost of emitter $i$ which is a function of its initial allocated quotas ($e_i^0$ ), and $e_i^{max}$ is the maximum emissions can be generated by emitter $i$. To estimate the emissions behavior under a cap-and-trade system with exchange rate, Eqs. (6.1a, 6.1b, and 6.1c) can be used after (6.1b) is revised as follows:

$$MD_i \left(e_i - \sum_{i \neq j} T_{ij} + \sum_{i \neq j} \alpha_{ji} T_{ji} - e_i^0\right) \leq D_i \quad i\&j = 1, 2, .. n \tag{6.2}$$

where $MD_i$ is the marginal damage to human health caused by emitter $i$; $D_i$ is a damage-based quota allocated to emitter $i$; $\alpha_{ij}$ is the exchange rate between emitters $i$ and $j$ which is defined as the ratios of their marginal damages (i.e., $\alpha_{ij} = MD_i/MD_j$). For an hourly-based exchange rate cap-and-trade system, the variable $e_i$, which represents the ozone season emissions, is replaced with 24 hourly-based emissions (i.e., $e_i = \sum_{t=1}^{24} e_{it}$) in Eqs. (6.1a and 6.1c). Furthermore, Eq. (6.2) is revised as follows:

$$MD_{it} \left(e_{it} - \sum_{i \neq j} T_{ijt} + \sum_{i \neq j} \alpha_{jit} T_{jit} - e_{it}^0\right) \leq D_{it} \quad i\&j = 1, .., n, \quad t = 1, .., 24 \tag{6.3}$$

Equation (6.3) is similar to Eq. (6.2), but has an extra index ($t$) which splits parameters to hourly sub-parameters. Details on estimation of source-specific marginal damages and abatement costs can be found elsewhere [3]. Air quality is

simulated the using Community Multiscale Air Quality Modeling System (CMAQ) version 4.5.1. The adjoint of the gas-phase CMAQ [1] is used to estimate source-specific marginal damages in a continental US domain with 34 vertical layers, and a 36 km grid size. CMAQ and its adjoint are run for the first week of July 2007. For cost minimization, KNITRO version 8.0 is used.

## 6.3 Results and Discussion

The performance of two cap-and-trade systems (with temporal (CaT-TMP) or non-temporal (CaT-EX) exchange rates) are compared to the current cap-and-trade system (CaT) with no exchange rate. To estimate emitters' post-trade emissions under each system, Eqs. (6.1a and 6.1c) are used with the corresponding constraints for each system (i.e., (6.1b) for the CaT, (6.2) for the CaT-EX, and (6.3) for CaT-TMP). Exchange rates are defined as the ratio of hourly MDs (Fig. 6.1b–f) under the CaT-TMP system to the average hourly MDs under the CaT-EX system (Fig. 6.1a). Hourly MDs indicate the damage to human health caused by 1 ton of emission from a particular emitter at a specific hour.

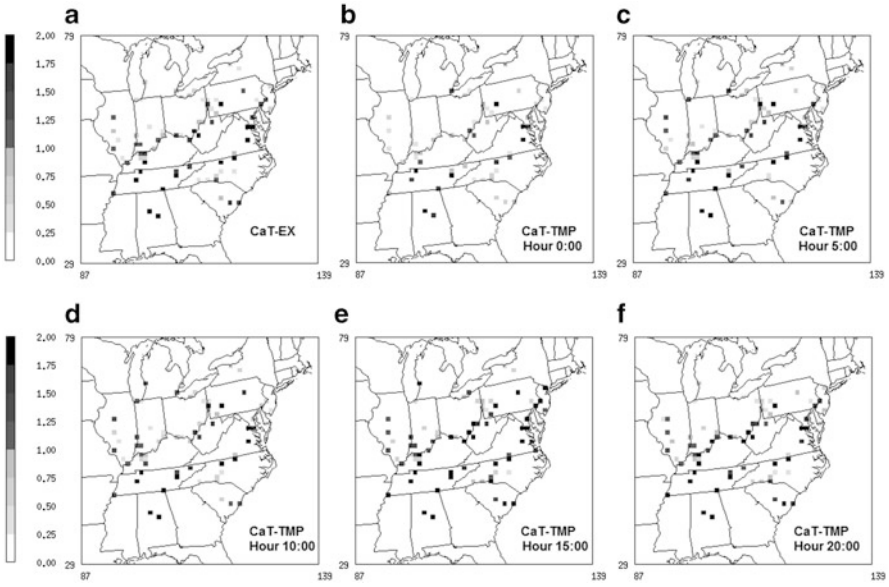


**Fig. 6.1** Exchange rates for the CaT-EX system (**a**), and for the CaT-TMP system (**b–f**) at different hours. The times are in GMT (the majority of the units are located in −5 GMT time zone). Negative hourly sensitivities are set to zero. Temporal exchange rates are the ratios of hourly MDs to the average marginal damage during the 24 h. Maximum exchange rates occur in time 17 GMT (not shown in Fig. 6.1) which corresponds to local time 12

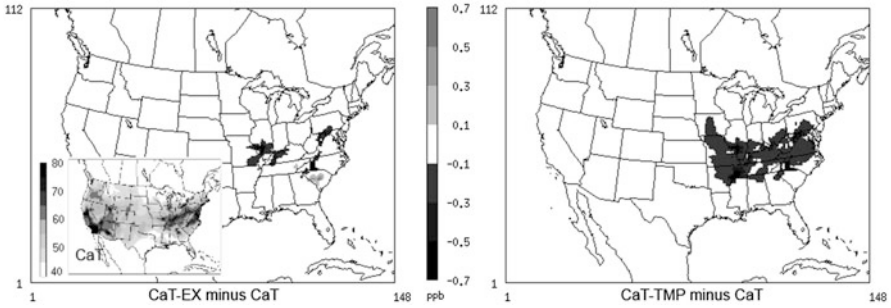


**Fig. 6.2** The average of daily 8 h ozone for 1 week modeling under the CaT system (small panel at the *bottom-left*), and the difference in average daily 8 h ozone between CaT and CaT-EX (*left*), or CaT-TMP (*right*) systems. Negative values indicate a decrease in health damage

**Table 6.1** Costs and benefits of exchange rate systems compared to the CaT system ($ million)

| | CaT-EX | CaT-TMP |
|---|---|---|
| Increase in abatement cost | 0.8 | 0.9 |
| Decrease in seasonal health damage | 64 | 174 |

Average 8 h ozone under the CaT system indicates a critical air quality condition in the eastern US (Fig. 6.2). Although switching from the CaT system to exchange rate systems results in an overall decrease in health damage (Table 6.1), an increase in local damage is observed in some locations (Fig. 6.2). However, this increase in local damage is negligible under the CaT-TMP system as compared to the CaT-EX system. Figure 6.2 also shows that regions where health benefits occur under the CaT-TMP system are also regions with high ozone concentration in the base case (CaT system). The summation of decreases in health damage in all locations under both CaT-TMP and CaT-EX as compared to CaT as well as the increase in abatement costs are listed in Table 6.1.

The net benefit (benefit minus cost) under the CaT-TMP system is about double that of under the CaT-EX system (Table 6.1). This is considered a significant benefit which is only achieved by redistributing the system-wide emissions in different locations and hours based on the ratio of MDs. Furthermore, the temporal exchange rates (Fig. 6.1) suggest that emissions reduction at hours with relatively higher exchange rates (10:00–15:00 local times) are more effective.

Note that under the proposed exchange rate systems, it is assumed that emissions can be transmitted from 1 h to another with no limitations. However, emission quantities from power plants depend on the electricity generation and shifting emissions between hours is affected by the electricity demand. Future research can investigate the effect of such limitations on hourly emissions transmission and the potential benefit of exchange rate systems. Furthermore, further research is required to investigate regulatory requirements for implementation of exchange rate systems.

## References

1. Hakami A, Henze DK, Seinfeld JH, Singh K, Sandu A, Kim S, Byun D, Li Q (2007) The adjoint of CMAQ. Environ Sci Technol 41(22):7807–7817
2. Mesbah SM, Hakami A, Schott S (2012) Improving NOx cap-and-trade system with adjoint-based emission exchange rates. Environ Sci Technol 46:11905–11912
3. Mesbah SM, Hakami A, Schott S (2014) Targeted NOx emissions control for improved environmental performance. In: Steyn Douw G, Builtjes Peter JH, Timmermans Renske MA (eds), Air pollution modeling and its application XXII. Springer, Dordrecht, pp 35–40

## Questions and Answers

**Questioner Name:** Douw Steyn

**Q:** If this scheme were implemented, how might industries "game" their emissions trading to gain economic advantage?

**A:** Under this scheme, the value of an emission quota for a high-damage industry is higher than that of a low-damage industry. Therefore, this scheme encourages the high-damage industries to lower their emissions and benefit by selling their unused high-value quotas in the market. In such a system, a polluter would benefit from being designated as a high-damage emitter, as its emissions become a higher-value commodity in the trading market. On the other hand, if the damage information presented here were used in a tax-based framework, the emitter would prefer a low-damage designation. So speculating on how the industry may react to this scheme would depend on the economic instrument of choice that would take into account the damage.

**Questioner Name:** Tianfeng Chai

**Q:** If the adjoint sensitivity is calculated based on model-ready emissions, isn't the spatial resolution of 36 km too coarse for the power plant emissions?

**A:** This is a valid point, and in some of the grid cells, there were multiple power plants. The 36 km resolution was chosen to reduce the high computational costs of adjoint modelling over a large-scale domain. The finer resolution can definitely help better distinguish between the plants.

# Chapter 7
# Source Attribution of Attainment and Exposure-Based Ozone Metrics in North America

**Amanda Pappin and Amir Hakami**

**Abstract** We use adjoint sensitivity analysis to examine the responses of a regulatory ozone attainment metric and adverse ozone health effects to location-specific reductions in anthropogenic $NO_x$ emissions. We find spatially heterogeneous responses among both attainment- and exposure-based metrics. Emission reductions in the western U.S. exert the most influence on attainment probability-weighted extreme concentrations (PWCs), while emission reductions in proximity to population centres in the eastern U.S. are most beneficial for reducing short-term ozone-related mortality.

## 7.1 Introduction

Ambient ozone standards in the U.S. currently specify that the fourth-highest daily maximum 8-h average (DM8A) ozone concentration measured in a year (and averaged over 3 years) must be below 0.075 ppm [3]. In air quality modelling studies, regulatory metrics have traditionally been modelled deterministically, where individual days of extreme concentrations define whether or not attainment is achieved. An alternative, probabilistic approach might consider the importance of modelled concentration-days to attainment demonstration using the probability distribution of ozone concentrations and the likelihood of any given day being among the four highest concentrations.

Human health metrics quantifying the adverse effects associated with ozone exposure can be used in tandem with regulatory attainment-based metrics in air quality management strategies. In comparison to attainment-based metrics that treat all locations equally so long as they are in nonattainment by the same degree,

A. Pappin • A. Hakami (✉)
Department of Civil and Environmental Engineering, Carleton University, Ottawa, ON, Canada
e-mail: amandapappin@cmail.carleton.ca; amir_hakami@carleton.ca

D. Steyn and R. Mathur (eds.), *Air Pollution Modeling and its Application XXIII*,
Springer Proceedings in Complexity, DOI 10.1007/978-3-319-04379-1_7,

human health metrics consider the size of populations in proximity to ozone concentrations in locations that violate standards. Furthermore, severe effects such as mortality have been shown to occur at concentrations far below current ozone standards [3]. Human health metrics thus provide a means of estimating the burden of ozone pollution on society regardless if locations are above or below ozone standards.

Prediction of the response of ozone metrics under various emission reduction programs requires estimating derivatives or sensitivities. Adjoint sensitivity analysis is a tool that can be used to quantify source-by-source influences on collective air quality metrics (e.g., ozone averaged over the U.S. or Canada). In this work, we estimate sensitivities or influences of location-specific reductions in anthropogenic $NO_x$ emissions on a national, probabilistic attainment-based ozone metric and short-term ozone mortality.

## 7.2 Methodology

Adjoint simulations require formulation of an adjoint cost function; a concentration-based metric defined over one or many receptors whose sensitivity is of interest in modelling. In this work, we define two adjoint cost functions for two sets of simulations. Our attainment-based metric, $J_1$, is a probability-weighted extreme concentration (PWC) summed or integrated over all locations in Canada and the U.S. whose local PWC exceeds 65 ppb, as formulated below,

$$J_1 = \sum_{(x,y)} \left( \frac{1}{\sum_{i=1}^{n} p_{i\,(x,y)}} \sum_{i=1}^{n} c_{i\,(\mathrm{x,y})}\, p_{i\,(x,y)} \right)$$

where $c_{i(\mathrm{x,y})}$ is the DM8A ozone concentration for day $i$ and location $(x, y)$, $p_{i(x,y)}$ is the probability that $c_{i(\mathrm{x,y})}$ is among the four highest simulated concentration-days of the ozone season (May–September) for location $i$ and is generated using binomial sampling of the ozone distribution with a successful event occurring when a randomly sampled concentration exceeds $c_{i(\mathrm{x,y})}$ for that concentration-day, and $n$ is the number of days in the ozone season. Ozone distributions used in estimation of $p_{i(x,y)}$ are location-specific probability distributions (assumed to be normal) for DM8A concentrations from a forward simulation using the Community Multiscale Air Quality model (CMAQ). Because attainment demonstration requires annual sets of measurements, we assume our sample ozone distributions for the ozone season of 2007 are representative of the full-year set of simulated concentrations.

For our exposure-based metric, $J_2$, we estimate premature mortality related to short-term ozone exposure in Canada and the U.S., as formulated below,

$$J_2 = \sum_{(\mathrm{x,y})} \sum_{i=1}^{n} M_{0_{i\,(\mathrm{x,y})}}\, P_{(x,y)}\; e^{\beta \cdot c_{i\,(\mathrm{x,y})}}$$

where $c_{i(x,y)}$ is as defined above, $M_{0_{i(x,y)}}$ is the non-accidental mortality rate and $P_{(x,y)}$ is the population (all ages) for location ($x$, $y$), and $\beta$ is the concentration-response factor of $4.27 \times 10^{-4}$ ppb$^{-1}$ for DM8A ozone [1]. For Canada, mortality rates and populations are based on 2007 from the Air Quality Benefits Assessment Tool (AQBAT), and data for the U.S. is from the Centers for Disease Control and Prevention (CDC).

We use the adjoint of CMAQ (version 4.5.1) to link attainment- and exposure-based ozone metrics to sources of anthropogenic $NO_x$ emissions within Canada and the U.S. Our simulations are conducted using a North American domain with a horizontal grid resolution of 36 km and 34 vertical layers. Our simulation episode is from July 1–15, 2007 using CMAQ-adjoint for gas-phase processes only. Meteorological inputs are produced from the Weather Research and Forecasting model (WRF), while emission inputs are projected to 2007 from the 2006 National Pollutant Release Inventory (NPRI) and the 2005 National Emissions Inventory (NEI) in Canada and the U.S., respectively.

## 7.3 Results and Discussion

Our adjoint sensitivities show the influence of $NO_x$ emissions reductions on (1) the national average PWC exceeding 65 ppb (Fig. 7.1a), and (2) nation-wide mortality from short-term ozone exposure (Fig. 7.1b). We scale our adjoint sensitivities to amount to the influence of a 10 % reduction in anthropogenic $NO_x$ emissions from any grid cell in the domain. A sensitivity of 0.1 in Fig. 7.1a or b indicates that a 10 % reduction in anthropogenic $NO_x$ from that grid cell reduces PWCs or short-term mortality within Canada and the U.S. by a cumulative 0.1 ppb or 0.1 deaths over the 15-day simulation episode. Our sensitivity maps thus show influences on a collective, national metric on a source-by-source basis but do not provide information as to where PWC or mortality effects occur within the boundaries of our adjoint cost functions.

Responses of ozone attainment- and exposure-based metrics vary substantially in magnitude from one source location to another (Fig. 7.1). Under the simulation period used in this study, mortality is most influenced by emission reductions in the eastern U.S., while PWCs are generally small or show negative sensitivities (with 10 % $NO_x$ emission reductions effectively increasing PWCs). The single largest influence on the attainment-based metric originates from emission reductions in the north-west of New Mexico state, where a 10 % reduction from a single grid cell reduces PWCs nationally by a cumulative 15.9 ppb. Within the Ohio River Valley, influences reach up to 6.8 ppb from a single grid cell, while in coastal California influences are as large as 6.1 ppb (2.9 ppb for Los Angeles). Although negative sensitivities are visible around the Great Lakes region and the southern U.S., they are generally small in magnitude, contributing up to a 0.9 ppb increase in PWCs within Canada and the U.S.

For nation-wide ozone mortality, source locations exerting the most influence are Memphis and Atlanta, where 10 % reductions in $NO_x$ emissions from each

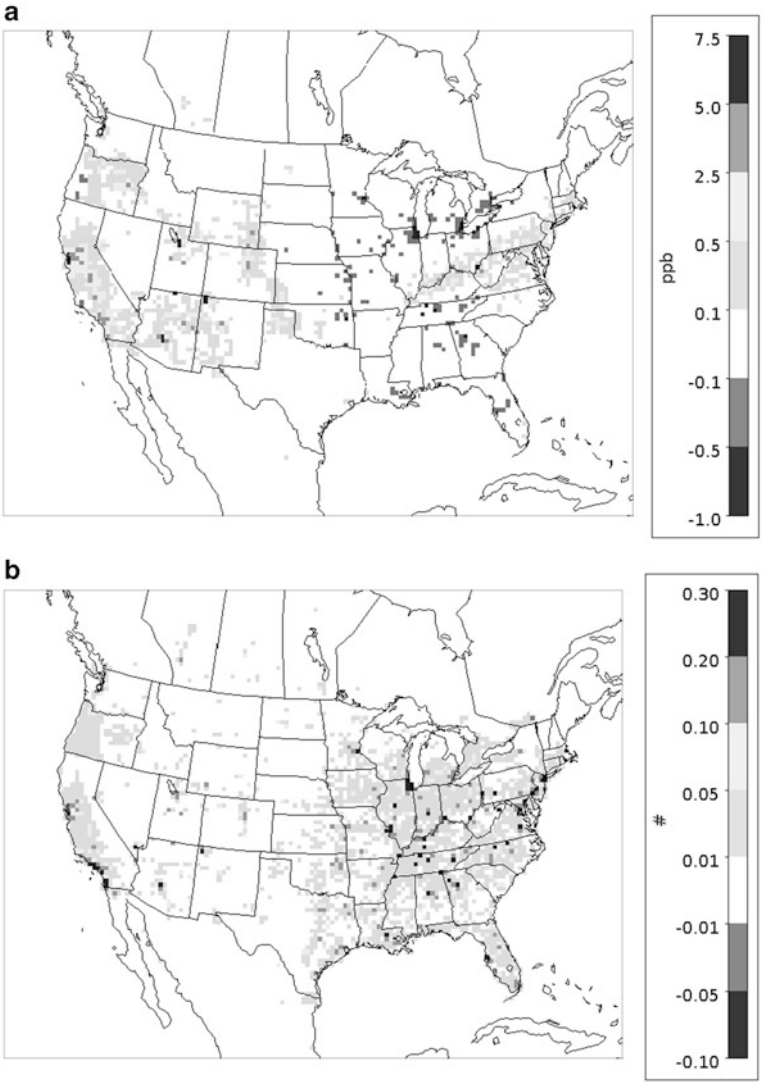


**Fig. 7.1** Influences of a 10 % anthropogenic $NO_x$ emission reduction in any grid cell on (**a**) national PWCs > 65 ppb, and (**b**) nation-wide short-term ozone mortality. Influences are integrated over July 1–15, 2007 and thus represent the reduction in either metric over the 15-day simulation period

grid cell reduce premature mortality nationwide by 0.43 and 0.3 deaths over the 15-day period simulated. When extrapolated to the full ozone season of 2007, these influences amount to 4.6 and 3.2 deaths, respectively. Negative sensitivities coincide with major urban areas and are sizable (such as Los Angeles, whose sensitivity is −0.59, or a seasonal influence of −6.3 deaths).

Interpretation of negative sensitivities for the attainment-based ozone metric modeled in this study requires consideration of the duration of the simulation episode. Over longer simulation periods, responses are likely to become more widespread and positive because days of extreme ozone concentrations captured in the adjoint cost function will fall within the timespan modelled. On the other hand, negative sensitivities for ozone mortality have been found in previous work and require consideration of long-term air quality management strategies that will change sensitivities to become more positive with increasingly stringent regional and local emission reductions [2].

## References

1. Bell ML, McDermott A, Zeger SL et al (2004) Ozone and short-term mortality in 95 US urban communities, 1987–2000. JAMA 292:2372–2378
2. Pappin AJ, Hakami A (2013) Source attribution of health benefits from air pollution abatement in Canada and the U.S.: an adjoint sensitivity analysis. Environ Health Perspect 121(5):572–579. doi:10.1289/ehp.1205561
3. U.S. EPA (2013) Integrated science assessment for ozone and related photochemical oxidants. EPA 600/R-10/076F Research Triangle Park, NC. http://cfpub.epa.gov/ncea/isa/recordisplay.cfm?deid=247492

## Questions and Answers

**Questioner Name:** Rohit Mathur

**Q:** You showed locations where there was an attainment benefit but not an exposure benefit – is that driven by population density?

**A:** Rather than distinguish between locations by the size of populations, attainment-based metrics treat all locations with the same degree of nonattainment as equal. By contrast, exposure-based metrics are more heavily influenced by ozone concentrations in the vicinity of large population centres. Source locations that show significant attainment-based sensitivities – but not exposure-based sensitivities – have widespread influence on ozone concentrations that do not generally coincide with locations of large populations.

**Questioner Name:** Paul Makar

**Q:** The model results are for gaseous metrics only while multi-pollutant metrics may give different policy advice. What are your plans for looking at multi-pollutant health metrics?

**A:** Once the adjoint of CMAQ for particle-phase species becomes available, we will quantify exposure-based sensitivities that consider both gaseous species and aerosols. In particular, multi-pollutant exposure-based sensitivities in regions such as Los Angeles would shed light on the true benefits of $NO_x$ reduction that

may be masked by our exclusion of aerosol health effects. Our exposure results look exclusively at mortality form short-term ozone exposure; however, a more inclusive approach would be to consider the morbidity or long-term effects of exposure to air pollution.

# Chapter 8
# CASTNET Methodology for Modeling Dry and Total Deposition

**Christopher M. Rogers, Thomas F. Lavery, Marcus O. Stewart, William R. Barnard, and H. Kemp Howell**

**Abstract** Gaseous and particulate pollutants are deposited to the environment through dry, wet, and occult atmospheric processes. The US Environmental Protection Agency (USEPA), in conjunction with the National Park Service (NPS), the Bureau of Land Management (BLM), and other partners, has established the Clean Air Status and Trends Network (CASTNET) to provide estimates of the dry deposition component of total deposition of sulfur and inorganic nitrogen across the United States. CASTNET began operation in 1991 and currently features 90 active sites with many partners including multiple federal agencies, tribal, state, and local entities, and educational institutions. Most CASTNET locations are rural and intended as long term monitoring sites. Previously, CASTNET used an inferential method to estimate dry deposition by combining measured pollutant concentrations and modeled deposition velocities. Until recently, deposition velocities were modeled using the NOAA/USEPA Multi-layer Model (MLM), which incorporated meteorological measurements and information on the vegetative cover within 1 km of each site. These values were combined with wet deposition values provided by the National Atmospheric Deposition Program's National Trends Network (NADP/NTN) to obtain total deposition. Recent changes to the methodology have improved data completeness.

C.M. Rogers (✉)
AMEC Environment & Infrastructure, Inc., 3901 Carmichael Ave., Jacksonville, FL 32207, USA
e-mail: christopher.rogers@amec.com

T.F. Lavery
Consultant, Cranston, RI, USA

M.O. Stewart • W.R. Barnard • H.K. Howell
AMEC Environment & Infrastructure, Inc., Newberry, FL, USA

D. Steyn and R. Mathur (eds.), *Air Pollution Modeling and its Application XXIII*, Springer Proceedings in Complexity, DOI 10.1007/978-3-319-04379-1_8,

## 8.1 Introduction

In 2011, CASTNET adopted a data substitution method developed by Bowker et al. [1] to allow for the estimation of deposition velocities in the absence of meteorological inputs whether due to invalid data or lack of monitoring. This results in nearly 100 % data completeness for dry deposition estimates at CASTNET sites. Also, the Parameter-elevation Regressions on Independent Slopes Model (PRISM) precipitation data set was utilized to improve the resolution of wet deposition estimates, particularly in high elevation areas. Using this method, CASTNET and NADP data show that total deposition of sulfur and nitrogen have decreased by approximately 47 % and 26 %, respectively, over the past 15 years.

The current methodology is part of a transition from the inferential method to a hybrid model that will incorporate deposition velocities produced using the Community Multiscale Air Quality (CMAQ) model with concentrations collected by CASTNET. The resulting dry deposition data set will have dramatically improved spatial resolution and will permit increased use of CASTNET data for applications such as analyzing critical loads throughout the United States.

## 8.2 Estimating Dry Deposition

Dry deposition processes are modeled as resistances to deposition. CASTNET's original network design was based on the assumption that dry deposition or flux could be estimated as the linear product of measured pollutant concentration (C) and modeled deposition velocity ($V_d$). $V_d$ is influenced by meteorological conditions, vegetation, and atmospheric and plant chemistry. The deposition velocity values for each site are calculated for each hour of each year using the MLM [3, 4]. The data used as inputs include meteorological measurements with an estimation of the vegetative species and associated characteristics including leaf-out timing and leaf area index (LAI).

In 2010, EPA discontinued meteorological measurements at all but four of the EPA-sponsored CASTNET sites. NPS- and BLM-sponsored sites continue to measure these parameters. The loss of this source of inputs for the MLM plus the need to improve $V_d$ data completeness resulted in the development of a method by EPA [1] to substitute historical average hourly $V_d$ values for missing MLM simulations. The substitution method was applied to the historical CASTNET database and used for dry deposition estimates beginning in 2012.

Historically, modeled $V_d$ values have been about 70 % complete for a given year. Bowker evaluated the new approach, which captures the site-specific diurnal and seasonal patterns in modeled $V_d$ values, by calculating the differences created by replacing missing $V_d$ values with the substituted data and calculating the percent error (%E) and percent difference (%D) between the original data and substituted data for 5,000 pairs of annual $V_d$ values.

Both measures of bias were found to be site dependent. The %E increased generally with the percentage of missing data for the 11 sites selected for evaluation. The %D showed both positive and negative average percent differences across the range of percent missing data. For a particular year at any given site, the annual mean $V_d$ resulting from substitution was either higher or lower than the true mean and, consequently, showed little bias. The results indicated that the average percent difference was relatively small (less than ±5 %).

## 8.3 Using PRISM to Estimate Wet Deposition for CASTNET Sites

NADP/NTN operates wet deposition samplers to measure concentrations of pollutants in precipitation and to calculate the deposition rate of air pollutants removed by precipitation. NADP/NTN operates more than 250 monitoring sites across the United States. Historically, wet deposition values were obtained from a grid of concentration and precipitation estimates derived from available NADP/NTN sites by using an inverse distance weighting (IDW) algorithm. Despite the equivalent precipitation and wet deposition values at NADP/NTN sites, this IDW approach produces interpolation errors, especially in regions with variable terrain and low geographic site density.

In 2011, the Parameter-elevation Relationships on Independent Slopes Model (PRISM) model [2] was selected by CASTNET and NADP as a source of precipitation data because it provides more accurate estimates of annual precipitation values in areas with complex terrain. The model was developed by the PRISM Climate Group at Oregon State University (OSU). PRISM uses point precipitation measurements, a digital elevation model (DEM), and other geographic data to estimate annual, monthly, and event-based precipitation data on a 4 km grid resolution.

Unlike statistical models such as IDW or kriging, PRISM is not a system of equations but a coordinated set of rules, decisions, and calculations designed to emulate the decision-making process a climatologist uses when creating a map of climatic data. The PRISM gridded data are adjusted to the precipitation measurements collected by NADP. Concentration in precipitation maps are then produced for the PRISM grid. The concentration values are multiplied by the precipitation rates to obtain gridded wet deposition fluxes. Gridded wet deposition fluxes are then interpolated to CASTNET monitoring locations [6].

The PRISM results indicate a significant improvement over the IDW estimates. Figure 8.1 presents scatter plots that show NADP/NTN measured precipitation rates compared to estimated IDW values and measured NADP/NTN rates compared to estimated PRISM values in the right diagram. In Fig. 8.1, the MARPD calculated using a bootstrapping method for PRISM and NADP/NTN precipitation data is 2.5 % versus an MARPD of 39 % between IDW-derived grid and NADP/NTN precipitation values.

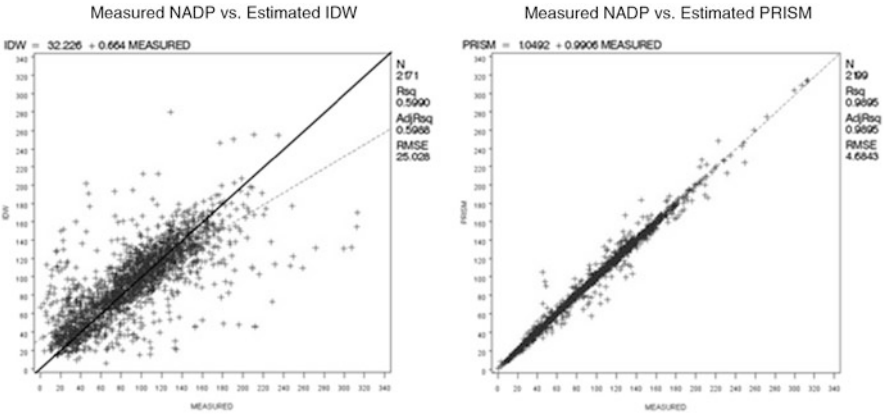


**Fig. 8.1** Comparison of NADP precipitation measurements with IDW estimates and PRISM estimates for 1999–2009 (Source: EPA Clean Air Markets Division)

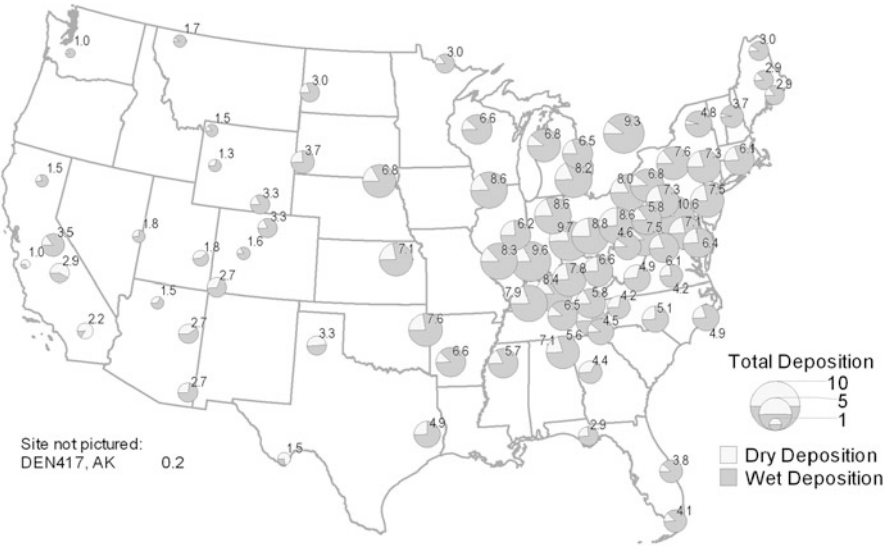


**Fig. 8.2** Total inorganic nitrogen deposition (kg/ha/year) for 2011

## 8.4 Estimates of Total Deposition

The MLM/Bowker approach was used to estimate dry deposition fluxes for 2011 for all CASTNET sites. These were combined with PRISM-adjusted wet deposition rates from NADP. Figure 8.2 presents a map of N deposition using

this method. The estimates updated using the Bowker approach and incorporating PRISM-adjusted NADP data indicate that total deposition of sulfur and nitrogen has declined by approximately 47 % and 26 %, respectively, over the past 15 years.

## 8.5 Summary

CASTNET and NADP/NTN data are used to produce estimates of total sulfur and inorganic nitrogen deposition. In 2011, both CASTNET and NADP began using revised procedures that produced improved total deposition estimates. As a next step for estimating dry deposition, CASTNET will transition from the inferential method to a hybrid model that will incorporate deposition velocities and concentration surfaces produced using the Community Multiscale Air Quality (CMAQ) model with concentrations measured by CASTNET [5]. The new method will include modeled species that are not measured at CASTNET sites. The resulting deposition data set will realize improved spatial resolution and will permit increased use of CASTNET data for applications such as analyzing critical loads.

## References

1. Bowker GE, Schwede DB, Lear GG, Warren-Hicks WJ, Finkelstein PL (2011) Quality assurance decisions with air models: a case study of imputation of missing input data using EPA's multilayer model. Water Air Soil Pollut 222:391–402
2. Daly C, Neilson RP, Phillips DL (1994) A statistical-topographic model for mapping climatological precipitation over mountainous terrain. J Appl Meteorol 33:140–158
3. Finkelstein PL, Ellestad TG, Clarke JF, Meyers TP, Schwede DB, Hebert EO, Neal JA (2000) Ozone and sulfur dioxide dry deposition to forests: observations and model evaluation. J Geophys Res 105(D12):15365–15377
4. Meyers TP, Finkelstein P, Clarke J, Ellestad TG, Sims PF (1998) A multilayer model for inferring dry deposition using standard meteorological measurements. J Geophys Res 103(D17):22645–22661
5. Schwede D, Lear G. A novel approach for estimating total deposition in the United States. In Press
6. U.S. Environmental Protection Agency (EPA) (2011) Using PRISM to estimate wet deposition for CASTNET. Presented at Spring 2011 NADP meeting Pensacola, FL. http://nadp.sws.uiuc.edu/committees/minutes.aspx

# Chapter 9
# ACCEPTED: An Assessment of Changing Conditions, Environmental Policies, Time-Activities, Exposure and Disease

**Andy Delcloo, Camilla Andersson, Bertil Forsberg, Tim Nawrot, and Myrto Valari**

**Abstract** Changes in urban design and traffic policy, demography, climate and associated adaptation, mitigation measures and environmental policies are likely to modify both outdoor and indoor air quality and therefore public health. The project aims to improve our understanding of future exposure situations and their impact on health, from an interdisciplinary approach. This will be achieved by using various state-of-the-art atmospheric models, measurements, epidemiological studies and reviews. To assess population full exposure, an integrated view accounting both for indoor and outdoor air pollution as well as for population time activity data will be developed. New dose-response functions will be estimated between health outcome, air pollution and temperature in order to better estimate the effects on the foetus and young children. Ultimately, scenarios of future urban climate and air quality will be simulated, combining future exposure scenarios, population scenarios and exposure-response functions to describe the effects of different trends and relevant policies on

A. Delcloo (✉)
Royal Meteorological Institute of Belgium, Brussels, Belgium
e-mail: Andy.Delcloo@meteo.be

C. Andersson
Swedish Meteorological and Hydrological Institute, Norrköping, Sweden
e-mail: Camilla.Andersson@smhi.se

B. Forsberg
Division of Occupational and Environmental Health, Department of Public Health and Clinical Studies, Umeå University, SE-90187 Umeå, Sweden
e-mail: Bertil.Forsberg@envmed.umu.se

T. Nawrot
Centre for Environmental Research, Hasselt University, Hasselt, Belgium
e-mail: Tim.Nawrot@uhasselt.be

M. Valari
Laboratoire de Meteorologie Dynamique, IPSL Ecole Polytechnique, 91128 Palaiseau Cedex, France
e-mail: Myrto.Valari@lmd.polytechnique.fr

D. Steyn and R. Mathur (eds.), *Air Pollution Modeling and its Application XXIII*, Springer Proceedings in Complexity, DOI 10.1007/978-3-319-04379-1_9,

relative risk and burden of illness attributed to urban pollutants and their interactions with extreme temperatures. Also the mitigation strategies that can be used to reduce urbanization and climate change effects on the local urban meteorology and air quality will be assessed. With applications in several large European cities, the project will study the impact of several alternative adaptation scenarios on urban air quality and human health to a mid-century horizon (2030–2060) accounting for the effects of a changing urban climate. Scenario-based health impact assessments will combine exposure information from climate models, emission scenarios, policy evaluation studies and concentration calculations with exposure-response functions from epidemiological studies of vulnerable groups within the project and previously published functions for mortality and hospital admissions. The effects of socioeconomic and demographic trends will be discussed, the predicted health impacts and benefits associated with different interventions and policies and other urban changes will be described.

## 9.1 Introduction

Changes in urban design, traffic policy, demography, climate, associated adaptation, mitigation measures, the energy choices made in front of resource shortage and environmental policies are likely to modify both outdoor and indoor air quality and therefore public health. The proposed project aims to improve our under-standing of future exposure situations and their impact on health, from an interdisciplinary approach. This will be achieved by using various state-of-the-art models and measurements, in particular as concerns indoor air quality. To assess population full exposure we will develop for the first time an integrated view accounting both for indoor and outdoor air pollution and their relations. Ultimately we will simulate scenarios of future urban climate and air quality, combine future exposure scenarios, population scenarios and exposure-response relationships to describe the effects of different trends and policies on relative risk and burden of illness attributed to urban pollutants and temperature. This will use a modeling suite from global climate, atmospheric composition, to urban scale climate weather and air quality. This will benefit from the recent climate simulations carried out in CMIP5 and CORDEX international projects and from simulations from the on-going project IMPACT2C. We will also perform epidemiological studies in three countries in order to better estimate the effects on the foetus and young children, and will use the results together with air quality scenario simulations to predict health impacts in scenarios. Besides coordination and knowledge transfer we plan four WPs.

## 9.2 WP1 Urban Scale Air-Quality and Climate

A major outcome of this WP will be to develop a modeling capacity for predictions of urban air quality resulting from a variety of planning and mitigation strategies, changes in residential density and taking into account climate change. This project

will in particular address the issue of the mitigation strategies that can be used to reduce urbanization and climate change effects on the local urban meteorology and air quality. The accurate determination of the impact of such scenarios is hindered, at the large scale end by the change in global climate and at the small scale end by the difficulty in modeling details of surface and emissions. The main objective of the project is to bridge processes across these scales using a suite of state-of-the-art atmospheric models. As an application we will focus on several European cities including Paris, Stockholm, Brussels and Augsburg to study the impact of several alternative adaptation scenarios on urban air-quality and human health for the period 1990–1999 and 2046–2055, accounting for the effects of changing urban climate. Some of the climate models (WRF, ALADIN) will use urban parameterizations involved in the urban heat island (TEB) to account for the impact of urbanization on large-scale air quality and meteorology. These include the turbulent fluxes into the boundary layer from areas covered by roads, buildings (including urban vegetation green roofs) and other artificial material.

State-of-the-art chemistry transport models (MATCH and CHIMERE) will be used to assess concentrations at urban scale and their change in the above strategies. Future emission projections for cities including Stockholm, Augsburg and Paris will be developed in collaboration with local agencies based on available scenarios on local policies, urban planning, traffic management, vehicle fleet, economic growth etc. Novel sub-grid scale approaches will be developed to describe air pollutant concentrations within the intra-urban canopy due to the heterogeneity of emission sources and local meteorology. Special attention will be given to street concentrations. Finally, we will evaluate the impact of the implementation of Low Emission Zones (LEZ) in several European cities in Germany, France and Sweden on traffic-related air pollutants levels. This assessment will be based both on analysis of the measured air pollutants levels by sophisticated statistical approach as well as on dispersion modeling.

The comparison of the different LEZ in terms of strategy, targeted vehicle fleet, area, etc. and impact (including health impact, see WP4) will result in recommendations for decision makers regarding the most effective design of LEZ.

## 9.3 WP2 Outdoor, Indoor and Personal Exposure

A study of outdoor and indoor concentration of ozone in Swedish homes and workplaces will describe how the indoor/outdoor ratio depends on the type of building, ventilation, environment and weather conditions in areas where very old and modern buildings coexist. In a second study we will investigate the associations between personal and ambient measurements of PM2.5, black carbon (soot) and particle number concentrations in different exposure situations (commuting by car or public transport, being at home or outdoors in different microenvironments). The subjects will keep a detailed diary and will record their whereabouts with geographic positioning systems (GPS) and motion detectors.

Finally, an exposure model will integrate outdoor levels of pollutant concentration with indoor air quality and time activity data to provide more realistic exposure metrics. Exposure inside characteristic types of buildings (e.g. residence, school, office) will be assessed as a function of outdoors air pollution, infiltration and ventilation. Alternative scenarios including variable levels of energy consumption by buildings and local policies for indoor air quality will be studied. We will study the variability in exposure levels depending on the proximity to roads, differences in indoor air quality between urban and rural locations. Time spent at different locations by several population groups (e.g. working adults, children, seniors) will be taken into account to estimate the total exposure. We plan to investigate how updated air quality modeling and/or measurement metrics may improve the effectiveness of the air quality alert system in reducing the exposure of vulnerable groups to air pollution. Several scenarios will be investigated to account for different adaptation practices including changes in the time spent indoors versus outdoors in response to air quality and issued warnings and alerts.

## 9.4 WP3 New Studies of Vulnerable Groups

Endpoints covered will include birth outcomes, biomarkers of effect (placental mitochondria) and respiratory health in childhood. A large birth register study will be performed for parts of Sweden and all Belgium investigating the effects of air pollution, especially PM from different sources and ozone, and temperature extremes on endpoints like preterm delivery. In addition to measured concentrations we will improve exposure data using modeled concentrations from WP1-2 with good temporal and spatial resolution.

Birth cohort studies with exposure at home modeled in detail will be used to study effects on placental mitochondria within three areas in Belgium. Measurements for WP2 will partly be done within these cohorts.

A large Stockholm cohort will be constructed by linkage of Swedish Medical Birth Registry, Patient Registry and Medication Registry. Recorded variation in concentrations at a few sites will be supplemented with high resolution modeled concentrations to study prenatal and early air pollution and pollen exposure and the risk of developing childhood asthma.

## 9.5 WP4 Scenario-Based Health Impact Assessments

In the final phase, scenario-based health impact assessments will combine exposure information from climate models, emission scenarios, policy evaluation studies and concentration calculations with exposure-response functions from epidemiological studies of vulnerable groups within the project and previously published functions

for mortality and hospital admissions. We will discuss effects of socioeconomic and demographic trends, describe the predicted health impacts and the benefits associated with different interventions and policies such as LEZ and other urban changes.

## 9.6 Consortium and Outcomes

The study will benefit from a large consortium with an interdisciplinary mix of experts involved in many projects (meteorology, air quality modeling, exposure measurements, epidemiology, environmental management, health impact assessment) and with large experience of interaction with policy-makers and stakeholders. There will be many partners in each WP and staff visiting and working in other partner organizations. We plan to produce novel scientific papers, policy-relevant end-user reports and arrange two final seminars for policy makers.

**Acknowledgements** ACCEPTED is carried out within the framework of the ERA-ENVHEALTH second call for transnational research projects on "Air pollution in urban areas: health impacts on vulnerable groups under changing conditions" launched in 2012. ERA-ENVHEALTH is a unique network striving towards better integrating environment and health research in policy. The research leading to these results is carried out under the ERA-ENVHEALTH 2nd call and has received funding from ANSES, ADEME, BelSPO, UBA and Swedish EPA. This publication reflects only the author's views and ERA-ENVHEALTH is not liable for any use that may be made of the information contained therein (http://www.acceptedera.eu).

# Chapter 10
# Studying Aerosol-Cloud-Climate Interactions over East Asia Using WRF/Chem

**Yang Zhang, Xin Zhang, Changjie Cai, Kai Wang, and Litao Wang**

**Abstract** East Asia provides an ideal testbed to study aerosol feedbacks into climate via direct and indirect effects because of high anthropogenic emissions and unique climatology. In this work, an online coupled meteorology-chemistry model, WRF/Chem, is applied to simulate air quality and climate interactions for multiple months in 2001, 2005, and 2008 to characterize long-term seasonal variations of pollutant concentrations and quantify the contributions of anthropogenic aerosols to aerosol direct and indirect effects. The results show a reasonably good performance for most meteorological variables and chemical species concentrations. Large biases in some variables may be caused by large uncertainties in emissions. Anthropogenic aerosols in East Asia can reduce the surface net solar radiation by up to 6 % and enhance cloud condensation nuclei and cloud droplet number concentrations by a factor of up to 3 on domain-average, with much greater impacts over urban areas. These results suggest that aerosol feedbacks are potentially important over polluted areas and should be taken into account in the development of emission control and climate mitigation policies for areas where the aerosol feedback signals are strong.

## 10.1 Introduction

Two major aerosol-radiation feedbacks (i.e., the aerosol direct effect by scattering and absorbing solar radiation and indirect effect by acting as cloud condensation nuclei (CCN)) are gaining extensive research attentions due to their importance in

Y. Zhang (✉) • X. Zhang • C. Cai • K. Wang
Department of Marine, Earth, and Atmospheric Sciences, North Carolina State University, Raleigh, NC 27695, USA
e-mail: yang_zhang@ncsu.edu

L. Wang
Department of Environmental Engineering, Hebei University of Engineering, Handan, Hebei 056038, China

D. Steyn and R. Mathur (eds.), *Air Pollution Modeling and its Application XXIII*, Springer Proceedings in Complexity, DOI 10.1007/978-3-319-04379-1_10,

climate change. Several recent studies (e.g. [1, 2, 4, 6, 18–23]) have shown the importance of these aerosol direct and indirect effects on a regional scale over continental U.S. and Europe. East Asia provides an ideal testbed to study aerosol feedbacks into climate via direct and indirect effects because of high anthropogenic emissions and special climatology that favor natural emissions of biogenic organic compounds and mineral dust as well as long range transport of pollutants. In this work, an online coupled meteorology-chemistry model, the Weather Research and Forecasting Model with Chemistry (WRF/Chem) is applied to simulate air quality and climate interactions for multiple months in 2001, 2005, and 2008. The objectives of this work are to enhance the model's capability through evaluating the model performance using observations from surface and satellite networks and improving model inputs and representations, characterize long-term seasonal variations of pollutant concentrations and their climate and chemical fingerprints, and quantify the contributions of anthropogenic aerosols to aerosol direct and indirect effects.

## 10.2 Model Setup

WRF/Chem simulations are conducted at a horizontal resolution of 36-km and a vertical resolution of 23 layers from 1,000 to 100 MB over East Asia for January, April, July, and October in 2001, 2005, and 2008. Meteorological initial conditions (ICON) and boundary conditions (BCON) are based on the National Centers for Environmental Predictions Final Analysis (NCEP-FNL) reanalysis data. Chemical ICON and BCON are based on previous simulations using the Community Multiscale Air Quality (CMAQ) modeling system [12, 13]. Anthropogenic/biogenic emissions are modified from Wang et al. [13], which is based on Streets et al. [10, 11] and Zhang et al. [15–17]. Our initial applications of WRF/Chem with default configurations indicated that inaccuracies in vertical distributions of anthropogenic emissions contribute significantly to poor model performance at surface and that the default dust emission module of Shaw [9] fails to capture dust emissions. In this work, those problems have been addressed by using a more realistic vertical distribution of emissions and incorporating a new online dust emission module of Zender et al. [14] into the model. Sea-salt emissions are simulated using the online scheme of Gong et al. [3] and O'Dowd et al. [8]. Biogenic volatile organic compound (VOC) emissions are based on the online module of MEGAN [5].

The meteorological predictions are evaluated using hourly global surface observational data from the National Climatic Data Center. The surface chemical predictions are evaluated using observational data from various sources including $SO_2$ and $PM_{10}$ derived from Air Pollution Index for major cities in China; CO, $SO_2$, NO, $NO_2$, $O_3$, and $PM_{10}$ measurements at more than 2000 sites from the National Institute for Environmental Studies in Japan and at 14 sites from Environmental Protection Department of Hong Kong; CO, $SO_2$, NO, $NO_2$, $O_3$, $PM_{2.5}$, and $PM_{10}$

measurement at ~80 sites from the Environmental Protection Administration of Taiwan; and $PM_{2.5}$ measurement from a site at Tsinghua University, Beijing, China. The predictions of column abundance of species mass concentrations and radiative properties are evaluated using satellite data, including the Measurements of Pollution in the Troposphere (MOPITT) for CO, the SCanning Imaging Absorption spectroMeter for Atmospheric CHartographY (SCIAMACHY) for $SO_2$ and $NO_2$, the Total Ozone Mapping Spectrometer (TOMS)/the Solar Backscatter UltraViolet (SBUV) and the Ozone Monitoring Instrument (OMI) for Tropospheric Ozone Residual (TOR), and the Moderate Resolution Imaging Spectoradiometer (MODIS) for aerosol optical depths (AOD).

In addition to the baseline simulations, additional simulations without anthropogenic aerosol emissions and secondary aerosol formation are performed. Feedbacks of anthropogenic aerosol are obtaining by taking the difference between the two sets of simulations.

## 10.3 Results and Conclusions

The WRF/Chem applications over East Asia for simulated months and evaluations with limited observations show good performance for $PM_{10}$ in mainland China (NMBs of −25 to −4.3 %), Hong Kong (NMBs of −30.4 to −1.1 %), and Japan in April, July, and Oct. (NMBs of −35.5 to −2.2 %), but larger underpredictions in Japan in January (NMBs of −60.4 to −44.1 %) and in Taiwan in all months (NMBs of −64 to −47.4 %). $PM_{2.5}$ performance in Taiwan is better (NMBs of −56.8 to −13.5 %) than that of $PM_{10}$. The model shows moderate to large underpredictions for $SO_2$, NO, $NO_2$, and CO but overpredictions for surface $O_3$ in Hong Kong, Taiwan, and Japan in most of months. It shows reasonable performance for column CO (NMBs of −23.6 to 24.6 %), column $NO_2$ (NMBs of 5.2–48.6 %), tropospheric ozone residual (NMBs of −10.5 to 50.6 %), and AOD (NMBs of −58.3 to 56.1 %), especially considering large uncertainties in Asian emissions. Site-specific evaluation over China/Japan shows reasonably good agreement for $O_3$, $PM_{2.5}$, and $PM_{10}$. Uncertainties in emissions may be the main reason for large biases in simulating concentrations and resultant variables such as AOD. In addition, limitations associated with model treatments of some atmospheric processes such as dust emission module, cloud microphysics, cumulus parameterizations, and aerosol-cloud interactions may also contribute to large biases in model predictions. For example, comparing model simulations using the default dust emission modules, the Zender et al. [14] dust emission module largely improves predictions of $PM_{10}$ and AOD.

Our results with adjusted anthropogenic emissions and improved dust emission module show that anthropogenic aerosol has a sizeable impact on radiation, cloud properties, and other boundary layer meteorological variables. For example, on domain-average, they act to decrease shortwave radiation by up to ~12 W $m^{-2}$ (or ~6 %), near surface temperature by as low as −0.07 °C, planetary boundary

layer height by up to ∼13 m (or ∼3 %), and increase AOD by up to 0.3 (or a factor of 4), column CCN at a supersaturation of 0.5 % by up to $3 \times 10^8$ $cm^{-2}$ (or ∼70 %), and column cloud droplet number concentrations by $2.4 \times 10^6$ $cm^{-2}$ (by a factor of 3). They can decrease precipitation in January but can either decrease or increase precipitation in July. The feedback signals and their impacts are much stronger over urban areas where the concentrations of $PM_{10}$ are higher. These feedbacks and resulting impacts show a strong seasonality (e.g., January vs. July) and some inter-annual variability (e.g., 2001 vs. 2005), due to variations of meteorology, climate, and emissions. These results are overall consistent with those of Jacobson et al. [7] and Zhang et al. [19] over CONUS, Zhang et al. [22, 23] over Europe, and Zhang et al. [20, 21] over globe.

These results suggest that aerosol feedbacks are important over polluted areas and should be considered in regulatory applications and development of emission control and climate mitigation policies for areas where the aerosol feedback signals are strong. They also indicate a need for accurate model inputs and treatments to reduce uncertainties in model predictions of air pollution and climate changes as well as a need to verify simulated feedbacks with observations from special field campaigns and long-term monitoring networks.

**Acknowledgments** This research was supported by the Office of Science, DOE climate modeling programs (DE-SC0006695) at NCSU and China's National Basic Research Program (2010CB951803). Thanks are due to David Streets, Argonne National Laboratory, and Qiang Zhang, Tsinghua University, for providing 2005 and 2008 emissions; Xuyan Liu, Tsinghua University, for performing 2008 simulation; Fengkui Duan and Kebin He, Tsinghua University, for proving observations at the Tsinghua site.

## References

1. Chapman EG, Gustafson WI Jr, Easter RC, Barnard JC, Ghan SJ, Pekour MS, Fast JD (2009) Coupling aerosol-cloud-radiative processes in the WRF-Chem model: investigating the radiative impact of elevated point sources. Atmos Chem Phys 9:945–964
2. Fast JD, Gustafson WI Jr, Easter RC, Zaveri RA, Barnard JC, Chapman EG, Grell GA, Peckham SE (2006) Evolution of ozone, particulates, and aerosol direct radiative forcing on the vicinity of Houston using a fully coupled meteorology-chemistry-aerosol model. J Geophys Res 111, D21305. doi:10.1029/2005JD006721
3. Gong S, Barrie LA, Blanchet JP (1997) Modeling sea salt aerosols in the atmosphere. 1: Model development. J Geophys Res 102:3805–3818
4. Grell GA, Peckham SE, Schmitz R, McKeen SA, Frost G, Skamarock WC, Eder B (2005) Fully coupled "online" chemistry within the WRF model. Atmos Environ 39:6957–6975
5. Guenther A, Karl T, Harley P, Wiedinmyer C, Palmer PI, Geron C (2006) Estimates of global terrestrial isoprene emissions using MEGAN (Model of Emissions of Gases and Aerosols from Nature). Atmos Chem Phys 6:3181–3210. www.atmos-chem-phys.net/6/3181/2006/
6. Gustafson WI, Chapman EG, Ghan SJ, Easter RC, Fast JD (2007) Impact on modeled cloud characteristics due to simplified treatment of uniform cloud condensation nuclei during NEAQS 2004. Geophys Res Lett 34:L19809. doi:10.1029/2007GL0300321

7. Jacobson MZ, Kaufmann YJ, Rudich Y (2007) Examining feedbacks of aerosols to urban climate with a model that treats 3-D clouds with aerosol inclusions. J Geophys Res 112, D24205. doi:10.1029/2007JD008922
8. O'Dowd CD, Michael HS, Consterdine IE, Lowe JA (1997) Marine aerosol, sea-salt, and the marine sulphur cycle: a short review. Atmos Environ 31:73–80
9. Shaw P (2008) Application of aerosol speciation data as an in situ dust proxy for validation of the Dust Regional Atmospheric Model (DREAM). Atmos Environ 42:7304–7309
10. Streets DG, Bond TC, Carmichael GR et al (2003) An inventory of gaseous and primary aerosol emissions in Asia in the year 2000. J Geophys Res 108(D21):8809. doi:10.1029/2002JD003093
11. Streets DG, Zhang Q, Wang L et al (2006) Revisiting China's CO emissions after TRACE-P: synthesis of inventories, atmospheric modeling, and observations. J Geophys Res 111, D14306. doi:10.1029/2006JD007118
12. Wang L-T (2006) Episodic study on the air quality simulation and control in Beijing, China. PhD dissertation. Tsinghua University, Beijing, China, 157 pp
13. Wang L-T, Jang C, Zhang Y, Wang K, Zhang Q, Streets D, Yu L, He K, Hao J-M, Fu J, Lam N, Lin J, Meskhidze N, Voorhees S, Schreifels J, Evarts D, Phillips S (2010) Assessment of air quality benefits from national air pollution control policies in China. I: background, emission scenarios and evaluation of meteorological predictions. Atmos Environ 44(28):3442–3448. doi:10.1016/j.atmosenv.2010.05.050
14. Zender CS, Bian H, Newman D (2003) Mineral Dust Entrainment and Deposition (DEAD) model: description and 1990s dust climatology. J Geophys Res 108(D14):4416. doi:10.1029/2002JD002775
15. Zhang Q, Streets DG, He K et al (2007) NOx emission trends for China, 1995–2004: the view from the ground and the view from space. J Geophys Res 112, D22306. doi:10.1029/2007JD008684
16. Zhang Q, Streets DG, He K, Klimont Z (2007) Major components of China's anthropogenic primary particulate emissions. Environ Res Lett 2:045027. doi:10.1088/1748-9326/2/4/045027
17. Zhang Q, Streets DG, Carmichael GR et al (2009) Asian emissions in 2006 for the NASA INTEX-B mission. Atmos Chem Phys 9:5131–5153
18. Zhang Y (2008) Online coupled meteorology and chemistry models: history, current status, and outlook. Atmos Chem Phys 8:2895–2932
19. Zhang Y, Wen X-Y, Jang CJ (2010) Simulating climate-chemistry-aerosol-cloud-radiation feedbacks in continental U.S. using online-coupled WRF/Chem. Atmos Environ 44(29): 3568–3582
20. Zhang Y, Chen Y-C, Sarwar G, Schere K (2012) Impact of gas-phase mechanisms on WRF/Chem predictions: mechanism implementation and comparative evaluation. J Geophys Res 117(D1):D01301. doi:10.1029/2011JD015775
21. Zhang Y, Karamchandani P, Glotfelty T, Streets DG, Grell G, Nenes A, Yu F-Q, Bennartz R (2012) Development and initial application of the global-through-urban weather research and forecasting model with chemistry (GU-WRF/Chem). J Geophys Res 117, D20206. doi:10.1029/2012JD017966
22. Zhang Y, Sartelet K, Wu S-Y, Seigneur C (2013) Application of WRF/Chem-MADRID and WRF/Polyphemus in Europe, Part I: Model description and evaluation of meteorological predictions. Atmos Chem Phys 13:3993–4058. doi:10.5194/acpd-13-3993-2013#_blank
23. Zhang Y, Sartelet K, Zhu S, Wang W, Wu S-Y, Zhang X, Wang K, Tran P, Seigneur C (2013) Application of WRF/Chem-MADRID and WRF/Polyphemus in Europe, Part II: Evaluation of chemical concentrations, sensitivity simulations, and aerosol-meteorology interactions. Atmos Chem Phys 13:6845–6875

## Questions and Answers

**Questioner Name:** Ted Russell

**Q:** How have you shown that you modeled precipitation response is not numerical noise and is significant ?

**A:** This is a very good question. We've seen similar responses from our multi-year simulations. As part of the QA steps, we first evaluated the simulated precipitation with the NCDC data to make sure the model performance is acceptable and consistent with other model applications. We then artificially increased the anthropogenic aerosol concentrations by a factor of 10 and found more robust responses of precipitation than the baseline, which indicated that modeled precipitation response is significant and is not numerical noise.

**Questioner Name:** K. Heinke Schlünzen

**Q:** How did you calculate the mean normalized bias?

**A:** What we calculated was normalized mean bias, instead of mean normalized bias. We took the sum of the differences between model predictions and observations at all monitoring stations (numerator), and divide it with the sum of all observations at all sites (denominator).

# Chapter 11
# Investigation of Trends in Aerosol Direct Radiative Effects over North America Using a Coupled Meteorology-Chemistry Model

**Rohit Mathur, Jonathan Pleim, David Wong, Christian Hogrefe, Jia Xing, Chao Wei, Chuen-Meei Gan, and Francis Binkowski**

**Abstract** A comprehensive investigation of the processes regulating tropospheric aerosol distributions, their optical properties, and their radiative effects in conjunction with verification of their simulated radiative effects for past conditions relative to measurements is needed in order to build confidence in their estimates of the projected impacts on future climate. This study aims at addressing this issue through a systematic investigation of changes in anthropogenic emissions of $SO_2$ and $NO_x$ over the past two decades in the United States, the consequent changes in anthropogenic aerosol loading in the North American troposphere, and subsequent impact on regional radiation budgets.

## 11.1 Introduction

A key uncertainty in quantification of aerosol radiative effects and their impact on climate change is the verification of the spatial and temporal variability in its magnitude and directionality and, consequently, its cumulative effect on the radiation balance of the earth-atmosphere system. While global numerical atmospheric models have recently been used to estimate the anthropogenic aerosol radiative effects for future changing emission scenarios, little effort has been devoted to verifying the fidelity of the simulated radiative effects relative to available

R. Mathur (✉)
Atmospheric Modeling and Analysis Division, United States Environmental Protection Agency, Research Triangle Park, NC, USA
e-mail: mathur.rohit@epa.gov

J. Pleim • D. Wong • C. Hogrefe • J. Xing • C. Wei • C.-M. Gan
U.S. Environmental Protection Agency, Research Triangle Park, NC, USA
e-mail: plein.jon@epa.gov; hogrefe.christian@epa.gov

F. Binkowski
Institute for the Environment, University of North Carolina at Chapel Hill, Chapel Hill, NC, USA

D. Steyn and R. Mathur (eds.), *Air Pollution Modeling and its Application XXIII*, Springer Proceedings in Complexity, DOI 10.1007/978-3-319-04379-1_11,

observations. A key outstanding question in addressing these uncertainties is how well do current models represent the regional and temporal variability of aerosol radiative forcing for current and past conditions?

There is increasing evidence that the amount of solar radiation incident at the Earth's surface is not stable and has undergone significant decadal variations. The variability in this surface solar radiation (also referred to as surface shortwave radiation) plays a prominent role in the earth's climate system as it is the source for energy exchanges between the atmosphere, and the land/biosphere/ocean components, and consequently can contribute to the modulation of the surface temperature, intensity of the hydrological cycle, and potentially the net ecosystem productivity [4]. Analyses of long-term records of surface radiation measurements have suggested a decreasing trend during the 1960–1980s time period, followed by period of leveling-out and to reversal (brightening) in the 1990s and thereafter. The documented long-term trends in surface solar radiation and their association with trends in emissions of aerosols and precursor species provide cases to test the representation of aerosol-radiation effects in current and evolving regional and global coupled chemistry/climate models.

## 11.2 Datasets and Model Overview

Title IV of the Clean Air Act Amendments (also known as the Acid Rain Program) has achieved substantial reductions in U.S. electric power industry emissions of $SO_2$ and $NO_x$ since the 1990s. Analysis of ambient measurements of gaseous and particulate phase sulfur concentrations at CASTNET and IMPROVE sites show significant decreasing trends during the 1995–2010 period. Observations of both all-sky and clear-sky surface short wave radiation at many sites in the eastern U.S. show an increasing trend during this period.

The coupled WRF-CMAQ modeling system [2, 5] is exercised for selected summer time slices (June–July–August for the years 1990, 1996, 2000, 2006) to simulate the changes in tropospheric aerosol loading and associated radiative effects resulting from the changes in anthropogenic emissions over the past two decades. Model simulations were performed over two domains: an outer hemispheric scale domain covering the Northern hemisphere, set on a polar stereographic projection and discretized with a horizontal resolution of 108 km (cf. [3]) and a nested 12 km resolution grid covering the Continental U.S. and portions of Canada and Mexico. Year specific emissions for the norther hemispheric domain were derived from the EDGARv4.2 global emission inventory. The regional 12 km resolution calculation employed emission estimates from recently developed inventory for 1990–2010 in which state-level anthropogenic emissions of $SO_2$, $NO_x$, CO, NMVOC, $NH_3$, $PM_{10}$ and $PM_{2.5}$ for a total of 49 sectors were estimated based on several long-term databases containing information about activity and emission controls [6].

## 11.3 Discussion

Simulated changes in tropospheric aerosol levels for different regions of the northern hemisphere are illustrated in Fig. 11.1 which shows summertime regional mean $SO_4^{2-}$ concentrations across the eastern U.S., western Europe, and eastern China. Systematic reductions in ambient $SO_4^{2-}$ levels in the east U.S. and western Europe are noted for the 1990–2006 period and are attributed to $SO_2$ emission reductions in these regions. In contrast a significant increase in $SO_4^{2-}$ levels across east China are noted post-2000 resulting from increase in industrial activity and energy demand and associated $SO_2$ emissions. These heterogeneities in changing tropospheric aerosol burden are likely to result in differences in regional radiation perturbation across these regions.

The simulated reductions in ambient $SO_4^{2-}$ over the eastern U.S. are consistent with trends in measured surface $SO_4^{2-}$ concentrations at several sites in the region [1]. Figure 11.2a presents spatial distributions of the modeled trends in surface-level $SO_4^{2-}$ inferred from a linear regression of simulated summer (June–July–August) average values for the four simulation years, 1990, 1995, 2000, 2006. Largest reductions in $SO_4^{2-}$ (>0.3 $\mu g/m^3$/year) are estimated downwind of the Ohio River valley where many electric generation units are based. The model estimated values in Fig. 11.2a are in the range of those inferred from observations in the eastern U.S. (−0.093 to −0.14 $\mu g/m^3$/year) as detailed in Gan et al. [1]. Regional reductions in ambient $PM_{2.5}$ are also simulated across the east U.S. for the period 1990–2006 (Fig. 11.2b). The corresponding changes in aerosol optical depth is illustrated in Fig. 11.2c which shows a systematic decreasing trend in tropospheric aerosol burden across the eastern U.S. Associated with the reductions in aerosol

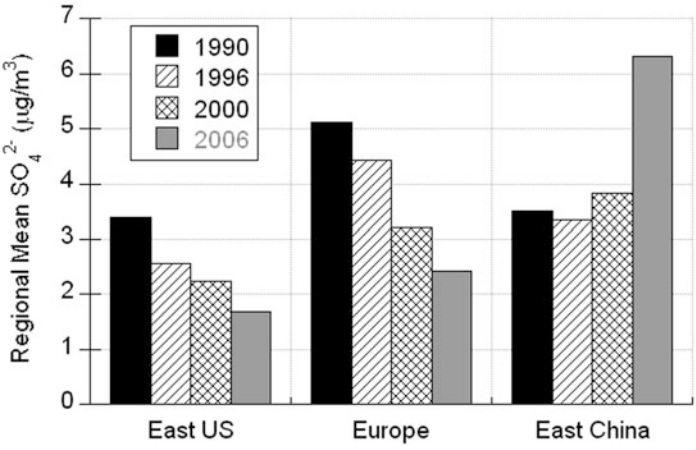


**Fig. 11.1** Simulated regional summertime mean $SO_4^{2-}$ concentrations

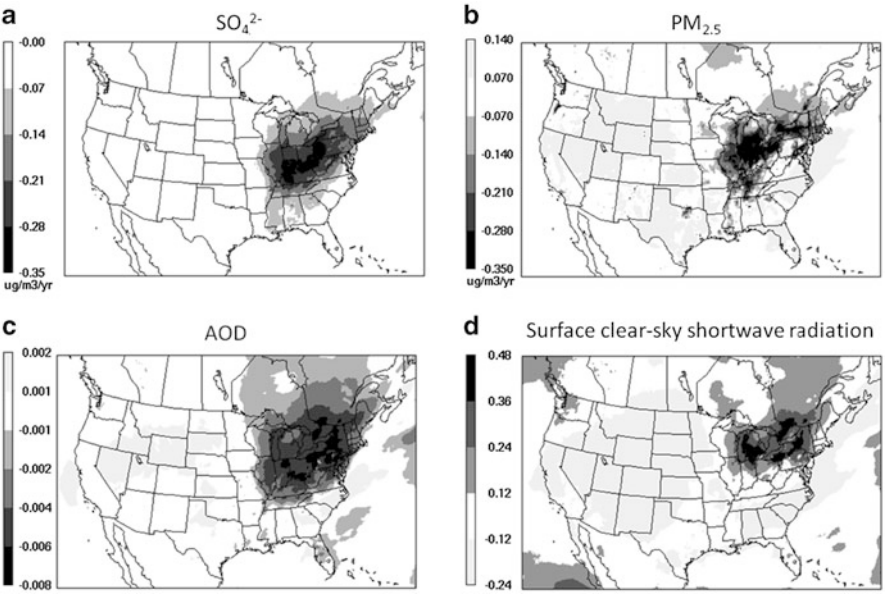


**Fig. 11.2** Spatial distribution of modeled trends during 1990–2006 in: (**a**) surface-level $SO_4^{2-}$ ($\mu g/m^3$/year), (**b**) surface-level $PM_{2.5}$ ($\mu g/m^3$/year), (**c**) aerosol optical depth, and (**d**) surface clear-sky shortwave radiation ($W/m^2$/year). All trends based on summer (June–July–August) values

burden in the region is a corresponding increase in simulated clear-sky surface shortwave radiation. Based on analysis of measurements at three eastern U.S. SURFRAD sites and the SGP site, we estimate an average increasing trend of 0.37 $W/m^2$/year in clear-sky shortwave radiation during 1995–2010 [1]. The corresponding model estimated trend is comparable in magnitude to the observed values and thus provide an estimate of the changes associated with direct aerosol radiative forcing in the east U.S.

**Disclaimer** This work was supported in part through an inter-Agency agreement between the U.S. Environmental Protection Agency and Department of Energy. Although this work has been reviewed and approved for publication by the U.S. EPA, it does not reflect the views and policies of the agency.

## References

1. Gan C-M, Pleim J, Mathur R, Hogrefe C, Long CN, Xing J, Roselle S, Wei C (2013) Assessment of the effect of air pollution controls on trends in shortwave radiation over the United States from 1995 through 2010 from multiple observation networks. Atmos Chem Phys Discuss 13:23719–23755. doi:10.5194/acpd-13-23719-2013

2. Mathur R, Pleim J, Wong D, Otte T, Gilliam R, Roselle S, Young J, Binkowski F, Xiu A (2010) The WRF-CMAQ integrated on-line modeling system: development, testing, and initial applications. In: Steyn DG, Rao ST (eds) Air pollution modeling and its application XX. Springer, Dordrecht, pp 155–159
3. Mathur R, Gilliam R, Bullock OR, Roselle S, Pleim J, Wong D, Binkowski F, Streets D (2012) Extending the applicability of the community multiscale air quality model to hemispheric scales: motivation, challenges, and progress. In: Steyn DG, Trini Castelli S (eds) Air pollution modeling and its applications, XXI. Springer, Dordrecht, pp 175–179
4. Wild M (2009) Global dimming and brightening: a review. J Geophys Res 114:D00D16. doi:10.1029/2008JD011470
5. Wong DC, Pleim J, Mathur R, Binkowski F, Otte T, Gilliam R, Pouliot G, Xiu A, Young JO, Kang D (2012) WRF-CMAQ two-way coupled system with aerosol feedback: software development and preliminary results. Geosci Model Dev 5:299–312. doi:10.5194/gmd-5-299-2012
6. Xing J, Pleim J, Mathur R, Pouliot G, Hogrefe C, Gan C-M, Wei C (2013) Historical gaseous and primary aerosol emissions in the United States from 1990 to 2010. Atmos Chem Phys 13:7531–7549. doi:10.5194/acp-13-7531-2013

## Questions and Answers

**Questioner Name**: Nicolas Moussiopoulos

**Q**: How do your model results regarding the direct effects compare against model uncertainty?

**A**: Unfortunately very few concurrent measurements of atmospheric aerosol size and composition profiles, their optical properties, and radiation are available to conduct a comprehensive closure experiment. We have used measurements from recent field campaigns to verify the model aerosol optics calculations and establish its credibility. We have also compared simulated surface solar radiation with measured values, under both moderate and high pollution episodes (e.g., wildfires) and found that including direct effects of aerosols helps improve the predictions of surface solar radiation. The long-term simulations discussed here are in fact another approach to build confidence in model predictions through comparison of trends for past conditions.

**Questioner Name**: Gabriele Curci

**Q**: In the comparison of $\Delta$AOD and corresponding $\Delta$ADRE it looks like positive $\Delta$AOD have larger impact on $\Delta$ADRE than negative changes: any hints why this is?

**A**: The aerosol optical properties (and consequently AOD) and their radiative effects are non-linearly dependent on a number of factor including aerosol size, composition, water content, albedo. The change in aerosol direct radiative effects ($\Delta$ADRE) thus should not be expected to strictly vary linearly with $\Delta$AOD.

**Questioner Name**: Yang Zhang

**Q**: In analyzing the trend in observed PM between 1990 and 2006, have the PM observations been adjusted for meteorological differences between a specific year and climatology?

**A**: In deriving the trends in observed PM, we did not perform any adjustment to account for year-to-year differences in meteorology. The model simulations for only the summer months for just four selected years in the 1990–2006 period presented here are preliminary, and are clearly not sufficient to infer a robust trend. We are currently completing model calculations for several 3-year long time slices during 1990–2010. We will then average both the model and the measurements for the appropriate periods to infer trends that can be cross-compared in a consistent manner.

# Chapter 12
# Future Year Air Quality Change Due to Growth in Aircraft Emissions and Changes in Climate

**Saravanan Arunachalam, Matthew Woody, Jared H. Bowden, and Mohammad Omary**

**Abstract** Increased growth in aviation activity in the future is projected to show increased emissions from this sector, and hence approximately proportional increases in concentrations if other factors were unchanging. However, emissions from other anthropogenic sources are generally expected to decrease due to several projected emissions control measures, and changes in climate will also occur. In this study, we evaluated air quality changes due to growth in aviation activities from 2005 to 2025, focusing on 99 major U.S. airports with aircraft activity data during landing and takeoff (LTO) activity developed for a growth scenario in 2025. We also assessed changes in climate based upon IPCC RCP 4.5 projections scenario, and used dynamically downscaled meteorology from the Climate Earth System Model (CESM) to WRF over the continental U.S. We performed six annual simulations at 36-km resolution using the WRF-SMOKE-CMAQ modeling system for 2005 and 2025, with and without aircraft emissions, and with and without changes in future year climate from CESM/WRF. We focused on assessing the incremental changes in $O_3$, $NO_2$ and $PM_{2.5}$ due to changes in emissions (due to aircraft and non-aviation sources) and meteorology. We see a net increase in annual average $PM_{2.5}$ due to aviation increase from a factor of 5.5 (2025 vs. 2005) without incorporating change in climate to 5.9 with change in climate. Similarly, the changes in summer season average of daily maximum 8-h $O_3$ due to aviation changes from a factor of 3.1–3.3 with change in climate. Both these changes translate to about a ~7 % additional increase in the future year that we attribute as the "climate penalty" factor. Detailed analyses of the $O_3$ changes show that the effect of change in climate is more pronounced at higher end of concentrations, where the grid-cells with values

S. Arunachalam (✉) • M. Woody • J.H. Bowden • M. Omary
Institute for the Environment, University of North Carolina at Chapel Hill, 137 E. Franklin St., #648A, Chapel Hill, NC 27599-6116, USA
e-mail: sarav@email.unc.edu

D. Steyn and R. Mathur (eds.), *Air Pollution Modeling and its Application XXIII*, Springer Proceedings in Complexity, DOI 10.1007/978-3-319-04379-1_12,

exceeding the U.S. NAAQS of 75 ppb see a 60 % increase due to change in climate. The changes in 1-h $NO_2$ due to aircraft increase by a factor of ~2 in 2025 vs. 2005, with increases around major airports being as high as a factor of 6.

## 12.1 Introduction

Aviation is a vital component of the U.S. infrastructure and activity is projected to grow steadily over the next 20 years. The Federal Aviation Administration (FAA) projects U.S. passenger enplanements to grow at an average annual rate of 2.5 % between 2011 and 2030. While an important mode of transportation, aircraft activities affect air quality due to emissions of CO, $NO_x$, Volatile Organic Compounds (VOCs), $SO_x$, $PM_{2.5}$, and numerous hazardous air pollutants. In light of the projected growth of aircraft usage and emissions, coupled with the expectation that emissions from non-aviation anthropogenic sources will decrease due to several emissions control measures that are likely to be in place as well as population size and age distribution changes over time, it is critical to understand the effects of aircraft on air quality from both an environmental and public health perspective. Here we extend an investigation of the simulated impacts of aviation emissions on current (2005) and future year (2025) air quality, using the CMAQ model. While we previously reported an assessment that looked only at emissions changes in the future, and their impacts on future air quality, the changes in climate was ignored [3]. In this study, we extend this analysis by incorporating changes in climate and looking at the nonlinearities in processes that impact future year air quality. To support this extension, we rely on Global Climate Models (GCMs) that model changes in climate and perform dynamic downscaling for regional scales.

Dynamical downscaling of climate change projections from GCMs requires large computational resources (high cost) because dynamical downscaling requires simulating multiple years to decades to provide statistics of the weather. In this study, we develop a cost-effective dynamical downscaling approach, by simulating a year each in the contemporary and future periods (low cost) to project the climate change signal. Our strategy is to understand and acknowledge potential limitations (effectiveness) of using a select few years while selecting years of interest using a quantitative measure. Such a strategy is important for applications wanting to use dynamical downscaling information for select years, like the AQ application here when emissions are available only one base year and one future year, as is typical for most air quality analyses.

## 12.2 Methodology

We performed WRF-SMOKE-CMAQ modeling to estimate the effects of current and future aircraft emissions on air quality within the continental U.S. GCM realizations for the contemporary and future climate scenarios were available from

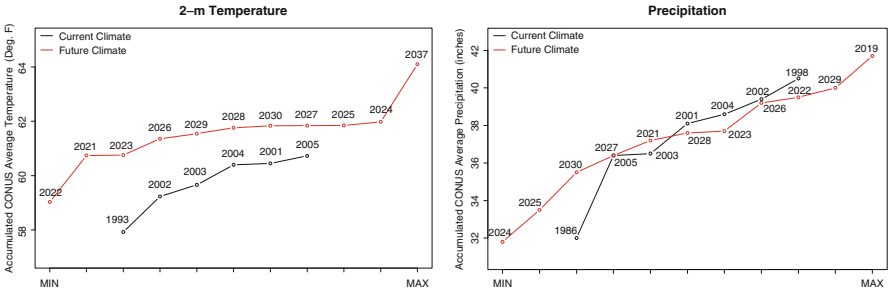


**Fig. 12.1** Selecting anomalous years from climate records

1850 to 2005 and from 2005 to 2100. We developed subjective criteria based on the availability of emissions and defining the extreme meteorological range. We then analyzed climatology from the contemporary and future year periods to identify a single year each to represent contemporary (2002) and future year (2024) meteorology for our modeling. We selected these 2 years that represent an extreme range in the meteorology to help provide an upper bound on climate change, while at the same time being within $\pm 5$ years from the years for which emissions are available, i.e. 2005 and 2025. There are other methods, such as the delta method; however, these methods tend to neglect potential changes in climate teleconnections (i.e. ENSO) as the climate changes. We then used the CESM simulation for these 2 years from the IPCC RCP4.5 scenario with a radiative forcing increase of 4.5 W/m$^2$ in the year 2100 to downscale to regional scale using the WRF model. We performed extensive comparisons between the dynamical downscaling projection to the GCM projection for both a 30-year mean climate and for the two select years, i.e., 2002 and 2024 (see Fig. 12.1).

Current year non-aviation emissions were estimated using the EPA's 2005 NEI and by excluding the NEI reported emissions from commercial aircraft. Future year non-aviation emissions for 2025 were interpolated from EPA's 2020 and 2030 projections of the 2005 NEI, which include existing or planned emission control programs for various sectors on the national and state level. Aircraft emissions data, based on Landing and Takeoff (LTO) cycles of commercial aircraft below 10,000 ft, were generated from a research version of EDMS, processed through the EDMS2Inv tool [1], and input into SMOKE. Aircraft emission estimates included CO, total organic gases (TOG), $NO_x$, $SO_x$, primary elemental carbon, and hazardous air pollutants (HAPS). Current year emissions estimates were based on hourly National Aerospace Standards (NAS) activity data from 99 major airports for February 19, 2004 and scaled up to compute an annual inventory. Specific annual scaling factors were applied to each airport based on flight schedules. Future year aviation estimates were scaled up using a growth scenario developed for the Interagency Portfolio and Systems Analysis Division of NextGen's Joint Planning and Development Office (JPDO) based on the methodologies of Gawdiak et al. [2]. Additional details about the aircraft emissions used and the modeling platform are

**Table 12.1** List of CMAQ simulations and input scenarios

| Scenario | Meteorology | Background emissions | Aircraft emissions |
|---|---|---|---|
| Base05 | 2005 | 2005 | None |
| Airp05 | 2005 | 2005 | 2005 |
| Base25M05 | 2005 | 2025 | None |
| Airp25M05 | 2005 | 2025 | 2025 |
| Base25M25 | 2025 | 2025 | None |
| Airp25M25 | 2025 | 2025 | 2025 |

described in Woody et al. [3]. Table 12.1 lists the six CMAQ simulations modeled, and we analyzed the results by computing differences between the "airp" and "base" cases for each pair of simulation to assess incremental contributions due to aircraft emissions.

## 12.3 Results

### *12.3.1 Changes in Climate*

Comparison of the upper threshold of the projected changes (Fig. 12.1) to the mean change in climate between 1976–2005 and 2016–2045 indicates that (a) for temperature, projected changes across parts of the U.S. are twice as large as the mean change, whereas (b) for precipitation, projected changes are much larger, up to 70 % change, relative to the mean change which is typically less than 10 %. This can have a significant impact on emissions estimates that are dependent on meteorology, as well as on air pollutants that respond to those. For e.g., climate change impacts on ozone, and volatile PM species that participate in heterogeneous chemistry in the future year will be exacerbated.

Downscaling CESM with WRF reveals large regional differences: (a) For temperature, the climate change signal is smaller in WRF by several degrees for many locations, but both CESM and WRF reveal largest increases for the central CONUS. (b) For precipitation, the magnitude of precipitation increases can change quickly over short geographical distances, which may be a problem for some applications.

### *12.3.2 Changes in Air Quality*

We focused our analyses on three criteria pollutants (that affect human health) – $O_3$, $NO_2$ and $PM_{2.5}$. Figure 12.2 shows ratios aviation-contributed impacts in 2025–2005 as domain-averaged bar plots. The bar plots (of domain averages) are presented

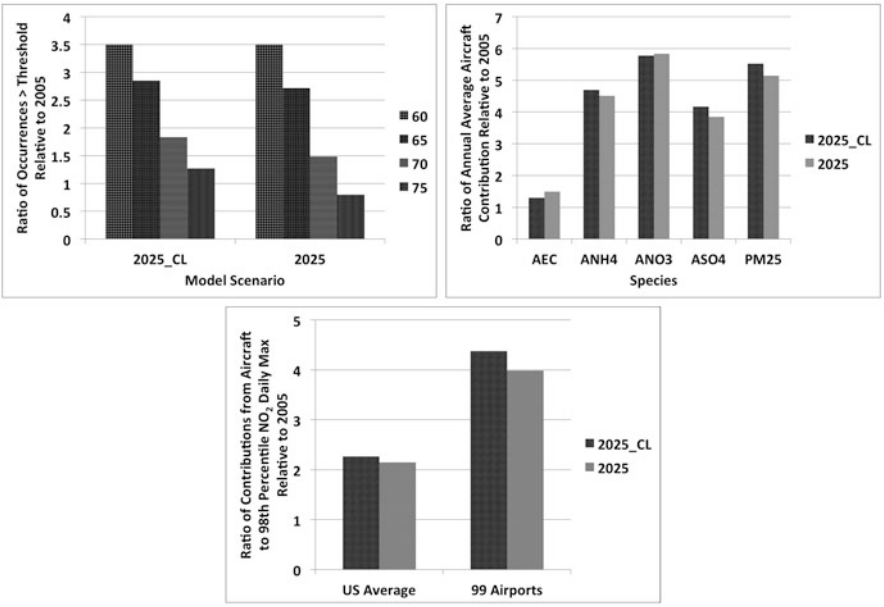


**Fig. 12.2** Ratios of aircraft-related impacts in 2025–2005 for $O_3$ (*top left*), $PM_{2.5}$ (*top right*), and $NO_2$ (*bottom*) using domain-averages

for both with and without climate change scenarios to show the impacts of climate change on these incremental aviation-related contributions. For all three pollutants, the impacts due to incorporating changes in climate are modest when compared to using constant meteorology. However, for $O_3$, we see that incorporating 2025 climate has an increase of up to 60 % in grid-cells exceeding the U.S. NAAQS levels (8 h $O_3 > 75$ ppb). For $NO_2$, the growth in aircraft emissions leads to a 2× increase in domain-average $NO_2$ in the future, the changes in 98th percentile 1-h $NO_2$ concentrations (new form of NAAQS in U.S.) can be as high as 6× in 2025 compared to 2005.

## 12.4 Conclusions

We have successfully developed a cost-effective downscaling technique from global to regional scale models, focused on emissions and AQ analyses, and applied this to extend a previous study focused on assessing future year AQ impacts due to growth in aircraft emissions, while incorporating changes in climate. The effect of this climate on assessing future year AQ due to growth in aircraft emissions is modest (∼7 %) on domain averages, but localized impacts are much higher especially when looking at NAAQS-relevant concentrations.

**Acknowledgements** This work was funded under the Partnership for Air Transportation Noise and Emissions Reduction (PARTNER) grants 09-CE-NE-UNC Amendments 001–005. PARTNER is funded by FAA, NASA, Transport Canada, U.S. Department of Defense and the U.S. EPA. Any opinions, findings, and conclusions or recommendations expressed in this material are those of the author(s) and do not necessarily reflect the views of PARTNER and its sponsors. We acknowledge CSSI, Inc. for providing the aircraft emissions from EDMS for this work, and to Christopher Sequeira and Mohan Gupta of the FAA for helpful discussions.

## References

1. Baek BH et al (2007) Development of an interface for the Emissions Dispersion and Modeling System (EDMS) with the SMOKE modeling system. In: Proceedings of the 16th annual emissions inventory conference, Raleigh, NC, May 2007
2. Gawdiak Y, Carr G, Hasan H (2009) JPDO case study of NextGen high density operations. In: 9th annual AIAA aviation, technology, integrations, and operations conference, Hilton Head, SC, September 2009
3. Woody M et al (2011) An assessment of aviation's contribution to current and future fine particulate matter in the United States. Atmos Environ 45(20):3424–3433

## Question and Answer

**Questioner Name:** Chris Nolte

Q: In choosing which years from the GCM to downscale, where the determinations based on conditions averaged over the globe, or over the regional modeling domain?

A: For this exercise, we focused only on the regional modeling domain, i.e., the continental U.S. and portions of Canada and Mexico.

# Chapter 13
# The Use of a Non Negative Matrix Factorization Method Combined to $PM_{2.5}$ Chemical Data for a Source Apportionment Study in Different Environments

**Adib Kfoury, Frédéric Ledoux, Abdelhakim Limem, Gilles Delmaire, Gilles Roussel, and Dominique Courcot**

**Abstract** This study revolves around the use of a Non Negative Matrix Factorization method under constraints for the identification sources profiles as well as their respective contributions in three sites in northern France. Using $PM_{2.5}$ chemical analysis data, the model identified eight background and four local industrial sources profiles. In addition, the contributions of these profiles showed that secondary aerosols and combustion sources are the major constituents of the analyzed $PM_{2.5}$, whereas industrial contributions were found majorly responsible for the elemental enrichments.

## 13.1 Introduction

The use of receptor modeling for atmospheric PM source apportionment studies has been largely applied around the world as a complementary method in addition to the analysis of chemical data. Matrix factorization based methods are well-known factor analysis models, from which the most famous applications are the Positive Matrix Factorization [4] and Non negative Matrix Factorization [3]. However, the extensive application of these models has shown the need to improve the manipulation conditions including calculations methods. Many gaps in the use of

A. Kfoury • F. Ledoux • D. Courcot (✉)
Université Lille Nord de France, F-59000 Lille, France

Unité de Chimie Environnementale et Interactions sur le Vivant, Université du Littoral Côte d'Opale, UCEIV EA4492, F-59140 Dunkerque, France
e-mail: adibkfoury@hotmail.com; Dominique.courcot@univ-littoral.fr

A. Limem • G. Delmaire • G. Roussel
Université Lille Nord de France, F-59000 Lille, France

Laboratoire d'Informatique, Signal et Image de la Côte d'Opale, Université du Littoral Côte d'Opale, LISIC EA4491, F-62228 Calais, France

D. Steyn and R. Mathur (eds.), *Air Pollution Modeling and its Application XXIII*, Springer Proceedings in Complexity, DOI 10.1007/978-3-319-04379-1_13,

mathematical modeling were revealed and addressed in reviews like Viana et al. [5] in 2008 and Bellis et al. [1] in 2013 for example. The first review proposed a list of research directions, from which we cite the use of hybrid models and the integration of *a priori* knowledge in the calculation procedures in order to distinguish some sources characterized by similar chemical species from each other. These propositions were taken in consideration in this work, in which we used a Constrained and Weighted Non-negative Matrix Factorization (CW-NMF) hybrid model [2] for source apportionment study of fine $PM_{2.5}$.

## 13.2 Constrained and Weighted NMF

The CW-NMF used in this study [2] takes in consideration measurements uncertainties related to the chemical data acquisition of the observations matrix, which lowers the effect of large errors on the criterion (13.1):

$$\{\boldsymbol{G}, \boldsymbol{F}\} = \underset{G,F}{\boldsymbol{arg\ min}} \sum_{i=1}^{n} \sum_{j=1}^{m} \left( \frac{x_{ij} - (\boldsymbol{GF})_{ij}}{\sigma_{ij}} \right)^2 \tag{13.1}$$

In this equation *"$x_{ij}$"* represents the current element drawn from the observations matrix, *"$\boldsymbol{G}$"* is the contributions matrix, *"$\boldsymbol{F}$"* is the source profiles matrix, and *"$\sigma_{ij}$"* is the general element of the uncertainties matrix $\boldsymbol{\Sigma}$.

In addition, this model has the possibility of including the *a priori* knowledge in the form of constraints within iterations. These constraints can be inserted in two forms: equality and inequality constraints. Equations (13.2, 13.3, and 13.4) explain how the algorithm searches iteratively for a profile vector while keeping equality (13.3) and inequality (13.4) constraints valid:

$$\{\boldsymbol{f}_i\} = \underset{f_i}{\boldsymbol{arg\ min}} \sum_{i=1}^{n} (\boldsymbol{x}_i - \boldsymbol{G}\,\boldsymbol{f}_i)^T \boldsymbol{W}_i\, (\boldsymbol{x}_i - \boldsymbol{G}\,\boldsymbol{f}_i) \tag{13.2}$$

$$\boldsymbol{M}_i\,\boldsymbol{f}_i - \boldsymbol{\delta}_i = \boldsymbol{0} \tag{13.3}$$

$$\boldsymbol{N}_i\,\boldsymbol{f}_i - \boldsymbol{\gamma}_i < \boldsymbol{0} \tag{13.4}$$

In Eq. (13.2), $\boldsymbol{W}$ represents the weight matrix. Each row of $\boldsymbol{M}_i$ includes only one element different from zero (13.3), whereas each row of $\boldsymbol{N}_i$ can include "1" or "−1" for constraints, and "0" everywhere else (13.4). $\boldsymbol{\delta}_i$ contains the set values of the profile vector while $\boldsymbol{\gamma}_i$ stands for the null vector. The first constraint allows the user to define specific values for chemical species in the sources profiles, while the second imposes an order of abundance for a given species between the different profiles (for example $f_{i1} - f_{i2} < 0$). The data used in these constraints were acquired from the chemical composition of emission sources samples and the literature.

## 13.3 Methodology

The acquisition of the observation data was achieved after two sampling campaigns and a series of chemical analysis. Sampling was conducted in three cities on the coast of Nord-Pas-de-Calais region (NPdC) in northern France, namely: Dunkerque (DK: industrial-urban), Boulogne-sur-Mer (BL: urban) and Saint-Omer (St-O: industrial-urban). Simultaneous sampling in DK and BL was achieved during winter (November–December, 2010) in addition to a spring campaign (April–May, 2010) between DK and St-O simultaneously. A Digitel® DA-80 high volume sampler was used to collect atmospheric $PM_{2.5}$ following a diurnal sampling method. Water soluble ions ($NH_4^+$, $Cl^-$, $NO_3^-$ and $SO_4^{2-}$) were analyzed using ion chromatography, total carbon (TC) using a CHNS-O analyzer, and major and trace elements (Al, Ca, Fe, K, Mg, Na, Ag, As, Ba, Cd, Co, Cr, Cu, Mn, Ni, Pb, Rb, Sb, Sn, Sr, Ti, V and Zn) using ICP-AES and ICP-MS respectively. A three step manipulation method was applied by CW-NMF using 357 samples to estimate the sources profiles and their respective contributions. The first manipulation was launched using the observed data of BL (86 samples), followed by a second calculation using St-O data (98 samples) and a final run using the observation data of DK (173 samples). The evaluation of the results quality was based on two main criteria: the shape of the identified profiles (convenience to the literature and/or *a priori* knowledge) as well as the correlation between CW-NMF estimated and observed concentrations.

## 13.4 Results

### *13.4.1 Sources Profiles (Matrix F)*

The use of the CW-NMF allowed us to identify 12 source profiles: 8 of which were common between the three study sites and are casually identified in coastal cities: sea-salts, aged sea-salts, crustal, secondary sulfates, secondary nitrates, combustion 1 (similar to traffic exhaust), traffic non-exhaust and combustion 2 (similar to biomass combustion). In addition, four industrial profiles were identified in Dunkerque and Saint-Omer, which are influenced by heavy and light industrial activities respectively: Integrated Steel Work (ISW)-fugitive, ISW-sintering stack, electric steel plant and glassmaking. The identification of these profiles was made possible through the integration of constraints which allowed taking in consideration the *a priori* knowledge on the sources in the calculations. The CW-NMF can also calculate the contributions of the industrial source profiles even if the chemical data set contains few samples impacted by these industrial sources.

**Table 13.1** Average contributions (in %) estimated by the CW-NMF

| | Average contributions (%) | | | |
|---|---|---|---|---|
| | Winter | | Spring | |
| Sources profiles | DK | BL | DK | St-O |
| Sea-salts | 2.9 | 2.4 | 2.3 | 2.6 |
| Aged sea-salts | 1.9 | 5.7 | 1.8 | 0.6 |
| Crustal | 0.2 | 0.3 | 0.3 | 0.3 |
| Secondary sulfates | 14.4 | 15.9 | 12.3 | 17.6 |
| Secondary nitrates | 34.3 | 39.8 | 61.8 | 57.4 |
| Traffic non-exhaust | 0.03 | 0.1 | 0.02 | 0.2 |
| Combustion 1 + 2 | 44.4 | 35.9 | 20.3 | 21.2 |
| ISW-fugitive emissions | 0.5 | – | 0.5 | 0.2[a] |
| ISW-sintering stack | 1.1 | – | 0.5 | |
| Electric steel plant | 0.3 | – | 0.2 | – |
| Glassmaking factory | – | – | – | 0.03 |

[a]This average contribution represents the ISW mixed emissions profile

## *13.4.2 Sources Contributions (Matrix G)*

### 13.4.2.1 Average Sources Contributions

For each identified source profile, the CW-NMF associates a specific contribution to the atmospheric $PM_{2.5}$ load in each sample. Hence we averaged the contribution of each source (Table 13.1) in all the samples collected at every sampling site.

Seasonal variations can be identified by studying these contributions. The secondary inorganic aerosols profiles (SIA: secondary sulfates and nitrates) contribute the most (49–75 %) in the global load of the analyzed $PM_{2.5}$ at the study sites (Table 13.1). Their contributions are higher during spring time, mostly during sunny days and dry and low speed winds anticyclone weather conditions, which favor the accumulation of $PM_{2.5}$. The combustion sources contributions ranged between 44 % in winter and 20 % in spring. This seasonal difference could be linked to the increased demand on heating during winter, and is around 24 % on average between winter and spring. This difference can be assumed to represent the contribution of heating activities. Finally, we can notice that these four previously mentioned sources constitute on average between 92 and 96 % of the total atmospheric $PM_{2.5}$.

### 13.4.2.2 Diurnal Sources Contributions

The analysis of the diurnal contributions showed that the evolution of SIA and marine salts contributions are synchronized between the sites of each sampling campaign: between Boulogne-sur-Mer and Dunkerque on one hand and Saint-Omer and Dunkerque on the other. This proves that the impact of these two sources is not linked to a local influence. Instead, it is found to be associated to a background $PM_{2.5}$ level that is fluctuating regionally. This regional scale variation is found to majorly

explain the levels fluctuations of these fine particles. The industrial sources are found to contribute in fewer amounts of $PM_{2.5}$ measured mass: 1–2 % in Dunkerque and about 0.2 % in Saint-Omer. However, these sources can significantly change the sampled particles composition, enriching this latter with elements such as: Fe, Zn, Pb, Cd, Sn, Cr, As, Ag, Cu and Rb in Dunkerque and Saint-Omer. In fact, we have observed that industrial contributions are found high in the total load of these elements in the samples. In addition, we should not neglect the indirect contributions from these industrial sources in the total $PM_{2.5}$ regional load, specifically through $NO_x$ and $SO_2$ emissions, which are precursors of inorganic aerosols formation.

## 13.5 Conclusion

The calculations made by CW-NMF using $PM_{2.5}$ chemical data lead to the identification of eight background sources profiles as well as four local industrial ones in three sites in northern France. The separation of very close sources profiles was achieved by the use of constraints representing the *a priori* knowledge. The contributions calculations showed that the weights of SIA and combustion sources are the highest in the total analyzed $PM_{2.5}$, whereas industrial contributions were found responsible of elemental enrichments.

## References

1. Bellis CA, Karagulian F, Larsen BR, Hopke PK (2013) Critical review and meta-analysis of ambient particulate matter source apportionment using receptor models in Europe. Atmos Environ 69:94–108
2. Delmaire G, Roussel G, Hleis D, Ledoux F (2010) Une version pondérée de la Factorisation Matricielle Non Negative pour l'identification de sources de particules atmosphériques: application au littoral de la Mer du Nord. Journal Européen des Systèmes Automatisés 44(4–5):547–566
3. Lee DD, Seung HS (1999) Learning the parts objects by non negative matrix factorization. Nature 401(6755):788–791
4. Paatero P, Tapper U (1994) Positive matrix factorization: a non-negative factor model with optional utilization of error estimates of data values. Environmentrics 5:111–126
5. Viana M, Kuhlbusch TAJ, Querol X, Alastuey A, Harrison RM, Hopke PK, Winiwarter W, Vallius M, Szidat S, Prévot ASH, Hueglin C, Bloemen H, Wahlin P, Vecchi R, Miranda AI, Kasper-Giebl A, Maenhaut W, Hitzenberger R (2008) Source apportionment of particulate matter in Europe: a review of methods and results. J Aerosol Sci 39:827–849

## Questions and Answers

**Questioner Name:** Roger Timmis

**Q:** How long was the sampling period, and how representative were the wind directions during the period; are you confident that source apportionments are representative of the long-term pollution climate?

**A:** The sampling period covered 46 days (1st campaign) and 52 days (2nd campaign) from early November 2010 to April 2011. The recorded meteorological data showed that wind directions fluctuated to include all major sectors: urban, marine, continental and industrial depending on the considered site. In addition, ambient temperatures also fluctuated between low (winter) and high (spring) values. Finally, we were able to divide the collected samples by wind sector to find that the major sectors are represented in an acceptable number of samples during each campaign. As for the seasonal behavior, the results are found to well represent the winter and spring period, but not the whole year.

**Questioner Name:** Tianfeng Chai

**Q:** How is the *a priori* uncertainty information used in the source apportionment?

**A:** The *a priori* knowledge was majorly used in the form of inequality constraints, meaning that this knowledge was introduced to give an order of abundance instead of a specific value that the model should consider. Therefore, the integration of uncertainties on the *a priori* knowledge is ineffective at this point.

# Chapter 14
# On the Interplay Between Upper and Ground Levels Dynamics and Chemistry in Determining the Surface Aerosol Budget

**G. Curci, L. Ferrero, P. Tuccella, F. Angelini, F. Barnaba, E. Bolzacchini, M.C. Facchini, G.P. Gobbi, T.C. Landi, M.G. Perrone, S. Sangiorgi, and P. Stocchi**

**Abstract** We use the WRF/Chem model to interpret observations of the aerosol concentration and its chemical composition both at surface level and along vertical profiles performed during an intensive campaign in July 2007 in Milan urban area. The model is added with a new diagnostic for aerosol budget analysis, building on that available for gas species, in order to study the contribution of upper levels processes on the aerosol formation at ground level. The analysis illustrates a quite variegated evolution of budget terms, which we found to depend strongly on the hour of the day, the vertical level, the aerosol compound, and the aerosol size. Primary components are generally emitted near the ground and rapidly transported by turbulent motions to the upper levels, where they gradually disperse and age. For some secondary components, such as nitrate, we calculate a net chemical destruction in the bottom layers, as opposed to a net chemical production higher in the boundary layer, which supply new material to ground level aerosol through turbulent mixing.

G. Curci (✉) • P. Tuccella
CETEMPS Centre of Excellence, Department of Physical and Chemical Sciences, University of L'Aquila, L'Aquila, Italy
e-mail: gabriele.curci@aquila.infn.it

L. Ferrero • E. Bolzacchini • M.G. Perrone • S. Sangiorgi
POLARIS Research Centre, Department of Environmental Sciences, University of Milano Bicocca, Milan, Italy

F. Angelini
Italian National Agency for New Technologies, Energy and Sustainable Economic Development (ENEA), Rome, Italy

F. Barnaba • G.P. Gobbi
Institute for Atmospheric and Climate Sciences (ISAC), National Research Council (CNR), Rome, Italy

M.C. Facchini • T.C. Landi • P. Stocchi
Institute for Atmospheric and Climate Sciences (ISAC), National Research Council (CNR), Bologna, Italy

D. Steyn and R. Mathur (eds.), *Air Pollution Modeling and its Application XXIII*, Springer Proceedings in Complexity, DOI 10.1007/978-3-319-04379-1_14,

**Table 14.1** WRF/Chem main options

| Physical process | WRF/Chem option |
|---|---|
| Microphysics | Morrison |
| Long-wave radiation | RRTMG |
| Short-wave radiation | RRTMG |
| Surface layer | Monin-Obukhov |
| Land-surface model | Noah LSM |
| Boundary layer scheme | Mellor-Yamada Nakanishi and Niino |
| Cumulus | New Grell scheme (G3) |
| Photolysis | Madronich |
| Chemistry model | New RACM-ESRL [2] |
| Aerosol model | MADE and VBS scheme for SOA [2] |
| Aerosol feedbacks | No |

## 14.1 Model Setup

WRF/Chem is a fully coupled "online" meteorology-radiation-chemistry model [1]. We use three nested domains at 30, 10, and 2 km horizontal resolution covering Europe, Northern Italy, and Po Valley, respectively, and 32 vertical levels extending up to 50 hPa. The initial and boundary meteorological conditions are provided by NCEP analyses every 6 h. The chemical initial and boundary conditions consist of time-invariant climatological profiles. We use an updated parameterization for the generation of secondary organic aerosols (SOA) based on the volatility basis set approach, as described in Ahmadov et al. [2]. More details on model configuration are reported in Table 14.1.

The anthropogenic emissions ($NO_x$, NMVOCs, CO, $SO_x$, $NH_3$ and unspeciated aerosol, elemental carbon and organic carbon) are taken from the TNO inventory at $7 \times 10$ km over Europe. The emissions are adapted to the chemical mechanism used in this study as described by Tuccella et al. [3]. Biogenic emissions are based on the MEGAN model. The chemidiag diagnostic option for gases [4] is added with aerosol species and processes, and used to build the budget analysis.

## 14.2 Results

In Table 14.2 we show statistical indices [5] of comparison of simulation on the inner domain at 2 km resolution with meteorological and chemical variables at the measurements site, located near downtown Milan, in the University campus of Milano Bicocca (45°31′19″ N, 9°12′46″ E). The meteorological bias is in the range of expected values for an urban environment. Temperature is underestimated by 2.4 °C, most probably because of misrepresentation of urban landuse and related energy fluxes with the default USGS database. Indeed, improvements were shown in a preliminary test employing CORINE database [6]. Relative humidity high bias is a consequence of that of temperature. Wind speed is overestimated by 0.55 m/s

**Table 14.2** Comparison of WRF/Chem with ground based hourly measurements for simulation period 5–18 July 2007 at University campus Milano Bicocca site (45°31′19″ N, 9°12′46″ E)

| Variable | Bias | NMB (%) | RMSE | r |
|---|---|---|---|---|
| T (°C) | −2.4 | −10 | 2.7 | 0.98 |
| RH (%) | 14 | 35 | 17 | 0.76 |
| WS (m/s) | 0.55 | 39 | 1.3 | 0.02 |
| WD (°) | 33 | 19 | 130 | 0.25 |
| NO (ppb) | −3.0 | −42 | 6.9 | 0.59 |
| $NO_2$ (ppb) | −9.7 | −39 | 14 | 0.43 |
| $O_3$ (ppb) | 3.2 | 9.8 | 12 | 0.64 |
| PM10 ($\mu g/m^3$) | −8.8 | −36 | 13 | 0.60 |
| PM2.5 ($\mu g/m^3$) | 1.9 | 17 | 5.7 | 0.57 |

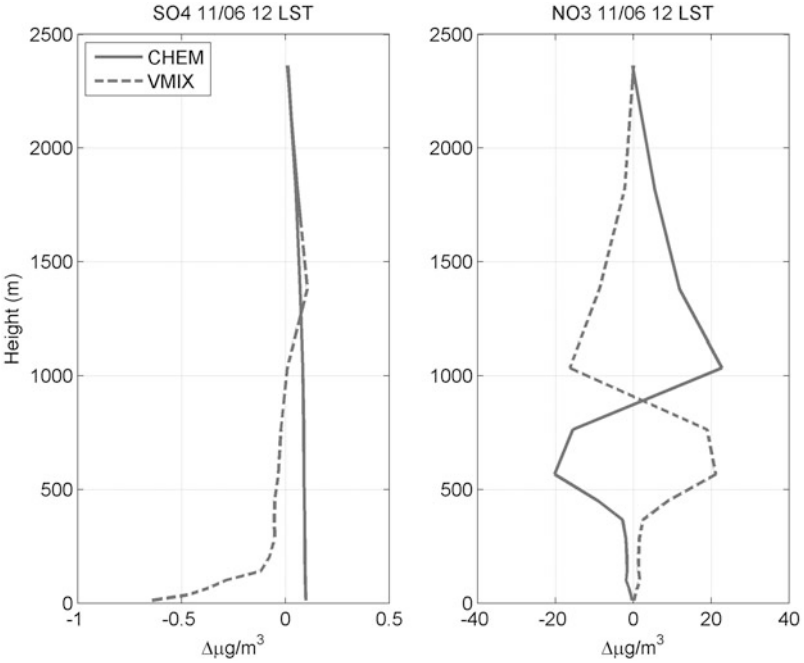


**Fig. 14.1** Sample budget profile of particulate sulfate (*left*) and nitrate (*right*) over Milan on June 11th 2007 at 12 local solar time. CHEM is the net production due to all aerosol processes, while VMIX is the vertical mixing plus dry deposition

(39 %). The bias is not systematic as for T and RH, but it concentrates nighttime (not shown), most probably because of difficulties in representing the transition from mixed to stable boundary layer in evening hours. Wind also shows larger fluctuations than observed, as denoted by an enhanced RMSE at 1.3 m/s and the null correlation.

Nitrogen oxides are underestimated by 40 % during the day, but the NO morning peak is well captured, indicating a potential important role of dynamics against emissions. Ozone is overestimated by about 10 %, especially nighttime and during

the afternoon (not shown). The significant difference between bias and RMSE denotes the presence of both systematic and unsystematic errors. PM10 and PM2.5 display a bias of −36 % and +17 % respectively, and are quite well correlated with measurements ($r \sim 0.6$). The low bias of PM10 may indicate a missing source from road dust resuspension.

In Fig. 14.1 we show a sample of the information derived from the budget analysis over Milan. Only the net chemical and vertical mixing terms for aerosol sulfate and nitrate are shown at noon. Sulfate is almost homogeneously produced throughout the PBL, it is deposited at the ground and mixed upward. On the other hand, nitrate is mostly produce above 800 m and destroyed below, so the nitrate concentrations we observe at the ground are actually those transported by turbulence from the upper levels.

**Acknowledgments** This work was funded by the Italian Space Agency (ASI) in the frame of the PRIMES project (contract n. I/017/11/0).

## References

1. Grell GA et al (2005) Fully coupled "online" chemistry within the WRF model. Atmos Environ 39:6957–6975
2. Ahmadov R et al (2012) A volatility basis set model for summertime secondary organic aerosols over the eastern U.S. in 2006. J Geophys Res 117:D06301. doi:10.1029/2011JD016831
3. Tuccella P et al (2012) Modeling of gas and aerosol with WRF/Chem over Europe: evaluation and sensitivity study. J Geophys Res 117:D03303. doi:10.1029/2011JD016302
4. Wong J et al, Budget and structural properties of the upper tropospheric ozone enhancement of North America in August 2006, in preparation
5. Thunis P et al (2012) Performance criteria to evaluate air quality modeling applications. Atmos Environ 59:476–482
6. Curci G et al (2012) Influenza su simulazioni meteo-chimiche dell'inventario di utilizzo del suolo: risultati preliminari dell'implementazione di CORINE in WRF/Chem, in Atti del V Convegno Nazionale "Il controllo degli agenti fisici: Ambiente, salute e qualità della vita". Torino, Italia. ISBN: 978-88-7479-118-7

## Questions and Answers

**Questioner name:** Sebnem Aksoyoglu

**Q:** Which precursors do you have for BSOA? Which one dominates BSOA formation?

**A:** BSOA precursors emissions are calculated with the MEGAN model and are isoprene and other lumped monoterpenes and sesquiterpenes as described in Ahmadov et al. (JGR 2012). Although isoprene emissions are generally predicted to be higher than monoterpenes in the Milan area, higher SOA yields of monoterpenes rank those compounds first in BSOA production.

**Questioner name:** Douw Steyn

**Q:** You note important chemical processes in the upper PBL, but this is where the vertical resolution becomes coarser. What was vertical resolution in the upper PBL, and do you think it was sufficiently fine?

**A:** The vertical resolution is of the order of 20–30 m near the surface and100 m up in the PBL. It would be certainly interesting to see how results changes with evenly spaced vertical levels, so that the volumes of the grid cells will be the same near the ground and up in the PBL. However, we already found that results don't change much with a finer resolution.

**Questioner name:** Roger Timmis

**Q:** How does the model resolve the effective emission heights of $SO_2$ and $NO_x$? Does the model resolve plume heights, which may be different for $SO_2$ (mainly from tall stacks) and $NO_x$ (more from low-level vehicle sources)?

**A:** Yes, but without on-line variation. The emissions are distributed in different vertical layers following the recommendations of EMEP modelling group, which vertically distributes emissions from different sources (i.e. SNAP sectors) with different profiles, that roughly also account for plume rise. However, these distributions are the same for all years and places, and do not vary with the meteorological situation.

# Chapter 15
# Modeling of Aerosol Indirect Effects with WRF/Chem over Europe

**Paolo Tuccella, Gabriele Curci, Suzanne Crumeyrolle, and Guido Visconti**

**Abstract** WRF/Chem has been updated in order to simulate the aerosol indirect effects using a new parameterization for production of secondary organic aerosol. The model has been evaluated over North Sea among the ATR-42 aircraft measurements of aerosol and cloud issued in frame European Integrated project on Aerosol Cloud Climate and Air Quality Interactions (EUCAARI). WRF/Chem tends to overpredict the number of condensation nuclei. Simulated liquid water content shows a bias of +15 %. Predicted cloud droplet number concentration is overestimated and radius effective droplet is underestimated.

## 15.1 Introduction

Aerosol particles play a key role in climate system by altering the global budget of radiation. They scatter and absorb directly (direct effect) the solar and thermal radiation [1] and affect indirectly (indirect effect) the patterns of clouds and precipitation [2]. The latter is usually referred to as "indirect effect" and arises from that the ability of aerosol particles to act as cloud condensation nuclei (CCN). An increase of aerosol particle concentration, for clouds with liquid water content (LWC) held constant, enhances the concentration of cloud droplets and reduces their size. This results in the increase of cloud albedo and is called "first indirect effect"

P. Tuccella (✉) • G. Curci • G. Visconti
CETEMPS- Dip. Scienze Fisiche e Chimiche, University of L'Aquila, L'Aquila, Italy
e-mail: paolo.tuccella@aquila.infn.it; gabriele.curci@aquila.infn.it

S. Crumeyrolle
Laboratoire de Météorologie Physique, Université Blaise Pascal,
UMR 6016 Clermont-Ferrand, France

NASA Langley Research Center, Hampton, VA 23666, USA

D. Steyn and R. Mathur (eds.), *Air Pollution Modeling and its Application XXIII*,
Springer Proceedings in Complexity, DOI 10.1007/978-3-319-04379-1_15,

or "Twomey's effect" [3]. Effects of first indirect effect on climate are still highly uncertain, and the representation of albedo effect is one of the most uncertainties in climatic projections [4].

In this work we present a preliminary evaluation of WRF/Chem model at medium resolution in order to assess the skill of the model to reproduce the main quantities in the aerosol-clouds interaction. The aim of the research is to understand how well a model reproduces the activation of aerosol particles in cloud droplets.

## 15.2 Methods

In this paper we use the version 3.4 of WRF/Chem model [5] with some news. The model has been updated in order to include the aerosol-cloud-interaction simulation using a new chemical mechanism for a better simulation of secondary organic aerosol [6], following the works of Fast et al. [7] and Chapman et al. [8].

A simulation is carried out on 15 May 2008 using two nested domains centered on Europe. First domain extent from 35°N to 57°N in latitude and from 15°W to 27°E in longitude. The horizontal resolution is 30 km with 41 vertical levels. Second domain is centered over the Netherlands, with horizontal resolution of 10 km. The model configuration is shown in Table 15.1. The anthropogenic emissions (gas and aerosol species) are taken from Nederlands Instituut Voor Toegepaste (TNO) inventory [9] and are adapted to WRF/Chem following Tuccella et al. [10].

WRF/Chem simulation results are then compared to measurements performed on-board the ATR-42 during the European Integrated project on Aerosol Cloud Climate and Air Quality Interactions (EUCAARI) [11]. The payload of the ATR-42 included a comprehensive suite of aerosol instrumentation including two Condensation Particle Counters (CPC3010, CPC3025), a Cloud Condensation Nuclei

**Table 15.1** WRF/Chem configuration

| Physical process | WRF/Chem option |
|---|---|
| Microphysics | Morrison |
| Long-wave radiation | RRTM |
| Short-wave radiation | RRTMg |
| Surface layer | Monin-Obukhov |
| Land-surface model | Noah LSM |
| Boundary layer scheme | Mellor-Yamada Nakanishi and Niino |
| Cumulus | G3 |
| Photolysis | Fast-J |
| Chemistry model | New RACM-ESRL [6] |
| Aerosol model | MADE and VBS scheme for SOA [6] |
| Biogenic emission | MEGAN |
| Direct aerosol feedback | Included [7] |
| Indirect aerosol feedback | Included [8] |

Chamber (CCNC), a custom scanning mobility particle sizer (SMPS), a comprehensive suite of cloud droplet instrumentation, and a Gerber PVM-100 Probe for cloud water mixing ratio. The Research Flight #52 flight is used in this study and was performed in clear sky, in the cloud vicinity as well as within the cloud layer. The flight was conducted on 15 May 2008 from 11:30 to 15:07 UTC above the North Sea.

## 15.3 Results

The number concentration of ultrafine particles (Dp < 15 nm) is obtained from difference between the two condensation particles counters (CPC3025 and CPC3010). Figure 15.1 shows the comparison of WRF/Chem results to the observed ultrafine particle number concentration and total aerosol concentration (Dp > 5 nm) as a function of altitude. The dots represent the 50th percentiles of the distribution, the error bars the 25th and 75th percentiles, respectively. Although the model tends to capture the dynamical range of the observations, it exhibits a larger variability than the one observed. Generally, WRF/Chem overestimates the particle number concentration by a factor of 2–2.5. This may be due to an excessive nucleation rate or to an overestimation of the ultrafine apportionment of anthropogenic emissions.

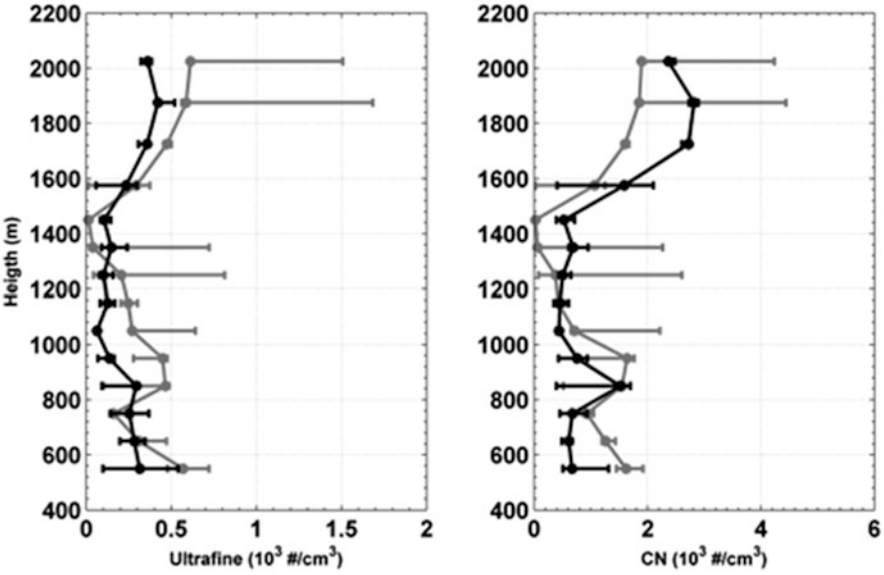


**Fig. 15.1** Vertical profile of ultrafine particle number condensation nuclei concentrations. *Black* and *gray lines* are the observed and modeled values, respectively. The dots represent the median of the distribution. The error bar denote the 25th and 75th, respectively

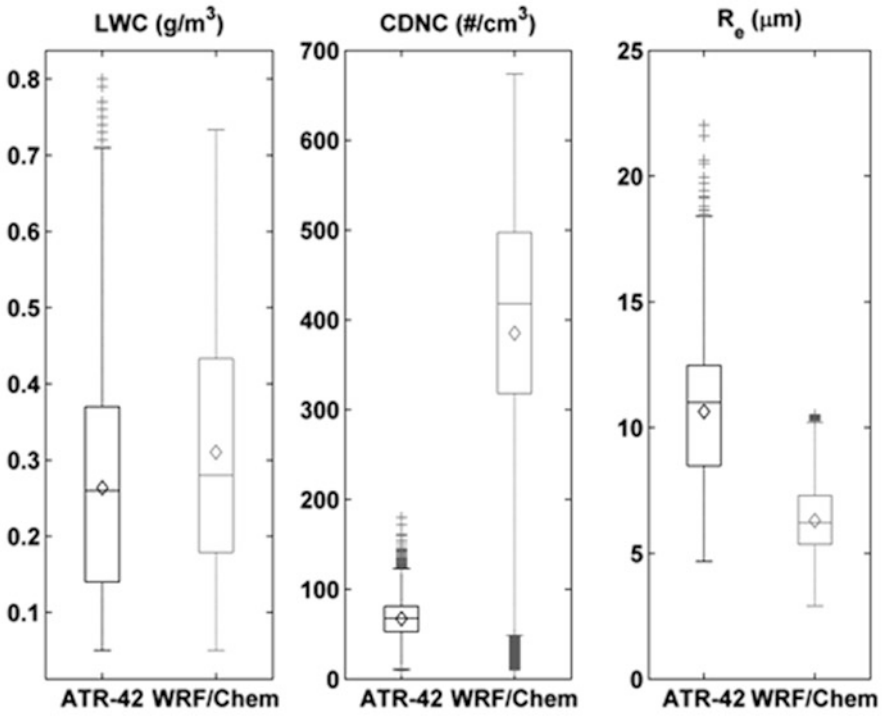


**Fig. 15.2** Box plot of observed and simulated LWC, CDNC and $R_e$ within the cloud layer. Whisker plots represent median, 25th and 75th percentiles, 1.5× (inter-quartile range), and outliers

During RF52 flight, the cloud layer is simulated by the model 100–200 m lower than observed (not shown). In Fig. 15.2, we compare through boxplots the simulated and observed boxplots of cloud liquid water content (LWC), cloud droplet number concentration (CDNC) and effective radius ($R_e$) of cloud droplets. WRF/Chem reproduces the observed dynamical range of LWC with a positive bias of 15–20 %. Predicted CDNC is overestimated about by a factor of 5. This bias could be due to a nonlinear response to the overestimation of CN, such as an alteration of the supersaturation profile evolution. The negative bias of modeled $R_e$ (about −30 %) is directly consequence of CDNC overestimation.

Next step is to evaluate the model above the land and increase the horizontal resolution at cloud scale (2 km).

**Acknowledgments** The work was founded by Italian Space Agency in the frame of the PRIMES (contract I/017/11/0) projects. The authors gratefully acknowledge Denier van der Gon and TNO to make available the anthropogenic emissions. The authors are grateful to NOAA for availability of the supercomputer to run the model. They also thank Fred Burnet, Bruno Piguet and Vincent Puygrenier to provide EUCAARI-IMPACT data.

## References

1. Haywood J, Boucher O (2000) Estimates of the direct and indirect aerosol radiative forcing due to tropospheric aerosols: a review. Rev Geophys 38:513–543
2. Lohmann H, Feichter J (2005) Global indirect effects: a review. Atmos Chem Phys 5:715–737
3. Twomey S (1974) Pollution and planetary albedo. Atmos Environ 8:1251–1256
4. Forster P et al (2007) Changes in atmospheric constituents and in radiative forcing. In: Climate change 2007: the physical science basis – Contribution of Working Group I to the fourth assessment report of the Intergovernmental Panel on Climate Change. Cambridge University Press, Cambridge
5. Grell GA et al (2005) Fully coupled "online" chemistry within the WRF model. Atmos Environ 39:6957–6975
6. Ahmadov R et al (2012) A volatility basis set model for summertime secondary organic aerosols over the eastern U.S. in 2006. J Geophys Res 117:D06301
7. Fast J et al (2006) Evolution of ozone, particulates, and aerosol direct radiative forcing in the vicinity of Houston using a fully coupled meteorology-chemistry-aerosol model. J Geophys Res 111:D21305
8. Chapman EG et al (2009) Coupling aerosol-cloud-radiative processes in the WRF-Chem model: investigating the radiative impact of elevated point sources. Atmos Chem Phys 9:945–964
9. van der Gon HD et al (2010) A high resolution European emission data base for the year 2005, A contribution to UBA-Projekt PAREST: Particle Reduction Strategie. In: TNO report, TNO-034-UT-2010-01895_RPT-ML
10. Tuccella P et al (2010) Modeling of gas and aerosol with WRF/Chem over Europe: evaluation and sensitivity study. J Geophys Res 117, D03303
11. Kulmala et al (2011) General overview: European Integrated project on Aerosol Cloud Climate and Air Quality interactions (EUCAARI) – integrating aerosol research from nano to global scales. Atmos Chem Phys V11:13061–13143. doi: 10.5194/acp-11-13061-2011

# Chapter 16
# The Influence of Cloud Chemical Processes on the Formation of Secondary Particulate Matter

**Roland Schroedner, Ralf Wolke, Andreas Tilgner, and Hartmut Herrmann**

**Abstract** As a pre-study for the 3-D-simulation of the hill cap cloud experiment HCCT 2010 the chemistry transport model COSMO-MUSCAT was tested in a 2-D-domain with a bell-shaped hill. The sensitivity of several target species (oxidants, pH, sulphate, organic mass, dicarboxylic acids, O/C-ratio) on the detail of the aqueous phase mechanism was investigated in a polluted urban and a clean continental rural air mass. For the treatment of aqueous phase chemistry the complex mechanism CAPRAM 3.0i in reduced version and the simple inorganic mechanism INORG was used. Differences between both mechanisms occurred for the oxidants which are not treated in INORG ($HO_2$, OH, $NO_3$) and the pH especially in the urban environment where much more organic reaction partners are also present in the aqueous phase. For $O_3$, $H_2O_2$ and the overall sulphate mass both mechanisms agree mostly within 5 %. Additionally, the composition of the organic mass has been analysed.

## 16.1 Introduction

The interaction of gases and aerosol particles with clouds entails a number of key environmental processes. On the one hand, they directly influence the life cycles of trace constituents and facilitate conversions of these trace constituents. On the other hand, multiphase transformations strongly influence cloud formation. Overall, both aerosol processing by clouds and cloud formation are subject to atmospheric dynamics. In the hill cap cloud experiment HCCT 2010 a relative enrichment of

R. Schroedner (✉) • R. Wolke • A. Tilgner • H. Herrmann
Department of Modeling of Atmospheric Processes, Leibniz Institute for Tropospheric Research (TROPOS), Permoserstrasse 15, 04303 Leipzig, Germany
e-mail: roland.schroedner@tropos.de; wolke@tropos.de

D. Steyn and R. Mathur (eds.), *Air Pollution Modeling and its Application XXIII*, Springer Proceedings in Complexity, DOI 10.1007/978-3-319-04379-1_16,

sulphate and organics on particles was observed after the cloud passage indicating production of these substances inside the cloud. In contrast, the total particulate mass dropped after the cloud passage. The interpretation of these results is difficult, because the influence of entrainment and deposition is not known. This gap can be bridged by 3-D chemistry transport models (CTMs). For this purpose the coupled CTM COSMO-MUSCAT was enhanced to consider cloud-chemical conversions. The model system was then tested in an artificial 2-D-domain simulating the flow over a hill including the evolution of a hill cap cloud.

## 16.2 The Model System COSMO-MUSCAT

The multiscale model system COSMO-MUSCAT ([7, 8]) is qualified for process studies as well as the operational forecast of pollutants in local and regional areas (e.g. [2]). It consists of two online-coupled codes: the CTM MUSCAT and the weather forecast model of the German Weather Service (DWD) COSMO [3]. The meteorological fields are provided by COSMO and are used by MUSCAT for transport and chemical processes for several gas phase species and particle populations.

For this study, the rather simple inorganic INORG [4] and the detailed organic aqueous phase mechanism CAPRAM 3.0i-RED (C3.0RED, [1, 6]) were compared to each other in a polluted urban and a rural continental air mass. Besides organics up to C4, C3.0RED treats also a complex $HO_x$- and transition metal ion chemistry (TMI), and reactions leading to sulphate and nitrate. In INORG the sulphate and nitrate production is implemented, as well as uptake and dissociation of $HNO_3$, $H_2SO_4$, HCl, $NH_3$ and $CO_2$.

## 16.3 Model Setup

Simulations were done for a vertical cross-section (2-D-domain, horizontal grid resolution: 1 km, vertical grid resolution: 25-100 m) lasting 48 h. The air streams over a bell-shaped hill (500 m high, 20 km half width) where a cap cloud forms shortly after the simulation starts. The initial chemical composition of the air and particles also enters the domain at the inlet boundary (left) during runtime. To ensure stable cloud conditions, radiative processes are only treated for photolysis. Aqueous phase processes are switched on for liquid water contents (LWC) above 0.01 g/m$^3$. Fast dissociations and all uptakes are balanced at this threshold value throughout the whole domain. The droplet number is held constant at 150 cm$^{-3}$ leading to droplets between 2 and 6.2 μm radius (depending on LWC).

## 16.4 Results and Discussion

For comparison, the behaviour of major chemical targets was examined. These are the oxidants OH, $HO_2$, $H_2O_2$, $NO_3$, $O_3$, the sulphate and organic mass, the pH, some dicarboxylic acids, and the O/C–ratio.

All oxidants, except $O_3$ which is almost not affected by the aqueous phase, are strongly depleted in the gas phase during the cloud passage due to uptake and reaction in the aqueous phase. The depletion is between 20 and 99 % with higher losses in the urban case. Besides $O_3$, $H_2O_2$ is the only oxidant present in both INORG and C3.0RED. Additionally, in both mechanisms its main fate in the aqueous phase is the production of sulphate. Therefore, only for these oxidants both mechanism show similar concentration patterns. However, there is a small depletion of OH, $HO_2$, and $NO_3$ present in INORG due to shading by the cloud and the loss of $H_2O_2$. After the cloud passage, reproduction of OH, $HO_2$, and $NO_3$ is quite fast, whereas $H_2O_2$ needs much more time to fill the loss.

The cloud water pH is slightly different between both mechanisms with more acidic cloud droplets for INORG. The differences are up to $-0.2$ for the rural and up to $-1$ for the urban case. Highest deviations occur during the day. In the urban case a diurnal cycle with higher pH during the night is observed in the model. The majority of the difference for the rural case can be explained by production of organic acids and to some extent by TMI-chemistry. For the urban air mass, this is more complex and also additional nitrate pathways come into consideration. The TMI-chemistry seems to have nearly no influence on the pH in the urban case.

Due to cloud chemistry, the sulphate mass is increased by a factor of 2–3 and $\sim$1.3 for the rural and the urban case, respectively. Downwind of the cloud the sulphate mass is up to 5 % lower for INORG compared to C3.0RED for the rural air mass. In contrast, the difference is opposite for urban daytime clouds. Only for the urban case during night-time, high deviations can be seen with up to 15 % lower sulphate using INORG. The production of sulphate is very sensitive to the pH. In the urban case, the oxidation via $H_2O_2$ is the most important during the daytime, whereas during the less acidic night-time also the $O_3$-pathway becomes essential (see Fig. 16.1). Consequently, in the more alkaline rural air mass the production via $O_3$ is responsible for the majority of sulphate present. Additionally, the reaction of $HNO_4$ with S(IV) can contribute up to 40 % to the urban daytime sulphate production.

The modelled organic mass using C3.0RED reaches in both cases values of up to 3.1 $\mu g/m^3$ inside of the cloud. The organic mass on cloud residuals is $\sim$1 and $\sim$0.8 $\mu g/m^3$ for the urban and rural case, respectively. The organic mass increases due to in-cloud production by a factor of 3–5. The modelled mass of glyoxalic acid is in the range of available measurements (e.g. [5]), whereas pyruvic acid is underestimated in the urban case and oxalic acid is underestimated in both air masses. Note that C3.0RED treats only some water-soluble organics with up to 4C-atoms and that no oligomerization reactions are present. Therefore, the modelled O/C-ratios of 1.6–1.8 are higher than observed in the atmosphere.

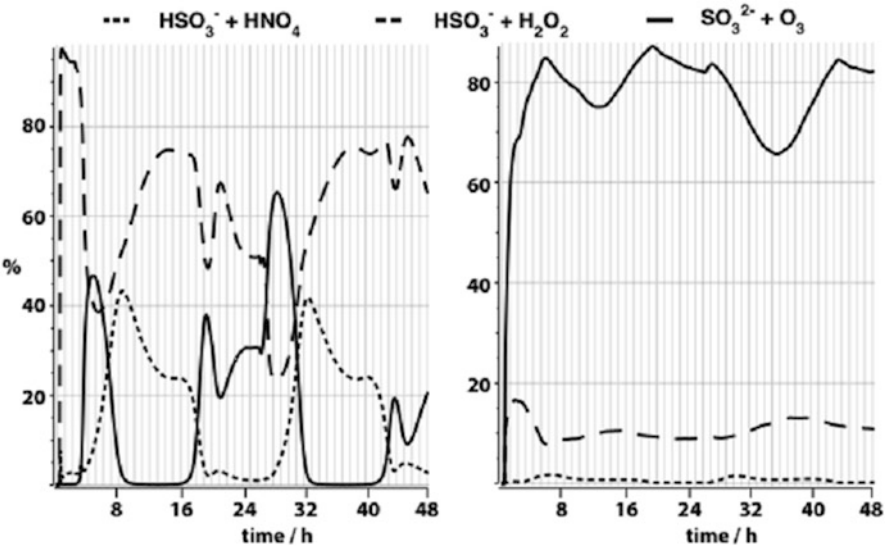


**Fig. 16.1** Relative contribution of the modelled reaction fluxes converting S(IV) to S(VI) for the urban (*left*) and rural case (*right*)

## 16.5 Conclusion

The regional chemistry transport model COSMO-MUSCAT has been used in a 2-D-domain. On top of a bell-shaped hill a cloud forms. The influence of the aqueous phase chemistry inside of this cloud on the overall chemical system was investigated. The detail of the aqueous phase chemistry mechanism was varied (simple inorganic INORG, and complex CAPRAM 3.0i reduced). The model was used in a polluted urban and a clean continental rural air mass. Both mechanisms agreed well for $H_2O_2$, $O_3$, and mostly the sulphate mass (all within 5 %). Differences showed up for the other examined oxidants (OH, $HO_2$, $NO_3$) which are not treated in INORG. In terms of pH, the differences reached sometimes extreme values up to 1. CAPRAM showed always a higher acidity which can be explained mainly by the production of organic acids, additional nitrate production, and transition metal ion chemistry. Glyoxalic acid is in the range of measurements, whereas pyruvic acid and oxalic acid are underestimated. The water soluble organic mass on cloud residuals reached values up to 0.8 and 1 $\mu g/m^3$ for the rural and urban case, respectively. The O/C-ratio lay within 1.6–1.8.

**Acknowledgments** R.S. acknowledges personal funding by the scholarship program of the German Federal Environmental Foundation (DBU). The ZIH Dresden and the NIC Jülich supported this work. We gratefully acknowledge the DWD Offenbach for good cooperation.

## References

1. Deguillaume L, Tilgner A, Schrodner R, Wolke R, Chaumerliac N, Herrmann H (2009) Towards an operational aqueous phase chemistry mechanism for regional chemistry-transport models: CAPRAM-RED and its application to the COSMO-MUSCAT model. J Atmos Chem 64(1):1–35. doi:10.1007/s10874-010-9168-8
2. Renner E, Wolke R (2010) Modelling the formation and atmospheric transport of secondary inorganic aerosols with special attention to regions with high ammonia emissions. Atmos Environ 44:1904–1912
3. Schättler U, Doms G, Schraff C (2013) A description of the nonhydrostatic regional COSMO-Model. Part I: Users guide. Deutscher Wetterdienst, Offenbach, 2013. Available from http://www.cosmo-model.org
4. Sehili AM, Wolke R, Knoth O, Simmel M, Tilgner A, Herrmann H (2005) Comparison of different model approaches for the simulation of multiphase processes. Atmos Environ 39:4403–4417
5. Sun J, Ariya PA (2006) Atmospheric organic and bio-aerosols as cloud condensation nuclei (CCN): a review. Atmos Environ 40:795–820
6. Tilgner A, Herrmann H (2010) Radical-driven carbonyl-to-acid conversion and acid degradation in tropospheric aqueous systems studied by CAPRAM. Atmos Environ 44:5415–5422
7. Wolke R, Schroder W, Schrodner R, Renner E (2012) Influence of grid resolution and meteorological forcing on simulated European air quality: a sensitivity study with the modeling system COSMO-MUSCAT. Atmos Environ 53:110–130
8. Wolke R, Knoth O, Hellmuth O, Schröder W, Renner E (2004) The parallel model system LM-MUSCAT for chemistry-transport simulations: coupling scheme, parallelization and application. In: Joubert GR, Nagel WE, Peters FJ, Walter WV (eds) Parallel computing: software technology, algorithms, architectures and applications. Elsevier, Amsterdam, pp 363–370

# Chapter 17
# An Improved Volatility Basis Set for Modeling Organic Aerosol in Both CAMx and CMAQ

**Bonyoung Koo, Eladio Knipping, and Greg Yarwood**

**Abstract** Atmospheric organic aerosol (OA) is highly complex and detailed mechanistic descriptions include hundreds or thousands of compounds and are impractical for use in photochemical grid models (PGMs). Therefore, PGMs adopt simplified OA modules where organic compounds with similar properties and/or origin are lumped together. The first generation volatility basis set (VBS) module grouped OA compounds by volatility and provided a unified framework for gas-aerosol partitioning of both primary and secondary OA and their chemical aging. However, a VBS approach with one dimension of variation (volatility) is unable to describe observed variations in OA oxidation state (i.e., O:C ratio) at a fixed volatility level. A two-dimensional VBS approach was introduced that tracks degree of oxidation in addition to volatility but further study is needed to fully parameterize 2-D VBS modules.

We developed a new OA module based on the VBS approach and implemented it in two widely-used PGMs. Our scheme uses four basis sets to describe oxidation state: two basis sets for oxygenated OA (anthropogenic and biogenic) and two for freshly emitted OA (from anthropogenic sources and biomass burning). Each basis set has five volatility bins including a zero-volatility bin for essentially non-volatile compounds. The scheme adjusts both carbon number and oxidation state in response to chemical aging by simplifying the 2-D VBS scheme. The new OA module is implemented in both the CAMx and CMAQ PGMs and evaluated for summer and winter 2005 episodes over the eastern US.

B. Koo (✉) • G. Yarwood
ENVIRON International Corporation, Novato, CA 94998, USA
e-mail: bkoo@environcorp.com; gyarwood@environcorp.com

E. Knipping
Electric Power Research Institute (EPRI), Washington, DC 20036, USA
e-mail: eknipping@epri.com

D. Steyn and R. Mathur (eds.), *Air Pollution Modeling and its Application XXIII*,
Springer Proceedings in Complexity, DOI 10.1007/978-3-319-04379-1_17,

## 17.1 Introduction

The volatility basis set (VBS) approach provides a unified framework for gas-aerosol partitioning of both primary and secondary OA (POA and SOA) and their chemical aging [1, 6]. It uses a set of semi-volatile OA species whose volatility is equally spaced in a logarithmic scale (the basis set), and the member species of the basis set are allowed to react further in the atmosphere (chemical aging) to describe volatility changes (i.e., shifting between volatility bins). The first generation VBS used one-dimensional basis sets where organic compounds are grouped only by their volatility and thus was unable to describe varying degree of oxidation observed in atmospheric OA of similar volatility. To address this shortcoming, a two dimensional VBS approach was proposed where organic compounds are grouped by oxidation state as well as volatility [2, 3]. However, full development of a 2-D VBS model will require further study.

## 17.2 Modeling Approach

Ambient aerosol mass spectrometer (AMS) measurement data have identified four characteristic groups of OA based on oxidation state, defined through O:C ratio: Hydrocarbon-like OA (HOA), biomass-burning OA (BBOA), and semi- and low-volatile oxygenated OA (SV-OOA and LV-OOA) [3]. The VBS framework developed here uses four basis sets to represent these ambient OA groups: Two for SOA or oxygenated POA (anthropogenic and biogenic), one for fresh POA from anthropogenic sources, and one for fresh POA from biomass-burning emissions. Each basis set includes 5 volatility bins ranging from 0 to $10^3$ $\mu g/m^3$ in saturation concentration ($C^*$). The molecular structures of OA compounds assigned to these volatility bins are determined by placing them on the 2-D VBS space (Fig. 17.1).

Aerosol yields from hydrocarbon precursors (aromatics, isoprene, monoterpenes and sesquiterpenes with $C^* > 10^7$) and intermediate-volatility organic compounds (IVOCs; $10^4 < C^* < 10^6$) were determined based on smog chamber data [4, 5]. Chemical aging shifts anthropogenic SOA into lower-volatility bins while aging of biogenic SOA was disabled as recommended by Murphy and Pandis [5]. Aging of POA is represented by partial conversion to OOA considering carbon and oxygen balances.

Emissions of IVOCs make important contributions to OA in the atmosphere but generally are missing from modeling emission inventories. If not provided, IVOC emissions are estimated by the VBS module by setting them equal to $1.5 \times$ POA emissions by default. We have also considered a higher SVOC ($10^{-2} < C^* < 10^3$) and IVOC emission case using estimates based on ambient measurements in Mexico City [7].

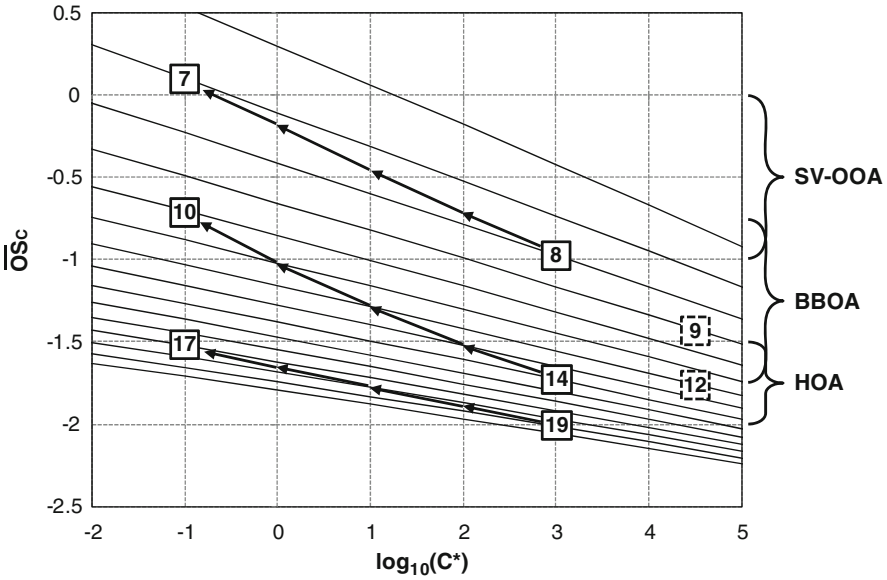


**Fig. 17.1** 2-D VBS space defined by $C^*$ and average oxidation state of carbon ($\overline{OS}_C$); contours of carbon numbers (in *square boxes*) are calculated using the 2-D VBS model by Donahue et al. [2]; IVOCs from biomass burning and anthropogenic sources are placed to have 9 and 12 carbons, respectively; chemical aging (indicated by *arrows*) accounts both for oxygenation (increase in oxidation state) and fragmentation (decrease in carbon number)

## 17.3 Model Evaluation

Two month-long (February and August) episodes based on the EPA's Cross-State Air Pollution Rule (CSAPR) base year (2005) modeling database were selected for evaluating the VBS module implemented in CAMx v5.41 and CMAQ v5. The modeling domain is shown in Fig. 17.2.

The model performance was evaluated using organic carbon (OC) measurement data collected at the Interagency Monitoring of Protected Visual Environments (IMPROVE) and EPA's Speciation Trends Network (STN) monitoring sites. Figure 17.3 shows fractional bias (FB) and fractional error (FE) of the modeled 24-h average OC concentrations for each of the winter and summer months over the 12 km modeling grid. FB and FE are defined as follows:

$$\mathrm{FB} = \frac{2}{N}\sum_{i=1}^{N}\left(\frac{P_i - O_i}{P_i + O_i}\right) \qquad \mathrm{FE} = \frac{2}{N}\sum_{i=1}^{N}\left|\frac{P_i - O_i}{P_i + O_i}\right|$$

where $P_i$ and $O_i$ represent model predicted and observed concentrations, respectively.

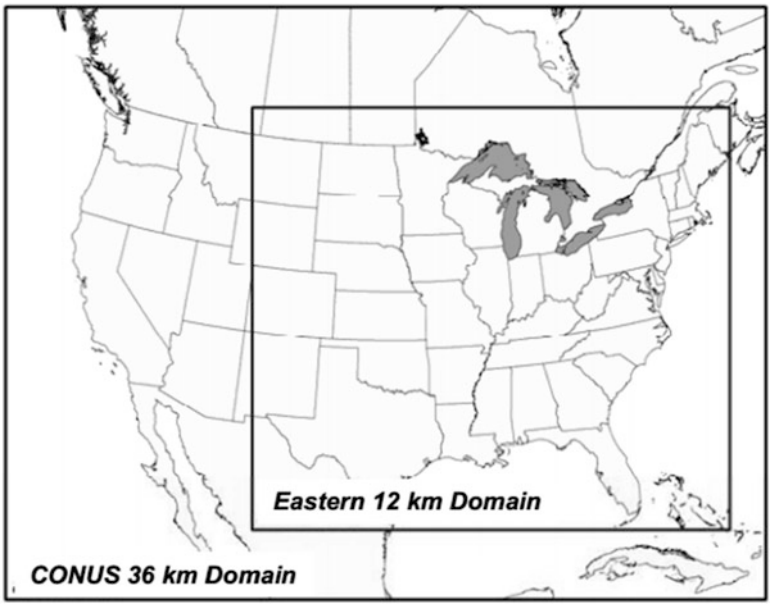


**Fig. 17.2** The 36 km modeling domain for the continental US with the 12 km grid covering the eastern US

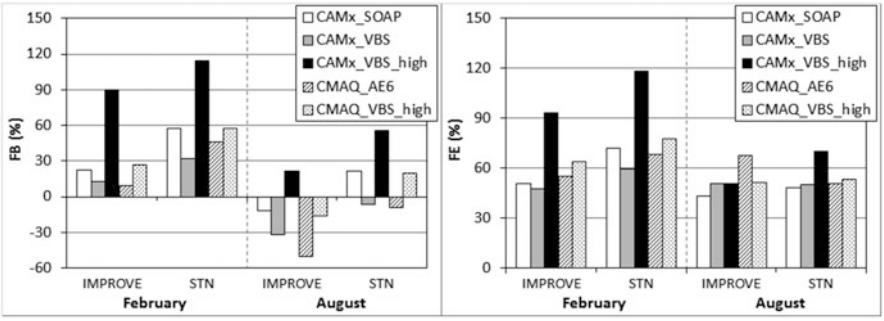


**Fig. 17.3** Fractional bias (*FB*) and error (*FE*) of the 24-h average OC concentrations modeled by CAMx and CMAQ with the standard and VBS OA formation schemes

The standard OA scheme in CAMx (CAMx_SOAP) overestimated observed OC except at rural sites (IMPROVE) in August. The base case VBS (CAMx_VBS) produced less OC than CAMx_SOAP due to POA evaporation, resulting in better performance in most cases. Higher SVOC/IVOC emissions (CAMx_VBS_high) produced too much OC. The standard CMAQ model (CMAQ_AE6) produced less OC than CAMx_SOAP, especially in summer. The VBS scheme with higher SVOC/IVOC emissions (CMAQ_VBS_high) improved summer time OC performance in rural sites, but showed overestimation biases in other cases.

## 17.4 Conclusion

A new VBS scheme was developed that describes atmospheric OA with varying volatility and degree of oxidation and implemented in both CAMx and CMAQ. Winter- and summer-time OC performance was evaluated using the EPA's CSAPR modeling database. SVOC and IVOC emissions were added to the modeling inventories in lower and higher amounts. OC performance of CAMx VBS was better than that of the standard CAMx in most cases but higher SVOC/IVOC emissions led to significant overestimation of OC, especially in winter. In CMAQ, VBS with higher SVOC/IVOC emissions made less difference from the standard OA module than in CAMx in winter. In August, the CMAQ VBS scheme improved OC performance at IMPROVE sites where the standard CMAQ showed significant underestimation bias. Additional research is needed to understand seasonal variations in SVOC/IVOC emission factors.

**Acknowledgments** This work was funded by the Electric Power Research Institute. We appreciate valuable discussion with Drs. Spyros Pandis, Neil Donahue and Allen Robinson at Carnegie Mellon University and Dr. Heather Simon at US Environmental Protection Agency.

## References

1. Donahue NM, Robinson AL, Stanier CO, Pandis SN (2006) Coupled partitioning, dilution, and chemical aging of semivolatile organics. Environ Sci Technol 40:2635–2643
2. Donahue NM, Epstein SA, Pandis SN, Robinson AL (2011) A two-dimensional volatility basis set: 1. Organic-aerosol mixing thermodynamics. Atmos Chem Phys 11:3303–3318
3. Donahue NM, Kroll JH, Pandis SN, Robinson AL (2012) A two-dimensional volatility basis set – Part 2: Diagnostics of organic-aerosol evolution. Atmos Chem Phys 12:615–634
4. Hildebrandt L, Donahue NM, Pandis SN (2009) High formation of secondary organic aerosol from the photo-oxidation of toluene. Atmos Chem Phys 9:2973–2986
5. Murphy BN, Pandis SN (2009) Simulating the formation of semivolatile primary and secondary organic aerosol in a regional chemical transport model. Environ Sci Technol 43:4722–4728
6. Robinson AL, Donahue NM, Shrivastava MK, Weitkamp EA, Sage AM, Grieshop AP, Lane TE, Pierce JR, Pandis SN (2007) Rethinking organic aerosols: semivolatile emissions and photochemical aging. Science 315:1259–1262
7. Shrivastava M, Fast J, Easter R, Gustafson WI Jr, Zaveri RA, Jimenez JL, Saide P, Hodzic A (2011) Modeling organic aerosols in a megacity: comparison of simple and complex representations of the volatility basis set approach. Atmos Chem Phys 11:6639–6662

## Question and Answer

**Questioner Name:** Sebnem Aksoyoglu

**Q:** It may be a challenge to modify emissions for use with CAMx VBS. Do you have any suggestions or procedures to modify emissions?

**A:** VBS can directly use CAMx emission input files that were prepared for the traditional SOAP organic aerosol scheme. However, if you can modify the emission inventory to provide additional details then you can make better use of capabilities in VBS. For example, if you can segregate the anthropogenic primary organic aerosol (POA) emissions to gasoline vs. diesel vehicles then you can use different volatility distributions. Also, if you provide emissions of intermediate VOCs (IVOCs) then you will supersede the default estimation of IVOC emissions using IVOC/POA ratios.

# Chapter 18
# Issues Related to On/Offline Meteorological and Atmospheric Chemistry Model Coupling

**Jonilda Kushta, Marina Astitha, Stavros Solomos, and George Kallos**

**Abstract** The online approach consists of the coupled treatment of chemical parameters, simultaneously with the meteorological parameters, in a single integrated modeling system that is referred to as chemical weather modeling. This approach offers the possibility to simulate the links and feedbacks between atmospheric processes that are traditionally neglected in air quality models. Both meteorological and chemical components are expected to benefit from this approach. Both approaches have advantages and disadvantages that make their use appropriate for different applications. This study discusses and evaluates the performance of the online Integrated Community Limited Area Modeling System (RAMS/ICLAMS) and the offline model, Comprehensive Air Quality Model with Extensions (CAMx), for a month long retrospective summertime text period, over Europe and the Greater Mediterranean Area (GMR). The implementation of the same chemical mechanisms, meteorological fields, emissions, initial and boundary conditions makes it easier to compare the results from the two models. However, there are some differences in the physical parameterizations utilized in the two models that are expected to result in differences between them. The feedback mechanisms are not activated in order to evaluate the performance of the two models regarding the advantages that the online approach offers (same projection, no interpolation in time and space, explicit calculation of the meteorological components, availability of the meteorological fields at each time step etc.). Results showed that the online approach gave better results regarding ground 1 h ozone and 24 h sulfate aerosol concentrations improving the main statistical parameters by roughly 20 % and

J. Kushta (✉) • M. Astitha • S. Solomos • G. Kallos
School of Physics, Atmospheric Modeling and Weather Forecasting Group, University of Athens, 15784 Athens, Greece
e-mail: kousta@mg.uoa.gr; kallos@mg.uoa.gr

D. Steyn and R. Mathur (eds.), *Air Pollution Modeling and its Application XXIII*, Springer Proceedings in Complexity, DOI 10.1007/978-3-319-04379-1_18,

increased correlation from 0.51 to 0.70. The differences may be mainly the outcome of the utilization of different methods for the calculation of the photolysis rates and the interpolation of the meteorological data for use in the offline model.

## 18.1 Introduction

The online approach consists of the coupled treatment of chemical parameters, simultaneously with the meteorological parameters, in a single integrated modelling system [1]. Online systems with their integrated approach have the advantage of using the same spatiotemporal resolution, projection and parameterization schemes minimizing inconsistencies, and can be used to assess links and feedbacks between chemical and meteorological components. Their increased computational requirements, however, remain an issue in several applications, making the offline approach, with its long developmental history, necessary. This study discusses and evaluates the performance of the online model RAMS/ICLAMS and the RAMS driven offline model CAMx, for a month long retrospective summertime text period, over Europe and GMR by making the two models as comparable as possible. The objective is to assess the differences between the two models and the points where their contribution can be more skillful.

## 18.2 Models Description

RAMS/ICLAMS is developed by the Atmospheric Modeling and Weather Forecasting Group at the University of Athens (AMWFG), in order to be used as a research and forecasting tool for air pollution and climate applications. The structure of the unified model and the new capabilities are described in detail in [2]. CAMx is an offline chemical transport model widely used and evaluated for several air quality applications [3]. The model domain for this study is Europe and GMR with a resolution of $0.22 \times 0.27°$ for CAMx and 24 km for RAMS/ICLAMS. The temporal resolution is 900 s for CAMx and 30 s for RAMS/ICLAMS. Both models use the same emissions (CIRCE 2005 $0.1 \times 0.1°$), the same gas phase scheme (SAPRC99 with EBI solver), the same initial and boundary conditions (from predefined look up tables) and ISORROPIA for the aerosol thermodynamic properties. However, the two models have different projections (CAMx latitude longitude geographical projection, RAMS/ICLAMS polar stereographic) and different advection schemes (BOTT for CAMx and Leapfrog/Forward upstream combination for RAMS/ICLAMS). The aerosol mechanism that comes with the SAPRC99 gas phase mechanism in CAMx is the CF mode (coarse-fine with only two size bin modes) while RAMS/ICLAMS utilizes the RPM scheme with three size modes. CAMx is driven from the meteorological datasets derived from RAMS/ICLAMS at

a frequency of 1 h. RAMS/ICLAMS utilizes an online module for the calculation of the photolysis frequencies that takes direct updated information regarding actinic fluxes from the RRTMG radiation Scheme.

## 18.3 Results and Discussion

The air pollution field is simulated with the two models and the comparison of model results with observations from the European Monitoring Evaluation Program network (EMEP http://www.emep.int) are shown in Fig. 18.1. The utilization of the online approach gives better results regarding 1 h $O_3$ compared to the offline model. The main characteristic is the decrease of the span of the modeled values. The overall correlation coefficient R is increased from 0.51 in the offline model to 0.70 in the online model. The normalized mean bias and error decrease from the offline to the online model ($-8.51$ μg m$^{-3}$ to 5.16 μg m$^{-3}$ for NMB and 31.20 μg m$^{-3}$ to 23.5 μg m$^{-3}$ for NME). RMSE and MB also improve from 30.98 μg m$^{-3}$ to 23.91 μg m$^{-3}$ and $-6.68$ μg m$^{-3}$ to 5.16 μg m$^{-3}$. CAMx exhibits an underestimation of the 1 h $O_3$ field while RAMS/ICLAMS overestimates it, but to a lower extent. This can be possibly attributed to differences in the simulation of the photolysis rates.

The improvement is evident for a number of stations over Europe, with different pollution and geographical characteristics. The online approach gives better results regarding ozone by simulating more accurately the peak values of 1 h $O_3$ during build-up hours as shown from the time series of modeled and observed concentrations over two selected stations in Fig. 18.2. The online approach exhibits a narrower span of the modeling values. Additionally, nighttime ozone concentrations from the online approach are in better agreement with the observations, probably due to the more accurate boundary layer and updraft simulation.

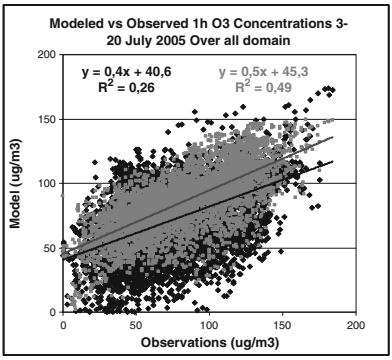


| | CAMX | ICLAMS |
|---|---|---|
| MEAN BIAS | -6,68 | 4,05 |
| RMSE | 30,98 | 23,91 |
| NMB | -8,51 | 5,16 |
| NME | 31,20 | 23,50 |
| R | 0,51 | 0,70 |

**Fig. 18.1** Scatter plot of modeled and observed ozone concentrations from EMEP stations over Europe for 3–20 July 2005 (*grey* – RAMS/ICLAMS, *black* – CAMx) and a table with the main statistical parameters

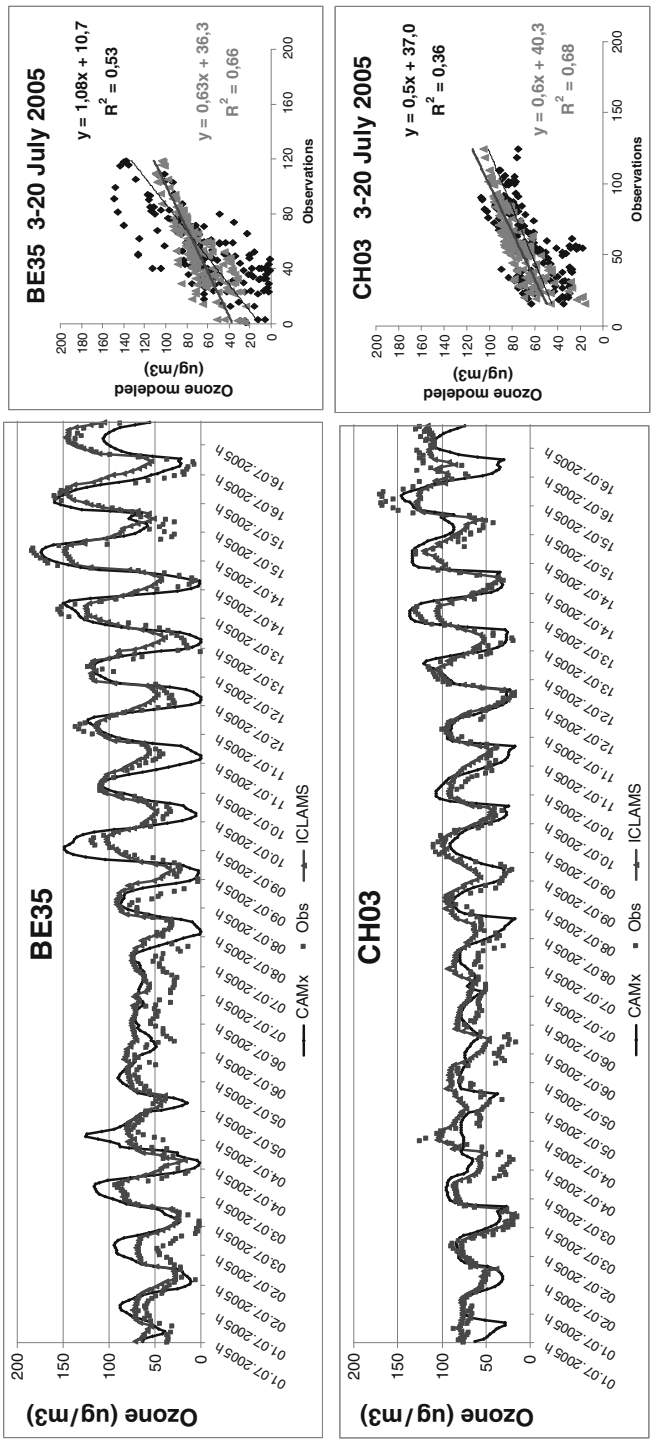


**Fig. 18.2** Time series of modeled and observed ozone concentrations over Vezin station (50° 30′ N 4° 59′ E) (*top plot*) and Tanikon station (47° 28′ N 8° 54′ E) (*bottom plot*) from the EMEP network (*black* – CAMx, *grey* – RAMS/ICLAMS, *dots* – observations) and the respective scatter plots from the comparison of CAMx results (*black*) and RAMS/ICLAMS results (*grey*) with the observations

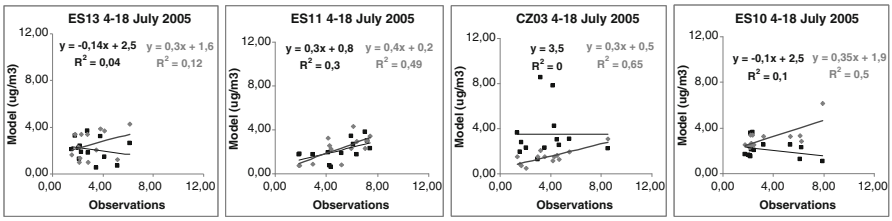


**Fig. 18.3** Time series of modeled and observed 24 h mean sulfate concentrations over Penausende (41° 17′ N 5° 52′ E), Barcarrola (38° 28′ N 6° 55′ E), Kosetice (49° 35′ N 15° 5′ E) and Cabo de Creus (42° 19′ N 3° 19′ E) (*blue* – CAMx, *green* – RAMS/ICLAMS)

Regarding sulfate aerosols both models exhibit a general underestimation that underlines the need for investigation of the role and accuracy of the primary $SO_2$ anthropogenic emissions. However, the online approach gives better results that are demonstrated by the increasing of the slope of the trend line and respective correlation as shown in Fig. 18.3.

## 18.4 Conclusions

Online models can have a more satisfactory performance than offline systems in air pollution studies due to their unified structure using the same projection, resolution and parameterization schemes (no spatiotemporal interpolation and parameterization inconsistencies). Additionally, the online approach gives the opportunity to assess feedback mechanisms that the offline approach neglects.

For a summer test period the online approach simulated in a more accurate way the ozone concentrations over Europe and GMR. The main improvements stand in the simulation of the concentrations during build-up hours (and daily maxima) and night-time lows. A slight improvement is also seen for 24 h mean sulfate concentrations. Taking into consideration the computational requirements of the online modelling systems and the type of the application, the offline approach may cover the needs of the user in several cases (i.e. simulating different emission scenarios with the same meteorological dataset). The online approach however, is necessary for applications where the feedback mechanisms are required (i.e. feedback of aerosols on radiation and clouds).

**Acknowledgments** This work was supported by EUROCONTROL Research Studentship Agreement no CO6/22048ST and FP6 project CIRCE contract no 036961.

## References

1. Grell G, Baklanov A (2011) Integrated modeling for forecasting weather and air quality: a call for fully coupled approaches. Atmos Environ. doi:10.1016/j.atmosenv.2011.01.017
2. Solomos S, Kallos G, Kushta J, Astitha M, Tremback C, Nenes A, Levin Z (2011) An integrated modeling study on the effects of mineral dust and sea salt particles on clouds and precipitation. Atmos Chem Phys 11:873–892. doi:10.5194/acp11-873-2011
3. ENVIRON (1998) User's guide to the Comprehensive Air Quality Model with Extensions (CAMx) Version 2.00. ENVIRON international corporation, 101 Rowland Way, Suite 220, Novato, CA 94945–5010

## Questions and Answers

**Questioner Name:** Yang Zhang

**Q:** Did you consider activation of insoluble aerosols such as dust and black carbon?
**A:** Yes we did.
**Q**: Is the insoluble fraction explicitly calculated or prescribed?
**A**: The insoluble fraction is prescribed.

# Chapter 19
# Increases in Wintertime Oxidation Capacity Counteract the Success of Emission Reduction Measures in Europe with Respect to Secondary Inorganic Aerosols

**Dominik Brunner, Christoph Knote, Lea Giordano, and Christoph Hueglin**

**Abstract** Air pollution reduction measures in Europe have led to marked decreases in the levels of primary pollutants such as $SO_2$ and $NO_x$ since the 1980s while for secondary pollutants like ozone and secondary inorganic aerosols (SIA) the effects of these measures are much less obvious. A recent extensive comparison of the composition of particulate matter smaller than 10 μm (PM10) in Switzerland between the years 1998/1999 and 2008/2009, for example, revealed no changes in the levels of nitrates despite large $NO_x$ emission reductions over this period. Similarly, aerosol sulphates decreased much less strongly than the precursor gas $SO_2$.

In this study we used the online coupled regional chemistry-transport model COSMO-ART to investigate these non-linear responses of SIA components to changes in their precursor gases $NO_x$, $SO_2$ and $NH_3$ focussing on wintertime conditions when PM concentrations are highest. We found that the reduced concentrations of $NO_x$ and NMVOC led to strong increases in the oxidation capacity of the European wintertime boundary layer as evidenced by pronounced enhancements in ozone, OH and $N_2O_5$ levels by sometimes more than 100 %. These changes resulted in accelerated formation of nitrates and sulphates and correspondingly smaller relative reductions in their concentrations as compared to the precursor gases, particularly within the densely populated and industrialized regions in Europe.

D. Brunner (✉) • L. Giordano • C. Hueglin
Laboratory for Air Pollution/Environmental Technology, Empa, Swiss Federal Laboratories for Materials Science and Technology, 8600 Dübendorf, Switzerland
e-mail: dominik.brunner@empa.ch; lea.giordano@empa.ch; christoph.hueglin@empa.ch

C. Knote
Atmospheric Chemistry Division, NCAR Earth System Laboratory, Boulder, CO 80301, USA
e-mail: knote@ucar.edu

D. Steyn and R. Mathur (eds.), *Air Pollution Modeling and its Application XXIII*, Springer Proceedings in Complexity, DOI 10.1007/978-3-319-04379-1_19,

## 19.1 Introduction

Despite significant reductions in $NO_x$ emissions in Switzerland and across most of Europe, nitrate concentration and deposition levels remained nearly constant in Switzerland during the past 20 years as indicated by measurements from the Swiss Air Pollution Monitoring Network NABEL [1]. Several hypotheses have been put forward to explain such a non-linear response of nitrate to its precursor gases $NO_x$:

Due to Europe-wide reductions in $SO_2$ emissions [2] the amount of ammonia required to neutralize sulfate has decreased with time potentially leaving more ammonia for the formation of ammonium nitrates [3, 4]. This hypothesis requires ammonia levels to be sufficiently low to be a limiting or at least partially/temporally limiting factor within the ammonium-sulfate/ammonium-nitrate system.

A second hypothesis is that the reduction in $NO_x$ emissions as well as the increase in the fraction of $NO_x$ emitted from vehicles in the form of $NO_2$ has led to reduced titration of ozone and a corresponding increase in ozone levels particularly in winter. The observed strong increase of the $NO_2$:NO ratio in vehicle emissions in Europe is due to the rising share of diesel cars and the introduction of diesel particulate filters which tend to oxidize NO to $NO_2$ already in the exhaust path [5]. Increased wintertime ozone levels may have accelerated photochemical processing and hence the formation of nitrates, e.g. through accelerated nighttime $N_2O_5$ chemistry.

To study these hypotheses and other potential explanations, we performed a range of sensitivity simulations using the online coupled chemistry transport model COSMO-ART [6] in a configuration including an advanced wet-phase chemistry and scavenging scheme [7]. This study describes the setup of the model simulations and presents a selection of results focusing on the simulations performed for winter.

## 19.2 COSMO-ART Model Simulations

COSMO-ART was setup to cover the domain of Europe at a horizontal resolution of $0.17° \times 0.17°$ and with 40 vertical levels. Chemical initial and boundary conditions (IC/BC) were obtained from NCAR-MOZART simulations available for the months of interest. Meteorological IC/BC were taken from ECMWF IFS model analyses. The following simulations were performed for the months of January 2009 and June 2009, representing typical winter- and summertime conditions, respectively:

- January 2009 with emissions from 1995 (experiment W95)
- January 2009 with emissions from 2009 (W09)
- June 2009 with emissions from 1995 (S95)
- June 2009 with emissions from 2009 (S09)

Emissions of $NO_x$, $SO_2$, $NH_3$, VOCs and PM were deduced from the TNO/MACC emission inventory [8] for the year 2003 and scaled to 1995 and

2009 based on country- and species-specific trends between 1995 and 2003 and between 2003 and 2009, respectively, as reported to EMEP. Hour-of-day, day-of-week and seasonal emission variations were considered separately for each country, emission category and species. The same meteorology (of the year 2009) was used for both the 1995 and 2009 simulations to exclude the influence of interannual meteorological variability on the results.

## 19.3 Results

In terms of emission changes from 1995 to 2009, the most relevant features are strong reductions in $SO_2$, $NO_x$, and NMVOC emissions by often more than 50 % in Western Europe. The reductions were typically smaller and more variable in Eastern Europe with some countries even showing increases for some species. Reductions in PM2.5 emissions were smaller, mostly between 10 and 40 % in Western Europe. Emissions of $NH_3$, which is dominated by agricultural activities, remained almost constant in most countries except for the Benelux countries and Denmark, where changes in agricultural practices led to notable reductions. $NO_x$ emissions are dominated by NO. When considering only the fraction emitted as $NO_2$, the trends are much less negative than those of $NO_x$ and in some countries including France and Austria even positive.

Figure 19.1 shows the mean surface (0–20 m) concentrations of $NO_x$ and of aerosol nitrate ($NO_3^-$) for the winter simulation W95 and the relative differences (W09-W95)/W95 due to the emission changes from 1995 to 2009. While $NO_x$ reductions were mostly in the range of 30–50 %, the reductions in nitrates were considerably smaller, typically by a factor of two. These differences are particularly large over Spain, the Po Valley in northern Italy and some regions in the UK. A similar non-linear relation between precursor emissions and photochemical products is also seen for $SO_2$ and its product sulfate, though with a somewhat different spatial distribution (not shown). The pattern of relative changes of ammonium shows no correspondence with the changes of ammonia but rather follows the patterns of nitrate changes, indicating that ammonia levels have never been a limiting factor in Europe.

The most striking differences between the two wintertime simulations are the strongly enhanced levels of photo-oxidants like ozone and $N_2O_5$ and of the OH radical in simulation W09 as compared to W95. Reduced titration by NO led to strong increases in ozone by typically 10–30 % and in some polluted regions like the Po Valley by more than 100 %. Similar findings apply to OH and $N_2O_5$ suggesting an acceleration in both daytime and nighttime radical chemistry. OH levels increased by 20–80 % across most of Europe, again most strongly in polluted areas where OH levels have been very low in 1995 due to rapid reaction with $NO_2$, VOCs and CO. $N_2O_5$, which is formed at night by reaction of $O_3$ with $NO_3$, shows a more variable pattern reflecting the interplay between $NO_x$ reductions and $O_3$ enhancements, with reductions in remote locations and increases in polluted areas with maximum

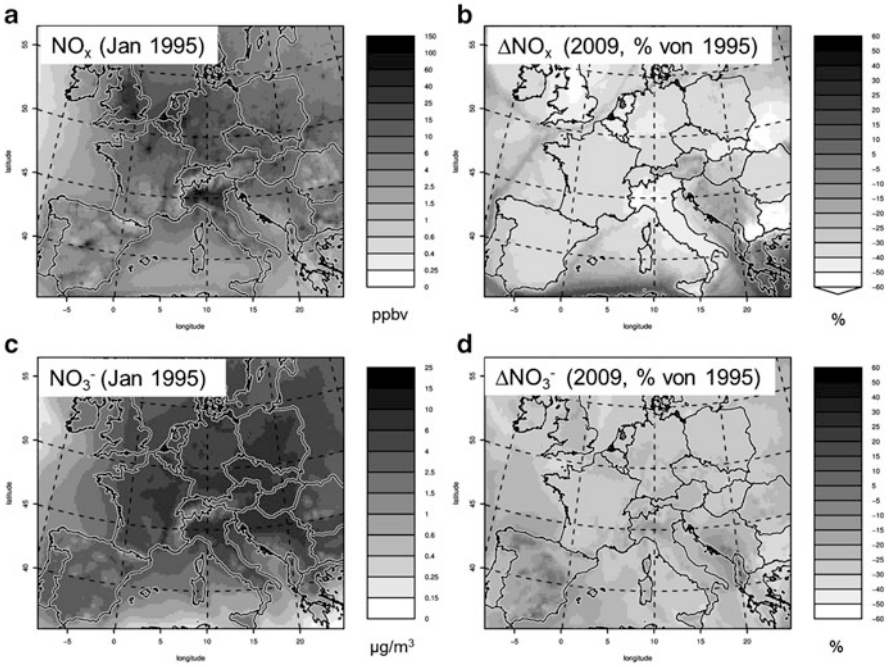


**Fig. 19.1** (**a**) Mean surface $NO_x$ concentration [ppb] for simulation W95. (**b**) Relative changes from 1995 to 2009 [%] (scale ranges from −60 to +60 %). (**c**) Mean surface aerosol nitrate concentration [$\mu g/m^3$] for simulation W95. (**d**) Relative changes from 1995 to 2009 [%] (scale ranges from −60 to +60 %)

values as large as +300 % in the Po Valley. The enhanced oxidation capacity of the wintertime atmosphere thus leads to a more rapid formation of nitrates and sulfate, which likely explains their highly non-linear response to precursor emission reductions.

## 19.4 Conclusions

Despite significant reductions of $SO_2$ and $NO_x$ emissions in Europe, nitrate levels in Switzerland remained approximately constant and sulfates were reduced much less than $SO_2$ during the past 15–20 years. The reasons for this non-linear response between aerosol components and precursor gases were investigated with the regional chemistry and transport model COSMO-ART by simulating winter and summer conditions using emissions representative of 1995 and of 2009, respectively. For wintertime we found a strong increase in $O_3$, OH and $N_2O_5$ levels from 1995 to 2009 due to reduced titration of $O_3$ by NO and reductions in NMVOC emissions. The strongly enhanced oxidation capacity of the wintertime

atmosphere in Europe leads to a more rapid formation of nitrates and sulfates and correspondingly higher concentrations at the surface and closer to the emission sources. Although the measured trends in Switzerland cannot be fully reproduced by the model, the simulations confirm the much smaller reduction of nitrates and sulfates as compared to their precursor gases and provide additional insight into the causes.

**Acknowledgments** We gratefully acknowledge the financial support for this study by the Swiss Federal Office for the Environment (FOEN). We further thank the developers of COSMO-ART, Heike and Bernhard Vogel at KIT, Germany, for great support and collaboration. Finally, we would like to thank Louisa Emmons (NCAR) for providing chemical IC/BC data, ECMWF for meteorological IC/BC, and TNO for the inventory of anthropogenic emissions.

## References

1. BAFU (2011) NABEL – Luftbelastung 2010. Messresultate des Nationalen Beobachtungsnetzes für Luftfremdstoffe (NABEL). Bundesamt für Umwelt, Bern. Umwelt-Zustand Nr. 1118: 126S
2. EMEP (2011) Transboundary acidification, eutrophication and ground level ozone in Europe in 2009. EMEP report 1/2011, Norwegian Meteorological Institute, Oslo
3. Seinfeld JH, Pandis SN (2009) Atmospheric chemistry and physics – From air pollution to climate change, 2nd edn. Wiley, New York
4. Bellouin N, Rae J, Jones A, Johnson C, Haywood J, Boucher O (2011) Aerosol forcing in the Climate Model Intercomparison Project (CMIP5) simulations by HadGEM2-ES and the role of ammonium nitrate. J Geophys Res 116:D20206. doi:10.1029/2011JD016074
5. Grice S, Stedman J, Kent A, Hobson M, Norris J, Abbott J, Cooke S (2009) Recent trends and projections of primary NO2 emissions in Europe. Atmos Environ 43(13):2154–2167
6. Vogel B, Vogel H, Bäumer D, Bangert M, Lundgren K, Rinke R, Stanelle T (2009) The comprehensive model system COSMO-ART–Radiative impact of aerosol on the state of the atmosphere on the regional scale. Atmos Chem Phys 9:8661–8680
7. Knote C, Brunner D (2013) An advanced scheme for wet scavenging and liquid-phase chemistry in a regional online-coupled chemistry transport model. Atmos Chem Phys 13:1177–1192. doi:10.5194/acp-13-1177-2013
8. Visschedijk A, Zandveld P, Denier van der Gon H (2007) High resolution gridded European emission database for the EU Integrate Project GEMS, TNO- report 2007-A-R0233/B, TNO, Apeldoorn, The Netherlands

## Question and Answer

**Questioner Name:** Heinke Schlünzen

**Q:** Did you also consider the reduction in VOC emissions in your simulations? Could this have added to the increased OH levels that you find for wintertime?

**A:** Yes, we did consider the changes in VOC emissions, and these were substantial in many countries over the period 1995–2009. Indeed, the increases in OH levels in polluted regions seen in winter is likely a combination of reductions in both NOx and VOC emissions.

# Chapter 20
# Investigating the Contribution of Biogenic Emissions to the Formation of Secondary Pollutants in Portugal

**Oxana Tchepel, Joana Ferreira, Helena Martins, Carlos Silveira, Ana Isabel Miranda, and Carlos Borrego**

**Abstract** This work aims to quantify the contribution of biogenic emissions to air quality levels of secondary pollutants in distinct areas of a study region taking into account the relevance of different processes, such as transport, deposition, and chemistry. In this sense the air quality model CAMx, with its source apportionment and process analysis tools, has been applied to Portugal, aiming to assess ozone ($O_3$) and secondary organic aerosol (SOA) levels during a summer month for three biogenic emission scenarios, which were defined considering the variability of emission factors. Results for secondary gases and particulate pollutants have been explored in terms of source and process contributions. The quantitative analysis showed that biogenic emissions contribute up to 90 % of SOA predictions. The uncertainty in isoprene emission factors may affect the concentration of SOA by ±30 % in average; however, because the $O_3$ production is NOx limited at the studied areas biogenic emissions scenarios did not affect $O_3$ concentration levels, which varied only ±1 % in average.

## 20.1 Introduction

Biogenic emissions, including isoprene and monoterpenes, play an important role in the formation of secondary gaseous and particulate pollutants in the atmosphere. Therefore, evaluation of the impact of biogenic emissions on the secondary

O. Tchepel (✉)
Faculty of Sciences and Technology, University of Coimbra, Rua Luis Reis Santos, Polo II, 3070-788 Coimbra, Portugal
e-mail: oxana@uc.pt

J. Ferreira • H. Martins • C. Silveira • A.I. Miranda • C. Borrego
CESAM & Department of Environment and Planning, University of Aveiro, 3810-193 Aveiro, Portugal
e-mail: jferreira@ua.pt; hmartins@ua.pt; carlos.silveira@ua.pt; miranda@ua.pt; cborrego@ua.pt

D. Steyn and R. Mathur (eds.), *Air Pollution Modeling and its Application XXIII*, Springer Proceedings in Complexity, DOI 10.1007/978-3-319-04379-1_20,

pollutants formation and distribution should be implemented in a comprehensive way [1]. To determine the contribution of different emission sources, in particular biogenic ones, to the observed pollution levels, source apportionment technology and process analysis implemented as part of a 3D photochemical grid model can be used. The CAMx Process Analysis (PA) tool allows a detailed model performance evaluation by tracking the contribution from individual physical and chemical processes governing the fate of the atmospheric pollutants. Additionally, the Ozone and Particulate Matter Source Apportioning Technologies (OSAT and PSAT) provide geographic region and source category "culpability". The SAT track $O_3$ and PMx (including secondary aerosols) formation based on how the groups of precursors contribute to pollutants formation and also investigate the contribution of boundary and initial conditions to the pollutants levels within the study domain.

This work aims to quantify the contribution of biogenic emissions and other processes (i.e. transport, deposition, emissions, and chemistry) to air quality levels of secondary pollutants in distinct areas of a study region, and to perform a sensitivity analysis of model predictions to isoprene and monoterpenes biogenic emissions.

## 20.2 Methodology

The air quality modelling system, composed by the WRF-ARW meteorological model and the CAMx chemical transport model (CTM) [2], was applied to Portugal, for 1 month period – June 2011. The modelling setup included 2 nesting domains covering Europe (D1) and Portugal (D2) with 27 and 9 km horizontal resolution, respectively. Initial and boundary conditions for D1 were taken from MOZART global CTM. EMEP emissions were used as inputs for D1, and the national anthropogenic emissions inventory for Portugal. Biogenic emissions were estimated based on country specific land use and vegetation data characterization and distribution.

Three scenarios of biogenic emissions for the study period were computed, considering a compilation of emission factors (EF) and biomass density for the vegetation species existing in Portugal. The reference scenario assumes EF and biomass values adjusted to the country environmental conditions. The other two scenarios represent extreme situations – minimum and maximum EF and biomass density encountered in literature per vegetation species [3].

Aiming to identify differences between distinct location types in terms of biogenic emission impact on secondary pollutants formation, for the three considered scenarios, the CAMx Source Apportionment (SAT) and Process Analysis (PA) tools were applied over Portugal focusing on four subdomains (see Fig. 20.3) that covered the main urban areas of Porto and Lisbon, one rural area north of a coastal industrial site, and a rural background area.

## 20.3 Results

The CAMx process analysis tool allowed quantifying the contribution of chemistry, deposition, top and lateral boundaries to the final concentration of each pollutant in each subdomain. Plots in Fig. 20.1 illustrates (Concentration + Process Contribution) versus Concentration for $O_3$ and biogenic SOA (SOAb) hourly modelled results for the reference scenario in an urban (SD1) and a rural (SD4) subdomain. For $O_3$ at the urban sub-domain, the chemistry contribution is mainly negative due to the consumption of ozone by precursors. At the rural site deposition assumes the main negative role. $O_3$ is transported into SD1 and SD4 through top and lateral boundaries. SOAb production (positive chemistry) occurs in both sub-domains.

The time series of hourly $O_3$ and SOAb modelled concentrations obtained for the three scenarios at each subdomain during June 2011 indicated that differences between scenarios are restricted to 2 periods when air temperatures were high. Thus, a deeper analysis was focused on the period 25–27th June. Figure 20.2 displays the hourly concentrations and the processes contribution, obtained for the reference scenario and this 3 days period. Positive contributions to $O_3$ are mainly coming from lateral boundaries, whereas SOAb are mostly influenced by local chemistry, especially in SD1, where maximum concentrations are higher. South wind may be affecting pollutant levels on the 25th and 26th (south boundary >0 and north boundary <0); and the opposite occurs on the 27th.

A statistical analysis of the hourly concentrations at the four subdomains showed that Smax emissions scenario may increase $O_3$ levels by 10 % in average in urban areas (with a maximum of 60 % increase at night). Moreover, Smin led to an average reduction of 8 %, achieving a maximum reduction of 44 %. Nevertheless, in rural areas, $O_3$ concentration is not sensitive to the biogenic emission scenarios. Regarding SOAb at all subdomains, Smax emissions contribute to 120 % increase of SOAb concentrations, in average, reaching maxima around 200 and 300 % in

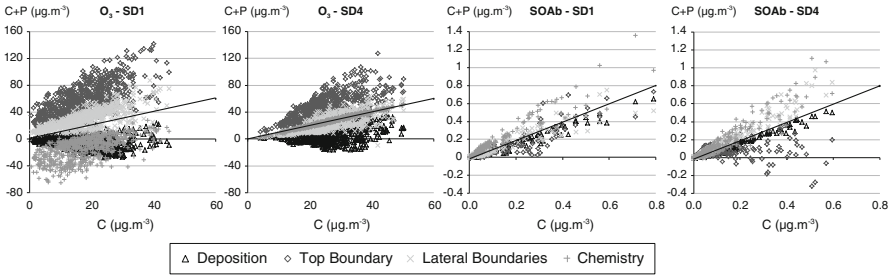


**Fig. 20.1** Positive and negative contribution ($\mu g.m^{-3}$) of different processes to the hourly $O_3$ and SOAb concentration for the reference scenario ([Concentration ($C$) + Process Contribution ($P$)] vs Concentration ($C$); values above the black line mean positive contribution and below the line negative contribution)

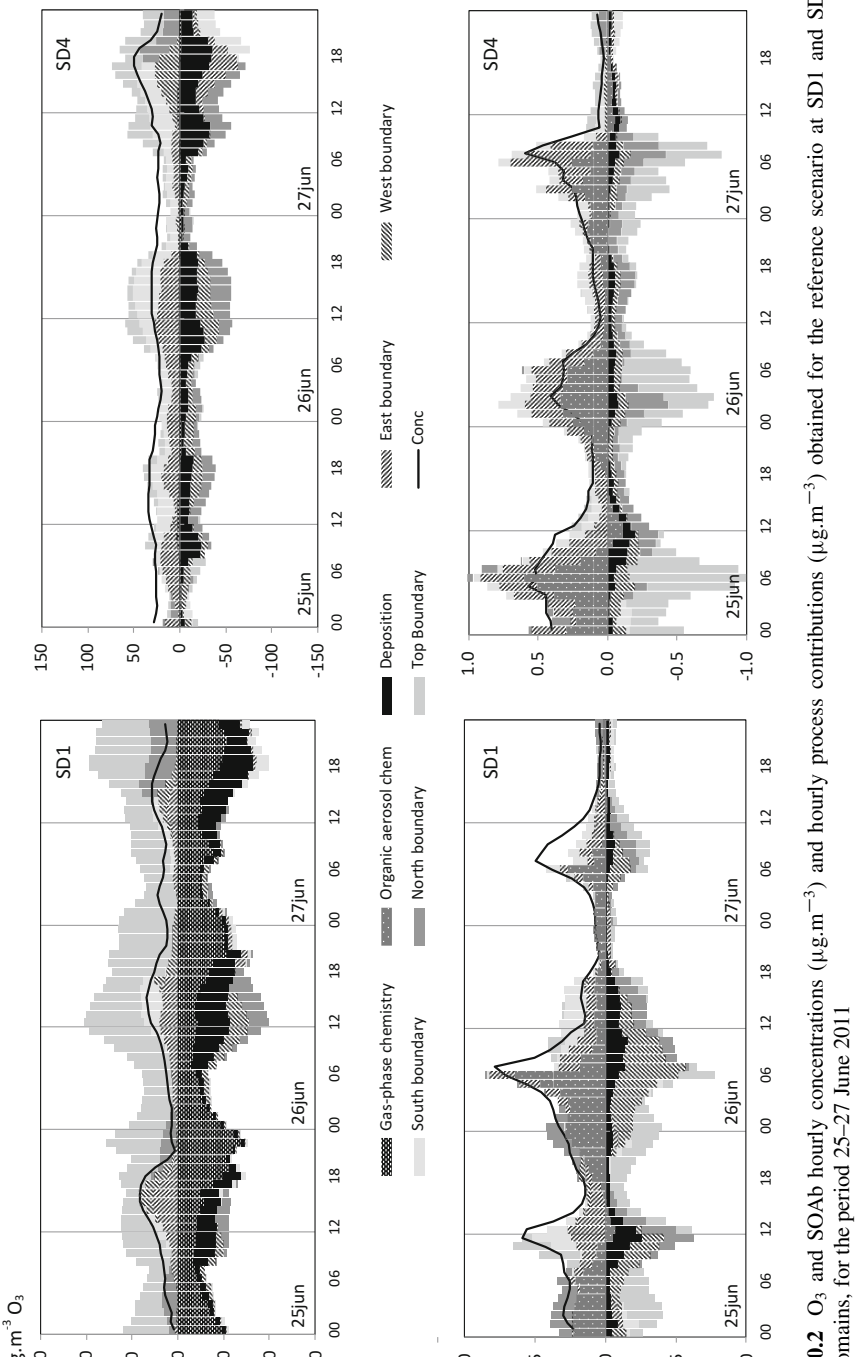


**Fig. 20.2** $O_3$ and SOAb hourly concentrations ($\mu g.m^{-3}$) and hourly process contributions ($\mu g.m^{-3}$) obtained for the reference scenario at SD1 and SD4 sub-domains, for the period 25–27 June 2011

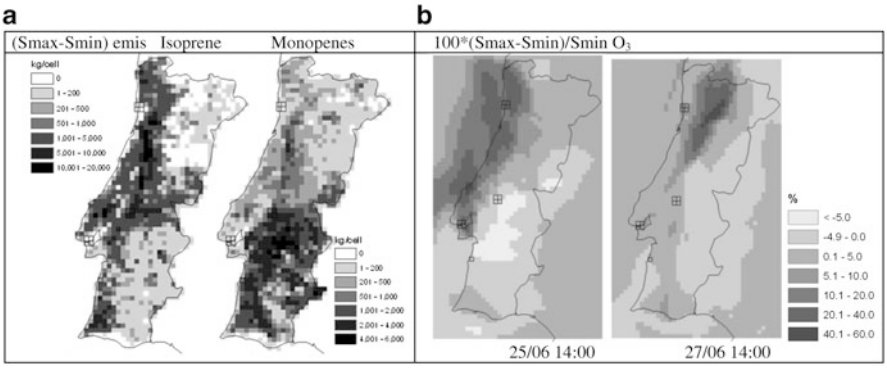


**Fig. 20.3** Differences between maximum (Smax) and minimum (Smin) scenarios regarding isoprene and monoterpene emissions (g.cell$^{-1}$.day$^{-1}$) (**a**) and $O_3$ concentration (difference in %) (**b**)

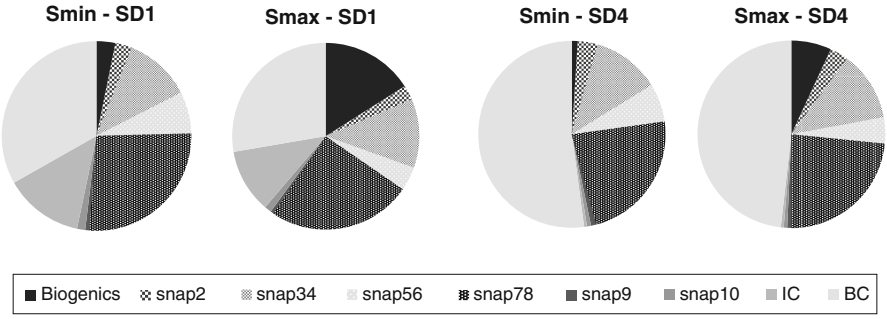


**Fig. 20.4** $O_3$ source contribution, by SNAP (Selected Nomenclature for sources of Air Pollution), obtained for the Smin and Smax scenarios at SD1 and SD4 sub-domains (8 h averaged maximum on June 27th)

urban and rural areas respectively. Smin decreases SOAb levels up to 86 % (average decrease around 70 %), in comparison with the reference scenario.

The analysis of spatial differences between scenarios revealed that the increase of emissions (from min to max scenario) (Fig. 20.3a for June, 25) may lead to $O_3$ concentration variations from −5 to +60 % at 14UTC of June 25th and 27th (Fig. 20.3b for June, 25 and 27). Maximum differences occur out of the most emitting regions, due to the secondary origin of this pollutant and the effect of meteorological conditions.

Figure 20.4 shows the contribution from different emission sectors, in particular from biogenic emissions, and from initial and boundary conditions (IC and BC, respectively) to the $O_3$ concentration values estimated by the OSAT tool for the Smin and Smax scenarios. The pie charts concerns the maximum 8-h average on 27th June for SD1 and SD4. The source sectors contribution is very different between scenarios for both subdomains: biogenic emissions increase its importance in $O_3$ formation from 3 to 16 % in the urban area (SD4) and from 1 to 7 % in the

rural area (SD4). However this does not affect the absolute 8-h averaged simulated concentration since the production of $O_3$ in both sub-domains is NOx-limited, an information also provided by OSAT.

## 20.4 Conclusion

Process Analysis and Source Apportionment tools within CAMx model were used to evaluate the impact of biogenic emissions on $O_3$ and biogenic SOA concentration values over Portugal. Three scenarios were considered based on maximum and minimum limits in emission factors. The results showed that chemistry positively affects SOAb, and has a negative contribution to $O_3$ in rural areas, while transport is the main factor that contributes positively to $O_3$ levels. The maximum and minimum emission scenarios contribute to vary SOAb concentrations by up to $-88$ to $+300$ %. $O_3$ levels may vary from $-40$ to $+60$ % and $\pm 15$ % in urban and rural areas, respectively. Despite the different role of biogenic emissions among scenarios and sub-domain types, $O_3$ concentration is not affected (varies in average $\pm 1$ %) since the production is NOx-limited.

**Acknowledgments** The Portuguese Foundation for Science and Technology (FCT) is acknowledged for the financial support of the project EMOSAT (PTDC/CTE-ATM/103253/2008, FCOMP-01-0124-FEDER-009305), post doc grants of J. Ferreira (SFRH/BPD/40620/2007) and H. Martins (SFRH/BPD/66874/2009).

## References

1. Curci G, Beekmann M, Vautard R, Smiatek G, Steinbrecher R, Theloke J, Friedrich R (2009) Modelling study of the impact of isoprene and terpene biogenic emissions on European ozone levels. Atmos Environ 43(7):1444–1455
2. ENVIRON (2011) User's guide to the comprehensive air quality model with extensions (CAMx) version 5.40 (September, 2011). http://www.camx.com
3. Oderbolz DC, Aksoyoglu S, Keller J, Barmpadimos I, Steinbrecher R, Skjøth CA, Plab-Dülmer C, Prévôt ASH (2013) A comprehensive emission inventory of biogenic volatile organic compounds in Europe: improved seasonality and land-cover. Atmos Chem Phys 13:1689–1712

## Questions and Answers

**Questioner Name**: Roger Jimmis

**Q**: What were the main reasons for the difference in estimated biogenic emissions between the maximum and minimum cases? Were differences because of alternative estimates of land use, biomass, emission factors per unit of vegetation, or temperature differences?

**A**: Maximum and minimum scenarios of biogenic emissions were built based on the ranges of emission factors and biomass densities found in the literature for each vegetation species. The minimum and maximum values of those ranges were considered to calculate the minimum and maximum isoprene and monoterpene emissions respectively.

**Questioner Name**: Dominik Brunner

**Q**: Why is contribution from chemistry negative in urban areas? Simple titration.
**A**: Yes, in fact, urban areas are characterized by the presence of ozone precursors emitted by local emission sources which affect the photochemical processes by consuming (negative chemistry) the ozone produced.

**Questioner Name**: Pins Lee

**Q**: The site south of Lisbon, on the coat was mentioned as a rural site, but you particularly underscored that this rural site has industry downwind from it. Why is that significant to your design of the measurement mix?
**A**: That is a rural EMEP station. It is classified as rural because it is located upwind an industrial site, since predominant winds are from north. However, this was chosen as an interesting area, requiring a more comprehensive analysis because historical measurements at the air quality station reveal that high levels of ozone can be observed in days with south wind. This indicates the influence of the industrial emissions in the air quality north of the industrial area as a result of the transport of air masses from south. This fact was already verified in previous modeling studies and is corroborated in the present study by the positive contribution of south boundaries in specific days with higher ozone concentrations.

**Questioner Name**: Oriol Jorba

**Q**: Do you have identified the reasons of your model underestimation of ozone?
**A**: The most probable explanation is related to anthropogenic emission inventory, specifically of NOx emissions. However, this was a particular month and a deeper analysis of results has to be performed to understand the reason of ozone underestimations by the model.

# Chapter 21
# Modelling Aerosol-Cloud-Meteorology Interaction: A Case Study with a Fully Coupled Air Quality Model (GEM-MACH)

**W. Gong, P.A. Makar, J. Zhang, J. Milbrandt, and S. Gravel**

**Abstract** A fully coupled on-line air quality forecast model, GEM-MACH, was used to study a case of cloud processing in an urban-industrial plume and aerosol-cloud-meteorology interaction. Preliminary results have shown a significant impact on modelled clouds and particulate sulfate concentrations due to the inclusion of the feedback from on-line aerosols to microphysics. Further tests and detailed comparison with in-situ measurements of this case are underway.

## 21.1 Introduction

Clouds play an important role in processing and cycling of atmospheric gaseous and aerosol tracers. A large portion of the atmospheric particulate sulphate is produced in cloud via aqueous-phase oxidation. Furthermore, cloud processed aerosols, often physically (size spectrum) and chemically (composition) modified, can behave differently in activating to form cloud droplets and/or ice crystals in subsequent cloud cycles, which will in turn impact precipitation generation, cloud life time, and cloud optical properties. Over the past decade a number of air quality forecasting systems have been developed with an on-line approach allowing varying levels of interaction amongst different atmospheric processes. Studies have

W. Gong (✉) • P.A. Makar • J. Zhang
Air Quality Research Division, Environment Canada, Toronto, ON, Canada
e-mail: wanmin.gong@ec.gc.ca; paul.makar@ec.gc.ca; junhua.zhang@ec.gc.ca

J. Milbrandt
Meteorological Research Division, Environment Canada, Dorval, QC, Canada
e-mail: jason.milbrandt@ec.gc.ca

S. Gravel
Air Quality Research Division, Environment Canada, Dorval, QC, Canada
e-mail: sylvie.gravel@ec.gc.ca

D. Steyn and R. Mathur (eds.), *Air Pollution Modeling and its Application XXIII*,
Springer Proceedings in Complexity, DOI 10.1007/978-3-319-04379-1_21,

shown a significant impact from aerosols and gases to weather predictions due to feedback through radiation and cloud microphysics, which in turn impact air quality predictions.

A major challenge in evaluating the model simulations of aerosol-cloud-meteorology feedbacks is often the lack of suitable observations. This work is a case study, based on airborne measurements from two flights during the ICARTT field campaign in summer 2004 [3], when the National Research Council of Canada Convair 580 sampled in and below stratocumulus downwind of Chicago along each of the 84 and 86°W meridians between 40.5 and 42.6°N. The Chicago urban plume was encountered along both meridians, and the observations indicated cloud processing. In this study, we use a fully coupled version of the Environment Canada's air quality forecast model (GEM-MACH) to assess the impact of feedbacks between chemistry and dynamics through aerosol-cloud-radiation interactions on modeled meteorology and air quality. Model results, with and without the feedbacks, are compared with the in-situ aircraft microphysics and chemistry measurements. The feedback mechanisms and their representations in the fully coupled GEM-MACH are examined.

## 21.2 The Model and Study Setup

GEM-MACH (**G**lobal **E**nvironmental **M**ultiscale model – **M**odelling **A**ir quality and **CH**emistry) is an on-line chemistry transport model embedded within GEM. A limited area version of GEM-MACH has been in use as Environment Canada's operational air quality prediction model since 2009 [5, 7].

Although on-line, the coupling between meteorology and chemistry in GEM-MACH has been one-way until recently, i.e., the chemistry portions of the model are influenced by meteorology, while feedbacks from chemistry to meteorology are not represented. As a participant in the 2nd phase of the Air-Quality Model Evaluation International Initiative (AQMEII), feedbacks between chemistry and meteorology have been introduced in GEM-MACH through the modifications made in two areas of the code: (1) changes to the droplet nucleation in the current microphysics scheme (in the physics module) to make use of the on-line, size and chemically resolved aerosols from the chemistry module, and (2) the replacement of the existing aerosol extinction (based on fixed, standard continental and marine aerosols) in the model radiation code with the extinction calculations based on the on-line aerosols [4].

The present study focuses on a particular day, August 10, 2004, when two research flights were conducted between 17 and 23 UTC. Model simulations with GEM-MACH were conducted at two horizontal resolutions, 15- and 2.5-km, in a nested cascading configuration over three model grids, shown in Fig. 21.1. The grids include: a continental domain at 15-km resolution covering most of the North American continent, an intermediate/regional 15-km domain, and a

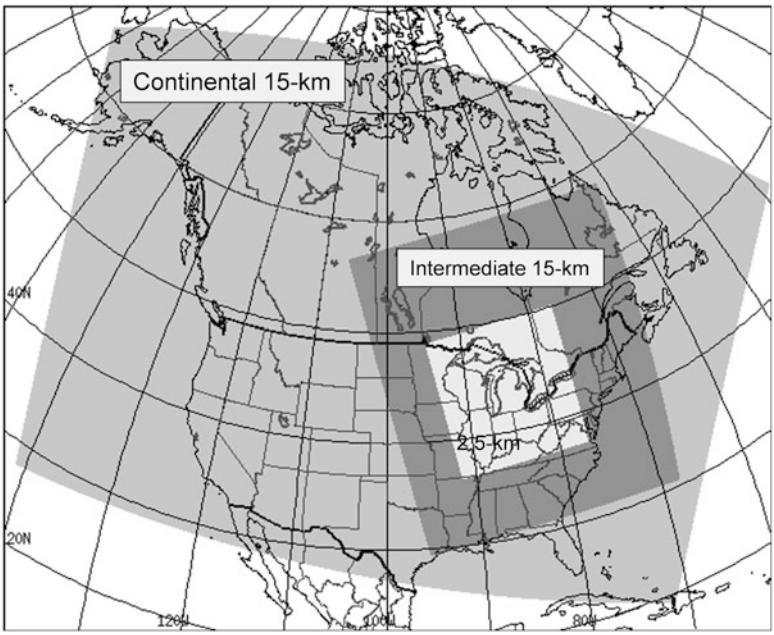


**Fig. 21.1** Nested model domains (continental 15-km, regional 15-km, and hi-res 2.5-km) used for the study

**Table 21.1** Key configurations for the various model runs in this study

| Runs | Grid-scale cond. | Sub-grid-scale convec. | Feedback[a] |
|---|---|---|---|
| Continental 15-km | Sundqvist[b] | Kain-Fritsch | No |
| Intermediate 15-km | M-Y double moment | Kain-Fritsch | No |
| 2.5-km | M-Y double moment | No | No/yes |

[a]Feedback through microphysics only
[b]The same as the physics configuration used in the operational GEM-MACH version

2.5-km resolution domain focusing on the flight area. Table 21.1 gives the key configurations for the various model runs. The continental 15-km simulations were conducted in 30-h segments starting daily at 00 Z from August 5–10, 2004; the first 6 h of each of the model runs are for meteorology-only spin-up while the chemistry (including tracer advection) starts at hour 6 from the concentration fields at the end of the previous 30-h run. The nested intermediate 15-km run was conducted for 24 h from 00 Z on August 10, 2004, and the 2.5-km runs were conducted for 18 h from 06 Z on August 10, 2004. A 12-bin representation of particle size spectrum is used in these simulations (in contrast to the 2-bin representation used in the operational version of the GEM-MACH). Anthropogenic emissions are based on the 2005 U.S. and 2006 Canadian national emission inventories.

## 21.3 Results and Discussion

The results discussed here are focused on the hi-resolution runs at 2.5-km, comparing the simulations with and without the on-line aerosol feedback through microphysics.

Model predicted cloud liquid water content (LWC) and cloud droplet number concentration ($N_c$) at 19 UTC 2004-08-10 are compared in Fig. 21.2. The GOES visible image (at 18:15 UTC) provides a view of the clouds at the time of the flight (FLT 16). The modelled LWC is significantly higher with relatively broader spatial coverage from the run with the on-line aerosol feedback than the one without the feedback. This corresponds to much higher $N_c$ predicted by the Abdul-Razzak and Ghan activation scheme [1] using the on-line aerosols (with feedback) than predicted by the original droplet nucleation scheme in MY-DM [6] with fixed generic "continental" aerosol (no feedback). The modelled precipitation (not shown here) is reduced with the feedback compared to the no-feedback run, consistent with less efficient coalescence process with smaller droplets. Also shown in Fig. 21.2 are comparisons with the in-situ measurements of LWC and $N_c$ from FLT 16 (along the in-cloud portion of the flight path). The modelled values were obtained by sampling through the modelled fields along the flight path (but with a vertical displacement of 225 m, up, as the modelled cloud base was higher than the observation by about 200 m). It appears that the model under-predicted LWC and $N_c$ without the on-line aerosol feedback but over-predicted with the feedback. The over-prediction of $N_c$ from the feedback run may be at least partly related to the particular updraft velocity parameterization used in the aerosol activation ([2]). Further test runs with different updraft velocities were conducted and preliminary examination of the results shows that the modelled $N_c$ and LWC are highly sensitive to the updraft velocity.

The impact of the feedback to modelled particulate sulfate is illustrated in Fig. 21.3. For this particular case, there is a predominant plume originating from the main $SO_2$ source region in eastern U.S. (along the Ohio River Valley) in the south-westerly flow of a frontal system. The comparison shows a considerable increase in modelled fine sulfate at cloud level (over the flight region and over upper Lake Michigan and Lake Superior) from the model run with the feedback corresponding to the greater predicted cloud LWC and hence increased aqueous phase production of sulfate.

## 21.4 Conclusion

Preliminary model simulations of a case from ICARTT field campaign using a fully coupled version of GEM-MACH have shown a significant impact on modelled clouds and chemical tracer concentrations due to the feedback of the on-line aerosols to microphysics. The model predicted much higher $N_c$ with feedback from the on-line aerosols, and consequently less rain and more cloud, in comparison with the

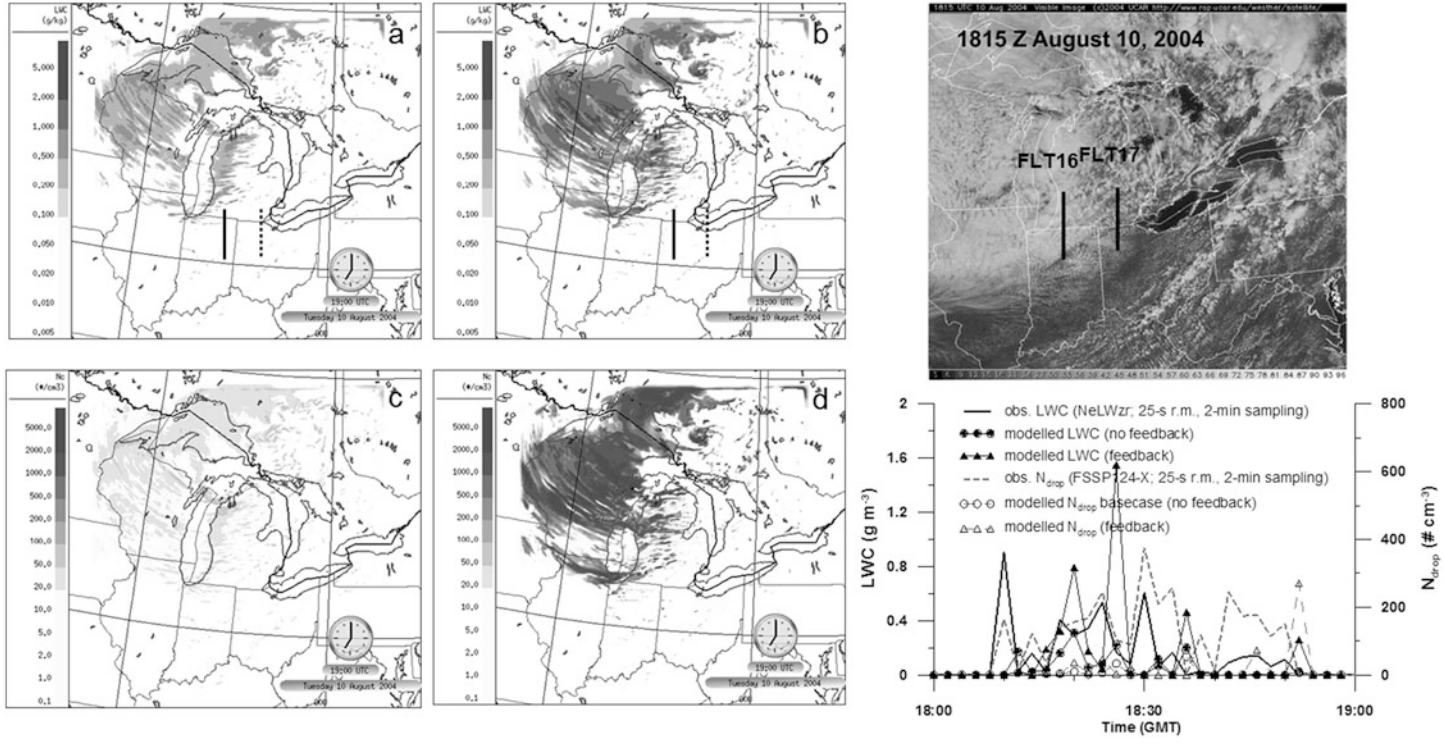


**Fig. 21.2** Four panels on the *left*: modelled LWC (in g/kg, *top panels*: **a** and **b**) and $N_{cld}$ (shown in #/cm$^3$, *bottom panels*: **c** and **d**) at model hybrid level of 0.8795; *left* (**a**, **c**) – without the feedback, *right* (**b**, **d**) – with the feedback. On the far *right*: GOES visible image at 1815 UTC 2004-08-10 (*top*), and comparison with in-situ aircraft observations of LWC (g/m$^3$) and droplet concentrations (#/cm$^3$) along the FLT 16 in-cloud flight path (*bottom*)

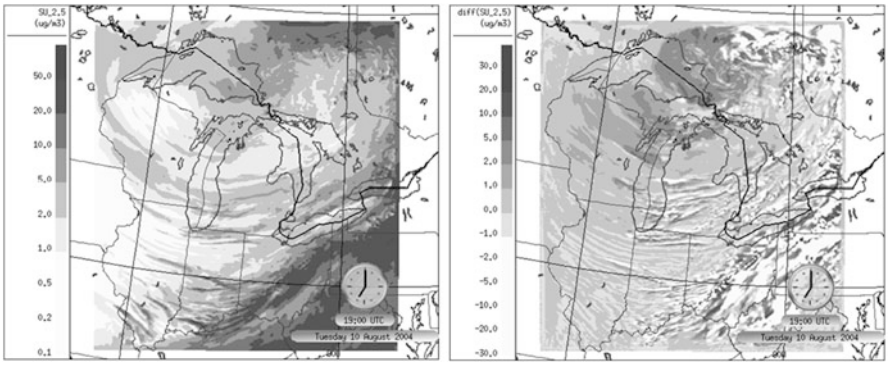


**Fig. 21.3** *Left panel*: modelled fine sulphate ($SU_{2.5}$) at model hybrid level of 0.8795 from the base-case simulation at 2.5-km resolution (no feedback); *right panel*: difference in modelled $SU_{2.5}$ at the same model level, [feedback on] – [feedback off]; all for 19 Z August 10, 2004

model run without the on-line aerosol feedback. As a consequence, model predicted sulfate concentration is increased due to the enhanced aqueous-phase production. Initial comparison with in-situ cloud microphysics measurements indicates that the current model simulation under-predicts cloud (both LWC and $N_c$) without the feedback from the on-line aerosols but over-predicts with the feedback for this case. A key variable, and a source of uncertainty, is updraft velocity in aerosol activation. The modelled $N_c$ and LWC are highly sensitive to the updraft velocity. Further investigation is needed.

**Acknowledgments** The authors would like to acknowledge Mr. Radenko Pavlovic (AQMAS/NPOD/MSC) for conducting a series of 12-h cycling runs using the standard operational GEM-MACH to generate chemical initial conditions for this study.

## References

1. Abdul-Razzak H, Ghan SJ (2002) A parameterization of aerosol activation. Part 3: Sectional representation. J Geophys Res 107(D3):4026. doi:10.1029/2001JD000483
2. Gong W et al (2013) Impact of aerosol activation on modelled regional particulate matter mass and size distribution due to cloud processing. In: Steyn DG, Timmermans R (eds) Air pollution modelling and its application XXII. Springer, Dordrecht
3. Hayden KL et al (2008) Cloud processing of nitrate. J Geophys Res 113(D18), D18201
4. Makar PA et al (2014) A process analysis of the impact of air-quality/weather feedbacks using GEM-MACH. In: Steyn D, Mathur R (eds) Proceedings of the 33rd ITM on air pollution modelling and its application. Springer, Dordrecht
5. Menard S et al (2014) Current and future developments in numerical air quality forecasting in Canada. In: Steyn D, Mathur R (eds) Proceedings of the 33rd ITM on air pollution modelling and its application. Springer, Dordrecht
6. Milbrandt JA, Yau MK (2005) A multimoment bulk microphysics parameterization. Part II: A proposed three-moment closure and scheme description. J Atmos Sci 62(9):3065–3081

7. Moran MD et al (2010) Particulate-matter forecasting with GEM-MACH15, a new Canadian air-quality forecast model. In: Steyn DG, Rao ST (eds) Air pollution modelling and its application XX. Springer, Dordrecht, pp 289–292

## Questions and Answers

**Questioner Name:** Dominik Brunner

Q: There is a large variability amongst the existing studies on aerosol indirect effect; some show a large effect while others show otherwise. What could be the reason for such large differences? Would a coordinated modelling effort make sense, (i.e., several models running the same cases)?

A: There could be a number of reasons for the differences, e.g., particular cases, differences in model representation of the feedback processes, etc. From the work carried out here, details of the cloud formation parameterizations within individual models, such as the assumptions used for cloud updraft velocity, can have a significant impact on model results. A coordinated multi-model inter-comparison study on selected cases would definitely be worthwhile.

**Questioner Name:** Pius Lee

Q: Our own experience with WRF-NMM is that, when cascading from a coarse grid to a finer grid, often stronger updraft and energetic convection result in triggering heavier precipitation. Is this the experience with GEM also? The AQ model (GEM-MACH), when cascading to finer (2.5-km) grid, has an effect of suppressing precipitation. These two effects seem to counter-act with each other. Have you quantified these effects individually? Are they physically based? If so, do you need "sponge-layers" in the grid-resolution transition to buffer the forcing?

A: The results that we have presented here show comparisons between the model runs with and without the feedback from the on-line aerosols, not between high and low model resolution. We have shown that, for the case studied, with the feedback from the on-line aerosols the modeled precipitation is reduced, as a result of enhanced cloud droplet number concentrations and less efficient coalescence process with smaller cloud droplets. All the model runs in question were conducted at high (2.5-km) resolution.

# Chapter 22
# Evaluation of Cloud Chemistry Mechanism Towards Laboratory Experiments

**Yoann Long, Laurent Deguillaume, and Nadine Chaumerliac**

**Abstract** Cloud chemistry models include more and more explicit multiphase mechanisms based on laboratory experiments that provide kinetic constants, stability constants of complexes, hydration constant, *etc.* However, they are still subject to many uncertainties, related to the aqueous chemical mechanism they used which most of the time has never been confronted against laboratory experimental data. To fill this gap, we propose to adapt the M2C2 model to simulate irradiation experiments on synthetic aqueous solutions under controlled conditions (pH, pressure, temperature, light intensity, . . . ) considering various chemical compounds that are supposed to contribute to the oxidative budget in cloud water (iron, oxidants such as $H_2O_2$). As target species, organic compounds (oxalic, formic, acetic acids) are taken into account since they are oxidized and are also good indicators of the oxidative capacity and potential iron complexant. Range of concentrations for all the studied chemical compounds are representative of *in situ* measurements. Numerical outputs are confronted to experimental data that consist in time evolution of the concentration of target species (Long Y, Charbouillot T, Brigante M, Mailhot G, Delort A-M, Chaumerliac N, Deguillaume L, Evaluation of modeled cloud chemistry mechanism against laboratory irradiation experiments: the HxOy/iron/carboxylic acid chemical system. Atmos Environ 77:686–695; 2013).

## 22.1 Introduction

Currently, cloud chemistry models consider both inorganic and organic mechanisms and chemical transformation are mainly driven by radical pathways that define the cloud oxidant capacity. Simulated oxidants concentrations such as $HO^{\bullet}$ strongly

Y. Long (✉) • L. Deguillaume • N. Chaumerliac
LaMP, CNRS, Université Blaise Pascal, 24 Av. des Landais, 63171 Aubière, France
e-mail: Y.Long@opgc.univ-bpclermont.fr; L.Deguillaume@opgc.univ-bpclermont.fr; N.Chaumerliac@opgc.univ-bpclermont.fr

D. Steyn and R. Mathur (eds.), *Air Pollution Modeling and its Application XXIII*, Springer Proceedings in Complexity, DOI 10.1007/978-3-319-04379-1_22,

depend on the chemical initialization (particularly iron under polluted conditions and organic matter amounts) and on the chemical mechanisms. The efficiency of chemical pathways that drive the oxidative capacity in these models has not been fully evaluated.

## 22.2 Modeling of Irradiation Experiments

The M2C2 model was adapted to simulate irradiation experiments using synthetic solutions under controlled conditions (pH, pressure, temperature, *etc.*) and considering chemical compounds that contribute to the oxidative budget in cloud water (iron and $H_2O_2$). Organic compounds (oxalic, formic, acetic acids) were taken into account as target species because they are oxidized by $HO^{\bullet}$ and are potential iron complexant especially oxalic acid which represents the most abundant diacid and an important component of the organic particulate matter. The concentration range for all chemical compounds is representative of *in situ* measurements [2] and values used to initialize the model are given in Table 22.1.

Figure 22.1 presents the simulated and experimental concentration time profiles of Fe(II), Fe(III), $HO^{\bullet}$ and $H_2O_2$ for experiment 1 which represents the $H_xO_y$/iron system. The degradation of $H_2O_2$ and Fe(II) under dark conditions (*i.e.* Fenton reaction) leads to the formation of Fe(III). Moreover, generated hydroxyl radicals react with Fe(II) explaining the quantitative (up to 95 %) Fe(III) formation. When irradiation starts Fe(III) concentration slightly decreases due to its photolysis partially counter-balanced by its formation via $HO^{\bullet}$ and Fe(II) reaction. Iron is stabilized at the end of simulation and experiment: Fe(III) photolysis could be then considered as the main source of $HO^{\bullet}$ (99 %) with a negligible contribution of $H_2O_2$ photolysis.

Then, in a second experiment carboxylic acids are added to the $H_xO_y$/iron system as observed in real clouds. The carboxylic acids play a double role of scavenger for generated hydroxyl radical and complexants of iron modifying the $H_xO_y$/iron reactivity. Comparisons between model outputs and measurements show that the chemical reactivity is correctly reproduced by the model (Fig. 22.2). As expected, time-evolution of iron and $H_2O_2$ concentrations are driven by photo-Fenton reactions. The Fe(II) concentration becomes constant (up to 90 %) at the end

**Table 22.1** Chemical concentrations (μM) of the synthetic solutions (1 and 2) and of the cloud sample (3)

| Exp. | $H_2O_2$ | Fe(II) | Fe(III) | Formic acid | Oxalic acid | Acetic acid | Succinic acid | Malonic acid | $NO_3^-$ | pH |
|---|---|---|---|---|---|---|---|---|---|---|
| 1 | 20 | 20 | 6 | | | | | | | 3.5 |
| 2 | 20 | 20 | 6 | 14.5 | 3 | 20 | | | | 3.8 |
| 3 | 5.85 | 2.38 | 0.7 | 35.34 | 11.22 | 42.53 | 2.82 | 2.4 | 414 | 5.0 |

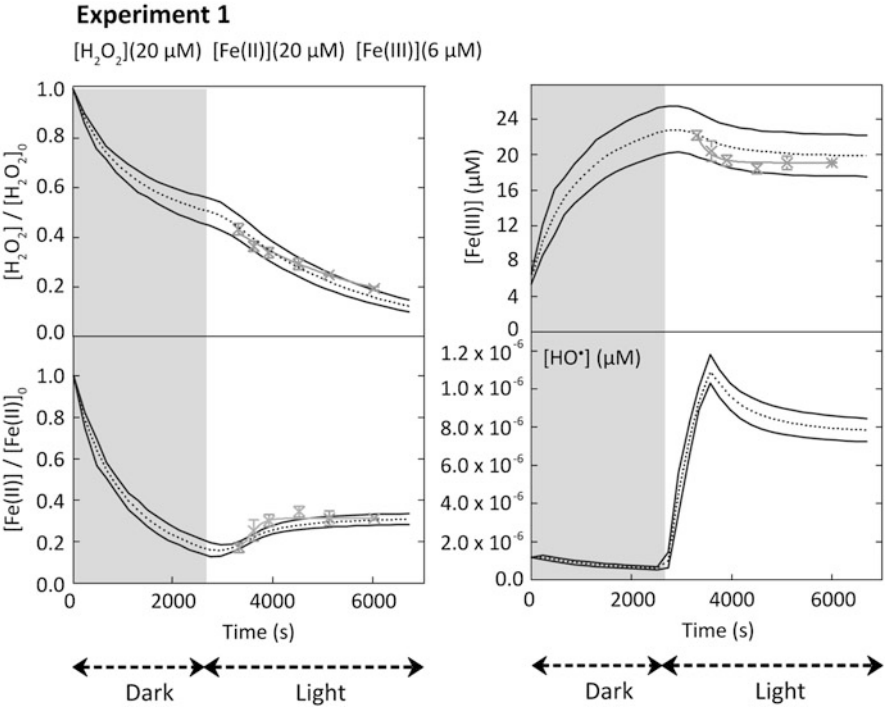


**Fig. 22.1** Comparison of concentration time evolutions of $H_2O_2$, Fe(II) and Fe(III) ($C/C_0$ with $C_0$ = initial concentration) between model (in *dark grey* with 10 % uncertainties on initial concentrations and ±0.3 on the pH value) and measurements (in *light grey*) for experiment 1 (Table 22.1). $HO^{\bullet}$ concentration time evolution simulated by the model is also presented

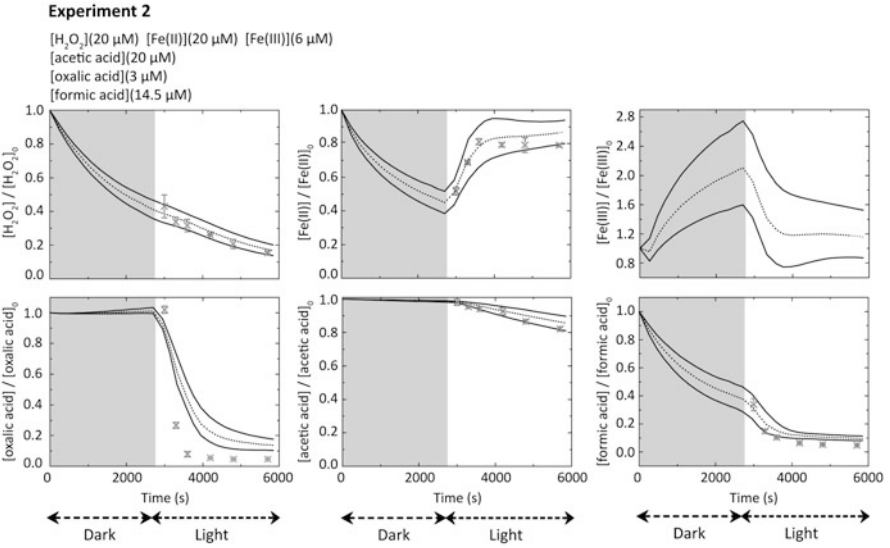


**Fig. 22.2** Same legend as Fig. 22.1 for the $H_xO_y$ iron/carboxylic acids chemical synthetic solution

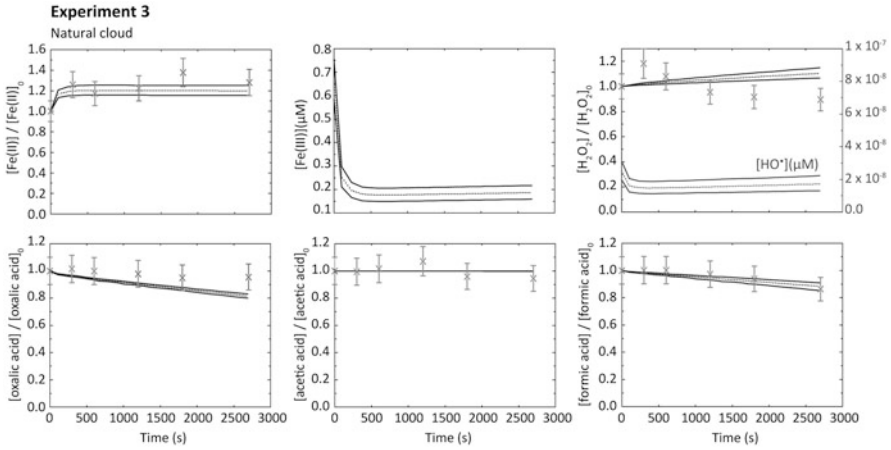


**Fig. 22.3** Same legend as Fig. 22.1 for the chemical natural cloud system

of the simulation. Acetic acid degradation by $HO^{\bullet}$ is slow compared to formic acid as observed by Charbouillot et al. [1] (20 % of degradation at the end of simulation).

Formic acid decreases quickly under irradiation and then stabilized (10 % of initial concentration) through its complexation with iron. Formic and acetic acid fates are mainly controlled by hydroxyl radical oxidation produced by photo-Fenton cycle. Oxalic acid degradation is driven by the formation and the direct photolysis of Fe(III) oxalic acid complexes whereas its formation by acetic acid oxidation is not enough sufficient to counterbalance its fate (an average of $3.44 \times 10^{-11}$ M $s^{-1}$ on the whole simulation). These final experiments showed that M2C2 model is able to explain time-concentration evolution of key chemicals involved in atmospheric cloud chemistry under controlled conditions *i.e.* initial concentrations, pH and T.

Finally, in the last experiment, a natural cloud sample was irradiated during 45 min. Model was constrained by the concentrations of major inorganic and organic ions measured in the cloud samples by ionic chromatography and pH (Table 22.1). The total iron concentration is 10 times lower than in experiment 1 whereas the organic amount is much higher with around 100 μM of measured organic acids. Comparisons between simulations and measurements of Fe(II), Fe(III), $HO^{\bullet}$ and $H_2O_2$ and VOCs concentration-time profiles are presented in Fig. 22.3.

For this particular cloud sample, the model properly reproduces the laboratory concentrations for the target species. The time evolution of iron speciation is driven by photo-Fenton reactivity and follows the same behavior than observed during irradiation of synthetic solutions. The concentration of hydroxyl radical at photostationary state is around $2 \times 10^{-14}$ M that is 100 times lower than in experiment 1. Consequently, the organic acids are slowly degraded in this case. Formic acid degradation is relatively slow and the contribution of acetic acid oxidation as a source of formic acid is negligible. Acetic acid stays constant

on the whole simulation time. The indirect source from acetic acid to formic acid is negligible. Conversely, oxalic acid concentration is underestimated by the model outputs up to 10 % at the end of the experiment. Higher molecular organic compounds such as malonic and succinic acids detected in our cloud sample might be precursors of oxalic acid through further oxidation pathways [3].

## 22.3 Conclusion

This study shows that the chemical mechanism describing the "oxidative engine" represented by the $H_xO_y$/iron chemical system is consistent with laboratory experiments under controlled conditions. Thus, the degradation of carboxylic acids commonly found in natural cloud waters is well reproduced by the M2C2 model. Confrontation of cloud chemistry model results with experimental data is a nice way to validate cloud chemistry models and their explicit chemical mechanisms [4].

## References

1. Charbouillot T, Gorini S, Voyard G, Parazols M, Brigante M, Deguillaume L, Delort A-M, Mailhot G (2012) Mechanism of carboxylic acid photooxidation in atmospheric aqueous phase: formation, fate and reactivity. Atmos Environ 56:1–8
2. Deguillaume L, Charbouillot T, Joly M, Vaïtilingom M, Parazols M, Marinoni A, Amato P, Delort A-M, Vinatier V, Flossmann A, Chaumerliac N, Pichon JM, Houdier S, Laj P, Sellegri K, Colomb A, Brigante M, Mailhot G (2013) Classification of clouds sampled at the puy de Dôme (France) from 10 yr monitoring: mean features of their physico-chemical properties. Atmos Chem Phys Discuss 13:22795–22846
3. Herrmann H, Tilgner A, Barzaghi P, Majdik Z, Gligorovski S, Poulain L, Monod A (2005) Towards a more detailed description of tropospheric aqueous phase organic chemistry: CAPRAM 3.0. Atmos Environ 39:4351–4363
4. Long Y, Charbouillot T, Brigante M, Mailhot G, Delort A-M, Chaumerliac N, Deguillaume L (2013) Evaluation of modeled cloud chemistry mechanism against laboratory irradiation experiments: the HxOy/iron/carboxylic acid chemical system. Atmos Environ 77:686–695

# Chapter 23
# Effects of Surf Zone Sea-Spray Particles on Aerosol Concentration in Coastal Area

**Gilles Tedeschi and Jacques Piazzola**

**Abstract** An experimental campaign has been conducted in Nov. 2007 in Duck, NC. Several sets of probes were used in various conditions, in order to measure either the marine aerosol vertical gradient and the flux emitted by the surf zone or the horizontal transport offshore. It was possible to find a new equation for the surf zone aerosol flux depending on the Wave Energy Dissipation (WED). The aerosol transport was simulated for offshore wind condition and compared to experimental data measured aboard a boat travelling along the offshore wind vector.

## 23.1 Introduction

The marine aerosol flux emitted in the surf zone (SZ) is several orders of magnitude higher than the open ocean (OO) flux. Even if the SZ size is only a few tens meters length, its effect may extend up to several tens of kilometres from the shoreline. One of the objectives of the study is to determine this distance, using a numerical transport model (MACMod [4]) dedicated to the simulation of marine aerosols transport, and to validate the modelling with the help of experimental data. Another objective is to validate the surf zone aerosol source function which is still not well determined.

G. Tedeschi (✉) • J. Piazzola
CNRS/INSU, IRD, Mediterranean Institute of Oceanography (MIO), Toulon University, UM 110, 83957 La Garde, France

CNRS/INSU, IRD, Mediterranean Institute of Oceanography (MIO), Aix Marseille University, UM 110, 13288 Marseille, France
e-mail: tedeschi@univ-tln.fr

D. Steyn and R. Mathur (eds.), *Air Pollution Modeling and its Application XXIII*, Springer Proceedings in Complexity, DOI 10.1007/978-3-319-04379-1_23,

## 23.2 Experimental Campaign

Data analyzed were collected in Duck, NC, in Nov. 2007, and were part of a larger experimental campaign, the Surf Zone Aerosol Experiment (SZAE), described by Van Eijk et al. [5].

The measurements were made at the 560 m long pier of the Field Research Facility (FRF) of the U. S. Army Corps of Engineers, equipped with the Sensor Insertion System (SIS), a crane-like device with two arms that can reach 15–25 m out from the side of the pier. The SIS can then be still positioned downwind of the SZ: close to the beach for onshore flows, and near the end of pier during offshore flows. Aerosol size distributions were measured at 6 and 16 m above the water level by 6 optical particle counters operated by TNO laboratory (The Hague, NL). Two probes were placed side by side in order to create 3 pairs and measure distributions over a wide radius range (0.21–45.5 μm). It was possible to obtain the aerosol vertical gradient and the flux emitted by the SZ. At the same time, wavefield data were obtained from the FRF array of pressure-gauges at 1 km offshore. The knowledge of the bathymetry profile allowed to calculate the wave energy dissipation (WED) in the surf zone.

The transport experiment took place during a 2 days offshore flow event on the 5th and the 6th November 2007. A commercial tuna fishing boat was chartered and a pair of probes was relocated from the SIS to the top of the boat's main cabin. During steady offshore flow conditions, the boat travelled from the end of the pier along the offshore wind vector to a distance of 13 km. Horizontal profiles of aerosol concentration could be measured.

## 23.3 Modelling of Sea-Spray Aerosol Particles Generated in the Surf Zone

Many studies have been devoted to the establishment of marine aerosol source functions at Open Ocean (OO), whereas the ones for the Surf Zone (SZ) are quite sparse. The wind speed is generally used to parameterize the aerosol production in terms of environmental conditions, which suggests that there is a strong correlation between aerosol production, wave breaking and wind speed. While this may be true in deep waters for wind-generated wavefields, wave breaking is a more complex process in the SZ, where the bathymetry should play an important role. In that case, the WED can be related to the bathymetry profile and the incident wavefield and can be thought as the governing parameter for the SZ aerosol generation. de Leeuw et al. [2] expressed the SZ source function with the help of wind speed $U$ at 10 m:

$$dF/dD = 1.1 \;\; 10^{7} e^{0.23U} D^{-1.65} \quad \left[\mu m^{-1}.m^{-2}.s^{-1}\right] \tag{23.1}$$

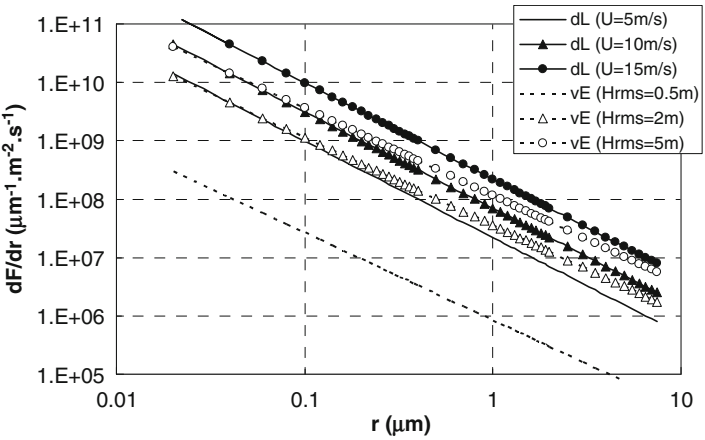


**Fig. 23.1** SZ sea-spray sources functions (dL and vE) for various conditions

called dL expression in the present paper. With the experimental data sets obtained during the SZAE, Van Eijk et al. [5] proposed the following expression:

$$dF/dD = 10^{\left[10\left(1-WED^{-0.35}\right)\right]} D^{-1.5} \quad \left[\mu m^{-1}.m^{-2}.s^{-1}\right] \tag{23.2}$$

called vE expression.

Figure 23.1 shows a comparison between the SZ source function calculated with dL et vE expressions. The wind speeds (5, 10 and 15 m/s) for dL and the wave heights (0.5, 2 and 5 m) for vE have been chosen to match roughly the oceanic conditions with the atmospheric ones. For low wind speed/wave height conditions, the fluxes differ by almost two orders of magnitude.

## 23.4 Modelling of the Aerosol Horizontal Transport

The MACMod model has been described extensively in a previous paper [4]. It is a 2D unsteady model resolving the budget equation for the sea-salt aerosol concentration using the finite volume method. Aerosol emission (production) and removal (deposition) at the sea surface are taken into account as additional terms for the vertical flux, in the first layer.

The MACMod model was used to perform numerical simulations of aerosol concentration up to tens km downwind of the surf zone. The horizontal (x coordinate) calculation domain was 50 km, divided in 1,000 cells of 50 m length. In the vertical (z) direction, the domain extended 600 m, divided in 25 cells with an irregular height step, stretched close to the sea surface. The height of the lowest grid cell was chosen to be 0.5 m. The lower layer (i.e. first 50 m) was represented by 10 grid

cells, and the remaining 15 grid cells were used to describe the upper layer (i.e. 50 up to 600 m). The simulations have been made for an offshore wind, with a main flow blowing from land to sea. At the upwind boundary, a vertical concentration profile was defined (set to zero in case of a clean atmosphere, i.e. no background component). In this paper, only the environmental conditions observed during the transport experiment ($U_{10} = 5$ m.s$^{-1}$ and ASTD $= -6$ K) are presented. The surf zone length was 30 m.

## 23.5 Results and Discussion

Figures 23.2, 23.3 and 23.4 show the horizontal profiles of SZ generated aerosol concentrations (as a function of the distance $X$ to the shore) both measured and computed, respectively for 1 μm, 0.5 μm and 0.1 μm radii. The modelled concentrations are presented for a 3 m height, corresponding to the probe height on the boat.

The dL law leads to very high aerosol concentrations compared to vE. For 1 and 0.5 μm radii, concentrations predicted by the model using vE are found close to measured ones. The WED is a more relevant parameter than the wind speed.

The decreasing of SZ generated sea-salt aerosols is very low (moreover here in unstable conditions with ASTD $= -6$ K) and influence of the SZ is found to be at least a few tens of km.

For the 0.1 μm radius, modelled aerosol concentrations are found to be 2 or 3 orders of magnitude lower than measured ones, as the modelling has been made with only marine aerosols and no continental ones. A new simulation was then made for the 0.1 μm radius, setting at the entrance boundary layer the concentration value measured on the shore, upwind the SZ, accounting for background continental

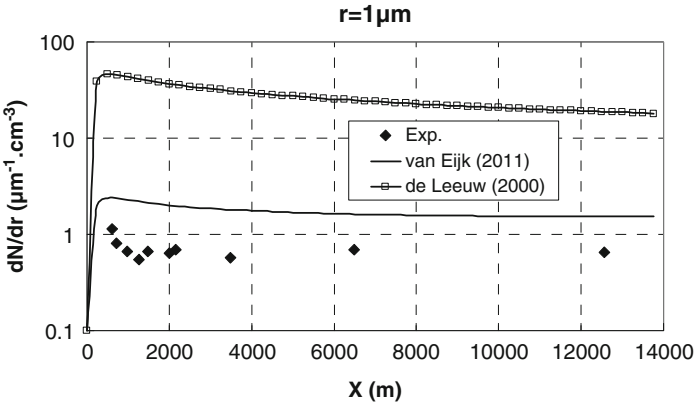


**Fig. 23.2** Aerosol concentration as a function of distance to the shore, $r = 1$ μm

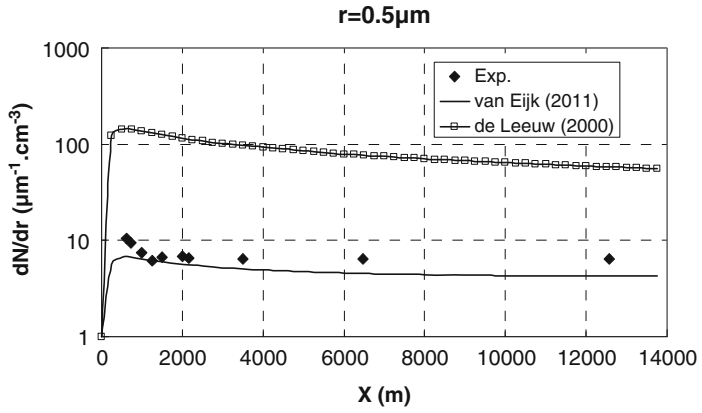


**Fig. 23.3** Aerosol concentration as a function of distance to the shore, $r = 0.5$ µm

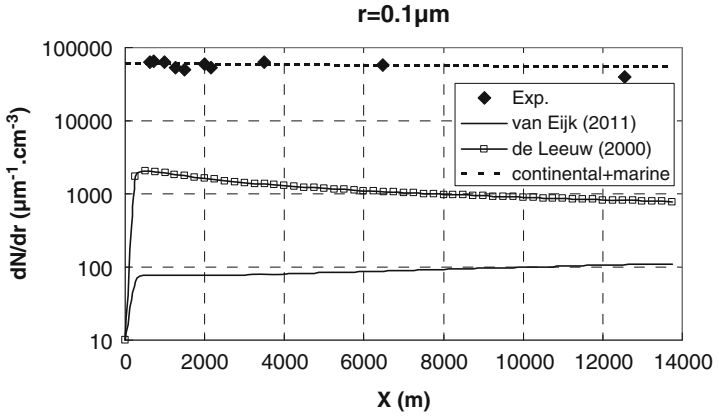


**Fig. 23.4** Aerosol concentration as a function of distance to the shore, $r = 0.1$ µm

particles only. The results are presented on Fig. 23.4, where it can be seen that the modelled concentration downwind the SZ fits exactly the measured ones, as expected. For very fine particles, the influence of the SZ is found negligible compared to background ones.

## References

1. Battjes JA, Janssen JPFM (1978) Energy loss and set-up due to breaking of random waves. In: Proceedings of the 16th international conference on coastal engineering. American Society of Civil Engineers, New York, pp 569–587
2. de Leeuw G, Neele FP, Hill M, Smith MH, Vignati E (2000) Production of sea spray in the surf zone. J Geophys Res 105:29,397–29,409
3. Longuet-Higgins MS, Stewart RW (1963) A note on wave set-up. J Mar Res 21:4–10

4. Tedeschi G, Piazzola J (2011) Development of a 2D marine aerosol transport model, application to the influence of thermal stability in the marine atmospheric boundary layer. Atmos Res 101:469–479
5. Van Eijk AMJ, Kusmierczyk-Michulec JT, Francius M, Tedeschi G, Piazzola J, Merritt DL, Fontana JD (2011) Sea-spray aerosol particles generated in the surf zone. J Geophys Res 116:D19210. doi:10.1029/2011JD015602

## Question and Answer

**Questioner Name:** Pavel Kishcha

**Q:** You found that the source function based on wave energy dissipation is better than the one based on 10 m wind. The wave energy dissipation is quite a complex parameter, which is not easy to obtain neither in theory nor in experiment. Could you elaborate how this parameter was defined in your study?

**A:** A semi-empirical model was used, based on the integration from an offshore position to the shoreline of the wave energy balance equation. It was assumed that reflection and bottom friction are negligible compared to depth-induced wave breaking. The dissipation function is modeled with Battjes and Janssen [1] model and the mean surface variation with Longuet-Higgins and Stewart [3] model. The bathymetry profile of the surf zone was surveyed 1 month prior to the experiment and incoming wavefield data were obtained from the FRF array of 15 pressure-gauges located at 8 m depth at 1 km offshore from the pier. It was then possible to compute mean wave energy dissipation.

# Chapter 24
# Novel Pathways to Form Secondary Organic Aerosols: Glyoxal SOA in WRF/Chem

**Christoph Knote, Alma Hodzic, Jose L. Jimenez, Rainer Volkamer, John J. Orlando, Sunil Baidar, Jerome Brioude, Jerome Fast, Drew R. Gentner, Allen H. Goldstein, Patrick L. Hayes, W. Berk Knighton, Hilke Oetjen, Ari Setyan, Harald Stark, Ryan M. Thalman, Geoffrey Tyndall, Rebecca Washenfelder, Eleanor Waxman, and Qi Zhang**

**Abstract** Current approaches to simulate secondary organic aerosols (SOA) in regional and global numerical models are based on parameterizations of the oxidation of precursor gases in the gas-phase and subsequent partitioning into particles. Recent findings suggest however that formation in the aqueous-phase of aerosols might contribute substantially to ambient SOA load. In this work we investigate the contribution of glyoxal to SOA through chemical processes associated with aerosols. Both a very simple and a more explicit mechanism of SOA formation from glyoxal was included in the regional chemistry transport model WRF/Chem. We simulated the first 2 weeks of June 2010 over the domain of California to make use of the extensive dataset collected during the CARES/CalNex field campaigns

C. Knote (✉) • A. Hodzic • J.J. Orlando • G. Tyndall
Atmospheric Chemistry Division, National Center for Atmospheric Research, Boulder, CO, USA
e-mail: knote@ucar.edu; alma@ucar.edu

J.L. Jimenez • R. Volkamer • S. Baidar • R.M. Thalman • E. Waxman
Department of Chemistry and Biochemistry, University of Colorado, Boulder, CO, USA

CIRES, University of Colorado, Boulder, CO, USA

H. Oetjen
Department of Chemistry and Biochemistry, University of Colorado, Boulder, CO, USA

P.L. Hayes
Department of Chemistry and Biochemistry, University of Colorado, Boulder, CO, USA

CIRES, University of Colorado, Boulder, CO, USA

Département de Chimie, Université de Montréal, Montréal, QC, Canada

J. Brioude • R. Washenfelder
CIRES, University of Colorado, Boulder, CO, USA

Chemical Sciences Division, NOAA Earth System Research Laboratory, Boulder, CO, USA

J. Fast
Pacific Northwest National Laboratory, Richland, WA, USA

D. Steyn and R. Mathur (eds.), *Air Pollution Modeling and its Application XXIII*,
Springer Proceedings in Complexity, DOI 10.1007/978-3-319-04379-1_24,

to evaluate our simulations. Contributions to total SOA mass were found to range from 1 to 15 % in the LA basin, and <1 to 9 % in the isoprene-rich eastern slopes of the Central Valley. We find that the simple approach previously used in box as well as global modeling studies gives the highest contributions. A combination of reversible partitioning and volume pathways can provide comparable amounts only if partitioning of glyoxal into the aerosol liquid-phase is instantaneous.

## 24.1 Introduction

A substantial fraction of ambient aerosols is organic matter. Most of this organic matter is not emitted as particles, but formed from precursor gases within the atmosphere. Besides pure gas phase oxidation pathways recent research also suggested considerable contributions of in-cloud and in-aerosol processing to organic aerosol load [2].

Glyoxal (CHOCHO), the smallest di-carbonyl, is one of the suggested precursors [3, 10]. It has both anthropogenic and biogenic precursors, a lifetime in the atmosphere between a few hours and a day, and was observed at sub ppbv levels in various environments. Its high solubility allows it to partition into cloud droplets and deliquesced aerosols. Recent results show an additional strong increase in partitioning into the liquid-phase in salt solutions [7]. Both reversible (hydration, oligomerization) and irreversible SOA formation has been observed in the laboratory. Box model studies were conducted to derive simple uptake coefficients that describe the formation of SOA from glyoxal as a surface process, and also to investigate its contribution employing more sophisticated chemistry. The results suggest that the contribution of glyoxal to SOA can be up to 15 % in Mexico City, but ranges from 0 to 4 % in Pasadena (CA) [10–12].

D.R. Gentner
Department of Civil and Environmental Engineering, University of California, Berkeley, CA, USA

A.H. Goldstein
Department of Civil and Environmental Engineering, University of California, Berkeley, CA, USA

Department of Environmental Science, Policy, and Management, University of California, Berkeley, CA, USA

W.B. Knighton
Montana State University, Bozeman, MT 59717, USA

A. Setyan • Q. Zhang
Department of Environmental Toxicology, University of California, Davis, CA, USA

H. Stark
Aerodyne Research, Inc., Billerica, MA, USA

CIRES, University of Colorado, Boulder, CO, USA

Here we show results of the implementation of the current state of knowledge on SOA formation from glyoxal into the regional chemistry transport model WRF/Chem and investigate its contribution to SOA on the regional scale. We made simulations over the Californian domain during the period of May 28th to June 15th 2010 to make use of the wealth of measurement data taken during the CARES/CalNex field campaigns to evaluate our model. A comparison of a simple surface uptake parameterization with a parameterization based on (volume) pathways based on laboratory evidence highlights the uncertainties currently associated with SOA formation from glyoxal. A comprehensive description of the work outlined here can be found in Knote et al. [8].

## 24.2 Methods

The chemistry transport model WRF/Chem [5] is used in version 3.4.1 with a grid resolution of 4 km and 40 vertical levels. We employ the Morrison double-moment scheme for cloud microphysics, RRTMG for short- and longwave radiation, the Noah land surface model, Mellor-Yamada Nakanishi and Niino 2.5 as planetary boundary layer scheme, and the Grell 3D ensemble for cumulus convection. NCEP Global Forecasting system (GFS) analyses are used as initial and boundary conditions for meteorology, and global MOZART-4 results for trace gases and aerosols. A combination of the US EPA National Emissions Inventory (NEI) 2005, the emission inventory of the California Air Resource Board (CARB) 2008, and inverse modeling results serves as the emissions input.

The MOZART mechanism to describe gas-phase chemistry [1] is used and has been extended for this work with a more explicit description of aromatics and isoprene oxidation, as well as the inclusion of $C_2H_2$ and HONO chemistry [8]. Aerosols are represented through the size-resolved Model for Simulating Interactions and Chemistry (MOSAIC, [13]) employing four size bins. The method described in Hodzic et al. [6], is used to describe traditional formation of SOA.

Different reversible and irreversible SOA formation pathways from glyoxal have been implemented. For reversible partitioning we first consider Henry's law partitioning between the gas-phase and the deliquesced aerosol including recent findings by Kampf et al. [7], who showed that the Henry's law constant of glyoxal can increase by up to three orders of magnitude in salt solutions. This is implemented as a time-dependent increase according to the current phase-state and salt concentration in aerosol water. We further include oligomer formation as a time-dependent equilibrium process involving glyoxal in aerosol water. Irreversible SOA formation from glyoxal can occur via three pathways. Two volume pathways use the amount of glyoxal that is partitioning into the deliquesced aerosol (see above): (1) an ammonium catalyzed pathway as described in Noziere et al. [9] as a function of the $NH_4^+$ ion concentration and particle pH, and (2) a reaction with OH as presented in Ervens and Volkamer [3]. Finally, we included a surface process with a fixed uptake coefficient ($\gamma = 1.0 \times 10^{-3}$). In the simulations with reversible partitioning and

volume pathways ("complex" mechanism), SOA formation only occurs if MOSAIC considers the aerosol to be deliquesced. This complex mechanism is contrasted with a simple parameterization that has been used in a previous global modeling study [4] that is based solely on the surface uptake. In this simple simulation the uptake does not depend on the aerosol phase-state and is always active.

## 24.3 Results

We found [8] the model is able to reasonably simulate meteorological conditions, the concentration levels of the main glyoxal precursor gases, aerosol amount and composition, and the major sinks for glyoxal (reaction with OH and photolysis). Two focus regions have been selected to investigate aggregated statistics on SOA formation from glyoxal: the Los Angeles Basin (LA) as a major urban area in California with high anthropogenic pollution, and the Eastern Slopes of the Central Valley (ESCV) as a clean region with high levels of isoprene. A budget analysis showed that in the LA basin formation from $C_2H_2$, aromatics and isoprene contribute with equal shares to glyoxal production, and that reaction with OH is a stronger sink (60 %) than photolysis (40 %). In the ESCV region isoprene oxidation is the main source of glyoxal (74 %), and destruction by photolysis is slightly more effective (54 %) than reaction with OH (46 %).

In all simulations we found that the LA basin is the hotspot for glyoxal SOA. The simple simulation, set up to resemble previous global and box model simulations, suggests that glyoxal contributes on average 15 % of SOA in the LA basin and 9.4 % in ESCV. In a simulation considering only reversible processing and the volume pathways we find 1.0 % in LA and 0.2 % in ESCV. If we add the (in this case aerosol phase-state dependent) surface uptake to the latter we get 5.5 % in LA and 1.7 % in ESCV. Hence, depending on the parameterization chosen, glyoxal can contribute substantially (15 % in LA using an always-active simple surface uptake) or be negligible (1 % in LA with only reversible partitioning and volume pathways).

We further found that the reason the volume/reversible pathways do not lead to larger contributions of glyoxal to SOA is not that the ($NH_4^+$-catalyzed/OH) reaction rates themselves are too slow, but rather that the supply of glyoxal to the aerosol liquid-phase is limiting. Kampf et al. [7], suggested a time-dependent increase in the glyoxal Henry's law constant, which we implemented into WRF/Chem. If we however assume that this increase is actually instantaneous, we find a contribution of glyoxal to SOA of 5.8 % in LA and 1.9 % in the ESCV region.

## 24.4 Conclusion

The formation of secondary organic aerosol from glyoxal has been investigated for the Californian domain during June 2010. The regional chemistry-transport model WRF/Chem has been extended for this purpose by a number of pathways to

describe this contribution, ranging from a simple surface uptake to explicit aerosol liquid-phase chemistry. This allows us to contrast between approaches taken in previous (global) modeling studies and those driven by evidence from laboratory experiments. The LA basin is always the hotspot for SOA formation from glyoxal. We find average contributions ranging from 1 to 15 % of SOA mass in the LA basin and 0.2 to 9.4 % in the Eastern slopes of the Central Valley. A parameterization based purely on laboratory evidence (reversible partitioning + volume pathways) is at the lower end of contributions, while the simple surface uptake method gives the largest values.

## References

1. Emmons LK, Walters S, Hess PG, Lamarque J-F, Pfister GG, Fillmore D, Granier C, Guenther A, Kinnison D, Laepple T, Orlando JJ, Tie X, Tyndall G, Wiedinmyer C, Baughcum SL, Kloster S (2010) Description and evaluation of the Model for Ozone and Related chemical Tracers, version 4 (MOZART-4). Geosci Model Dev 3:43–67
2. Ervens B, Turpin BJ, Weber RJ (2011) Secondary organic aerosol formation in cloud droplets and aqueous particles (aqSOA): a review of laboratory, field and model studies. Atmos Chem Phys 11:11069–11102
3. Ervens B, Volkamer R (2010) Glyoxal processing by aerosol multiphase chemistry: towards a kinetic modeling framework of secondary organic aerosol formation in aqueous particles. Atmos Chem Phys 10:8219–8244
4. Fu T-M, Jacob DJ, Wittrock F, Burrows JP, Vrekoussis M, Henze DK (2008) Global budgets of atmospheric glyoxal and methylglyoxal, and implications for formation of secondary organic aerosols. J Geophys Res-Atmos 113:D15303
5. Grell G, Peckham S, Schmitz R, McKeen S, Frost G, Skamarock W, Eder B (2005) Fully coupled online chemistry within the WRF model. Atmos Environ 39:6957–6975
6. Hodzic A, Jimenez JL (2011) Modeling anthropogenically controlled secondary organic aerosols in a megacity: a simplified framework for global and climate models. Geosci Model Dev 4:901–917
7. Kampf CJ, Waxman EM, Slowik JG, Dommen J, Pfaffenberger L, Praplan AP, Prevot ASH, Baltensperger U, Hoffmann T, Volkamer R (2013) Effective Henrys Law partitioning and the salting constant of glyoxal in aerosols containing sulfate. Environ Sci Technol 47:4236–4244
8. Knote C, Hodzic A, Jimenez JL, Volkamer R, Orlando JJ, Baidar S, Brioude J, Fast J, Gentner DR, Goldstein AH, Hayes PL, Knighton WB, Oetjen H, Setyan A, Stark H, Thalman R, Tyndall G, Washenfelder R, Waxman E, Zhang Q (2013) Simulation of semi-explicit mechanisms of SOA formation from glyoxal in a 3-D model. Atmos Chem Phys Discuss 13:26699–26759
9. Noziere B, Dziedzic P, Cordova A (2009) Products and kinetics of the liquid-phase reaction of glyoxal catalyzed by ammonium ions ($NH_4^+$). J Phys Chem A 113:231–237
10. Volkamer R, Martini FS, Molina LT, Salcedo D, Jimenez JL, Molina MJ (2007) A missing sink for gas-phase glyoxal in Mexico City: formation of secondary organic aerosol. Geophys Res Lett 34:L19807
11. Washenfelder R, Young C, Brown S, Angevine W, Atlas E, Blake D, Bon D, Cubison M, de Gouw J, Dusanter S, Flynn J, Gilman JB, Graus M, Griffith S, Grossberg N, Hayes PL, Jimenez JL, Kuster W, Lefer BL, Pollack I, Ryerson T, Stark H, Stevens PS, Trainer M (2010) The glyoxal budget and its contribution to organic aerosol for Los Angeles, California, during CalNex 2010. J Geophys Res 116:D00V02

12. Waxman EM, Dzepina K, Ervens B, Lee-Taylor J, Aumont B, Jimenez JL, Madronich S, Volkamer R (2013) Secondary organic aerosol formation from semi-and intermediate-volatility organic compounds and glyoxal: relevance of O/C as a tracer for aqueous multiphase chemistry. Geophys Res Lett 40:978–982
13. Zaveri R, Easter R, Fast J, Peters L (2008) Model for simulating aerosol interactions and chemistry (MOSAIC). J Geophys Res 113:D13204

## Questions from the Audience and Answers

**Q:** *In the detailed approach, did you consider dimer formation and oligomerization?*

**A:** Yes, di- and oligomer formation is considered as being in time-dependent equilibrium with the amount of glyoxal that partitions into aerosol liquid water (see [7, 8] for details).

**Q:** *How is your definition of "kinetic limitation" different from the traditional definition which may be important to be considered for coarse particles (sea salt in coastal regions) & winter conditions? (Note that the rate of gas to particle mass transport is proportional to temperature but anti-proportional to particle diameter)*

**A:** There has been a misunderstanding. The important parameter is the time-dependence of the partitioning. [7], suggest that there is a time delay in which the Henry's law increases to high values in the case of a salt solution. This is the reason for the low contributions of glyoxal to SOA through reversible partitioning/volume pathways. If we assume instantaneous Henry's law partitioning according to the Henry's law constant appropriate for the current salt concentrations, contributions to SOA from reversible partitioning/volume pathways are higher.

**Q:** *You consider the formation of oligomers in your model. These oligomers can be formed by photo-chemical reactions or by "dark" reactions. Do you consider these kinds of reactions in your chemical scheme?*

**A:** Oligomers are "formed" as being in time-dependent equilibrium (see question 1 and main text). What we consider a "dark" pathway are the findings of [9]. This is modeled as an irreversible SOA formation pathway (and is based on a study of non-irradiated bulk liquid samples), so it possibly includes oligomers formed by a dark reaction.

# Chapter 25
# Modeling Seasonal Changes in Organic Aerosol Composition at the puy de Dôme (France)

**Christelle Barbet, Laurent Deguillaume, and Nadine Chaumerliac**

**Abstract** In the atmosphere, a significant fraction of organic aerosol (OA) makes up the particulate matter. Since OA consists of thousands of complex molecules, uncertainties remain concerning their sources and atmospheric processes leading to their transformation (Hallquist M et al. Atmos Chem Phys 9:5155–5236, 2009). OA are, in principle, divided into two categories: primary organic aerosol (POA), which is emitted directly into the atmosphere, and secondary organic aerosol (SOA), which is formed by the photo-chemical oxidation of volatile organic compounds (VOC). VOC emissions and consequently OA formation are strongly linked to the season of the year. To that purpose, simulations were performed in autumn (September 2008) and summer (June 2010) with the WRF-CHEM model including more precisely RACM (Stockwell WR et al. J Geophys Res 102:25847–25879, 1997) chemical mechanism for gas phase associated with MADE for aerosols (Ackermann IJ et al. Atmos Environ 32(17):2981–2999, 1998) and VBS (Ahmadov et al. J Geophys Res 117:D06301, 2012) for SOA. Moreover, model outputs are compared with measurements performed during each season (Freney EJ et al. Atmos Chem Phys 11:13047–13059, 2011) at the puy de Dôme monitoring site which is located in central France (45°46 N 2°57 E) and is a part of the ACTRIS (Aerosols, Clouds, and Trace gases Research InfraStructure) and GAW (Global Atmospheric Watch) network.

## 25.1 Introduction

Atmospheric particles have negative effects on climate, air quality and human health. Organic aerosols represent a large fraction of the particulate mass at both urban and remote locations [15], but there are still large gaps in understanding their

C. Barbet (✉) • L. Deguillaume • N. Chaumerliac
LaMP, CNRS, Université Blaise Pascal, 24 Av. des Landais, BP 80026, 63171 Aubière, France
e-mail: C.Barbet@opgc.univ-bpclermont.fr; L.Deguillaume@opgc.univ-bpclermont.fr; N.Chaumerliac@opgc.univ-bpclermont.fr

D. Steyn and R. Mathur (eds.), *Air Pollution Modeling and its Application XXIII*, Springer Proceedings in Complexity, DOI 10.1007/978-3-319-04379-1_25,

formation pathways and there is considerable uncertainty in their representation in 3-D models [5, 14]. Despite the importance of organic aerosols (OA) in the environment, data sets to constrain models are limited. Nevertheless, based on available data sets it appears that models tend to underestimate SOA concentrations in the boundary layer (e.g., [7, 8, 12, 14]) as well as in the free troposphere [6]. The reasons for the differences between measured vs. modeled SOA in different regions remain unclear due to the numerous and complex chemical and physical phenomena involved in SOA formation [5, 11]. One major uncertainty relates to the formation of gaseous secondary organics. The aim of this study is to model organic aerosols using data available from the puy de Dôme station in France, where both aerosol and VOCs are monitored for two seasons and two air masses.

## 25.2 Model Description

WRF-chem model results from the coupling of the WRF model (Weather Research and Forecast) with a chemistry module. This coupling between dynamics, radiation and chemistry allows for simulating gases and aerosols. The chemical mechanism, RACM, includes 17 inorganic and 32 organic stable species, 28 reactive intermediates (4 inorganic and 24 organic species) for 237 reactions. In order to limit number of model groups, similar organic compounds are grouped together based on the principle of reactivity weighting. Aggregation factors, computed by Middleton et al. [10], are used for VOC. RACM chemical mechanism [13] is coupled with MADE-VBS [1, 2]. The dynamical processes include condensation, coagulation, size-dependent dry deposition and sedimentation, advection and diffusion. Particle formation is treated by two processes: direct particle emission and secondary formation by gas to particle conversion.

Anthropogenic emissions come from MACCity [9]. Biogenic emissions are provided by MEGAN [4]. Biomass burning emissions are derived from the Fire Inventory from NCAR version 1.0 (FINNv1).

## 25.3 Model Comparisons with Observations at the puy de Dôme

Detailed investigations of the chemical and microphysical properties of atmospheric aerosol particles were performed at the puy de Dôme research station (1,465 m) in autumn (September 2008) and in summer (June 2010) using a compact Time-of-Flight Aerosol Mass Spectrometer [3]. This data set is used together with VOCs measurements available solely on the June 2010 case.

The simulations last 5 days and two nested domains are defined over Europe and France respectively with a resolution of 30 and 10 km for the inner domain.

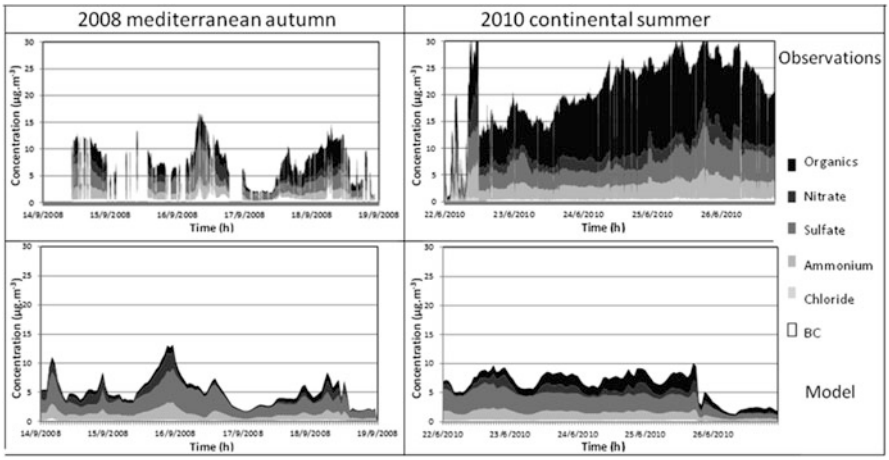


**Fig. 25.1** Comparisons between model outputs and observations at the puy de Dôme site

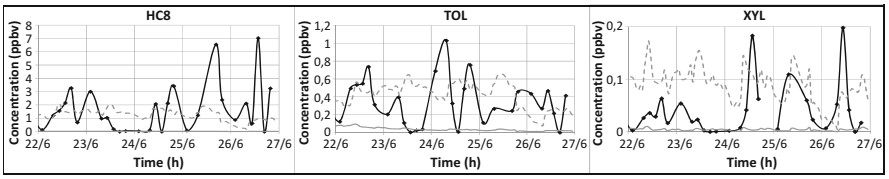


**Fig. 25.2** Results of a sensitivity test on anthropogenic VOCs emissions

Figure 25.1 provides a sample of comparisons between AMS data and model outputs for aerosol concentrations for the two seasons. The model captures the variability of the concentrations induced by the diurnal cycle and topographic forcing but underestimates organic aerosol especially for the second case.

For the 2010 polluted summer event, VOCs concentrations observed at the puy de Dôme are well reproduced by the model when they originate from biogenic emissions but are not correctly simulated in case of anthropogenic VOCs such as alkanes with high OH reactivity, toluene and xylene.

In Fig. 25.2, concentrations of alkanes are reported together with the observations (in black) in the base run (in grey full line) and in a run where their emissions have been increased by a factor 50 (in grey with dotted line). Also, toluene and xylene are multiplied by a factor 10 to fit to the observations.

A new simulation is performed in these conditions and increasing the VOCs concentrations provide much higher SOA which seems more realistic when comparing to the data (Fig. 25.3).

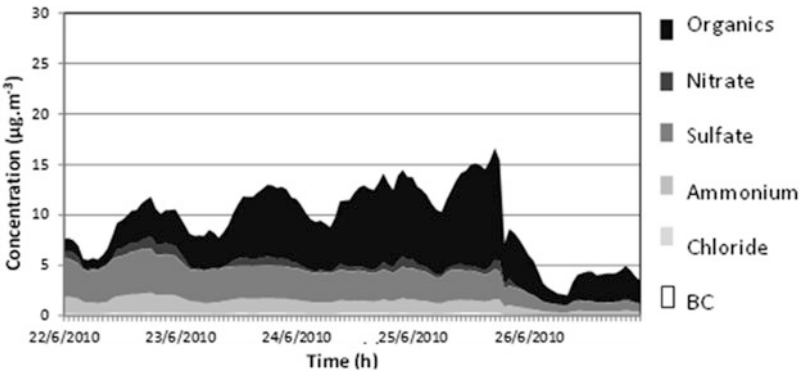


**Fig. 25.3** SOA concentrations simulated assuming higher anthropogenic VOCs emissions

## 25.4 Conclusion

Data from the puy de Dôme station in France have been used to validate SOA formation mechanism used in WRFCHEM, based on VBS scheme from Ahmadov et al. [2]. Results show that SOA are underestimated by the model in case of polluted air mass in summer partly due to too low anthropogenic VOCs emissions.

## References

1. Ackermann IJ, Hass H, Memmesheimer M, Ebel A, Binkowski FS, Shankar U (1998) Modal aerosol dynamics model for Europe: development and first applications. Atmos Environ 32(17):2981–2999
2. Ahmadov R et al (2012) A volatility basis set model for summertime secondary organic aerosols over the eastern United States in 2006. J Geophys Res 117:D06301
3. Freney EJ et al (2011) Seasonal variations in aerosol particle composition at the puy-de-Dôme research station in France. Atmos Chem Phys 11:13047–13059
4. Guenther A, Karl T, Harley P, Wiedinmyer C, Palmer PI, Geron C (2006) Estimates of global terrestrial isoprene emissions using MEGAN (Model of Emissions of Gases and Aerosols from Nature). Atmos Chem Phys 6:3181–3210
5. Hallquist M et al (2009) The formation, properties and impact of secondary organic aerosol: current and emerging issues. Atmos Chem Phys 9:5155–5236
6. Heald CL, Jacob DJ, Park RJ, Russell LM, Huebert BJ, Seinfeld JH, Liao H, Weber RJ (2005) A large organic aerosol source in the free troposphere missing from current models. Geophys Res Lett 32:L18809
7. Johnson D, Utembe SR, Jenkin ME (2006) Simulating the detailed chemical composition of secondary organic aerosol formed on a regional scale during the TORCH 2003 campaign in the southern UK. Atmos Chem Phys 6:419–431
8. Kleinman LI et al (2008) The time evolution of aerosol composition over the Mexico City plateau. Atmos Chem Phys 8:1559–1575
9. Lamarque JF et al (2010) Historical (1850–2000) gridded anthropogenic and biomass burning emissions of reactive gases and aerosols: methodology and application. Atmos Chem Phys 10:7017–7039

10. Middleton P, Stockwell WR, Carter WPL (1990) Aggregation and analysis of volatile organic compound emissions for regional modeling. Atmos Environ 24A:1107–1113
11. Pankow JF, Barsanti KC (2009) The carbon number-polarity grid: a means to manage the complexity of the mix of organic compounds when modeling atmospheric organic particulate matter. Atmos Environ 43:2829–2835
12. Simpson D et al (2007) Modeling carbonaceous aerosol over Europe: analysis of the CARBOSOL and EMEP EC/OC campaigns. J Geophys Res 112:D23S14
13. Stockwell WR, Middleton P, Chang JS, Tang X (1997) A new mechanism for regional atmospheric chemistry modeling. J Geophys Res 102:25847–25879
14. Volkamer R, Jimenez JL, San Martini F, Dzepina K, Zhang Q, Salcedo D, Molina LT, Worsnop DR, Molina MJ (2006) Secondary organic aerosol formation from anthropogenic air pollution: rapid and higher than expected. Geophys Res Lett 33:L17811
15. Zhang Q et al (2007) Ubiquity and dominance of oxygenated species in organic aerosols in anthropogenically-influenced Northern Hemisphere midlatitudes. Geophys Res Lett 34:L13801

# Chapter 26
# Using WRF-CMAQ Air Quality Modelling System to Estimate BaP Concentrations over Zaragoza (Spain)

**Roberto San José, Juan Luis Pérez, Marisol Callen, José Manuel López, and Ana Mastral**

**Abstract** The main aim is to estimate the BaP concentrations in the atmosphere and know the main influences on BaP ground level concentrations. We have utilized CMAQ 4.7 version as core for our system. BaP degradation and adsorption mechanism have been integrated into the chemical-transport model. Emissions have been processed the EMIMO-UPM emission model with a top-down approach including detailed GIS data. The air quality model has been driven by the WRF meteorological model. Urban particulate material generally contains a significant amount of amorphous organic carbon. Absorptive mechanism plays the dominant role in the urban air and also in air affected by urban sources. Equilibrium partitioning calculations are based on absorptive partitioning model. Gas/particle partitioning of BaP is simulated as an absorption process into the organic mass on the aerosol particle assuming the formation of a quasi-ideal solution. BaP reaction with ozone is an important degradation pathway of the particulate BaP in the atmosphere. The degradation rate constant depends on the ozone gas to surface equilibrium constant and the maximum rate coefficient that would be observed at high ozone concentrations. A validation process of the BaP and other pollutant results has been conducted in the urban area of Zaragoza (Spain) during 10 weeks in 2010. The agreement is generally satisfactory. The simulated concentrations depend on the meteorological and emission inputs.

R. San José (✉) • J.L. Pérez
Technical University of Madrid (UPM), Boadilla del Monte, 28660 Madrid, Spain
e-mail: roberto@fi.upm.es

M. Callen • J.M. López • A. Mastral
Instituto de Carboquímica (ICB-CSIC), c/Miguel Luesma Castán, 4, 50018 Zaragoza, Spain

D. Steyn and R. Mathur (eds.), *Air Pollution Modeling and its Application XXIII*,
Springer Proceedings in Complexity, DOI 10.1007/978-3-319-04379-1_26,

## 26.1 Introduction

Benzo(a)pyrene (BaP) is polycyclic aromatic hydrocarbon whose adverse effects on human health have been demonstrated [1]. Because of this reason, the Directive 2004/107/CE of the European Union establishes a target value of 1 ng/m$^3$ of BaP in the atmosphere.

Accurate calculation of gas/particle partitioning on a regional/local scale re-quires information about the spatially and temporally resolved physical characteristics and chemical compositions of atmospheric aerosols. To simulate adequately the processes that determine the transport, degradation and deposition of BaP and other PAHs, it is essential to have a chemical transport model that represents the state of the art in atmospheric modelling as well as in aerosol chemistry and dynamics. In this paper, the BaP concentrations in the atmosphere have also been estimated by using last generation of air quality dispersion models, a 3D Eulerian regional model, with the inclusion of the transport, scavenging and deposition processes for the BaP. The modifications of the model with the inclusion of the new specie and related mechanisms are fully described including some parameters used.

## 26.2 BaP Extension

We used the Community Multiscale Air Quality (CMAQ) model of the US-EPA [2, 3]. It can be conveniently linked to the mesoscale meteorological model Weather & Research Forecasting system (WRF) developed by NCAR and others [5], which is used here to calculate the meteorological input fields so CMAQ model is driven by WRF meteorological model with 1 h temporal resolution. WRF model can be directly linked to CMAQ via a Meteorological Chemistry Interface Preprocessors (MCIP). The purpose of this study is to add modules to simulate BaP with the CMAQ model version 4.7.1 (June 2010).

In this contribution, an extension to CMAQ (CMAQ-BaP) is presented. We use the new extended version of CMAQ (CMAQ-BaP) developed by us to investigate BaP spatial and temporal distribution over Iberian Peninsula and Zaragoza area. The basic version of CMAQ is modified to read emissions and to simulate the transport, scavenging, and deposition of BaP. CMAQ wet deposition includes rainout and washout from convective precipitation and scavenging. Two new BaP species have been added, aerosol (BAP) and gas (SV_BAP). BaP in the gas-phase primarily react with OH although, the representative lifetime with respect to reaction with OH is higher than BaP in the particulate-phase, so the BaP in gas phase is treated as inert gas (no chemical reactions). BaP is emitted in particle phase. Deposition and scavenging of the aerosol BaP is the same parameterizations as for CMAQ organic aerosols. Deposition velocity of BaP gas is the same as the semi-volatile alkanes that is calculated by CMAQ. We added new developments to simulate gas phase and

organic carbon (OC)-bound particulate transport and chemistry. The BaP extension to CMAQ calculates the partition of the compound between the gas and the particle phase. An OC absorption model is implemented to model gas-particle partitioning of BaP based on the absorptive partitioning model of Pankow [7] and Odum et al. [6]). We incorporate also BaP loss due to oxidation by Ozone ($O_3$) with a first order reaction. Reaction with ozone can be an important degradation pathway for the particulate BaP in the atmosphere. Degradation of the aerosol BaP by the Ozone has been implemented into CMAQ based on Kwamena et al. [4].

## 26.3 Results and Conclusion

The simulation is developed with a nesting approach, the mother domain cover the Iberian Peninsula with 27 km. resolution and the three nesting domains have been setup centred over Zaragoza city. First nesting level is 9 km. resolution, second 3 km and finally 1 km. resolution. We use 15 vertical terrain following levels up to 100 hPa.

Model runs for 12 weeks (11 weeks from 2010 and 1 from 2011) corresponding to the field campaign. The measurement data are used to examine the model results under very different meteorological conditions. These 12 weeks are representative for a year simulation. To evaluate the atmospheric concentrations calculated with the new CMAQ-BaP extension, modelled values are compared to observation. BaP modelled concentrations for the monitoring location was then compared to the actual daily mean measurements (Fig. 26.1). The CMAQ-BaP model shows mean concentration of 0.10 (ng/m$^3$) and measurement is 0.09 (ng/m$^3$), so good results are obtained because model and measurement values are quite close.

The agreement is generally satisfactory, the best results are observed in winter period, which is the most important for the BaP concentrations. The model

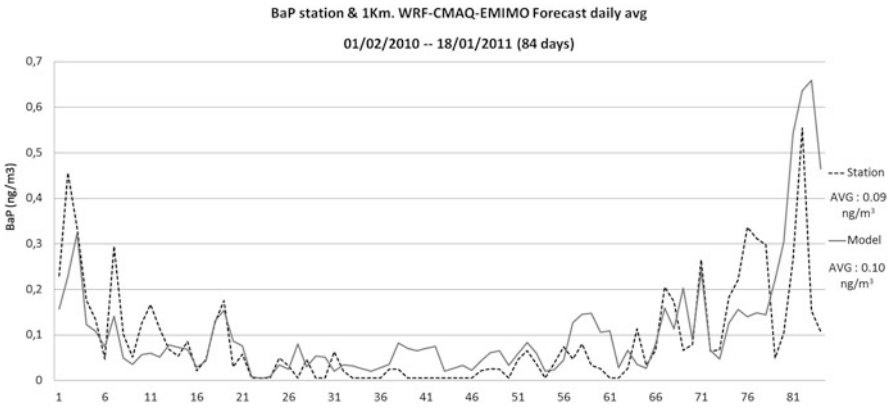


**Fig. 26.1** Comparison BaP model 1 km. resolution (*solid line*) and BaP monitoring station

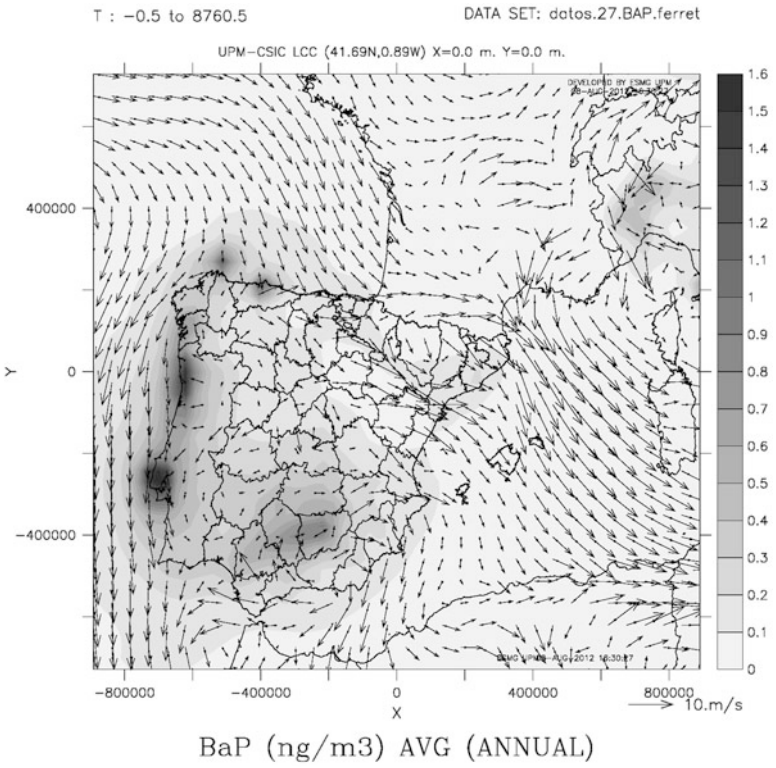


**Fig. 26.2** BaP surface results, temporal average. over Iberian Peninsula with wind vectors

validation shows the BaP extension performance is correct over the modelled area. The BaP concentrations agree well with the observations, particularly very high BaP peaks are resolved by the extended model. The modelling system reproduces the degree of seasonality of the BaP, with higher concentrations in the winter months.

Now we can see in (Fig. 26.2) the BaP spatial surface results over Iberian Peninsula (27 km. resolution). The data are average of the 12 weeks simulated. The simulation shows the BaP hot spots over Iberian Peninsula.

We have added the ability to simulate the atmospheric behaviour of BaP to CMAQ model. This includes the addition of two processes: gas/particle partitioning and degradation by ozone. Other aspects such as transport and diffusion are developed using de CMAQ framework. Also the CMAQ aerosol module provides the necessary aerosol parameters to the gas/particle partitioning model. WRF-CMAQ modelling system, which has been extended to simulate BaP concentrations, can be used to get the spatial and temporal distribution of BaP concentrations across large areas domain and to also assess the impact of different emissions reduction strategies. The evaluation results in this paper suggest that the new CMAQ-BaP

is able to simulate fairly well the ambient air concentrations of BaP. For further verification of the model performance, long-term runs will be carried out and more measurement points will be used.

**Acknowledgments** Authors would like to thank Aula Dei-CSIC (R. Gracia), the Ministry of Science and Innovation (MICIIN) and the E plan for supporting the project CGL2009-14113-C02-01. J.M. López would also like to thank the MICIIN for his Ramón y Cajal contract. Also to thank Departamento de Medio Ambiente del Gobierno de Aragón, Dirección General del Catastro del Gobierno de Aragón, Sistema de Información Territorial del Gobierno de Aragón and Ayuntamiento de Zaragoza. Authors thankfully acknowledge the computer resources, technical expertise and assistance provided by the Centro de Supercomputación y Visualización de Madrid (CeSVIMa) and the Spanish Supercomputing Network (BSC).

## References

1. Boström CE, Gerde P, Hanberg A, Jernström B, Johansson C, Kyrklund T, Rannug A, Törnqvist M, Victorin K, Westerholm R (2002) Cancer risk assessment, indicators and guidelines for polycyclic aromatic hydrocarbons in the ambient air. Environ Health Perspect 110:451–488
2. Byun D, Ching J (1999) Science algorithms of the EPA Models-3 Community Multiscale Air Quality (CMAQ) Modeling System EPA/600/R-99/030. Office of Research and Development, United States Environment Protection Agency, Washington, DC
3. Byun D, Schere K (2006) Review of the governing equations, computational algorithms, and other components of the models-3 Community Multiscale Air Quality (CMAQ) modeling system. Appl Mech Rev 59:51–77
4. Kwamena N, Thornton J, Abbatt J (2004) Kinetics of surface-bound benzo[a]pyrene and ozone on solid organic and salt aerosols. J Phys Chem A 108(52):11626–11634
5. Michalakes J, Chen S, Dudhia J, Hart L, Klemp J, Middlecoff J, Skamarock W (2001) Development of a next generation regional weather research and forecast model. Developments in teracomputing. In: Zwieflhofer W, Kreitz N (eds) Proceedings of the ninth ECMWF workshop on the use of high performance computing in meteorology. World Scientific, Singapore
6. Odum JR, Hoffmann T, Bowman F, Collins D, Flagan RC, Seinfeld JH (1996) Gas/particle partitioning and secondary organic aerosol yields. Environ Sci Technol 30:2580–2585
7. Pankow JF (1994) An absorption model of gas-particle partitioning of organic compounds in the atmosphere. Atmos Environ 28:185–188

# Chapter 27
# The POAEMM Project: Prediction of Spatial and Temporal Variation of Marine Aerosols in Coastal Area

**Gilles Tedeschi, J. Piazzola, L. Gardenal, V. Pourret, and M. Martet**

**Abstract** The POAEMM project consists of developing a tool for predicting the spatial and temporal variation of aerosols particles in a marine coastal environment. This is achieved by coupling the MEDEX parametric model (MIO) and the fine mesh meteorological model AROME developed by Meteo France. The first step has been to do the semi-automation of the MIO experimental station. Based on semi-empirical formulations, MEDEX is then revised in order to take better account of oceanographic and meteorological conditions.

## 27.1 Introduction

In coastal areas, the presence of the shoreline modifies the wave and wind fields. As the marine aerosol concentration depends both on the local production (correlated to wave breaking) and on the atmospheric transport (correlated to wind), strong heterogeneities may appear in the horizontal aerosol concentration. The POAEMM project aims to improve the prediction of such concentrations. This will be done

G. Tedeschi (✉) • J. Piazzola
CNRS/INSU, IRD, Mediterranean Institute of Oceanography (MIO), Toulon University, UM 110, 83957 La Garde, France

CNRS/INSU, IRD, Mediterranean Institute of Oceanography (MIO), Aix Marseille University, UM 110, 13288 Marseille, France
e-mail: tedeschi@univ-tln.fr

L. Gardenal
CS Système d'information, 230 rue Marcellin Berthelot, 83079 Toulon Cedex 9, France

V. Pourret • M. Martet
Meteo-France, DP/SERV/BEC, 42 av. G. Coriolis, 31057 Toulouse Cedex, France

D. Steyn and R. Mathur (eds.), *Air Pollution Modeling and its Application XXIII*,
Springer Proceedings in Complexity, DOI 10.1007/978-3-319-04379-1_27,

by coupling the parametric model MEDEX to a meteorological model and by improving MEDEX with the help of hundreds hours of measurements according to the semi-automation of the MIO experimental station of Porquerolles island.

## 27.2 Porquerolles Island Experimental Station

The MIO experimental station is located at the Westside of Porquerolles Island, near Toulon on the French Mediterranean coast (see Fig. 27.1). It allows measurements for specific meteorological conditions: winds blowing from Westerly to Northerly directions. In such conditions, the fetch is considered either 25 km long (NW winds) or infinite as defined by the criterion applied for fully developed sea conditions (W to SW winds), *i.e.,* more than 100 km for our simulations. Such a location allows working with a full set of probes in a marine environment protected from direct anthropogenic pollution (national park), but without chartering a (expensive) ship. On the other hand, until a few months ago, a daily human presence was required to operate the probes, collect data and fill the power generator tank (no energy supply from the network is available). The operator had to stay at the station the whole day, as the time needed to travel from the laboratory to the station (car + boat + car on a ground path) is about 2 h. Due to this inconvenience, the use of the station was limited to a few days per year.

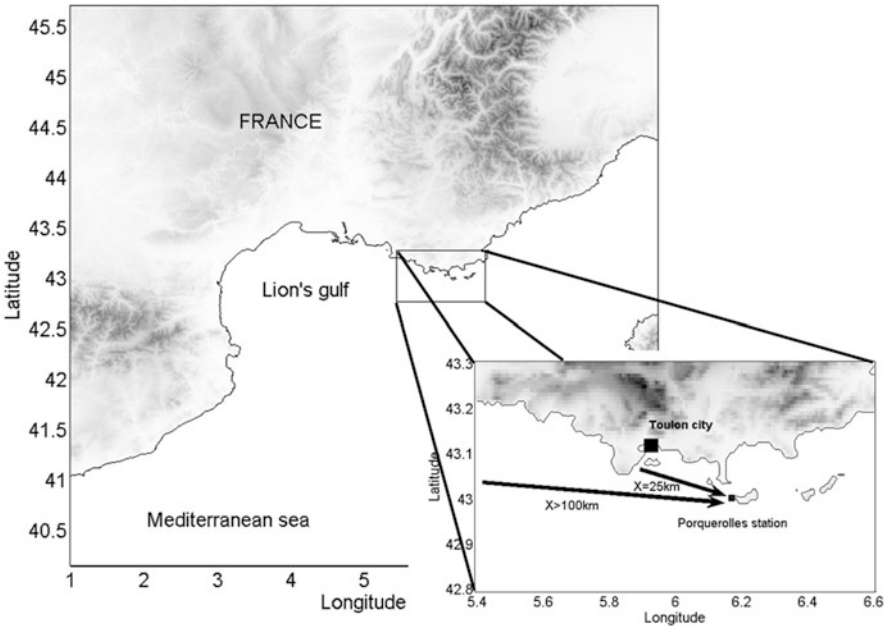


**Fig. 27.1** Porquerolles Island station on the French Mediterranean coast

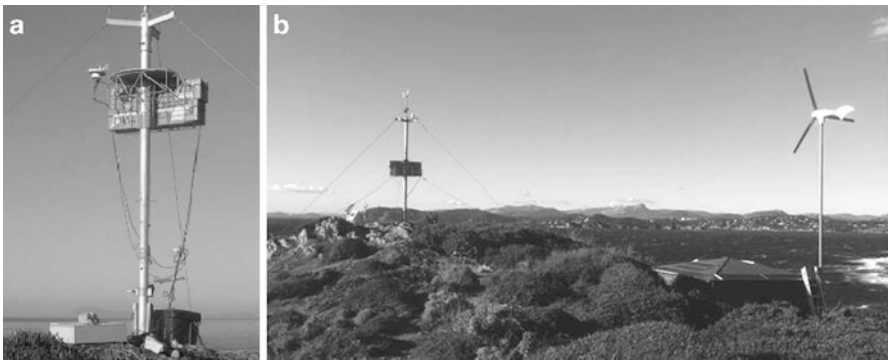


**Fig. 27.2** (**a**) PMS probes. (**b**) The station with solar panels and wind mill

The station is equipped with aerosol optical counters (PMS) to measure size distributions: the CSASP-200 (TNO laboratory, The Hague, NL) for particles diameters from 0.21 to 18.5 μm and the CSASP-100HV-ER (MIO laboratory) from 1.5 to 92 μm. The probes are mounted on a mast at 20 m above sea level (Fig. 27.2a). Meteorological data are collected at the same time: wind speed and direction, pressure, relative humidity, temperature. The optical depth is measured with a CIMEL CE 318, connected to the Aeronet network.

For a few months, the station has been equipped with solar panels (500 W), a wind mill (600 W), batteries and an inverter to reach a full energy autonomy (Fig. 27.2b). Moreover, a GSM link allows the probes to be remotely switched on (during meteorological situations of interest) or off (if not) in order to manage and save energy. The GSM link also allows recovering measured data.

## 27.3 Modelling of the Horizontal Aerosol Concentration Distribution

The marine aerosol concentration at a given location is calculated with the parametric model MEDEX [2]. The particle size distribution dN/dr is calculated as the sum of modified lognormal functions:

$$\frac{dN}{dr}(r) = \sum_{m=1}^{4} \frac{A_m}{f} . e^{-C_m \ln^2\left(\frac{r}{f.r0_m}\right)} \tag{27.1}$$

where the coefficients $A_m$ and $C_m$ of the various modes $r_0$ are parameterized as a function of wind speed and fetch, and $f$ is the growth factor accounting for relative humidity. The wind speed and the fetch are supposed to be correlated to the wave breaking and the aerosol production, as well as the particles transport over the sea.

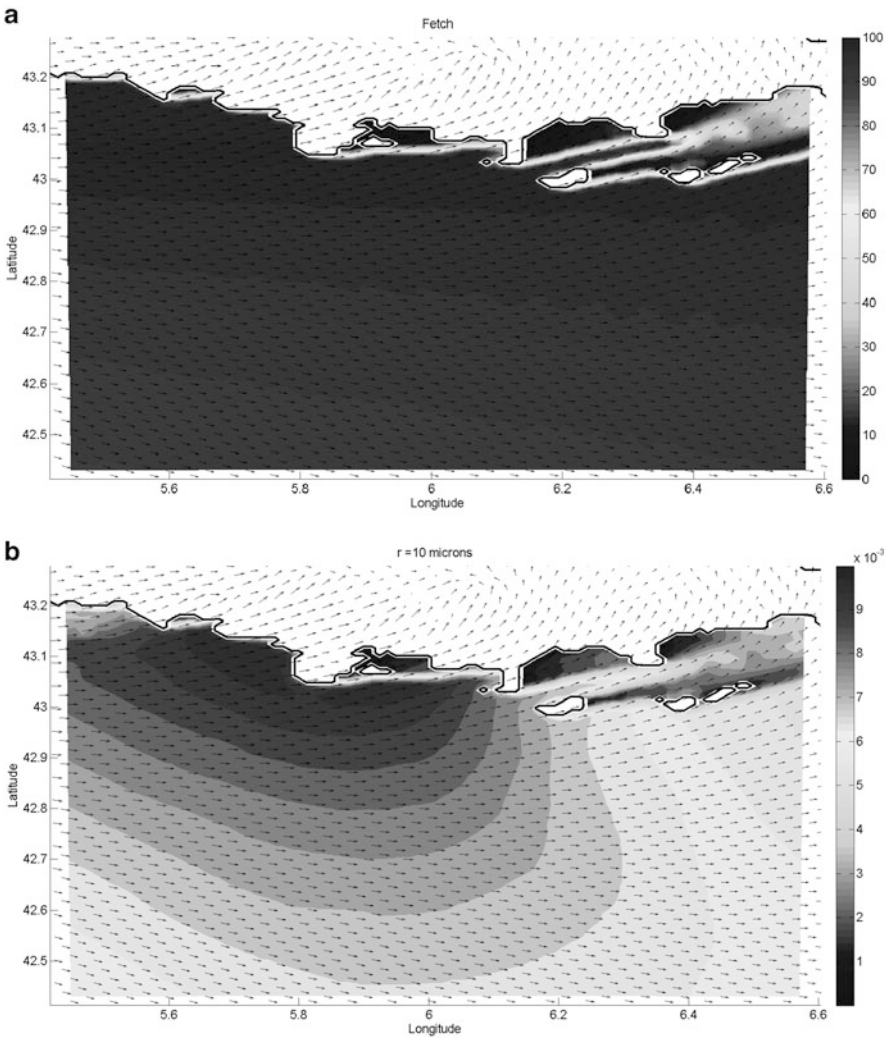


**Fig. 27.3** (**a**) Calculated fetch (km). (**b**) Aerosol concentration at 10 m ASL, $r = 10\ \mu m$

The parametric model is coupled with a meteorological model: RAMS with a 1 km grid mesh (for a research application) or AROME (Meteo France) with a 2.5 km grid mesh (for an operational aim). For each grid cell, the fetch is calculated going upwind along the stream line. When the shoreline is reached or when the wind vector is significantly different from the original cell one (and thus thought to be no more representative of its sea state), the distance calculated over the sea is taken as the fetch. An example of the fetch map and the horizontal aerosol concentration distribution is shown on Fig. 27.3a, b, for a 1 km mesh.

## 27.4 One Year Experimental Campaign

The experimental campaign using the new station configuration began on Nov. 2012 and will end on Nov. 2013. Meteo France provides a prediction of the meteorological field with AROME and an estimate of aerosol concentration and origin (marine or anthropogenic) at the station with the MOCAGE model [1]. If the environmental conditions are of interest (quite steady NW to SW wind, mainly marine aerosols), concentration measurements are recorded during several hours. At present time (June 2013), data have been recorded during 300 h and will be used to improve MEDEX model. An example of comparison between modelled and measured aerosol concentrations is shown on Fig. 27.4a ($U_{10} = 10$ m/s) and Fig. 27.4b ($U_{10} = 6$ m/s).

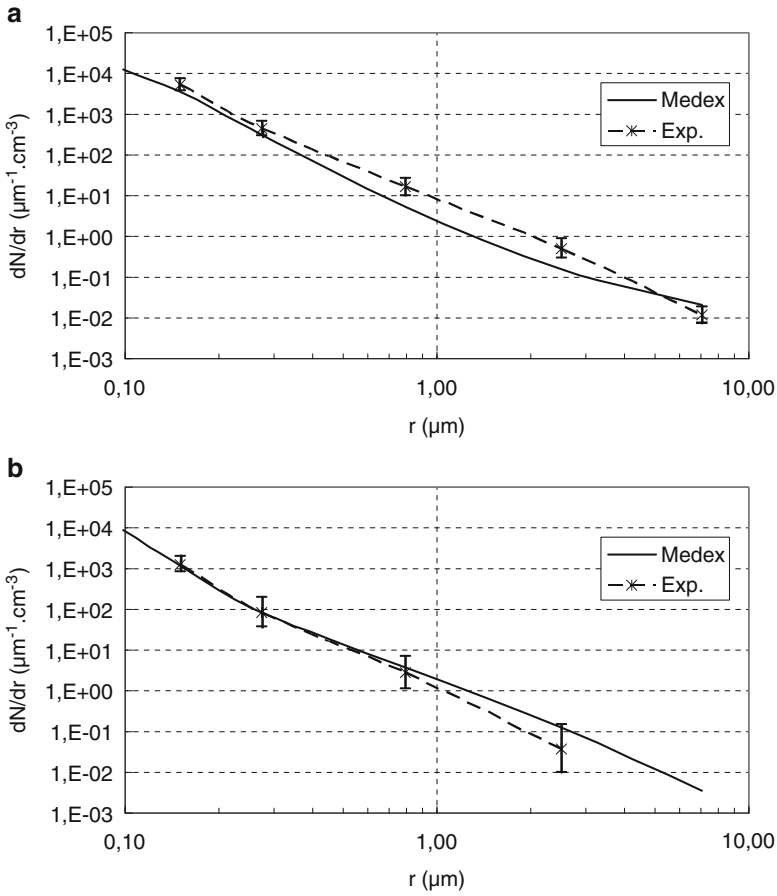


**Fig. 27.4** (**a**) Aerosol concentration, 29/11/12. (**b**) Aerosol concentration, 11/12/12

**Acknowledgment** The authors wish to thank the French DGA and ANR for the support to this study (contract n° ANR-11-ASTR-008-02).

## References

1. Martet M, Peuch VH, Laurent B, Marticorena B, Bergametti G (2009) Evaluation of long-range transport and deposition of desert dust with the CTM MOCAGE. Tellus 61B:449–463
2. Piazzola J, Bouchara F, Van Eijk AMJ, de Leeuw G (2003) Development of the Mediterranean extinction code MEDEX. Opt Eng 42(4):912–924

# Chapter 28
# An Integrated Weather and Sea State Forecasting System for the Arabian Peninsula (WASSF)

**Jumaan Al Qahtani, Elyas Alaa, George Kallos, George Galanis, Sarantis Sofianos, Christina Mitsakou, Chris Spyrou, Christina Kalogeri, Nikolaos Bartsotas, John Athanaselis, Vassilios Vervatis, Stavros Solomos, Panagiotis Axaopoulos, Daniel W. Beard, and Ioannis Alexiou**

**Abstract** Saudi Aramco is the oil industry of the Kingdom of Saudi Arabia with several activities related to the environment. In order to optimize daily operations and minimize environmental risks a forecasting system has been employed and setup in operations. The objectives of the system include prevention and mitigation of environmental problems, as well as early warning of local conditions associated with extreme weather events. The management and operations part is related to early warning of weather and dust storms that affect operations of various facilities, whereas the environmental part is mainly focused on air quality and desert dust levels in the atmosphere.

## 28.1 System Overview

The operational components of the integrated system include: (i) a weather and desert dust prediction system with a forecasting horizon of 5 days, (ii) a wave analysis and prediction component for Red Sea and Arabian Gulf, (iii) an ocean circulation, tidal analysis and prediction of both Red Sea and Arabian Gulf and (iv) an aviation part specializing in the vertical structure of the atmosphere

J. Al Qahtani (✉) • E. Alaa • D.W. Beard • I. Alexiou
Environmental Protection Department, Saudi Aramco, Dhahran, Saudi Arabia
e-mail: jqahtani@yahoo.com

G. Kallos • G. Galanis • C. Mitsakou • C. Spyrou • C. Kalogeri • N. Bartsotas
J. Athanaselis • S. Solomos
Faculty of Physics, Atmospheric Modeling and Weather Forecasting Group,
University of Athens, Athens, Greece
e-mail: kallos@mg.uoa.gr; http://forecast.uoa.gr

S. Sofianos • V. Vervatis • P. Axaopoulos
Faculty of Physics, Ocean Physics and Modeling Group, University of Athens, Athens, Greece

D. Steyn and R. Mathur (eds.), *Air Pollution Modeling and its Application XXIII*,
Springer Proceedings in Complexity, DOI 10.1007/978-3-319-04379-1_28,


**Fig. 28.1** WASSF overview

and extreme events that affect air transport and other operations. A graphical representation of the system's current structure is summarized in Fig. 28.1.

The parts under development are related to aerosol characterization and study of fog formation mechanisms. In situ dust sampling and laboratory spectral and chemical characterization will be done to determine the pollution level associated with dust particles and specific dust events (such as Al-Shamal winds). The synergetic use of modeling and sampling allows for a complete assessment of the dust quality and origin in the area of interest, which is among the most important (globally) hot spots of photochemical smog and particulate matter levels, as indicated by satellite measurements. The correlation between dust events and dust composition will contribute to developing a source apportionment of particular pollution signatures.

## 28.2 Atmospheric Model

The core of the WASSF suite is SKIRON, the modeling system developed at the University of Athens from the AM&WFG [1]. SKIRON is appropriately modified to capture the key processes that dominate the region (desert meteorology) and was recently updated with a brand new desert classification scheme that consists of seven discrete categories, which further assist in the accurate estimation of dust uptake areas.

The model runs twice daily at a horizontal resolution of $0.033° \times 0.033°$ with a forecast horizon that stretches to 5 days and outputs include a full list of meteorological as well as dust related parameters (Fig. 28.2). Visibility maps and meteograms

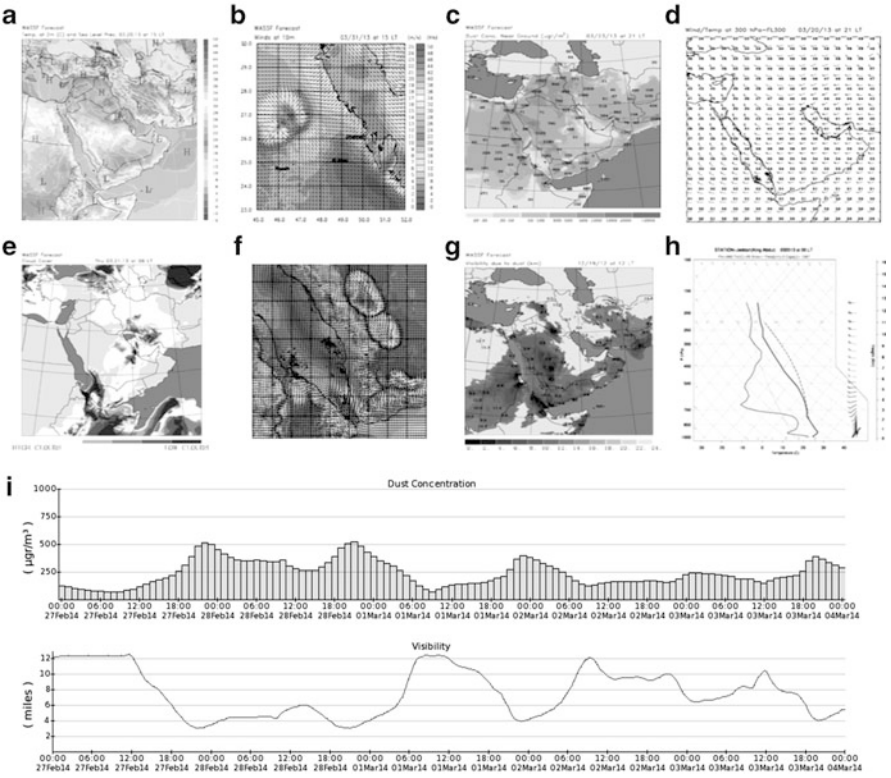


**Fig. 28.2** Atmospheric model outputs: (**a**) temperature at 2 m (°C) (**b**) East coast – wind at 10 m (m/s) (**c**) dust concentration near ground ($\mu gr/m^3$) (**d**) Aviation maps – wind and temperature at FL300 (m/s) (**e**) cloud coverage (%) (**f**) Red Sea – wind at 10 m (m/s) (**g**) visibility due to dust (km) (**h**) airport skew-T diagram (**i**) dustgrams – dust concentration ($\mu gr/m^3$) and visibility (miles)

are produced through a new parametrization that takes into consideration the role of dust levels, relative humidity and precipitation. Specialized data sets required for on/offshore operations are also provided on a regular basis.

The SKIRON forecasts serve as the driving force for both wave and ocean circulation models.

## 28.3 Marine Components

The wave forecasts are based on the latest version of the WAM model – ECMWF parallel version, cycle 33R1, which is used by a number of operational and research centers worldwide (ECMWF, UK Met Office, US Navy) [2]. The version adopted

includes a new advection scheme that provides a more uniform propagation in all directions as well as a novel shallow water scheme providing new potential for near-shore behavior, something essential for the area under study. MICOM (Miami Isopycnic Coordinate Ocean Model) is a primitive equation ocean model that has its vertical discretization in layers of constant potential density. The vertical grid consists of seven isopycnal layers. The ocean circulation model is combined with a barotropic tidal prediction based on a global model of ocean tides. The model combines inverse methods and hydrodynamics to compute and predict tidal elevation and tidal currents.

## 28.4 Additional Products

Special focus has been given to provide a user friendly platform, that will assist company employees in their everyday planning. The homepage presents current weather conditions, an hour-by-hour forecast, a 5-day overview with weather icons and automated text reports. METAR/TAF reports from airports across KSA and neighboring countries alongside station data from Saudi Aramco's AMMNET network are imported in a MySQL database. Web display on Google Maps features weather icons for a quick overview and info bubbles that activate on mouseover. An interactive forecast section allows the user to select the place of interest by entering either a location name, a set of coordinates, or by dragging a map marker. Satellite images are offered through EUMETSAT and INSAT (Fig. 28.3).

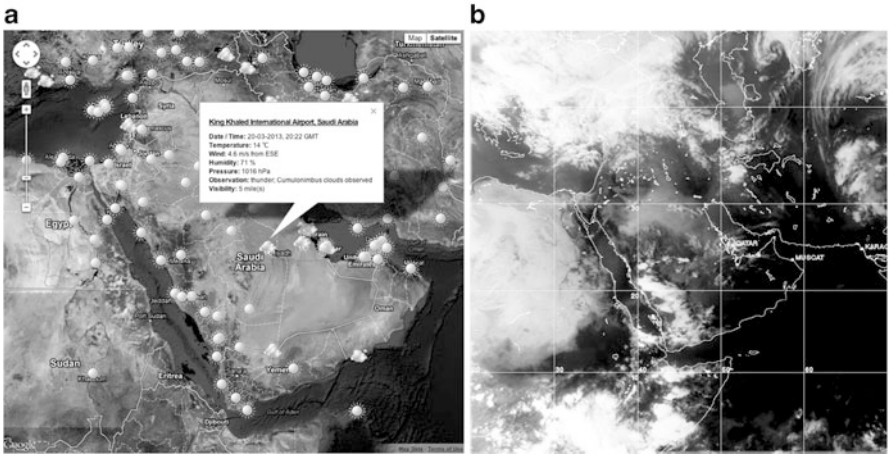


**Fig. 28.3** (**a**) Web display of hourly collected METAR reports and (**b**) satellite imagery from INSAT

## 28.5 Concluding Remarks

WASSF is an integrated weather suite for the Arabian Peninsula. It provides specialized environmental products for industrial operations along with sufficient warnings for various extreme environmental conditions. Aerosol characterization and fog formation are the two most recent parts of its ongoing evolving process.

**Acknowledgments** This work was supported by the Environmental Protection Department of Saudi Aramco.

## References

1. Spyrou C, Mitsakou C, Kallos G, Louka P, Vlastou G (2010) An improved limited area model for describing the dust cycle in the atmosphere. J Geophys Res 115:D17211. doi:10.1029/2009JD013682
2. Hasselmann S, Hasselmann K, Bauer E, Bertotti L, Cardone CV, Ewing JA, Greenwood JA, Guillaume A, Janssen P, Komen G, Lionello P, Reistad M, Zambresky L (1988) The WAM model – a third generation ocean wave prediction model. J Phys Oceanogr 18(12):1775–1810

# Chapter 29
# Modelling Past and Future Changes in Secondary Inorganic Aerosol Concentrations in the UK

**Riinu Ots, Anthony Dore, Y. Sim Tang, Christine F. Braban, Massimo Vieno, and Mark Sutton**

**Abstract** The FRAME (Fine Resolution Atmospheric Multi-pollutant Exchange) model is a Lagrangian atmospheric transport model with a horizontal grid resolution of $5 \times 5$ km$^2$. This work uses FRAME to calculate annual average concentrations of three secondary inorganic aerosol species ($NH_4^+$, $NO_3^-$, $SO_4^{2-}$) and gas phase $SO_2$ over the United Kingdom for the years 2000–2010. Modelled concentrations are compared to measurements from 12 monitoring sites which are operated with the UK Eutrophying and Acidifying Air Pollutants (UKEAP) Acid Gases and Aerosols Network (AGANet). The results showed good spatial correlation between measurements of gas and aerosol concentrations and modelled values ($R^2 > 0.8$). However FRAME underestimated decreases in sulphate and ammonium aerosol concentrations over the 11-year period and overestimated changes in $SO_2$ concentrations relative to measurements. Ongoing work to investigate temporal changes in atmospheric oxidation rates should clarify this difference. FRAME showed a more modest reduction in nitrate concentrations (compared to ammonium and sulphate), which is in agreement with measurements.

FRAME was used to estimate air concentrations for two future scenarios based on emissions predictions for the years 2020 and 2030 in which significant reductions

R. Ots (✉)
Centre for Ecology and Hydrology, Bush Estate, Penicuik, Midlothian EH26 OQB, UK

School of Chemistry, University of Edinburgh, Joseph Black Building, West Mains Road, Edinburgh EH9 3JJ, UK
e-mail: R.Ots@ed.ac.uk

A. Dore • Y.S. Tang • C.F. Braban • M. Sutton
Centre for Ecology and Hydrology, Bush Estate, Penicuik, Midlothian EH26 OQB, UK
e-mail: todo@ceh.ac.uk

M. Vieno
Centre for Ecology and Hydrology, Bush Estate, Penicuik, Midlothian EH26 OQB, UK

School of GeoSciences, University of Edinburgh, Crew Building, West Mains Road, Edinburgh EH9 3JN, UK

D. Steyn and R. Mathur (eds.), *Air Pollution Modeling and its Application XXIII*, Springer Proceedings in Complexity, DOI 10.1007/978-3-319-04379-1_29,

in UK emissions in the UK are forecast (40 % for $SO_2$ and 47 % for $NO_x$ between 2010 and 2030). The relationships between long term changes in precursor gas emissions and the formation of secondary inorganic aerosol are discussed in terms of the modelling results.

## 29.1 Introduction and Model Description

In this study a simple Lagrangian model using annually averaged meteorology has been used to simulate the concentrations of secondary inorganic aerosol species in the UK. The FRAME model has been previously applied to calculate the deposition of sulphur and nitrogen and exceedance of critical loads (i.e. [1, 2]) and was found to perform well when compared to more complex Eulerian models. FRAME is a Lagrangian model using straight line trajectories with a 1° angular resolution which runs at a 5 km resolution over the British Isles and 50 km resolution over Europe with a fine vertical grid spacing (1 m at the surface). Area emissions are injected into sector dependent levels and point source emissions are treated with a plume rise routine. Vertical diffusion in the air column is calculated using K-theory eddy diffusivity. Wet deposition is calculated using a 'constant drizzle' approximation driven by an annual rainfall map. Five land classes are considered and a vegetation specific canopy resistance parameterization is employed to calculate dry deposition of particulates.

Modelled concentrations are compared to measurements from 12 monitoring sites which are operated with the UK Eutrophying and Acidifying Air Pollutants (UKEAP) Acid Gases and Aerosols Network (AGANet). Monitoring work commenced in September 1999, providing continuous monthly data on nitric acid, particulate nitrate and other inorganic species. For our model validation, we averaged these monthly measurements to annual means.

Future emissions that were used for our future scenario runs have been estimated by the UK Department of Energy and Climate Change Updated Energy Projections (UEP43). They forecast a 40 % reduction in $SO_2$ and 47 % in $NO_x$ emissions between the years 2010 and 2030. However $NH_3$ emissions from agricultural sources in the UK are expected to fall by only 5 % over the next decade. Similar levels of $SO_2$ and $NO_x$ emissions reductions are forecast for Europe by the International Institute for Applied Systems Analysis (www.iiasa.ac.at). This emissions data will be used to estimate future reductions in secondary inorganic concentrations (see results in Table 29.1).

**Table 29.1** Modelled changes in annual average surface concentrations over the UK

| | 2000–2010 (%) | 2010–2020 (%) | 2010–2030 (%) |
|---|---|---|---|
| $SO_2$ | −77 | −5 | −21 |
| $SO_4$ | −30 | −26 | −32 |
| $NH_4$ | −26 | −25 | −33 |
| $NO_3$ | −21 | −24 | −35 |

## 29.2 Results

The results showed good spatial correlation between measurements of gas and aerosol concentrations and modelled values ($R^2 > 0.8$ – Fig. 29.1). Figure 29.1 also shows the normalized mean bias over the years for all four pollutants and the percentage of modelled annual concentrations in the 12 measurement stations that fell in the range of a factor 2 from the measurements. A curious discrepancy between the modelled and measured concentrations of $SO_2$ and $SO_4$ appears for the later (2008–2010) years – the model starts to underestimate $SO_2$ and overestimate $SO_4$. Sensitivity studies will be performed, to uncover the possible reason for this. We also

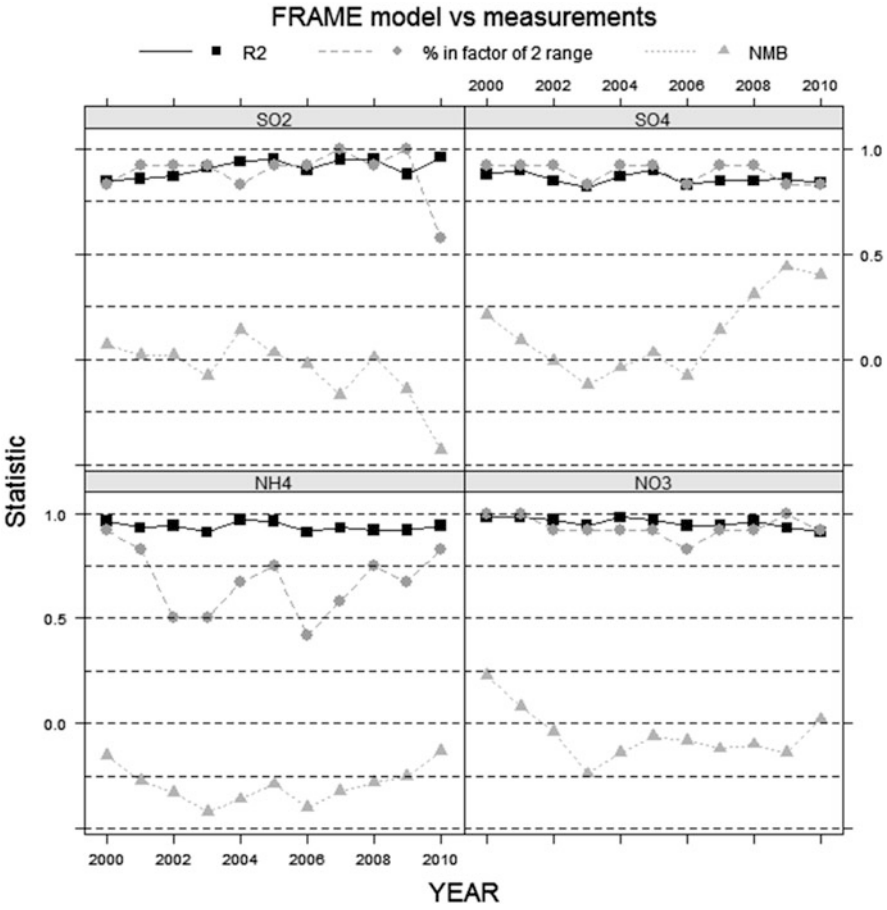


**Fig. 29.1** Statistics (R2 – coefficient of determination, NMB – normalized mean bias) between the modeled and measured annual average concentrations of $NH_4^+$, $NO_3^-$, $SO_4^{2-}$ and $SO_2$

noticed that the model tends to underestimate concentrations in more remote regions (i.e. Scotland), implying an underestimation of long range transport (from the source regions in England).

## 29.3 Conclusions

- In general, the FRAME model reproduces annual concentrations of $NH_4^+$, $NO_3^-$, $SO_4^{2-}$ and $SO_2$ very well.
- The model under-estimates lower concentrations of $SO_4^{2-}$ due to an underestimation of long range transport from source regions (i.e. England) to more remote regions (i.e. Scotland).
- The strong agreement between the modelled and measured values for the past years indicates the applicability of FRAME to future air pollution scenarios.

**Acknowledgments** This work was funded by the UK Natural Environment Research Council and the Department for the Environment, Food and Rural Affairs. The authors are also thankful for the R-project (www.R-project.org) and its packages Lattice and Openair (www.openair-project.org).

## References

1. Matejko M, Dore AJ, Hall J, Dore CJ, Blas M, Kryza M, Smith R, Fowler D (2009) The influence of long term trends in pollutant emissions on deposition of sulphur and nitrogen and exceedance of critical loads in the United Kingdom. Environ Sci Policy 12:882–896
2. Dore AJ, Vieno M, Tang YS, Dragosits U, Dosio A, Weston KJ, Sutton MA (2007) Modelling the atmospheric transport and deposition of sulphur and nitrogen over the United Kingdom and assessment of the influence of SO2 emissions from international shipping. Atmos Environ 41(11):2355–2367

# Chapter 30
# Modelling the Impact of Energy Transitions on Air Quality and Source Receptor Relations

**C. Hendriks, J. Kuenen, R. Kranenburg, M. Schaap, and P. Builtjes**

**Abstract** Air pollution is associated with adverse effects on human health through exposure to PM and ozone. To design effective air pollution mitigation strategies it is essential to quantify the effect of pollutant emission reductions on their concentrations as well as health and ecosystem impacts. Within integrated assessment modeling source-receptor relationships (SRRs) are used that are based on chemistry transport modelling. Currently, these SRRs are made using invariant emission time profiles. The LOTOS-EUROS model equipped with a source attribution module was used to test this assumptions for renewable energy scenarios. Renewable energy availability and thereby fossil fuel back up are strongly dependent on meteorological conditions. We have used the spatially and temporally explicit energy model REMix to derive time profiles for backup power generation. These time profiles were used in LOTOS-EUROS to investigate the effect of emission timing on air pollutant concentrations and SRRs. It is found that the effectiveness of emission reduction in the power sector is significantly lower when accounting for the shift in the way emissions are divided over the year and the correlation of emissions with synoptic situations. The source receptor relationships also changed significantly. This effect was found for both primary and secondary pollutants. Our results indicate that emission timing deserves explicit attention when assessing the impacts of system changes on air quality.

## 30.1 Introduction

To reduce greenhouse gas emissions from energy consumption, large-scale deployment of solar and wind power is a promising strategy. However, these systems are intermittent electricity sources. As storage of electricity is expensive, there is a need

C. Hendriks (✉) • J. Kuenen • R. Kranenburg • M. Schaap • P. Builtjes
TNO, Department of Climate, Air and Sustainability, Utrecht, The Netherlands
e-mail: carlijn.hendriks@tno.n

D. Steyn and R. Mathur (eds.), *Air Pollution Modeling and its Application XXIII*,
Springer Proceedings in Complexity, DOI 10.1007/978-3-319-04379-1_30,

for back-up electricity generation capacity that will most likely consist of fossil fuel fired plants. Hence, a solid environmental impact assessment for fossil fuel combustion remains necessary in the future. The transition to renewable energy will reduce air pollutant concentrations, as emissions from fossil fuel fired power plants will be reduced dramatically. However, apart from an absolute reduction in emissions there will also be a significant change to the timing of the emissions because power plants used as back-up capacity will operate when not enough renewable electricity is available, not necessarily at times when demand peaks. This means that the relation between an emission from a certain source and its impact on air pollutant concentrations in a certain receptor region (source receptor relations, SRRs) might also change. Source receptor relations are commonly used in integrated assessment models to assess the impact of emission reduction measures and are assumed to be linear for emission changes <15 %. For system changes that involve shifts in the temporal and geographical profile of emissions, SRRs may be non-linear for much smaller changes in the total emissions than currently assumed. In this study, we assess the impact of changing time profiles of emissions from the power sector on source receptor relations. Two simple renewable energy scenarios with corresponding emission time profiles were developed. The air quality impacts of these scenarios and the impacts on SRRs are assessed using the Chemistry Transport Model (CTM) LOTOS-EUROS equipped with a source attribution module.

## 30.2 Set-Up of Scenarios and Model Runs

Four emission scenarios for Europe were defined to investigate the effect of a high deployment of renewable electricity on air quality. For the baseline scenario, the current electricity mix is used, consisting of fossil fuels (54 % of the electricity generated in Europe), nuclear power (25 %) hydroelectric power (16 %), wind (4 %) and solar energy (<1 %). In the scenarios with high renewable electricity production, the share of renewable electricity production (i.e. solar and wind power) is increased, replacing fossil-fuel based electricity. In the so-called 50/50 scenario, the contribution of PV and wind to the electricity mix is equal, together totalling 25 % of the electricity demand on average for Europe. In the 'high wind' scenario, wind energy produces 25 % of the electricity demand in each country where possible. Solar power is used to reach the 25 % renewables if wind energy potential is too low. To keep the scenarios as simple as possible, storage and trade of electricity are not included in our scenarios. Furthermore, nuclear and hydroelectric power are assumed to generate the same power output each hour of the year and the mix of fossil fuel-fired power plants is assumed to remain the same. The electricity load at each hour should equal the sum of the electricity generation from all sources. Hourly renewable electricity generation potentials $P_{ren}(x,t)$ were calculated using the REMix model [4].

The annual total emissions for all sectors are taken from the TNO-MACC database [1]. In all except the baseline scenario, the emissions of the power sector

are reduced by the percentage of fossil fuels replaced by renewables. The share of fossil fuels in the electricity mix is 57 % in the baseline scenario and 34 % for the 50/50 and high wind scenarios. Therefore, in the scenarios assuming a high deployment of renewable electricity, the annual emissions from the European power sector are effectively reduced by 40 %. For all scenarios including the baseline, the annual total emissions from the power sector for each country were divided over the year assuming a linear relation to the fossil fuel based electricity generated.

Additional to the baseline, 50/50 and high wind scenarios, a control scenario was defined to be able to distinguish the impact of the emission reduction and of the change in timing. This scenario consists of the emission totals of the '50/50' scenario and the time profiles of the baseline scenario.

The distribution of the fossil-based electricity varies considerably between the scenarios. In the equal solar/wind scenario, the relative difference between summer and winter becomes larger due to the abundant availability of solar-based power in the summer months. The high wind scenario shows more fluctuations throughout the year because high wind speed conditions come in episodes.

The scenarios described above were used as input to the chemistry transport model LOTOS-EUROS [2] version 1.8 to calculate the effects of a high deployment of solar and wind energy on air pollutant concentrations.

## 30.3 Results

Sulfate aerosol is for a large part emitted by coal-fired power plants. The reduction of power plant emissions in our scenarios causes a reduction in ambient fine sulfate, especially in Eastern Europe (−35 %) where coal is an important fuel for power plants. However, when more realistic power plant emission time profiles are used the annual average concentrations are up to 20 % higher compared to the situation in which the time profiles are kept as they are now. Using the time profiles calculated for the scenario with maximum deployment of wind energy, half of the reduction in concentration because of the lower emissions from the power sector is canceled when the time profiles are adapted. These trends are also observed for fine nitrate aerosol, whereas for other substances, changing the time profiles has no or only a small effect on the average annual concentrations.

Additional to the effect on annual average concentrations, the effect of timing of power plant emissions on source receptor relations is investigated. Figure 30.1 shows the effect of SO2 emissions from German and Czech power plants on the concentrations of sulphate aerosol for ten European countries. The figure shows the average SO4 concentration due to the German/Czech power sector to ten receptor countries, divided by the total SO2 emissions from Germany/Czech republic in each scenario. The result is a measure for the 'effectivity' of emissions in terms of resulting air pollution. As Fig. 30.1 illustrates, reducing SO2 emissions without changing the time profile yields slightly higher concentrations of SO4 per unit of SO2 emission. Looking at the effect of the change in time profile (compare

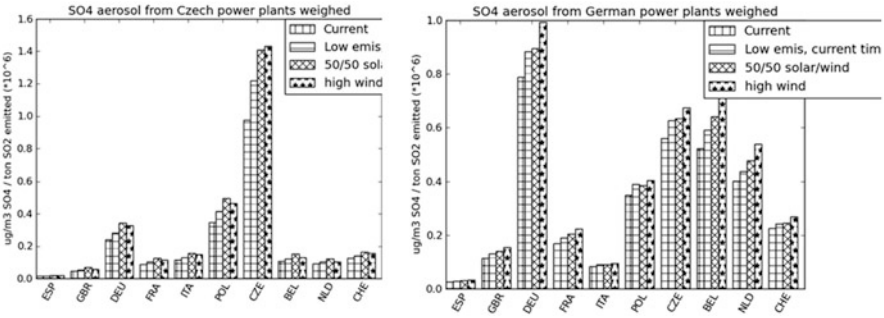


**Fig. 30.1** Sulfate concentrations per unit emission from Czech (*left*) and German (*right*) power plants for ten receptor countries

second and third bars for each country) shows that this increases the effectivity of SO2 emissions from German/Czech power plants for all receptor countries. This effect is strongest for countries close to the source country and can amount to 40 % of the original pollutant/emission ratio (e.g. for sulphate aerosol from Czech power plants). For the high wind scenario, the concentration per unit emission also increases compared to the baseline scenario. The increase in effectivity of power plant emissions for the high renewable scenarios is found for all substances and also for other countries.

## 30.4 Conclusion

We demonstrated that the representation of temporal profiles in air quality models is important and might have a large impact on the results of such modeling studies. The impact of the power sector on air pollutant concentrations was assessed given several simple scenarios in which renewable electricity production is increased. The source receptor relations for the power sector for several countries in Europe were investigated, and we found that using a different temporal profile might significantly impact the source receptor relations. In integrated assessment modeling, usually linear source receptor relations are used. The assumption that these relations behave linearly when the change in annual total emissions is limited should be evaluated carefully given our results.

**Acknowledgments** This study was funded by the 7th Framework Programme of the European Commission EnerGEO (http://www.energeo-project.eu/).

## References

1. Kuenen JJP, Denier van der Gon HAC, Visschedijk A, Van der Brugh H, Van Gijlswijk R (2011) MACC European emission inventory for the years 2003–2007. TNO report TNO-060-UT-2011–00588, Utrecht
2. Schaap M, Timmermans RMA, Sauter FJ, Roemer M, Velders GJM, Boersen GAC, Beck JP, Builtjes PJH (2008) The LOTOS-EUROS model: description, validation and latest developments. Int J Environ Pollut 32:270–289
3. Mues A, Kuenen J, Hendriks C, Manders A, Segers A, Scholz Y, Hueglin C, Builtjes P, Schaap M (2013) Sensitivity of air pollution simulations with LOTOS-EUROS to temporal distribution of anthropogenic emissions. Atmos Chem Phys Discuss 13:19311–19350
4. Scholz Y (2012) Renewable energy based electricity supply at low costs: development of the REMix model and application for Europe. PhD thesis, University of Stuttgart, Germany, 199 p

## Questions and Answers

**Questioner Name:** Roger Timmis

**Q:** Will an expansion of renewables mean that fossil fuel power stations are used more for short-term responsive (back-up) energy generation? If so, do you expect more use of gas-fuelled power stations that emit $NO_x$, rather than more use of coal-fired stations that emit $SO_2$? How appropriate is it to focus the scenarios on $SO_2$ – which is not particularly associated with rapid 'back-up' power stations?

**A:** We indeed expect that an increase in renewable electricity production from intermittent sources such as sun and wind will cause fossil fueled power stations to be used more as a back-up electricity source. With the current technology, gas-fueled power stations are more fit to take this role than coal-fired plants, because switching on and off is easier for gas-fired stations. However, as the price difference between gas and coal increases and energy companies keep investing in new coal-fired power plants, coal-fired stations may also be used as back-up capacity in the future, although they are less flexible than gas-fired plants. In this paper, we show examples of sulfate because the effects we discuss were most prominent for this substance. This is mainly because the energy industry is an important source of $SO_2$, whereas e.g. $NO_x$ is also emitted in large amounts by traffic and industry. A correct representation of emission timing is also important for $NO_x$ and PM (see e.g. Mues et al. [3]).

# Chapter 31
# Impact of Mercury Chemistry on Regional Concentration and Deposition Patterns

**Johannes Bieser, Volker Matthias, Armin Aulinger, Beate Geyer, Ian Hedgecock, Francesco DeSimone, Christoph Gencarelli, and Oleg Travnikov**

**Abstract** In the atmosphere mercury exists in three forms: Gaseous Elemental Mercury (GEM), Gaseous Oxidized Mercury (GOM), and Particle Bound Mercury (PBM). GOM and PBM make up only 1 % of the total. But deposition, which is the only sink for atmospheric mercury, is dominated by these two species. Therefore, oxidation processes are key to understand the behaviour of mercury in the atmosphere. However, in the scientific community a consensus on the importance of oxidizing reactants, namely ozone, hydroxy radicals, and halogens, has not been reached.

This model study about the influence of chemical reactants on the regional transport of mercury is part of the European Union FP7 Research Project GMOS (Global Mercury Observation System). GMOS focuses on the improvement and validation of mercury models to assist establishing a global monitoring network and to support political decisions.

In the course of this study the Community Multiscale Air Quality (CMAQ) model was used to simulate the transport and deposition of mercury. CMAQ was run on a regional domain over Europe using different chemical mechanisms for

J. Bieser (✉) • V. Matthias • A. Aulinger • B. Geyer
Helmholtz-Zentrum Geesthacht, Institute of Coastal Research, Max-Planck-Strasse 1, 21502 Geesthacht, Germany
e-mail: johannes.bieser@hzg.de

I. Hedgecock • F. DeSimone • C. Gencarelli
CNR – Institut Inquinamento Atmosferico, U.O.S. Di Rende, UNICAL-Polifunzionale, 87036 Rende, Italy

O. Travnikov
Meteorological Synthesizing Center-East of EMEP, 2nd Roshchinsky proezd., 8/5, Moscow 115419, Russia

D. Steyn and R. Mathur (eds.), *Air Pollution Modeling and its Application XXIII*, Springer Proceedings in Complexity, DOI 10.1007/978-3-319-04379-1_31,

the oxidation of mercury. The model results were compared to newly available long term observations of speciated mercury. Based on this unique dataset, the relevance of different chemical reactions for the oxidation and reduction of mercury were investigated. The main finding was that the emissions of GOM as well as the production of GOM by oxidation processes is vastly overestimated. Moreover, there are indicators that the fraction of PBM, produced by reaction of GEM with ozone and OH is overestimated.

## 31.1 Introduction

Mercury is a global pollutant that is known to have adverse effects on human health [14]. Because of anthropogenic emissions from fossil fuel burning the amount of mercury available in the environment is steadily increasing. Recent studies have shown that the atmospheric mercury burden has tripled since pre-industrial times [1, 13]. Due to its severity, the problem of global mercury pollution is in the focus of several international conventions such as the UNEP mercury program [15] and the UN-ECE Long-Range Transport of Atmospheric Pollution Convention-Task Force on Hemispheric Transport of Air pollution (HTAP) [7]. Major scientific questions about atmospheric mercury are the oxidization processes of elemental mercury, global and regional transport patterns, and a better understanding of mercury emissions.

In the atmosphere mercury exists in three forms: Gaseous Elemental Mercury (GEM), Gaseous Oxidized Mercury (GOM), and Particle Bound Mercury (PBM). For the atmospheric long range transport GEM is the most important mercury species. This is due to the long life time of the species and the fact that it represents the largest fraction (99 %) of the total atmospheric mercury. However, an extremely important question in order to understand the global mercury cycle is the deposition of mercury from the atmosphere. GOM and PBM make up only 1 % of the total, but deposition, which is the only sink for atmospheric mercury, is dominated by these two species. Therefore, it is very important that CTMs are able to calculate the atmospheric concentration as well as the deposition of these species. Previous studies about mercury deposition found that models generally overestimate the amount of wet deposition. But due to a lack of PBM and GOM measurements it was not possible to further investigate the underlying mechanisms [5]. Due to the very low concentrations of GOM and PBM (1–100 pg/m$^3$) until recently no continuous measurements for these species were available. This lack of observation data is now being addressed by the Global Mercury Observation System (GMOS). As part of the GMOS project, Weigelt et al. [16] recently published the first full-speciation long-term measurement series for atmospheric mercury in Europe. For the first time, this study utilizes these speciated observations to evaluate an atmospheric mercury model.

## 31.2 Methods

The chemistry transport model (CTM) CMAQ [6] was set up on a $72 \times 72$ km$^2$ domain over Europe with a $24 \times 24$ km$^2$ nested domain over the North- and Baltic Sea region. To account for the uncertainty in input datasets the model was run with meteorological fields from COSMO-CLM [10] and WRF [11]. The outer domain was forced with 6 hourly boundary conditions from the global Hg CTMs ECHMERIT [8] and GLEMOS [12]. Hourly anthropogenic and biogenic emissions were created with the SMOKE-EU emissions model [2, 3]. Annual total mercury emissions were obtained from the $0.5 \times 0.5°$ global emission inventory for 2005 from Pacyna et al. [9].

Modelled concentrations of PBM and GOM, as well as wet deposition of mercury were compared with observations at the German measurement station Waldhof. At Waldhof for the years 2009–2012 hourly observations of GEM and 3-hourly observations of PBM and GOM are available. The detection limit of the applied method is 0.4 pg/m$^3$. Additionally, daily precipitation and weekly wet deposition measurements are available. Based on this dataset the capability of CMAQ to reproduce atmospheric concentrations of oxidized mercury and the removal of mercury out of the atmosphere is investigated. For this purpose several scenarios were calculated with CMAQ, where the different sources of PBM and GOM were removed from the input fields.

$$\mathrm{GEM} + \mathrm{O_3} \rightarrow 0.5\ \mathrm{PBM} + 0.5\ \mathrm{GOM} \tag{31.1}$$

$$\mathrm{GEM} + \mathrm{OH} \rightarrow 0.5\ \mathrm{PBM} + 0.5\ \mathrm{GOM} \tag{31.2}$$

$$\mathrm{GEM} + \mathrm{H_2O_2} \rightarrow \mathrm{GOM} \tag{31.3}$$

$$\mathrm{GEM} + \mathrm{Cl_2} \rightarrow \mathrm{GOM} \tag{31.4}$$

$$\mathrm{GEM} + \mathrm{Cl} + \mathrm{M} \rightarrow 0.5\ \mathrm{HG} + 0.5\ \mathrm{GOM} + \mathrm{M} \tag{31.5}$$

Finally, the chemical reactions for mercury oxidation were evaluated. In the heavy metal version of CMAQ, GEM can be oxidized by ozone (Eq. 31.1), OH (Eqs. 31.2 and 31.3), and chlorine (Eqs. 31.4 and 31.5). Bromine reactions are not implemented into the model. To evaluate the influence of the different reactions additional CMAQ runs were performed for each reactant and each product.

## 31.3 Results

It was found that CMAQ generally overestimates the amount of oxidized mercury in the atmosphere. On average PBM is overestimated by a factor of 2 and GOM by a factor of 5. A source attribution by means of different CTM scenarios revealed that

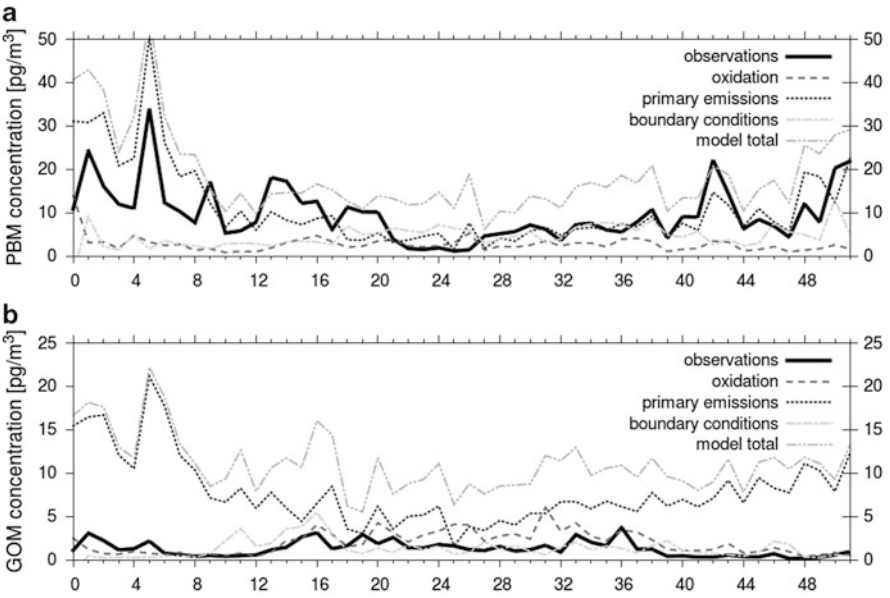


**Fig. 31.1** Comparison of modelled concentrations of (**a**) PBM and (**b**) GOM with observations at Walfhof. Additionally, results from source attribution scenarios with only a single source for PBM and GOM are depicted. All values are based on 3-hourly data for 2009

primary emissions are the largest contributor to PBM and GOM concentrations. For PBM the primary emissions alone can explain the observed concentrations (Fig. 31.1a *'primary emissions'*). For GOM the strong overestimation by the model could be explained by the primary emissions. CMAQ runs without direct emissions of GOM lead to good agreement with observations (Fig. 31.1b *'oxidation'*). The assumption form these findings is that PBM is mainly created by emissions and GOM mainly by oxidation reactions.

These assumptions are confirmed by the observed annual and diurnal variabilities. PBM exhibits a strong diurnal variability which is in accordance with the primary mercury emissions. The production of PBM by oxidation, however, is anti-correlated to the observations with slightly higher reaction rates in summer. This can be explained by the increased availability of ozone and OH. GOM, on the other hand, correlates significantly with the diurnal ozone and OH cycles.

Moreover, an evaluation of modelled GOM concentrations for different reactants (ozone, OH, $H_2O_2$, chlorine) was performed (Fig. 31.2). It was found, that the best agreement with observations were obtained by the oxidation of GEM by ozone. The overestimation of GOM in weeks 40–45 could be explained by an strong overestimation of modelled ozone concentrations during that period. The combined OH and $H_2O_2$ reaction lead to good agreement during summer but produced too low GOM concentrations during winter. The chlorine reaction produced only negligible amounts of GOM at Waldhof.

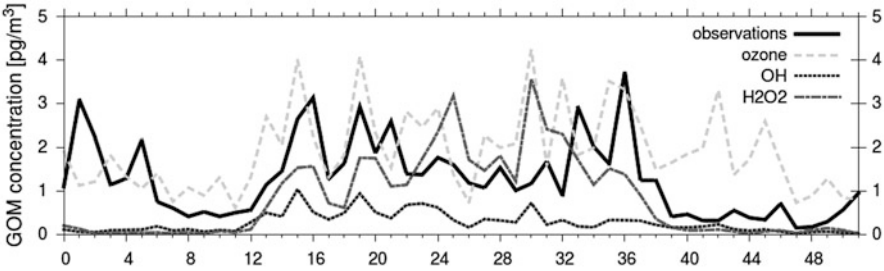


**Fig. 31.2** Comparison of observations to modelled GOM concentrations for different chemical reactants

Finally, we investigated the deposition of mercury. Only little is known about the dry deposition of mercury. The model indicates that the annual average wet and dry deposition over Europe are in the same order of magnitude. However, there are no direct measurements of mercury dry deposition available for evaluation of the model. For wet deposition daily precipitation and weekly deposition from wet only samplers are available at Waldhof. It was found, that the model generally overestimates the concentration of mercury in rain water. A model comparison with observed monthly wet deposition at 18 EMEP stations gave similar results [4]. The bias of modelled wet depositions was much lower when the modelled values were corrected with measured concentrations of PBM and GOM. A correction with the observed precipitation improved the correlation but did not improve the model bias. Using a modified version of CMAQ that was set up according to the findings described above lead to better agreement with observed mercury wet deposition.

## 31.4 Conclusion

A comparison of high resolution speciated mercury and wet deposition measurements revealed that the reaction rates currently used in atmospheric CTMs overestimate the production of PBM and GOM. For PBM, the primary emissions lead to an annual cycle and PBM concentrations that were in accordance with observations, while the oxidation reactions led to an unrealistic increase of PBM during summer. For GOM the model overestimated concentrations by a factor of 5. The modelled concentrations were inside a factor of 2 of observations if primary GOM emissions were completely neglected. In this case the model was also able to reproduce the strong annual and diurnal cycle of GOM.

This leads to the assumption that the reaction rates for mercury oxidation need to be revised and that the current split of products overestimates the production of PBM (Eqs. 31.1 and 31.2). Moreover, the speciation of emissions in current inventories is deemed to overestimate the amount of GOM emitted by combustion processes.

The results of this study are based on a single measurement station. With additional high resolution long-term speciated mercury measurements becoming available through the GMOS project, during the next years the presented findings will be evaluated for further observations in Europe and other regions.

**Acknowledgments** We acknowledge the European Commission for funding this work under the EU-FP 7 project GMOS. We want to thank Elke Bieber from the German Umwelt Bundesamt (UBA) and Andreas Schwerin from the Waldhof station for their support and the measurement data used for this study. Further, our thanks go to Andreas Weigelt, who operates the Tekran instruments at Waldhof.

## References

1. Amos HM, Jacob DJ, Holmes CD, Fisher JA, Wang Q, Yantosca RM, Corbitt ES, Galarneau E, Rutter AP, Gustion MS, Steffen A, Schauer JJ, Graydon JA, St Louis VL, Talbot RW, Edgerton ES, Sunderland EM (2011) Gas-particle partitioning of atmospheric Hg(II) and its effect on global mercury deposition. Atmos Chem Phys Discuss 11:29441–29477
2. Bieser J, Aulinger A, Matthias V, Quante M, Builtjes P (2011) SMOKE for Europe – adaptation, modification and evaluation of a comprehensive emission model for Europe. Geosci Model Dev 4:1–22. doi:10.5194/gmd-4-1-2011
3. Bieser J, Aulinger A, Matthias V, Quante M, Denier van der Gon HAC (2011) Vertical emission profiles for Europe based on plume rise calculations. Environ Pollut 159:2935–2946. doi:10.1016/j.envpol.2011.04.030
4. Bieser J, Matthias V, Geyer B, Hedgeckock I, DeSimone F, Gencarelli C, Travnikov O, Weigelt A (2013) A diagnostic evaluation of modelled mercury wet depositions in Europe using speciated high resolution observations. Submitted to ESPR, November 2013
5. Bullock OR, Atkinson D, Braverman T, Civolo K, Dastoot A, Davignon D, Ku JY, Lohmann K, Myers TC, Park RJ, Seigneur C, Selin NE, Sistla G, Vijayaraghavan K (2009) An analysis of simulated wet deposition of mercury from the North American Mercury Model Intercomparison Study. J Geophys Res Atmos 14:D08301
6. Byun DW, Schere K (2010) Review of the governing equations, computational algorithms, and other components of the models-3 Community Multiscale Air Quality (CMAQ) modeling system. Appl Mech Rev 59(2):51–77
7. ECE (Economic Commission for Europe), Pirrone N, Keating T (eds) (2010) Hemispheric transport of air pollution. Part-B: Mercury. United Nations, New York/Geneva
8. Jung G, Hedgecock I, Pirrone N (2009) ECHMERIT V1.0 – a new global fully coupled mercury-chemistry and transport model. Geosci Model Dev 2:175–195
9. Pacyna EG, Pacyna JM, Steenhuisen F, Wilson S (2006) Global anthropogenic mercury emission inventory for 2000. Atmos Environ 40(22):4048–4063
10. Rockel B, Will A, Hense A (2008) The regional climate model COSMO-CLM (CCLM). Meteorol Z 17:347–348
11. Skamarock WC, Klemp JB, Dudhia J, Gill DO, Barker DM, Duda MG, Huang WX-Y Wang, Powers JG (2008) A description of the advanced research WRF Version 3. Technical report, National Center for Atmospheric Research, Boulder
12. Travnikov O, Ilyin I (2009) The EMEP/MSC-E mercury modeling system. In: Pirrone N, Mason RP (eds) Mercury fate and transport in the global atmosphere. Springer, Dordrecht, pp 571–587
13. UNEP (United Nations Environment Programme) (2008) Global atmospheric mercury assessment: sources, emissions and transport. UNEP, Geneva

14. UNEP (United Nations Environment Programme) (2013) Global mercury report. UNEP, Geneva
15. UNEP (United Nations Environment Programme) (2013) Mercury: time to act. Technical report. Chemicals Branch, Division of Technology, Industry and Economics, United Nations Environment Programme (UNEP), Geneva
16. Weigelt A, Temme C, Bieber E, Schwerin A, Schuetz M, Ebinghaus R, Kock HH (2013) Measurements of atmospheric mercury species at a German rural background site from 2009 to 2011 – methods and results. Environ Chem 10(2):102–110. Available online: http://dx.doi.org/10.1071/EN12107

# Chapter 32
# A Multiscale Modeling Study to Assess Impacts of Full-Flight Aircraft Emissions on Upper Troposphere and Surface Air Quality

**Lakshmi Pradeepa Vennam, Saravanan Arunachalam, B.H. Baek, Mohammad Omary, Francis Binkowski, Seth Olsen, Rohit Mathur, William Vizuete, and Gregg Fleming**

**Abstract** Aviation is a unique anthropogenic source with 4-dimensional varying emissions, emitting 90 % of their emissions in upper troposphere at cruise altitudes (9–12 km). Aircraft emissions budgets in upper troposphere lower stratosphere (UTLS) region and their potential impacts on upper troposphere and surface air quality are not well understood. The key objective of this study is to characterize the aircraft emissions during full-flight activity in regional and hemispheric modeling scales, and assess their impacts on upper tropospheric chemistry and surface air quality. Using detailed spatio-temporal characterization of aircraft emissions along with other background emissions in the modeling domains, we studied incremental impacts of aircraft emissions focusing mainly on $O_3$, $NO_x$ and $PM_{2.5}$ species. Comparison of modeling results with aircraft measurements showed improvement of model performance due to enhanced modeling platform and consideration of cruise altitude aviation emissions in the upper troposphere.

## 32.1 Introduction

Pollutants that occur in upper atmosphere possess longer lifetimes, which can also be subjected to intercontinental transport due to strong winds and complex chemistry in UTLS. Aviation is one anthropogenic source that emits emissions

L.P. Vennam • S. Arunachalam (✉) • B.H. Baek • M. Omary • F. Binkowski • W. Vizuete
The University of North Carolina at Chapel Hill, NC, USA
e-mail: sarav@email.unc.edu

S. Olsen
University of Illinois at Urbana-Champaign, IL, USA

R. Mathur
Atmospheric Modeling and Analysis Division, United States Environmental Protection Agency, Research Triangle Park, NC, USA

G. Fleming
Volpe National Transportation Systems Center, U.S. DOT, Cambridge, MA, USA

D. Steyn and R. Mathur (eds.), *Air Pollution Modeling and its Application XXIII*, Springer Proceedings in Complexity, DOI 10.1007/978-3-319-04379-1_32,

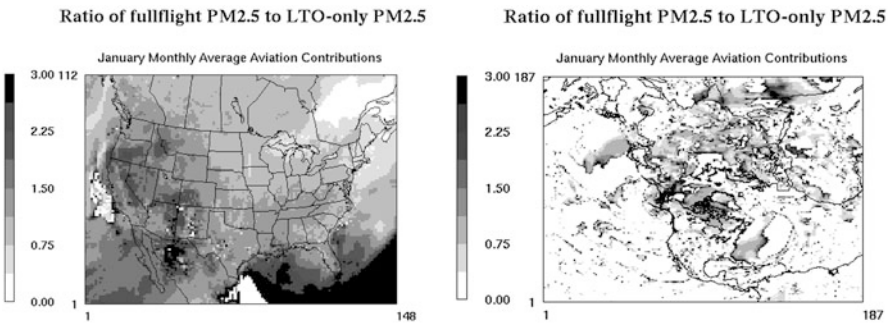


**Fig. 32.1** Ratio of fullflight to LTO-only PM2.5 impacts for ConUS (*left*) and Northern Hemispheric (*right*) modeling domains

directly in the upper and lower atmospheres. Globally, 92.5 % of aviation fuel burn occurs in the northern hemisphere with 69 % occurring in mid-latitudes and 74.6 % of them occurring in cruise altitudes [5, 6]. Majority of aviation emissions occur at cruise altitudes, limited studies to date have concentrated on impact of those emissions on UTLS and surface layer, especially for regional-scale studies. However most of these studies are based on global models that have a coarser spatial resolution (2.5° = ∼250 km) than typical regional (36 km, 34 layers, ∼65 hPa (top layer)) and hemispheric (108 km, 35 layers, ∼61 hPa (top layer), polar stereographic projection) air quality model applications considered in this study (Fig. 32.1).

Lamarque et al. [3] have shown that a relatively smaller source of $NO_x$, such as from aviation in the upper troposphere could play an unexpectedly huge role in enhancing the ozone production near tropopause level. Given the nonlinear chemistry, consideration of background $NO_x$ budgets (including another $NO_x$ source aloft, such as from lightning) are important to clearly emphasize the role of aviation $NO_x$ near cruise altitude. Allen et al. [1] showed that including lightning NO emissions in a regional-scale model enhances upper troposphere budgets of $NO_2$, but still underpredict aircraft measurements (INTEX-A) aloft which could be due to missing aircraft emissions as a source in the model. A new global aircraft inventory from the Aviation Environmental Design Tool (AEDT, [6]) with commercial aircraft activity between all airports during all modes represented as chorded segments is now available. This dataset provides motivation for this study to address and distinguish between the effects of aircraft emissions during cruise activity and landing and takeoff (LTO) cycles on surface as well as upper troposphere air quality.

## 32.2 Methodology

In this study we considered the US EPA's Community Multi-scale Air Quality (CMAQv5) model to perform simulations over the continental U.S. (ConUS). We used 2005 NEI emissions for background sources, the Weather Research Forecast

**Table 32.1** List of CMAQ model simulations and their configurations

| | Model scenario | Description |
|---|---|---|
| Standard | Base | All background emissions sources; Profile-based BCs |
| | Sensairp_full | Background + **full-flight aircraft emissions**; Profile-based BCs |
| | Sensairp_LTO | Background + only LTO aircraft emissions; Profile-based BCs |
| Enhanced | Base_s01 | All background emissions sources + **LNOx emissions; CAMChem BCs and online photolysis** |
| | Sensairp_s01_full | Background + **full-flight emissions** + LNOx emissions; CAMChem BCs and online photolysis |
| | Sensairp_s01_LTO | Background + only LTO aviation emissions + LNOx emissions; CAMChem BCs and online photolysis |

(WRF) model to develop input meteorology, and climatological averages for CMAQ IC/BCs. Aircraft emissions were based on AEDT [2, 6] that included emissions from 31 million commercial flights (13.6 million in the U.S.). We processed these for CMAQ using AEDTProc, a new tool to create gridded aircraft emissions in CMAQ's 3D grid structure. While we refer to this as the "standard" model application, we also created an "enhanced" model application with three specific improvements: lightning NOx based upon methodology by Allen et al. [1], IC/BCs from CAMChem – a global model which also included AEDT global inventories, and use of the new online photolysis module in CMAQv5 (instead of the lookup table approach) that incorporates modeled aerosol loading and effects of aerosols to modulate photolysis rates.

We then performed CMAQ simulations for January and July 2005 using the standard and enhanced configurations for three cases each no aircraft emissions, include aircraft emissions only within the LTO cycle, and include aircraft emissions during full flight as shown in Table 32.1. We then assessed incremental aviation contributions by computing differences of sensairp (with aircraft) and base case (without aircraft) scenarios.

## 32.3 Results

### *32.3.1 Impact of Aviation on Surface Layer Concentration*

We assessed aircraft emissions impacts on surface air quality by computing modeled absolute concentration differences (sensairp – base) of $NO_x$, $O_3$ and $PM_{2.5}$ in both winter and summer months as represented in Table 32.2. An increase in surface layer concentrations of $O_3$ and $PM_{2.5}$ was observed in full-flight runs when compared with LTO runs. Further, an increase in $O_3$ (0.2–0.4 %), $PM_{2.5}$ (0.05–0.15 %), $NO_x$ (0.2 %) during July, and decrease in $NO_x$ (during January) domain-average aviation-attributable concentrations are observed in regional scale. The $NO_x$ decrease is likely due to reaction of increased $O_3$ with available $NO_x$ species to produce $HNO_3$, which is a termination reaction for $NO_x$ (also observed by [4]).

**Table 32.2** Domain-average aircraft-related contribution during January and July 2005

| | Modelling scenarios | $NO_x$, ppbV (Jan, July) | | $O_3$, ppbV (Jan, July) | | $PM_{2.5}$, $\mu g/m^3$ (Jan, July) | |
|---|---|---|---|---|---|---|---|
| Enhanced (US from CONUS domain) | Aviation_full | −0.001 | 0.006 | 0.153 | 0.214 | 0.015 | 0.007 |
| | Aviation_LTO | −0.0002 | 0.006 | 0.130 | 0.095 | 0.013 | 0.003 |
| | **Ratio of full flight to LTO-only impacts** | **5** | **1** | **1.2** | **2.3** | **1.2** | **2.3** |
| Enhanced (HEMI) | Aviation_full | −0.629 | −0.017 | −2.401 | 2.393 | −0.300 | 0.134 |
| | Aviation_LTO | −0.077 | 0.0007 | −0.348 | 0.0081 | −0.0167 | −0.0036 |
| | **Ratio of full flight to LTO-only impacts** | **8.2** | **−24.2** | **6.9** | **295.4** | **17.9** | **−37.2** |
| Enhanced (US from HEMI domain) | Aviation_full | −0.107 | −0.004 | −0.226 | 0.338 | −0.0019 | 0.0305 |
| | Aviation_LTO | −0.122 | 0.0013 | −0.2106 | 0.0072 | 0.013 | −0.0615 |
| | **Ratio of full flight to LTO-only impacts** | **0.87** | **−3.07** | **1.07** | **46.9** | **−0.1** | **−0.5** |

In the case of $PM_{2.5}$, the full-flight case predicted higher aviation-attributable concentrations than LTO-only case (Fig. 32.1). Total aviation-related $PM_{2.5}$ is higher in January, and $ANO_3$ (nitrate aerosol) dominates among the individual aerosol contributions to total $PM_{2.5}$. However in July, $ASO_4$ (sulfate aerosol) dominates the total $PM_{2.5}$ contributions due to aircraft. In hemispheric scale, we see an overall decrease in aviation-attributable concentrations for all three pollutants, except in July where full-flight case showed 5 % (full flight) increase in domain-average $O_3$. However, spatial plots (not presented here) showed some $NO_2$ local increases in CMAQ hemispheric scale providing additional spatially-resolved information on aviation impacts than prior global-scale model studies. We also compared CONUS domain US aviation concentrations with HEMI do-main US aviation concentrations (Table 32.2); high concentrations are observed in the latter case due to full flight scenario in the month of July due to higher transport in the hemispheric-scale than regional-scale. But overall we saw a decrease in the hemispheric-scale US domain average concentrations due to higher background decreases though the airport regions showed localized increases.

### *32.3.2 Impact of Aviation and Model Evaluation in Upper Troposphere*

To assess aviation impacts in the upper troposphere, we instrumented CMAQ with the advanced process analysis tool over the entire ConUS to study UTLS chemistry. We looked at individual $NO_x$ and $NO_y$ production, and consumption from major reactions based on mass throughput near cruise altitude layers. Overall $HNO_3$ and PAN showed increase in concentrations in their net reaction, which could be generated from reaction of aviation produced $NO_x$ with $O_3$ and OH radical. These species can even deposit on soot particles (elemental carbon) emitted from aircraft and further increase aerosol concentrations. Finally, we compared different model scenarios (Table 32.1) with observations from aircraft during INTEX-NA and found that sensairp-enhanced case showed better match with observations in upper troposphere (see Fig. 32.2) when compared to prior CMAQ applications with addition of lightning $NO_x$ but not aircraft emissions [1].

## 32.4 Conclusion

We developed an enhanced modeling framework to incorporate a new anthropogenic source that is not traditionally used in regional-scale applications. Incorporating full flight aircraft emissions along with other background sources improved the model performance mainly near upper troposphere, which can be useful to modeling community in creating better model predictions in upper atmosphere. We will

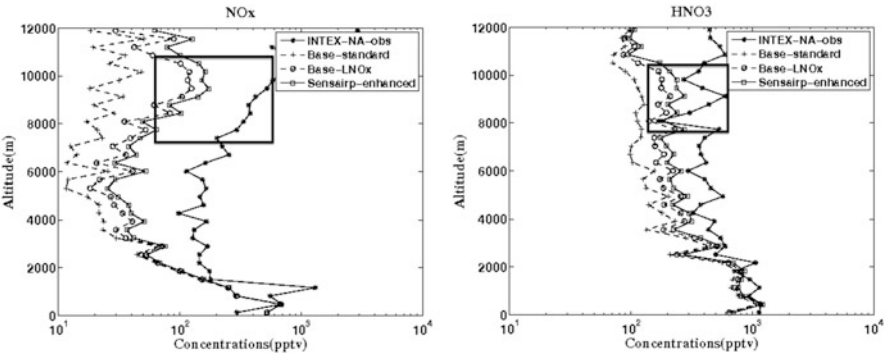


**Fig. 32.2** Comparison of modeled $NO_x$ and $HNO_3$ vertical profile with INTEX-NA observational data

continue this investigation by studying inter-continental transport with CMAQ hemispheric-scale application and will perform detailed model evaluation against satellite-based observations. Overall, aircraft emissions during full flight activities contribute <1 % to surface air quality, for all three pollutants studied. However, the contribution to surface $O_3$ and $PM_{2.5}$ due to full flight can be ~2.5× (particularly July) higher compared to LTO-only emissions. Though our results are generally comparable to prior global studies [4], we see localized increases of species such as $NO_x$ and $PM_{2.5}$ near urban and airport locations both at regional and hemispheric scale, illustrating the benefit of enhanced resolution to study air quality. We also note the influence of boundary conditions and background concentrations on the incremental contributions of aviation in regional scale AQ, specifically by enhancing $O_3$ levels at the surface due to aircraft.

**Acknowledgments** The emissions inventories used for this work were provided by U.S. DOT Volpe Center and are based on data provided by the U.S. FAA and EUROCONTROL in support of the objectives of the International Civil Aviation Organization Committee on Aviation Environmental Projection CO2 Task Group. Any opinions, finding, and conclusions or recommendations expressed in this material are those of the author(s) and do not necessarily reflect the views of the U.S. DOT, Volpe Center, the U.S., FAA, EUROCONTROL or ICAO.

## References

1. Allen DJ, Pickering KE, Pinder RW, Henderson BH, Appel KW, Prados A (2012) Impact of lightning NO on eastern United States photochemistry during the summer of 2006 as determined using the CMAQ model. Atmos Chem Phys 12:1737–1758
2. Barrett S, Prather M, Penner J, Selkirk H, Balasubramanian S, Dopelheuer A, Fleming G, Gupta M, Halthore R, Hileman J, Jacobson M, Kuhn S, Lukachko S, Miake-Lye R, Petzold A, Roof C, Schaefer M, Schumann U, Waitz I, Wayson R (2010) Guidance on the use of AEDT gridded aircraft emissions in atmospheric models, version 2.0. Technical report, Federal Aviation Administration, Washington, DC

3. Lamarque JF, Brasseur GP, Hess PG, Muller JF (1996) Three-dimensional study of relative contributions of the different nitrogen sources in the troposphere. J Geophys Res 101(17):22955–22968
4. Lee H, Olsen SC, Wuebbles DJ, Youn D (2013) Impacts of aircraft emissions on the air quality near the ground. Atmos Chem Phys 13:5505–5522
5. Olsen SC, Wuebbles DJ, Owen B (2013) Comparison of global 3-D aviation emissions datasets. Atmos Chem Phys 13:429–441
6. Wilkerson JT, Jacobson MZ, Malwitz A, Balasubramanian S, Wayson R, Fleming G, Naiman AD, Lele SK (2010) Analysis of emission data from global commercial aviation: 2004 and 2006. Atmos Chem Phys 10:6391–6408

## Question and Answer

**Questioner Name:** Amir Hakami

**Q:** Have you considered emissions of water vapor and its potential impact on chemistry?

**A:** We did not consider $H_2O$ emissions in our aircraft emissions, but consideration of the actual aircraft $H_2O$ emissions can impact the chemistry at cruise altitude to very small extent. Given the high amount of OH radical concentrations present in the upper troposphere, the perturbations from aircraft water vapor could be relatively small to affect the chemistry. But due to lower temperatures near UTLS, water vapor from aircraft can undergo condensation followed by freezing and sedimentation of ice crystals on the contrails impacting the radiative forcing. Study of atmospheric impacts of contrails and water vapor is another ongoing research area under climate impacts, and is not considered part of this study, which is focused on air quality impacts of aviation emissions.

# Chapter 33
# Relevance of Photolysis Frequencies Calculation Aspects to the Ozone Concentration Simulation

**Malte Uphoff, David Grawe, Ole Ross, and K. Heinke Schlünzen**

**Abstract** For the simulation of photochemically created pollutants like ozone it is essential to correctly consider reaction rates induced by short-wave radiation. In atmospheric chemistry transport models this is achieved by the use of either off- or online calculated photolysis frequencies. In this study the effect of different input parameters of a radiation model on the calculated photolysis frequencies have been investigated. In the second step an atmospheric chemistry transport model was used to assess the impact of changed photolysis frequencies on the simulation of ozone concentrations. The impact of changed radiation model input parameters on the calculated photolysis frequencies vary not only with regard to the changed parameter but also with regard to the to the species to be dissociated. Furthermore the impact of different sets of photolysis rates employed in a chemical transport simulation on the modelled concentrations is differed and likely to be less important than other aspects of the simulation like the resolution of the grid and the emissions used. Apart from major surface albedo changes (grass to snow) and extreme changes in total ozone column content for $J_{O3}$ clouds are the dominating factor in modifying the photolysis frequencies especially as they feature a highly temporal and special variation. The results show that simulated maximum ozone concentrations in areas with clouds are reduced.

M. Uphoff (✉) • D. Grawe • K.H. Schlünzen
Meteorological Institute, Klima Campus, University of Hamburg, Bundesstrasse 55, 20416 Hamburg, Germany
e-mail: malte.uphoff@zmaw.de

O. Ross
Meteorological Institute, Klima Campus, University of Hamburg, Bundesstrasse 55, 20416 Hamburg, Germany

Bundesanstalt für Geowissenschaften und Rohstoffe, Stillweg 2, 30655 Hannover, Germany

D. Steyn and R. Mathur (eds.), *Air Pollution Modeling and its Application XXIII*, Springer Proceedings in Complexity, DOI 10.1007/978-3-319-04379-1_33,

## 33.1 Introduction

Human health and vegetation growth are negatively affected by high concentrations of ground level ozone. Although there is a long history in studying ozone pollution and developing and implementing mitigation measures exceedances of regulatory standards in 2012 remain at serious levels in the European Union [1]. Ozone as a secondary pollutant is not directly emitted to the atmosphere but formed in a series of (photochemical) reactions from other directly emitted pollutants like nitrogen oxide ($NO_X$), carbon monoxide (CO) and primary hydrocarbons (RH) (e.g. methane ($CH_4$), formaldehyde (HCHO)). Photolysis frequencies are the rate coefficients in the respective photolytic reactions and as such have to been known to solve the set of ordinary differential equations composing the employed chemical reaction mechanism like RADM2 [5]. The Photolysis frequency $J_A$ (or J value for short) of species A is determined by integrating the product of the absorption cross section of the molecule A $\sigma_A$, its photodissociation quantum yield $\varphi_A$ and the spectral actinic flux $F_\lambda$ over the spectral interval of wavelengths which provide enough energy for photodissociation of the molecule A (33.1).

$$J_A = \int_{\lambda_1}^{\lambda_2} \sigma_A(\lambda, p, T)\varphi_A(\lambda, p, T)\, F_\lambda(\lambda)\, d\lambda \tag{33.1}$$

While absorption cross section and quantum yield depend strongly on the respective molecule under investigation the spectral actinic flux is completely determined by the shortwave radiation field in theatmosphere.

## 33.2 Methodology

To assess the importance of the radiation modifying processes on the modelled photolysis frequencies the radiation model STAR (System for Transfer of Atmospheric Radiation) [4] was used to calculated photolysis frequencies. The impact of clouds was assessed by using two different parameterisations. The first parameterisation [P1] is empirical and based on the cloud liquid water path [3] while the second parameterisation [P2] is based on the ratio of cloudy-sky to clear-sky actinic fluxes which were calculated by the radiation scheme of the mesoscale atmospheric model METRAS (MEsoscale TRAnsport and Stream model) [2]. The next question to be investigated is how modified sets of photolysis frequencies will influence the surface concentration of pollutants. Due to their scale of impact as well as their temporal and spatial variability the changes in J values due to clouds were selected to study the influence on chemistry simulations. The model M-SYS [6] composed of METRAS, the chemistry transport model MECTM (MEsoscale Chemistry Transport Model) which is based on the RADM2 chemistry mechanism [5] and STAR was used to model a period with high ozone concentrations in June of 2005 for the Rhine-Ruhr

area in Germany. The simulations were performed with a 12 km and a 4 km spatial resolution. The simulation with 4 km grid resolution was nested into the 12 km result.

## 33.3 Results and Discussion

Results from the different sensitivities are summarized in Fig. 33.1. Albedo changes cause the largest variation in the J values. A surface cover change from grass to fresh snow may cause an increase in the J values up to 250 %. An extreme increase

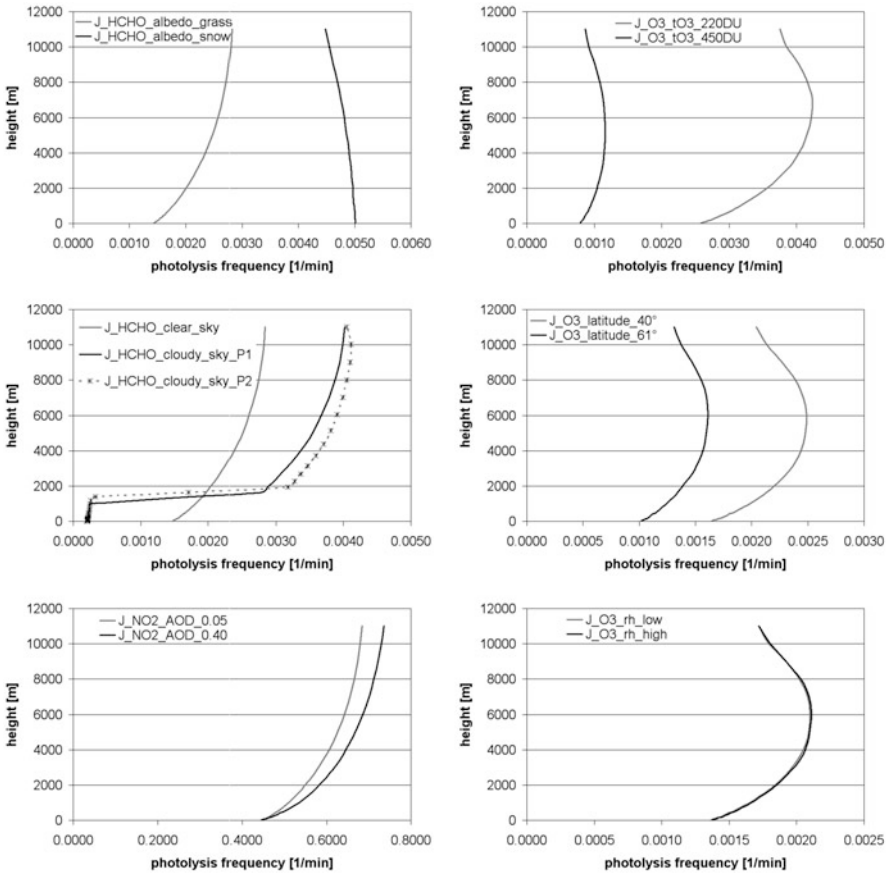


**Fig. 33.1** Vertical profiles of the photolysis frequencies at noon for varied conditions. *Upper left*: for different surface albedos, *upper right*: for different ozone column contents, *center left*: for different cloud parameterisations, *center right*: for different latitudes (viz. different solar zenith angles), *lower left*: for different aerosol optical depths and *lower right*: for different relative humidities

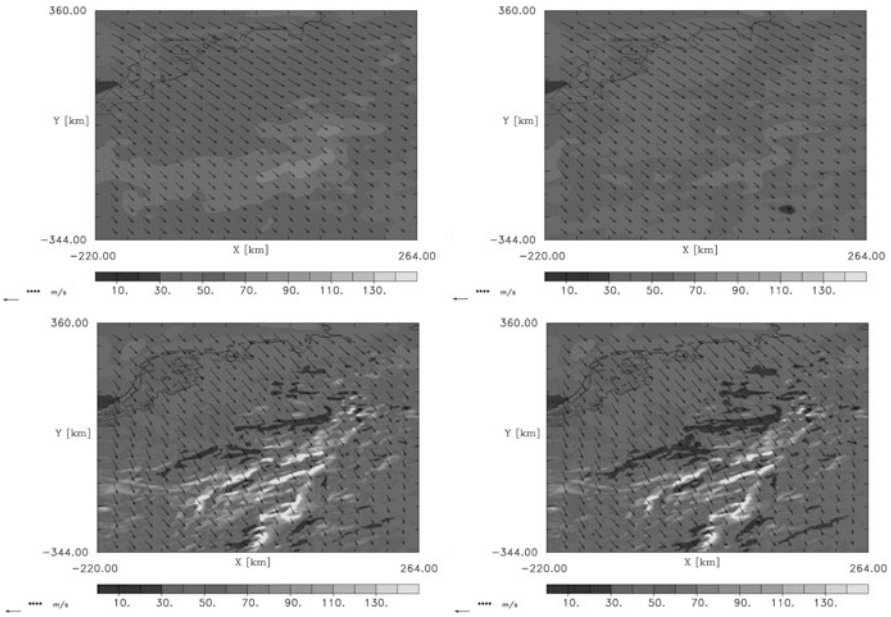


**Fig. 33.2** Ozone concentration in [ppb] at the surface for 5 pm at 21 June 2005. 12 km resolution (*top*), 4 km resolution (*bottom*), without cloud impact (*left*) with cloud impact (*right*)

in the total ozone column content causes a strong decrease in the $J_{O3}$ but does affect other photolytic reactions to a (much) lesser extent. In accordance with previous findings J values are increased above clouds and are reduced below by scattering and absorption. The geographical latitude and the time of the day determine the solar zenith angle. A low solar altitude corresponds to less extraterrestrial solar radiation received and hence lower J values but the extent of the decrease depends on the respective photolytic reactions ($-35$ % for $O_3 \rightarrow O(^1D)$ and $-5$ % for $NO_2 \rightarrow O(^3P) + NO$). Heavier polluted air features a higher aerosol optical depth (AOD). Strongly absorbing aerosols reduce the actinic flux at the earth's surface whereas strongly scattering aerosols increase it. Photolysis frequencies for $NO_2$ and HCHO are slightly increased while $J_{O3}$ remains almost unaffected. Photolysis frequencies showed little sensitivity towards changes in the relative humidity and air pressure profiles. Changes in the temperature profiles mainly affect the ozone photolysis frequency.

The spatial resolution of the chemistry simulation clearly has a pronounced effect on the modeled ozone concentrations. The results in the 4 km resolution feature higher ozone maximum concentrations and a much larger affected area (Fig. 33.2) though this is most likely due to finer resolved orography and emissions which translates into different initial mixing ratios and therefore different chemical developments. The presence of clouds in the model domain reduces the photolysis frequencies in the chemistry simulation. This in turn leads to reduced ozone concentration at the surface.

## 33.4 Conclusion

Photolysis frequencies depend individually on typical radiation calculation input parameters. Surface albedo, ozone column content and clouds are among the most important aspects to be considered. Clouds cause an increase above and a decrease below in photolysis frequencies and consequently lower surface ozone concentrations. However the effect of resolution of the simulation grid as well as of the emissions feature a more pronounced impact on the concentrations levels and their spatial extent.

**Acknowledgements** This work was supported in parts by the German Science Foundation (DFG) under grant number SCHL 499-4 and the Cluster of Excellence CLISAP (EXC177). Emission data have been provided by the MEGAPOLI project which is funded as part of the European Union's Seventh Framework Programme FP/2007-2011.

## References

1. European Environmental Agency (EEA) (2013) Air pollution by ozone across Europe during summer 2012, EAA Technical report no 3/2013. European Environmental Agency, Copenhagen, 48 p
2. Meyer EMI, Schlünzen KH (2011) The influence of emission changes on ozone concentrations and nitrogen deposition into the southern North Sea. Meteorol Z 20(1):75–84
3. Pour-Biazar A, McNider RT, Roselle SJ, Suggs R, Jedlovec G, Byun DW, Kim S, Lin CJ, Ho TC, Haines S, Dornblaser B, Cameron R (2007) Correcting photolysis rates on the basis of satellite observed clouds. J Geophys Res 112(D910302):1–17
4. Ruggaber A, Dlugi R, Nakajima T (1994) Modelling radiation quantities and photolysis frequencies in the troposphere. J Atmos Chem 18(2):171–210
5. Stockwell WR, Middleton P, Chang JS, Tang X (1990) The second generation regional acid deposition model chemical mechanism for regional air quality modelling. J Geophys Res 95(D10):16343–16367
6. Trukenmüller A, Grawe D, Schlünzen KH (2004) A model system for the assessment of ambient air quality conforming to EC directives. Meteorol Z 13(5):387–394

## Questions and Answers

**Questioner Name:** Rohit Mathur

**Q:** You showed some relatively large $O_3$ sensitivity to the $O_3$ column used in photolysis rates. Are the perturbations in $O_3$ column used in the sensitivity runs representative of the uncertainty in its specification?

**A:** Maximum natural variation of total $O_3$ column content of about 100 DU can be observed in a few days for mid-latitude locations like the Hohenpeißenberg in Southern Germany. Whereas the used differences in the sensitivity study reflects more the annual cycle of about 200 DU. Depending on the location uncertainties in measured total $O_3$ column content are way smaller, about 5 %.

**Questioner Name:** Roger Timmis

**Q:** Could you say more about the reflectance processes in the model for (a) clouds and (b) snow. Does the reflectance for clouds take into account of different cloud types and possible multiple reflections for some cloud types like cumulus. What albedo is assumed for snow?

**A:** Two parameterizations have been used to include the impact of clouds on modeled photolysis rates in the CTM simulation. The first is an empirical approach based on the total liquid water path of the respective atmospheric column and the second parameterization is based on the ratio of cloudy-to-clear sky actinic fluxes which are calculated in the driving atmospheric model. Clouds are differential by the location, vertical extent and cloud liquid water pathway. The radiation module of the atmospheric model METRAS features a basic approach to account for multiple reflection in the vertical direction but not in the horizontal direction therefore does not feature increased actinic fluxes between broken cumulus cloud fields. The albedo of snow is used in a wavelength depending setting ranging from 0.86 at 0.28 $\mu$m to 0.907 at 0.7 $\mu$m.

**Questioner Name:** Christian Hogrefe

**Q:** How sensitive do you expect your results to be to grid resolution?

**A:** At least for coarser grid and emission resolutions ($\Delta x = 12$ and 4 km) this parameter has proven to have a more pronounced effect on surface ozone levels than changes to other factors e.g. like photolysis rates. However, I expect that in finer resolutions (e.g. $\Delta x = 1$ km) physical processes like varying photolysis frequencies with become more dominant.

# Chapter 34
# Air Pollution in China in January 2013

**Volker Matthias, Armin Aulinger, Johannes Bieser, Beate Geyer, and Markus Quante**

**Abstract** In January 2013 exceptionally high levels of particulate matter (PM) concentrations were reported for the area around Beijing (40 N, 116 E) with maximum concentrations exceeding 500 $\mu g/m^3$. Observations of the aerosol optical depth (AOD) within the Aeronet sun-photometer network showed an AOD of more than 2 on several days. In order to analyze this high pollution episode PM concentrations in China were simulated with the Community Multiscale Air Quality (CMAQ) model for the period from 10 December 2012 to 31 January 2013. Emissions were taken from the EDGAR data base. The most recent emission rates from 2008 were further increased considering the growth of China's gross domestic product. The results were compared to ground based PM2.5 measurements taken at the US embassy in Beijing and to Aeronet sun-photometer observations. The model was generally able to reproduce the high PM levels measured in situ close to ground, however the largest peak on 12 January was not captured, because of an exceptionally strong temperature inversion close to ground that was not reproduced in the meteorological fields. The meteorological model significantly underestimated the relative humidity in the lowest layer, leading to some underestimations of the aerosol optical depth. An analysis of the most important source sectors showed that residential heating was the main emission source sector on those days with the highest aerosol concentrations.

V. Matthias (✉) • A. Aulinger • J. Bieser • B. Geyer • M. Quante
Helmholtz-Zentrum Geesthacht, Institute of Coastal Research, Max-Planck-Strasse 1, 21502 Geesthacht, Germany
e-mail: volker.matthias@hzg.de; armin.aulinger@hzg.de; johannes.bieser@hzg.de

D. Steyn and R. Mathur (eds.), *Air Pollution Modeling and its Application XXIII*, Springer Proceedings in Complexity, DOI 10.1007/978-3-319-04379-1_34,

## 34.1 Introduction

Chinas economy has grown rapidly in the last 20 years. This coincides with a drastically increased energy demand, increased traffic and a raised industrial production. All these activities cause large emissions of air pollutants. Therefore, eastern China is known as one of the areas with highest air pollution in the world.

In January 2013 exceptionally high levels of particulate matter (PM) concentrations were reported for the area around Beijing (40 N, 116 E) with maximum concentrations of particles smaller than 2.5 $\mu$m (PM2.5) exceeding 500 $\mu g/m^3$ on several days in a row. This coincided with low temperatures and calm winds in entire North East China.

A model study has been set up at Helmholtz-Zentrum Geesthacht which aimed at answering the following questions related to this exceptional situation:

- Which emission sectors contribute most to the high aerosol concentrations?
- What is the impact of the meteorological situation on the high pollution level?
- How accurately can state of the art air quality models simulate extreme pollution events?

## 34.2 Methods

The regional atmospheric chemistry transport model CMAQ (Community Multiscale Air Quality) was set up on a $72 \times 72$ km$^2$ grid for South East Asia with a nested $24 \times 24$ km$^2$ grid covering mainly North East China, Korea and parts of Russia and Japan. 30 vertical layers up to 20 hPa were implemented on the coarse grid, the finer grid contained 40 vertical layers. CMAQ was driven with meteorological fields from the mesoscale meteorological model COSMO-CLM (CCLM). The model was run for the period from 10 December 2012 until 31 January 2013.

For the coarse grid simulation of COSMO-CLM the model setup of Feser and Barcikowska [2] was used. The simulation was once initialized in 1948 and then done continuously with a resolution of 0.5°, and 32 vertical levels. The nested simulation with 0.22° resolution and 40 vertical levels started in Dec. 2012. Spectral nudging of NCEP data was applied for large scale wind speed components in the upper levels to enforce the observed large scale circulation.

No actual, freely available emission inventory for China is existing. The most recent comprehensive emission data set is the EDGAR emission data from 2008. It is delivered as annual totals on $0.1 \times 0.1$ degrees for the entire globe. These emissions were adapted for the current situation by extrapolating the emission increase between 2004 and 2008 until the year 2012. This was done on a grid cell basis in order to apply different growth factors in different areas of the grid. The emissions were then distributed in time according to seasonal, weekly and annual factors determined in the SMOKE for Europe emission model [1], which was adapted to the region.

Constant concentration profiles were used as boundary conditions outside the large grid. The influence of the boundary conditions on the air pollution levels in the Beijing area was investigated through sensitivity runs. It was found that their influence was negligible during this specific time period characterized by low wind speeds.

## 34.3 Results

Figure 34.1 shows a map of the PM2.5 concentrations on the $24 \times 24$ km$^2$ grid in the lowest model layer. The average concentration during the second week in January (7–13 January) was higher than 85 $\mu$g/m$^3$ in large areas of North East China. The time series of the PM2.5 concentration (Fig. 34.2) shows modelled PM2.5 concentrations up to 500 $\mu$g/m$^3$. No officially measured PM2.5 concentrations were available to the authors, however observations made at the US embassy in Beijing were reported in the internet. The corresponding PM2.5 concentrations were even higher than the modelled values. In particular on 12 January PM2.5 concentrations of more than 800 $\mu$g/m$^3$ were reported. These values were not reproduced by the model. During the other periods, the model captured the pollution levels and their variability quite well.

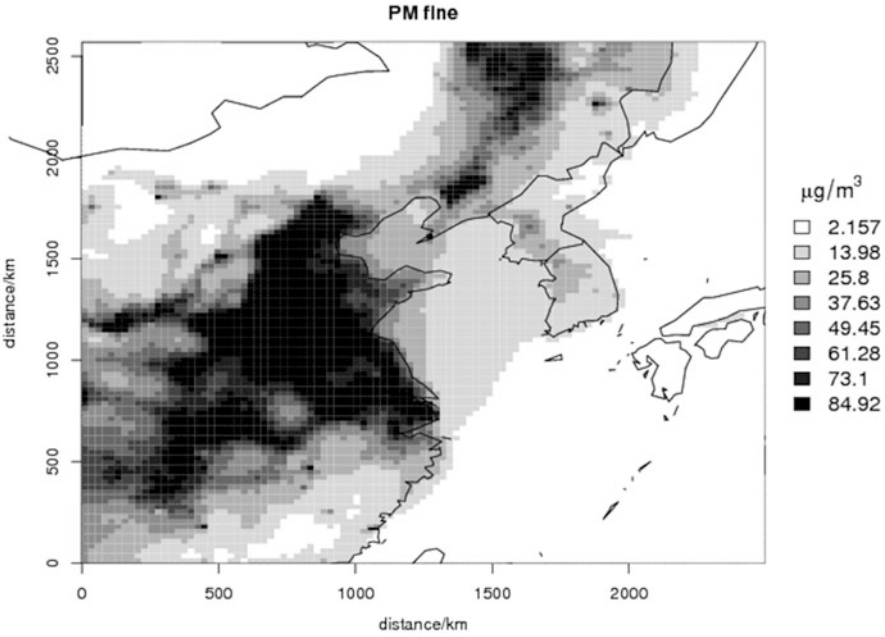


**Fig. 34.1** CMAQ model results: Mean PM2.5 concentration in the lowest model layer between 7 and 13 January 2013 in North East China

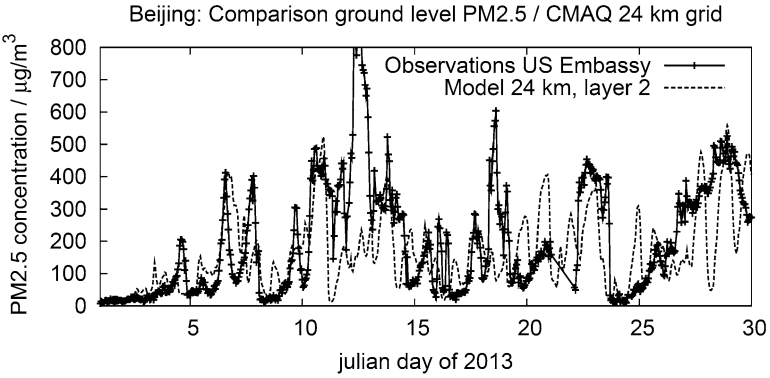


**Fig. 34.2** Comparison of modelled PM2.5 concentrations in the second model layer (20–40 m above ground) (*dashed lines*) and observations at the US embassy (*solid lines*)

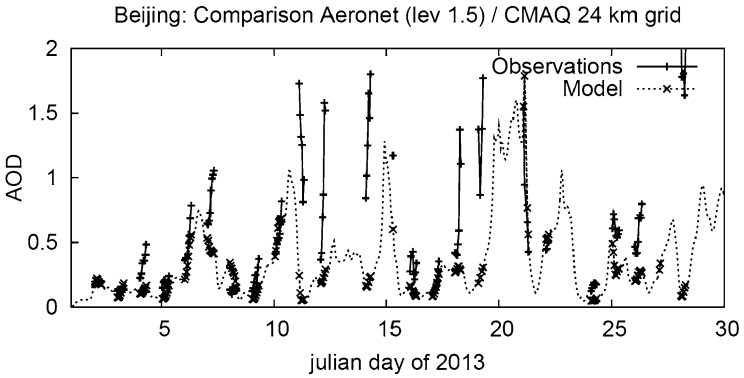


**Fig. 34.3** Aerosol optical depth in Beijing measured with Aeronet sun-photometer (*solid lines*) compared to CMAQ model results (*dashed lines*). Crosses denote model values corresponding to the observation times

The model results were also compared against aerosol optical depth (AOD) observations gathered within the Aeronet sun-photometer network [3]. As an example Fig. 34.3 shows the time series for January 2013 at Beijing. Again the model underestimates the highest observations, in particular between 10 and 15 January, on 18/19 and on 28 January. There are two important reasons for this which are closely related to the meteorological situation. One is that extreme temperature inversions and very shallow boundary layers are not well simulated by the model. This was likely the case e.g. on 12 January, when the ground level concentrations were much too low in the model. The second reason is that AOD depends critically on relative humidity (RH) at values above 80 %. Such high values were frequently observed in Beijing, as was seen in data from radiosoundings. The model typically showed much lower RH in the boundary layer.

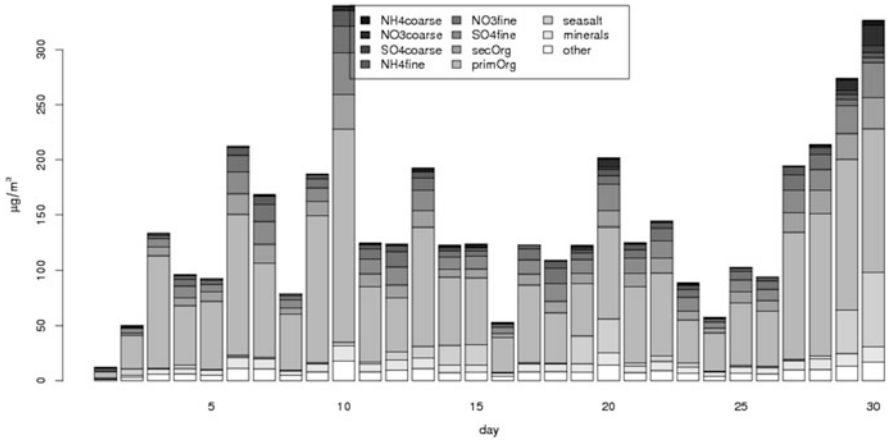


**Fig. 34.4** Chemical composition of PM2.5 in Beijing from 1 to 30 January 2013

An analysis of the modelled chemical species of the fine aerosol at Beijing (Fig. 34.4) reveals that the aerosol is to a large extent composed of primary and secondary organics. These species have a particularly high share of 60–70 % in the total emissions in sector 2 (residential heating). A further analysis of the contribution of the different emission sectors to the total PM2.5 showed that only the contribution of sector 2 to the total PM2.5 was positively correlated ($R = 0.54$) to the total concentration. This indicates that the highest PM2.5 concentrations are significantly influenced by emissions from residential heating. Calm winds and a significant temperature inversion contribute to the accumulation of aerosols from nearby ground based sources in a very shallow boundary layer. Traffic emissions were found to be of minor importance for the aerosol formation.

## 34.4 Conclusion

The exceptionally high air pollution in China in January 2013 was simulated with the CMAQ model system using extrapolated EDGAR emission data from 2008 and COSMO-CLM meteorological fields. In general, the level of PM2.5 was matched well according to the few available observations. However, the highest PM2.5 concentrations were not adequately reproduced because the very shallow boundary layer could not be captured by the meteorological model. According to the CMAQ model, primary and secondary organics are the largest fractions in the chemical composition of the aerosol in Beijing. Emissions from residential heating contributed more than on average to the aerosol concentrations on those days with the highest aerosol load.

**Acknowledgments** The authors thank US EPA for the development and distribution of CMAQ and the EDGAR community for the provision of emission data. We would like to thank the AERONET sun-photometer network and their PIs for their important observations. Special thanks to David Black and Ajay Pillarisetti for collecting the PM2.5 observations at the US embassy in Beijing.

## References

1. Bieser J et al (2011) SMOKE for Europe – adaptation, modification and evaluation of a comprehensive emission model for Europe. Geosci Model Dev 4(1):47–68
2. Feser F, Barcikowska M (2012) The influence of spectral nudging on typhoon formation in regional climate models. Environ Res Lett 7:014024. doi:10.1088/1748-9326/7/1/014024
3. Holben BN et al (1998) AERONET – a federated instrument network and data archive for aerosol characterization. Remote Sens Environ 66:1–16

## Questions and Answers

**Questioner Name:** Clemens Mensink

**Q:** Why is your meteorological model not catching the temperature inversion and resulting shallow PBL?

**A:** Several aspects could play an important role. These are radiative effects because of lacking aerosols in the meteorological model, a too coarse vertical resolution of the model and larger scale effects that result from errors in the driving meteorological data from NCEP. Some of the parameterizations that treat the turbulent kinetic energy under stable conditions in the COSMO model might also be relevant. We did not investigate this in detail until now.

**Questioner Name:** Christian Hogrefe

**Q:** This episode would be a good test for applying a coupled model. Do you have plans to do so?

**A:** Yes, we agree that this is an interesting episode for studying the interaction between solar radiation, high aerosol loads and reduced vertical mixing due to high atmospheric attenuation of sunlight. In our research group we currently do not use online coupled CTMs. We have plans to install either WRF-CMAQ or COSMO-ART in order to test the performance of online coupled models in complex situations like this one. However, currently we are lacking enough man-power to get these plans realized, soon.

**Questioner Name:** Jonathan Pleim

**Q:** My comment follows up from the previous two questions. Our collaborators at Tsinghua University in Beijing have done similar modeling for a different case using the two-way coupled WRF-CMAQ with direct aerosol feedback. They

have shown large effects of direct aerosol feedback to greatly reduce PBL height and greatly increase PM2.5 concentrations for extreme episodes.

**A:** We think this could be an important effect which is not considered in our current simulation. It would be worth to see results from an online model for the same period.

**Questioner Name:** Yang Zhang

**Q:** Did you have a chance to compare your emissions with MEIC (multi-resolution emission inventory for China), www.meicmodel.org?

**A:** Unfortunately, we were not aware of this emission inventory, but we are highly interested to do another model run with this alternative data set.

# Chapter 35
# Impact on Ontario's Air Quality due to Changes in North American Emission from 2005 to 2020

**Andrei Chtcherbakov, R. Bloxam, S. Wong, and Y. Hall**

**Abstract** This paper shows the effects of emission reductions from 2005 to 2020 levels on ozone and PM2.5 concentrations in Ontario based on modelling results. To assess the effect of these changes on Ontario's air quality, the modelling system WRF – SMOKE – CMAQ was run with 2010 meteorology for the entire year. Emission estimates were based on US EPA Cross-State Air Pollution Rule Final CAP – BAFM 2005-Based Platform, version 4.2, Toxic rule 2016 with updates projected to 2020 for mobile emissions and Environment Canada 2005 and 2020 emission inventories.

Emission changes in Ontario and in the neighbouring US states (Ohio, Michigan, Indiana, etc.) from 2005 levels to projected values of 2020 are discussed. Modelling results were summarized to show spatial and temporal variability in ozone and PM2.5 concentration over Ontario due to emission reduction in the whole domain. Analysis was performed on annual values and on values obtained on days with high concentrations only.

## 35.1 Introduction

Analysis of emissions trends for recent years for both US and Canada shows reductions in almost all sectors – point, area, off road and on road mobile sources. These changes are mainly due to the implementation of control strategies, efficiency gains and global economic downturn. These emission reductions have contributed to lower ambient pollutant concentrations in the province of Ontario (Canada) and all over North America.

A. Chtcherbakov (✉) • R. Bloxam • S. Wong • Y. Hall
Air Monitoring and Transboundary Air Sciences Section, Environmental Monitoring and Reporting Branch, Ontario Ministry of Environment, Toronto, ON, Canada
e-mail: Andrei.Chtcherbakov@ontario.ca

D. Steyn and R. Mathur (eds.), *Air Pollution Modeling and its Application XXIII*,
Springer Proceedings in Complexity, DOI 10.1007/978-3-319-04379-1_35,

In this study modelling results were analyzed to evaluate the effect of emission reductions from 2005 levels to projected 2020 levels on air concentrations of ozone (8 h maximum concentration) and fine fraction of particulate matter (PM2.5) in Ontario, Canada, are shown.

To perform the analysis, a modelling system consisting of WRFv3.11 – Weather Research and Forecast meso-meteorological model, SMOKEv2.4/3.0 – emission processing model, and CMAQv4.6 – regional chemical transport model were used.

## 35.2 Modelling System Set Up

The setup of modelling system was as follows.

To obtain the meteorological input, WRFv3.11 was run for the entire year of 2010. Initialization of WRF was done every 12 h with the Eta analysis of 3D meteorological fields. The model used default settings for the microphysics and numerics, a 36 km horizontal resolution, a spatial coverage including all of North America, and 22 vertical layers with finest resolution up to 20 m in the surface layer. To transform WRF3.11 output files to the files used in emission processing (SMOKEv 2.4/3.0), the regional chemical transport model (CMAQ4.6), postprocessor MCIPv3.4/4.0 was used. The model's output was enhanced by incorporating urban heat island effect based on including anthropogenic heat flux in the surface layer, recalculating parameters related to vertical mixing and applying changes to selected grid cells representing major Canadian cities (Toronto and Montréal areas). This resulted in improvements to the CMAQ performance in these urban areas. Emissions were processed separately for US and Canada with 2010 meteorology using the SMOKE2.4/3.0 emission processor and the SAPRC99 chemical mechanism.

For year 2005, US EPA Cross-State Air Pollution Rule Final CAP – BAFM 2005-Based Platform, version 4.2 was used for US emissions and emission inventory files from Environment Canada (EC) with updates and addendums related to Ontario region were used for Canada.

For year 2020, US emission inventories for the Toxic Rule 2016 along with updated ancillary files were processed. Mobile emissions were projected from 2016 to 2020 levels based on factors provided by US EPA.

Regional scale chemical transport model CMAQ4.6 with the SAPRC99 chemical mechanism with default physical and chemical settings, default boundary and initial conditions, derived from the supplied vertical profiles was run for 2005 and 2020 emission scenarios to calculate ambient air concentrations of major atmospheric pollutants. The model was run with horizontal resolution of 36 km, in a domain of $71 \times 79$ grid cells, covering an area stretching from South Carolina to Hudson Bay and from eastern Manitoba to the Maritime Provinces. A vertical resolution with the same structure as the meteorological model (WRF) was used to eliminate possible interpolation errors.

## 35.3 Emissions and Ozone and PM2.5 Concentration Changes from 2005 to 2020

Emission reduction from 2005 levels to the projected 2020 levels occurred in all major sectors resulting in provincial emission decreases of 30–40 %.

Primary PM2.5 emissions decreased considerably both in US and Canada. The most noticeable emission reductions can be seen close to the Ohio/Pennsylvania border, Indiana, and southwestern Ontario. Changes in the Greater Toronto Area (GTA) are not as noteworthy.

Even more significant reductions can be seen in SO2 emissions with the most affected areas being in Indiana, Ohio, Pennsylvania and Illinois and Detroit region. All these regions are located upwind to prevailing air mass flows into southern Ontario and thus emitted species are likely involved in long-range transboundary advection to Ontario, thereby contributing to air pollution and affecting air quality in Ontario.

Annual PM2.5 and 8-h maximum ozone concentrations on high concentrations days show a noticeable reductions in ozone (8–16 %) and PM2.5 (10–40 %) concentrations across Ontario due to emission reduction from 2005 to 2020 levels. The spatial distribution of reductions varies depending on location (urban vs. rural), chemical and physical processes involved in contaminant formation (local vs. long range transportable influences) and prevailing wind directions relative to emission sources (upwind vs. downwind).

On Fig. 35.1, percent changes in ozone and PM2.5 concentrations in selected counties across Ontario are presented.

The smallest impact on PM2.5 concentrations due to emission reduction was found in highly urbanized municipalities, including 9–19 %, in Toronto and York counties, and 17 % in Ottawa county as opposed to more rural communities, for example Wellington and Middlesex counties, where the reductions in concentrations were more than 40 % . These differences can be explained by the fact that PM2.5 concentrations at rural regions are dominated by secondary components. Precursors which transform during long transport to form secondary components, such as sulfates (SO4), nitrates (NO3), and secondary organic aerosol (SOA), have decreased significantly. On the contrary, urban PM2.5 composition is dominated by local, primarily emitted species, with spatially limited impacts. Additionally, emission reductions of primary PM2.5 species in the GTA from 2005 to 2020 were not as significant as compared to other contaminants, including SO2, a PM2.5 precursor.

Communities in southwestern Ontario, closest to the Canada/US border (such as Essex County – Windsor area), are under the influence of long range transboundary ozone transport. Ozone reduction in these areas ranged from 12 to 13 %. In urban areas, especially the GTA, less regional ozone production due to reductions of elevated emitted ozone precursor pollutants upwind is compensated by less ozone titration by local low level NOx emissions because of the changes from 2005 to

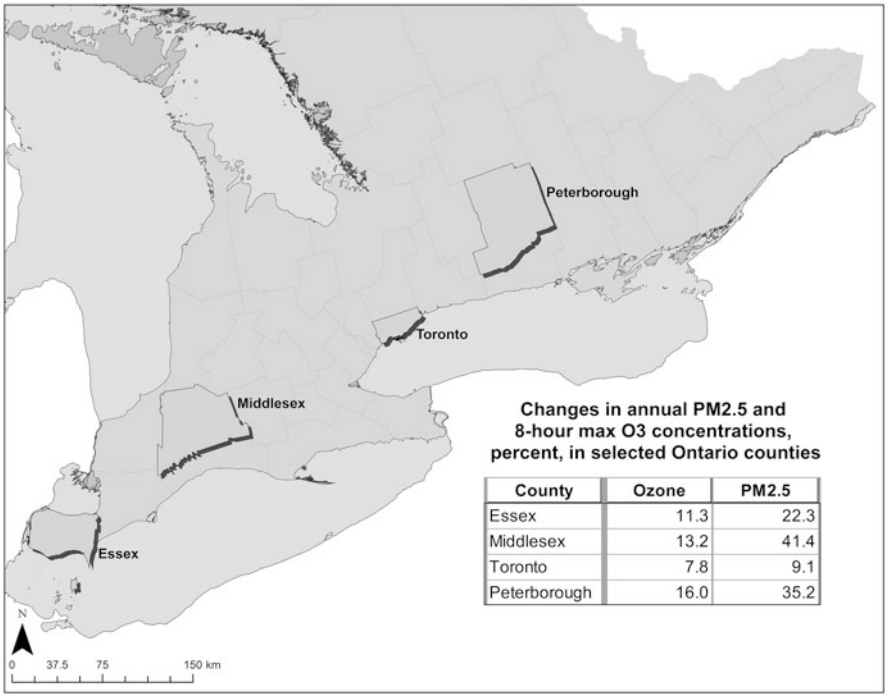


| County | Ozone | PM2.5 |
|---|---|---|
| Essex | 11.3 | 22.3 |
| Middlesex | 13.2 | 41.4 |
| Toronto | 7.8 | 9.1 |
| Peterborough | 16.0 | 35.2 |

**Fig. 35.1** Changes in annual PM2.5 and 8-h max ozone concentrations, percent, due to emission reduction from 2005 to 2020 level in selected Ontario counties

2020 levels. That explains why the impact in the GTA on ozone reductions is the lowest, only 7–8 %. On the contrary, the areas with the greatest ozone reduction, 16 %, are located downwind of the GTA in Peterborough and Frontenac counties (Kingston).

## Question and Answer

**Questioner Name:** Christian Hogrefe

**Q:** How do the modelled concentration reductions compare to regulatory air quality standards. Will additional emission reductions be required to meet these standards?

**A:** For ozone concentrations additional reductions in precursor emissions will be required to meet existing Canada wide standard, controls should be implemented mostly south of Canada – US border.

# Chapter 36
# Modelling the Concentration and Deposition of Heavy Metals in the UK

**Anthony Dore, Stephen Hallsworth, Małgorzata Werner, Maciej Kryza, Eiko Nemitz, Heath Malcolm, Stefan Reis, and David Fowler**

**Abstract** A relatively simple Lagrangian atmospheric transport model (FRAME) was adapted to simulate the concentration and deposition of nine heavy metals (As, Cd, Cr, Cu, Pb, Ni, Se, V and Zn) in the UK. The modelled data was compared with annually averaged measured wet deposition of metals and concentrations in air. The model obtained good correlation with measurements of metal concentrations in air but with very large underestimates (normalised mean biases in the range −0.64 to −0.93), indicating a major under-estimate in total atmospheric emissions. Wet deposition was less closely correlated to measurements. Inclusion of estimates of spatial re-suspension of wind-driven dust for the UK in the model simulation led to an improvement in agreement with measured concentrations. However the amount of re-suspended material was considered to be highly uncertain due to the limited availability of measurement data of the heavy metal content of surface soil and dust.

## 36.1 Introduction and Model Description

Heavy metals are a concern for both human health and natural ecosystems. As a multi-organ system toxicant, Pb can have chronic and acute affects on human health. Cadmium is carcinogenic by inhalation. Cd, Pb, Cu, Ni and Zn are detrimental to soil microbes when critical loads are exceeded [3]. The 1998 UNECE protocol on heavy metals committed all participating countries to reduce their emissions of Pd and Cd to levels below those of 1990 as well as phasing out leaded petrol. As a result

A. Dore (✉) • S. Hallsworth • E. Nemitz • H. Malcolm • S. Reis • D. Fowler
Centre for Ecology and Hydrology, Bush Estate, Penicuik, Midlothian EH26 OQB, UK
e-mail: todo@ceh.ac.uk

M. Werner • M. Kryza
Department of Climatology and Atmosphere Protection, University of Wrocław, ul. Kosiby 8, 51-621 Wrocław, Poland
e-mail: malgorzata.werner@uni.wroc.pl; maciel.kryza@uni.wroc.pl

D. Steyn and R. Mathur (eds.), *Air Pollution Modeling and its Application XXIII*, Springer Proceedings in Complexity, DOI 10.1007/978-3-319-04379-1_36,

of this, as well as growing environmental awareness, emissions of Cd and Pb in the UK fell by 85 and 97 % respectively in the UK between 1990 and 2006.

In this study a simple Lagrangian model using annually averaged meteorology has been adapted to simulate the concentration and deposition of nine heavy metals in the UK. The FRAME model has been previously applied to calculate the deposition of sulphur and nitrogen and exceedance of critical loads (i.e. [2]) and was found to perform well when compared to more complex Eulerian models. FRAME is a Lagrangian model using straight line trajectories with a 1° angular resolution which runs at a 5 km resolution over the British Isles and 50 km resolution over Europe with a fine vertical grid spacing (1 m at the surface). Area emissions are injected into sector dependent levels and point source emissions are treated with a plume rise routine. Vertical diffusion in the air column is calculated using K-theory eddy diffusivity. Wet deposition is calculated using a 'constant drizzle' approximation driven by an annual rainfall map. Five land classes are considered and a vegetation specific canopy resistance parameterization is employed to calculate dry deposition of particulates. For this work the model was modified to simulate nine non-reactive heavy metals (As, Cd, Cr, Cu, Pb, Ni, Se, V and Zn) including size-segregated particulate concentrations using four size categories.

## 36.2 Results

The modelled dry and wet deposition of Pb over the UK for the year 2006 is illustrated in Fig. 36.1. In general a strong gradient is evident, with the higher concentrations found in the central and southern part of the country, due to both long the range transport of pollutants from European sources as well as the greater intensity of emissions sources in the southern part of the UK. High values for wet deposition occur in more remote areas with lower air concentrations but high annual precipitation, such as the Highlands of Scotland and the Welsh hills.

A rural network for monitoring the concentrations of heavy metals in air and precipitation has been in operation in the UK since the year 2004. For the year 2006 the network consisted of 13 sites at which samples of precipitation were collected every 4 weeks for analysis of concentrations. Measurements of the concentration of heavy metals in air using a Partisol $PM_{10}$ sampler were also made with a weekly sample collection at ten of these sites. The concentrations of the nine trace metals included in this study were measured by ICP-MS analysis. Deposition of heavy metals at the sites was calculated by combining the measured concentrations in precipitation with annual precipitation measured at the sites with tipping bucket rain gauges. Figure 36.2 illustrates the correlation with measurements for Pb. Both air concentration and wet deposition are significantly under-estimated by the model. There is evidence of a much stronger correlation with measured air concentrations ($R^2$ of 0.89) than with wet deposition ($R^2$ of 0.67). This may reflect the complexity of the wet deposition process which is not fully captured by the model or the influence of dry deposition to the collector surface. The low slope of the Pb

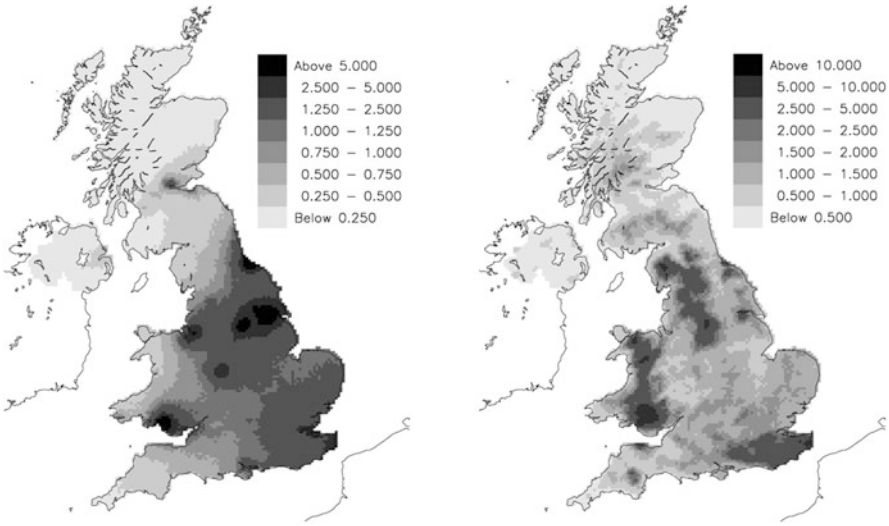


**Fig. 36.1** Dry deposition of Pb (*left*); wet deposition of Pb (*right*) g $Ha^{-1}$

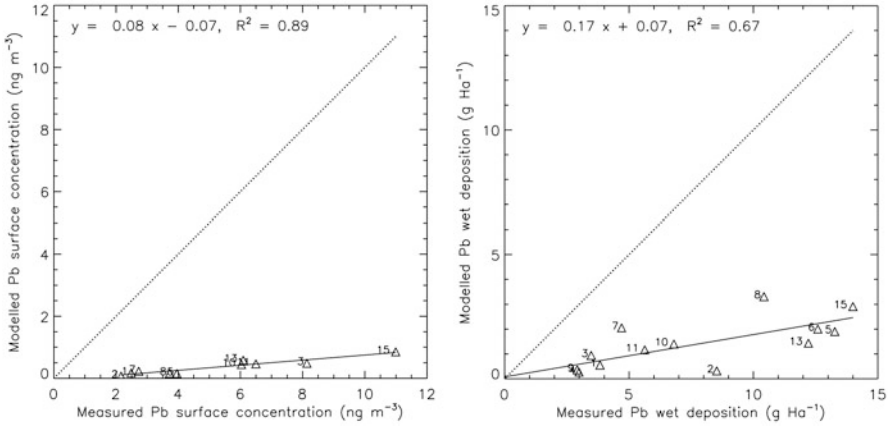


**Fig. 36.2** Correlation of the model with: measurements of Pb concentration in air (*left*); measurements of Pb wet deposition (*right*)

correlation plots (0.08 for air concentration; 0.17 for wet deposition) illustrates that overall Pb concentrations in both air and precipitation are greatly under-estimated by the model. This is a clear indication of missing or under-estimated emissions sources.

The modelled annual average air concentration and wet deposition for all metals has been compared with the values obtained by measurement at the monitoring

**Table 36.1** Estimates of primary and re-suspended emissions of Cd and Pb for the UK for 2006 (Mg year$^{-1}$)

| Variable | Cd | Pb |
|---|---|---|
| Primary | 3.6 | 87.9 |
| Re-suspended (a) | 0.52 | 40.8 |
| Resuspended (b) | 3.1 | 469 |

networks. These results suggest that the official National Atmospheric Emissions Inventory estimates are insufficient to account for observed concentrations of As, Cd, Cr, Cu, Ni, Pb and Zn by factors ranging from 2 to 10.

Additional model simulations were undertaken which included spatial estimates of the wind-driven re-suspension of surface dust [1, 4]. The surface dust layer is known to contain high concentrations of heavy metals which are still present in the environment due to the legacy of higher atmospheric metal emissions during the preceding decade. Estimates of the annual emissions of re-suspended metals for the UK vary significantly depending on the technique used to estimate metal concentrations in the surface dust layer. Both the total primary emissions of Cd and Pb as well as re-suspension estimates using (a) measured metal concentrations in a 15 cm surface soil core and (b) an algorithm based on use of 'enhancement factors' in the surface dust layer are illustrated in Table 36.1.

With re-suspension scenario (a) (including surface metal concentrations based on measurements from soil cores) only a moderate improvement in the model comparison with measurements was observed. However with scenario (b) the much larger estimates of the mass of re-suspended metals led to a significant improvement in the comparison with measurements. The normalised bias for correlation with measured Pb concentrations in air changed from −0.93 for the primary emissions scenario to −0.45 for scenario (b).

## 36.3 Conclusion

An atmospheric transport model was used to calculate the wet deposition and air concentrations of heavy metals (As, Cd, Cr, Cu, Pb, Ni, Se, V and Zn) in the UK. Comparison with measurements from a national monitoring network revealed the large magnitude of missing emissions sources. Inclusion of secondary 'legacy' emissions caused by the wind-driven re-suspension of surface dust led to improved agreement with measurements. However the contribution from this source remains highly uncertain due to the lack of measurements of metal concentrations in the surface dust layer. Other possible sources of emissions not included in the study include those from natural sources and sea water as well as fugitive emissions and the possibility of under-estimated primary emissions sources.

**Acknowledgments** This work was funded by the Natural Environment Research Council.

## References

1. Abbott J (2008) Modelling re-suspended heavy metal emissions. Report to the Department for the environment, food and rural affairs. ED 05450303, issue number 2, October 2008
2. Matejko M, Dore AJ, Hall J, Dore CJ, Błaś M, Kryza M, Smith R, Fowler D (2009) The influence of long term trends in pollutant emissions on deposition of sulphur and nitrogen and exceedance of critical loads in the United Kingdom. Environ Sci Policy 12:882–896
3. RoTAP (2012) Review of transboundary air pollution. Acidification, eutrophication, ground-level ozone and heavy metals in the UK. http://www.rotap.ceh.ac.uk/
4. Travnikov O, Ilyin I, Rozovskaya O, Varygina M, Aas W, Uggerud HT, Mareckova K, Wankmueller R (2012) Long-term changes of heavy metal transboundary pollution of the environment (1990–2010) EMEP contribution to the revision of the heavy metal protocol. http://www.emep.int/publ/common_publications.html#2012. Accessed 17 May 2013

## Questions and Answers

**Questioner Name:** Roger Timmis

**Q:** Have you considered comparing model performance for particularly wet and particularly dry years (or seasons) when re-suspension could be suppressed or enhanced respectively? 2012 was especially wet in England when dust (e.g. from steel works) was suppressed compared to other years – so 2012 may be a possible "wet" year compared to other years.

**A:** The re-suspended emissions values calculated by MSC-east covered a 20 year period and these did indeed show considerable inter-annual variability due to meteorology (i.e. both soil wetness and wind speed). A regional multi-year study would therefore certainly be of interest.

**Questioner Name:** Steve Hanna

**Q:** There is much uncertainty in published re-suspension factors. Sehmel's chapter on observations of re-suspension in a U.S. SOE Workbook suggests, for the same chemical and oil type, re-suspension can vary over many orders of magnitude depending on moisture content and packing (e.g. by vehicles). Does your model account for these uncertainties?

**A:** Two independent estimates of heavy metal re-suspension were used in the model and these were calculated externally in separate studies. These re-suspension estimates did account for soil wetness, soil type and particle size as well as vehicle packing. However it should be acknowledged that the values of many of these input parameters and their spatial distribution in the re-suspension calculation are highly uncertain. The range of uncertainty in re-suspension estimates due to imprecise knowledge of input parameters has not been assessed.

# Chapter 37
# A Process Analysis of the Impact of Air-Quality/Weather Feedbacks Using GEM-MACH

**Paul A. Makar, Wanmin Gong, Junhua Zhang, Jason Milbrandt, Sylvie Gravel, Balbir Pabla, and Philip Cheung**

**Abstract** Environment Canada's "Global Environmental Multiscale – Modelling Air-quality and Chemistry" (GEM-MACH) is the Canadian operational air-quality model, used to provide forecasts of ozone, $PM_{2.5}$ and air-quality health metrics to the Canadian public. The operational GEM-MACH is an on-line model, but is not fully coupled, in that the chemical variables are not used to modify the weather. The model was converted to fully coupled status as part of Environment Canada's participation in phase 2 of the Air-Quality Model Evaluation International Initiative, with three classes of modifications: (1) Additions required in order to allow feedbacks to take place between weather and chemistry; (2) Model improvements necessary to ensure feedback accuracy; (3) Model improvements to allow the use of AQMEII-2 prescribed inputs and diagnostic outputs.

The revised model is being used to generate four annual simulations of air-quality over North America, for "feedback" and "base-case" simulations for the years 2006 and 2010. Here, the initial test simulation results for 2006 of surface $O_3$ and $PM_{2.5}$ are compared using a simple statistical package, as a means of identifying cases wherein feedbacks have the greatest influence on the model's chemical output. These instances will be put forward for further study under the multi-model framework of AQMEII-2.

P.A. Makar (✉) • W. Gong • J. Zhang • B. Pabla • P. Cheung
Air Quality Research Division, Environment Canada, Toronto, ON, Canada M3H 5 T4
e-mail: paul.makar@ec.gc.ca; wanmin.gong@ec.gc.ca; junhua.zhang@ec.gc.ca; balbir.pabla@ec.gc.ca; philip.cheung@ec.gc.ca

J. Milbrandt
Recherche en Prévision Numérique, Environment Canada, Dorval, QC, Canada HP9 1 J3
e-mail: jason.milbrandt@ec.gc.ca

S. Gravel
Air Quality Research Division, Environment Canada, Dorval, QC, Canada HP9 1 J3
e-mail: sylvie.gravel@ec.gc.ca

D. Steyn and R. Mathur (eds.), *Air Pollution Modeling and its Application XXIII*,
Springer Proceedings in Complexity, DOI 10.1007/978-3-319-04379-1_37,

## 37.1 Introduction

The Global Environmental Multiscale model [4], coupled with chemistry modules first described in Gong et al. [5] comprise the main building blocks of the operational GEM-MACH model. Background information on the model, its evaluation, etc., appear elsewhere in the proceedings for this and previous ITM conferences (cf. [8]). The operational model is "on-line" in that the model's chemistry package runs within the weather forecast model's physics (the chemistry includes 42 gas-phase species, a 9 species/2 bin aerosol microphysics package, modules for inorganic and organic heterogeneous chemistry, cloud processing of aerosols, and packages for the input and use of SMOKE-generated emissions data). The operational model is not, however, fully coupled: the resulting chemistry is not allowed to impact the meteorological model's radiative transfer and cloud microphysics. We describe below the suite of changes to upgrade the operational GEM-MACH model to a fully coupled status.

## 37.2 Implementing Feedbacks: Modifications and Upgrades to the Model Code

### *37.2.1 Code Modifications for Feedbacks*

*Aerosol Indirect Effect* The operational GEM-MACH code uses the Sundqvist and Kain-Fritsch schemes for resolved-scale condensation processes and sub-grid scale deep convective processes, respectively. The Kain-Fritsch convective scheme does not lend itself to easy incorporation of the aerosol feedback to microphysics: the feedback of on-line aerosols to the model microphysical processes was incorporated via upgrading from Sundqvist to the 2-moment explicit microphysics scheme of Milbrandt and Yau [9] (used here at 15-km resolution to allow at least some of the aerosol indirect effect to influence model results, and for consistency with higher resolution studies currently underway). The scheme solves the bulk prognostic equations for number density and mass mixing ratio of 6 hydrometeors (cloud droplets, rain, ice, snow, graupel and hail). The default cloud condensation nuclei (CCN) activation at a given supersaturation follows Cohard et al. [3], with a fixed CCN spectrum for generic "continental" or "maritime" aerosols, but has been replaced here with the Abdul-Razzak and Ghan (2002) scheme, to use the on-line sectional and chemically-speciated aerosols. Aerosol activation is determined through comparing the upper and lower bounds of critical supersaturation of each size bin to the maximum supersaturation in an updraft, parameterized through a number-weighted effective critical supersaturation [6]. The model aerosols thus influence the meteorology through cloud droplet nucleation, while the cloud droplet number concentrations are in turn used in cloud processing of gases and aerosols in the chemistry module.

*Aerosol Direct Effect* The operational radiative transfer modules [7] use specified latitudinally varying incremental aerosol optical depths, and assume uniform aerosol concentrations from 0 to 1,500 m, and single values of asymmetry factor and single-scattering albedo (with different numbers for oceanic and continental airmasses). These simple parameterizations were replaced with large ($10^5$ member) lookup tables for the three aerosol optical properties (layer optical depth, asymmetry factor and single-scattering albedo). The tables were generated using the Mie code of Bohren and Huffmann [2], have axes of aerosol water content versus size, and employ a complex refractive index for aerosols of $[(1.5-0.17\ W_f)+(0.01*(1.0-W_f))i]$, where $W_f$ is the volume fraction of aerosol water. The aerosol wet and dry mass and the particle numbers within each bin are used to create bin-specific values for the three optical properties, which are summed to determine the net properties across the distribution. Implementation of a speciation-resolved set of tables will take place in future work.

### 37.2.2 Code Modifications to Ensure Feedback Accuracy

*Aerosol Size Distribution* Cloud droplet nucleation and radiative properties of aerosols are strong functions of aerosol size and number (poorly resolved in a 2 bin model such as the operational GEM-MACH). Consequently, GEM-MACH was used in a 12-bin configuration for these simulations, in order to better resolve the aerosol size distribution.

*Sea-Salt Emissions Flux Improvement* The operational GEM-MACH included the mass flux of sea-salt aerosols into the lowest model layer as a separate operator at the end of the sequence of operators affecting aerosol mass, while more recent versions of GEM-MACH (cf. [8]) include sea-salt emissions as a flux boundary condition on the diffusion equation; this improvement has been added to the GEM-MACH version used here.

*Particle Settling and Deposition Velocity Corrections* The operational model formulation for settling velocities [1] is strictly valid only for particles $< 19$ $\mu$m diameter, leading to large overestimates for particles under humid conditions. Formulae covering larger particles and droplets and the Cunningham slip correction factor were incorporated [1]. The operational model algorithm using the settling velocities calculates aerosol mass flux between model layers as an exponential decay rate to estimate transport out of the bottom of the layer. Tests with high resolution versions of GEM-MACH showed that this methodology could sometimes lead to erroneously high particle masses due to conflicts with the model's semi-Lagrangian advection algorithm. Particle settling and deposition are estimated using a one-dimensional semi-Lagrangian advection approach, with a clipped and column-mass-conserving cubic Lagrange interpolant, eliminating this problem.

### 37.2.3 Code Modifications for AQMEII-2 Inputs and Enhanced Diagnostic Outputs

*Regenerated Emissions* The gridded and speciated AQMEII-2 emissions for North America were available under the study protocol from the US EPA for a single model speciation and grid. The emissions inventory was reprocessed with the SMOKE emission processing system to create new emissions for GEM-MACH on its native grid and chemical speciation.

*Emissions Input Capabilities* The GEM-MACH model and emissions preprocessor codes were modified to allow the number and location of major point sources to vary on a daily or hourly basis, to accommodate daily changes in wildfire emissions in the AQMEII-2 database.

*Accumulated Field Output* The operational model's capability to output total PM2.5 and PM10 as accumulated fields was extended for output of speciated $PM_1$, $PM_{2.5}$, $PM_{10}$, and total PM.

*Deposition Field Output* No provision was available in the operational model for the diagnostic output of deposition of gases and particles; output diagnostics were added for wet deposition of $HSO_3^-$, $H_2O_2$, organic peroxide, $SO_4^{2-}$, $NO_3^-$, $NH_4^+$, base cations, $HCO_3^-$, $H^+$, sea-salt, secondary organic aerosol, crustal material, black carbon, primary organic carbon and aerosol-bound water, and dry deposition of particle sulphate, sea-salt, secondary and primary organic matter, crustal material elemental carbon, and gases ($SO_2$, $H_2SO_4$, NO, $NO_2$, $O_3$, $HNO_3$, PAN, HONO, organic nitrate, $NH_3$, $NO_y$, $H_2O_2$, and HCHO).

*Satellite Comparison Diagnostics.* Diagnostics for total column densities of NO, $NO_2$, $SO_2$, CO, $NH_3$, $C_2H_4$, toluene, formaldehyde, isoprene, $PM_{2.5}$ and $PM_{10}$, and total column emissions of NO, $NO_2$, $SO_2$, CO, $NH_3$,.biogenic NO, $C_2H_4$, toluene, HCHO, isoprene, monoterpenes, biogenic "other VOC", biogenic isoprene, $PM_{2.5}$ and $PM_{10}$, were added to the model.

*Diagnostics for Tracking Feedbacks.* Additional outputs for the total column and individual layer aerosol optical depths at 4 radiative transfer and 5 diagnostic wavelengths (444.8, 940.1, 1785.7, 3190.5, and 470, 550, 555, 650, 675 nm) were added, as were the aerosol asymmetry factor and single scattering albedo, fine and coarse mode aerosol number density, VOC branching ratio ($NO_x$ versus VOC paths), total VOC concentration, total VOC reactivity, and $NO_2$ photolysis rate.

*Boundary Conditions* MACC MOZART-IFS reanalysis fields were converted to the model units and interpolated to the model grid, as stipulated under the AQMEII-2 protocol.

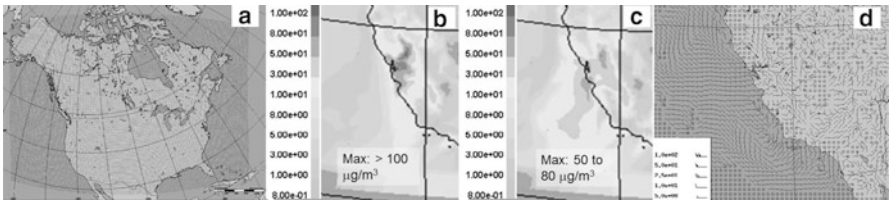


**Fig. 37.1** (**a**) GEM-MACH 15 km grid used in AQMEII-2 simulations; Surface $PM_{2.5}$ concentrations, San Francisco, 12UT, February 10th, 2006 for (**b**) base case and (**c**) feedback; (**d**); residual wind field (f.b. – base case)

## 37.3 Model Setup and Run Procedure

Model simulations are being carried out on a North American grid with a 15 km grid spacing (Fig. 37.1a). For the GEM-MACH simulations, the model is run in a "12 h of meteorology only/48 h of chemistry" configuration; the first 12 h of the simulation are used to spin-up the meteorological fields, and the remaining 48 h include chemistry, with and without feedbacks. For the GEM-MACH simulations, meteorological initial conditions come from operational analyses, while meteorological boundary conditions are derived from GEM simulations that start from operational analyses. Correlation coefficients between hourly "feedback" and "base case" simulations are being used to identify case studies where feedbacks have the greatest impact on both meteorology and chemistry, with $PM_{2.5}$ and residual wind fields off the coast of San Francisco as an example (Fig. 37.1b, c). These changes resulted from differences in radiative transfer and cloud cover on previous days. Summer simulations (Fig. 37.2) have substantial differences in urban PBL heights (higher with feedbacks), suggesting that feedbacks may help improve model performance by reducing existing primary emitted species positive biases in cities. The work is ongoing, with completion in late 2013/2014.

## 37.4 Current Status and Ongoing Work

Model simulations are underway at the time of writing of this abstract. As part of the workup of the model output for AQMEII-2, statistical comparisons between model surface fields between feedback and non-feedback simulations are being carried out to allow the identification of times with the largest divergence between the simulations, hence the situations and locations in which feedbacks have the greatest influence on the forecast.

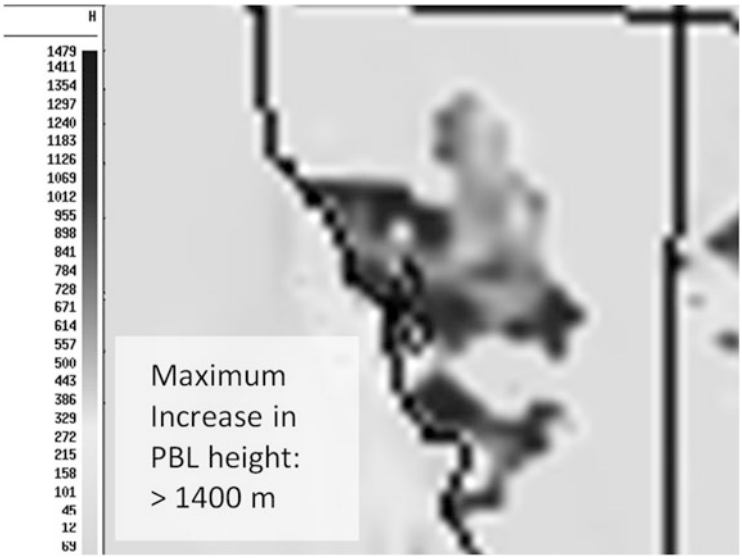


**Fig. 37.2** Increases in urban PBL height (f.b.- base case), July 19, 2006, San Francisco area

## References

1. Beard KV (1976) Terminal velocity & shape of cloud and precipitation drops aloft. J Atmos Sci 22:851–864
2. Bohren CF, Huffman DR (1983) Absorption and scattering of light by small particles. Wiley and Sons, Toronto, 530 pp
3. Cohard J-M et al (1998) Extending Twomey's analytical estimate of nucleated cloud droplet concentrations from CCN spectra. J Atmos Sci 55:3348–3357
4. Côté J et al (1998) The operational CMC-MRB global environmental multiscale (GEM) model. Part 1: design considerations and formulation. Mon Weather Rev 126:1373–1395
5. Gong W et al (2006) Cloud processing of gases and aerosols in a regional air quality model (AURAMS). Atmos Res 82:248–275
6. Gong W et al (2012) Impact of aerosol activation on modelled regional particulate matter mass and size distribution due to cloud processing. In: Steyn DG, Timmermans R (eds) Air pollution modelling and its application XXII. Springer, Dordrecht, in press
7. Li J, Barker HW (2005) A radiation algorithm with correlated-k distribution. Part I: local thermal equilibrium. J Atmos Sci 62:286–309
8. Ménard S et al (2013) Current and future developments in numerical air quality forecasting in Canada, these proceedings
9. Milbrandt JA, Yau MK (2005) A multimoment bulk microphysics parameterization. Part II: a proposed three-moment closure and scheme description. J Atmos Sci 62(9):3065–3081

## Questions and Answers

**Questioner Name:** Roger Timmis

**Q:** Are periods with strong feedback effects associated with particular steady (non-changing) synoptic conditions, i.e. with "spells" of weather when similar conditions persist for a few days? If so, could the feedback effects be made clearer + more process-related by grouping together results for these similar synoptic conditions? This could identify conditions when/where it is important to include feedback processes in order to improve model performance.

**A:** The analysis done so far is not sufficient to answer the question fully, though once the runs for both years are completed this could be checked. For the two episodes studied so far, the conditions over which the two runs differ do seem to occur on a synoptic time scale (the low correlations are present over 4 days in each case). So there may well be sets of synoptic conditions that are associated with a larger impact of the feedbacks, but it's too early to say yet whether these conditions are sufficiently frequent or unique to allow identification of "feedback-important" days by synoptic weather pattern. It's a good idea, and one that we should follow up on in AQMEII-2.

**Questioner Name:** Douw Steyn

**Q:** It would seem that the short-wave radiation (and associated temperature) changes would weaken, rather than strengthen, the sea breeze?

**A:** The increase in downward SW radiation at the surface occurs during the daytime, whereas the increase in residual sea-breeze strength is occurring on the subsequent night and early morning, when the short-wave input is zero. One would indeed expect the *daytime* land breeze to be strengthened by this effect – however, the sea-breeze increase occurs later, at night. At night, surface temperatures over the land have dropped when feedback effects are included; this implies that subsidence has increased at night over the land, and this subsidence is driving the nighttime sea-breeze. What is unclear as of yet is the connection between the day and subsequent night conditions – what has caused the additional nighttime cooling over the land? For example, the addition of feedbacks may have reduced cloud cover, allowing for greater radiative cooling in the subsequent night, in addition to allowing more shortwave to reach the ground in the afternoon. The additional short-wave radiation reaching the surface may also have caused daytime convection, followed by rainfall then clearing skies and more radiative cooling at night. More work will be required with the full set of model outputs to track down the causes behind the sequence of events shown here.

# Chapter 38
# Analog-Based Postprocessing Methods for Air Quality Forecasting

**Luca Delle Monache, Irina Djalalova, and James Wilczak**

**Abstract** Two new postprocessing methods based on analogs are proposed to reduce the systematic and random errors of air quality prediction. The analog of a forecast for a given location and time is defined as a past prediction that matches selected features of the current forecast. The first method is the weighted average of the observations that verified when the best analogs were valid (AN). The second method consists in applying a postprocessing algorithm inspired by the Kalman filter (KF) to AN (KFAN). The AN and KFAN are tested for ground level ozone and PM2.5 0–48 h predictions from the Community Multiscale Air Quality (CMAQ) model, with observations from 1602 surface stations from the EPA AirNow network over the continental United States for a 1-year period. Preliminary results of the new methods include a large reduction of the systematic and random errors of the direct model output, with an increase of the correlation between observations and predictions at all forecast lead times.

L.D. Monache (✉)
National Center for Atmospheric Research (NCAR), Boulder, CO, USA
e-mail: lucadm@ucar.edu

I. Djalalova
Cooperative Institute for Research in Environmental Sciences (CIRES),
University of Colorado, Boulder, CO, USA

National Oceanic and Atmospheric Administration (NOAA), Boulder, CO, USA
e-mail: irina.v.djalalova@noaa.gov

J. Wilczak
National Oceanic and Atmospheric Administration (NOAA), Boulder, CO, USA
e-mail: james.m.wilczak@noaa.gov

D. Steyn and R. Mathur (eds.), *Air Pollution Modeling and its Application XXIII*,
Springer Proceedings in Complexity, DOI 10.1007/978-3-319-04379-1_38,

## 38.1 Introduction

Forecast systematic and random errors are a problem common to all chemistry transport models [5]. In this paper we present preliminary results of a comparison of different postprocessing methods that aim at estimating these errors in real-time, to increase the accuracy of air quality predictions. These methods include simple approaches as persistence (PERS) and a 7-day running-mean bias correction (7DAY, [6]), a state-of-the-science postprocessing algorithm inspired by the Kalman filter [1, 2], and two new analog-based approaches. The analog of a forecast for a given location and time is defined as a past prediction that matches selected features of the current forecast. The first method is the weighted average of the observations that verified when the best analogs were valid (AN). The second method consists in applying a postprocessing algorithm inspired by the Kalman filter (KF) to AN (KFAN) [3, 4].

The PERS, 7DAY, AN and KFAN were tested for ground level ozone and PM2.5 0–48 h predictions from the Community Multiscale Air Quality (CMAQ) model, with observations from 1602 surface stations from the EPA AirNow network over the continental United States for a 1-year period.

## 38.2 Conclusion

Preliminary results are based on root-mean-square-error (RMSE), RMSE components [i.e., centered RMSE (CRMSE) and bias], and correlation, for both ground-level ozone and PM2.5. Based on these metrics, the methods rank (from the best to the worst) as follows: KFAN, KF, AN, PERS, 7DAY and the direct model output (RAW).

The best method, KFAN, improves the raw model prediction by more than 50 % base on RMSE, and about 35 % for correlation. Future work will focus on a sensitivity analysis of key aspects of the analog-based procedures, including the number of analogs, the predictor variables use for the analog search, and the amplitude of the time windows over which the analog matching is performed.

## References

1. Delle Monache L, Nipen T, Deng X, Zhou Y, Stull RB (2006) Ozone ensemble forecasts: 2. A Kalman-filter predictor bias correction. J Geophys Res 111:D05308. doi:10.1029/2005JD006311
2. Delle Monache L, Wilczak J, McKeen S, Grell G, Pagowski M, Peckham S, Stull R, McHenry J, McQueen J (2008) A Kalman-filter bias correction of ozone deterministic, ensemble-averaged, and probabilistic forecasts. Tellus 60B:238–249

3. Delle Monache L, Nipen T, Liu Y, Roux G, Stull R (2011) Kalman filter and analog schemes to post-process numerical weather predictions. Mon Weather Rev 139:3554–3570
4. Delle Monache L, Eckel T, Rife D, Nagarajan B, Searight K (2013) Probabilistic weather predictions with an analog ensemble. Mon Weather Rev 141:3498–3516
5. Russell A, Dennis R (2000) NARSTO critical review of photochemical models and modeling. Atmos Environ 34:2283–2324
6. Wilczak JM, McKeen SA, Djalalova I, Grell G (2006) Bias-corrected ensemble predictions of surface $O_3$. J Geophys Res 111:D23S28. doi:10.1029/2006JD007598

## Questions and Answers

**Questioner Name:** Heinke Schlunzen

**Q:** How do you treat measurement errors?

**A:** We agree that is important to consider observational errors while evaluation air quality predictions. It is worth noticing that the analog-based methods, particularly AN, are based on past observations of the quantity to be predicted, and therefore they include observational errors in their estimates.

**Questioner Name:** Stefano Galmarini

**Q:** Your analog-based methods produce an estimate where observations are available. What about locations where observations are not available?

**A:** In applications where observations over a gridded domain are necessary, the analog-based methods could be generated by using as the "ground-truth" not the observation, but rather an analysis (which merges observations with model estimates) over the same grid. Such approach will be considered for future research efforts.

# Chapter 39
# Comparing Different Modeling Approaches in Obtaining Regional Scale Concentration Maps

**Bino Maiheu, Nele Veldeman, Peter Viaene, Koen De Ridder, Dirk Lauwaet, Felix Deutsch, Stijn Janssen, and Clemens Mensink**

**Abstract** We studied and compared different operational modeling techniques that are used to generate regional scale concentration maps for $PM_{10}$, $PM_{2,5}$, $NO_2$ and $O_3$ over Belgium. The various techniques and resulting maps were analyzed, validated and compared aiming at identifying the best possible regional scale concentration map for each pollutant. A distinction was made between a temporal and a spatial validation. The temporal analysis revealed that an intelligent interpolation technique based on land use characteristics in general performs best in capturing the temporal aspects of air quality in Belgium for the investigated pollutants. For $PM_{10}$ and $PM_{2.5}$ this technique also performs best in generating the spatial pattern of the observed annually averaged concentrations. A deterministic model combined with a corrective 'Optimal Interpolation' data assimilation technique performs best in reproducing the spatial pattern of $O_3$. For $NO_2$ the interpolation technique manages best in explaining the spatial pattern of the observed annually averaged concentrations in Belgium, but when restricted to the region of Flanders, it competes with a thoroughly calibrated Lagrangian type of modeling.

## 39.1 Introduction

Detailed regional scale concentration maps are important in the framework of environmental assessment studies, preparing action plans and documents supporting EU infringement procedures, as well as a basis for negotiations with stakeholders such as federations, (industrial) sectors and local authorities. We studied and compared different operational modeling techniques that are used to generate such maps for $PM_{10}$, $PM_{2,5}$, $NO_2$ and $O_3$ over Belgium. The different techniques include

B. Maiheu • N. Veldeman • P. Viaene • K. De Ridder • D. Lauwaet • F. Deutsch • S. Janssen • C. Mensink (✉)
VITO, Environmental Modeling Unit, Boeretang 200, 2400 Mol, Belgium
e-mail: Clemens.mensink@vito.be

D. Steyn and R. Mathur (eds.), *Air Pollution Modeling and its Application XXIII*, Springer Proceedings in Complexity, DOI 10.1007/978-3-319-04379-1_39,

(i) an intelligent interpolation technique based on land use characteristics (RIO model, [1–3]); (ii) a deterministic Eulerian modeling approach (AURORA model, [4, 6]) taking into account four different methods of calibration (simple classical bias correction, simple bias correction according to orthogonal regression, advanced bias correction based on '*Kalman Filtering*' and '*Optimal Interpolation*' data assimilation); and (iii) a Lagrangian model calibrated for $NO_2$ and $PM_{10}$ (VLOPS model, based on van Jaarsveld [7]).

## 39.2 Methodology

The various techniques and resulting maps were analyzed, validated and compared aiming at identifying the best possible regional scale concentration map for each pollutant. The validation was based on the jackknife resampling technique or '*leaving-one-out*' technique comparing the model results with the measurements obtained from 58 monitoring stations for $PM_{10}$, 34 stations for $PM_{2,5}$, 67 stations for $NO_2$ and 39 stations for $O_3$. Furthermore, a distinction was made between a temporal and a spatial validation. The spatial resolution for the models was set at $4 \times 4$ km$^2$. The year 2009 was used as reference year for both the modeling and the observations.

The model results were evaluated on various statistical indicators, such as RMSE, $R^2$, BIAS, but also target plots, QQ plots and a comparative RMSE for the time series. The JRC DELTA tool [5] was used to perform the various evaluations. By lack of time to do a thorough Monte Carlo analysis to obtain weighted score distributions, the assignment of the model scores was based on the simple assumption that the best performing model gets 10 points, the median of the contributing models gets 5 points and on this basis the remainder model scores are rescaled. This is carried out for each statistical indicator after which a summation is made to obtain the overall scores.

The model versions that took part in the evaluation were the following ones: "rio" indicates the generally applied RIO model based on land use regression and Ordinary Kriging of the residuals; "rio09" indicates the same model, but with its trend functions exclusively based on the observations for 2009; "aur" indicates a straight forward application of the AURORA model; "auroi" stands for the version using optimal interpolation as a data assimilation technique; "aurkf" relates to the AURORA results using Kalman filtering as a data assimilation technique and "aurbias" indicates the AURORA application using a bias correction.

## 39.3 Results and Discussion

The temporal analysis revealed that the RIO model in general performs best in capturing the temporal aspects of air quality in Belgium for the investigated pollutants, as shown in Table 39.1 for $PM_{10}$ and in Table 39.2 for the $NO_2$

**Table 39.1** Temporal validation results and overall score for six different model approaches comparing model results and observations (58 stations) for $PM_{10}$

| Model | Zone | rio | rio09 | aur | auroi | aurkf | aurbias |
|---|---|---|---|---|---|---|---|
| *PM10_MEDIAN_STATION_BIAS* | *0* | 9.28 | 8.94 | 0.00 | 0.00 | 1.06 | 10.00 |
| *PM10_MEDIAN_STATION_RMSE* | *0* | 9.79 | 10.00 | 0.00 | 5.98 | 4.02 | 3.38 |
| *PM10_MEDIAN_STATION_TCOR* | *0* | 9.84 | 10.00 | 0.00 | 6.11 | 3.89 | 0.87 |
| *PM10_MEDIAN_STATION_TARGET* | *0* | 10.00 | 9.92 | 0.00 | 5.32 | 3.43 | 4.68 |
| *PM10_MEDIAN_STATION_QQID* | *0* | 9.02 | 10.00 | 0.11 | 1.58 | 2.40 | 7.60 |
| **Score** | | **47.93** | **48.86** | **0.11** | **18.99** | **14.79** | **26.54** |

**Table 39.2** Temporal validation results and overall score for six different model approaches comparing model results and observations (67 stations) for $NO_2$

| Model | Zone | rio | rio09 | aur | auroi | aurkf | aurorth | aurbias |
|---|---|---|---|---|---|---|---|---|
| *NO2_MEDIAN_STATION_BIAS* | *0* | 8.36 | 9.29 | 0.02 | 10.00 | 2.75 | 5.00 | 3.74 |
| *NO2_MEDIAN_STATION_RMSE* | *0* | 10.00 | 10.00 | 0.00 | 7.25 | 4.08 | 3.47 | 5.00 |
| *NO2_MEDIAN_STATION_TCOR* | *0* | 10.00 | 9.90 | 0.00 | 6.33 | 5.00 | 1.54 | 3.27 |
| *NO2_MEDIAN_STATION_TARGET* | *0* | 10.00 | 9.54 | 0.00 | 6.87 | 4.50 | 2.71 | 5.00 |
| *NO2_MEDIAN_STATION_QQID* | *0* | 7.78 | 5.00 | 4.23 | 10.00 | 0.00 | 4.37 | 5.82 |
| **Score** | | **46.13** | **43.73** | **4.25** | **40.44** | **16.33** | **17.09** | **22.83** |

**Table 39.3** Spatial validation results and overall score for six different model approaches comparing model results and observations (58 stations) for $PM_{10}$

| Model | Zone | rio | rio09 | aur | auroi | aurorth | aurbias |
|---|---|---|---|---|---|---|---|
| *PM10_SPATIAL_CORR* | *0* | 9.79 | 10.00 | 3.81 | 6.19 | 3.54 | 1.31 |
| *PM10_SPATIAL_DSLOPE* | *0* | 6.50 | 7.26 | 1.92 | 3.50 | 10.00 | 1.77 |
| *PM10_SPATIAL_MEDERR* | *0* | 5.40 | 4.60 | 0.00 | 9.14 | 3.92 | 10.00 |
| *PM10_SPATIAL_RMSE* | *0* | 10.00 | 8.00 | 0.00 | 7.14 | 0.00 | 2.86 |
| **Score** | | **31.70** | **29.85** | **5.73** | **25.97** | **17.46** | **15.95** |

concentrations. The uncorrected, deterministic AURORA model scores the least. The AURORA model calibrated with measurements using different techniques ('*Optimal Interpolation*', *'Kalman Filtering'* and bias correction) provides significantly better results than the uncorrected AURORA model, but not better than the RIO model. With the Lagrangian approach no time series can be generated due to technical model restrictions.

From the spatial analysis it became clear that distinction between the considered pollutants should be made. For $PM_{10}$ and $PM_{2.5}$ the RIO model performs best in generating the spatial pattern of the observed annually averaged concentrations, as for example shown for $PM_{10}$ in Table 39.3. The deterministic model AURORA remains behind, even when corrected with different correction and data assimilation techniques. The AURORA model corrected with '*Optimal Interpolation*' performs best in reproducing the spatial pattern of $O_3$. At the Belgian level the RIO model manages best in explaining the spatial pattern of the observed annually averaged

**Table 39.4** Spatial validation results and overall score for six different model approaches comparing model results and observations (67 stations) for $NO_2$

| Model | Zone | rio | rio09 | aur | auroi | aurorth | aurbias |
|---|---|---|---|---|---|---|---|
| *NO2_SPATIAL_CORR* | *0* | 10.00 | 9.72 | 4.21 | 5.79 | 3.39 | 3.83 |
| *NO2_SPATIAL_DSLOPE* | *0* | 4.18 | 10.00 | 6.10 | 0.00 | 0.00 | 5.82 |
| *NO2_SPATIAL_MEDERR* | *0* | 7.35 | 10.00 | 0.00 | 9.89 | 0.00 | 2.65 |
| *NO2_SPATIAL_RMSE* | *0* | 10.00 | 9.34 | 2.65 | 6.42 | 3.58 | 2.88 |
| **Score** | | **31.5** | **39.1** | **13** | **22.1** | **6.97** | **15.2** |

$NO_2$ concentrations (see Table 39.4). At Flemish level, the RIO model and the VLOPS model for which a bias correction is applied (simple bias correction or based on orthogonal regression) are competitive.

## 39.4 Conclusion

To ensure a balanced decision making, different aspects have to be considered when creating the "best" or "most accurate" concentration map. Both quantitative and qualitative aspects have to be taken into account. The initial question "Which technology is best suited for modeling large-scale concentration maps over Belgium?" therefore requires a well balanced answer. First of all the preferred technique depends on whether one is more focused on the temporal aspect of the behavior of pollutants or on the spatial aspects. The temporal analysis reveals that the interpolation technique presented in this paper outperforms the deterministic modeling approach. For the spatial assessment this depends on the pollutant. Note however, that these conclusions are restricted to assessments of the actual situation or situations in the past. When the decision making involves forecasts or scenario calculations, deterministic models are probably the only way to provide answers.

**Acknowledgement** This research has been carried out in the framework of the Flanders Environmental Report and was financially supported by the Flemish Environmental Agency.

## References

1. Hooyberghs J, Mensink C, Dumont G, Fierens F (2006) Spatial interpolation of ambient ozone concentrations from sparse monitoring points in Belgium. J Environ Monit 8:1129–1135
2. Janssen S, Dumont G, Fierens F, Mensink C (2008) Spatial interpolation of air pollution measurements using CORINE land cover data. Atmos Environ 42:4884–4903
3. Janssen S, Dumont G, Fierens F, Deutsch F, Maiheu B, Celis D, Trimpeneers E, Mensink C (2012) Land use to characterize spatial representativeness of air quality monitoring stations and its relevance for model validation. Atmos Environ 59:492–500

4. Mensink C, De Ridder K, Lewyckyj N, Delobbe L, Janssen L, Van Haver P (2001) Computational aspects of air quality modelling in urban regions using an optimal resolution approach. In: Margenov S, Wasniewski J, Yamalov P (eds) Large-scale scientific computing, Lecture notes in computer science, 2179., Springer Berlin Heidelberg, pp 299–308
5. Thunis P, Georgieva E, Pederzoli A (2011) The DELTA tool and Benchmarking report, concepts and user's guide. Version 1 – 18 February 2011. Joint Research Centre, Ispra
6. Van de Vel K, Mensink C, De Ridder K, Deutsch F, Maes J, Vliegen J, Aloyan A, Yermakov A, Arytyunyan V, Khodzher T, Mijling B (2010) Air quality modelling in the lake Baikal region. Environ Monit Assess 165:665–674
7. van Jaarsveld J (2004) Description and validation of OPS-Pro 4.1, 2004, RIVM report 500045001

## Questions and Answers

**Questioner Name:** Jeremy Silver

**Q:** Were the data assimilation treatments applied as a post hoc correction, or were they applied online?

**A:** All data assimilation techniques were applied in post-processing, thus offline and after results were obtained by the AURORA model.

**Questioner Name:** Pius Lee

**Q:** Your concentration map from your data assimilation scheme seemed to depend on the availability of a dense monitoring network. The $NO_2$ network contains 67 stations, whereas in contrast, the $O_3$ network has 39 stations. Does this difference have an impact on the quality of the resulting concentration maps?

**A:** This certainly has an impact on the quality of the concentration maps, but the effect will also be related to the concentration gradients obtained by the model. If gradients are strong, e.g. for $NO_2$ concentrations in cities, a more dense network would help to improve the results, whereas if gradients are smoother, e.g. for changes of $O_3$ over larger areas, adding monitoring stations would have less effect.

# Chapter 40
# Impact of RACM2, Halogen Chemistry, and Updated Ozone Deposition Velocity on Hemispheric Ozone Predictions

**Golam Sarwar, Jia Xing, James Godowitch, Donna Schwede, and Rohit Mathur**

**Abstract** We incorporate the Regional Atmospheric Chemistry Mechanism (RACM2) into the Community Multiscale Air Quality (CMAQ) hemispheric model and compare model predictions to those obtained using the existing Carbon Bond chemical mechanism with the updated toluene chemistry (CB05TU). The RACM2 enhances monthly mean ozone by 2–10 ppbv in polluted areas compared to the CB05TU while reducing mean ozone by 2–6 ppbv in remote areas. We develop an effective halogen reaction that can consume ozone over the gulfs and oceans. The current CMAQ model uses substantially lower ozone deposition velocity over water compared to observed data. We modify the CMAQ deposition velocity to account for the enhanced deposition due to chemical interactions between ozone and oceanic iodide. The effective halogen reaction and enhanced deposition velocity reduce monthly mean ozone by 2–8 ppbv over water. The majority of the reduction occurs via the halogen reaction. A comparison of model predictions with available observed profile reveals that the RACM2 over-predicts surface ozone in polluted areas while improving the comparison in remote areas. Model predictions with the halogen chemistry and enhanced deposition velocity compare better with the observed data.

## 40.1 Introduction

The Carbon Bond chemical mechanism uses a lumped structure approach and was originally developed for modeling polluted urban conditions though it has been revised in recent years for applications to cleaner and remote conditions.

G. Sarwar (✉) • J. Xing • J. Godowitch • D. Schwede
National Exposure Research Laboratory, U.S. Environmental Protection Agency, Research Triangle Park, NC, USA
e-mail: sarwar.golam@epa.gov

R. Mathur
Atmospheric Modeling and Analysis Division, United States Environmental Protection Agency, Research Triangle Park, NC, USA
e-mail: mathur.rohit@epa.gov

D. Steyn and R. Mathur (eds.), *Air Pollution Modeling and its Application XXIII*, Springer Proceedings in Complexity, DOI 10.1007/978-3-319-04379-1_40,

The Regional Atmospheric Chemistry Mechanism (RACM2) uses a lumped molecular approach and was specifically designed for regional applications ranging from the Earth's surface to the upper troposphere [3]. In this study, we examine the impacts of the Carbon Bond 2005 chemical mechanism with the updated toluene chemistry (CB05TU) [7] and the RACM2 on air quality using the Community Multiscale Air Quality (CMAQ) model. A comparison of ozone ($O_3$) deposition velocities in CMAQ with observed data [4] suggests that CMAQ uses substantially lower values than observed data over water. Results of recent field studies also suggest that halogens can be emitted over gulfs and oceans and destroy $O_3$ [5]. However, the CMAQ model does not employ such reaction. We develop and employ an effective halogen reaction for $O_3$ destruction over oceans and gulfs. Additionally, we revise the treatment of model $O_3$ deposition velocities over water to account for the chemical enhancement of deposition due to the interaction of $O_3$ and oceanic iodide. We also examine impacts of these two additional processes on air quality in the northern hemisphere.

## 40.2 Method

The study uses the WRF-CMAQ coupled modeling system [8] to simulate air quality. Evaluations for the CMAQ model have previously been conducted by comparing model predictions to measured ambient pollutants [2]. The CMAQ model has displayed considerable skill in simulating $O_3$ and other chemical species in the atmosphere. The modeling domain for this study covers the entire northern hemisphere using 108-km grid spacings and 44 vertical layers. Model simulations are performed for three summer months in 2006. Initial conditions are obtained from a different CMAQ simulation with 1 month spin-up period. The study uses Emissions Database for Global Atmospheric Research (http://edgar.jrc.ec.europa.eu/index.php) for generating model-ready emissions. The first simulation uses the CB05TU while the second simulation uses the RACM2. Differences in the results are attributed to the changes in the chemical mechanisms.

Helmig et al. [4] reported measurements of $O_3$ deposition velocities over oceanic areas. Observed median values ranged from 0.009 to 0.27 cm $s^{-1}$ while CMAQ currently uses values less than 0.001 cm $s^{-1}$. We follow the procedures of Chang et al. [1] to revise model $O_3$ deposition velocities over water. The revised treatment produces deposition velocities similar to the observed $O_3$ deposition velocities over water.

Using long-term measurements in the Cape Verde archipelago in Atlantic Ocean, Read et al. [5] suggested that halogens, emitted from oceans and gulfs, chemically destroy $O_3$. However, the details of these emissions and their atmospheric reactions are complex and emerging, and are not included in any air quality models. Here, we develop an effective halogen reaction that can destroy $O_3$ over gulfs and oceans only during the day and within the planetary boundary layer. We derive a first order rate constant of $2.0 \times 10^{-6}$ $s^{-1}$ for the reaction using observed data of Read et al. [5]. It

is an effective surrogate reaction of the detailed halogen chemistry that can occur in the atmosphere and allows examining their impacts without knowing the detailed halogen emissions and associated chemical reactions. The third simulation was conducted using the RACM2 with the effective halogen reaction and the enhanced $O_3$ deposition velocities. Differences in the results are attributed to the halogen chemistry and enhanced $O_3$ deposition velocities over water.

## 40.3 Results and Discussion

Predicted monthly-mean (August) surface $O_3$ with the CB05TU and differences in the model predictions due to the RACM2 are shown in Fig. 40.1. The CB05TU predicts values of 20–60 ppbv in North America and 20–80 ppbv in Europe and Asia. The RACM2 enhances $O_3$ by 2–10 ppbv in polluted areas due primarily to greater recycling of nitrogen oxides and more active organic chemistry. It reduces $O_3$ by 2–6 ppbv in remote clean areas due primarily to differences in organic nitrate representation. The CB05TU predicts a maximum value of 103 ppbv in the modeling domain while the RACM2-predicted maximum value is reduced to 97 ppbv. Sarwar et al. [6] examined the impacts of the two mechanisms and reported that RACM2 enhances $O_3$ in the continental United States. Results presented here over the continental United States are consistent with their findings. The effective halogen reaction and enhanced deposition velocity reduce $O_3$ by 2–8 ppbv over water bodies (Fig. 40.1c). The majority of the reduction occurs due to the halogen chemistry. Results obtained for other months are similar and not shown due to space limitation.

Model predictions are compared to observed ozonesonde profiles from four sites in Fig. 40.2. The RACM2 over-predicts $O_3$ near the surface at Sable Island, Gulf of Mexico, and Trinidad Head. However, its predictions aloft tend to agree better with the observations from Sable Island and Trinidad Head. The RACM2 predictions also agree better with the observed data at Hilo than the CB05TU predictions. Model predictions with the halogen reaction and enhanced $O_3$ deposition velocity improve the comparison with observed data at all sites.

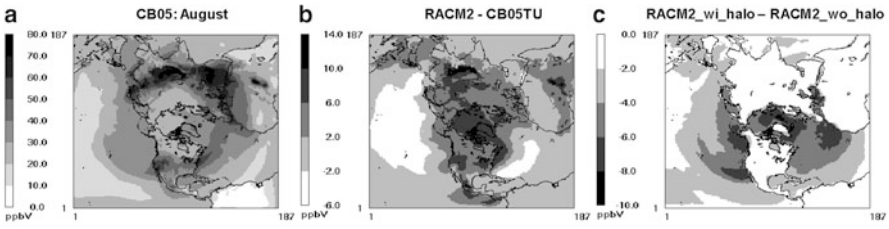


**Fig. 40.1** (**a**) Monthly-mean (August) $O_3$ obtained with the CB05TU (**b**) differences in monthly-mean $O_3$ obtained with the RACM2 and CB05TU (**c**) differences in monthly-mean $O_3$ obtained with the effective halogen reaction and enhanced $O_3$ deposition velocity and without any halogen reaction and the existing $O_3$ deposition velocity (using RACM2)

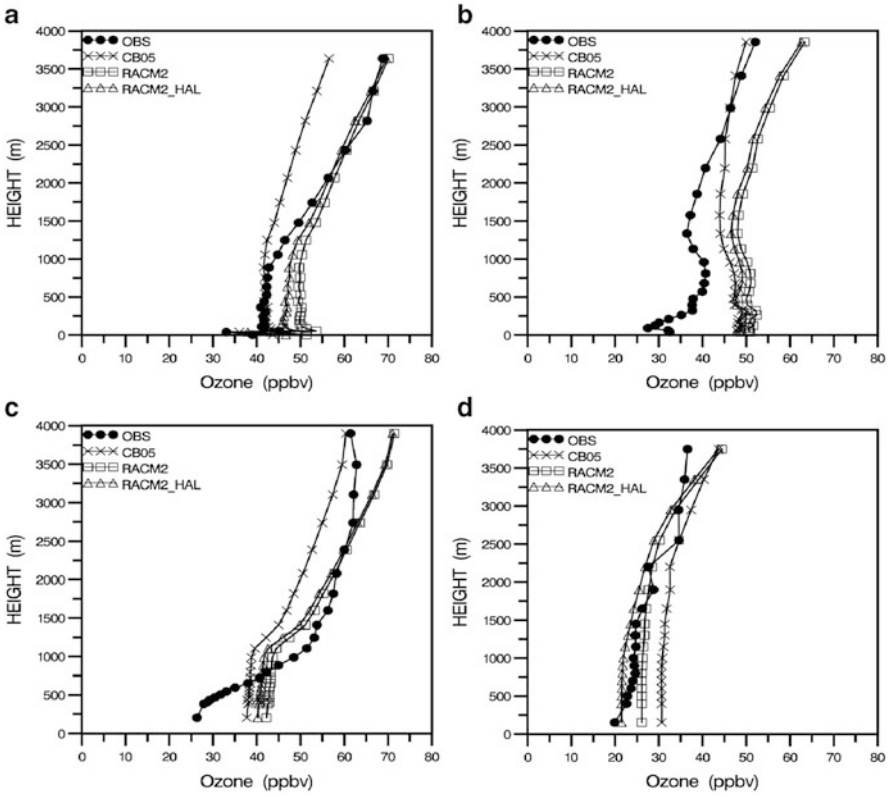


**Fig. 40.2** A comparison of model $O_3$ predictions to observed data (August) at (**a**) Sable Island, NS (**b**) Gulf of Mexico (**c**) Trinidad Head, CA (**d**) Hilo, HI

## 40.4 Summary

We compare model predictions with RACM2 to those obtained with the CB05TU. The RACM2 enhances $O_3$ in polluted areas while reducing $O_3$ in remote clean areas. The RACM2 over-predicts surface ozone in polluted areas; however, it tends to improve the predictions aloft in these areas. The RACM2 improves the predictions in remote clean areas. We develop an effective halogen reaction for simulating $O_3$ loss due to the halogen chemistry and revise $O_3$ deposition treatment. Predictions obtained with these additional processes reduce $O_3$ over water and improve the comparison with the observed data, particularly at Hilo, HI.

**Disclaimer** Although this paper has been reviewed by EPA and approved for publication, it does not necessarily reflect EPA's policies or views.

## References

1. Chang W et al (2004) Ozone deposition to the sea surface: chemical enhancement and wind speed dependence. Atmos Environ 38:1053–1059
2. Foley KM et al (2010) Incremental testing of the CMAQ modeling system version 4.7. Geosci Model Dev 3:205–226
3. Goliff WS et al (2013) The regional atmospheric chemistry mechanism, version 2. Atmos Environ 68:174–185
4. Helmig D et al (2012) Atmosphere-ocean ozone fluxes during the TexAQS 2006, STRATUS 2006, GOMECC 2007, GasEx 2008 and AMMA 2008 cruises. J Geophys Res 117:D04305. doi:10.1029/2011JD015955
5. Read KA et al (2008) Extensive halogen-mediated ozone destruction over the Atlantic ocean. Nature 453:1232–1235
6. Sarwar G et al (2013) A comparison of atmospheric composition predicted with the carbon bond and the RACM. Atmos Chem Phys Discuss 13:1–47
7. Whitten G et al (2010) A new condensed toluene mechanism for carbon bond: CB05-TU. Atmos Environ 44:5346–5355
8. Wong DC et al (2012) WRF-CMAQ two-way coupled system with aerosol feedback: software development and preliminary results. Geosci Model Dev 5:299–312

## Questions and Answers

**Questioner Name:** Douw Steyn

**Q:** I noticed notable ozone reductions over east Greenland Sea which is frozen for much of the year. How did you model ozone deposition over frozen area?

**A:** The current model treats all oceans same way. Thus, it currently does not differentiate between frozen and liquid water in the oceans.

**Questioner Name:** Amir Hakami

**Q:** Did you consider differences between CB05 and RACM2 separately for day and night?

**A:** Indeed we evaluated the diurnal pattern of model predictions obtained with the two mechanisms. Model predictions with RACM2 are consistently higher than those obtained with the CB05 during the day as well as at night.

# Chapter 41
# A Global Wildfire Emission and Atmospheric Composition: Refinement of the Integrated System for Wild-Land Fires IS4FIRES

**Joana Soares and Mikhail Sofiev**

**Abstract** The current study intends to evaluate the fire emission estimates obtained from IS4FIRES v1.5. The system provides spatially and temporally resolved emission fluxes originated from wild-land fires. The emissions were obtained by utilising remote-sensing products of MODIS and SEVIRI instruments: TA and FRP. The primary scaling is based on emission factors for PM2.5 determined for seven land-use types: grass, crop residue, shrub, tropical, temperate and boreal forest, and peat. The PM2.5 emission fluxes can be converted to total PM and gaseous species using literature-reported scaling factors.

To evaluate the system, the fire emission fluxes were used as input to the SILAM model, which evaluated the dispersion and transformation of the released smoke. The observational datasets included AOD observations from MODIS. To facilitate the comparison and estimate the contribution from fires to AOD, SILAM inorganic chemistry calculated formation of secondary inorganic aerosol. Primary PM emissions from anthropogenic and natural sources were also included.

The model-measurement comparison showed that spatial and temporal distributions of the fire smoke are well reproduced. Nevertheless, the smoke from fires occurring in central Africa and South America are overestimated, and fires occurring in areas where peat and crop are dominant are underestimated. The optimization of the system, in general, results on a reduction of the emission coefficients, with exception of peat and crop, as expected; it reduces emission substantially especially for the areas where tropical and grass are dominating and fires tend to be very intense (Africa). Nevertheless, in some cases reduction seems to be counterproductive, emissions are heavily reduced.

J. Soares (✉) • M. Sofiev
Air Quality Department, Finnish Meteorological Institute, FI-00101 Helsinki, Finland
e-mail: joana.soares@fmi.fi

D. Steyn and R. Mathur (eds.), *Air Pollution Modeling and its Application XXIII*,
Springer Proceedings in Complexity, DOI 10.1007/978-3-319-04379-1_41,

## 41.1 Introduction

The quantification of fire emissions and its impact, in terms of atmospheric composition, air quality, human health and climate forcing, is a continuous challenge due to numerous uncertainties and stochastic behaviour of wild-land fires. This study intends to evaluate the fire emission estimates obtained from IS4FIRES v1.5.

## 41.2 Methodology

### *41.2.1 Fire Input Data: IS4Fires v.1.5*

The FAS provides spatially and temporally resolved emission fluxes originated from wild-land fires. IS4Fires consists of two parallel branches based on partly independent Level 2 MODIS Collection 4 and 5 active-fire products: the Temperature Anomaly (TA) and Fire Radiative Power (FRP). The TA and FRP-based branches are partly independent and demonstrate somewhat different features: the first is more sensitive to small-scale fires, but the latter is based on a physically a better grounded quantity for the determination of the fire emissions, since the release of radiative energy is approximately proportional to the number of carbon atoms oxidised per second. Sofiev et al. [7] showed that the combination of both methods improves the representation of emission of small fires. The algorithms of converting the fire information to the emission fluxes of atmospheric pollutants are described in Sofiev et al. [7]. The primary scaling is the emission factor to total PM and other species are obtained with cross-scaling factors from the review of Andreae and Merlet [2]. However, the simulations discussed in this study are based on optimized emission factors, which were obtained for seven land-use classes (grass, crop residue, shrub, tropical, temperate and boreal forest, and peat) using Akagi et al. [1] and merged with the original coefficients of Sofiev et al. [7], are in use on the IS4Fires v1.5. In addition, the emission injection is dynamic; with the injection height being calculated using the formula suggested by Sofiev et al. [9]. The diurnal variation of emissions is static and taken from SEVIRI re-analysis.

### *41.2.2 Modelling Tool: SILAM v.5.3*

The modelling tool used in this study is the System for Integrated modeLling of Atmospheric composition, SILAM ([5]; Sofiev et al. [6]). For aerosols, the mechanisms of dry deposition varies from primarily turbulent diffusion driven removal of fine aerosols to primarily gravitational settling of coarse particles [4]. The wet deposition distinguishes between sub- and in-cloud scavenging and

between rain and snow [5]. The physical-chemical modules of SILAM cover inorganic chemistry, size-resolved primary particles of various types, radioactive nuclides and probability distribution. For the current study, the SILAM simulations included anthropogenic [3], fire-induced (described in Sect. 41.2.1) and sea salt Sofiev et al. [8] emissions. Meteorological information and necessary geophysical and land cover maps are taken from ECMWF meteorological models. Wild-land fires source was obtained from FAS v1.5 system described above. To facilitate the comparison and estimate the contribution from fires to AOD, SILAM inorganic chemistry calculated formation of secondary inorganic aerosol. Primary PM emissions from anthropogenic and natural sources were also included. The results shown in this study are based on global runs for time period between 2001 and 2012 with a horizontal resolution of 1*1° and the vertical profile was represented by nine uneven layers reaching up to the tropopause, the lowest layer is 50 m thick. All simulations had 15 min internal time-step while the output was averaged over 1 h.

### *41.2.3 Environmental Monitoring Data*

The predicted aerosol optical thickness of aerosols has been compared with remote-sensing observations. The results of the simulations were compared with MODIS (Aqua and Terra) AOD, at 550 nm wavelength, using full collocation of the datasets. Firstly, MODIS observations were projected to the grid of SILAM output and all grid cells with less than 50 MODIS pixels excluded – for each hour. Secondly, SILAM results were filtered using mask built of existing MODIS data (also for each hour): SILAM results with no counterpart in MODIS observations were excluded. Finally, the AOD in the grid cells that pass all filters was averaged to daily and monthly levels and compared with the corresponding MODIS data.

### *41.2.4 Optimization of IS4Fires*

The optimization was based on the AOD predicted and the AOD obtained by remote sensing data, as described in Sect. 41.2.3. The selection of data was based only on the fire dominating cells – all active fires are accounted for: a temporal and spatial selection was done based on the grid cells where the daily average for fire PM AOD was bigger than non-fire PM AOD. Values for MODIS AOD where collected for the same time and grid cell, resulting two vectors: one of modelled and one of predicted values. Subsequently, seven vectors with modelled values will be obtained, one for each individual land-use type fire computation, based on these spatial and temporal records. Meaning that for the same day and grid-location there is a value for each land-use category fire-related concentrations: the matrix for the optimization process. The observation vector was obtained by subtracting the MODIS AOD and the non-fire PM AOD estimated by SILAM, so that only fire

AOD is evaluated. The final step of the optimization fit was to run an unconstrained nonlinear optimization, a function that finds the minimum of a scalar function of several variables, starting at an initial estimate:

$$\left(A\overrightarrow{X} - \overrightarrow{y}\right)^T \left(A\overrightarrow{X} - \overrightarrow{y}\right) \rightarrow \min \overrightarrow{X} \tag{41.1}$$

where A is the matrix of estimated values (no. land-use types*no. predicted values), $\overrightarrow{y}$ is the vector with observed values (1*no. observations), and $\overrightarrow{X}$ is the vector of the emissions factors for each land-use type presently in use in IS4Fires system (1*no. emissions factors per land-use), the initial estimate.

## 41.3 Results and Discussion

The model-measurement comparison showed that spatial and temporal distributions of the fire smoke are, in general, well reproduced. Routinely the smoke from fires occurring in central Africa and Amazonia is overestimated and fires occurring in areas where peat and crop are abundant are occasionally underestimated. The overestimation is possible due to under-representation of local phenomena facilitating fast dispersal of plumes, such as deep convection and/or misattribution of land-use types. The latter was responsible for ∼10 %, in average, for the overestimation of the plumes (not shown here). The optimization of the system revealed, as expected, reduction of the emission coefficients, with exception of peat and crop (Fig. 41.1). The signal for each land-use type is similar, year to year, with exception of crop. Figure 41.2 shows an example of the spatial distribution of SILAM AOD for October 2008 before and after the optimization, and the spatial distribution for MODIS AOD, both at 550 nm. The figure shows that the optimization of the systems brings closer the model to the remote sensing measurements.

## 41.4 Conclusion

The IS4FIRESv1.5 clearly shows improvement compared to its previous version. The model-measurement comparison showed that spatial and temporal distributions of the fire smoke are well reproduced. Nevertheless, the smoke from fires occurring in central Africa and South America are overestimated, possibly due under-representation of local phenomena facilitating fast dispersal of plumes, such as deep convection. On the other hand, fires occurring in areas where peat and crop are dominant are underestimated. A better distribution of land-use improves the model results by reducing the overestimation of the plumes in ∼10 % and brings the predictions closer to the measurements. The optimization of the system, in general, results on a reduction of the emission coefficients, with exception of peat and crop,

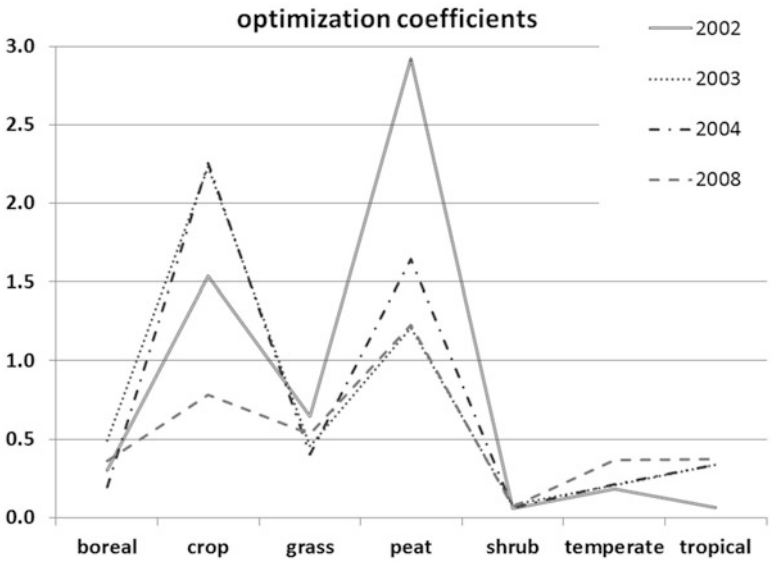


**Fig. 41.1** Optimization of the emission coefficient for each land-use type, year 2002–2004 and 2008

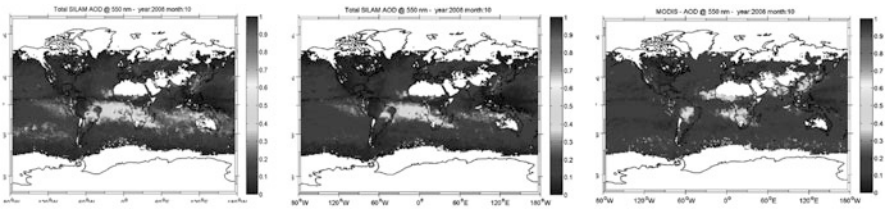

**Fig. 41.2** AOD spatial distribution for SILAM before (*left*) and after (*centre*) optimization, and MODIS (*right*). Monthly average for October, 2008

as expected; it reduces emission substantially especially for the areas where tropical and grass are dominating and fires tend to be very intense (Africa). Nevertheless, in some cases reduction seems to be counterproductive, emissions are heavily reduced.

**Acknowledgments** The study has been funded by the Academy of Finland, project IS4FIRES.

## References

1. Akagi SK, Yokelson RJ, Wiedinmyer C, Alvarado MJ, Reid JS, Karl T, Crounse JD, Wennberg PO (2011) Emission factors for open and domestic biomass burning for use in atmospheric models. Atmos Chem Phys Discuss 11:4039–4072. doi:10.5194/acp-11-4039-2011

2. Andreae MO, Merlet P (2001) Emission of trace gases and aerosols from biomass burning. Glob Biogeochem Cycle 15:955–966
3. Granier C, Bessagnet B, Bond T, D'Angiola A, van der Gon HD, Frost GJ, Heil A, Kaiser JW, Kinne S, Klimont Z, Kloster S, Lamarque J, Liousse C, Masui T, Meleux F, Mieville A, Ohara T, Raut J, Riahi K, Schultz MG, Smith SJ, Thompson A, van Aardenne J, van der Werf GR, van Vuuren DP (2011) Evolution of anthropogenic and biomass burning emissions of air pollutants at global and regional scales during the 1980–2010 period. Climate Change 109(1–2):163–190
4. Kouznetsov R, Sofiev M (2012) A methodology for evaluation of vertical dispersion and dry deposition of atmospheric aerosols. J Geophys Res 117:D01202. doi:10.1029/2011JD016366
5. Sofiev M, Siljamo P, Valkama I, Ilvonen M, Kukkonen J (2006) A dispersion modeling system SILAM and its evaluation against ETEX data. Atmos Environ 40:674–685
6. Sofiev M, Galperin M, Genikhovich E (2008) A construction and evaluation of Eulerian dynamic core for the air quality and emergency modelling system SILAM. In: Borrego C, Miranda AI (eds) Air pollution modeling and its application XIX, Nato science for peace and security series C – environmental security. Springer, Dordrecht, pp 699–701. NATO; CCMS; Univ Aveiro, 10.1007/978-1-4020-835 8453–9 94, 29th NATO/CCMS international technical meeting on air pollution modeling and its application, Aveiro, Portugal, 24–28 Sept 2007
7. Sofiev M, Vankevich R, Lotjonen M, Prank M, Petukhov V, Ermakova T, Koskinen J, Kukkonen J (2009) An operational system for the assimilation of the satellite information on wild-land fires for the needs of air quality modelling and forecasting. Atmos Chem Phys 9:6833
8. Sofiev M, Soares J, Prank M, de Leeuw G, Kukkonen J (2011) A regional-to-global model of emission and transport of sea salt particles in the atmosphere. J Geophys Res 116:D21302. doi:10.1029/2010JD014713
9. Sofiev M, Ermakova T, Vankevich R (2012) Evaluation of the smoke-injection height from wild-land fires using remote-sensing data. Atmos Chem Phys 12(4):1995–2006. doi:10.5194/acp-12-1995-2012

## Question and Answer

**Questioner Name:** George Pouliot

**Q:** Explain the optimization that was done for the wild Fire emissions.

**A:** The optimization is described on the Sect. 41.2.3.

# Chapter 42
# The Regional LOTOS-EUROS Model on Tour

**Renske Timmermans, Carlijn Hendriks, Richard Kranenburg, Arjo Segers, and Roy Wichink Kruit**

**Abstract** While emissions in Europe tend to show negative trends and are relatively well known, for some other regions in the world largely positive emission trends are visible and accurate information on these emissions is lacking. Over these regions satellite observations can play a large role, especially when there are few ground based observations available. Satellite observations have been successfully combined with regional chemistry transport models to provide best possible air quality analyses and forecasts and to derive important information on emission sources.

LOTOS-EUROS is a regional chemistry transport model with an active data assimilation system aimed at modeling the European air quality. To be able to answer the air quality and emission information needs over regions outside Europe a new LOTOS-EUROS version has been developed which can in principle be applied over any region of the world. First calculations have been performed over China. Resulting $NO_2$ and PM fields have been compared to satellite observations from the OMI instrument and ground based observations in Beijing and Shanghai. The results look promising as the model is able to reproduce the spatial and temporal variability within the $NO_2$ and PM concentrations. Absolute differences between model and observations can be attributed to missing sources in the model, scaling issues and observational errors.

In this paper we will present the steps that have been taken to develop the new LOTOS-EUROS version, show results over China and discuss encountered issues and further development plans.

R. Timmermans (✉) • C. Hendriks • R. Kranenburg • A. Segers • R.W. Kruit
Department of Climate, Air and Sustainability, TNO, Princetonlaan 6,
3584 CB Utrecht, The Netherlands
e-mail: renske.timmermans@tno.nl

D. Steyn and R. Mathur (eds.), *Air Pollution Modeling and its Application XXIII*,
Springer Proceedings in Complexity, DOI 10.1007/978-3-319-04379-1_42,

## 42.1 Introduction

The LOTOS-EUROS model is a regional chemistry transport model currently aimed at modeling the air pollutant concentrations and depositions over Europe. Emissions of pollutants are one of the driving forces of the model. To improve our knowledge on air quality and its drivers, the model is often combined with observations from in-situ as well as satellite instruments. For example, within the EU FP7 project ENERGEO, it has been shown that with the LOTOS-EUROS model it is possible to determine NOx emissions and their location as well as their trends over Europe by making use of satellite observations from the OMI instrument [2]. Such an application is very useful as it improves our knowledge on the emissions and the resulting air pollutant concentrations and deposition.

The added value of using satellite observations for emission monitoring will be larger over areas where emission knowledge is lacking, e.g. over China where emissions have increased dramatically during the past decades. To be able to extend our applications to areas outside of Europe, the model needs to be adapted in such a way that it can run over any part of the globe.

## 42.2 Model Developments

**Meteorology:** The LOTOS-EUROS model is driven by meteorological fields from the ECWMF. These data are also available for other parts of the world.

**Land use:** The land use (e.g., grass, water, arable land, coniferous trees) is used for both the deposition and the biogenic emissions. For the European LOTOS-EUROS version we use the CORINE/PHARE (EEA) database. For the global version, the global land cover 2000 (GLC2000) with 23 land use classes and a spatial resolution of $1 \times 1$ km at the equator, was found to be best suited. It is a harmonized land cover database over the whole globe for the year 2000.

**Deposition:** For the deposition in LOTOS-EUROS, 9 DEPAC land use classes are used. In the new version the land use classes from GLC2000 have been translated to the DEPAC land use classes for which deposition values are available.

**Emissions:** In the European version of the model anthropogenic emissions are provided by the TNO-MACC emission inventory, which covers Europe only. As a global alternative, we are using the EDGAR database version 4.2 provided by JRC. The composition of emitted substances and the height profiles were taken constant over the globe. For the time profiles, geographical zones were defined to be able to account for different time zones and climate.

**Biogenic emissions:** The current biogenic emissions in LOTOS-EUROS are based on vegetation maps that only cover Europe. It is not clear whether the used parameterizations could be applied to other regions too. It was therefore decided to include the MEGAN biogenic emission module, which is applicable on the global scale.

**Initial and Boundary conditions:** in this study are taken from the MACC re-analysis data which are available globally from 2003 until now, every 3 h.

## 42.3 Results

First calculations with the new version of the model have been performed over China for the period of July 2006. The model resolution is ∼25–20 km. Results have been compared to OMI $NO_2$ observations and ground based observations where available.

Figure 42.1 shows the average modeled and OMI data for July 2006 and the difference between both. The comparison shows a very good agreement when we look at the distribution of high $NO_2$ values, the patterns are very similar in model and satellite observations. We do see that the model produces lower $NO_2$ columns than the OMI observations both in background values as over large urban source areas. Similarly, previous studies have shown that our model produces lower results than OMI, also over Europe [3]. One of the explanations for this is the overestimation of $NO_2$ columns by OMI by 0–40 % especially in summer [1]. Other causes could be soil NOx emission, which are largest in summer, and NOx produced by lightning, two processes that are not included in the used model version.

Figure 42.2 shows the modeled and measured time series of daily PM10 and $NO_2$ in Shanghai and Beijing, where observed regional API indices are converted to concentrations. The modeled values over Shanghai are an average over four grid cells covering the eight stations used for the measured regional average API. The modeled values over Beijing are taken from one central grid cell in Beijing. The stations in Beijing which are used for the regional average API are widely spread within at least 20 model grid cells. This distribution of stations hampers the comparison as only a regional average observation is available and the exact location of the 27 stations was not known to us.

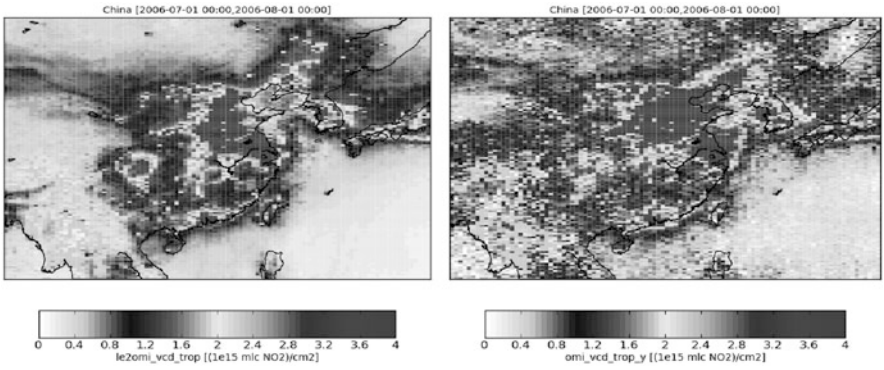


**Fig. 42.1** Average LOTOS-EUROS modeled tropospheric $NO_2$ column (*left*) and OMI tropospheric $NO_2$ column (*right*) for July 2006 over China

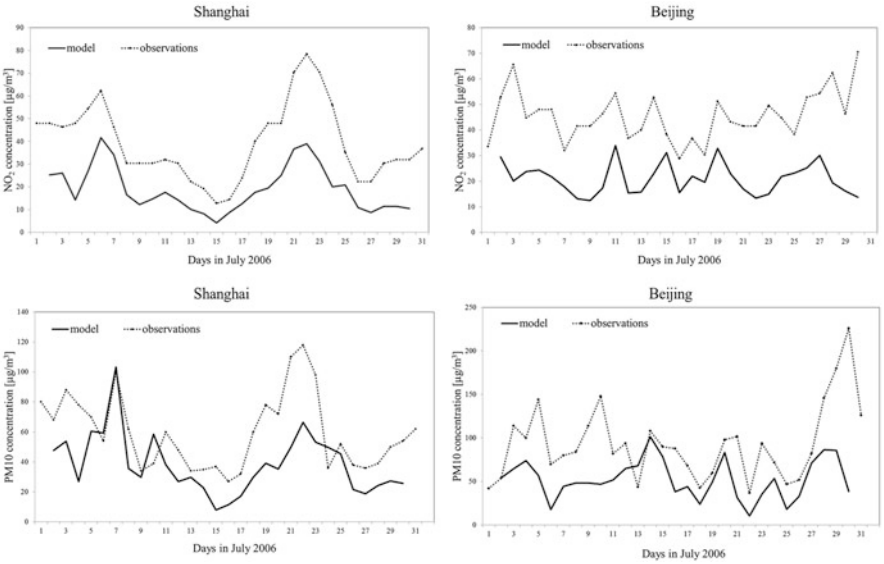


**Fig. 42.2** Time series of $NO_2$ (*top row*) and PM10 (*bottom row*) for Shanghai (*left*) and Beijing (*right*). Comparison between regional averaged observations (*dotted line*) and modeled values (*solid line*). The modeled values are taken as average over four grid cells for Shanghai and one central grid cell for Beijing

The model is able to well reproduce the temporal variability in the observations. The temporal correlation for $NO_2$ for Shanghai is very high with a value of 0.9, for Beijing the temporal correlation is lower, 0.21 (0.42 for the grid cell east of the central grid cell). The temporal correlation for PM10 for Shanghai is 0.67 and for Beijing 0.37. As mentioned above the comparison over Beijing is hampered due to the wide spread of the observation locations and the lack of information on the exact locations of the stations. On average the model underestimates the PM10 and $NO_2$ concentrations, this could be due to a representativity problem. The observations stations are all urban stations which are not representative for the model grid size of ∼25–30 km. For PM10 discrepancies might also be due to an underestimation of dust concentrations. Dust from traffic resuspension, urban sources and agricultural activities have not been taken into account in the current model simulation. The windblown dust routine could be another source of error as it is probably parameterized based on dust flux measurements for arid or desert areas, and might be inaccurate for dust emissions in agriculture areas.

## 42.4 Conclusion and Outlook

We have created a model version that can run over any part of the world when the necessary input data has been downloaded. First test results over China look promising. The model is able to reproduce the temporal variability in PM10, and

NO2 concentrations. On average the model underestimates observations both from satellite (OMI for NO2) and in-situ instruments (PM10 and NO2). This can at least partly be accounted to an overestimation by the OMI instrument for $NO_2$ in summer and representativity errors of the urban monitoring stations for the used model resolution. For more dedicated applications over China, one should consider using a dedicated Chinese emission and land use data.

During this study several assumptions were made or processes were neglected. In the future one should consider the following suggestions for improvements:

- Include country specific temporal emission profiles. Emissions are now assumed to follow the default daily and hourly profiles for LOTOS-EUROS, including rush hour and weekends, which is of course not valid for all countries.
- Improve emission composition per country (e.g. now assumption 3 % of NOx emissions is NO2, 1 % of PM10 emissions is EC).
- Implement traffic resuspension and dust emissions from agricultural activity
- The use of an extended model top (at 9,500 m) instead of the standard 3,500 m. This will be needed especially for tropical regions where the tropospheric boundary layer can be very large and regions which are more than 2,000 m above sea level.
- Extension of current deposition routines by adding classes and defining the deposition values for the classes available in GLC2000.
- Inclusion of convection
- Inclusion of lightning emissions

## References

1. Boersma KF, Eskes HJ, Brinksma EJ (2004) Error analysis for tropospheric $NO_2$ retrievals from space. J Geophys Res 109:D04311. doi:10.1029/2003JD003962
2. Curier L et al (2013) Synergistic use of LOTOS-EUROS and $NO_2$ tropospheric columns to evaluate the NOX emission trends over Europe. In: Steyn D, Builtjes P, Timmermans R (eds) Air pollution modeling and its application XXII. Springer, Dordrecht
3. Timmermans R, Eskes H, Builtjes P, Segers A, Swart D, Schaap M (2012) LOTOS-EUROS air quality forecasts by assimilation of OMI tropospheric NO2 columns. In: Steyn D, Trini Castelli S (eds) Air pollution modeling and its application XXI. Springer, Dordrecht, pp 347–351

## Question and Answer

**Questioner Name:** Yang Zhang

**Q:** Was the ground-based $NO_2$ concentrations used in the comparisons derived based on API.

**A:** Yes, the $NO_2$ observations that were available to us were all derived from API values, we are aware that these observations might have a low quality, however access to observations in China is often complicated, and we hope to get access to better validation observations in the near future.

# Chapter 43
# The Incorporation of the US National Emission Inventory into Version 2 of the Hemispheric Transport of Air Pollutants Inventory

**George Pouliot, Terry Keating, Greet Maenhout, Charles Chang, James Beidler, and Ryan Cleary**

**Abstract** EPA's 2008 National Emission Inventory has been incorporated into version 2 of the Hemispheric Transport of Air Pollutants Inventory. This work involves the creation of a detailed mapping of EPA Source Classification Codes (SCC) to the International Nomenclature for Reporting System (NFR). The mapping of SCC codes to the NFR system allows for comparison of USA emission inventories with other national inventories on a consistent basis. We summarize the emission estimates for 2008 and 2010 and provide a useful reference for linking USA inventories to Global inventories for use in regional and global chemical transport models.

## 43.1 Introduction

The Task Force on Hemispheric Transport of Air Pollution (TF-HTAP) is an international scientific cooperative effort to improve the understanding of the intercontinental transport of air pollution across the North Hemisphere. It was organized in 2005 under the auspices of the UNENC Convention on Long-range Transboundary Air Pollution and is open to all interested experts. In 2010, TF-HTAP

G. Pouliot (✉)
Atmospheric Modeling and Analysis Division, U.S. EPA, Research Triangle Park, NC 27711, USA
e-mail: pouliot.george@epa.gov

T. Keating
Office of Air and Radiation/Office of Policy Analysis and Review, U.S. EPA, Washington, DC 20460, USA

G. Maenhout
Joint Research Centre, Institute for Environment and Sustainability, Ispra, Italy

C. Chang • J. Beidler • R. Cleary
Computer Sciences Corporation, Research Triangle Park, NC 27711, USA

D. Steyn and R. Mathur (eds.), *Air Pollution Modeling and its Application XXIII*, Springer Proceedings in Complexity, DOI 10.1007/978-3-319-04379-1_43,

produced the first comprehensive assessment of the intercontinental transport of air pollution in the Northern Hemisphere. In 2012, TF-HTAP launched a new phase of cooperative experiments and analysis that is intended to inform the LRTAP Convention and other multi-lateral cooperative efforts, as well as national actions to decrease air pollution and its impacts. The first objective in this new phase is to provide a single global annual dataset that draws from the "best available" inventories developed on a regional basis and filled in with global inventories. This new dataset is called HTAP_V2 and consists of $0.1° \times 0.1°$ grid maps of CO, $SO_2$, $NO_x$, NMVOC, $NH_3$, $PM_{10}$, $PM_{2.5}$, BC and OC for the years 2008 and 2010. HTAP_V2 uses nationally reported emissions combined with regional scientific inventories in the format of sector-specific grid maps. The grid maps are complemented with EDGARv4.3 data for those regions where data are absent. The global grid maps are a joint effort from US-EPA, the MICS-Asia group, EMEP/TNO, the REAS and the EDGAR group to serve in the first place the scientific community for hemispheric transport of air pollution. This work describes the incorporation of EPA's National Emission Inventory into HTAP_V2.

## 43.2 2008 EPA NEI

An Emission modeling platform includes annual emission inventories, emission processing tools and methods, and a collection of ancillary files detailing temporal allocation, spatial allocation, speciation, and other parameters. The 2008 Emission Modeling platform (http://www.epa.gov/ttn/chief/emch/index.html#2008) was the starting point for the emissions used in HTAP_V2. The software used to complete the processing includes the following: Sparse Matrix Operator Kernel Emissions (SMOKE) model version 3.1 (http://www.smoke-model.org/index.cfm) processed utilizing the US EPA Emissions Modeling Framework (EMF) version 2.5; Multimedia Integrated Modeling System (MIMS) Spatial Allocator version 3.6 (http://www.ie.unc.edu/cempd/projects/mims/spatial/); Python version 2.6 for generation of on road inventories by SCC based on EPA's Office of Transportation and Air Quality (OTAQ) MOtor Vehicle Emission Simulator (MOVES) MOVES2010b activity data (http://www.epa.gov/otaq/models/moves/index.htm).

The annual county level emissions from all sources except mobile sources were speciated into 25 non-methane VOC aggregation groups based on the Global Emissions Initiative (GEIA). However, for the purpose of summarizing the emissions in this paper, we will report the sum of the non-methane VOC emissions rather than each of the 25 groups. Mobile Source emission estimates were based on MOVES emission factors with 2007 meteorology processed with the SMOKE/MOVES system. A fleet year of 2007 was assumed for the mobile sources in the MOVES system. Surrogates were calculated with the spatial allocator version 3.6 and were based on the same inputs as in the 2008 modeling platform but revised for the 0.1° resolution of a global domain on latitude-longitude grid which includes the entire 50 states and Puerto Rico.

## 43.3 Summary of Emission Estimates

We summarize the emission estimates provided for version 2 of the HTAP inventory for the United States in the following tables. Table 43.1 contains a description of each sector and a numerical number used in subsequent tables. Tables 43.2 and 43.3 contain emission estimates for all criteria pollutants for the CONUS plus Alaska and Hawaii for 2008 and 2010. We have used a more detailed grouping of emissions by source category than actually implemented in the version 2 of the HTAP inventory. In addition, some sources which were not used by the HTAP inventory are included for completeness.

**Table 43.1** Description of emissions sectors and numerical code

| Sector description | Number |
|---|---|
| Aviation | 1 |
| Shipping except international waters | 2 |
| Energy point sources | 3 |
| Industry except dust | 4 |
| Ground transport except dust | 5 |
| Building heating, cooling, and equipment | 6 |
| Solvents | 7 |
| Crop cultivation | 8 |
| Agricultural waste | 9 |
| Waste disposal | 10 |
| Dust from industrial sources | 4.5 |
| Dust from ground transport | 5.5 |
| International shipping | 2.5 |
| Energy area sources | 3.5 |

**Table 43.2** US 2008 emission estimates in Tg/year by sector codes

| Sector number | CO | $NO_x$ | VOC | EC | OC | $PM_{10}$ | $NH_3$ | $SO_2$ | Non-carbon $PM_{2.5}$ |
|---|---|---|---|---|---|---|---|---|---|
| **1** | 920 | 116 | 59 | 5 | 1 | 19 | 0 | 13 | 0 |
| **2** | 2,360 | 514 | 826 | 13 | 11 | 29 | 0 | 34 | 3 |
| **3** | 679 | 3,077 | 53 | 14 | 15 | 384 | 25 | 8,202 | 263 |
| **4** | 4,431 | 3,187 | 4,425 | 78 | 71 | 641 | 85 | 1,666 | 313 |
| **5** | 35,246 | 7,164 | 4,189 | 43 | 2 | 279 | 136 | 152 | 95 |
| **6** | 12,174 | 769 | 1,152 | 33 | 233 | 435 | 58 | 279 | 155 |
| **7** | 5 | 5 | 3,632 | 0 | 1 | 4 | 0 | 0 | 2 |
| **8** | 541 | 477 | 189 | 35 | 10 | 75 | 3,262 | 30 | 8 |
| **9** | 346 | 16 | 32 | 5 | 17 | 45 | 0 | 3 | 23 |
| **10** | 1,192 | 86 | 211 | 19 | 67 | 213 | 62 | 19 | 95 |
| **4.5** | 0 | 0 | 0 | 0 | 5 | 1,283 | 0 | 0 | 138 |
| **5.5** | 0 | 0 | 0 | 1 | 30 | 3,940 | 0 | 0 | 430 |
| **2.5** | 178 | 1,927 | 83 | 2 | 2 | 177 | 0 | 1,329 | 160 |
| **3.5** | 352 | 568 | 3,368 | 3 | 6 | 39 | 3 | 151 | 19 |

**Table 43.3** US 2010 emission estimates in Tg/year by sector codes

| Sector number | CO | $NO_x$ | VOC | EC | OC | $PM_{10}$ | $NH_3$ | $SO_2$ | Non-carbon $PM_{2.5}$ |
|---|---|---|---|---|---|---|---|---|---|
| **1** | 920 | 116 | 59 | 5 | 1 | 19 | 0 | 13 | 0 |
| **2** | 1,873 | 532 | 709 | 13 | 9 | 25 | 0 | 32 | 3 |
| **3** | 679 | 3,077 | 53 | 14 | 15 | 384 | 25 | 8,202 | 263 |
| **4** | 3,987 | 3,006 | 4,379 | 73 | 69 | 634 | 85 | 1,622 | 312 |
| **5** | 27,229 | 6,111 | 3,379 | 143 | 73 | 275 | 112 | 41 | 43 |
| **6** | 11,340 | 791 | 1,095 | 33 | 236 | 439 | 58 | 273 | 156 |
| **7** | 5 | 5 | 3,632 | 0 | 1 | 4 | 0 | 0 | 2 |
| **8** | 437 | 416 | 173 | 28 | 9 | 67 | 3,262 | 4 | 8 |
| **9** | 346 | 16 | 32 | 5 | 17 | 45 | 0 | 3 | 23 |
| **10** | 1,192 | 86 | 211 | 19 | 67 | 213 | 62 | 19 | 95 |
| **4.5** | 0 | 0 | 0 | 0 | 5 | 1,283 | 0 | 0 | 138 |
| **5.5** | 0 | 0 | 0 | 1 | 30 | 3,940 | 0 | 0 | 430 |
| **2.5** | 178 | 1,927 | 83 | 2 | 2 | 177 | 0 | 1,329 | 160 |
| **3.5** | 352 | 568 | 3,368 | 3 | 6 | 39 | 3 | 151 | 19 |

## 43.4 Further Information

Documentation and additional details are available at http://edgar.jrc.europa.eu/htap_v2/index.php?SECURE=123. The final data sets used for the HTAP_V2 inventory will be posted at http://www.geicenter.org and http://eccad.sedoo.fr.

**Disclaimer** Although this paper has been reviewed by EPA and approved for publication, it does not necessarily reflect EPA's policies or views.

## Question and Answer

**Questioner Name:** Paul Makar

**Q:** "You mentioned that no temporal allocation is being done (at this stage). Will HTAP impose (a) temporal allocation(s) on the emissions prior to the use of the merged inventory? Temporal allocation can have a very big impact on model results."

**A:** The HTAP_V2 inventories are being created as annual estimates. However, we have created monthly temporal allocation factors for each of the emission sectors which could be used at least for the US. Temporal allocation for other parts of the world remains a challenge.

# Chapter 44
# Impact of Vertical and Horizontal Resolutions on Chemistry Transport Modelling

**Bertrand Bessagnet, Augustin Colette, Etienne Terrenoire, Laurent Menut, and Philippe Thunis**

**Abstract** This paper presents the main results of two specific studies related to the sensitivity of spatial resolution on chemistry transport modeling. The horizontal scale is addressed by simulating the air quality in Europe for the full year 2009 at 50 and 8 km resolutions on a very high performance computing infrastructure. An additional 2 km resolution was performed on a smaller period to assess the added value of a very high horizontal resolution during the air pollution outbreak of January 2009 when particulate and nitrogen dioxide levels reached alert levels. We reveal small scale air pollution patterns that highlight the contribution of city plumes to background air pollution levels. The influence of the vertical resolution on air pollutant concentrations near the surface is studied. The results are discussed in terms of differences on surface concentrations between the reference case and an improved resolution. Adding a point close to the surface appears to be important mainly for high nocturnal concentrations in very stable boundary layers.

B. Bessagnet (✉) • A. Colette • E. Terrenoire
Institut National de l'Environnement Industriel et des Risques, INERIS, 60550 Verneuil en Halatte, France
e-mail: bertrand.bessagnet@ineris.fr; fabienne.carette@ineris.fr; augustin.colette@ineris.fr; etienne.terrenoire@ineris.fr

L. Menut
Laboratoire de Météorologie Dynamique, École Polytechnique, ENS, UPMC, CNRS, IPSL, 91128 Palaiseau, France
e-mail: laurent.menut@lmd.polytechnique.fr

P. Thunis
European Commission, JRC, Institute for Environment and Sustainability, Climate Change and Air Quality Unit, Via E. Fermi 2749, 21027 Ispra, VA, Italy
e-mail: philippe.thunis@jrc.ec.europa.eu

D. Steyn and R. Mathur (eds.), *Air Pollution Modeling and its Application XXIII*, Springer Proceedings in Complexity, DOI 10.1007/978-3-319-04379-1_44,

## 44.1 Introduction

Beside the challenges in understanding and representing physical and chemical processes, the most common limitation in geophysical modelling studies regards spatial resolution, often restricted because of computational cost. With the ever growing computing facilities, such limitations are pushed back and we are now able to introduce a continental scale atmospheric chemistry simulation at 8 km and up to 2 km resolution. To assess the added value of high vertical resolution continental-scale atmospheric chemistry simulations we investigate air quality simulations in 2009 over Europe. A specific pollution outbreak in January 2009 was analyzed. The main driving factor for this event was an intense cold spell during which the stable meteorological situation enhanced the accumulation of air pollution while anthropogenic emissions of pollutants from domestic heating were high. The highest horizontal resolution in the simulation proposed here is about 2 km whereas current practices are in the range of 10 km, for instance in the Modelling Atmospheric Composition Change project (MACC) of the Global Monitoring for Environment and Security programme of the European Commission. The computational demand of the simulation presented here is thus two orders of magnitude above current practices. The impact of the vertical resolution is assessed with a simulation over the Paris basin for a winter and a summer month in 2009 with three different vertical resolutions.

## 44.2 Impact of the Horizontal Resolution

The off-line Chemistry Transport Model (CTM) CHIMERE [1] was used to model the transport and transformation of trace species. The model is being used by several international teams for research and environmental policy underpinning. It has been involved in many model intercomparison initiatives and is now part of the European pre-operational air composition forecasting system MACC. As an offline CTM, CHIMERE requires prescribed meteorological fields which were provided here by ECMWF (IFS model at 16 km resolution). The resolution of the meteorological model does not match that of the CTM, but performing a continental scale high-resolution meteorological simulation is a challenge in itself that was ruled out of the present initiative. Pan-European high-resolution air pollutant emission fluxes are computed using a top-down approach (a downscaling technique to disaggregate coarse inventories using proxies such as point source location and population density map) to cope with the lack of input data to propose a bottom-up approach at the continental scale. Two simulations at 50 km and about 8 km resolutions were performed over Europe for the full year 2009. A resolution of $0.03125 \times 0.015625°$ (i.e. about 2 km at the centre of the domain) of longitude and latitude, respectively, was chosen for the highest resolution; this high resolution simulation is performed over a 10 day period in winter 2009. On average there is a clear improvement of the

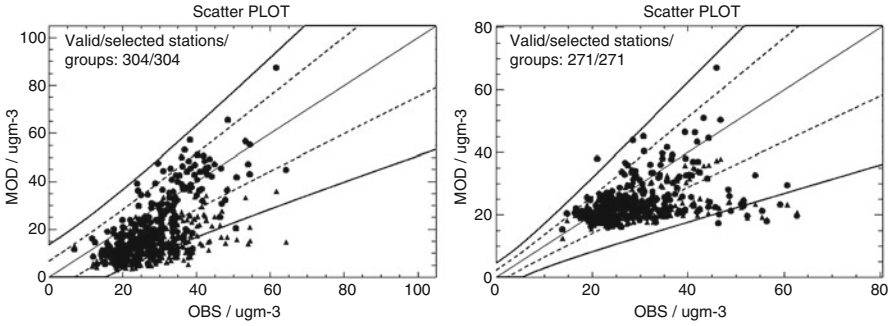


**Fig. 44.1** Model *versus* Observations scatter plots at 50 km (*triangles*) and 8 km (*dots*) for all urban stations in Europe for $NO_2$ (*left*) and $PM_{10}$ (*right*) (full year 2009)

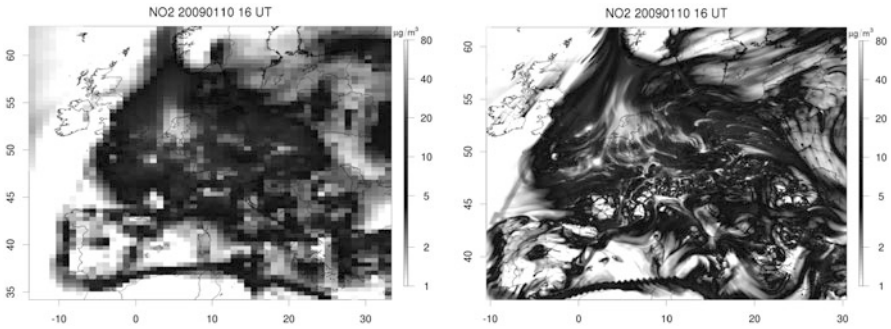


**Fig. 44.2** Map of $NO_2$ ($\mu g/m^3$) on January 10, 2009 at 16:00 UTC in the 50 km (*left*) and 2 km (*right*) resolution CHIMERE simulations

modelled $NO_2$ and $PM_{10}$ between the 50 and 8 km resolution respectively in term of bias for the whole year 2009 (Fig. 44.1). The shaded area indicates a minimum level of quality a model should fulfill for a given application; this "model quality objective" is based on the measurement uncertainty [3].

The maps in Fig. 44.2 provide snapshots of the simulations of nitrogen dioxide at about 50 and 2 km of resolution. While the coarse run captures well the main emission hotspots, local maxima are smeared out because of the numerical diffusion of the Eulerian CTM. The improvement brought about by the increased resolution is assessed by comparison with observed $NO_2$ and $PM_{10}$ concentrations across Europe as reported in the AIRBASE repository (Table 44.1). We find that increasing the resolution improves significantly the root mean square error (RMSE), especially at urban sites. The difference between the RMSE at urban, suburban and rural stations decreases with the resolution showing that we resolve better spatial gradients. This feature is more sensitive for $NO_2$ than $PM_{10}$ because of the lower spatial variability of the later.

Table 44.1 somehow questions the relevance of very high resolution simulations since the bulk of the improvement is achieved at 8 km resolution for which the

**Table 44.1** Model performances of each configuration over the whole modelling domain between January 9 and 16, 2009

| | | 50 km | | 8 km | | 2 km | |
|---|---|---|---|---|---|---|---|
| Pollutant | Station type | RMSE ($\mu g/m^3$) | Corr | RMSE ($\mu g/m^3$) | Corr | RMSE ($\mu g/m^3$) | Corr |
| $NO_2$ | *Urban* | 29.95 | 0.70 | 21.52 | 0.65 | 18.93 | 0.62 |
| | *Suburban* | 17.03 | 0.60 | 12.30 | 0.58 | 11,77 | 0.56 |
| | *Rural* | 7.80 | 0.54 | 6.67 | 0.64 | 6.68 | 0.68 |
| $PM_{10}$ | *Urban* | 34.14 | 0.57 | 31.28 | 0.46 | 30.42 | 0.43 |
| | *Suburban* | 17.55 | 0.49 | 15.42 | 0.51 | 14.54 | 0.53 |
| | *Rural* | 6.96 | 0.51 | 6.26 | 0.63 | 6.01 | 0.63 |

*RMSE* root mean square error, *Corr* average spatial correlation

RMSE of daily mean $NO_2$ averaged over the whole monitoring network is 26 % (10 % for $PM_{10}$) lower than the 50 km simulation. The 2 km resolution adds only another 5 % (3 % for $PM_{10}$) to achieve an average RMSE 32 % (13 % for $PM_{10}$) lower than the coarse configuration. In addition, the improvement in the spatial correlation is only seen at rural sites (and suburban sites for $PM_{10}$). These findings illustrate the need to develop more sophisticated emission downscaling algorithms for such high resolution scales.

## 44.3 Impact of the Vertical Resolution

Three model configurations are used: (i) the CHIMERE mesh in the default set-up (C8: 8 levels from 995 to 500 hPa), (ii) a mesh refined along the whole vertical axis (C20: 20 levels from 995 to 500 hPa) and (iii) a mesh with a refinement near the surface (C9: 9 levels from 999 to 500 hPa). The heights of the first level are respectively 40 m, 40 m and 8 m respectively for C8, C20 and C9 simulations. The set-up is presented in Menut et al. [2], the domain covers the Paris basin with a resolution of 5 km. For ozone, concentrations usually increase with altitude. This leads to lower values near the surface with C9. The C20 concentrations are lower between 40 and 1,500 m, but higher up to 1,500 m (Fig. 44.3). The same impact is observed on the January profile, but with an inversion of differences around 700 m. This feature reflects the impact of a refined vertical transport, between the boundary layer and the free troposphere. Over Paris there is a decrease of ozone concentrations due to the titration effect between 40 and 8 m for the C9 simulation. An increase is observed for $NO_2$ concentrations because of emissions, helping to get better urban increments over urban areas (not shown here).

This study was conducted over a highly urbanised area, known to be poorly represented in terms of sub-grid scale dynamical processes. While the first layer of C8 and C20 (40 m) is more related to the buildings top heights, C9 (8 m) is representative of the urban canopy layer and this should be expressed in the vertical mixing representation.

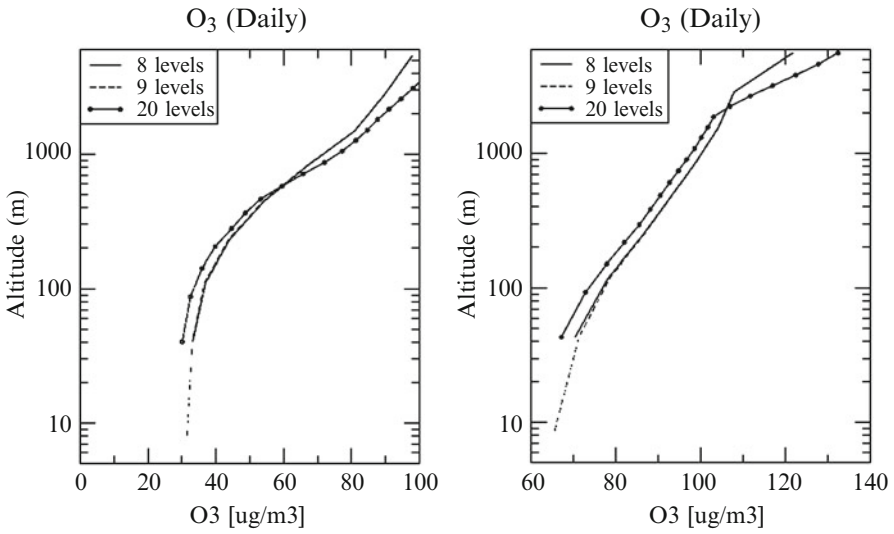


**Fig. 44.3** Mean modelled ozone vertical profiles at 15:00 UTC in January and August 2009 over Paris. The profiles are averaged for each month of January (*left side*) and August (*right side*)

## 44.4 Conclusion

Achieving a very high horizontal resolution simulation demonstrates the robustness of the selected air quality model. We discussed the added value in terms of air pollution modelling and decision support. The comparison with in-situ observations shows that model biases are significantly improved despite some spurious added spatial variability attributed to shortcomings in the emission downscaling process and coarse resolution of the meteorological fields. Regarding the vertical resolution, the relevance of adding a point close to the surface has been shown and this corresponds to modify the 'urban increment' roughly defined as the difference between the city and background concentrations. This expected change is due to the combined effects of (i) higher deposition rates in remote areas (over vegetative covers) and (ii) higher concentrations of primary pollutants emitted within the urban canopy (or lower for ozone) over cities.

**Acknowledgments** This study was funded by the French Ministry in charge of Environment. European funding also benefited to this initiative through the EC4MACS project of the Life Programme of the European Commission (LIFE06 ENV/AT/PREP/06).

## References

1. Bessagnet B, Menut L, Curci G, Hodzic A, Guillaume B, Liousse C, Moukhtar S, Pun B, Seigneur C, Schulz M (2008) Regional modeling of carbonaceous aerosols over Europe – focus on secondary organic aerosols. J Atmos Chem 61:175–202

2. Menut L, Bessagnet B, Colette A, Khvorostiyanov D (2013) On the impact of the vertical resolution on chemistry-transport modelling. Atmos Environ 67:370–384
3. Thunis P, Pederzoli A, Pernigotti D (2012) Performance criteria to evaluate air quality modeling applications. Atmos Environ 59:476–482

## Question and Answer

**Questioner Name:** Dominik BRUNNER

**Q:** Did you ensure mass conservation when modifying the wind speed over the urban areas?

**A:** Yes, the divergence budget is made after the correction (calculation of the vertical wind speed).

# Chapter 45
# A Model Study on the Effects of Emission Reductions on European Air Quality Between 1990 and 2020

**Sebnem Aksoyoglu and André S.H. Prévôt**

**Abstract** We simulated the ozone and particulate matter (PM) concentrations in Europe with the regional air quality model CAMx for 1990 (reference year for the Gothenburg Protocol), 2005 (reference year for the revised Gothenburg protocol), 2006 (for model validation) and 2020 (target year for the revised Gothenburg protocol) to investigate the effects of emission reductions on air quality. The three emission scenarios used for 2020 were Baseline, Mid and MTFR, prepared by IIASA using the GAINS model. Comparisons between 1990 and 2005 suggested a large decrease (up to 50 %) in PM2.5 concentrations as shown also by observations. PM2.5 levels were predicted to decrease further by about 35 % (Baseline) and 45 % (MTFR) until 2020. Although ozone damage indicators AOT40 and SOMO35 were modeled reasonably well for the reference case 2005, the relative change between 1990 and 2005 did not match some of the observations. The significant decrease in indicators predicted for 2020 should be further investigated, because background ozone concentrations might have a strong influence on correct prediction of these indicators with thresholds. Our results suggested that the deposition of nitrogen compounds decreased by 20–50 % between 1990 and 2005 and the main reduction was due to the oxidized nitrogen species. On the other hand, the modeled deposition of the reduced nitrogen species in 2005 was higher than in 1990. The deposition of the oxidized nitrogen species was predicted to decrease further by about 40 % until 2020 while deposition of reduced nitrogen species would be higher in the future.

S. Aksoyoglu (✉) • A.S.H. Prévôt
Laboratory of Atmospheric Chemistry, Paul Scherrer Institute, 5232 Villigen, PSI, Switzerland
e-mail: sebnem.aksoyoglu@psi.ch; andre.prevot@psi.ch

D. Steyn and R. Mathur (eds.), *Air Pollution Modeling and its Application XXIII*,
Springer Proceedings in Complexity, DOI 10.1007/978-3-319-04379-1_45,

## 45.1 Introduction

In spite of the current legislation devoted to air pollution control, ozone and PM10 levels often exceed the ambient air quality standards in Europe (for ozone: 120 $\mu g\ m^{-3}$ maximum daily 8-h mean, for PM10: 50 $\mu g\ m^{-3}$ daily mean). An earlier study suggested that the decrease in local ozone production due to emission reductions between 1985 and 2010 might have been partly or completely compensated by the simultaneous increase in the background ozone [2]. The ozone precursor emissions in Europe and in North America have decreased significantly since 1980s while $NO_x$ emissions increased dramatically in Asia in the last decade [8]. Ozone concentrations in Europe can therefore be affected by emissions from other continents due to its sufficiently long lifetime. The revised Gothenburg Protocol was signed in 2012 including the fine particulate matter (PM2.5). The EMEP Centre for Integrated Assessment Modelling (CIAM) at IIASA prepared various emission control scenarios for cost-effective improvements of air quality in Europe in 2020 using the GAINS (Greenhouse gas – Air pollution Interactions and Synergies) model within the framework of revised Gothenburg Protocol. In this paper, we discussed the annual changes in particulate matter, ozone damage indicators AOT40 and SOMO35 and nitrogen deposition between 1990 and 2005 as well as between 2005 and 2020.

## 45.2 Method

We used the 3-dimensional air quality model CAMx (Comprehensive Air quality Model with extensions, http://www.camx.com) and meteorological model WRF (Weather Research and Forecasting Model, http://wrf-model.org/index.php). The model domain covered whole Europe with a horizontal resolution of $0.250° \times 0.125°$. A nested domain around Switzerland had three times higher resolution. Details on model parameterization can be found in Aksoyoglu et al. [3]. The biogenic emissions were calculated using the meteorological data from WRF output according to the method described in Andreani-Aksoyoglu et al. [1]. European emissions for anthropogenic sources for 2006 are from TNO (http://www.gmes-atmosphere.eu/).

We calculated the meteorological fields for 2006 with the WRF model and used them for all the CAMx simulations with different emission scenarios for the entire year. The modeled scenarios are: 1990 (retrospective), 2006 (model validation), 2005 (reference case), BL 2020 (baseline scenario), MID 2020 (mid scenario), MTFR 2020 (maximum technically feasible reduction scenario). Emission scenarios for 2020 were selected from the emission scenarios prepared by IIASA using the GAINS model in the framework of the revision of the Gothenburg Protocol (http://gains.iiasa.ac.at/index.php/policyapplications/gothenburg-protocol-revision). The relative reductions in three emission scenarios for 2020 are shown in Table 45.1

**Table 45.1** Emission reductions for 2020 relative to 2005 [4]

| Pollutant | BL scenario (%) | Mid scenario (%) | MTFR scenario (%) | Revised Gothenburg Protocol (%) |
|---|---|---|---|---|
| $SO_2$ | 66 | 69 | 78 | 59 |
| $NO_x$ | 50 | 54 | 59 | 43 |
| NMVOC | 36 | 42 | 56 | 28 |
| $NH_3$ | 4 | 24 | 35 | 6 |
| PM2.5 | 34 | 42 | 64 | 22 |

together with the reductions according to the revised Gothenburg Protocol, which was not yet signed when this study was carried out. Initial and boundary concentrations were obtained from the global model MOZART [5]. We kept the background ozone concentrations constant for the reference case (RC 2005) and for 2020 scenarios based on the information in the literature [6, 7]. The simulations for 1990 however, were carried out with lower background ozone concentrations.

## 45.3 Results

Model performance was found to be reasonably good in rural sites for gaseous as well as particulate species except for some days in winter that occurred mainly during periods of strong inversions (Fig. 45.1). The model results suggest that PM2.5 concentrations in central Europe decreased by about 40–50 % between 1990 and 2005, as shown by the observations at various sites. Assuming the baseline (BL) scenario-which is the closest scenario to the revised Gothenburg Protocol- a further decrease of about 35 % in PM2.5 was predicted for 2020 in Europe (Fig. 45.2). The MTFR scenario with the highest ambition on the other hand, would lead to about 45 % reduction in the European PM2.5 concentrations. Although peak ozone levels decreased between 1990 and 2005, the annual ozone concentrations increased in Europe.

The modeled ozone damage indicators AOT40 (Accumulated dose of ozone Over the Threshold of 40 ppb) for vegetation and SOMO35 (Sum of Ozone Means Over 35 ppb) for health impacts for 2005 were reasonable when compared to measurements. However, there was a discrepancy between predictions and observations for the change between 1990 and 2005, showing the sensitivity of parameters such as AOT40 and SOMO35 to threshold values. Assuming a constant background ozone concentration in Europe between 2005 and 2020, model predicts a large decrease in AOT40 and SOMO35 ($\sim$50 %). However, changes in the background ozone concentrations in Europe might affect the modeling of damage indicators significantly and therefore this issue needs further investigation.

Our results suggested that the deposition of nitrogen compounds decreased by 20–50 % between 1990 and 2005 and the largest reductions were predicted in eastern part of Europe. The results indicated that the main reduction in nitrogen

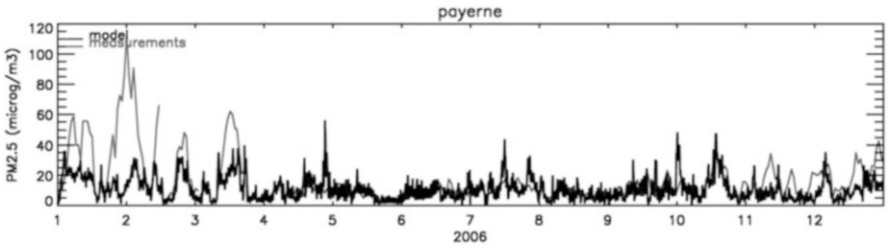


**Fig. 45.1** Comparison of modeled and measured PM2.5 concentrations ($\mu g\ m^{-3}$) in 2006 at Payerne (CH)

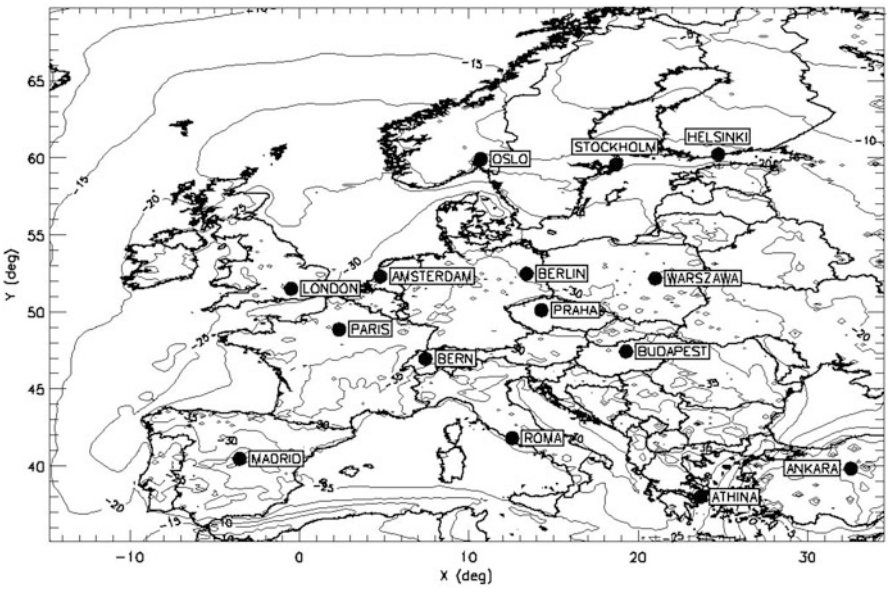


**Fig. 45.2** Change in annual average of PM2.5 (%), BL 2020 – RC 2005

deposition was due to the decrease in the deposition of oxidized nitrogen species. On the other hand, the modeled deposition of the reduced nitrogen species ($NH_3$ and particulate $NH_4$) in 2005 was higher than in 1990. The deposition of the oxidized nitrogen species was predicted to decrease further by about 40 % until 2020 while deposition of reduced nitrogen species would continue to increase.

## 45.4 Conclusion

The results of this study suggested that PM2.5 concentrations in Europe have decreased by up to 50 % between 1990 and 2005 as shown also by measurements. PM2.5 levels were predicted to continue decreasing until 2020 by 30 and 50 %

according to the Baseline and MTFR emission scenarios, respectively. Our results also showed that reductions in ozone precursor emissions would lead to a decrease in peak ozone levels while concentrations at urban sites would increase. Although the modeled ozone damage indicators AOT40 and SOMO35 for 2005 were similar to observations, there was a discrepancy in the relative change since 1990. Under the assumptions used in this study, both indicators were predicted to decrease significantly until 2020. Such predictions however, should be further investigated carefully, because background ozone concentrations might have a strong influence on modeling of these indicators. The model results suggested that the deposition of oxidized nitrogen compounds decreased since 1990. They were predicted to decrease further until 2020 while deposition of reduced species would continue to increase.

**Acknowledgments** This study was financially supported by the Swiss Federal Office of Environment, FOEN. We are grateful to ECMWF, TNO, IIASA, INFRAS, Meteotest, NABEL/EMPA, ENVIRON, and M. Tinguely for providing us with various data or help.

## References

1. Andreani-Aksoyoglu S, Keller J (1995) Estimates of monoterpene and isoprene emissions from the forests in Switzerland. J Atmos Chem 20:71–87
2. Andreani-Aksoyoglu S, Keller J, Ordonez C, Tinguely M, Schultz M, Prevot ASH (2008) Influence of various emission scenarios on ozone in Europe. Ecol Model 217:1209–1218. doi:10.1016/j.ecolmodel.2008.1006.1022
3. Aksoyoglu S, Keller J, Barmpadimos I, Oderbolz D, Lanz VA, Prévôt ASH, Baltensperger U (2011) Aerosol modelling in Europe with a focus on Switzerland during summer and winter episodes. Atmos Chem Phys 11(14):7355–7373. doi:10.5194/acp-5111-7355-2011
4. CIAM (2011) An updated set of scenarios of cost-effective emission reductions for the revision of the Gothenburg Protocol. http://gains.iiasa.ac.at/index.php/policyapplications/gothenburg-protocol-revision/369-ciam-report-4-2011
5. Horowitz LW, Walters S, Mauzerall DL, Emmons LK, Rasch PJ, Granier C, Tie X, Lamarque J-F, Schultz MG, Tyndall GS, Orlando JJ, Brasseur GP (2003) A global simulation of tropospheric ozone and related tracers: description and evaluation of MOZART, version 2. J Geophys Res 108:4784. doi:10.1029/2002JD002853
6. Logan JA, Staehelin J, Megretskaia IA, Cammas JP, Thouret V, Claude H, De Backer H, Steinbacher M, Scheel HE, Stübi R, Fröhlich M, Derwent R (2012) Changes in ozone over Europe: analysis of ozone measurements from sondes, regular aircraft (MOZAIC) and alpine surface sites. J Geophys Res 117(D9):D09301
7. Wilson RC, Fleming ZL, Monks PS, Clain G, Henne S, Konovalov IB, Szopa S, Menut L (2012) Have primary emission reduction measures reduced ozone across Europe? An analysis of European rural background ozone trends 1996–2005. Atmos Chem Phys 12(1):437–454
8. Zhang Y, Olsen SC, Dubey MK (2010) WRF/chem simulated springtime impact of rising Asian emissions on air quality over the U.S. Atmos Environ 44(24):2799–2812

## Questions and Answers

**Questioner Name:** Dominik Brunner

**Q:** How exactly was background at borders of domain simulated?
**A:** Boundary conditions were obtained from the global model MOZART for the year of interest. In case of 1990, we used literature values.

**Questioner Name:** Douw Steyn

**Q:** In a similar retrospective study in the Vancouver region, we found an increase in the NOx efficiency for $O_3$ production. Did you find similar chemical process changes over decadal scales in your study?
**A:** Not yet. We will investigate the detailed ozone chemistry and trends since 1990 in a follow-up study.

# Chapter 46
# Analysis and Modelling of Ambient Air Toxics Pollutants in Canada with Environment Canada AURAMS Model

**Jack Chen, Craig Stroud, Calin Zaganescu, Gilles Morneau, and Daniel Wang**

**Abstract** In Canada, air toxic pollutants are regulated under Schedule 1 of the Canadian Environmental Protection Act-1999. As part of the Canadian government's Clean Air Regulatory Agenda (CARA), Environment Canada is working with Health Canada to develop air quality modelling capabilities to support assessments of health and environmental impacts from mobile source emissions. In current phase, there are 6 compounds of interest: benzene, 1-3 butadiene, formaldehyde, acetaldehyde, acrolein and 1-2-4 trimethylbenzene. Environment Canada's AURAMS air quality model was modified to explicitly simulate the chemistry of these compounds with the SAPRC07-toxics mechanism. National emissions inventories were processed for air toxics species with source-specific VOC profiles, while on-road mobile sources were explicitly modeled. AURAMS was applied on a 45-km grid spaced domain covering Canada and the US, and over a summer and a winter period. Long-term analysis of >5 years of surface measurements from National Air Pollutant Surveillance (NAPS) Network for 10–54 stations were used to compare with this first model analysis. This paper will focus on the analysis of long-term ambient concentrations of air toxics in Canada, as well as initial results from the AURAMS model with air toxics capability for a summer and a winter period.

J. Chen (✉) • C. Zaganescu • G. Morneau
Meteorological Services Canada, Environment Canada, Montreal, QC, Canada
e-mail: jack.chen@ec.gc.ca

C. Stroud • D. Wang
Science and Technology Branch, Environment Canada, Toronto, ON, Canada

D. Steyn and R. Mathur (eds.), *Air Pollution Modeling and its Application XXIII*,
Springer Proceedings in Complexity, DOI 10.1007/978-3-319-04379-1_46,

## 46.1 Introduction

In 2006, the Canadian government introduced the Clean Air Regulatory Agenda (CARA), which aimed, in part, to reduce emissions of air pollutants and to protect the health and wellness of Canadians. In order to understand the source, evolution, and fate of air toxics compounds, Environment Canada is developing regional air quality modelling capabilities for six toxics associated with mobile exhausts and industrial sectors, they are: benzene (BENZ), 1-3 butadiene (BD13), formaldehyde (HCHO), acetaldehyde (CCHO), acrolein (ACRO) and 1-2-4 trimethylbenzene (B124).

AURAMS is a regional air quality modelling system developed by Environment Canada. It was developed as a 'unified' regional photochemical modelling system, and has been utilized in many science and policy applications [5, 7, 8, 10]. The model is comparable in scope to the Community Multiscale Air Quality (CMAQ) model developed by the U.S. EPA. Both simulate the formation and evolution of gas-phase species, particulate matter, and their interactions [9].

The default chemical representation in AURAMS is the revised ADOM-II mechanism [6] with 42 gas-phase species and 13 VOC species. Except for formaldehyde, there are no explicit formulations for air toxics. In this experiment, the mechanism was replaced with the SAPRC-07-tx mechanism, available in the CMAQ model. The mechanism has 125 gas-phase species and explicit representation of the toxic species of interest [1].

This modified AURAMS model was applied to simulate air toxics ambient concentration for the winter (Jan-Feb-Mar) and summer (Jun-Jul-Aug) seasons for year 2006. The model setup is similar to previous exercises with a domain covering the contiguous US and Canada at 45-km grid resolution [3]. Emission inputs were based on the 2005 and 2006 national inventories from the US and Canada, respectively, and processed using the SMOKE processor [2]. Air toxics emissions were estimated using source-specific VOC speciation profiles, except for on-road mobile sources, where specific toxics species were generated using the MOBILE6C model.

## 46.2 Air Toxics Measurements

Surface measurements of the six air toxics were obtained from the Canadian National Air Pollution Network (NAPS) for years 2004–2010. While most measurements were on a frequency of once-every-6-days at 24-h sampling period, measurement frequencies do vary by station, species and year. To ensure enough observations for monthly representativeness, a simple completeness criterion was applied where stations with less than 3 measurements per month were dropped from the analysis. Overall, between 17 and 47 % of data was eliminated depending

on species. BENZ, BD13 and B124, were sampled in canisters and measured by gas chromatography with mass spectrometric detector, while ACRO, HCHO and CCHO were derivatized on DNPH cartridges, separated by liquid chromatography and measured by UV-absorption detector.

Most stations in the analysis are from urban, populated cities, while about ~25 % of all stations are of rural category. For BENZ, BD13, and B124, there were, on average, 12,198 measurements from 52 stations. The variability in annual sample frequency and number of available stations was small for some toxics; for example the BENZ station count was highest in 2009 (# station = 39, n = 2,023) and lowest in 2010 (# station = 34, n = 1,755). However, there were significantly less measurements for HCHO, CCHO and ACRO (average of 2,099 measurements from 17 stations), leading to greater variability in annual sample frequency; for instance, the HCHO station count was highest in 2008 (# station = 13, n = 322), and lowest in 2005 (# station = 6, n = 177). It is important to note that, due to variability in sample time, frequency and location, the analysis presented may not be sufficient to represent ambient concentration trends across all of Canada. It is, however, a good representation for locations near urban areas where measurement stations were located.

All six toxics species exhibit high concentration variability over 2004–2010. Figure 46.1 shows the month and annual concentration ranges by percentile values as well as overall means and trends. Except for ACRO, all species showed clear decreasing trends over the years. The reduction rate (slope) is largest for HCHO (−0.11) followed by BENZ (−0.09) and CCHO (−0.07). Concentration variability also decreased over the years especially for BENZ, BD13 and B124 where there were more measurement data. There was apparent concentration seasonality for most species. HCHO and CCHO have similar trends with a summer maximum (2.53 $\mu g/m^3$ and 1.48 $\mu g/m^3$, respectively) and a winter minimum (1.37 $\mu g/m^3$ and 0.87 $\mu g/m^3/m^3$, respectively), while BENZ showed a winter maximum (1.18 $\mu g/m^3$) and a summer minimum (0.81 $\mu g/m^3$). The variations were less obvious for BD13, B124 and ACRO due to their low overall concentrations.

## 46.3 AURAMS Model Assessment

Hourly model outputs were averaged by sampling periods and paired spatiotemporally for comparison. Figure 46.2 shows the analysis for the six toxics over the two modelled seasons in 2006. In general, the model showed ability in capturing seasonal concentration ranges. There were obvious seasonal biases that vary by species. For both seasons, AURAMS under-predicted the mean, median and variability for both ACRO and B124. A more rigorous comparison by scatter plot showed model performed better for CCHO and HCHO, likely due to their detailed representations in SAPRC07-toxics; while BENZ and BD13 showed slight over

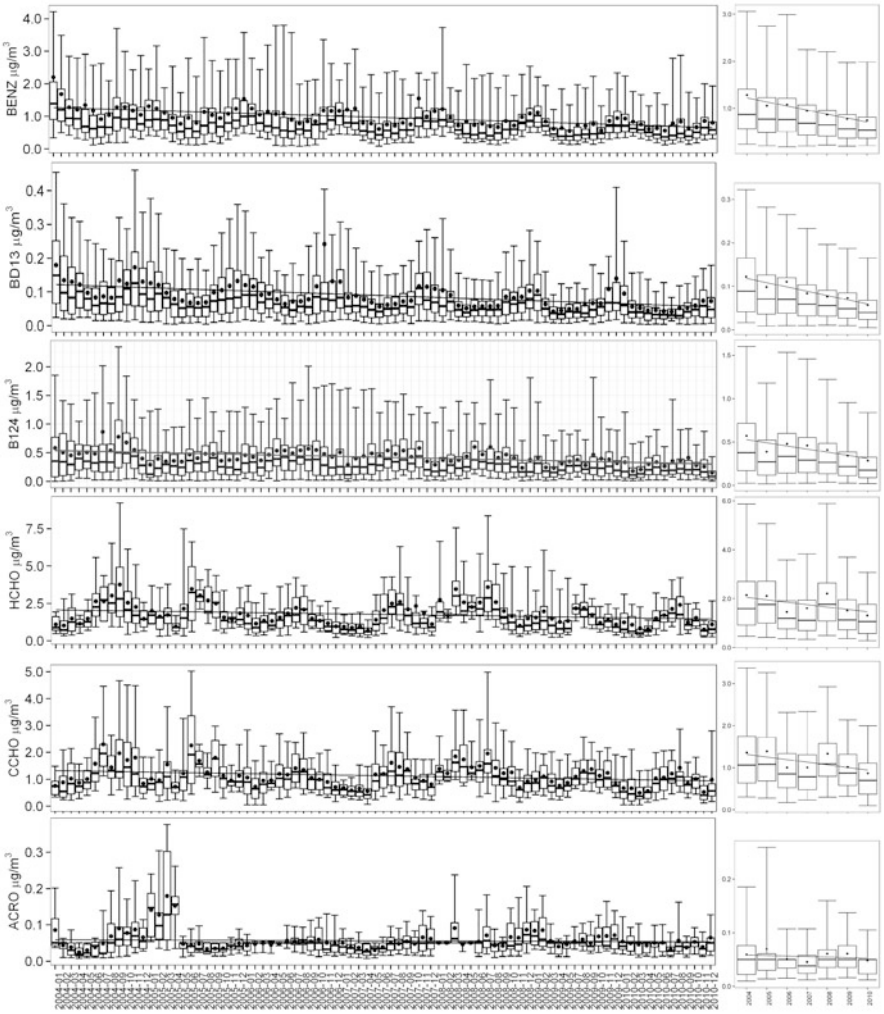


**Fig. 46.1** Box-n-whisker plots of observed air toxic species by month (*left*) and year (*right*). The *error-bars* and *boxes* represent 95th/75th/50th/25th/5th percentile. Overall monthly mean is noted by dots

predictions during winter, mostly from urban stations in Vancouver and Toronto areas. The performance was slightly worse for ACRO with model under-prediction in the summer time concentrations with a normalized mean bias of −86 %. This may be partly due to possible uncertainties in measurement techniques as well as few sample stations available [4]. Overall, by species, the fraction of modelled data that is within a factor of two of measured data ranges from HCHO at 73 % and CCHO at 67 %, to B124 at 28 % and ACRO at 19 %.

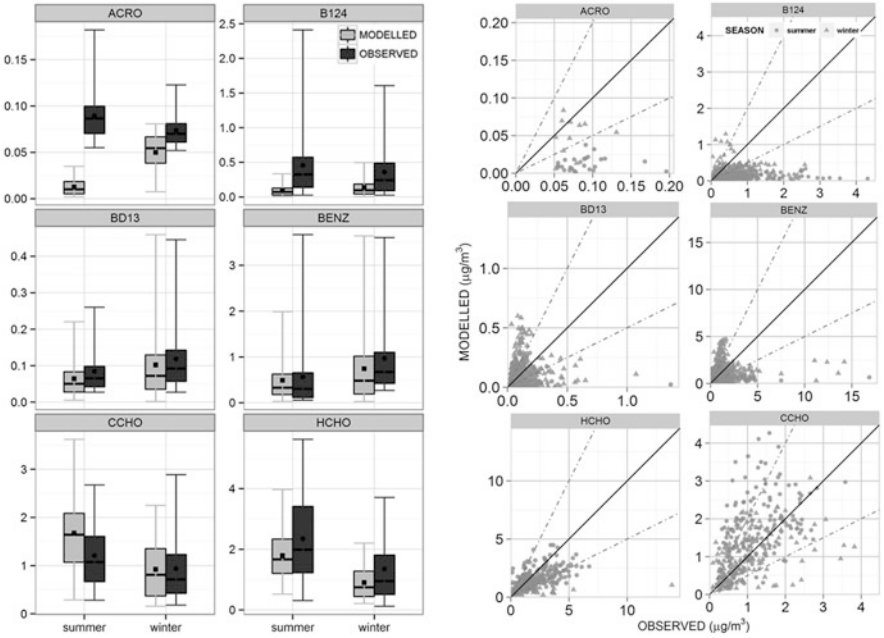


**Fig. 46.2** (*Left*) Box-n-whisker plot of 2006 seasonal observed and modelled air toxics. The *error-bars* and *boxes* represent 98th/75th/50th/25th/2nd percentiles, overall means are marked by black dots. (*Right*) Scattered plot of observed and modelled air toxics paired by both time and space. The *solid line* denotes 1:1 while *dotted-lines* mark areas of 2:1

## 46.4 Summary

Environment Canada is developing predictive capabilities with the AURAMS air quality model for selected air toxics: benzene (BENZ), 1-3 butadiene (BD13), formaldehyde (HCHO), acetaldehyde (CCHO), acrolein (ACRO) and 1-2-4 trimethylbenzene (B124). Analysis of long-term ambient concentrations (2004–2010) showed decreasing trends and variability for all species except ACRO. Many species also exhibited seasonality in ambient concentrations. Preliminary AURAMS results for the 2006 summer and winter seasons showed skills in capturing seasonal ranges as well as site-specific concentrations. There were seasonal biases for ACRO and B124, and the performance metrics were generally better for CCHO and HCHO but poor for ACRO.

## References

1. Carter WP (2010) Development of the SAPRC-07 chemical mechanism. Atmos Environ 44(40):5324–5335

2. CEMPD, Center for Environmental Modeling for Policy Development – Sparse Matrix Operator Kernel Emissions (SMOKE) Modeling system website available from: http://www.smoke-model.org
3. Chen J, Cousineau S, Davignon D, Duhamel A, Gilbert S, Menard V, Racine J, Sassi M, Samaali M (2010) Proceedings to 9th annual CMAS conference. Available online: http://www.cmascenter.org/conference/2010/abstracts/chen_2006_annual_2010.pdf
4. Herrington JS, Zhang JJ (2008) Development of a method for time-resolved measurement of airborne acrolein. Atmos Environ 42(10):2429–2436
5. Kelly J, Makar PA, Plummer DA (2012) Projections of mid-century summer air-quality for North America: effects of changes in climate and precursor emissions. Atmos Chem Phys 12:5367–5390
6. Stockwell WR, Lurmann FW (1989) Intercomparison of the ADOM and RADM gas-phase chemistry mechanisms. Report prepared for the Electric Power Research Institute, June. Electric Power Research Institute, Palo Alto, CA, 260pp
7. McKeen S, Chung SH, Wilczak J, Grell G, Djalalova I, Peckham S, Gong W, Bouchet V, Moffet R, Tang Y, Carmichael GR, Mathur R, Yu S (2007) Evaluation of several real-time PM2.5 forecast models using data collected during the ICARTT/NEAQS 2004 field study. J Geophys Res 112:D10S20
8. Moran MD, Dastoor A, Gong SL, Gong W, Makar PA (1998) Conceptual design for the AES regional particulate-matter model/unified air quality model. October, Atmospheric Environment Service, Downsview, ON, 100 pp
9. Smyth SC, Jiang W, Roth H, Moran MD, Makar PA, Yang F, Bouchet VS, Landry H (2009) A comparative performance evaluation of the AURAMS and CMAQ air quality modelling systems. Atmos Environ 43:1059–1070
10. Stroud CA, Morneau G, Makar PA, Moran MD, Gong W, Pabla B, Zhang J, Bouchet VS, Fox D, Venkatesh S, Wang D, Dann T (2008) OH-reactivity of volatile organic compounds at urban and rural sites across Canada: evaluation of air quality model predictions using speciated VOC measurements. Atmos Environ 42:7746–7756

## Questions and Answers

### Questioner Name: Pradeepa Vennan

**Q:** In the case of acrolein, CMAQ showed similar under-prediction and some papers pointed out that it could be due to uncertainty in the measurements, have you looked into it?

**A:** Yes, we have looked into it, and you are correct that the measurement uncertainties do partly explain the model under-predictions. In this case, the measurements from NAPS network were conducted via the DNPH cartridges (TO11A method). It is known that the method can cause negative biases due to decomposition of acrolein on DNPH substrate. However, how much this uncertainty contributed to the model performance is unknown. Given that the model comparison is worse in the summer, with large under-predictions, we do suspect that an incomplete acrolein emission in the model input (i.e. no wild fire sources) is likely to contribute more to model error than measurement uncertainty.

**Questioner Name: Armin Aulinger**

**Q:** Did you perform any statistical tests for trends in the time series of the measurements of air pollutants?

**A:** The presentation showed seasonal box plots with trend lines calculated from the overall averages. The box plot whiskers represents 98th and 2nd percentile values, thus extreme outliers were removed, in addition, a simple sample completeness criteria was applied such that only stations with more than 3 measurements per month was used in the analysis. Considering that the sample dataset is relatively large, we did not apply additional statistical tests on significance.

**Questioner Name: Roger Timmis**

**Q:** With reference to the unusual trends of increasing acrolein at Port Moody, BC, were seasonal variations at Port Moody similar to those in other cities? Also, would you see signals from wildfire acrolein at Port Moody similar to wildfire signal from elsewhere?

**A:** Given the steady increasing of annual acrolein ambient concentrations from 2004 to 2010, we have indeed looked into the seasonal variations of acrolein in Port Moody. However, the trend does not support source contributions from wildfires. Average seasonal concentrations over the period (7 years) for this site showed summer-fall concentrations at 0.05 $\mu g/m^3$ and winter-spring concentrations at 0.07 $\mu g/m^3$.

Another possible attribution to the ambient acrolein may due to anthropogenic sources from urban growth. According to the most recent census from Statistics Canada (http://www12.statcan.gc.ca/census-recensement/index-eng.cfm; accessed 2013-Sept), Port Moody is the fastest growing city by population in Metro Vancouver, and 24th overall across Canada. Between 2006 and 2011 the city had $\sim$20 % growth in population. The steady increase in population and its related activities may partly explain the increases in acrolein ambient levels in the area.

# Chapter 47
# Investigating the Coherence Between a Global and a Limited Area Model for Dust Particle Production and Distribution in N-Africa

**Marina Astitha, Chris Spyrou, Serafim Kontos, George Kallos, and Jos Lelieveld**

**Abstract** The choice of the parameterization scheme, the input parameters and the spatial resolution are options that can provide significantly different modelling results for the processes of desert dust production and transport. This work will discuss the level of coherence between a regional and a global modelling system with regards to the simulation of desert dust production and transport in N-Africa. The limited-area model SKIRON/Dust and the atmospheric chemistry general circulation model EMAC (ECHAM5/MESSy2 Atmospheric Chemistry) have been applied using a common physically-based dust emission scheme. The differences between the two modelling systems and the comparison with the observations will be analysed and discussed, as well as the plans for future work in their offline coupling.

## 47.1 Introduction

Desert dust particles are significant atmospheric constituents, which affect air quality and climate in various ways. The dust transport in regional and global scales might be of episodic nature but the overall effect in the atmospheric circulation is

M. Astitha (✉)
Department of Civil and Environmental Engineering, University of Connecticut, 261 Glenbrook Road, Storrs, CT 06269-3037, USA
e-mail: astitha@engr.uconn.edu

C. Spyrou • S. Kontos • G. Kallos
Atmospheric Modeling and Weather Forecasting Group, University of Athens, School of Physics, University Campus, Bldg PHYS-V, 15784 Athens, Greece
e-mail: kallos@mg.uoa.gr

J. Lelieveld
EEWRC, The Cyprus Institute, Athalassa Campus, Nicosia, Cyprus

Max Planck Institute for Chemistry, Becherweg 27, 55128 Mainz, Germany

D. Steyn and R. Mathur (eds.), *Air Pollution Modeling and its Application XXIII*, Springer Proceedings in Complexity, DOI 10.1007/978-3-319-04379-1_47,

considered non-negligible. Thus, the need to improve the modelling of the emission, transport and deposition of dust particles is of scientific interest, especially when the combination of different scales is possible.

The motivation for this work originated from the need to adopt the offline coupling between two modelling systems, a global and a regional, and manage to exploit each model's advantages towards a hybrid dust modelling scheme. In the first phase that is discussed in this paper, the limited-area model SKIRON/Dust and the atmospheric chemistry-climate model EMAC were applied with conformity in the parameterization of desert dust emissions. The SKIRON/Dust dust module was re-coded to include the updated dust emission scheme as implemented in the EMAC model [1]. The performed case studies are compared with satellite and remote sensing retrievals to explore the level of coherence in the horizontal and vertical distribution of Saharan dust particles, as well as the dust size distribution during transport. This presentation will elaborate on the differences and similarities between the two models and discuss the results from the dust simulations for June 2006.

## 47.2 Methodology for Modelling the Dust Production in Regional and Global Scale

The SKIRON/Dust modeling system is based on the atmospheric model SKIRON, which has been developed at the University of Athens from the Atmospheric Modeling and Weather Forecasting Group [5, 6]. During the SKIRON/Dust simulations, the prognostic atmospheric and hydrological conditions are used to calculate the effective rates of the injected dust concentration based on viscous/turbulent mixing, soil composition, soil moisture, shear-free convection and diffusion. The model has been configured with a $0.15° \times 0.15°$ spatial resolution and the simulation period was February-June 2006.

The ECHAM5/MESSy2.41 Atmospheric Chemistry (EMAC) model is a combination of the ECHAM5 general circulation model and the Modular Earth Submodel System [2]. The EMAC model runs with a spectral resolution of T106 ($\sim 1.1° \times 1.1°$) and 31 vertical levels up to 10 hPa for the year 2006. The difference with the implementation in Astitha et al. [1] is the explicit treatment of the soil characteristics in the N-African and NE-Asian deserts that influence the horizontal movement of desert dust particles [4]. The vertical flux of emitted particles is also changed, based on the particle populations that can be released from soil, following Laurent et al. [3]. Detailed region-specific input data have been used by both models that include up-to-date surface soil data sets (aerodynamic and smooth roughness length, dry soil size distribution and texture) in $0.25° \times 0.25°$ spatial resolution. Both models use the 8-size bin distribution (lognormally distributed in each bin)

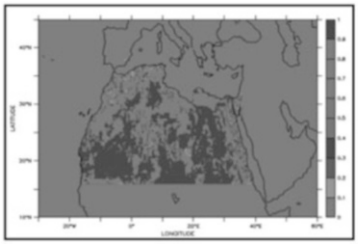

N-AFRICA PARTICLE POPULATIONS THAT CAN BE RELEASED FROM SOIL (Laurent et al. 2010)

| $D_v$(μm) | $\sigma_g$ |
|---|---|
| 1.5 | 1.7 |
| 6.7 | 1.6 |
| 14.2 | 1.5 |

8 SIZE BIN DISTRIBUTION DURING TRANSPORT (Perez et al. 2006)

| Dmin(μm) | Dmax(μm) | Density (g/cm³) |
|---|---|---|
| 0.2 | 0.36 | 2.65 |
| 0.36 | 0.6 | 2.65 |
| 0.6 | 1.2 | 2.65 |
| 1.2 | 2 | 2.65 |
| 2 | 3.6 | 2.65 |
| 3.6 | 6 | 2.65 |
| 6 | 12 | 2.65 |
| 12 | 20 | 2.65 |

**Fig. 47.1** *Left*: Erodibility of the soil in N-Africa. *Middle*: Particle populations as adopted in Laurent et al. [3]. *Left*: Size distribution during transport

during transport (Fig. 47.1), though, in EMAC, these bins are grouped into the accumulation and coarse insoluble modes used for all aerosol physical and chemical processes.

## 47.3 Results and Discussion

The first phase of the coupling between the global atmospheric chemistry-climate model EMAC and the limited-area model SKIRON/Dust has been completed with the implementation of a common desert dust parameterization scheme. The same input files of soil texture and size distribution for N-Africa have been used in both models. The differences between the two modeling systems are concentrated in the atmospheric part as well as the aerosol deposition processes and the horizontal resolution. Also, the SKIRON/Dust model includes a high resolution (30s) land-use/land-cover database, the radiative effect of dust within the Rapid Radiative Transfer Model (RRMTG) and the viscous sublayer/turbulent mixing that is important for such small scale perturbations.

The simulations for June 2006 have shown that the new implementation of the dust emission scheme has improved the qualitative correlation of SKIRON/Dust with the MODIS-Aqua satellite AOD at 550 nm (Fig. 47.2) and the quantitative correlation with the AERONET AOD (Fig. 47.3), compared to the original version of the model. The global model overestimates the AOD which becomes more apparent in the quantitative comparison with the AERONET AOD at 550 nm (Fig. 47.3). The selection of the 8 AERONET stations was based on the characterization of a 'dusty' station if the AOD $>0.2$ and Angstrom $<0.75$ for at least 30 % of the data.

Both models simulate very well the dust outbreak towards the CE-Atlantic Ocean (Dakar and Capo Verde), as well as the stations located inland (Agoufou, Banizoumbou and Tamanrasset) and in Algeria (Blida). The biggest discrepancy is found on the NW part of the African continent, where the global model overestimates the AOD by a factor of 2–3. This might be an effect of the

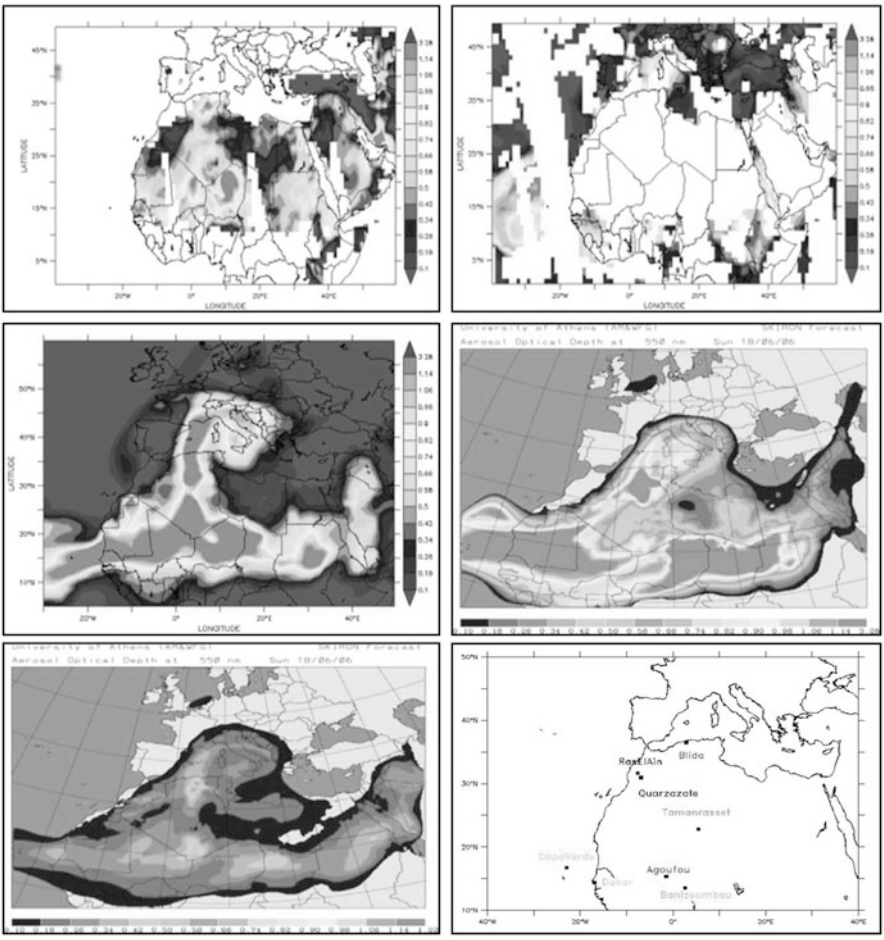


**Fig. 47.2** Daily aerosol optical depth at 550 nm for June 18, 2006. *Upper plots*: MODIS-Aqua (v5.1). *Middle plots*: EMAC model (*left*), SKIRON/Dust new (*right*). *Lower plots*: SKIRON/Dust original scheme (*left*), AERONET stations (*right*)

horizontal resolution, as the global model cannot adequately resolve the complex terrain features in this area (Atlas mountain range). Differences are also found in the vertical distribution of the dust particles, which is better described by the SKIRON/Dust model. The second stage of the offline coupling between the two modeling systems will give an overview of the advantages and disadvantages of this methodology to the simulation of the regional desert dust outbreaks.

**Acknowledgments** Part of the research leading to these results has received funding from the European Research Council under the European Union's Seventh Framework Programme (FP7/2007-2013)/ERC grant agreement n° 226144. We also thank Dr B. Marticorena for kindly providing us with the surface features for N-Africa and NE-Asia.

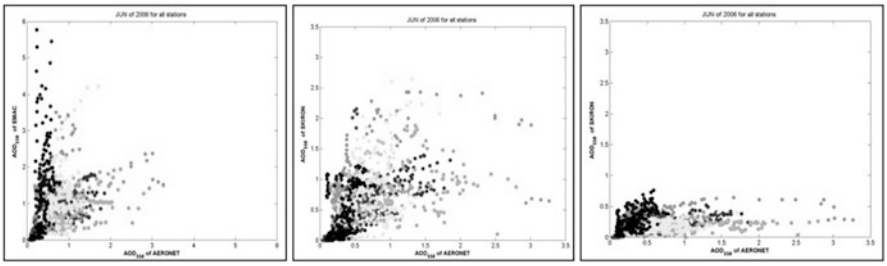

**Fig. 47.3** AOD@550nm from AERONET in comparison with the EMAC model (*left*), SKIRON/Dust with the new dust scheme (*middle*) and SKIRON/Dust with the original scheme (*right*). The color of the points denotes the location of the AERONET station

## References

1. Astitha M, Lelieveld J, Abdel Kader M, Pozzer A, de Meij A (2012) Parameterization of dust emissions in the global atmospheric chemistry-climate model EMAC: impact of nudging and soil properties. Atmos Chem Phys 12:11057–11083. doi:10.5194/acp-12-11057-2012
2. Jöckel P, Kerkweg A, Pozzer A, Sander R, Tost H, Riede H, Baumgaertner A, Gromov S, Kern B (2010) Development cycle 2 of the Modular Earth Submodel System (MESSy2). Geosci Model Dev 3:717–752. doi:10.5194/gmd-3-717-2010
3. Laurent B, Tegen I, Heinold B, Schepanski K, Weinzierl B, Esselborn M (2010) A model study of Saharan dust emissions and distributions during the SAMUM-1 campaign. J Geophys Res 115:D21210. doi:10.1029/2009JD012995
4. Marticorena B et al (1997) Modeling the atmospheric dust cycle: 2. Simulation of Saharan dust sources. J Geophys Res 102:4387–4404
5. Spyrou C, Kallos G, Mitsakou C, Athanasiadis P, Kalogeri C, Iacono MJ (2013) Modeling the radiative effects of desert dust on weather and regional climate. Atmos Chem Phys 13:5489–5504
6. Spyrou C, Mitsakou C, Kallos G, Louka P, Vlastou G (2010) An improved limited area model for describing the dust cycle in the atmosphere. J Geophys Res 115:D17211. doi:10.1029/2009JD013682

# Chapter 48
# Effects of Future Ship Emissions in the North Sea on Air Quality

**Armin Aulinger, Volker Matthias, Johannes Bieser, and Markus Quante**

**Abstract** By means of model simulations with the chemistry transport model CMAQ the influence of ship emissions in the North Sea on concentrations and depositions of sulfur and nitrogen oxides over Europe was investigated. Ship emissions for the North Sea of the base year 2008 were provided by the Dutch research institute MARIN. Based on this, emission scenarios were developed that comply to ECA regulations at different levels. Finally, the emissions were fed into the CMAQ model that simulates the fate of pollutants in the atmosphere in order to estimate concentrations and depositions of the pollutants of interest for each scenario. A comparison of the simulation results yielded a quantification of the changes of air pollution levels over the North Sea riparian states and, hence, provided information for estimating the benefit of installing ECAs in the North Sea. Concentration differences can reach up to 50 % close to shipping lines and still 25 % ashore. The ECA regulations to lower nitrogen and sulfur exhaust take effect at different time scales and are counteracted by the expected increase of fuel use due to increased ship traffic.

## 48.1 Introduction

Land based sources of $SO_x$ and $NO_x$ have decreased substantially in Europe during the last 20 years, partly because of technical progress in the sectors of traffic, heating and industrial production, and partly because of the political and economic changes in Eastern Europe since 1990. In contrast, measures to control ship emissions have been disregarded for a long time. Since recently, however, the awareness of air pollution by shipping in particular concerning the emission of precursors for particulates

A. Aulinger (✉) • V. Matthias • J. Bieser • M. Quante
Helmholtz-Zentrum Geesthacht, Institute of Coastal Research, Max-Planck-Strasse 1, 21502 Geesthacht, Germany
e-mail: armin.aulinger@hzg.de; volker.matthias@hzg.de; johannes.bieser@hzg.de

D. Steyn and R. Mathur (eds.), *Air Pollution Modeling and its Application XXIII*, Springer Proceedings in Complexity, DOI 10.1007/978-3-319-04379-1_48,

is rising (Lauer et al. [4]; Corbett et al. [2]) and political options to decrease ship emissions are discussed. Ship traffic in the North Sea is now recognized by the riparian states as a relevant source for air pollutants, especially because it is likely to grow further during the coming decades. For this reason, the North Sea is accounted for Emission Control Area (ECA) with the objective to reduce the emissions of $NO_x$ and $SO_x$. In the second IMO GHG study [1] both the increase of ship traffic for the next 40 years and implications of introducing ECAs on emission factors for $NO_x$ and $SO_x$ are described. Reducing emissions, however, does not necessarily allow to draw conclusions about the actual concentration levels distant from the sources, i.e. ashore. This is even more true for secondary pollutants like particulate ammonium sulphate or ammonium nitrate that undergo chemical transformations while being transported in the atmosphere. In this study, the authors develop several emission scenarios for $NO_x$ and $SO_x$ derived from base case emissions of 2008 and depending on ECA regulations and use these scenarios to simulate concentrations and depositions of particulate nitrate and sulfate over Europe.

## 48.2 Methods

The Dutch research institutes MARIN and TNO provided ship emissions for the North Sea as yearly totals projected on a spherical grid of 5 km grid cell width [3] which were then used for simulations with the Community Multiscale Air Quality (CMAQ) modeling system. The ship emissions data have been interpolated to a lambert conformal grid of 24 km cell width spanning the CMAQ model domain. The yearly totals in kg were transformed to g/s as required by the model without a temporal profile. The model runs covered the months December to February representing winter and June to August for summer. Meteorological fields were produced with the climate version of the weather forecast model of the German weather service (CLM), land based emissions and boundary conditions were calculated from results of the MOZART global model of 2008. To estimate the influence of ship emissions on pollutant concentrations one model run performed with ship emissions was compared to one without ship emissions.

The authors of the second IMO GHG study propose specific emission factors for $NO_x$ and $SO_x$ in g/kg fuel consumed. Concerning $SO_x$ emissions, the emission factors decrease with the sulfur content in ship fuel that is in ECA zones 1.5 % for the base year 2008, 1.0 % since 2010, 0.1 % from 2015 on. Outside of ECAs the content was assumed to be 2.7 % in 2008 and will be reduced to 0.5 % in 2020. Emissions of $NO_x$ depend on the engines rather than on the fuel used, and the MARPOL directives prescribe that new built ships have to fulfill Tier I – III regulations depending on the keel laying year. Taking this into account and assuming 3 % growth of the fleet as well as an average vessel life time of 30 years IMO provides steadily decreasing emission factors for $NO_x$ between 2007 and 2050.

Using the emission factors that reflect the non-ECA emissions of 2008 as reference the authors of this study developed fractional scaling factors to calculate

**Table 48.1** Fractional emission increases coming from the base year 2008

| Pollutant | Scenario (year) | No ECA | ECA |
|---|---|---|---|
| $NO_x$ | 2020 | 1.2 | 0.94 |
| | 2030 | 1.44 | 0.61 |
| $SO_x$ | 2020 | 0.45 | 0.1 |
| | 2030 | 0.58 | 0.13 |

emissions for 2020 and 2030 both for ECA and non-ECA cases based on the MARIN emissions of 2008 (Table 48.1). Because the IMO emission factors are in g/kg fuel the scaling factors additionally consider an annual increase of fuel use of 2.7 % which is the assumed increase of $CO_2$ emissions from ships in the A1 IPCC base scenario. In this way, we developed emission scenarios for 2020 and 2030 both for ECA and non-ECA cases which we used for CMAQ simulations. The results were compared to the base case run.

## 48.3 Results and Discussion

The difference of pollutant concentrations between simulations with and without ship emissions was, of course, the largest along the major shipping lines, above all the English Channel. $NO_2$ which is almost equivalent to $NO_x$ emissions increased in the winter months from about 12 $\mu g/m^3$ by 25 % in the Channel. In areas ashore where no large industries or high population densities are found like in Denmark the increase is still 15 %. In industrialized areas, however, even if close to the shore like Belgium where concentrations of 20 $\mu g/m^3$ and more were found the increase of 0.4 % is nearly negligible. The same trends hold for $SO_2$ which is the largest part of $SO_x$ emissions. However, the increase is a little lower with 20 % at the most. Even if the absolute concentration increases are almost equal in winter and summer the relative increases are higher in Summer because emissions from heating which is an important land based source is much lower in summer. Thus, $SO_2$ concentrations rise in summer in the Channel by about 40 % and by more than 20 % in Denmark. The emission of these compounds influences of course also the concentrations of nitrate and sulfate the formation of which requires heat and sunlight. Therefore, it is straightforward that the concentration differences of sulfate in summer are the largest reaching 50 % over the Channel and about 25 % in Denmark (Fig. 48.1).

Until 2020 the sulfate content in fuels will decrease both inside and outside ECAs compared to 2008. Within the ECA zone it will drop to 0.1 % starting 2015. Thus, the effects on sulfur emissions and concentrations will be seen immediately. The decrease of sulfate concentrations over the North Sea will be 20 % according to the simulation results considering the ECA requirements and 15 % without considering them. Until 2030 the sulfate concentrations will rise by 4 % compared to 2020 even in ECA zones. The reason is that there is no emission reduction scheduled beyond 2015 while the ship traffic and, thus, the amount of fuel consumed is expected to increase.

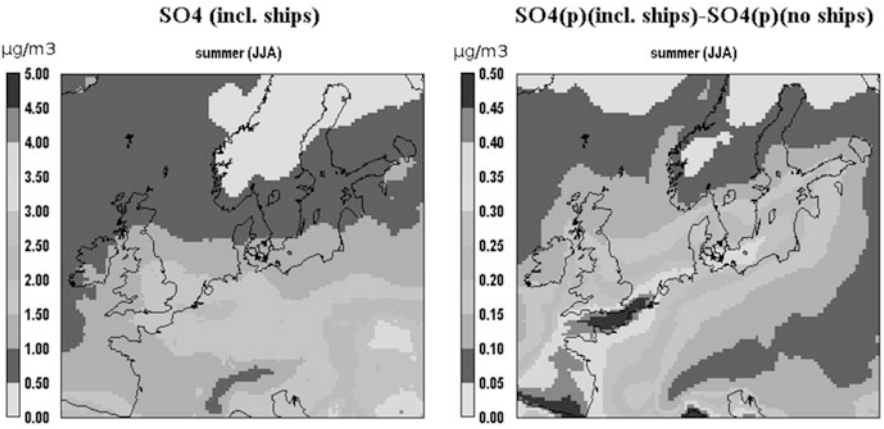


**Fig. 48.1** Map showing the sulfate concentrations in summer (*left*) and the increase by ship emissions (*right*)

Nitrogen emissions and thus nitrate concentrations and depositions depend on the rate by which old vessels are replaced by new builts. Therefore, the influence of ECA regulations on ship emissions and air quality will need more time to take effect on the one hand. On the other hand there will be steady reduction of nitrogen emissions also after 2020. For this reason, in spite of the increasing ship traffic, the nitrate depositions for example will decrease by only 2 % until 2020 and by at about 5 % until 2030.

## 48.4 Conclusion

Considering different ship emission scenarios, concentrations and deposition of gaseous and particulate inorganic nitrogen and sulfur compounds over the North Sea and its riparian states were studied using the CMAQ modeling system. Scenarios for 2020 and 2030 were inspired by the ECA regulations of MARPOL Annex VI. The influence of ships is notable directly at the ship tracks and in coastal regions where no major land based sources are present like in Denmark. The relative concentration increases are larger in summer than in winter due to the different source strengths of land based sources, whereby the formation of particulates in summer is additionally enhanced because of higher air temperature and UV radiation.

A positive effect of the reduction of nitrogen exhaust on air quality will only be visible in 2030 when most of the older ships are replaced by newer ones that comply to the Tier III regulations of MARPOL Annex VI. In contrast to that, the reduction of sulfur emissions is the largest in the scenario for 2020. After that, sulfur emissions will increase again because ship traffic and thus fuel use will increase and

a further reduction of the sulfur fuel content is hardly achievable due to the high costs. A sustainable reduction of sulfur from ships would probably only be possible if alternative fuels like LNG or exhaust gas cleaning techniques like scrubbers were introduced.

## References

1. Buhaug Ø, Corbett JJ, Endresen Ø, Eyring V, Faber J, Hanayama S, Lee DS, Lee D, Lindstad H, Markowska AZ, Mjelde A, Nelissen D, Nilsen J, Pålsson C, Winebrake JJ, Wu W, Yoshida K (2009) Second IMO GHG study 2009. International Maritime Organization (IMO), London, April 2009
2. Corbett JJ, Winebrake JJ, Green EH, Kasibhatla P, Eyring V, Lauer A (2007) Mortality from ship emissions: a global assessment. Environ Sci Technol 41:8512–8518
3. Denier van der Gon H, Hulskotte J (2010) Methodologies for estimating shipping emissions in the Netherlands: a documentation of currently used emission factors and data on related activity. Report 500099012, ISSN: 1875–2322 (print) ISSN: 1875–2314 (on line)
4. Lauer A, Eyring V, Corbett JJ, Wang C, Winebrake JJ (2009) Assessment of near-future policy instruments for ocean going shipping: impact on atmospheric aerosol burdens and the earth's radiation budget. Environ Sci Technol 43:5592–5598

# Chapter 49
# Temporally and Spatially Resolved Air Pollution in Georgia Using Fused Ambient Monitor Data and Chemical Transport Model Results

**Sheila A. Sororian, Heather A. Holmes, Mariel Friberg, Cesunica Ivey, Yongtao Hu, James A. Mulholland, Armistead G. Russell, and Matthew J. Strickland**

**Abstract** Health data geo-coded with residential coordinates are being used to investigate the relationship between ambient air quality and pediatric emergency department visits in the State of Georgia over the time period 2000–2010. Two types of ambient air quality data – observed concentrations from ambient monitors and predicted concentrations from a chemical transport model (CMAQ) – are being fused to provide spatially resolved daily metrics of five air pollutant gases (CO, $NO_2$, $NO_x$, $SO_2$ and $O_3$) and seven airborne particulate matter measures ($PM_{10}$, $PM_{2.5}$, and $PM_{2.5}$ constituents $SO_4^{2-}$, $NO_3^-$, $NH_4^+$, EC, OC). The observational data provide reliable temporal trends at and near monitors, but limited spatial information due to the sparse monitoring network; CMAQ data, on the other hand, provide rich spatial information but less reliable temporal information. Four data fusion techniques were applied to provide daily spatial fields of ambient air pollutant concentrations, with data withholding used to evaluate model performance. Two of the data fusion methods were combined to provide results that minimized bias and maximized correlation over time and space with withheld data. Results vary widely across pollutants. These results provide health researchers with complete temporal and spatial air pollutant fields, as well as with temporal and spatial error estimate fields that can be incorporated into health risk models. Future work will apply these methods to five cities for use in ongoing air pollution health studies and to examine strategies for incorporating land use regression variables for spatial downscaling of data fusion results.

S.A. Sororian • H.A. Holmes • M. Friberg • C. Ivey • Y. Hu • J.A. Mulholland (✉) • A.G. Russell
School of Civil and Environmental Engineering, Georgia Institute of Technology, Atlanta, GA 30332, USA
e-mail: heather.holmes@ce.gatech.edu; james.mulholland@ce.gatech.edu; ted.russell@gatech.edu

M.J. Strickland
Department of Environmental Health, Emory University, Atlanta, GA 30322, USA

D. Steyn and R. Mathur (eds.), *Air Pollution Modeling and its Application XXIII*, Springer Proceedings in Complexity, DOI 10.1007/978-3-319-04379-1_49,

## 49.1 Introduction

Large population studies of human health effects associated with air pollution can take advantage of both temporal and spatial variation in ambient air quality levels when such estimates are available. As a part of the Southeastern Center for Air Pollution and Epidemiology (SCAPE), we are examining relationships of health outcomes with ambient air pollution resolved temporally to a daily level and resolved spatially to a 4 km and smaller scale. Presented here is an approach for estimating daily spatial fields of air pollution in the State of Georgia for use in an investigation of the relationship with pediatric emergency department visits, geocoded with residential coordinates, that builds on previous work [2].

## 49.2 Methods

Observed concentrations of five air pollutant gases (CO, $NO_2$, $NO_x$, $SO_2$ and $O_3$) and seven airborne particulate matter measures ($PM_{10}$, $PM_{2.5}$, and $PM_{2.5}$ constituents $SO_4^{2-}$, $NO_3^-$, $NH_4^+$, EC, OC) were obtained from EPA's Air Quality System (AQS), the Southeastern Aerosol Research Characterization (SEARCH) [3], and the Assessment of the Spatial Aerosol Composition in Atlanta (ASACA) [1] networks for Georgia for the 2000–2010 time period. The number of monitors and daily metrics calculated are listed in Table 49.1. Locations of monitors are shown in Fig. 49.1. The observational data provide reliable temporal trends at and near monitors [6], but limited spatial information due to the sparse monitoring network. Predicted hourly concentrations from CMAQ were obtained for the Georgia domain at the 12 km scale for 2002–2008 [5] and at the 4 km scale for 2009–2010 [4]; daily metrics were computed from these datasets. The CMAQ data provide rich spatial information but less reliable temporal information. Four data fusion techniques are applied and evaluated for 2010. Two methods use regression models of observational and CMAQ annual mean data for scaling (Eq. 49.1). One of these methods involves daily kriging of the ratio of the observation (OBS) to its annual mean and then rescaling by the predicted annual mean ($C^*_1$, Eq. 49.2). The second

**Table 49.1** Ambient air pollutant metrics and monitors

| | 8-h max $O_3$ | 1-h max $NO_2/NO_x$ | 1-h max CO | 1-h max $SO_2$ | 24-h avg $PM_{10}$ | 24-h avg $PM_{2.5}$ | 24-h speciated $PM_{2.5}$ |
|---|---|---|---|---|---|---|---|
| North GA mt | 3 | 0 | 0 | 2 | 3 | 2 | 2 |
| Metro Atlanta | 14 | 7 | 5 | 5 | 8 | 16 | 6 |
| Piedmont | 4 | 0 | 0 | 2 | 1 | 5 | 2 |
| Upper coastal | 4 | 0 | 0 | 1 | 4 | 7 | 2 |
| Lower coastal | 2 | 0 | 0 | 3 | 3 | 4 | 2 |
| Total | 27 | 7 | 5 | 13 | 19 | 34 | 14 |

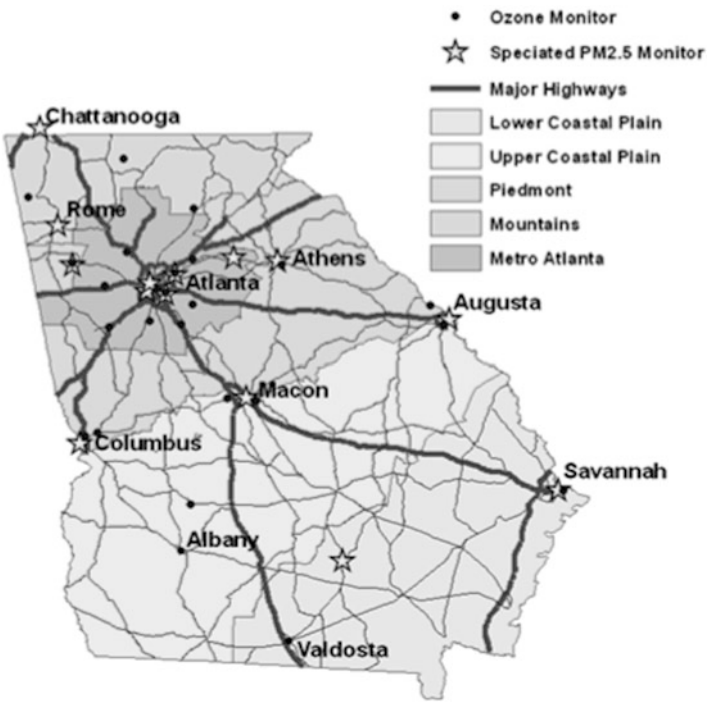


**Fig. 49.1** Map of Georgia showing regions and major cities, major roadways, and locations of speciated $PM_{2.5}$ and ozone monitors

of these methods involves rescaling the CMAQ data ($C^*_2$, Eq. 49.3). The other two methods involve kriging error on a multiplicative ($C^*_3$, Eq. 49.4) and additive ($C^*_4$, Eq. 49.5) basis. Data withholding was used to evaluate model performance. Two of the methods were then selected and combined to provide results that minimized bias and maximized correlation over time and space with withheld data.

$$\langle C^* \rangle = \alpha_{yr} \langle CMAQ \rangle^{\beta} \tag{49.1}$$

$$C_1^* = (OBS/\langle OBS \rangle)_{krig} \times \langle C^* \rangle \tag{49.2}$$

$$C_2^* = CMAQ \times \langle C^* \rangle / \langle CMAQ \rangle \tag{49.3}$$

$$C_3^* = CMAQ \div (CMAQ/OBS)_{krig} \tag{49.4}$$

$$C_4^* = CMAQ - (CMAQ - OBS)_{krig} \tag{49.5}$$

## 49.3 Results

The four data fusion methods yield similar spatial fields (e.g. Fig. 49.2). However, the methods that involved daily kriging of error (Eqs. 49.4 and 49.5) were less stable, performing less well in terms of both bias and correlation for most pollutants. Therefore, the methods that involved using the annual mean model (Eq. 49.1) were selected. The first approach involving kriging daily observation ratios (OBS method) yields results with a spatial structure of CMAQ and perfectly correlated temporally with observations at monitor locations. As the distance from monitors increases, the Pearson correlation coefficient decreases (exponential correlogram model: $R_1 = e^{\gamma D}$ where D is a weighted distance to monitors). The second approach that involves rescaling CMAQ predictions (CMAQ method) yields results that have similar correlations with observations across monitors (average Pearson correlation coefficient of $R_2$). Thus, the OBS method performs best near monitors and the CMAQ method performs best far from monitors.

The OBS and CMAQ methods were combined to provide the best overall prediction. A correction was added to the CMAQ method prediction to correct for seasonal bias. The daily spatial fields generated by the OBS and CMAQ methods were averaged by weighting based on their temporal correlation coefficients ($R_1$ and $R_2$). Thus, at monitor locations the OBS data fusion method prediction was used and far from monitors the CMAQ data fusion method was used. Combined data fusion method results minimize bias and maximize temporal correlation over space. Results shown in Fig. 49.3 show the percent biases and temporal correlations in

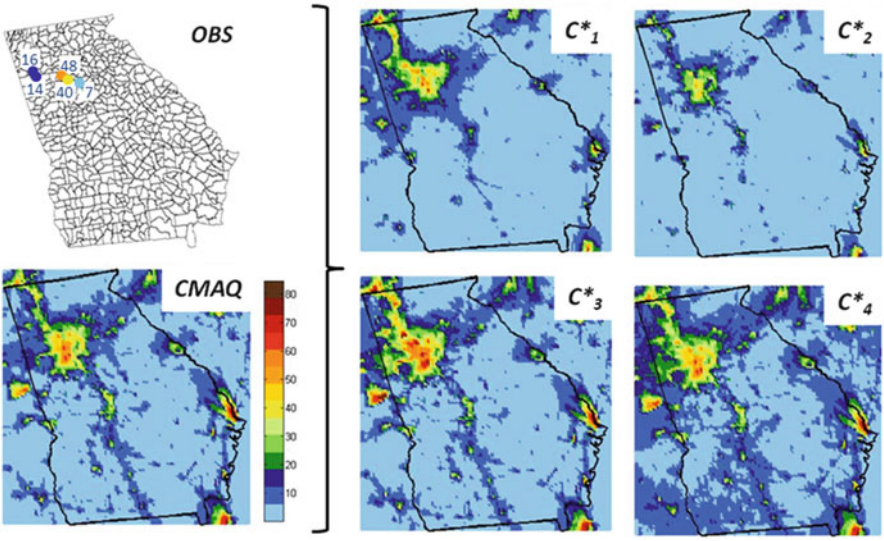


**Fig. 49.2** Predicted 1-h max $NO_2$ fields by four data fusion methods, 9/21/10

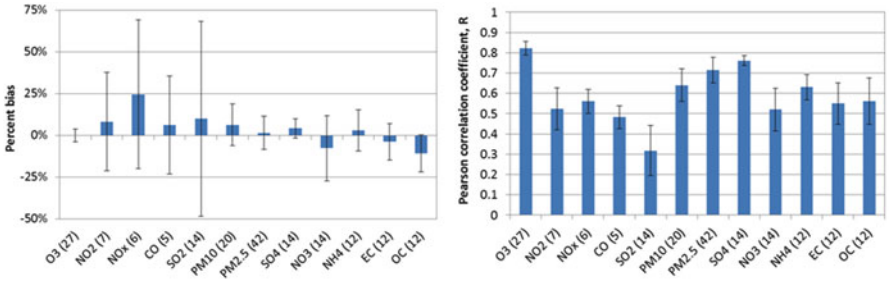


**Fig. 49.3** Percent bias (*left*) and Pearson correlation coefficient (*right*) for CMAQ method predictions, 2002–2008. *Bars* represent averages and *error bars* represent standard deviations across all monitors. The number of monitors for each pollutant is given in *parentheses*

the CMAQ method predictions for the 2002–2008 time period using 12 km CMAQ data. When combined with OBS method predictions, temporal correlations increase near monitors.

Results vary widely across pollutants. Estimates of primary pollutants largely from mobile sources (i.e. CO, $NO_2$, $NO_x$, and EC) rely largely on CMAQ data because they are spatially heterogeneous and have low spatial autocorrelation, whereas estimates of largely secondary pollutants (i.e. $O_3$, $SO_4^{2-}$, $NO_3^-$, $NH_4^+$) and pollutants of mixed origin ($PM_{10}$, $PM_{2.5}$ and OC) rely to a greater extent on observations because they are spatially more homogeneous and have high spatial autocorrelation. $SO_2$, largely from coal combustion, is the most difficult pollutant to estimate due to the inability of monitors to capture and CMAQ to predict accurately point source plume dispersion.

These results provide health researchers with complete temporal and spatial air pollutant fields, as well as with temporal and spatial error estimate fields that can be incorporated into health risk models. Future work will apply these methods to five cities for use in ongoing air pollution health studies and to examine strategies for incorporating land use regression variables for spatial downscaling of data fusion results.

**Acknowledgments** This publication was made possible by USEPA grant R834799. Its contents are solely the responsibility of the grantee and do not necessarily represent the official views of the USEPA. Further, USEPA does not endorse the purchase of any commercial products or services mentioned in the publication.

## References

1. Butler AJ, Andrew MS, Russell AG (2003) Daily sampling of PM2.5 in Atlanta: results of the first year of the assessment of spatial aerosol composition in Atlanta study. J Geophys Res 108(D7):8415

2. Darrow LA, Klein M, Flanders WD, Waller LA, Correa A, Marcus M, Mulholland JA, Russell AG, Tolbert PE (2009) Ambient air pollution and preterm birth: a time-series analysis. Epidemiology 20(5):689–698
3. Hansen DA, Edgerton ES, Hartsell BE, Jansen JJ, Kandasamy N, Hidy GM, Blanchard CL (2003) The southeastern aerosol research and characterization study: Part 1 – overview. J Air Waste Manage Assoc 53(12):1460–1471
4. Hu Y, Chang M, Russell A, Odman M (2010) Using synoptic classification to evaluate an operational air quality forecasting system in Atlanta. Atmos Pollut Res 1:280–287
5. PHASE (2013) Air quality data for the CDC national environmental public health tracking network. URL http://www.epa.gov/heasd/research/cdc.html. Accessed 2013
6. Wade KS, Mulholland JA, Marmur A, Russell AG, Hartsell B, Edgerton E, Klein M, Waller L, Peel JL, Tolbert PE (2006) Effects of instrument precision and spatial variability on the assessment of the temporal variation of ambient air pollution in Atlanta, Georgia. J Air Waste Manage Assoc 56(6):876–888

# Chapter 50
# Maritime Sector Emissions Contribution to the Particulate Matter Pollution in a Mediterranean City-Port: A Modeling Approach

**A. Poupkou, N. Liora, A. Karagiannidis, T. Giannaros, C. Giannaros, D. Melas, and A. Argiriou**

**Abstract** The main aim of this work is the investigation of the contribution of different emission sources to the concentrations of the fine Particulate Matter (PM2.5) in the city-port of Patras in Greece using a meteorological and a photochemical model. Emphasis is given on the contribution of the maritime transport and the activities within the Patras harbor area for which the existing environmental information is very limited.

## 50.1 Introduction

During the last decades, there has been an increasing urbanization pressure on the Mediterranean port-cities with impacts on their economic growth but also on their environment. PM is a key pollutant in the urban atmosphere of Patras. Although the frequency of the days, when the observed daily PM10 concentrations in the Patras city center exceed the corresponding EU air quality standard, is declining in the period 2001–2010, it is still well above the EU limits (i.e. 24-h PM10 values higher than 50 $\mu g/m^3$ permitted for 35 days per year).

A. Poupkou (✉) • N. Liora • A. Karagiannidis • A. Argiriou
Department of Physics, University of Patras, Patras 26500, Greece
e-mail: poupkou@auth.gr

T. Giannaros • C. Giannaros • D. Melas
Department of Physics, Aristotle University of Thessaloniki, Thessaloniki 54124, Greece

D. Steyn and R. Mathur (eds.), *Air Pollution Modeling and its Application XXIII*,
Springer Proceedings in Complexity, DOI 10.1007/978-3-319-04379-1_50,

## 50.2 Data and Methodology

The modeling system used in the framework of the present study consisted of the Weather Research and Forecasting (WRF) model and the photochemical model Comprehensive Air Quality Model with Extensions (CAMx). Source apportionment was performed for PM10 and PM2.5 using the Particulate Source Apportionment Technology (PSAT) tool of CAMx. The modeling system was applied over a 10 km resolution grid that covered the Balkan Peninsula and a $124 \times 74$ km$^2$ grid over Patras in 2 km spatial resolution (Fig. 50.1). The chemical boundary conditions for the Balkan modeling domain were taken from the IFS-MOZART global modeling system while those for the domain of Patras were taken from the Balkan coarse domain. The modeling system was applied for a summer period extending from 1 July to 31 August 2010.

The MOdel for the Spatial and tEmporal diStribution of emissionS (MOSESS) [2] was applied in order to compile a spatially (2 km resolution) and temporally resolved inventory for the CO, NOx, $SO_2$, $NH_3$, NMVOCs, PM10 and PM2.5 emissions of the anthropogenic sources in Patras on the basis of the European scale emission inventory for the year 2007 of The Netherlands Organisation [1]. Emphasis was given on the emissions from the various activities inside the area of the harbor (stockpiles, unloading processes, harbor machineries etc.) as well as on those from the maritime transport (cargo, passenger ships etc.), for which a detailed inventory was compiled on the basis of activity data provided by the Patras Port Authority for the reference year 2010. Figure 50.2 shows the contribution of different activities to the maritime/harbor sector annual pollutant emissions in the Patras domain. Passenger ships are the major source with contributions of more than 60 % to all pollutant emissions. Fishing boats have an about 20 % contribution to NOx emissions. Inland waterways vessels (e.g. pleasure boats) contribute with about 10 % to PM10 and PM2.5 emissions. Sea salt, windblown dust and biogenic NMVOCs emissions were calculated employing the Natural Emission Model (NEMO) [3] driven by WRF.

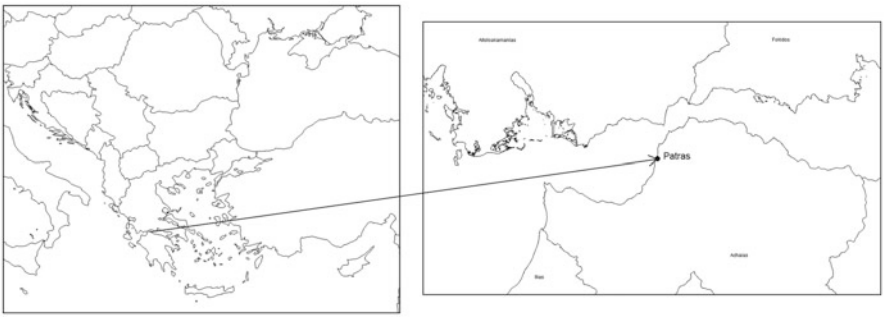


**Fig. 50.1** The Balkan and Patras CAMx domains

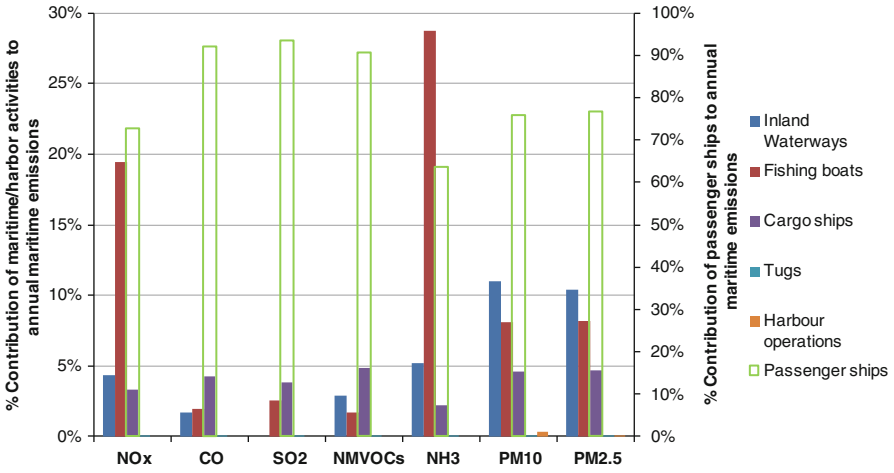


**Fig. 50.2** % Contribution of activities to the maritime/harbor sector annual pollutant emissions

The emission sources apportioned for Patras were the following: (1) Road transport, (2) Maritime and harbor activities, (3) Non industrial combustion plants, (4) Industries, (5) Soil (windblown dust), (6) Vegetation (biogenic NMVOCs) and (7) Left over sources (e.g. non-road vehicles, waste treatment, agriculture, solvent use, distribution of fuels).

## 50.3 Results and Conclusions

Figure 50.3 presents the results of the contribution of selected emission sources inside the modeling domain to the PM2.5 atmospheric levels in the greater Patras area (the influence of pollution sources outside the Patras domain is not considered). CAMx results show that the contribution of maritime and harbor activities is higher over the maritime than over the coastal and continental areas of the study domain. Over the former areas, the contribution can be very significant in the summer (more than 80 %) and is higher over the maritime areas to the west of Patras where the ship routes are found. The contribution of road transport in Patras is important and may be up to 30 %. Finally, NMVOCs emitted from vegetation produce secondary organic aerosols that have a small contribution to the PM2.5 levels in Patra (up to 5 %), which is more significant though (contribution up to about 50 %) over the forested areas of the study domain.

The work presented is a first effort to provide some insight on the issue of PM pollution in Patras, in relation also with the presence of the port in the city, and allow the policy makers to develop effective control strategies for the reduction of atmospheric pollution.

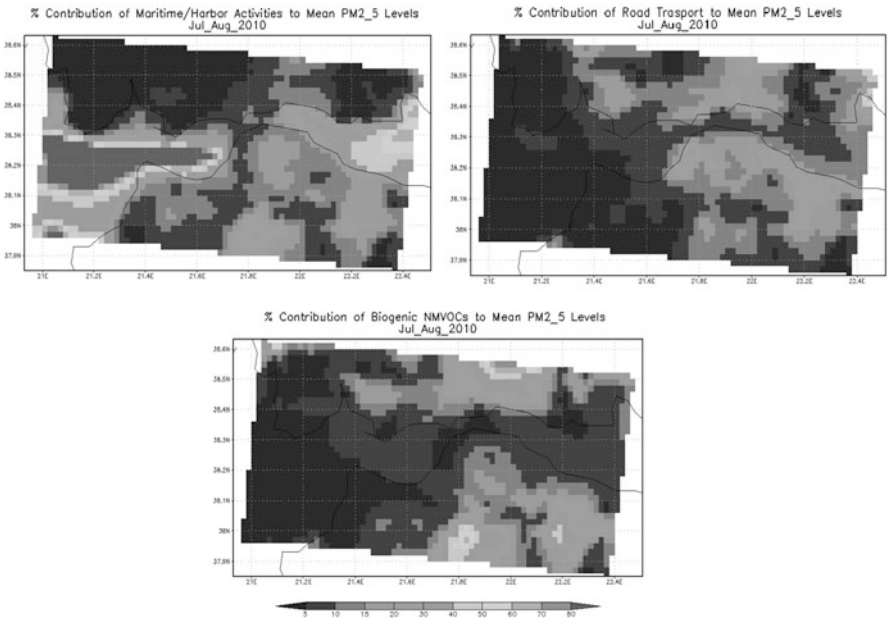


**Fig. 50.3** Spatial distribution of the % contribution of emission sources to the mean PM2.5 concentrations in the Patras domain for the summer period July to August 2010

**Acknowledgments** This work is financed by the European Territorial Cooperation Programme Greece-Italy 2007–2013 project CESAPO, co-financed by the European Union (ERDF) and by National Funds of Greece and Italy. We would like to thank for the IFS-MOZART model data and for the TNO anthropogenic emission data provided in the framework of the EU FP7 project MACC II (Grant agreement no: 283576).

## References

1. Kuenen J, van der Gon HD, Visschedijk A, Dröge R, van Gijlswijk R (2011) MACC European emission inventory for the years 2003–2007. The Netherlands Organisation report, TNO-060-UT-2011-00588, Utrecht, The Netherlands
2. Markakis K, Katragkou E, Poupkou A, Melas D (2013) MOSESS: a new emission model for the compilation of model-ready emission inventories. Application in a coal mining area in Northern Greece. Environ Model Assess 18:509–521. doi:10.1007/s10666-013-9360-8
3. Poupkou A, Giannaros T, Markakis K, Kioutsioukis I, Curci G, Melas D, Zerefos C (2010) A model for European biogenic volatile organic compound emissions: software development and first validation. Environ Model Softw 25:1845–1856. doi:10.1016/j.envsoft.2010.05.004

# Chapter 51
# Application and Evaluation of the High-Resolution Regional Scale FRAME Model for Calculation of Ammonia and Ammonium Air Concentrations for Poland for the Years 2002–2008

**Maciej Kryza, Anthony J. Dore, Małgorzata Werner, and Kinga Wałaszek**

**Abstract** Over 98 % of ammonia ($NH_3$) emission in Poland comes from agricultural activity. Compared to oxidised sulphur and nitrogen, which show significant downward trends after the year 1990, national total $NH_3$ emission is fairly stable at around 320 Gg. In this work, the Fine Resolution Atmospheric Multi-pollutant Exchange (FRAME) model is used to assess the long-term information on annual $NH_3$ and $NH_4^+$ air concentrations.

The main findings of our work show that the FRAME model is capable of reproducing air concentrations of $NH_3$ and $NH_4^+$ well for all selected years. There is no tendency for under or overestimation of the observed air concentrations. The FRAME model results are also in general agreement with the EMEP-Unified model results, though the differences in spatial resolutions of both models are important (FRAME 5 km grid and EMEP-Unified 50 km grid). There no significant trend in $NH_3$ annual air concentration in Poland if country average values are compared.

## 51.1 Introduction

Over 98 % of ammonia ($NH_3$) emission in Poland comes from agricultural activity. Compared to oxidised sulphur and nitrogen, which show significant downward trends after the year 1990, national total $NH_3$ emission abatements are less

M. Kryza (✉) • M. Werner • K. Wałaszek
Department of Climatology and Atmosphere Protection, Wroclaw University, Wroclaw, Poland
e-mail: maciej.kryza@uni.wroc.pl; malgorzata.werner@uni.wroc.pl; kinga.walaszek@uni.wroc.pl

A.J. Dore
Centre for Ecology and Hydrology, Edinburgh, UK
e-mail: todo@ceh.ac.uk

D. Steyn and R. Mathur (eds.), *Air Pollution Modeling and its Application XXIII*,
Springer Proceedings in Complexity, DOI 10.1007/978-3-319-04379-1_51,

pronounced, especially over the last decade. Poland is still in a group of European countries with the highest emissions of $NH_3$, together with France, Italy, Spain and the United Kingdom. High emission of $NH_3$ in Poland leads to serious environmental problems related to acidification and eutrophication, with further consequences in e.g. biodiversity loss [6].

In this work, the Fine Resolution Atmospheric Multi-pollutant Exchange (FRAME) model is used to assess the long-term information on annual $NH_3$ and $NH_4^+$ air concentrations. The country average is calculated to describe the changes in $NH_3$ and $NH_4^+$ air concentrations during a period of 2002–2008. The evaluation of the model is presented by comparison of the FRAME results with the air concentrations of $NH_3$ and $NH_4^+$ measurements from the EMEP network.

## 51.2 Data and Methods

### *51.2.1 FRAME Model Description and Emission Data*

FRAME is a statistical trajectory model that describes the main atmospheric processes in a column of air that travels along straight-line trajectories over the model domain. A detailed description of the model and its application for the United Kingdom is provided by Dore et al. [3] and Fournier et al. [4]. Here the model was applied for the area of Poland, with a domain of $160 \times 160$ grid cells of size 5 km $\times$ 5 km [7]. In the vertical, FRAME consists of 33 layers with thickness changing from 1 m at the surface to 100 m at the top of the domain. Boundary conditions for the model run are calculated with the FRAME-Europe model, that runs for the entire Europe with spatial resolution of 50 km $\times$ 50 km. The FRAME model was run here separately for years 2002–2008, with year specific meteorological and emission data.

The Polish national emission inventory for years 2002–2008 was used in this study [2], and re-gridded onto the model grid [7]. For each year considered in this work, year specific meteorological data were used for modeling. Total $NH_3$ emission read in by the model is summarized in Table 51.1. There is a decreasing trend in $NH_3$ emission within the study period, but not stable, with a large drop in emission in year 2005 and relatively small changes during the years 2002–2004 and 2006–2008.

**Table 51.1** National total $NH_3$ emission (Gg of $NH_3$) for years 2002–2008

| | 2002 | 2003 | 2004 | 2005 | 2006 | 2007 | 2008 |
|---|---|---|---|---|---|---|---|
| $NH_3$ | 325.0 | 322.6 | 316.5 | 269.6 | 287.2 | 283.9 | 279.5 |

### *51.2.2 Model Evaluation*

$NH_3$ gas concentration measurements were not available for the model evaluation. We used the annual average $NH_3 + NH_4^+$ (gas + aerosol) concentrations measured by the EMEP monitoring sites in the FRAME model domain. Two sites were located in the Czech Republic and Germany and four sites representing Poland. For each year, the model performance was summarized with the Mean Bias (MB), Mean Absolute Error (MAE) and Fraction of Two (FAC2) statistics.

## 51.3 Results

The spatial pattern of annual average air concentration of $NH_3$ is presented in Fig. 51.1 for year 2002 (the highest $NH_3$ annual emission) and 2005 (the lowest emission in the period considered). The spatial distribution of $NH_3$ air concentration is similar for both years compared. The highest air concentrations are calculated over the central area of Poland, which is the source region for ammonia emission from agriculture. There are large areas with annual average $NH_3$ air concentrations above 3 $\mu g\ m^{-3}$, which is the critical level threshold for higher plants [1] (Fig. 51.1).

For all years considered, the FRAME model performance is stable, with the error statistics at a similar level (Table 51.2). The $NH_3 + NH_4^+$ air concentrations are overestimated except for the year 2006. All measuring sites are within the factor of two range for the years 2002–2005. For the 2006–2008 period, one site is outside of this threshold.

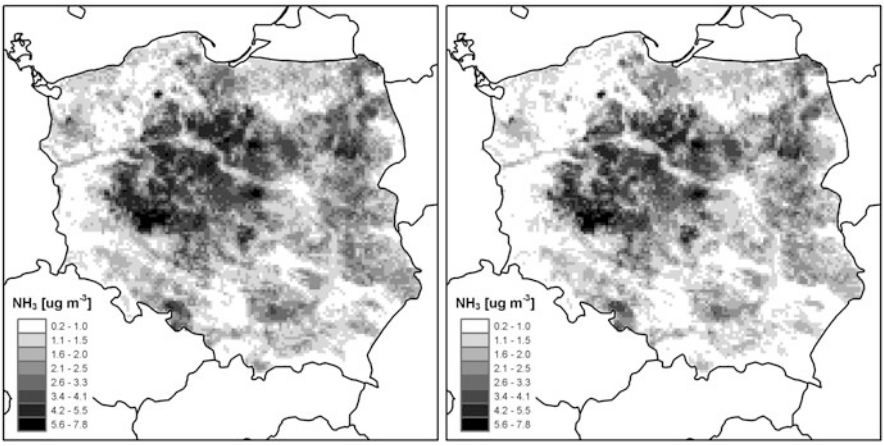


**Fig. 51.1** Annual average air concentrations of $NH_3$ for year 2002 (*left plot*) and 2005 (*right plot*)

**Table 51.2** Model evaluation statistics for year 2002–2008

| | 2002 | 2003 | 2004 | 2005 | 2006 | 2007 | 2008 |
|---|---|---|---|---|---|---|---|
| MB | 0.33 | 0.26 | 0.26 | 0.05 | –0.25 | 0.02 | 0.07 |
| MAE | 0.53 | 0.51 | 0.47 | 0.49 | 0.55 | 0.49 | 0.50 |
| FAC2 | 1.0 | 1.0 | 1.0 | 1.0 | 0.88 | 0.88 | 0.88 |

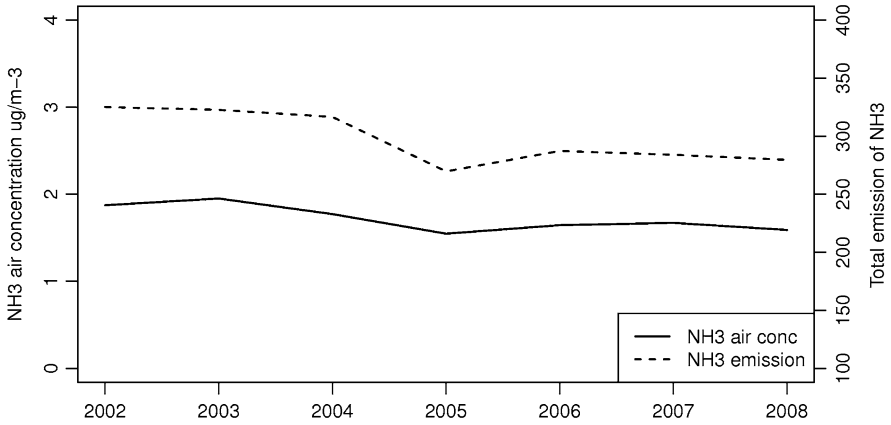


**Fig. 51.2** Country average $NH_3$ air concentration and national total emission of ammonia

Country average $NH_3$ air concentration was compared with the annual national total emission of ammonia, to check what is the relation between the atmospheric level of ammonia and local emission (Fig. 51.2). The relation is strong, but there are also some non-linearities. These should be attributed to the variability in meteorological conditions and transboundary transport of ammonia [8, 9]. The other reason for non-linearities may be related with changes in $SO_2$ and $NO_x$ emissions.

## 51.4 Summary and Conclusions

In this paper the preliminary results of FRAME modeled changes in $NH_3$ air concentrations over the period of 2002–2008 were presented. The main findings are:

- The FRAME model is capable in reproducing the annual average concentrations of ammonia and ammonium. The results may be applied in further studies related with critical level thresholds exceedances [5].
- The areas of high $NH_3$ annual average concentrations do not change significantly from year to year, despite the large changes in national total emission.

- There is a strong correlation between the national total emission and country average $NH_3$ air concentration, which has previously been suggested by Kryza et al. [7, 8]. There are also some nonlinearities in the emission-concentration relation due to variability in annual meteorological conditions and emissions of acidifying gases [9].

**Acknowledgments** This work was funded by the Polish National Science Centre grant no UMO-2012/05/B/ST10/00446.

## References

1. Cape JN, van der Eerden LJ, Sheppard LJ, Leith ID, Sutton MA (2009) Evidence for changing the critical level for ammonia. Environ Pollut 157:1033–1037
2. Dębski B, Olendrzyński K, Cieślińska J, Kargulewicz I, Skośkiewicz I, Olecka A, Kania K (2009) Inwentaryzacja emisji do powietrza $SO_2$, $NO_2$, CO, $NH_3$, pyłów, metali ciężkich, NMZO, TZO w Polsce za rok 2005, Institute of Environmental Protection
3. Dore AJ, Vieno M, Fournier N, Weston KJ, Sutton MA (2006) Development of a new wind-rose for the British Isles using radiosonde data, and application to an atmospheric transport model. Q J Roy Meteorol Soc 132:2769–2784
4. Fournier N, Dore AJ, Vieno M, Weston KJ, Dragosits U, Sutton MA (2004) Modelling the deposition of atmospheric oxidised nitrogen and sulphur to the United Kingdom using a multi-layer long-range transport model. Atmos Environ 38:683–694
5. Hallsworth S, Dore AJ, Bealey WI, Dragosits U, Vieno M, Hellsten S, Tang YS, Sutton MA (2010) The role of indicator choice in quantifying the threat of atmospheric ammonia to the 'Natura 2000' network. Environ Sci Pol 13:671–687
6. Krupa SV (2003) Effects of atmospheric ammonia ($NH_3$) on terrestrial vegetation: a review. Environ Pollut 124:179–221
7. Kryza M, Werner M, Blas M, Dore AJ, Sobik M (2010) The effect of emission from coal combustion in nonindustrial sources on deposition of sulfur and oxidized nitrogen in Poland. J Air Waste Manage Assoc 60:856–866
8. Kryza M, Werner M, Dore AJ, Blas M, Sobik M (2012) The role of annual circulation and precipitation on national scale deposition of atmospheric sulphur and nitrogen compounds. J Environ Manage 109:70–79
9. Matejko M, Dore AJ, Hall J, Dore CJ, Blas M, Kryza M, Smith R, Fowler D (2009) The influence of long term trends in pollutant emissions on deposition of sulphur and nitrogen and exceedance of critical loads in the United Kingdom. Environ Sci Policy 12:882–896

# Chapter 52
# Regional Transports of Atmospheric $NO_x$ and $HNO_3$ over Cape Town

**Babatunde J. Abiodun, Adefolake M. Ojumu, Samantha Jenner, and Tunde V. Ojumu**

**Abstract** This study examines the contribution of pollutants (NOx and HNO3) from Highveld on pollution in Cape Town. For the study, we analyzed observation data (2001–2008) from the City of Cape Town air quality network and regional climate model (RegCM4) simulations (2001–2004) over southern Africa. The model accounts for the influence of complex topography, atmospheric condition, and chemical reactions among the atmospheric gases in simulating the emission and transport of the pollutants over southern Africa. The model results show that north-easterly flows can transport pollutants (especially HNO3) at low level (surface – 850 hPa) from Highveld to Cape Town. And in April, a tongue of high concentration of NOx and HNO3 extends from Highveld to Cape Town along southern coast. The study shows two dominant paths through which pollutants from Mpumalanga Highveld are transported to Cape Town. The first path follows the borders of South Africa, Botswana and Namibia, and along Western Cape to Cape Town while the second path is moves southward over South Africa to the south coast and then eastward along south coast to Cape Town.

B.J. Abiodun (✉) • S. Jenner
Climate Systems Analysis Group, Department of Environmental and Geographical Science, University of Cape Town, Cape Town, South Africa
e-mail: babiodun@csag.uct.ac.za

A.M. Ojumu
Department of Environmental and Agricultural Sciences, University of South Africa, Pretoria, South Africa

T.V. Ojumu
Department of Chemical Engineering, Cape Peninsula University of Technology, Cape Town, South Africa

D. Steyn and R. Mathur (eds.), *Air Pollution Modeling and its Application XXIII*, Springer Proceedings in Complexity, DOI 10.1007/978-3-319-04379-1_52,

## 52.1 Introduction

Cape Town, the most popular tourist city in Africa, experiences air pollution with unpleasant odour in winter. A combination of geographical and meteorological factors makes Cape Town favourable for accumulation of air pollutants. For instance, the city is bordered by the Table Mountain complex to the south-west, False Bay to the south and Table Bay to the west. The location of Cape Town (33.9°S, 18.4°E) at the south-west tip of Africa (Fig. 52.1) influences the wind patterns. At this subtropical latitude, calm conditions are sometimes produced over the city under stagnant anticyclonic flows; the associated subsidence temperature inversion can suppresses vertical exchange of air and pollutants during most periods of the year. Furthermore, the South Atlantic anticyclone and the cold Benguela current induce surface inversion, which strengths over the Cape Town [5]. Consequently, extreme high pollution events occur from April to September; and whenever the brown haze occurs during this period, it extends over most of the Cape Town and shifts according to the prevailing wind direction [7].

Previous studies have associated the pollution with local emission of pollutants within the city. But, since secondary pollutants like $HNO_3$ can be transported by wind to cause health impact far from their original sources, it is important to investigate how pollutants transported from remote sources in South Africa can contribute to the air quality problem in Cape Town. The present study examines how the transport of atmospheric pollutants ($NO_x$ and $HNO_3$) from the Mpumalanga Highveld may contribute to the pollution in Cape Town.

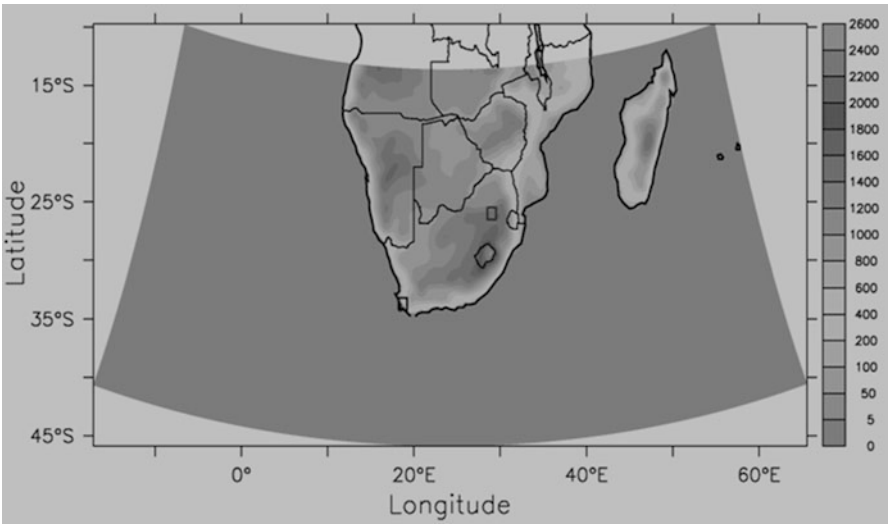


**Fig. 52.1** The RegCM simulation domain indicating Southern Africa topography (meters), Cape Town at the south western tip of South Africa, and Mpumalanga Highveld at the north eastern part of South Africa

## 52.2 Models Description and Set-Ups

The study applied the International Centre for Theoretical Physics (ICTP) Regional Climate model (version 4) with chemistry (hereafter, RegCM) to simulate the climate and pollution transport over Southern Africa (Fig. 52.2). RegCM is a hydrostatic, sigma-coordinate model [2, 4] that allows online coupling of atmospheric and chemistry parameters. The model has been successfully tested over Southern Africa [1, 3, 6]. For the present study, RegCM simulation was set up with a 35 km horizontal resolution. The simulation domain centres on 33°S and 24°E and extends, with the Lambert conformal projection, from 16.62°W to 54.41°E and from 10.5°S to 40.45°S (Fig. 52.2). In the vertical, the domain spans 18 sigma levels, with highest resolution near the surface and lowest resolution near the model top. Initial and lateral boundary meteorological conditions were provided by ERA-Interim 1.5° × 1.5° gridded reanalysis data from ECMWF (European Centre for Medium-Range Weather Forecasts). Emissions data with a 1° × 1° resolution was provided by the RCP (Representative Concentration Pathways) global dataset that accompanies the standard RegCM package. The simulation covers a period of 4 years 3 months (i.e. October 2000–December 2004). The first 3 months simulations were discarded as model spin-up, while the remaining 4 years simulations were analysed for the study.

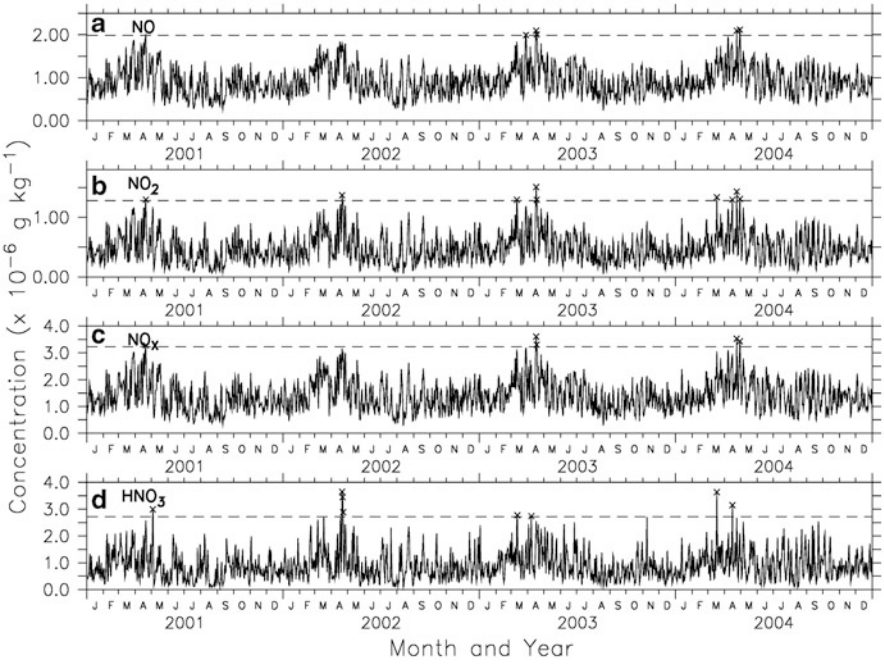


**Fig. 52.2** The time series of the simulated pollutants concentration over Cape Town in 2001–2004. The extreme values (99 percentiles) are indicated with *dashed*

## 52.3 Results and Discussion

Details on the performance of the simulation can be found Abiodun et al. [1]. Overall, the comparison showed that RegCM3 captures well the seasonal variation of the pollutants concentration of Cape Town, except that the simulated peak occurs in April instead of July, and the correlation between the observed and simulated daily concentration is weak ($r = 0.43$) [1].

The time series of the simulated pollutants concentration over Cape Town (Fig. 52.2) shows that the extreme concentration events (defined as 99 percentiles; $\geq 3.3 \times 10^{-6}$ g kg$^{-1}$ for NOx; $\geq 2.8 \times 10^{-6}$ g kg$^{-1}$ for $HNO_3$) mostly occur in April. However, the extreme event for $NO_x$ and $HNO_3$ rarely occur on the same day, suggesting that, in Cape Town, the atmospheric conditions that induce $NO_x$ extreme events may be different from those that induces of $HNO_3$ extreme events. The composite of wind flow during extreme pollution events in Cape Town shows a transport of pollutant from the Mpumalanga Highveld to Cape Town at surface (Fig. 52.3). For NOx extreme events, the low-level wind pattern is characterized with northerly and north-easterly flows, transporting the pollutant from the Mpumalanga Highveld towards Cape Town and south coast. Along the south coast, there is a confluence of the northerly flow and easterly flow. The easterly flow also transports pollutants from eastern part of South Africa towards Cape Town. The wind pattern also features a calm or light variable wind which causes stagnation of air flow. This will provides a favourable atmospheric condition for accumulation

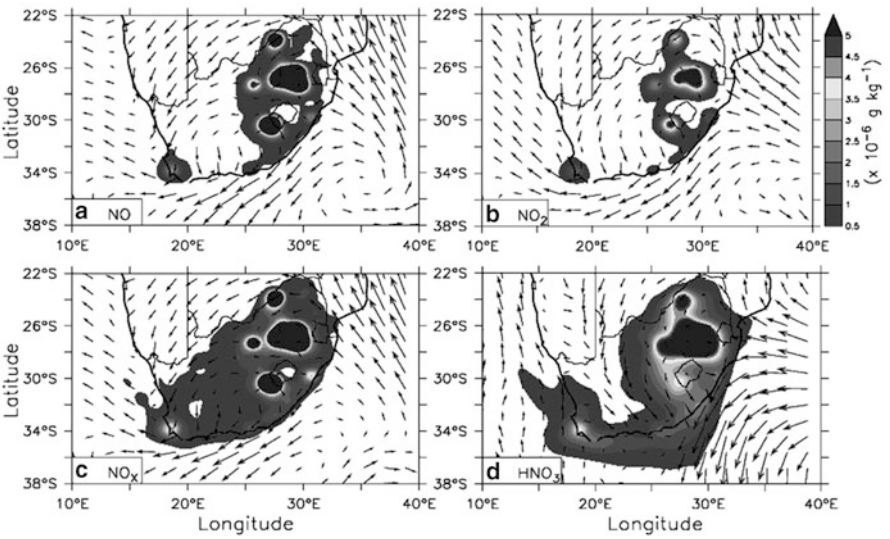


**Fig. 52.3** The composite of low-level (surface – 850 hPa) wind flow (*arrow*) during the extreme pollution events in Cape Town. The corresponding pollutant concentration (NO, NO2, NOx and HNO3; $\times 10^{-6}$ g kg$^{-1}$) are *shaded*

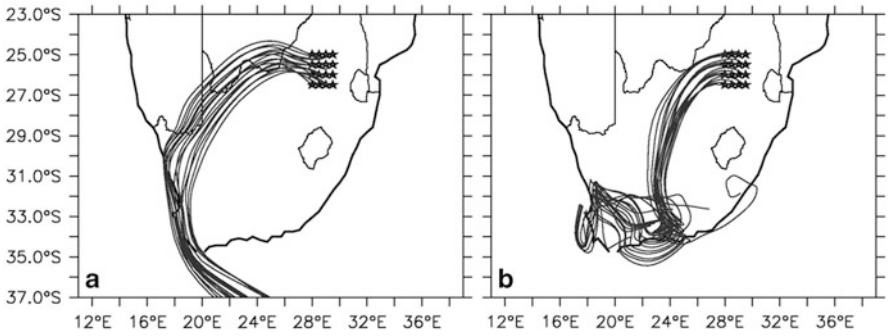


**Fig. 52.4** The simulated paths for low-level transports of pollutants from Mpumalanga Highveld to Cape Town

of the pollutants over the city during the extreme events. At 700 hPa (not shown), there is a strong anticyclonic flow over southern Africa. This anticyclone will produce a strong subsidence over South Africa, and the subsidence will prevent a vertical mixing of the pollutants, capping the high concentrations of pollutants close to the surface as they are transported toward from the Mpumalanga Highveld toward Cape Town.

The synoptic wind patterns that induce the extreme $HNO_3$ events differ from those that induce the extreme $NO_x$ events (Fig. 52.3d). With $HNO_3$ extreme event, the low-level wind pattern features a strong north-westerly flow transporting $HNO_3$ from the Mpumalanga Highveld to the south coast. In addition, it shows a strong easterly flow transporting fresh air from Indian Ocean, but turns poleward as it approaches the escarpment, thereby deflecting the fresh air from the continent, at same time, forming a confluence flow with the north-westerly flow along the coast. The wind patterns also feature a weak wind along the south coast and a col over Cape Town. Hence, there is a band of high $HNO_3$ concentration along the coast, linking the peak $HNO_3$ concentration at Cape Town with that over the Mpumalanga Highveld. As with $NO_x$ extreme event, the 700 hPa wind pattern features a strong anticyclone (centering over the border between South Africa and Botswana) but with a stronger north-westerly flow over the western flank of South Africa.

To indentify the paths for the low-level transport of pollutants from Mpumalanga Highveld to Cape Town, we used the RegCM simulated surface wind in a Lagrangian particle model. In the particle model, particles were released daily over Mpumalanga Highveld and the positions of the pollutants were monitored for 10 days as they were transported by the winds away from the source. Figure 52.4 shows examples of two dominant paths through which the pollutants are transported from the Highveld Cape Town. In first case, the pollutants are transported along borders of South Africa, Botswana and Namibia, then along Western Cape into Cape Town. In the second case, the pollutants are transported southward over South Africa to the south coast, then westerly along south coast into Cape Town. These two paths occur in March–September and are consistent with the wind patterns in Fig. 52.3.

## 52.4 Conclusion

This study has applied a regional climate model (RegCM) to study the transport of NOx and $HNO_3$ over South Africa, with emphasis on pollutants transport from Mpumalanga Highveld to Cape Town. The study shows that during the extreme events, the north-easterly flow transports NOx directly from The Mpumalanga Highveld to Cape Town, a band high concentration of $HNO_3$ links the peak $HNO_3$ concentration at Cape Town with that of the Mpumalanga Highveld. The study indentifies two dominant paths through which pollutants from Mpumalanga Highveld are transported to Cape Town. The first path follows the borders of South Africa, Botswana and Namibia, and along Western Cape to Cape Town while the second path is moves southward over South Africa to the south coast and then eastward along south coast to Cape Town.

Since the results of this study are based on only 4 years simulation from a single model, there is need for longer simulations with multi-models to establish the robustness of the findings. A longer simulation will account for the influence inter-annual variability on the results while using multi-model simulations will provide opportunity for models comparisons and for assessing the degree of inter-model variability. However, the present study suggests that the transport of NOx and HNO3 from Mpumalanga Highveld may contribute to the pollutants concentration in Cape Town.

**Acknowledgement** The project was supported with grants from National Research Foundation (NRF, South Africa) and the Applied Centre for Climate and Earth Sciences (ACCESS). The third author was supported with grants from African Centre for Cities (ACC). Computations facility was provided by Centre for High Performance Computing (CHPC, South Africa).

## References

1. Abiodun BJ, Ojumu AM, Jenner S, Ojumu TV (2013) Transport of atmospheric NOx and $HNO_3$ over Cape Town. Atmos Chem Phys Discuss 13:11827–11862
2. Giorgi F, Anyah RO (2012) The road towards RegCM4. Climate Res 52:3–6
3. Jenner SL, Abiodun BJ (2013) The transport of atmospheric sulfur over Cape Town. Atmos Environ. doi:10.1016/j.atmosenv.2013.06.010
4. Pal JS, Giorgi F, Bi X, Elguindi N, Solmon F, Gao X, Rauscher SA et al (2007) Regional climate modeling for the developing world: the ICTP RegCM3 and RegCNET. Bull Am Meteorol Soc 88(9):1395–1409
5. Preston-Whyte RA, Diab RD, Tyson PD (1977) Towards an inversion climatology of southern Africa, II, non-surface inversions in the lower atmosphere. S Afr Geogr J 59:47–59
6. Sylla MB et al (2009) Multiyear simulation of the African climate using a regional climate model (RegCM3) with the high resolution ERA-interim reanalysis. Climate Dyn 35(1):231–247
7. Wicking-Baird MC, De Villiers MG, Dutkiewicz R (1997) Cape Town brown haze study. Report No. Gen 192, Cape Town

# Chapter 53
# The Impact of Transboundary Transport of Air Pollutants on Air Quality in the United Kingdom and Poland

**Małgorzata Werner, Maciej Kryza, Anthony J. Dore, and Kinga Wałaszek**

**Abstract** Precursors of particulate matter, as well as particulate matter (PM) itself can be transported in the atmosphere over long distances, thus the problem of air pollution should be considered in the cross-border context. We used the Fine Resolution Atmospheric Multi-pollutant Exchange model to calculate the import and export of sulphur and nitrogen compounds and primary particulate matter ($PPM_{2.5}$ and $PPM_{10}$) for the year 2007, separately for a central European country (Poland) and an island nation (the UK). For PPM the analysis was done for two cases – including and excluding sea salt aerosol (SSA). The absolute mass of import is higher for Poland than the UK in the case of pollutants for which SSA is not the main contributor (e. g. $NO_3^-$, $NH_4^+$). Excluding SSA the import of $PPM_{2.5}$ and $PPM_{10}$ is higher for Poland than the UK. Including SSA, for both countries the mass of imported $PPM_{10}$ and $PPM_{2.5}$ is higher than the national total emission. For most of the considered pollutants the highest contribution of import was calculated for the north-west and west part of the UK and the west and south-west part of Poland.

## 53.1 Introduction

Due to a large amount of anthropogenic and natural emission sources of pollutants and their existence time in the atmosphere, which allows for transport over long distances, the concentration of pollutants and chemical composition are highly

M. Werner (✉) • M. Kryza • K. Wałaszek
Department of Climatology and Atmosphere Protection, University of Wrocław, Wrocław, Poland
e-mail: malgorzata.werner@uni.wroc.pl; maciej.kryza@uni.wroc.pl; kinga.walaszek@uni.wroc.pl

A.J. Dore
Natural Environment Research Council, Centre for Ecology and Hydrology, Edinburgh, UK
e-mail: todo@ceh.ac.uk

D. Steyn and R. Mathur (eds.), *Air Pollution Modeling and its Application XXIII*, Springer Proceedings in Complexity, DOI 10.1007/978-3-319-04379-1_53,

variable in space and time [6]. The role of transboundary transport is assessed by the Clean Air for Europe Directive (CAFE, 2008/50/EC) which emphasises the need for coordination amongst neighbouring countries in preparing and implementing air quality improvement plans.

In this study we used a Lagrangian atmospheric transport model to calculate the contribution of import and national emissions of sulphur and nitrogen compounds and primary particulate matter. The calculation was made for two European countries (the UK and Poland), which differ in respect of geographical location (maritime and inland), meteorological conditions and emission structure, for one selected year – 2007.

## 53.2 The Atmospheric Transport Model FRAME

FRAME is a Lagrangian statistical trajectory model that is used for the United Kingdom and Poland to support environmental management and protection. The fundamentals of the model are described by Fournier et al. [3], Dore et al. [1], Vieno et al. [9] and, for the FRAME model for Poland, by Kryza et al. [5]. FRAME is used here with a grid resolution of 5 km × 5 km and grid dimensions of 172 × 244 cells for the UK and 160 × 160 cells for Poland. The import of particles from outside of both domains is calculated with FRAME-Europe – a similar model to FRAME, which runs for the entire Europe on the EMEP grid at 50 km × 50 km resolution and grid dimension of 123 × 119 cells. For this study FRAME was run for secondary inorganic aerosols (SIA), primary particulate matter (PPM, without the contribution of sea salts) and sea salt aerosol (SSA). Import was understood here as the influx of pollutants into the administrative boundaries of the UK and Poland (not within the model domain). Similarly, export was calculated for pollutants emitted within the administrative borders of the analysed countries.

Evaluations of the FRAME model results for SIA ($SO_4^{2-}$, $NO_3^-$, $NH_4^+$), SSA and particulate matter (PM) concentrations were undertaken in earlier studies for both countries and were found to be in good agreement with measurements. The details are provided by Dore et al. [1, 2], Kryza et al. [4, 5], Werner et al. [8, 9].

## 53.3 Results and Discussion

Absolute import is higher for Poland than for the UK in the case of pollutants, for which sea surface is not the main contributor of emission (e.g. N-NOy ÷ nitrogen from oxidised nitrogen, N-NHx ÷ nitrogen from reduced nitrogen). In the case of sulphur and nitrogen compounds, the highest import is for N-NOy, both for the UK and Poland. For PPM the role of import and export was calculated twice: including and excluding SSA. When we do not take into account SSA, import of $PPM_{2.5}$ and

**Table 53.1** National emission (National, Gg) of pollutants, import from outside of the considered countries (Import, Gg), which includes sea salt aerosol emission and the relation of export to import for the UK and Poland in 2007

| | UK | | | | Poland | | | |
|---|---|---|---|---|---|---|---|---|
| Pollutants | S-SOx | N-NOy | N-NHx | PPM10 | S-SOx | N-NOy | N-NHx | PPM10 |
| National | 298.9 | 428.3 | 243.6 | 144.4 | 393.0 | 269.0 | 237.7 | 328.0 |
| Import | 114.2 | 128.9 | 47.5 | 2643.6 | 126.5 | 236.9 | 101.0 | 793.1 |
| Export/Import | 1.6 | 2.4 | 2.3 | 0.0 | 1.5 | 0.5 | 0.7 | 0.1 |

$PPM_{10}$ is higher for Poland than for the UK. In this case, import is slightly higher than national emission of $PPM_{2.5}$ and $PPM_{10}$ in Poland by about 10 %, whereas in the UK the import is lower than national emission, in both cases ($PM_{2.5}$ and $PM_{10}$) by about 30 %. When we take SSA into consideration (Table 53.1), the highest value of import is for $PM_{10}$ in the UK. For both counties the import of $PPM_{10}$ and $PPM_{2.5}$ is higher than national emission.

The spatial distribution of imported pollutants in total concentrations of $SO_4^{2-}$, and $NO_3^-$ is presented in Fig. 53.1. The highest contribution of imported $SO_4^{2-}$ in the UK is related with the coastal areas, especially in the western part of the country (contribution >80 %). Inland, the contribution of pollutants coming from other countries is less than 20 % (locally below 10 %). The highest role of import for $NO_3^-$ concentrations in the UK is in the north-western part of the country (contribution about 30 %), as well as in the south-east. A similar spatial pattern to that for $NO_3^-$ is observed for $PPM_{2.5}$ and $PPM_{10}$. The increased contribution of import reaches further inland in the case of $PPM_{2.5}$ than $PPM_{10}$ due to the slower removal rate from the atmosphere of fine particles.

For Poland the highest contribution of import (for SIA and PPM) is in the west and partially also in the south-west (for $SO_4^{2-}$ import locally reaches 80 %). The variability of the $NO_3^-$ contribution is small – for most of Poland this amounts to 60–70 %, and only in western parts locally exceeds 70 %. The decreased role of import is observed in urban areas in the case of $NO_3^-$ because of the large contribution of local emission.

## 53.4 Summary and Conclusions

- The absolute mass of imported pollutants is higher for the UK than Poland only for species for which the main source is the sea surface. For the remaining chemical components considered (e.g. $SO_4^{2-}$, $NO_3^-$) import for Poland is higher
- Lower absolute mass of import for the UK in comparison to Poland in the case of nitrogen compounds or PPM (without SSA) results from larger distance to the UK from emission sources (e.g. continental Europe). Simultaneously in prevailing westerly circulation, more often a relatively clean mass of air

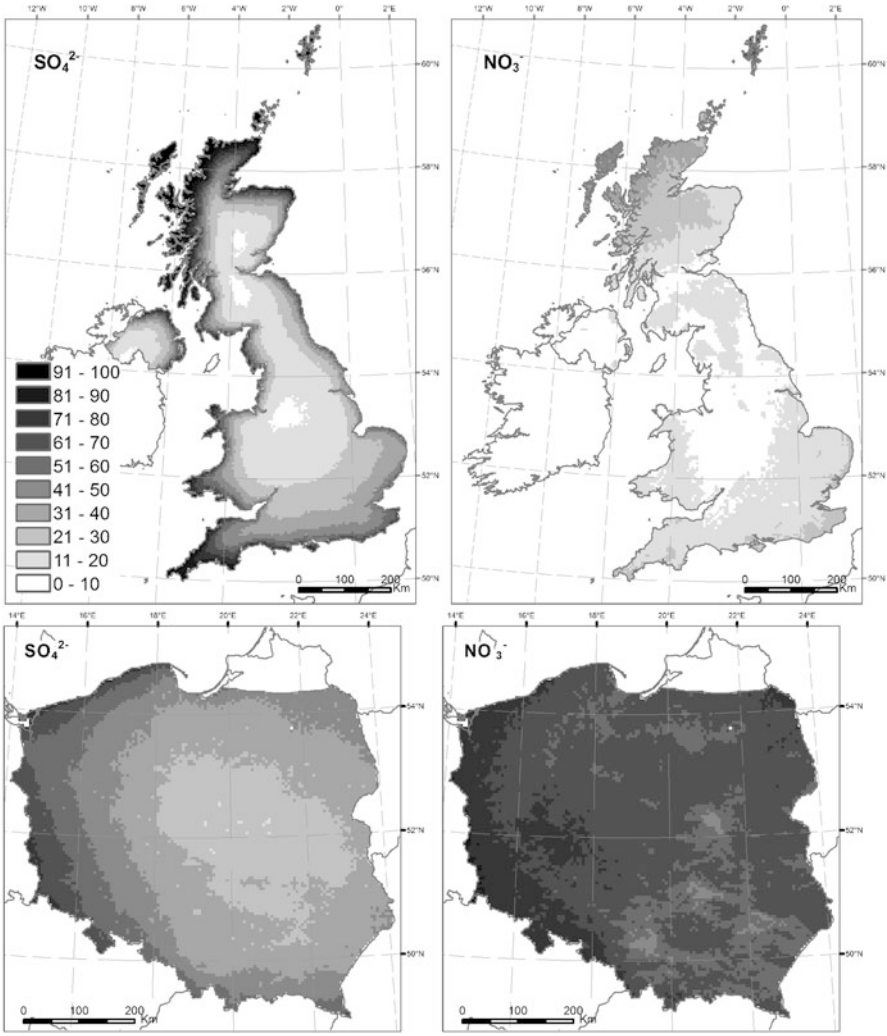


**Fig. 53.1** Contribution of imported particles in total $SO_4^{2-}$ and $NO_3^-$ concentrations in 2007 (Unit: %, the same legend for all maps)

come from oceanic areas than from the continent. Poland, surrounded by many neighbouring emission sources receives a large contribution from pollutants emitted outside the border.

- The relatively high contribution of import in total concentrations of SIA or PPM in the north-west part of the UK is related to a lack of local emission sources in this region (Grampian Mts), whereas increased import on the south-east is related to the transport of pollutants from the continental part of Europe.

**Acknowledgments** This work was supported by the Department for the Environment, Food and Rural Affairs (DEFRA, UK) and The Polish National Science Centre (UMO-2012/05/B/ST10/00446). Calculations have been carried out in Wroclaw Centre for Networking and Supercomputing (http://www.wcss.wroc.pl), Grant No. 170.

## References

1. Dore AJ, Vieno M, Tang YS, Dragosits U, Dosio A, Weston KJ, Sutton MA (2007) Modelling the atmospheric transport and deposition of sulphur and nitrogen over the United Kingdom and assessment of the influence of SO2 emissions from international shipping. Atmos Environ 41:2355–2367
2. Dore AJ, Kryza M, Hall J, Hallsworth S, Keller V, Vieno M, Sutton MA (2012) The influence of model grid resolution on estimation of national scale nitrogen deposition and exceedance of critical loads. Biogeosciences 9:1597–1609
3. Fournier N, Dore A, Vieno M, Weston K, Dragosits U, Sutton M (2004) Modelling the deposition of atmospheric oxidized nitrogen and sulphur to the UK using a multi-layer long-range transport model. Atmos Environ 38:683–694
4. Kryza M, Matejko M, Błaś M, Dore A, Sobik M (2010) The effect of emission from coal combustion in non-industrial sources on deposition of sulphur and nitrogen oxides in Poland. J Air Waste Manag Assoc 60:856–866. doi:10.3155/1047-3289.60.7.856
5. Kryza M, Werner M, Dore AJ, Błaś M, Sobik M (2012) The role of annual circulation and precipitation on national scale deposition of atmospheric sulphur and nitrogen compounds. J Environ Manag 109:70–79. doi:10.1016/j.jenvman.2012.04.048
6. Maenhaut W (2008) New directions: future needs for global monitoring and research of aerosol chemical composition. Atmos Environ 42:1070–1072
7. Vieno M, Dore AJ, Stevenson DS, Doherty R, Heal M, Reis S, Sutton MA (2010) Modelling surface ozone during the 2003 heat-wave in the UK. Atmos Chem Phys 10:7963–7978
8. Werner M, Kryza M, Dore AJ, Błaś M, Hallsworth S, Vieno M, Smith RI (2011) Modelling of marine base cation emissions, concentrations and deposition in the UK. Atmos Chem Phys 11:1023–1037
9. Werner M, Kryza M, Dore AJ, Wałaszek K (2013) Differences in the spatial distribution and chemical composition of PM10 between the United Kingdom and Poland. Environ Model Assess (under review). doi:10.1007/s10666-013-9384-0

# Chapter 54
# A 40-Year History of a Simple Urban Dispersion Model and Its Evaluation

**Steven Hanna**

**Abstract** This paper traces the evolution of my "simple urban dispersion model", beginning with the 1971 Atmospheric Turbulence and Diffusion Laboratory (ATDL) urban dispersion model, which was developed for application to urban area sources of radon. The Gaussian plume model is the basis, with use of Gifford's novel derivation involving integration over upwind sources. The development continued with the addition of an urban meteorological preprocessor in the Hybrid Plume Dispersion Model (HPDM), accounting for the effects of strong mechanical mixing and increases in turbulence intensity in urban areas. Since 2000, the simple urban model was modified for US Department of Defense applications regarding toxic gas releases in built-up city centers, and tested with extensive field data. One model option is the Gaussian formula and another is an even simpler dimensionless relation.

## 54.1 Introduction

In the early 1970s, Dr. Frank Gifford and I developed a simple urban dispersion model and named it the ATDL (Atmospheric Turbulence and Dispersion Laboratory) urban dispersion model. Gifford [3] developed the mathematical theory that justified the integration over the upwind area and allowed the resulting simplifications. The ATDL model was originally used for calculating the dispersion of radon emissions from cooking stoves across an urban area, where the emissions could be expressed as area sources. The model was subsequently further developed and evaluated with urban field experiment data from St.Louis and elsewhere.

S. Hanna (✉)
Hanna Consultants, 7 Crescent Ave., Kennebunkport, ME 04046-7235, USA
e-mail: hannaconsult@roadrunner.com

D. Steyn and R. Mathur (eds.), *Air Pollution Modeling and its Application XXIII*,
Springer Proceedings in Complexity, DOI 10.1007/978-3-319-04379-1_54,

The basic formulation was adopted by the US EPA and others in their operational dispersion models for urban areas (e.g., see [12]).

Hanna and Chang [10] analyzed urban boundary layer field data and suggested several modifications to the meteorological preprocessor of their Hybrid Plume Dispersion Model (HPDM). These accounted for the facts that, at night, there may be an upward heat flux in urban areas, and that there is enhanced mechanical turbulence over rough urban surfaces and therefore a tendency towards neutral conditions.

The simple urban dispersion model concept was revived and modified in the past 15 years because of a resurgence of interest in urban dispersion, especially related to security issues, such as the threat of deliberate releases of hazardous gases in highly-populated areas of cities. Collaborating with Prof. Rex Britter, we modified the ATDL urban dispersion model so that it better applied to near-surface point sources in the midst of building obstacles [2, 6, 8]. The scaling "constants" and power laws in the model were fit to the many urban field and wind tunnel observations that became available in the past 15 years (such as DAPPLE, Urban 2000, MUST, JU2003, MSG05, and MID05), leading to a simple but robust formulation that provides good agreement with observations. It has been shown that, probably due to the large natural variability of the urban boundary layer, the simple model produces as good statistical agreement with the field observations as much more complex models, such as CFD models.

## 54.2 The ATDL Urban Dispersion Model

At NOAA's Atmospheric Turbulence and Diffusion Lab (ATDL) in Oak Ridge, TN, Frank Gifford and I developed and tested the simple ATDL urban dispersion model (e.g., [4, 5, 7]) over the course of several years beginning in about 1969. At the time, the U.S. Atomic Energy Commission (AEC) was concerned about the health effects of radon released by fossil-fuel-fired combustion sources in large urban areas. The radon source emissions were known approximately as averages across square grid systems (with size about 0.5–1 km) covering the urban area. The Gifford paper [3] on computation of pollution from several sources described an elegant and fast solution where the Gaussian plume is turned "upwind" from a given receptor location and an integration is made over the upwind area sources. This method avoided the need to apply the Gaussian plume model to thousands of individual point sources. The Gaussian plume formula was used with $\sigma_y$ and $\sigma_z$, estimated using a simple power law function of downwind distance, and Pasquill stability class. For a uniform square grid system of area source emissions, the solution for the concentration in any grid square could be written analytically on a single line.

The ATDL urban dispersion model was most frequently applied to calculations of annual averages, which depend on the distribution of area source strengths and the wind direction rose. Gifford and Hanna [4] found that, for fairly evenly distributed source emissions across an urban grid network, the ATDL model could

be even further simplified to $C = AQ_{ao}/u$, where A is a dimensionless "constant", $Q_{ao}$(g m$^{-2}$ s$^{-1}$) is the average area source strength and u (m s$^{-1}$) is the average wind speed in the urban surface layer. Comparisons with PM, CO, and $SO_2$ observations from several cities led to a determination that $A = 200$ best fit the observations for neutral conditions and for average annual conditions.

## 54.3 The HPDM Urban Meteorological Preprocessor

The Hybrid Plume Dispersion Model (HPDM) was developed under EPRI sponsorship during the period from about 1985 to 1995. HPDM was intended for plumes from industrial stacks. Many of the scientific modules in HPDM became incorporated into AERMOD, the US EPA's current recommended model for industrial point sources. In the early 1990's, after data became available from the tracer study at the Indianapolis Power and Light power plant stack, which was located on the edge of the Indianapolis urban area, we modified the HPDM meteorological preprocessor to account for urban effects such as increased roughness and anthropogenic heat fluxes [10]. Like AERMOD, HPDM does not use the Pasquill $\sigma_y$ and $\sigma_z$ curves and stability classification scheme. Instead, HPDM and AERMOD estimate u* and L using Monin-Obukhov similarity theory, from which turbulence intensities, Lagrangian time scales, and dispersion parameters $\sigma_y$ and $\sigma_z$ can be calculated. For a given sun's intensity and geostrophic wind speed, over the urban area the wind speed near the surface is less, the friction velocity u* is greater, the sensible heat flux $H_s$ at night is of smaller magnitude or even slightly positive, and the magnitude of L is much greater than in the surrounding rural area.

Although the meteorological preprocessor can make use of observations of u, $\sigma_v$ and $\sigma_w$ from several levels on a tower, most of the time only a wind observation is available at a single height. Also, a measure of cloudiness is usually available. Land-use information is used to estimate surface roughness, $z_o$, Bowen Ratio, and albedo. Just from the larger $z_o$ over an urban area, the calculated u* (and $\sigma_v$ and $\sigma_w$) will be larger, as well as the calculated mixing depth. Being proportional to $u^{*3}$, L will also be larger (i.e., closer to neutrality) over the urban area. Urban HPDM also prescribed a "minimum L magnitude $= 3h_b$" over the urban surface with average building height, $h_b$. This was based on the rationale that the magnitude of L is proportional to the depth dominated by mechanical mixing. Hanna and Chang [10] demonstrated that the urban version of HPDM provided good agreement in predicted u*, $\sigma_v$ and $\sigma_w$, and concentrations in Indianapolis and in other cities such as St. Louis.

## 54.4 Revised Simple Urban Dispersion Model

A resurgence of interest in urban dispersion occurred in the late 1990s and continues to the present time. This is fueled by air quality concerns (e.g., impacts of PM and NOx from traffic sources on urban populations) as well as national security concerns

(e.g., impacts of releases of chem.-bio agents in busy downtown venues). Although many scientists are using CFD models for these applications (see [9]), we felt that simple models are likely to perform just as well when compared with the highly variable urban field observations. We attempted to slightly revise the ATDL urban dispersion model (Gaussian based), and also to investigate the performance of even simpler formulas from dimensional analysis such as $Cu/Q = A/x^2$.

### *54.4.1 Revisions to ATDL Gaussian-Based Urban Dispersion Formula*

Hanna et al. [8] and Hanna and Baja [6] describe a revised version of the decades-old ATDL urban dispersion model. The model focuses on point sources and uses dispersion coefficients, $\sigma_y$ and $\sigma_z$, consistent with the so-called Briggs urban formulas [1, 7], which were primarily based on observations from the St. Louis field experiment involving tracer gas releases [13]. Venkatram [15] reanalyzed those data from a modern vantage point and compared them with his recent observations and updated theories. McElroy and Pooler [13] suggested that there may be an initial $\sigma_{yo}$ and $\sigma_{zo}$ of about 40 m, due to mixing around building obstacles and in street canyons near the source. However, McElroy and Pooler [13] and Briggs [1] did not use this initial value, perhaps because they felt that there were insufficient data close to the source (the nearest samplers were 800 m away in St. Louis).

The latest version of the simple model used by Hanna and Baja [6] reincarnates the initial $\sigma_{yo}$ and $\sigma_{zo}$ of 40 m assumption and tests it with data near the source. The model is evaluated with the extensive tracer data from the Joint Urban 2003 (JU2003) and the Madison Square Garden 2005 (MSG05) field experiments, where source releases and samplers were in built-up downtown areas with deep street canyons and nearby tall buildings with heights exceeding 100 m.

Assume that the source is emitted at ground level, which is a valid assumption even if the release height is as high as 10 m in an urban environment, because of the large initial plume spread. Also assume that the receptor is located at $z = 0$, for the same reason. The Gaussian formula can be written:

$$C/Q = \left(1/\left(\pi u \sigma_y \sigma_z\right)\right) \exp\left(-y^2/2{\sigma_y}^2\right) \qquad x > 0 \tag{54.1}$$

where C/Q has units $s/m^3$, y is the lateral distance from the plume centerline (assuming that the x axis has been lined up along the plume axis), and the wind speed, u, is the averaged wind speed for the plume as it is transported in the urban canopy.

The standard deviations are assumed to be made up of two parts, an initial $\sigma_o$ due to the mixing in the street canyons at the source location, and a turbulent $\sigma_t$ due to the usual ambient turbulence, which exists over all types of terrain. The initial $\sigma_{yo} = \sigma_{zo} = 40$ m is based on McElroy and Pooler [13] and also appear to be valid

at JU2003 and MSG05. It is assumed that in downtown urban areas, $\sigma_y = \sigma_z$. We then have the following formula:

$$\sigma_y = \sigma_z = \sigma_{yo} + \sigma_{yt} = 40\ \text{m} + \text{Bx} \tag{54.2}$$

The parameter (or "constant") B equals 0.25 in Briggs' urban sigma formulas for neutral conditions. The stability is assumed nearly neutral during the daytime in built-up downtown areas. Large mechanical mixing is expected in the urban canopy, as confirmed by observations of JU2003 and MSG05 heat fluxes and Monin length, L, reported by Hanna et al. [11]. At night, the stabilities are on the stable side of neutral, thus suggesting that the Briggs' [1] slightly stable value of B = 0.08 be used. The linear relation in Eq. (54.2) is valid only at short distances, x, less than about 1 or 2 km from the source.

It is implied that the cloud of material initially spreads out into a hemispherical shape around the source area. Thus there is material dispersing even in the upwind direction (at $x < 0.0$), as confirmed by JU2003, MSG05, and MID05 observations. This can be handled by the following correction for $x < 0$ where the along wind $\sigma_{xo}$ is assumed to also equal 40 m.

$$C/Q = \left(1/\left(\pi u \sigma_{yo} \sigma_{zo}\right)\right) \exp\left(-y^2/2{\sigma_{yo}}^2\right) \exp\left(-x^2/2{\sigma_{xo}}^2\right) \qquad x < 0 \tag{54.3}$$

The simple urban model described above assumes that there is large initial mixing due to the influence of recirculating wakes and street canyon vortices caused by several buildings. Thus the model is most valid after the plume has passed around and/or over several buildings. It can be hypothesized that a downwind distance equal roughly to the average building height is necessary for this initial mixing to take place. Thus in comparisons with JU2003 and MSG05 data, the above model is assumed valid for downwind distances greater than about 50 or100 m. This parameter can also be varied in sensitivity studies.

For samplers at distances from the source less than about 50 or 100 m, or when the line-of-sight is unobstructed between the release point and the sampler, it is assumed that the plume remains in the initial street canyon or courtyard and travels more or less unimpeded without being extensively mixed laterally by the multiple large buildings. In this case, we assume that the initial dispersion ($\sigma_{yo} = \sigma_{zo} = \sigma_{xo}$) is smaller. A value of 10 m is assumed, but this is also subject to sensitivity analyses. The turbulent dispersion (i.e., 0.08× or 0.25×) remains the same.

An estimate of the urban wind speed is needed. Hanna et al. [11] show that the average magnitude of the street-level wind speed is about 2 m/s during JU2003 and MSG05.

Because of the initial plume size $\sigma_o$ assumed at $x = 0.0$, the Cu/Q solution in Eq. (54.1) becomes independent of x near the source, approaching about 0.0002 $m^{-2}$ (for $\sigma_o = 40$ m) or about 0.003 $m^{-2}$ (for $\sigma_o = 10$ m) as x approaches 0.0 during both day and night. These limits were verified using observations at receptors within about 100 m of the source during JU2003, MSG05 and MID05.

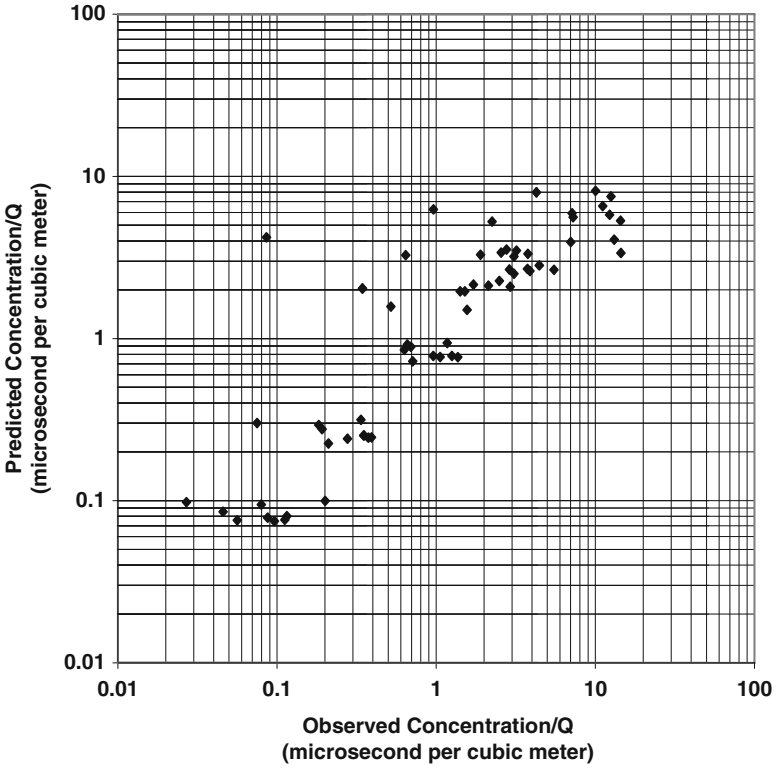


**Fig. 54.1** Simple urban model predicted versus observed C/Q ($\mu s/m^3$) for arc maximum 30-min average concentrations per trial for daytime JU2003 IOPs (3, 4, and 6)

Figures 54.1 and 54.2 contain scatter plots of the above simple urban model and of the DTRA HPAC UDM/MM5 model predictions, respectively, versus observations for the daytime tracer trials at JU2003. HPAC UDM/MM5 is DTRA's operational model and is based on the SCIPUFF Lagrangian puff dispersion model, with meteorological inputs from the MM5 mesoscale meteorological model. It is evident to the eye that there is little difference in performance between the simple model and the more complex model.

### *54.4.2 Simple Scaling Relation*

In Sect. 54.1, it was stated that a simplified version of the ATDL urban model was found to provide a reasonable estimate of annual average concentrations in urban areas when emissions from area sources are dominant and are widespread. That is $C = AQ_a/u$, where $Q_a$ is area source strength and A is a dimensionless

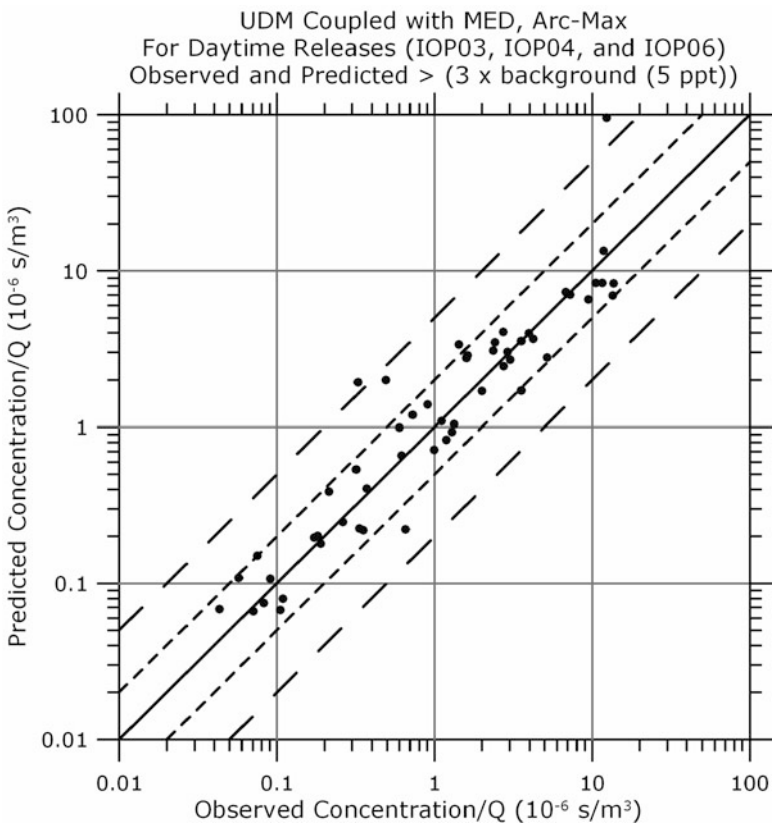


**Fig. 54.2** HPAC UDM/MM5 predicted versus observed C/Q ($\mu s/m^3$) for arc maximum 30-min average concentrations per trial for daytime JU2003 IOPs (3, 4, and 6)

constant that depends somewhat on city size. 30 years later, Britter and Hanna [2] suggested a slightly different dimensionless relation for point sources in urban areas based on analyses of the London DAPPLE field and wind tunnel data (e.g., [14]): $C = DQ/(ux^2)$, valid for $x < 50\ h_b$, where $h_b$ is average building height, and u is the average urban canopy wind speed. The concentration, C, is assumed to be the maximum on the plume centerline at the distance, x. Neutral conditions are assumed in the downtown area and the "constant", D, is said to be of order 10. Hanna et al. [11] use the observations at JU2003 and MSG05 and MID05 to "tune" this scaling relation (e.g., see Fig. 54.3) so that the following formulas are valid, at downwind distances less than about 1 or 2 km:

$$C = 4Q/\left(ux^2\right) \text{ daytime} \tag{54.4}$$

$$C = 10Q/\left(ux^2\right) \text{ nighttime} \tag{54.5}$$

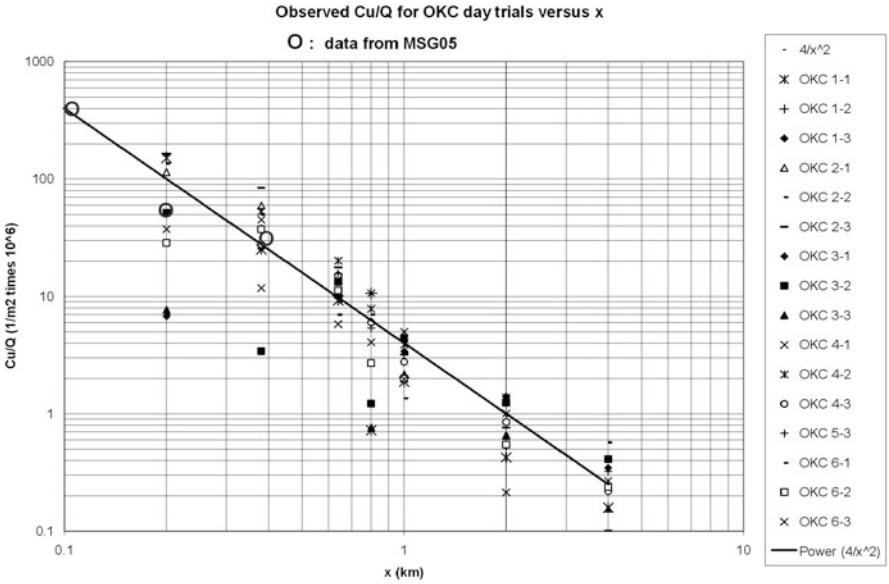


**Fig. 54.3** Summary plot of observed *Cu*/*Q* versus *x* for daytime trials during JU2003 at Oklahoma City (*OKC*), and averaged over all PFT tracers and release trials for MSG05. C is the maximum 30-min averaged concentration observed along a cross-wind arc of monitors at a given downwind distance, *x*. The line given by $Cu/Q = 4/x^2$ is drawn

These solutions can be compared with the asymptotic limits for Eq. (54.1). On the plume centerline ($y = z = 0.0$) at large downwind distances, x, during the day, the Gaussian solution in Eq. (54.1) approaches the limit $C/Q = 5.1/(ux^2)$, which is close to (about 25 % larger than) the relation observed at JU2003 and MSG05 and listed in Eq. (54.4).

## 54.5 Further Comments

Why does a simple urban dispersion model perform just as well as much more complex and detailed models such as CFD models or the DTRA HPAC/UDM model system? The answer can be seen when the observed concentration distributions in space are plotted for the JU2003, MSG05, and MID05 tracer experiments. In all experiment trials, the observed distribution is broad (i.e., it is not a narrow plume), with the plume initially spreading overran angle of 100° or so and continuing to cover a wide area at larger distances. Similarly, the samplers at building rooftops indicate that there has been rapid vertical dispersion. The large turbulence intensities in the very rough urban area contribute to this large spread. Thus it is "easy" for a simple dispersion model to capture this broad plume.

Additionally, there are many causes of large natural variability or randomness in urban areas. Turbulence intensities are on the order of unity for wind speeds of 1 or 2 m/s. Slow meanders of the incoming flow can cause the local plume to first follow a certain street orientation, but then shift to a street orientation perpendicular to the first. Thus there are large natural fluctuations in concentration, too, that can not be directly accounted for by any modeling system, including CFD models.

Because of the fundamental natural uncertainty in urban boundary layer turbulence and dispersion, the models are up against a "minimum RMSE" that "can't be beat". For example, once a pair of dispersion models are able to produce a relative mean bias less than about 50 % and a relative RMSE less than about unity, there is no more significant improvement possible. Thus the performance measures for the two models cannot be shown to be significantly different at the 95 % confidence level.

## References

1. Briggs GA (1973) Diffusion estimation for small emissions. ATDL report no. 79, ATDL, NOAA/ARL, Oak Ridge
2. Britter RE, Hanna SR (2003) Flow and dispersion in urban areas. Annu Rev Fluid Mech 35:469–496
3. Gifford FA (1959) Computation of pollution from several sources. Int J Air Water Pollut 2:109–110
4. Gifford FA, Hanna SR (1973) Modeling urban air pollution. Atmos Environ 7:131–136
5. Hanna SR (1971) A simple method of calculating dispersion from urban area sources. J Air Pollut Control Assoc 21:774–777
6. Hanna SR, Baja E (2009) A simple urban dispersion model tested with field data from Oklahoma City and Manhattan. Atmos Environ 43:778–885
7. Hanna SR, Briggs GA, Hosker RP (1982) Handbook on atmospheric diffusion, DOE/TIC-11223 (DE82-002045). NTIS/USDOC, Springfield, 102 p
8. Hanna SR, Britter R, Franzese P (2003) A baseline urban dispersion model evaluated with Salt Lake City and Los Angeles tracer data. Atmos Environ 37:5069–5082
9. Hanna SR, Brown MJ, Camelli FE, Chan S, Coirier WJ, Hansen OR, Huber AH, Kim S, Reynolds RM (2006) Detailed simulations of atmospheric flow and dispersion in urban downtown areas by computational fluid dynamics (CFD) models – an application of five CFD models to Manhattan. Bull Am Meteorol Soc 87:1713–1726
10. Hanna SR, Chang JC (1992) Boundary layer parameterizations for applied dispersion modeling over urban areas. Bound-Lay Meteorol 58:229–259
11. Hanna SR, White J, Zhou Y (2007) Observed winds turbulence, and dispersion in built-up downtown areas in Oklahoma city and Manhattan. Bound-Lay Meteorol 125:441–468
12. Jensen SS, Larson T, Deepti KC, Kaufman JD (2009) Modeling traffic air pollution in street canyons in New York City for intra-urban exposure assessment in the US Multi-Ethnic Study of atherosclerosis and air pollution. Atmos Environ 43:4544–4556
13. McElroy JL, Pooler F (1968) The St. Louis dispersion study, vol II –Analysis. National Air Pollution Control Admin. Pub. No. AP-53. USDHEW, Arlington, 50 p
14. Neophytou MK, Britter R, Martin D, Price C, Nickless G, Shallcross D (2005) Results from a tracer field experiment in London (UK) and comparisons with predictions from urban dispersion models. In: Proceedings of the 5th international conference on urban air quality, Valencia, 29–31 Mar 2005
15. Venkatram A (2005) An examination of the urban dispersion curves derived from the St. Louis dispersion study. Atmos Environ 39:3813–3822

## Questions and Answers

**Questioner Name:** Luca Delle Monache

**Q:** In your talk you mentioned that there may be an "error threshold", below which it may be difficult to go with any modeling approach, because of the intrinsic limited predictability of the phenomena we are trying to model. My question is: Can we come up with an estimate of such an error threshold, either theoretical or empirical? You suggested some values for wind speed (about 1 m/s) and other variables, based on your experience over the years. A discussion on how we could estimate this threshold from a theoretical point of view perhaps could enrich your paper.

**A:** Our models cannot satisfactorily account for the full spectrum of atmospheric motions. There is inherent or natural uncertainty (random variability) at all time and distance scales. Consequently, observed time series of, say, wind speed or pollutant concentration exhibit more fluctuations than model-predicted time series. I do not know how this inherent uncertainty can be estimated from a theoretical point of view. The basic uncertainty (error threshold) numbers that I quote are based more on empirical evidence than theory. However, it is important to base these empirical numbers on as large a set of modeling studies and evaluations with field data as possible.

**Questioner Name:** Clemens Mensink

**Q:** If you would be able to spend another one million dollars by means of a two page proposal (as you managed to do 40 years ago . . . ), what would be in that proposal? In other words: according to your expertise and experience, where should we focus on in the (near) future?

**A:** As I mentioned in my presentation, our proposals to the US Department of Energy (DOE) in the 1970s were quite general, so my answer will also be general. Keeping to the topic area of dispersion within urban metropolitan areas, I would focus on study of vertical profiles of turbulence and Lagrangian time scales in the layer from the ground surface to several times the mean building height. Also, it is important to determine the horizontal variation of boundary layer variables and hence dispersion as a plume is transported across the variable urban surface, from the suburbs to the commercial area to the dense residential area to the built-up downtown, and out of the city on the other side. A challenge is to decide the optimum averaging distance for defining urban surface characteristics (e.g., street, bock, or neighborhood).

**Questioner Name:** Stefano Galmarini

**Q:** Can I interpret your conclusions in the sense that, in complex urban condition, there are few regulating features and any effort to pursue the details is futile, and in principle not as cost/effective as a simple solution?

**A:** Yes, that is one interpretation. The bottom line is that there is so much natural variability in urban areas that it is difficult to demonstrate statistically-significant differences in performance measures for two dispersion models, once the models have managed to remove any large mean bias and have avoided obvious outliers.

**Questioner Name:** Sylvia Trini-Castelli

**Q:** About random variability and uncertainty: They are not uniquely related to urban canopy conditions, but they characterize the atmospheric processes themselves. In your opinion, should the modeling community spend more effort investigating and addressing uncertainties? Are you aware of specific studies in this direction?

**A:** Yes, estimates of the expected uncertainties are needed. These can be obtained from a combination of field experiments and theoretical analysis. SCIPUFF is an example of a dispersion model that can make use of inputs of mesoscale variabilities. It originally included a parameterization of this component (a function of the length scale of mesoscale motions and an estimate of the variance of the mesoscale speed variations in time and space), but recently has added a new methodology based on parameterizations of ensembles of mesoscale meteorological model runs.

# Chapter 55
# Assessment of the Effect of Multiscale Interactions on the Atmospheric Flow and the Dispersion of Air Pollution in the City of Paris

**Ph. Barmpas, G. Tsegas, I. Douros, N. Moussiopoulos, and V. Akylas**

**Abstract** Interactions between different spatial and temporal scales play a major role in determining the flow structure over the urban canopy in densely built agglomerations. The intense surface in-homogeneities result in the generation of additional terms in the turbulent transport within the urban atmospheric boundary layer (ABL), which in effect generate equally intense temporal in-homogeneities. Aiming to address the limitations which arise as a result of physical disparities between the scales involved, a novel two-way scheme has been developed within the frame of the EU MEGAPOLI project to couple the mesoscale model MEMO and the microscale model MIMO, utilising a collection of interpolating metamodels. The methodology developed was employed for assessing the effects of multiscale interactions on turbulent transport in the city of Paris using the MARS-aero model, and was validated based on comparisons with monitoring measurements. Simulation results reveal an improvement of the prediction skill over non-coupled models in accurately resolving scale interactions on the atmospheric flow within the urban ABL.

## 55.1 Introduction

Interactions between different spatial and temporal scales play a major role in determining the flow structure over the urban canopy in densely built agglomerations. Recent efforts to resolve obstacle-induced influences on the mesoscale

Ph. Barmpas (✉) • G. Tsegas • I. Douros • N. Moussiopoulos • V. Akylas
Laboratory of Heat Transfer and Environmental Engineering, Aristotle University, Thessaloniki GR-54124, Greece
e-mail: fotis@aix.meng.auth.gr; gtseg@aix.meng.auth.gr; jdouros@aix.meng.auth.gr; moussio@eng.auth.gr; vasilis@aix.meng.auth.gr

D. Steyn and R. Mathur (eds.), *Air Pollution Modeling and its Application XXIII*, Springer Proceedings in Complexity, DOI 10.1007/978-3-319-04379-1_55,

structure of the urban atmospheric boundary layer (UABL) have been reviewed by Schlünzen et al. [4]. Aiming to address the limitations which arise as a result of the physical disparities between the different scales involved, a novel two-way scheme has been proposed within the frame of the EU MEGAPOLI [2] project for coupling the mesoscale model MEMO [3] and the microscale model MIMO [1], utilising a collection of multi-dimensional interpolating metamodels. The coupled MEMO-MIMO system was used to simulate meteorological fields over the Greater Paris Area during a 12-day wintertime case from 12 to 23 January 2010. The performance of the coupled system was further evaluated by introducing the calculated meteorological fields as driving meteorological input for dispersion calculations using the Eulerian chemical dispersion model MARS-aero.

## 55.2 Methodology

The metamodel can be viewed as an interpolation scheme: for any state of the "input" condition vector $x = (u_{\text{in1,2}}, \alpha_{\text{in1,2}}, E_{\text{in1,2}})$ the corresponding "output" state vector $y = (u_{\text{out1,2}}, \alpha_{\text{out1,2}}, E_{\text{out1,2}})$ is calculated, with the two vectors consisting of the wind speed ($u$), wind direction ($a$) and turbulent kinetic energy ($E$) vertical profiles, averaged over the two inflow and outflow lateral boundaries of a given microscale computational domain. For each metamodel, a calibration set of input and output states ($x_k$, $y_k$), $k = 1$. $N_{\text{cal}}$ has to be determined by explicitly simulating $N_{\text{cal}}$ microscale cases during a initialisation-calibration stage. In the coupling stage, forcing terms provided by each calibrated metamodel are numerically introduced in the discretised mesoscale fields by means of Newtonian relaxation, while a dimensionless coupling coefficient $g$ adjusts the relative strength of the Newtonian forcing. Details of the methodology can be found in Tsegas et al. [6].

## 55.3 Application: The MEGAPOLI Paris Case

### *55.3.1 Case Setup and Input Data*

In the frame of the MEGAPOLI project, Paris was assigned as the target mega-city. An urban structure database was created using optical images, digital maps and Synthetic Aperture Radar (SAR) interferometry for an area of Paris of $6 \times 3$ km$^2$ with the centre of the area being the Place d' Italie, Southeast of the city hub. Sievinen et al. [5] have prepared a set of digital elevation maps (DEMs) covering an extended central area in Paris (shown in white in Fig. 55.1c).

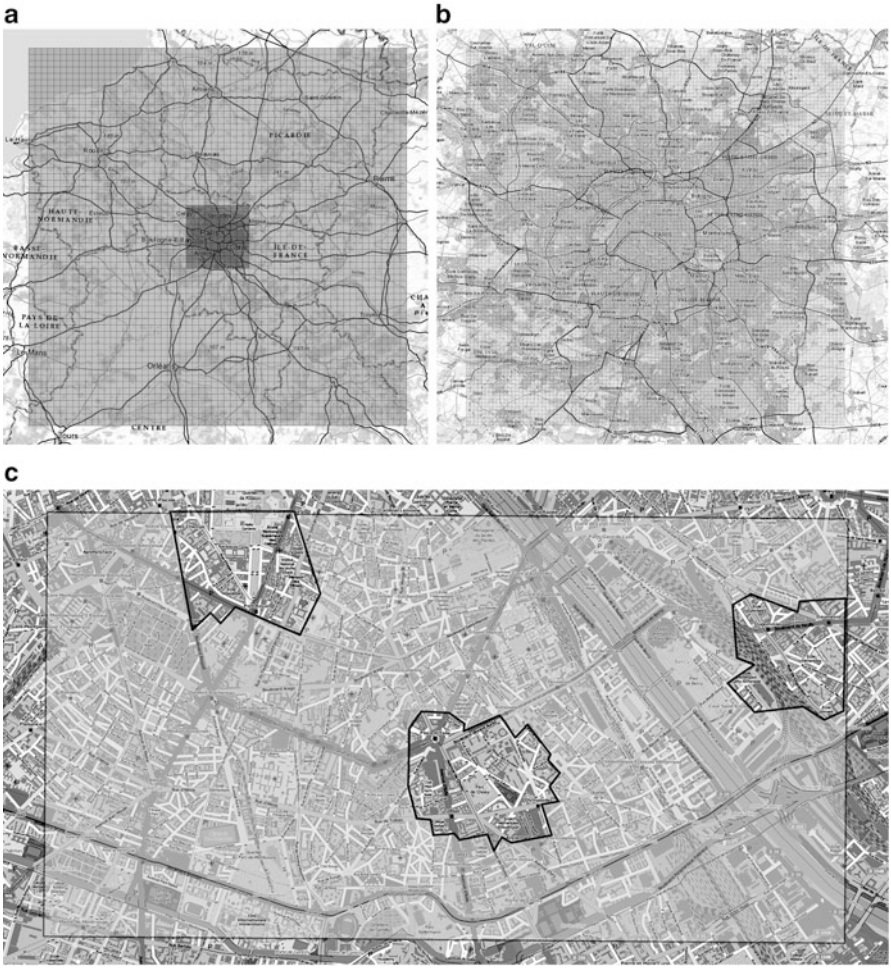


**Fig. 55.1** The coarse (**a**) and fine (**b**) Paris mesoscale domains, and the three areas of microscale application (**c**)

### *55.3.2 Microscale Calculations*

Based on previous urban studies, in order to account for the microscale effects on the UABL, depending on the size and the degree of the surface in-homogeneities of the city under investigation, it is normally enough to consider a finite number of characteristic city sectors. For the needs of the present study, three such sectors in the centre of Paris were considered, each one with an approximate size of $3 \times 3$ km$^2$, whose borders are shown by the filled polygons in Fig. 55.1c. A total of48 Unsteady

Reynolds Averaged Navier Stokes (URANS) simulations were performed, 16 for each one of the three sectors covering a period of 4 days, with each individual simulation corresponding to a period of 6 h.

Microscale calculation results predict a substantial increase of Turbulent Kinetic Energy (TKE) downstream of the sector, with a corresponding decrease within the street, in accordance with Tsegas et al. [6].

### *55.3.3 Coupled Mesoscale-Microscale Calculations*

For the mesoscale calculations two concentric computational grids were defined in a nested configuration: a coarse grid with an extent of $300 \times 300$ km$^2$ and resolution of 5 km (Fig. 55.1a) and a fine grid extending to $50 \times 50$ km$^2$ with a resolution of 500 m (Fig. 55.1b), covering the central areas of Paris. Initial and lateral boundary conditions for the outer mesoscale grid were obtained from meteorological sounding data. Model calculations were performed under three different configurations: (a) standard MEMO runs; (b) MEMO coupled with MIMO using a coupling coefficient of $g = 10^{-2}$; and (c) the coupled configuration with $g = 10^{-3}$.

The performance of the mesoscale model was evaluated by comparing calculated quantities to measurements of meteorological parameters at 18 locations in and around the Paris area during the simulation period. In Fig. 55.2, the Index of Agreement (IA) of the surface temperature and wind calculated using the standard mesoscale and coupled configurations is shown for the station locations. In most cases the $g = 10^{-2}$ coupled configuration is achieving the highest scores.

### *55.3.4 Pollutant Dispersion Calculations*

The performance of the coupled system was further evaluated by using the calculated meteorological fields for driving pollutant dispersion calculations with the Eulerian chemical dispersion model MARS-aero. Two sets of dispersion calculations were evaluated on the basis of monitoring data, one driven by the stand-alone MEMO meteorological fields and the other using fields calculated by the coupled system with $g = 10^{-2}$, respectively. The size and configuration of the calculation grid was kept identical to those of the meteorological model while the required gridded emission data for Paris were provided by AirParif in the framework of the MEGAPOLI project.

A comparison of the calculated concentration time series with monitoring data indicates that the coupled model as a meteorological driver results in improved bias at most of the station locations, irrespective of the bias sign. The improvement appears more significant for photochemically active pollutants like ozone and $NO_2$, less so for $PM_{10}$ and $PM_{2.5}$. An improved correlation is also observed for $SO_2$ at several stations, indicating the ability of the coupled model to better reproduce

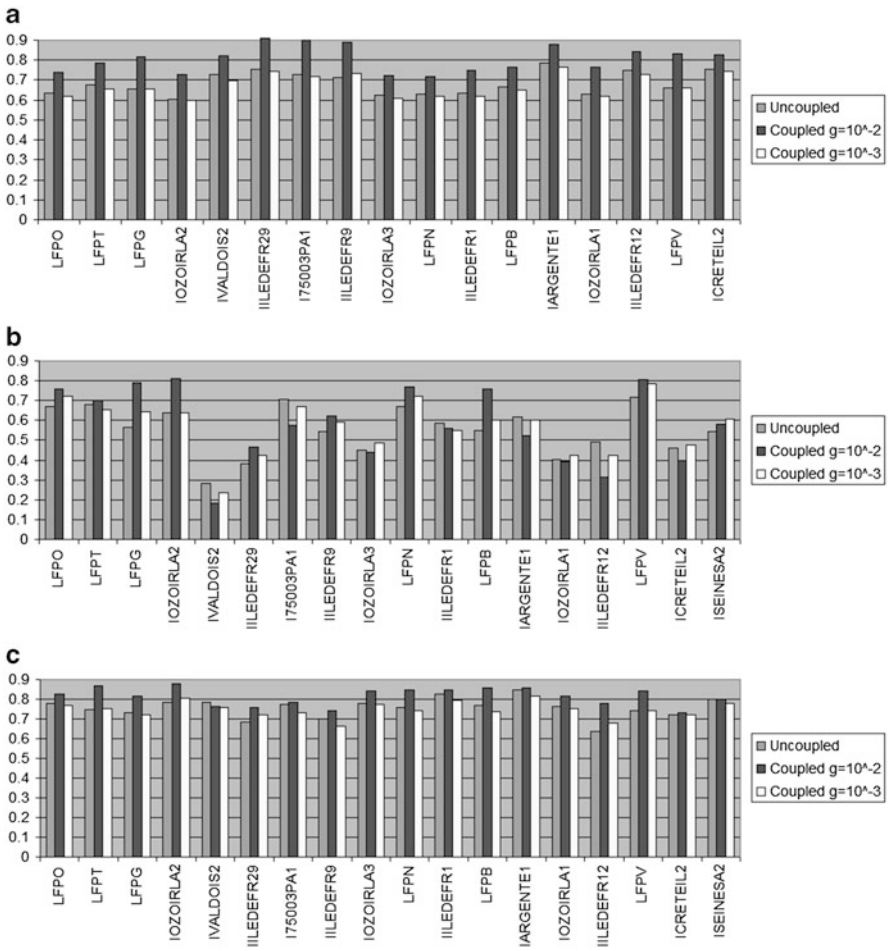


**Fig. 55.2** Index of Agreement (*IA*) between calculated and observed time series of temperature (**a**), wind speed (**b**) and wind direction (**c**)

the development and dispersion of the wintertime city plume under variable wind conditions. In Fig. 55.3, two indicative cases of the observed improvements are illustrated.

## 55.4 Conclusions

A novel two-way coupling scheme between the mesoscale model MEMO and the microscale model MIMO has been applied for assessing the effects of multiscale interactions on the turbulent transport in the city of Paris, over a multi-day

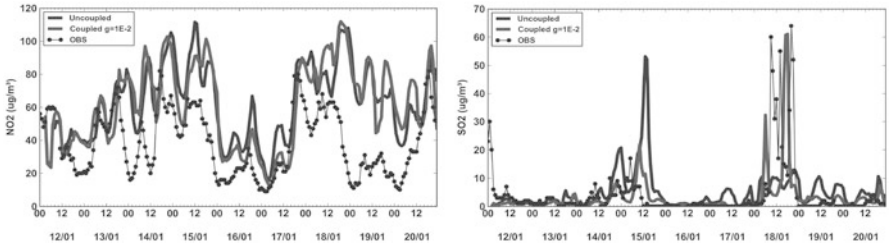


**Fig. 55.3** Calculated and observed time series of $NO_2$ at the Lognes monitoring station (*left*), and of $SO_2$ at the Ivry-sur-Seine monitoring station (*right*)

wintertime period. Validation of the coupled system using monitoring measurements indicates an overall improvement of the model predictive skill compared to mesoscale calculations that use standard urban canopy parameterisations.

**Acknowledgments** The research leading to these results has received funding from the European Union's Seventh Framework Programme FP/2007–2011 within the project MEGAPOLI, grant agreement n°212520.

## References

1. Ehrhard J, Khatib IA, Winkler C, Kunz R, Moussiopoulos N, Ernst G (2000) The microscale model MIMO: development and assessment. J Wind Eng Ind Aerodyn 85:163–176
2. MEGAPOLI Scientific Report 11-24 (2011) MEGAPOLI-50-REP-2011-10, 104 p. Available online at http://megapoli.dmi.dk/publ/MEGAPOLI_sr11-24.pdf
3. Moussiopoulos N, Flassak T, Berlowitz D, Sahm P (1993) Simulations of the wind field in Athens with the nonhydrostatic mesoscale model MEMO. Environ Model Softw 8:29–42
4. Schlünzen KH, Grawe D, Bohnenstenge SI, Schlüter I, Koppmann R (2011) Joint modelling of obstacle induced and mesoscale changes – current limits and challenges. J Wind Eng Ind Aerodyn 99:217–225. doi:10.1016/j.jweia.2011.01.009
5. Sievinen P, Praks J, Hallikainen M, Koskinen J, Hellsten A, Kukkonen J (2009) Urban morphology retrieval by means of remote sensing for the modelling of atmospheric dispersion and micro-meteorology. In: Digest IEEE international symposium on Geoscience and Remote Sensing (IGARSS'09), Cape Town, South Africa, 4 pp
6. Tsegas G, Barmpas P, Douros I, Moussiopoulos N (2011) A metamodelling implementation of a two-way coupled mesoscale-microscale flow model for urban area simulations. Int J Environ Pollut 47(1/2/3/4):278–289

## Questions and Answers

**Questioner Name:** Gabriele Curci

**Q:** Can you add more detail on the meta-model used for meso- to micro-scale coupling?

**A:** The metamodelling formulation has been previously described in more detail in Tsegas et al. [6]. The essential forcing terms are introduced back into the mesoscale equations using Newtonian relaxation, followed by a correction step for ensuring overall mass conservation.

**Questioner Name:** Steve Hanna

**Q:** Have you compared the results of your model of Paris with the results of the MICROSWIFT-SPRAY model application to Paris, which have been recently extensively described in presentations at other conferences?

**A:** We are aware of the very interesting work presented by the MICROSWIFT-SPRAY group, but we have not yet attempted any validation or cross-comparison with their results. Certainly, the availability of high-resolution measurements performed in the framework of this project offers the possibility of validating our model at a scale previously unavailable.

**Questioner Name:** Heinke Schlünzen

**Q:** Are thermal effects taken into consideration in your model?

**A:** Thermal effects are obviously taken into consideration in the mesoscale model (MEMO), including a parameterisation of anthropogenic heating and radiation trapping in the urban canopy. Our microscale model (MIMO) does support the calculation of thermal effects from urban structures but these terms were not explicitly taken into account in the Paris calculations.

**Questioner Name:** Greg Yarwood

**Q:** Does the coupling between models conserve the mass of trace species?

**A:** Our implementation of Newtonian relaxation should ensure mass conservation at all scales, however this has not yet been numerically tested. The mesoscale and microscale models include modules for dispersion of inert species, so this would be relatively straightforward to check.

# Chapter 56
# PAHs Modelling over Urban Area of Rome: Integration of Models Results with Experimental Data

**Claudio Gariazzo, Camillo Silibello, Sandro Finardi, Paola Radice, Alessio D'Allura, Monica Gherardi, and Angelo Cecinato**

**Abstract** The identification and quantification of population exposure of children and elderly people to PAHs in urban areas are the major goals of the EXPAH LIFE+ Project (www.ispesl.it/expah). To reach these objectives an integrated approach, based on measurements and modeling techniques, has been set up to preliminarily reconstruct PAHs levels in the Rome metropolitan area. Field campaigns of particulate PAHs and $PM_{2.5}$ have been performed in different sites and microenvironments from December 2011 to July 2012. These data were essential to evaluate and integrate results of the Flexible Air quality Regional Model (FARM) that has been run from June 2011 to May 2012. PAHs modeled concentrations are presented for the city of Rome as well as a comparison with observations. Capabilities and limits in modeling PAHs in urban areas are then discussed.

## 56.1 Introduction

Polycyclic Aromatic Hydrocarbons (PAHs) are a class of complex organic chemicals of increasing concern for their occurrence in the environment, produced by the incomplete combustion of organic material. PAHs can be found in the

C. Gariazzo (✉) • M. Gherardi
Department of Technology Innovation, Department of Medicine Epidemiology and Occupational Hygiene, INAIL Research Center, Via Fontana Candida 1, 00040 Monteporzio Catone (RM), Italy
e-mail: c.gariazzo@inail.it; m.gherardi@inail.it

C. Silibello • S. Finardi • P. Radice • A. D'Allura
Arianet, via Gilino 9, 20128 Milan, Italy
e-mail: c.silibello@aria-net.it; s.finardi@aria-net.it; p.radice@aria-net.it; a.dallura@aria-net.it

A. Cecinato
U.O.S. Rome, CNR-IIA, Via Salaria km 29.3, I-00015 Montelibretti (RM), Italy
e-mail: cecinato@iia.cnr.it

D. Steyn and R. Mathur (eds.), *Air Pollution Modeling and its Application XXIII*, Springer Proceedings in Complexity, DOI 10.1007/978-3-319-04379-1_56,

atmosphere in both gaseous and particulate forms. The best known PAH is the benzo[a]pyrene (B[a]P). DNA damage induced by PAHs exposure was demonstrated by different authors (e.g. [8]). PAHs are emitted by many sources, including motor vehicles, domestic burning of coal and wood, power generation via combustion and waste processing. In highly urbanized areas the sources are almost exclusively anthropogenic: domestic heating and mobile (vehicles) sources [7]. Population living in urban areas, where elevated levels are typically found (in the range of ng $m^{-3}$), have a significant risk to contract lung, skin, and bladder cancers due to the exposure to these pollutants. The identification and quantification of population exposure of children and elderly people to PAHs in urban areas are the major goals of the EXPAH LIFE+ Project (www.ispesl.it/expah). To reach these objectives an integrated approach, based on measurements and modeling techniques, has been set up to preliminarily reconstruct PAHs levels in the Rome metropolitan area. In this paper PAHs modeled concentrations are presented for the city of Rome as well as a comparison with observations.

## 56.2 Material and Methods

### *56.2.1 Inclusion of PAHs Processes in FARM Model*

The Atmospheric Modelling System (AMS) used to reconstruct PAHs levels is based on FARM (Flexible Air quality Regional Model; [4]), a three-dimensional Eulerian chemical-transport model that accounts for the transport, chemical conversion and deposition of atmospheric pollutants. Among PAHs, four indicator compounds, considered by the UNECE Protocol on POPs on the basis of their low volatility combined to their carcinogenicity, have been included in the model: namely benzo(a)pyrene (B[a]P), benzo(b)fluoranthene (B[b]F), benzo(k)fluoranthene (B[k]F) and indeno(1,2,3-cd)pyrene (I_P). The SAPRC-99 gas-phase chemical mechanism and the modal AERO3 aerosol module (U.S. EPA CMAQ modeling system), have been consequently updated in order to include the PAHs reactions with hydroxyl radical [5] and their partitioning between gas and aerosol phases following the approach suggested by Aulinger et al. [1].

### *56.2.2 Study Area and PAHs Emission Inventory*

Rome, one of the greatest urbanized cities of the Mediterranean area with an extension of 1,290 $km^2$ and about three million inhabitants, has been selected as a target site for a detailed study of population exposure of children and elderly people

to PAHs. The air pollution in the city is mainly characterized by high levels of $NO_2$, $O_3$ and $PM_{10}$. Several studies have reported severe health effects due to air pollution in this urban area [3]. In order to estimate PAHs levels over this area, FARM has been applied to two nested domains: a larger domain including Lazio Region ($61 \times 51$ grid cells with an horizontal resolution of 4 km) and the target domain including Rome metropolitan area ($60 \times 60$ cells with an horizontal resolution of 1 km). Emission data have been derived from the Lazio Region inventory and from the reference national emission inventory ISPRA2005. The latter has been used to assign emission data to surrounding regions included in the larger domain and has been updated to the year 2009, coherently with the regional inventory, using historical trends. Details about the PAHs emission inventory can be found in a proper EXPAH technical report [6]. Spatial disaggregation, time modulation and speciation (for PAHs, VOCs and PM) of emission data were made according to thematic layers (e.g. EU CORINE Land Cover), typical trends (yearly, monthly and daily) and speciation profiles depending on SNAP source classification. The analysis of PAHs emissions over Lazio Region, Rome Province and Rome Municipality evidences that residential heating represents by far the major source accounting for 73 % (which corresponds to 4,389 kg/year), 86 % (3,086 kg/year) and 92 % (2,010 kg/year), respectively. Waste treatment contribution is the second main contribution with 22 % of emissions over the Region (1,310 kg/year), 9 % over the province (334 kg/year) and 3 % over Rome municipality (64 kg/year). Road transport contributes to PAHs emissions in the 3–4 % range over these areas. PAHs emissions have been also compared with the European scale inventory developed by TNO evidencing the significant uncertainty affecting these data that can generally be considered larger than that associated to the other pollutants.

### *56.2.3 PAHs Monitoring Field Campaigns*

Experimental campaigns have been performed in the frame of EXPAH project with the aim to measure PAHs and $PM_{2.5}$ at different living/working microenvironments in Rome. $PM_{2.5}$ was sampled, on a daily basis, at low volume conditions using PTFE filters, and then analysed for higher carcinogenic PAH contents by means of gas chromatography/mass spectrometry, using 5 days aggregated sampled filters to increase signal-noise ratio. Two seasonal in-field campaigns (summer (May–July 2012) and winter-spring (December 2011–March 2012)) have been performed by sampling both indoor and outdoor living/working microenvironments. During each seasonal campaign, 20 living environments have been monitored among houses, schools, offices and transport vehicles. In winter-spring in-field campaign, B[a]P outdoor levels ranged from 1.4 to 2.0 ng/m$^3$, while target PAHs ranged $8.4 \div 13.2$ ng/m$^3$. At summer lower levels have been measured: the ambient air B[a]P ranged from 0.06 to 0.19 ng/m$^3$, while PAHs ranged $0.62 \div 1.52$ ng/m$^3$.

## 56.3 Results and Discussion

The simulation period lasted from June 2011 to May 2012 including almost all EXPAH experimental campaigns. Meteorological fields needed by FARM have been reconstructed by the limited area non-hydrostatic weather prediction model RAMS driven by ECMWF analyses. Measured data collected during the experimental campaigns permitted to evaluate the performance of the modeling system during different periods of the year. The comparison between observed and predicted PAHs concentrations has evidenced the capability of the modeling system to reconstruct PAHs concentration levels over Rome conurbation and to describe their seasonal variation (see Fig. 56.1). Nonetheless, an overestimation of observed concentrations was identified during colder periods probably determined by: (1) the large uncertainty affecting PAHs emission estimates from the house heating sector due to the significant emission factors variations depending on the fuel burned; (2) difficulties in distributing emissions within the urban texture.

To reduce model uncertainty and obtain more reliable gridded pollution fields for further epidemiological studies, two approaches, based on "data fusion" techniques and on a simplified method have been used. The former combines background concentration fields with observed information using Successive Correction Method (SCM) [2]. The latter consists in multiplying daily PAHs concentrations by a correction factor computed as the ratio between observed and predicted monthly average concentrations ($f_c$). In Table 56.1, the statistical analysis for B[a]P is presented, confirming the capability of the adopted approaches to improve model result.

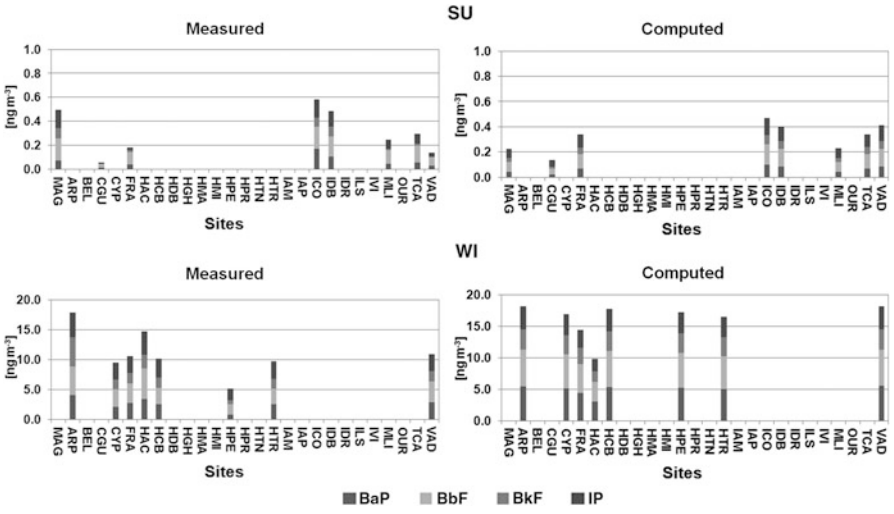


**Fig. 56.1** Observed and computed PAHs concentrations during summer (*SU*: August, 2–7, 2011) and winter (*WI*: January, 16–20, 2012) at monitoring sites (x-axis) operating during EXPAH field campaigns

**Table 56.1** Statistical analysis of simulated yearly averaged B[a]P concentrations over Rome

| Run | IOA (**1**) | R (**1**) | FAC2 (**100 %**) | MFE (**0 %**) | RMSE (**0 ng m$^{-3}$**) |
|---|---|---|---|---|---|
| Base case | 0.59 | 0.67 | 44.4 | 79.3 | 1.45 |
| Data fusion | 0.95 | 0.83 | 93.0 | 25.1 | 0.20 |
| $f_c$ | 0.79 | 0.67 | 80.7 | 39.3 | 0.35 |

*Bold* values in parenthesis are referred to ideal values of the considered metrics

Nevertheless, since EXPAH measurement field campaigns did not cover the whole modeled year and PAHs are not routinely measured at the stations of the local monitoring network, the data fusion approach could not be used to reduce predicted concentrations bias along the simulated year. So the "$f_c$" approach has been considered to provide more realistic concentration fields.

## 56.4 Conclusions

The upgraded version of FARM model, including PAHs chemistry, has been applied to Rome metropolitan area (1 km resolution) from June 2011 to May 2012 (1 year run). This application represents one of the earlier high resolution simulations performed over one of the mostly significant urban area in Europe. PAHs results evidenced the capability of the modeling system to reconstruct their levels over Rome conurbation and to describe their seasonal variation. However, since an overestimation of observed values has been identified during colder periods, possibly due to inaccuracies in the PAHs emission inventory, a simplified approach, consisting in multiplying predicted concentrations by a monthly correction factor, has been adopted to reduce PAHs concentrations bias. This correction provided an improvement of model results confirmed by the statistical analysis. Results addresses for an improvement of PAHs emission inventory and its speciation.

**Acknowledgments** The LIFE+ EU financial program (EC 614/2007) is acknowledged for the provision of funding for EXPAH project (LIFE09 ENV/IT/082).

## References

1. Aulinger A, Volker M, Quante M (2007) Introducing a partitioning mechanism for PAHs into the community multiscale air quality modeling system and its application to simulating the transport of benzo(a)pyrene over Europe. J Appl Meteorol Climatol 46(11):1718–1730
2. Bratseth AM (1986) Statistical interpolation by means of successive corrections. Tellus 38A:439–447
3. Cesaroni G, Badaloni C, Gariazzo C, Stafoggia M, Sozzi R, Davoli M, Forastiere F (2013) Long-term exposure to urban air pollution and mortality in a cohort of more than a million adults in Rome. Environ Health Perspect 121:324–331. http://dx.doi.org/10.1289/ehp.1205862

4. Gariazzo C, Silibello C, Finardi S, Radice P, Piersanti A, Calori G, Cucinato A, Perrino C, Nussio F, Cagnoli M, Pelliccioni A, Gobbi GP, Di Filippo P (2007) A gas/aerosol air pollutants study over the urban area of Rome using a comprehensive chemical transport model. Atmos Environ 41:7286–7303
5. Gusev A, Mantseva E, Shatalov V, Strukov B (2005) Regional multicompartment model MSCE-POP. EMEP/MSC-E technical report 5/2005
6. Radice P, Smith P, Costa MP, D'Allura A, Pozzi C, Nanni A, Finardi S (2012) EXPAH – ACTIONS 4.3-4.4: calculation and integration of traffic emissions with the updated Lazio Region inventory. Spatial, temporal and chemical disaggregation of the emission inventory. EXPAH technical report, April 2012. http://www.ispesl.it/expah/documenti/R2012-05_ARIANET_EXPAH_A4.3-4_final.pdf
7. Ravindra K, Sokhi R, Van Grieken R (2008) Atmospheric polycyclic aromatic hydrocarbons: source attribution, emission factors and regulation. Atmos Environ 42:2895–2921
8. Taioli E, Sram R, Binkova B, Kalina I, Popov TA, Garte S, Farmer PB (2007) Biomarkers of exposure to carcinogenic PAHs and their relationship with environmental factors. Mutat Res Fundam Mol Mech Mutagen 620(1/2):16–21, 6p

## Questions and Answers

**Questioner Name:** Johanner Bieser

**Q**. As your only degradation reaction is a gas-phase reaction with OH, my question is whether this reaction takes place in your model at all?
**A**. Yes, the fraction of PAHs in the gas-phase is not homogeneous within the studied area. Outside Rome urban area is higher and not negligible. So we can confirm that gas-phase with OH take actually place;
**Q**. In your model in what percentage are B[a]P, B[h]F, B[k]F in the gas-phase?
**A**. The four PAHs are distributed in the gas-phase as follows: B[a]P about 50–60 %, B[k]F about 20–30 %; B[b]F about 15–25 %. Indeno-Pyrene is negligible;
**Q**. Are your primary emissions gaseous or particulate?
**A**. Primary emissions of PAHs are in the gas-phase.

**Questioner Name:** Armin Aulinger

**Q**. Do you plan to include degradation of particulate PAHs, because it is the major degradation path of PAHs and it could explain overestimations?
**A**. Yes, we plan to integrate degradation processes of particulate PAHs. Preliminary results considering $O_3$ degradation confirm the relevance of these processes. However we think inaccuracies in the PAHs emission inventory is the main reason of the PAHs overestimation in winter, as the latter is not observed at summer time with the same extent when ozone reaches maximum values.

# Chapter 57
# Modelling the Effects of Urban Morphology, Traffic and Pedestrian Dynamics on Students' Exposure to Air Pollution

**Jorge Humberto Amorim, Joana Valente, Cláudia Pimentel, Pedro Cascão, Vera Rodrigues, Ana Isabel Miranda, and Carlos Borrego**

**Abstract** The United Nations Environment Programme stated that the human exposure to air pollutants primarily emitted by road traffic is associated to nearly 0.8 million premature deaths annually, especially in sensitive groups such as children. This paper evaluates the individual exposure of students in a Portuguese town accounting for their walk to school and the time spent in the classroom. The analysis was carried out for 8 hypothetical walking routes that were tracked and profiled with a GPS. Ambient air pollutant concentrations of CO and PM10 were simulated with a Computational Fluid Dynamics (CFD) model, while indoor air pollutant levels were estimated for different classrooms using the simulated outdoor concentrations and a mass transfer approach. Results show that the individual exposure of pedestrians in a city is extremely spatially dependent, as a consequence of air pollutant dispersion patterns, leading to significant disparities between the children's exposure. A tendency between the orientation of classroom's façade and resulting exposure was not found, but in the case of the outdoor exposure the children coming from N and NE have the highest values. The variability of the estimated exposure values shows the magnitude of the error that can be committed when using a single value of air quality as a surrogate of air pollution exposure. This problem can be overcome by using building-resolving CFD models that provide an accurate and detailed understanding of how human behaviour and habits can affect the exposure of urban citizens and ultimately their health.

J.H. Amorim (✉) • J. Valente • C. Pimentel • P. Cascão • V. Rodrigues • A.I. Miranda • C. Borrego
CESAM & Department of Environment and Planning, University of Aveiro,
3810-193 Aveiro, Portugal
e-mail: amorim@ua.pt; joanavalente@ua.pt; claudiapimentel@ua.pt; pmcascao@ua.pt; vera.rodrigues@ua.pt; miranda@ua.pt; cborrego@ua.pt

D. Steyn and R. Mathur (eds.), *Air Pollution Modeling and its Application XXIII*,
Springer Proceedings in Complexity, DOI 10.1007/978-3-319-04379-1_57,

## 57.1 Introduction

Air pollution is the environmental factor with the highest impact on health in Europe and is responsible for the largest burden of environment-related diseases [6]. Since the 1990s numerous studies have demonstrated the association between the outdoor air pollutants concentration and the occurrence of health related problems (e.g., [7]). In particular, some authors (e.g., [4]) have found associations between exposure to traffic and adverse health effects, such as hypertension, myocardial infarction, stroke, atherosclerosis, heart disease and mortality. Most studies on health effects of traffic exposure mostly rely on associations between hospital records and data from air quality monitoring stations, considered as representative of exposure in a specific geographical area. Due to the limited spatial representativeness and high cost of exposure measurements, the use of building-resolving air quality models is a reliable and useful tool.

## 57.2 Methodology

Personal exposure to CO and PM10 of 8 hypothetical children was calculated for a typical school morning (from 8h30 to 13h30), including the time spent in the classroom but also the exposure during the walk to school. The 3D fields of wind and air pollutant concentration, and the resulting exposure, were calculated with a local scale modelling system.

### *57.2.1 Study Area*

The study domain, with $0.4 \times 0.2$ km$^2$, is located at the centre of Aveiro town, in Northwest Portugal. The selected area is predominantly residential with a school where an urban traffic' air quality monitoring station (AQS) from the national Portuguese network is located at the front yard. In the definition of the virtual domain, neighbouring buildings were assembled based on their configuration, while trees were defined as blocks with a porosity proportional to their leaf area density. Aiming to obtain a reasonable time profile for each route, the 8 pathways were tracked using a GPS. Then, children were randomly distributed by different classrooms, one in each façade of the building, as indicated in Fig. 57.1.

### *57.2.2 Air Quality and Exposure Modelling*

Local scale air quality modelling was carried out using the Computational Fluid Dynamics (CFD) model VADIS [1], a RANS prognostic model that produces the turbulent 3D wind flow with a k-$\varepsilon$ turbulence closure coupled with the green canopy

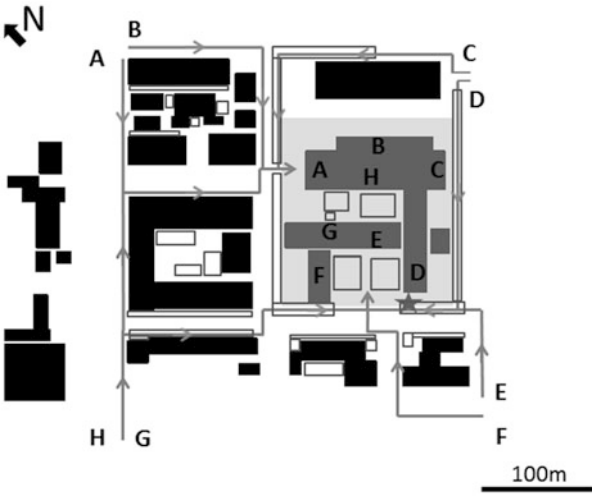


**Fig. 57.1** *Top view* of the virtual domain. Buildings are shown as *black boxes* and tree blocks as *unfilled boxes*. The *arrows* indicate the different walking routes. The *grey rectangle* shows the school, where the *letters* indicate the classroom of the corresponding children and the *star* is the AQS.

module URVE [1] and a Lagrangian method for dispersion. For the calculation of the outdoor exposure we have used the microenvironment approach from Hertel et al. [3], while for the indoor exposure the method found in Guo [2] was applied, as given by Eq. 57.1:

$$Eout_{i,c} = Cout_{i,xy} \times t_{c,xy}; \quad Ein_{i,c} = \left[ \left( \frac{S_r + pQ_{i,r}Cout_{i,xy} - Q_{i,r}Cin_{i,r}}{V_r} \right) \times t_{c,r} + Cin_{i,r} \right] \times t_{c,r} \tag{57.1}$$

where $Eout_{i,c}$ ($\mu g.m^{-3}.h$) is the outdoor exposure of children $c$ over the time $t_{c,xy}$ that was spent in a given location $xy$ with a concentration of pollutant $i$ equal to $Cout_{i,xy}$ ($\mu g.m^{-3}$), $Ein_{i,c}$ is the indoor exposure of children $c$ over the time $t_{c,r}$ spent in room $r$, $S_r$ is the indoor emission rate (assumed as 0 $\mu g.h^{-1}$), $p$ is the penetration factor (=1, following [5]), $Q_{i,r}$ is the ventilation rate of room $r$ (=33 $m^3.h^{-1}$, which is the average of ventilation data acquired in 9 Portuguese classrooms under the scope of the SINPHONIE project), and $Cin_{i,r}$ is the indoor concentration in the previous time-step ($\mu g.m^{-3}$). The output data produced by the modelling system are both instant and mean exposure values.

## 57.3 Results and Discussion

Air quality simulations were done on an hourly basis for the period between 8 and 14 h on May 5th, 2004. Examples of concentration fields are shown in Fig. 57.2. The comparison of model results against data collected at the AQS indicated a

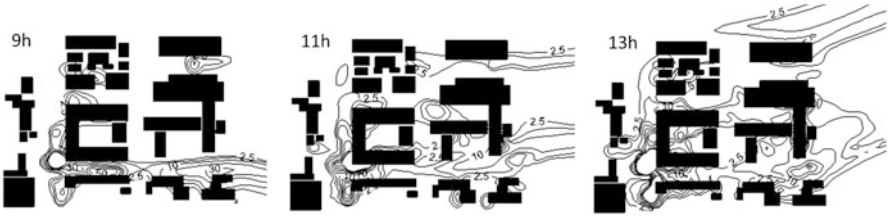


**Fig. 57.2** Representation of hourly averaged PM10 concentration isolines ($\mu g.m^{-3}$) in a 1.5 m high horizontal plane. Buildings are shown as *black rectangles* and tree blocks were omitted for simplification

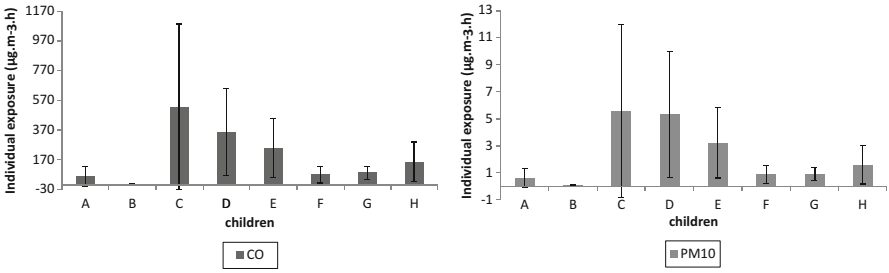


**Fig. 57.3** Average values (*bars*) and standard deviation (*lines*) of individual exposure ($\mu g.m^{-3}.h$) to PM10 and CO for the 8 considered children, in the period from 8 to 14 h

very good performance according to the acceptance criteria defined by COST732 (NMSE: 0.07; correlation coefficient: 0.999; factor of two: 1.00). More details about the air quality simulations can be found in Amorim et al. [1].

The time evolution of the spatial distribution of PM10 (as also for CO, not shown in Fig. 57.2) indicates a strong synergy between the incoming wind direction, traffic emissions and the characteristics and location of buildings and trees. In Fig. 57.3 the average and standard deviation of the resulting children's exposure to PM10 and CO is presented, including both the time spent walking from home to school and inside the classroom.

The analysis shows a significant disparity between children's average exposure, which varies between 0.1 and 5.6 $\mu g.m^{-3}.h$ for PM10 and between 9 and 527 $\mu g.m^{-3}.h$ for CO. A tendency between the orientation of classroom's façade and resulting exposure was not found, but in the case of the outdoor exposure the children coming from N and NE have the lowest values. The outdoor exposure contribution for the total morning exposure varies significantly among the selected children, from 0.03 to 23 % for PM10 and from 0.04 to 17 % for CO, despite the fact that, in average, the time spent outdoors is only 1.2 % of the total. The purpose of this paper was to evaluate the contribution of outdoor air pollution on exposure. For this reason, the indoor emission of particles (mainly due to resuspension) was neglected, which would have increased the exposure.

## 57.4 Conclusions

This study shows, through a local scale modelling approach, that the individual exposure of students in a city is extremely time and spatial dependent, as a consequence of the complex wind flow and air pollutant dispersion patterns. From the health point of view, these results suggest that even in a small domain a significant error can potentially occur if a mean air quality value is used as a proxy for the exposure of the individuals that use that specific microenvironment. This problem can be overcome by using building-resolving CFD models that are able to provide an accurate and highly detailed understanding of how human behaviour and habits can affect the exposure of urban citizens and ultimately their health. In this sense, modelling exposure studies can be of great importance in planning studies, particularly in the case of environmentally sensitive buildings, such as schools and hospitals.

**Acknowledgments** This work was supported by European Funds through COMPETE and by National Funds through the Portuguese Science Foundation (FCT) within projects PEst-C/MAR/LA0017/2013, INSPIRAR (PTDC/AAC-AMB/103895/2008) and CLICURB (EXCL/AAG-MAA/0383/2012), and the Post-Doc grants of J.H. Amorim (SFRH/BPD/48121/2008) and J. Valente (SFRH/BPD/78933/2011). An acknowledgment also to C. Alves, J. Silva, M. Duarte and T. Nunes for the ventilation data collected under SINPHONIE project ("Schools Indoor Pollution and Health: Observatory Network in Europe", DG SANCO).

## References

1. Amorim JH, Rodrigues V, Tavares R, Valente J, Borrego C (2013) CFD modelling of the aerodynamic effect of trees on urban air pollution dispersion. Sci Total Environ 461–462:541–551
2. Guo Z (2002) Review of indoor emission source models Part 1. Overview. Environ Pollut 120:533–549
3. Hertel O, Leeuw FD, Raaschou-Nielsen O, Jensen SS, Gee D, Herbarth O, Pryor S, Palmgren F, Olsen E (2001) Human exposure to outdoor air pollution – IUPAC technical report. Pure Appl Chem 73(6):933–958
4. Hoek G, Brunekreef B, Goldbohm S, Fischer P, van den Brandt PA (2002) Association between mortality and indicators of traffic-related air pollution in the Netherlands: a cohort study. Lancet 360:1203–1209
5. Thatcher TL, Layton DW (1995) Deposition, resuspension, and penetration of particles within a residence. Atmos Environ 29(13):1487–1497
6. WHO (2006) Air quality guidelines – global update 2005, Regional Office for Europe, pp 484
7. WHO (2010) Development of WHO guidelines for indoor air quality, Regional Office for Europe, pp 27

## Questions and Answers

**Questioner name:** Jeremy Silver

**Q:** Have you considered the influence of which side of the street the subject walks along?

**A:** The exact pathway of the student was considered by feeding the CFD model with the trajectory (position versus time) given by the GPS. In that sense, it was considered in which side of the street the individual was walking. Nevertheless, we did not analyze the differences between the exposure of individuals making the same pathway in opposite sides of the street.

**Questioner name:** Christof Gromke

**Q:** What explains the different characteristics (seen in the comparison of observations and modeling results) in the CO and PM10 concentrations?

**A:** In this work we have only considered as sources the traffic exhaust emissions. Although traffic is the main source of air pollution in that specific area, pollutants of other sources (e.g., the resuspension of PM10 caused by traffic dynamics) are measured too. These other sources have distinct contributions for the CO and PM10 concentrations in ambient air, which explain the different characteristics shown in the graphs. Nevertheless, qualitatively both pollutants follow similar trends. Also, the statistical comparison of simulation outputs against observations led to similar results.

**Questioner name:** Roger Timmis

**Q:** Does your study take into account different respiration rates between walking (outdoor) and sitting (indoor) students?

**A:** No, not in this particular study. The calculation of exposure does not take into account respiration rates. To take those into account the inhaled dose has to be calculated by multiplying exposure by respiration rate.

**Q:** When ventilating classrooms, can your model be used to advise which windows should be open (or kept closed) in the different façades of the school building, in order to minimize inflows of outdoor pollution into classrooms during different wind directions?

**A:** This model uses a simple approach that considers the mass transfer with the windows closed (we have the information from the school that they usually don't open windows). The suggested study could be done by using the estimated mass transfer rates for open windows, and guidelines could be established taking into account both the wind direction and the outdoor concentrations.

# Chapter 58
# LES of Advective and Turbulent Passive Scalar Fluxes in a Street Intersection

**Vladimir Fuka, Libor Kukačka, and Josef Brechler**

**Abstract** The effect of varying complexity of idealized urban canopy on street traffic generated air pollution is simulated using large eddy simulation. The geometry is modeled as an approximation to typical city centers in Central Europe and is also used for wind tunnel measurements. Four configurations have with increasing complexity have been considered. In this paper we examine average scalar concentrations and the scalar fluxes decomposed to the advective and turbulent parts.

## 58.1 Introduction

The geometry of the streets and buildings in a city plays an important role in the pollution dispersion [1]. Significant influence of building geometry was also shown by computer simulation [8]. Kukačka et al. [4] presented detailed measurement of advective scalar fluxes from a point source in an intersection with a pollution source was and the quadrant analysis of vertical scalar fluxes in the same configuration was introduced in [5], but the geometry in these studies was relatively simple.

V. Fuka (✉) • J. Brechler
Department of Meteorology and Environment Protection, Faculty of Mathematics and Physics, Charles University in Prague, Prague 18000, Czech Republic
e-mail: Vladimir.Fuka@mff.cuni.cz; Josef.Brechler@mff.cuni.cz

L. Kukačka
Department of Meteorology and Environment Protection, Faculty of Mathematics and Physics, Charles University in Prague, Prague 18000, Czech Republic

Institute of Thermomechanics, Academy of Sciences of the Czech Republic, v. v. i., Prague 18200, Czech Republic
e-mail: Kukacka@it.cas.cz

D. Steyn and R. Mathur (eds.), *Air Pollution Modeling and its Application XXIII*, Springer Proceedings in Complexity, DOI 10.1007/978-3-319-04379-1_58,

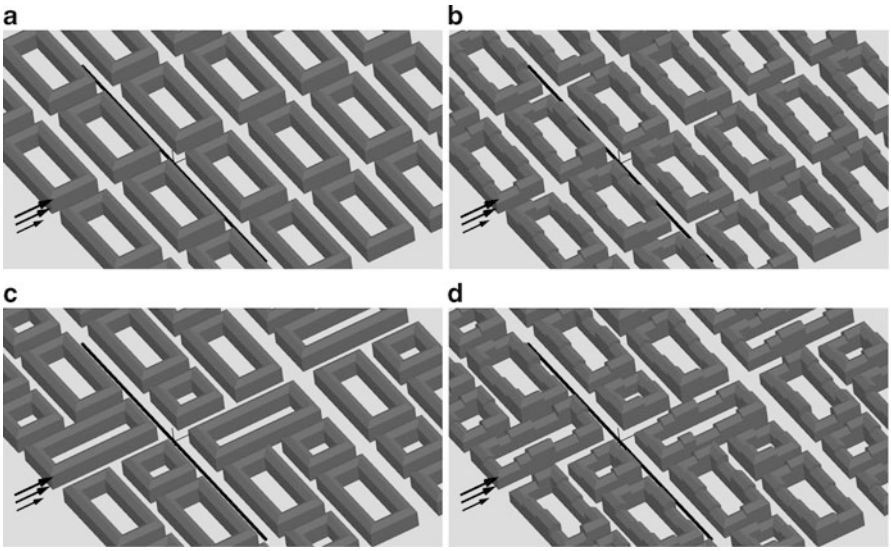


**Fig. 58.1** The urban geometries used for the simulations: (**a**) A1 (**b**) A2 (**c**) B1 (**d**) B2. The height of the medium building is 25 m. The origin of the coordinate system is shown by a cross of *thin lines*. The *thick line* is the line source, which is placed on the *y* axis from points [0,−200,0] to [0,200,0]. The wind flows in the x direction as shown by the *arrows*

This paper shows first results of the project, which aims to quantify the effect of varying urban geometry complexity on turbulence and pollution dispersion using both wind tunnel experiments and a numerical simulations. At this time, only small amount of experimental results is available and therefore this paper concentrates on simulation results, which will be used also as an aid for determining interesting areas for detailed measurements.

### *58.1.1 Problem Geometry*

We chose four types of geometry that will be denoted A1, A2, B1 and B2. The letter indicates ground plan of the buildings which can be seen in Fig. 58.1. All buildings in geometries with number 1 have the same height (25 m full-scale, 6.25 cm model scale). For geometries with number 2 there are three heights of buildings (20, 25 and 30 m) placed pseudo-randomly in a periodically placed Template.

A line source of passive scalar is placed in the center of the main street as shown in Fig. 58.1. The center of the line source is in the center of a main intersection Here we consider only flow perpendicular to this street and to the line source.

### *58.1.2 Numerical Model*

We used our in-house numerical model CLMM (Charles University Large-eddy Microscale Model) for presented computations [2]. The model uses large eddy simulation (LES) for the turbulent flow and solves the incompressible Navier-Stokes equations using the fractional step method.

The equations are discretized using the third order Runge-Kutta method and the semi-implicit Crank-Nicolson method. In space it uses the finite volume method on a uniform Cartesian grid. The spatial discretization of the fluxes is second order central with the exception of the momentum advection, which is fourth order central and scalar advection, which uses a third order positive method [3]. The nonlinear terms are filtered with filter width equal to two cell widths [7]. The sigma subgrid model [6] is used for computation of the subfilter (subgrid) scales.

## 58.2 Boundary Conditions

All current simulations were performed at the model scale (1:400) with a finite (1 m long) line source to be as close to the wind tunnel experiment as possible. The boundary conditions on horizontal domain boundaries were periodic. The flow was driven by a constant pressure gradient. The top boundary was a zero stress (free-slip) wall. The computational domain had dimensions 320 m × 560 m × 200 m for geometry A and 320 m × 585 m × 200 m for geometry B. The resolution was 2 m in all directions.

All concentration results were made non-dimensional using the formula

$$C^* = C\frac{UHL}{Q}, \tag{58.1}$$

where $C^*$ is the non-dimensional concentration, $C$ is the real concentration, $H$ is the reference height 25 m, $U$ is the reference velocity (average velocity above the intersection with the line source center in the height $2H$), $L$ is the source length and $Q$ is the source intensity. Velocities were made non-dimensional by dividing by $U$.

## 58.3 Results

The pedestrian level (1.5 m) concentration in the center of the main road parallel with the wind direction is plotted in Fig. 58.2a. The most distinctive feature of the cases with varying building height (A2 and B2) is sharper decrease of concentration

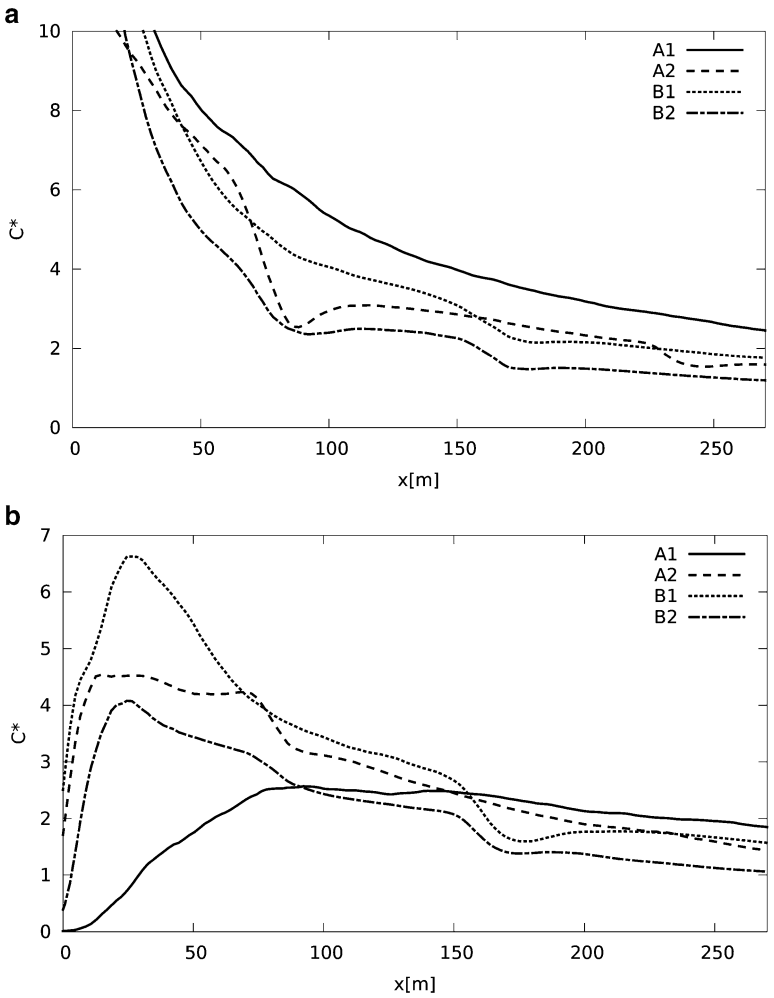


**Fig. 58.2** The graphs of the concentrations at line y = 0 m and (**a**) z = 1.5 m (**b**) z = 10 m

to distance around 80 m (the next intersection). Unlike the homogenous cases, the flow is asymmetric there, and the air is being mixed with the air from the other street, not directly influenced by the source. Behind this local minimum the curve is flat and approaches the curves of the homogenous cases. Case A1 has the highest concentrations and case B2 has the lowest concentration for all distances shown.

Higher, at the height of 10 m (Fig. 58.2b) another interesting feature exists. Here the air is the cleanest for case A1 up to the distance 90 m. It is because of a jet of clean air from area before the source, which is much longer in this (artificially) highly symmetric case.

**Table 58.1** The average scalar fluxes above the street with the source at the height 20 m

| Case | $<w^*c^*> 10^{-3}$ | $<w^*><c^*> 10^{-3}$ | $<w^{*\prime}c^{*\prime}> 10^{-3}$ |
|---|---|---|---|
| A1 | 2.28 | 3.04 | −0.77 |
| A2 | 3.00 | 2.61 | 0.39 |
| B1 | 5.17 | 4.80 | 0.38 |
| B2 | 4.75 | 4.39 | 0.36 |

Finally, in Table 58.1 we present the average vertical scalar fluxes above the street containing the source at the height of 20 m for all configurations. The fluxes are averaged over the domain $(-10\text{ m}, 10\text{ m}) \times (-140\text{ m}, 140\text{ m}) \times (20\text{ m})$ for geometries A and over $(-12.5\text{ m}, 12.5\text{ m}) \times (-210\text{ m}, 210\text{ m}) \times (20\text{ m})$.

## 58.4 Conclusions

First results of LES of air pollution dispersion in the idealized urban canopy with four cases with different geometry complexity showed the influence of the geometry on the dispersion. In most parts of the domain turbulent fluxes are smaller than advective fluxes, but they cannot be neglected. The results of this study will be re-evaluated after higher resolution runs, together with cases with different wind angles and compared to the wind-tunnel measurements that are to be conducted soon.

**Acknowledgments** This work has been supported by the Grant Agency of the Charles University under the grant no. 535412. The wind tunnel measurements for this project are performed in the environmental wind tunnel of the Institute of Thermomechanics, AS CR.

## References

1. Dabbert W, Hoydysh W, Schoring M, Yang F, Holynskyi O (1995) Dispersion modelling at urban intersection. Sci Total Environ 169:93–102
2. Fuka V, Brechler J (2011) Large eddy simulation of the stable boundary layer. In: Fořt J, Fürst J, Halama J, Herbin R, Hubert F (eds) Finite volumes for complex applications VI problems & perspectives, vol 4, Springer proceedings in mathematics. Springer, Heidelberg, pp 485–493
3. Hundsdorfer W, Koren B, vanLoon M, Verwer JG (1995) A positive finite-difference advection scheme. J Comput Phys 117:35–46
4. Kukačka L, Kellnerová R, Jurčáková K, Jaňour Z (2012) Analysis of scalar fluxes and flow within modelled intersection depending on the approach flow direction. In: Steyn DG, Trini Castelli S (eds) Air pollution modeling and its application XXI. Springer, Dordrecht, pp 113–118
5. Kukačka L, Nosek Š, Kellnerová R, Jurčáková K, Jaňour Z (2013) Quadrant analysis of turbulent pollution flux above the modelled street intersection. EPJ web of conferences, vol 45, p 01053. http://dx.doi.org/10.1051/epjconf/20134501053
6. Nicoud F, Toda HB, Cabrit O, Bose S, Lee J (2011) Using singular values to build a subgrid-scale model for large eddy simulations. Phys Fluids 23:085106

7. Vasilyev OV, Lund TS, Moin P (1998) A general class of commutative filters for LES in complex geometries. J Comput Phys 146:82–104
8. Wang X, McNamara KF (2007) Effects of street orientation on dispersion at or near urban street intersections. J Wind Eng Ind Aerodyn 95:1526–1540

## Questions and Answers

**Questioner name:** Christof Gromke

**Q:** Do your simulations substantiate that the more irregular the building arrangement is, the lower the (average) concentrations in the street network are?

**A:** Our results seem to suggest this conclusion; however, we must be careful. Especially in the simplest case, the regularity is artificial and does not exist in reality. Also, the wind is never exactly aligned to the streets for a long time. More wind directions have to be simulated.

**Questioner name:** Silvia Trini-Castelli

**Q:** Are you going to apply the same modelling system in the frame of Michelstadt modelling exercise in COST Action ES1006?

**A:** Yes, the model CLMM is being actively used in COST ES1006. Especially for the puff releases of hazardous substances LES offers possibility to assess the variability of individual puffs, but only of limited number of them, due to long computational times.

# Chapter 59
# Two-Phase Accidental Dense Gas Releases Simulations with the Lagrangian Particle Model Microspray

**L. Mortarini, G. Tinarelli, S. Trini Castelli, G. Carlino, and D. Anfossi**

**Abstract** In this work we simulated the Macdona (USA) chlorine railway accident with the Lagrangian dispersion model MicroSpray, twice: firstly by using the standard version and then by using a recently developed new two-phase module. MicroSpray was coupled with the diagnostic MicroSwift model, which provides the 3-D wind field in presence of obstacles and orography, and was used to test the two options. The results obtained in the two simulations, with and without the new module, are presented and the differences are discussed.

## 59.1 Introduction

In order to model the atmospheric dispersion of accidentally released dense gases, it is necessary to include algorithms accounting for the heat exchanges due to phase changes. When using dispersion models two options are possible: (i) to calculate source emissions rates by means of appropriate equations describing the two-phase dynamics, (ii) to use "off-line" calculation of these inputs.

Here we compare these two options, by simulating the Macdona (USA) chlorine railway accident [3] with the Lagrangian dispersion model MicroSpray. In the

L. Mortarini (✉) • S. Trini Castelli • D. Anfossi
Institute of Atmospheric Sciences and Climate, CNR, Torino I-10133, Italy
e-mail: L.Mortarini@isac.cnr.it; S.TriniCastelli@isac.cnr.it; D.Anfossi@isac.cnr.it

G. Tinarelli
ARIANET S.r.l., Milan I-20128, Italy
e-mail: G.Tinarelli@aria-net.it

G. Carlino
SIMULARIA S.r.l., Torino I-10125, Italy
e-mail: G.Carlino@simularia.it

D. Steyn and R. Mathur (eds.), *Air Pollution Modeling and its Application XXIII*,
Springer Proceedings in Complexity, DOI 10.1007/978-3-319-04379-1_59,

first run the standard dense-gas version was used, in the second one a recently developed two-phase module was tested. In the standard version the negative buoyancy effect is modeled coupling a modified set of Glendening et al. [2] equations with the energy conservation and state equations. A system of differential equations is solved for each stochastic particle to simultaneously evaluate the dynamics and the thermodynamics of the plume. In the new module, the two-phase dynamics is modeled accounting for the density effects and the thermodynamic transformations, assuming homogeneous thermodynamic equilibrium at each time step. After the initial flashing, the evolution of the liquid and vapor mass fraction of the contaminant, of the water vapor and dry air is evaluated. Information on the accident were taken from Hanna [3]. This yields the possibility or to start the simulations with source emissions estimated by widely used models, or to calculate the source emissions during the first stage of the simulation, when the contaminant is still in its liquid phase.

MicroSpray [5] was driven by the diagnostic MicroSwift model [4], which provides the 3-D wind field in presence of obstacles and orography, and it was used to test the two options.

## 59.2 Model Description

In the standard MicroSpray version the flashing of the liquid is not accounted for and an input source emission model is needed. The new version is able to deal with two-phase releases (vapor–liquid), aerosol evaporation and latent heat processes in the dispersing plume.

Immediately after the flashing the release is mostly vapor by volume and liquid by mass. Therefore, dealing with the physics of the aerosols implies the introduction of the liquid phase of the contaminant and, if necessary, of the water vapor entrained. The entrainment of ambient air produces a decreasing of the partial pressure and hence a cooling of the mixture below its boiling point and the condensation of water. The total mass of each particle needs to be split in five contributing parts: contaminant in vapor phase, contaminant in liquid phase, water in vapor phase, water in liquid phase and dry air. Consequently, a mass conservation equation needs to be written for each specie, contaminant, water and dry air. These equations are coupled with three momenta conservation equations and with the energy conservation equation (enthalpy balance). The horizontal momenta conservation equations were modified, introducing a negative term that represents the drag force, which strongly influences the dynamics of turbulent jets close to the source. The liquid aerosol and vapor are taken to be in thermodynamic equilibrium, therefore a single temperature characterizes the cloud (homogeneous equilibrium model). To solve the new system of equations we utilized the equation of state for vapor mixtures proposed by Ermak [1].

## 59.3 Results and Discussion

Figure 59.1 shows the evolution of the vertical velocity and the density evaluated by the model for a chlorine release with different initial conditions [3]. To compare the two cases, we fix the origin of the axes of the pseudo-gas simulation at the instant when the liquid phase is exhausted in the two-phases runs (dashed vertical line and top labels in Fig. 59.1). The black triangles refer to a simulation where there is no liquid phase and the initial condition is set after the evaporation process took place: this corresponds to method 2 in Hanna [3] and to the previous version of MicroSpray. The grey triangles refer to a mixture of vapor (20 %) and liquid (80 %) released in dry ambient air, while the dots represent the same two-phase mixture released in an environment with the 10 % of relative humidity. The density evolution with time shows that after 0.1 s the two-phase simulations have reached the pseudo-gas initial density and after 0.4 s the liquid contaminant mass fraction

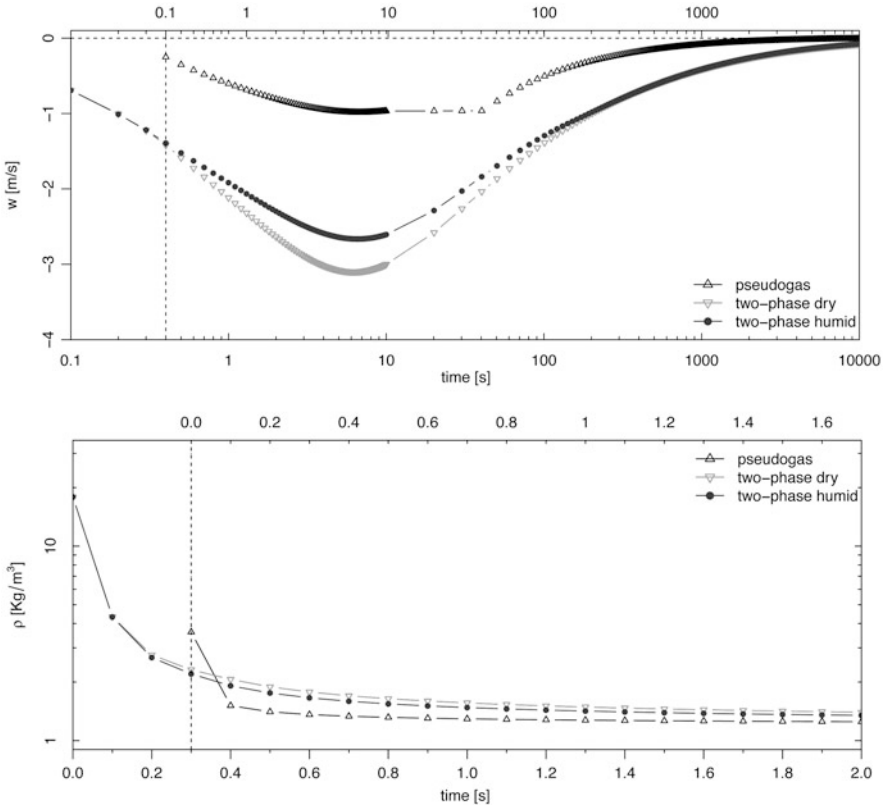


**Fig. 59.1** Vertical velocity (*top*) and density (*bottom*) as functions of the simulation time

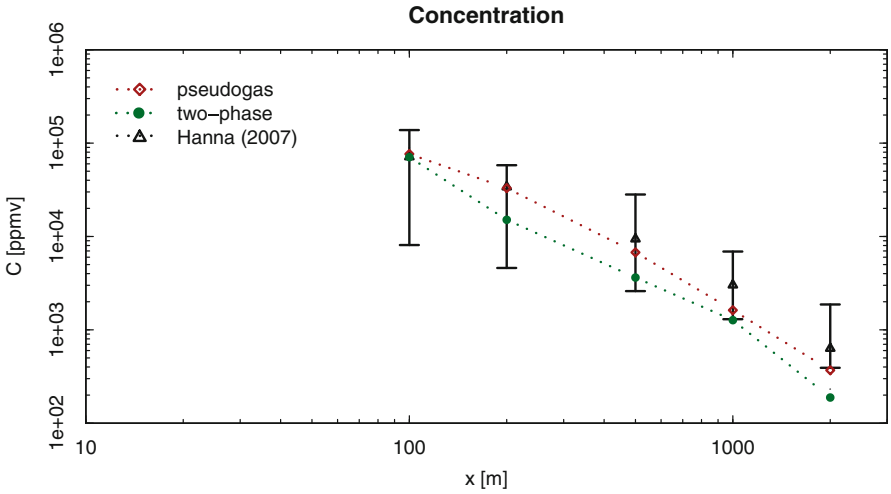


**Fig. 59.2** Ten-minutes averaged concentration as a function of the distance from the emission

is zero (not shown). In the two-phase approach the vertical velocity becomes larger than in the pseudo-gas because the liquid phase causes a smoother decrease of the plume density. A second consequence of the density difference is found close to the ground where the density produces an outflow velocity that accelerates the plume in a different amount. Figure 59.2 shows the chlorine maximum concentration averaged on 10 min: the two-phase model results are slightly smaller and this is probably due to the initial faster horizontal speed. The figures well highlight the different evolution of the dynamics and thermodynamics in the first stage after the emission, with its consequences on the estimation of the ground level concentrations.

## References

1. Ermak D (1990) User's manual for SLAB: an atmospheric dispersion model for denser-than-air releases. UCRL-MA-105607, Lawrence Livermore National Laboratory, Livermore, 144 pp
2. Glendening JW, Businger JA, Farber RJ (1984) Improving plume rise prediction accuracy for stable atmospheres with complex vertical structure. J Air Pollut Control Assoc 34:1128–1133
3. Hanna S (2007) Comparisons of six models using three chlorine release scenarios (Festus, Macdona, Graniteville). Report number P082. Research Foundation for Health and Environmental Effects, Arlington, VA, 58 pp
4. Tinarelli G, Brusasca G, Oldrini O, Anfossi D, Trini Castelli S, Moussafir J (2007) Micro-Swift-Spray (MSS) a new modelling system for the simulation of dispersion at microscale. General description and validation. In: Air pollution modelling and its applications XVII. Springer, New York, pp 449–458

5. Tinarelli G, Mortarini L, Trini Castelli S, Carlino G, Moussafir J, Olry C, Armand P, Anfossi D (2012) Review and validation of MicroSpray, a Lagrangian particle model of turbulent dispersion. In: Lin JC, Brunner D, Gerbig C, Stohl A, Luhar A, Webley P (eds) Lagrangian modeling of the atmosphere, AGU geophysical monograph 200. American Geophysical Union, Washington, DC, pp 311–327

## Questions and Answers

**Questioner Name:** Paul Makar

**Q:** (1) Are aerosol microphysics' properties included in the model? Or are the thermodynamics of the model bulk phase only? Factors like the Kohler effect could affect the timing of the approach to equilibrium for liquid/gas, for example.

**A:** In Lagrangian particle models the single particle has no volume and represents a given tracer mass, therefore it does not correspond to, for instance, a drop. In our approach we assign to the particle five mass fractions: tracer, liquid and gas, water, vapor and liquid, dry air. The model treats the thermodynamics with a bulk approach and the particle's mass fraction evolution is driven by it.

**Q:** (2) Have you considered estimating the emissions of 'intermediate volatility compounds' using your model?

**A:** Given the former answer, this approach was not considered.

**Questioner Name:** Steve Hanna

**Q:** Can your model treat

1. jets at any angle
2. deposition to the ground or vegetation and
3. underlying complex terrain?

**A:** Microspray includes deposition to the ground and explicitly accounts for the complex terrain. The model can also treat jets at any angle. Vegetation is not treated in an explicit way but enters through the roughness and land use parameters.

# Chapter 60
# Modeling of the Urban Heat Island and its effect on Air Quality using WRF/WRF-Chem – Assessment of mitigation strategies for a Central European city

**Joachim Fallmann, Stefan Emeis, and Peter Suppan**

**Abstract** In 2050 the global fraction of urban population will increase to over 69 %, which means that around 6.3 billion people are expected to live in urban areas (UN, Urban population, development and environment. http://www.un.org/esa/population/publications/2011UrbanPopDevEnv_Chart/urban_wallchart_2011-web-smaller.pdf, 9 May 2013, 2011). Cities are the predominant places for human beings to settle down, thus becoming more vulnerable to extreme weather events aggravating phenomena like heat stress and decreasing air quality aroused by inner city pollution. Affecting human health and having the tendency to occur more likely in the future (Solomon et al. Contribution of working group I to the fourth assessment report of the intergovernmental panel on climate change, 2007. Cambridge University Press, Cambridge/New York, 2007), finding mitigation strategies to counteract future air quality related problems and ways to sustain development is of great importance. In this study, the mesoscale numerical model WRF/WRF-Chem is used on regional scale to simulate the effect of urban planning scenarios on dynamical processes impressing urban climate and air quality.

## 60.1 Introduction

Urban Heat Island (UHI) describes the tendency for an urbanized area, because of its radiative and geometrical features, to remain warmer than its rural surroundings and thus generating its own microclimate [3]. Low albedo materials of impervious surfaces like pavements, roofs and asphalt tend to absorb a bulk of the incoming

J. Fallmann (✉) • S. Emeis • P. Suppan
Institute of Meteorology and Climate Research, Atmospheric Environmental Research (IMK-IFU), Campus Alpin, Karlsruhe Institute of Technology (KIT), Kreuzeckbahnstr. 19, 82467 Garmisch-Partenkirchen, Germany
e-mail: joachim.fallmann@kit.edu

D. Steyn and R. Mathur (eds.), *Air Pollution Modeling and its Application XXIII*, Springer Proceedings in Complexity, DOI 10.1007/978-3-319-04379-1_60,

solar radiation, and re-radiate solar energy in form of infrared heat [5]. The annual mean temperature of a large city is about 1–3 °C (UHI intensity) higher than in the outer areas, on individual calm, clear nights even up to 12 °C [3]. In addition to health problems produced by rising temperatures itself, the effect of accelerating photochemical reaction rates will in turn worsen the inner-city air quality [2]. Specific urban planning strategies like green roofs or facades and highly reflective materials are able to reduce the negative effects of the UHI and mitigate future problems connected to air quality. By using WRF/WRF-Chem on regional scale, coupled to urban parameterization schemes [1], it is the goal to analyze the evolution of urban climate while applying common mitigation strategies Area of interest is the area of Stuttgart, located in a valley, in one of the warmest regions around Germany.

## 60.2 Modelling System

For representing the 3-dimensional structures of urban areas, urban parameterization schemes are applied [1] and coupled to NOAH Land Surface Model LSM. By using 33 classes CORINE land cover classification, the distinction between three urban subclasses (high- and low density residential and commercial), serving as input for the urban canopy model, is possible. A three domain basic nesting is conducted, with the finest resolution reaching 1 km (Fig. 60.1).

Amongst others, two urban approaches are discussed in this study and applied for the urban area of Stuttgart for different urban planning scenarios. The Single Layer Urban Canopy Model SLUCM and the multi layer Building Effect Parameterization approach BEP (Fig. 60.2) [1].

For each urban class, parameters are defined to represent urban properties (e.g. building height, street width, surface albedo or vegetation cover) according city structure accounting for building and street orientation and characteristics of buildings, as well as thermodynamic properties and roughness features.

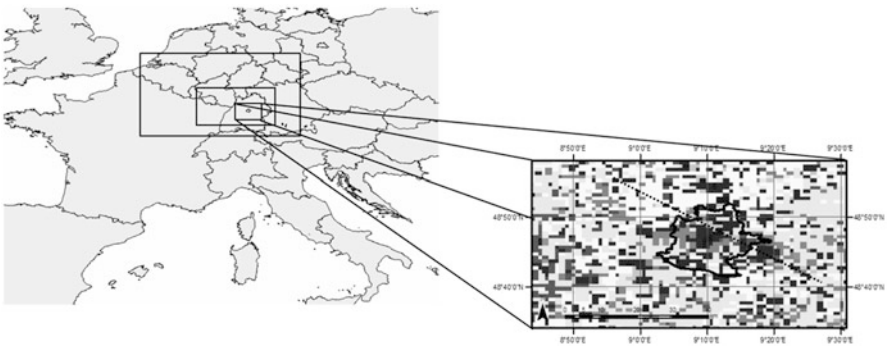

**Fig. 60.1** Location of modelling domains (*left*) (Source: map adapted from [9]) and urban area of Stuttgart, equal to size of domain 3 (*right*) representing an area of 61 × 49 km, and USGS classified land cover with 1 km resolution [10]

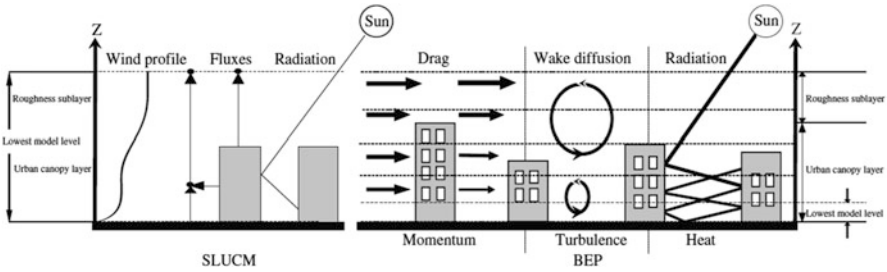


**Fig. 60.2** Schematic figure of SLUCM [7] – *left* and BEP [8] – *right*; both show differences in representing the processes in the urban canopy layer [1]

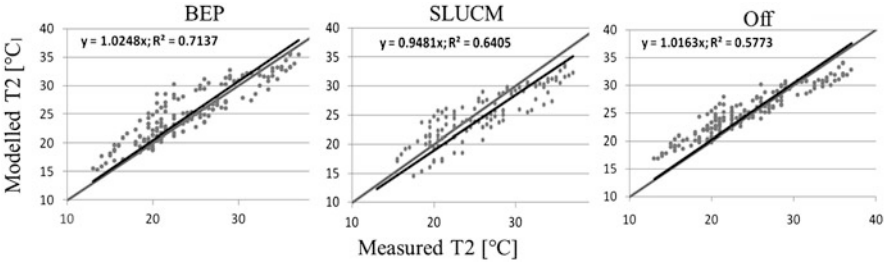


**Fig. 60.3** Measurement compared with modeled temperature for the particular parameterization scheme respectively, BEP (Martilli 2002) and SLUCM (Kusaka 2001) and 'switch off' mode were the urban canopy parameterization is neglected and the different surface properties are defined only over land use tables

In the course of a sensitivity study, modeled 2 m potential temperatures are being compared against observation data, the canopy model which reveals the largest correlation coefficient is applied for further investigations (Fig. 60.3). For the numerical study a time period with stable weather conditions was chosen; with clear sky, weak wind speeds and regular incoming solar radiation (Aug 11 – Aug 18, 2003).

## 60.3 Results and Discussion

In response to extreme heat events like during the 11–18 Aug 2003, city planners often introduce green surfaces as tools to reduce the effects of heat. This scenario will be simulated in the model by making two 'City Park' simulations. The first is a 'Central Park' scenario where 25 urban classified grid cells in the center of Stuttgart are replaced by natural vegetation. This change accounts for 25 $km^2$, or approximately 12 % of the total city area. The other urban greening scenario ('Many Parks') will be represented by the inclusion of several smaller parks scattered across the urban area. The sizes of the parks within the city borders are

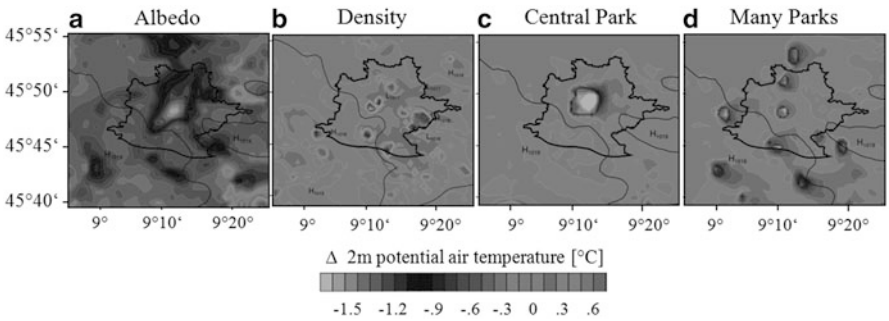


**Fig. 60.4** Difference in potential 2 m-air temperature between ‘Real Case’ and ‘Scenario’. From *left* to *right*: ‘Albedo’ case with changed albedo for roofs and walls (**a**), Density with modified proportion street width/building height (**b**) and the two urban greening scenarios with one big park (**c**) and a number of smaller parks (**d**)

**Table 60.1** Impact of scenarios on UHI formation expressed as difference between mean urban and mean rural 2 m potential temperatures, the maximum in modeled temperature for the period Aug 11–18 as well as standard deviation and mean value of the urban temperatures

| Scenario | Albedo | Density | Many parks | Big park | Real case |
|---|---|---|---|---|---|
| ⊖ mean urban [°C] | 31.5 | 32.4 | 32.5 | 32.3 | 33.1 |
| ⊖ max [°C] | 31.9 | 33 | 33.5 | 33.3 | 34.3 |
| Std dev. [°C] | 0.32 | 0.48 | 0.5 | 0.43 | 0.6 |
| **UHI;** delta ⊖ | **0.84** | **1.32** | **1.47** | **1.19** | **2.52** |

equal and their total area is the same as in the ‘Central Park’ simulation. Another commonly known measure to reduce surface temperatures is the modification of the reflective characteristics of impervious surfaces Changing the albedo of rooftops and building walls in the urban parameter table from 0.2 to 0.7 (‘Albedo’), this would represent reflective white paintings. The third case study ‘Density’ reflects a direct intervention in the urban landscape, by increasing the proportions of roof width to street width by 20 %.

Referring to Fig. 60.4 and Table 60.1, the changing of reflective properties of roof and wall surfaces (‘Albedo’) case, tends to have the biggest impact on UHI formation. To investigate the scenario-effect on air quality, in this case surface ozone, WRF-Chem is coupled to urban WRF model, using the MACC 7 km emission inventory. Finest resolution is decreased to 3 km and domain size is $\sim 150 \times 200$km.

Figure 60.5 shows the development of near surface ozone concentration in the course of a day (August 13 2003) comparing different urban planning scenarios. The 8-h mean (12–20) for the real case without applying any measure accounts for 150 $\mu g/m^3$. Using extensive roof greening, can reduce this amount by 14 % down to 130 $\mu g/m^3$, whereas changed roof albedo or building density is able to decrease the 8-h mean of surface ozone by 7 % (140 $\mu g/m^3$). For Ozone being

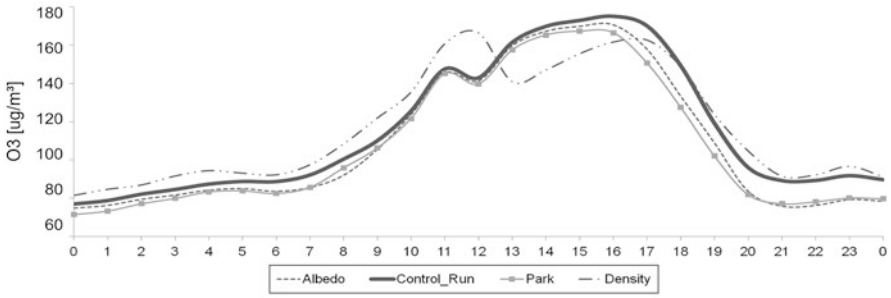


**Fig. 60.5** Near surface ozone concentration in the course of a day for August 13 2003 for 'Real Case' (Control Run) and 'Scenario' expressed in $\mu g/m^3$, for an urban location within the city centre of Stuttgart

a secondary compound, closely linked to NO2 and NO concentration through photolysis reactions, it is also advisable to look at these concentrations as well. For this reason it is planned for further studies to concentrate on these processes and further to analyze the effect of UHI mitigation strategies on aerosol formation.

## References

1. Chen F et al (2011) The integrated WRF/urban modelling system: development, evaluation, and applications to urban environmental problems. Int J Climatol 31(2):273–288; Wiley
2. EPA (2008) Reducing urban heat Islands: compendium of strategies – urban heat Island basics; http://www.epa.gov/hiri/resources/pdf/BasicsCompendium.pdf. 08/04/2013
3. Oke TR (1982) The energetic basis of the urban heat island. John Wiley & Sons, Ltd; Quart J R Meteorol Soc 108(455):1–24
4. Solomon S et al (2007) Contribution of working group I to the fourth assessment report of the intergovernmental panel on climate change, 2007. Cambridge University Press, Cambridge/ New York
5. Taha H (1997) Urban climates and heat islands: albedo, evapotranspiration, and anthropogenic heat. Energy Build 25(2):99–103
6. UN (2011) Urban population, development and environment. http://www.un.org/esa/population/publications/2011UrbanPopDevEnv_Chart/urban_wallchart_2011-web-smaller.pdf. 09/05/2013
7. Kusaka H, Kondo H, Kikegawa Y, Kimura F (2001) A simple single-layer urban canopy model for atmospheric models: comparison with multi-layer and slab models. Bound-Layer Meteor 101(3):329–358
8. Martilli A, Clappier A, Rotach MW (2002) An urban surface exchange parameterisation for mesoscale models. Bound-Layer Meteorol 104(2):261–304
9. Sandvik B (2009) World borders dataset. Online available at: http://thematicmapping.org/downloads/world_borders.php. 20/01/2014
10. USGS (2006) USGS land cover classification. Online available at: http://landcover.usgs.gov/pdf/anderson.pdf. 02/11/2013

# Chapter 61
# Assessment of Three Dynamical Urban Climate Downscaling Methods

**Rafiq Hamdi, Hans Van De Vyver, Rozemien De Troch, Piet Termonia, and Andy Delcloo**

**Abstract** A new high-resolution dynamical downscaling strategy to examine how rural and urban areas respond to change in future climate, is presented. The regional climate simulations have been performed with a new version of the limited-area model of the ARPEGE-IFS system running at 4-km resolution coupled with the Town Energy Balance scheme (TEB). In order to downscale further the regional climate projections to a urban scale, at 1 km resolution, a stand-alone surface scheme is employed in offline mode. We performed downscaling simulations according to three model set-ups: (i) reference run, where TEB is not activated neither in 4-km simulations nor in 1-km urban simulation, (ii) offline run, where TEB is activated only for 1-km urban simulation and (iii) inline run, where TEB is activated both for regional and urban simulations. The applicability of this method is demonstrated for Brussels Capital Region, Belgium. For present climate conditions, another set of simulations were performed using European Center for Medium-Range Weather Forecasts global reanalysis ERA40 data. Results from our simulations indicate that the reference and offline runs have comparable values of daytime and nocturnal urban heat island (UHI) and lower values than the inline run. The inline values are closer to observations. In the future climate, under and A1B emission scenario, the three downscaling methods project a decrease of daytime UHI between −0.24 and −0.20 °C, however, their responses are different for nocturnal UHI: (i) reference run values remains unaltered, (ii) for the offline runs, the frequency of present

R. Hamdi (✉) • H. Van De Vyver • A. Delcloo
Royal Meteorological Institute of Belgium, Brussels, Belgium
e-mail: rafiq.hamdi@meteo.be; hans.vandevyver@meteo.be; andy.delcloo@meteo.be

R. De Troch • P. Termonia
Royal Meteorological Institute of Belgium, Brussels, Belgium

Department of Physics and Astronomy, Ghent University, Ghent, Belgium
e-mail: rozemien.detroch@ugent.be; piet.termonia@ugent.be

D. Steyn and R. Mathur (eds.), *Air Pollution Modeling and its Application XXIII*,
Springer Proceedings in Complexity, DOI 10.1007/978-3-319-04379-1_61,

climate weak nocturnal UHI decreases to the benefit of negative UHIs leading to a significant decrease in the nocturnal UHI over the city, (iii) for the inline run, nocturnal UHIs stays always positive but the frequency of the strong UHI decreases significantly in the future by 1 °C.

## 61.1 Introduction

Today, scientists, urban planners and policy makers are beginning to work together to understand and monitor the interaction between urban areas and climate change and to consider adaptation and mitigation strategies. To maintain or improve the quality of living in cities, urban planners need detailed information on future urban climate on residential scale. Such information is provided by climate models. However, because impervious surfaces cover only less than 1 % of the world's land area, most of the global circulation models that are utilized for climate change research do not account for urban surfaces. In fact, cities affect the local weather by perturbing the wind, temperature, moisture, turbulence, and surface energy budget field. One very known phenomena is the so-called urban heat island (UHI) effect where urban air temperatures are substantially higher than corresponding temperatures in the surrounding rural areas. The last official report from the Intergovernmental Panel on Climate Change IPCC AR4 recognizes that urban warming in addition to greenhouse gas has not explicitly been taken into account in global climate change simulations. Therefore, in order to provide detailed climate change projections to the regional scale required for impact studies over urban areas, researchers from the RMI have proposed in 2012 a new method to quantify the averaged present and future UHI for each square kilometer over an area that covers the entire Brussels capital area [2]. The regional climate simulations have been performed with a new version of the limited-area model of the ARPEGE-IFS system running at 4-km [1] resolution coupled with the Town Energy Balance scheme (TEB) [3]. In order to downscale further the regional climate projections to a urban scale, at 1 km resolution, a stand-alone surface scheme is employed in offline mode. As a first step, the applicability of the method was demonstrated for the period 1961–1990. Then, the evolution of UHI of Brussels (Belgium) for the period 2071–2100 was studied in the context of the ARPEGE global climate model scenario A1B that was proposed by the IPCC. We performed downscaling simulations according to three model set-ups: (i) the reference run representing a control simulation where the TEB scheme is not activated neither in the 4-km regional climate simulation nor in the 1-km urban climate simulation, (ii) the offline run where the TEB scheme is activated only for the 1-km urban climate simulation. This run mimics the situation where the atmospheric forcing coming from the regional climate simulations did not include any signature of the urban heat island. And (iii) the inline run where the TEB scheme is activated both for the regional and urban climate simulations.

## 61.2 UHI of Brussels for the Present Climate

The nocturnal and daily UHI intensity is defined as the difference in minimum and maximum, respectively, temperature between Uccle (suburban area 6 km south of the city center of Brussels) and the rural station Brussegem. The observed summer mean of each year between 1955 and 2006 is plotted with the linear trends. The UHI calculated in the period 1961–1990 with the ARPEGE-Climate driven simulations for the reference (ARP_RF), offline (ARP_OF), and inline (ARP_IN) runs are also plotted. It can be noticed that the urban simulations using TEB in offline mode results in an underestimation of nocturnal and daytime UHI (Fig. 61.1).

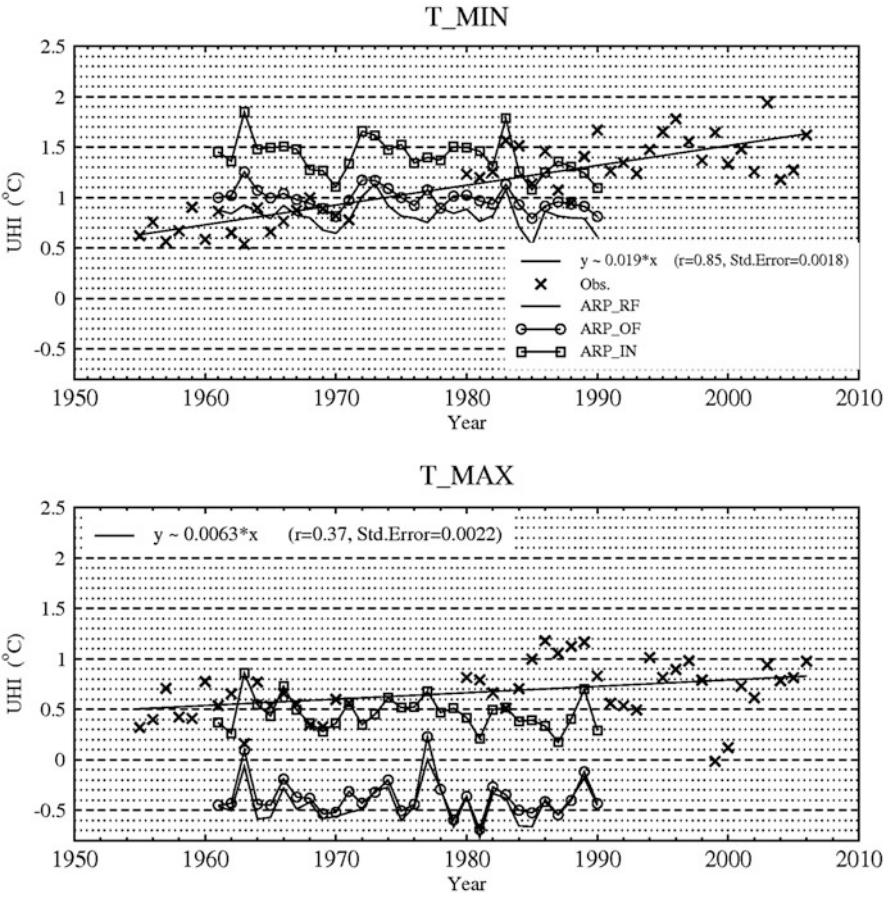


**Fig. 61.1** Time series (1955–2006) of the summer-mean UHI [°C] at Uccle for the minimum (*top*) and maximum (*bottom*) temperature estimated as the difference between Uccle and the rural station Brussegem with the linear trend (r is the correlation coefficient and Std. Error is the standard error of the regression coefficient, no data were found for Brussegem between 1972 and 1979). Also shown are the UHI calculated in the period 1961–1990 with the ARPEGE-Climate driven simulations for the reference (ARP_RF), offline (ARP_OF), and inline (ARP_IN) runs

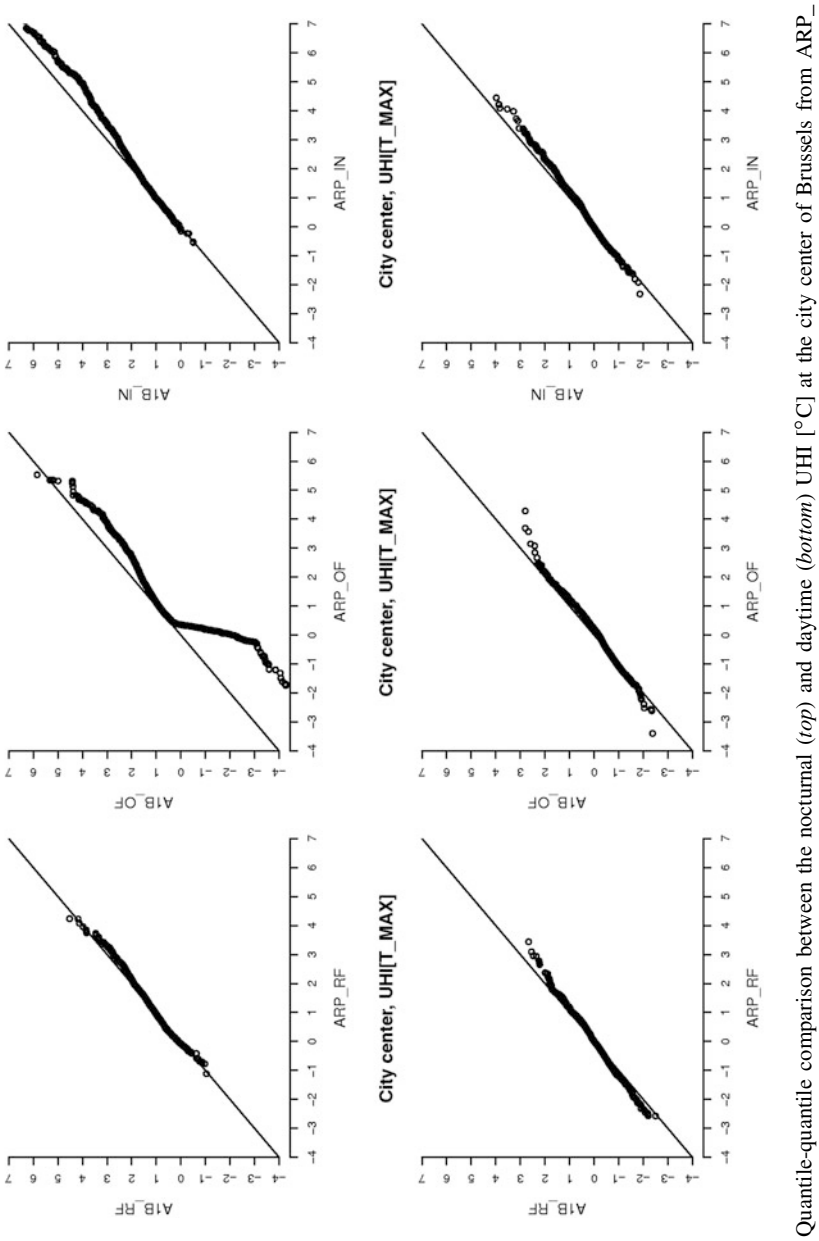


**Fig. 61.2** Quantile-quantile comparison between the nocturnal (*top*) and daytime (*bottom*) UHI [°C] at the city center of Brussels from ARP_ and A1B_ ARPEGE-Climate driven experiment. The *three columns* correspond to the reference, offline, and inline runs

## 61.3 UHI of Brussels for the Future Climate

The figure below presents a quantile-quantile comparison between the nocturnal and daytime UHI at the city center of Brussels from present climate conditions and A1B_ ARPEGE-Climate driven experiment. The nocturnal UHI simulated by the reference run remains unaltered and there are no changes in either the frequency or magnitude of the extreme heat islands. The offline run presents a significant decrease in the nocturnal UHI over the city center (−0.36 °C) and the suburban areas (−0.28 °C) while there is an increase over the rural areas. The frequency of present climate weak nocturnal UHI (between 0 and 1 °C) decreases to the benefit of negative UHIs in the future climate. The mechanism by which this occurs is related to changes in incoming long-wave radiation at night. For the inline run the nocturnal UHIs stays always positive with values between 0 and 7 °C. However, the frequency of the strong UHI (>3 °C) decreases significantly in the future climate by 1 °C (Fig. 61.2). This is linked with a soil dryness during the summer where the projected cumulated summer precipitation over the Brussels Capital Region decreased by 35 %.

## References

1. Gerard L, Piriou JM, Brozková R, Geleyn JF, Banciu D (2009) Cloud and Precipitation parameterization in a Meso-Gamma-Scale operational weather prediction model. Mon Weather Rev 137:3960–3977
2. Hamdi R, Van de Vyver H, De Troch R, Termonia P (2013) Assessment of three dynamical urban climate downscaling methods: Brussels's future urban heat island under an A1B emission scenario. Int J Climatol. doi:10.1002/joc.3734
3. Masson V (2000) A physically-based scheme for the urban energy budget in atmospheric models. Bound Layer Meteorol 94:357–397

# Chapter 62
# Validating the RIO-IFDM Street Canyon Coupling over Antwerp, Belgium

**Wouter Lefebvre, Martine Van Poppel, Bino Maiheu, Stijn Janssen, Evi Dons, and Clemens Mensink**

**Abstract** Further integration of different spatial scales in concentration modeling is important for assessing the European limit values for $NO_2$. The local $NO_2$-concentrations are influenced by the regional background, the local emissions and the street canyon effects. Therefore, it is important to combine all these contributions in the model chain that one wants to use for such an assessment. In this paper, we present the results of a coupled model chain, using an intelligent measurement interpolation tool, a bi-gaussian plume model and a street canyon model to simulate the concentrations over the city of Antwerp, Belgium. The results of this model campaign are validated against weekly averaged $NO_2$ measurements at 49 locations in the city of Antwerp, during both a winter and a summer week. It is shown that the model performed well, with an $R^2$ between 0.73 and 0.90, RMSE around 5 $\mu g/m^3$ and small biases. Next to this validation, the performance of different model parts is shown, in order to provide information on the importance of the different components.

## 62.1 Introduction

It is essential for the modelling community to create a reliable modelling framework which is able to capture both the spatial diverseness of the concentrations on a street-level scale, while still providing complete coverage over the studied region. This paper evaluates such an integrated modeling framework against independent measurements in the city of Antwerp. A comparison with measured concentration

W. Lefebvre (✉) • M. Van Poppel • B. Maiheu • S. Janssen • E. Dons • C. Mensink
VITO, Boeretang 200, 2400 Mol, Belgium
e-mail: Wouter.lefebvre@vito.be; martine.vanpoppel@vito.be; bino.maiheu@vito.be; stijn.janssen@vito.be; evi.dons@vito.be; Clemens.mensink@vito.be

D. Steyn and R. Mathur (eds.), *Air Pollution Modeling and its Application XXIII*, Springer Proceedings in Complexity, DOI 10.1007/978-3-319-04379-1_62,

over two seasons is presented and the performance of different model components is discussed. As such, we can be assured that major characteristics of the concentration distribution are captured by the model.

## 62.2 Measurements

Measurements reported in this paper are part of a larger multidisciplinary study (HAEPS; Health Effects of Air Pollution in Antwerp Schools) dealing with health impact of traffic related air pollution on school children. To assess the exposure of the children at home, air quality measurements were performed at selected home locations.

$NO_2$ was measured over 7 days at different locations (chosen to represent different ranges in concentration fields such as street canyon locations, urban traffic locations and urban background locations) in an urban area using diffusive sampling tubes (IVL, Sweden; Ferm and Svanberg [1]) resulting in weekly average concentrations. The locations are characterised by differences in traffic exposure. Diffusive samplers are placed in a dedicated rain shield attached to a rainwater pipe, a balcony or a streetlamp, near the front door.

At each location, $NO_2$ was monitored during late spring (May–June 2011) and late autumn (November–December 2011). In both seasons, measurements were performed at 8 locations simultaneously during 5 consecutive weeks resulting in 40 locations sampled. In addition, all 40 locations were sampled simultaneously for 1 week in each season, including also 12 extra locations, resulting in 52 locations. During the entire sampling campaign, $NO_2$ was measured at an urban location of the AQ monitoring network.

## 62.3 Model Setup

An integrated model chain has been set up to assess the air quality at the local (street level) scale, including both regional variability as well as local variation in sources of air pollution. The different components of the model chain are discussed in the next paragraphs. The MIMOSA4 emission model [7, 8] is used to calculate local traffic emissions. The resulting spatially and temporally distributed emissions are used in the bi-Gaussian model IFDM [4, 5]. These results are coupled to output of the land-use regression model RIO [2, 3]. A method to avoid double counting of the (local) emissions by the different models is applied [5]. Finally the output of the IFDM model is coupled as boundary conditions to the IFDM street canyon module. In all these coupling steps, care is taken to consistently take into account the fast $NO_x$-$O_3$-chemistry. Finally, the results of the IFDM model and the IFDM street canyon module are combined using a post processing tool, so that the street canyon concentrations are confined to the street canyons, and the IFDM roof top concentrations are used outside of the canyons.

The integrated model chain has been used to perform simulations for the city of Antwerp, using meteorological data of a local meteo station, situated in the northern part of the city.

## 62.4 Validation

First of all, we compare all weekly model values to all weekly measurement values (not shown). This yields a very good correlation ($R^2 = 0.86$), combined with a small RMSE (5.28 $\mu g/m^3$) and a low bias (1.5 $\mu g/m^3$). However, as we have combined measurements at different locations in both seasons for several separate weeks the resulting correlation might be artificially increased. This is due to the fact that the late autumn concentrations are systematically higher than the late spring concentrations. As this seasonal effect is covered by RIO (which takes into account the concentrations measured in the stations of the telemetric network around Antwerp), we automatically get a large $R^2$ by using all the measurement values together. Therefore, we will focus our analysis on the two weeks with the majority of the data, one in autumn, and one in spring (Fig. 62.1, lower right). This leads to a similar $R^2$ (0.87), RMSE (5.31 $\mu g/m^3$) and a somewhat higher bias (1.91 $\mu g/m^3$). However, if we only look at concurrent measurements, i.e., measurements that have been made during the same week, we get an $R^2$ of respectively 0.80 and 0.62 in spring and autumn, an RMSE between 5 and 6 $\mu g/m^3$ for both weeks and a bias ranging from almost 5 $\mu g/m^3$ in spring to about $-1$ $\mu g/m^3$ in autumn. The latter values do not mix spatial and temporal correlation and are thus a good indication of the spatial predictive power of the model. As can be seen in Fig. 62.1, lower right, the model underestimates the higher concentrations and overestimates the lower concentrations. The spatial and temporal variability of the model is thus slightly too small. The underestimation of the spatial variability is also represented by the slope of the linear regression of the modeled values on the measurements. This slope is found to be 0.67, well under the ideal case of slope 1.

## 62.5 Conclusion

This paper presents an integrated model framework for calculating concentrations at the urban to street level scale. The method is validated by an $NO_2$ monitoring campaign, using passive samplers in a late spring and late autumn period. The validation analysis show that the model is able to represent the spatial variability within an urban environment. As a result, the model can be used to improve the exposure assessment of people living in the urban area and to complement fixed monitoring stations that are often only limited in number in a city.

The validation analysis was performed for the different steps in the model chain revealing the strengths of the different components in creating these concentration maps. First of all, it was shown that RIO is well able to represent the differences

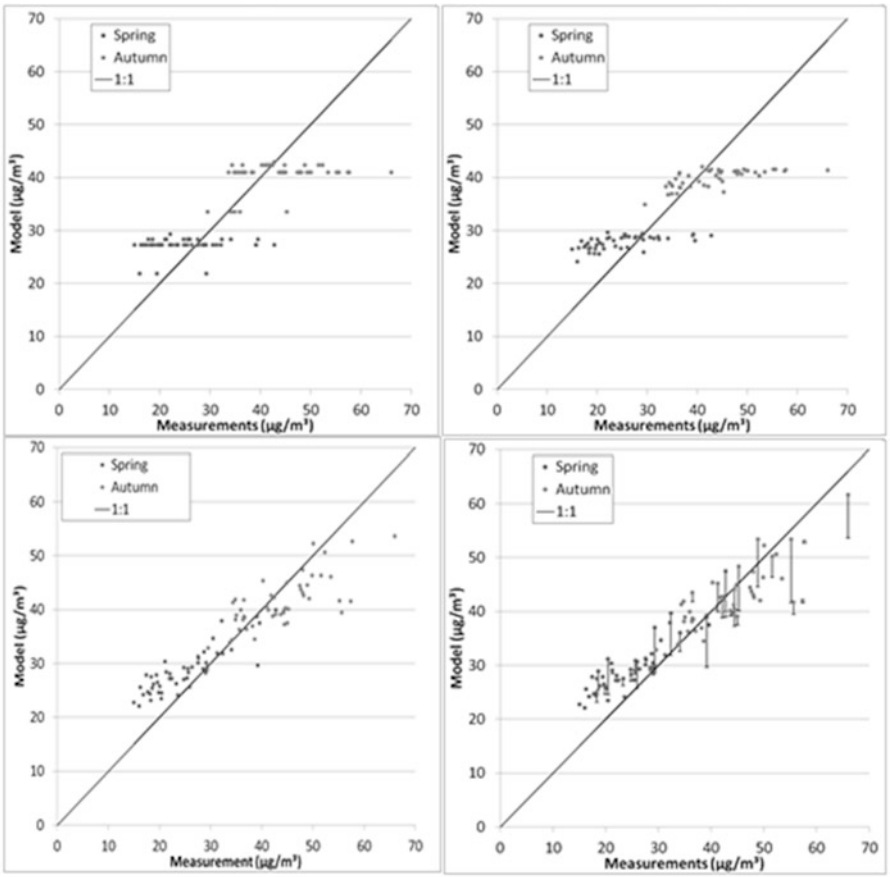


**Fig. 62.1** Validation plots for different steps in the methodology. *Upper left*: for RIO. *Upper right*: for the interpolated RIO. *Lower left*: for RIO + IFDM. *Lower right*: the complete model chain. Every point represents the weekly averaged concentration (in $\mu g/m^3$) measured (X-axis) and modeled (Y-axis). The *black lines* on the graph represent the street canyon contribution

between the seasons. However, due to the relatively low resolution, it is not capable of representing the spatial variability between the different locations. Interpolating these RIO-results to the measured locations does not add much skill to the model. The use of the plume model improves strongly the accuracy of the results. In particular, the RMSE decreases and the $R^2$ soars. This last parameter improves even more when taking into account street canyons.

More information can be found in Lefebvre et al. [6].

## References

1. Ferm M, Svanberg P-A (1998) Cost-efficient techniques for urban- and background measurements of $SO_2$ and $NO_2$. Atmos Environ 32:1377–1381
2. Hooyberghs J, Mensink C, Dumont G, Fierens F (2006) Spatial interpolation of ambient ozone concentrations from sparse monitoring points in Belgium. J Environ Monit 8:1129–1135. doi:10.1039/b612607n
3. Janssen S, Dumont G, Fierens F, Mensink C (2008) Spatial interpolation of air pollution measurements using CORINE land cover data. Atmos Environ 42(20):4884–4903. doi:10.1016/j.atmosenv.2008.02.043
4. Lefebvre W, Fierens F, Trimpeneers E, Janssen S, Van de Vel K, Deutsch F, Viaene P, Vankerkom J, Dumont G, Vanpoucke C, Mensink C, Peelaerts W, Vliegen J (2011) Modeling the effects of a speed limit reduction on traffic-related elemental carbon (EC) concentrations and population exposure to EC. Atmos Environ 45:197–207. doi:10.1016/j.atmosenv.2010.09.026
5. Lefebvre W, Vercauteren J, Schrooten L, Janssen S, Degraeuwe B, Maenhaut W, de Vlieger I, Vankerkom J, Cosemans G, Mensink C, Veldeman N, Deutsch F, Van Looy S, Peelaerts W, Lefebre F (2011) Validation of the MIMOSA-AURORA-IFDM model chain for policy support: modeling concentrations of elemental carbon in Flanders. Atmos Environ 45(37):6705–6713. doi:10.1016/j.atmosenv.2011.08.033
6. Lefebvre W, Van Poppel M, Maiheu B, Janssen S, Dons E (2013) The RIO-IFDM-street canyon model chain: a validation study in Antwerp, Belgium. Atmos Environ 77:325–337
7. Mensink C, De Vlieger I, Nys J (2000) An urban transport emission model for the Antwerp area. Atmos Environ 34:4595–4602
8. Vankerkom J, De Vlieger I, Schrooten L, Vliegen J, Styns K (2009) Beleidsondersteunend onderzoek: Aanpassingen aan het emissiemodel voor wegtransport MIMOSA. Studie uitgevoerd in opdracht van VMM – MIRA, 2009/TEM/R/084

# Chapter 63
# The Influence of the Changing $NO_x$-Split for Compliance to the European Limit Values in Urban Areas

**Wouter Lefebvre, Charlotte Vanpoucke, Frans Fierens, Stijn Janssen, Bart Degraeuwe, and Clemens Mensink**

**Abstract** In this paper, we investigate the influence of the changing NOx-split in traffic emissions on the ambient NO2-concentrations. First of all, we show that the NOx-split is indeed changing, by looking at measurements in tunnels and at urban locations. Secondly, we analyze on a local scale the effect of this changing split. It is shown that the a large influence can be found. Finally, we discuss some of the consequences of these changes, for instance, on the effectiveness of the EU-legislation.

## 63.1 Introduction

The city of Antwerp has not yet been able to comply to the European limit values for $NO_2$ (annual mean concentration of 40 $\mu g/m^3$), despite relatively strong decreases in $NO_x$-emissions both in the city itself, in the Flemish region and in the whole of Western Europe. However, the decline in ambient $NO_2$-concentrations did not mirror these strong decreases. We investigate the role of the changing $NO_x$-split of traffic emissions in these trends.

W. Lefebvre (✉) • S. Janssen • B. Degraeuwe • C. Mensink
VITO, Boeretang 200, B-2400 Mol, Belgium
e-mail: Wouter.lefebvre@vito.be; stijn.janssen@vito.be; bart.degraeuwe@vito.be; Clemens.mensink@vito.be

C. Vanpoucke • F. Fierens
Belgian Interregional Environment Agency, Kunstlaan 10-11, 1210 Brussels, Belgium
e-mail: Vanpoucke@irceline.be; fierens@irceline.be

D. Steyn and R. Mathur (eds.), *Air Pollution Modeling and its Application XXIII*,
Springer Proceedings in Complexity, DOI 10.1007/978-3-319-04379-1_63,

## 63.2 Results

First of all, we show that the average traffic $NO_x$-split is indeed changing strongly (estimations of this $NO_x$-split in Flanders range from 5 % NO2 in the early 1990s, around 20 % in 2007, 27 % in 2010 to estimations of respectively 35 and 40 % in 2015 and 2020, Lefebvre et al. [3]). This change can be seen both in measurements in tunnels, where the $NO_x$-concentrations decrease despite increasing $NO_2$-concentrations and, to a lesser extent, at traffic and urban measurement locations (Fig. 63.1). Indeed, at these locations, a decrease in $NO_x$-concentrations is found, whereas the $NO_2$-concentrations decrease only slightly or show even an increase (Fig. 63.1). However, the rate of increase is rather variable.

Secondly, we analyze on a local scale the effect of the changing $NO_2$-$NO_x$ emissions over time, based on the COPERT emission functions and a combination of a Gaussian and a street-box model. Using a coupling of a bi-gaussian and a street box model to regional background concentrations [4, 5], we can test the influence of this split change. In these model results, we see that the marked change over time in the $NO_2/NO_x$ ratio does play an important role on the urban scale, with increasing $NO_2$-concentrations originating from a higher $NO_2/NO_x$-split. The effects are ranging from 0.5 at urban background locations to more than 4 $\mu g/m^3$ close to the Antwerp ring road and in major street canyons (Fig. 63.2). Therefore, it is important to take this changing $NO_x$-split into account in any assessment and scenario work which aims at predicting ambient $NO_2$ concentrations at present or under changing policy conditions. Nevertheless, the change in $NO_x$-split is different between the traffic emissions on different types of roads, as roads with a larger amount of heavy duty vehicles will have smaller changes in this split over time. This spatial variability in the changing $NO_x$-split is shown to be not important for the ambient concentrations (effects smaller than 1 $\mu g/m^3$ except at some locations within major street canyons, Fig. 63.2). In other words, while it is important to take into account the general trend in the $NO_x$-split, it does not seem important to take into account the local variability of this split.

## 63.3 Discussion and Conclusions

This paper has shown the major effect of the changing $NO_x$-split on the ambient $NO_2$-concentrations. This has important implications for the consistency of the emission and ambient air quality legislation at an European level. Indeed, emission standards on $NO_x$-emissions could lead to decreasing $NO_x$-emission, but with a higher $NO_2/NO_x$-ratio and will thus yield lower decreases in the ambient $NO_2$-concentrations than expected.

This changing $NO_x$-split should also be taken into account in scientific studies, extending to a regional scale. One can imagine that studies estimating for instance the amount of $NO_x$-emission reductions in a certain region based on the satellite

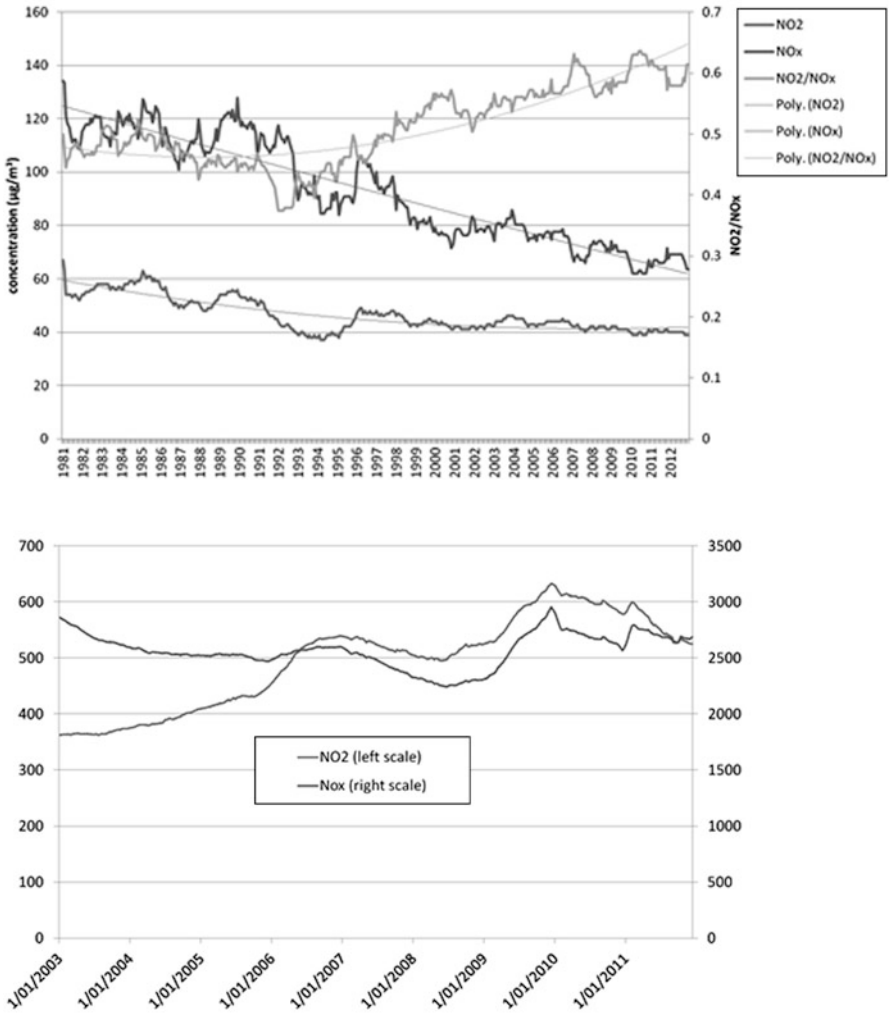


**Fig. 63.1** 12-month running average of $NO_2$-concentrations (*lower line*), $NO_x$-concentrations (*middle line*) in an average of three urban location (*above*) and in a tunnel (*below*). On the *upper chart*, the ratio between the two is also given and in fine lines a second order trend line is included. All concentrations are in $\mu g/m^3$

measurements of $NO_2$ to be significantly affected by this trend in $NO_x$-splits [1]. Furthermore, in many studies on the combination of the effect of changing emissions and climate change, the change in $NO_x$-split is not taken into account [2]. However, it could be important for both $NO_2$-concentrations (directly) and for $O_3$-concentrations (indirectly, due to effects on titration).

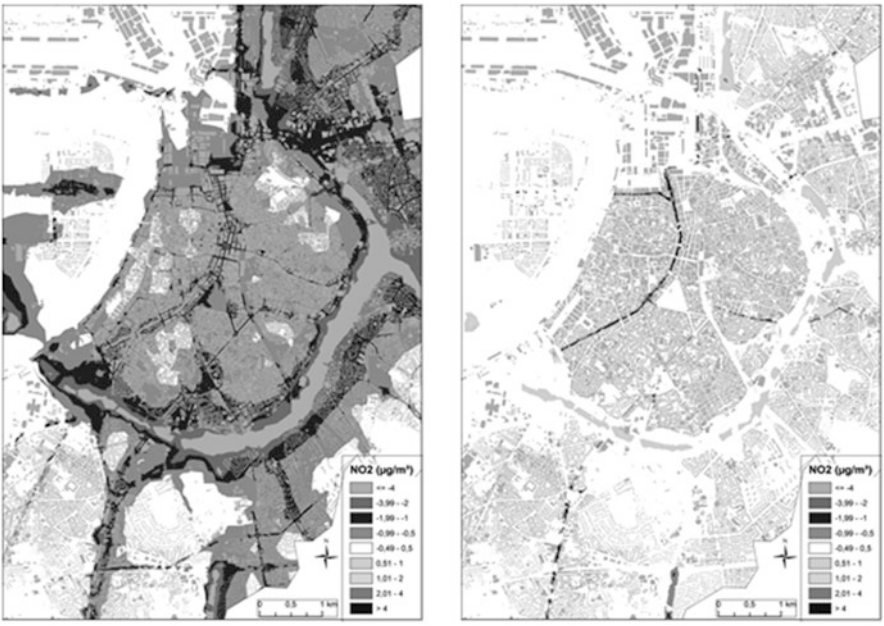


**Fig. 63.2** Difference in annual mean $NO_2$-concentrations as estimated for 2015 between a scenario with a $NO_2/NO_x$-ratio of 5 % and a scenario with a $NO_2/NO_x$-ratio of 31.5 % (*left*). Difference in annual mean $NO_2$-concentrations as estimated for 2015 between a scenario with a homogeneous $NO_2/NO_x$-ratio of 31.5 % and a scenario with a traffic-composition dependent $NO_2/NO_x$-ratio of 31.5 % (*right*). In all scenarios, the total $NO_x$-emissions were equal

## References

1. Eskes H, Timmermans R, Curier L, de Ruyter de Wildt M, Segers A, Sauter F, Schaap M (2012) Data assimilation and air quality forecasting, abstract book and presentation 32nd ITM, Utrecht
2. Lauwaet D, Viaene P, Brisson E, van Noije T, Strunk A, Van Looy S, Veldeman N, Blyth L, De Ridder K, Janssen S, Lefebvre W (2013) High resolution climate change and air quality modelling for policy support over Belgium. Conference proceedings, extended abstract, HARMO Madrid
3. Lefebvre W, Janssen S, Schrooten L, Deutsch F, Vankerkom J, Degraeuwe B, Veldeman N, Peelaerts W, Van Looy S, Lodewijks P, Meynaerts E, De Vlieger I, Op't Eyndt T, Schepens J, Lefebre F, Blyth L (2010) Luchtkwaliteit langs snelwegen en belangrijke gewestwegen in Vlaanderen, Studie uitgevoerd in opdracht van LNE, departement ALHRMG, 2010/RMA/R/255
4. Lefebvre W, Van Poppel M, Maiheu B, Janssen S, Dons E (2013) Evaluation of the RIO-IFDM-street canyon model chain. Atmos Environ 77:325–337. doi:10.1016/j.atmosenv.2013.05.026
5. Lefebvre W, Van Poppel M, Maiheu B, Janssen S, Dons E, Mensink C (2013) Validation the RIO-IFDM-street canyon coupling over Antwerp, Belgium, elsewhere in this edition

# Chapter 64
# Evaluation of Air Pollution Models for Their Use in Emergency Response Tools in Built Environments: The 'Michelstadt' Case Study in COST ES1006 ACTION

**Bernd Leitl, Silvia Trini Castelli, Kathrin Baumann-Stanzer, Tamir G. Reisin, Photios Barmpas, Marton Balczo, Spyros Andronopoulos, Patrick Armand, Klara Jurcakova, Maya Milliez, and All COST ES1006 Members**

**Abstract** The first results of a model validation test case, carried out in the research context of the COST ES1006 Action, are outlined and discussed. The validation exercise was established with an application-oriented approach, devoted to the investigation of the modeling performances in the emergency-response framework.

B. Leitl
Meteorological Institute, University of Hamburg, Hamburg, Germany

S. Trini Castelli (✉)
Institute of Atmospheric Sciences and Climate (ISAC), National Research Council (CNR), I-10133 Torino, Italy
e-mail: s.trinicastelli@isac.cnr.it

K. Baumann-Stanzer
Central Institute for Meteorology and Geodynamics, Vienna, Austria

T.G. Reisin
SOREQ NRC, Yavne, Israel

P. Barmpas
Aristotle University of Thessaloniki, Laboratory of Heat Transfer and Environmental Engineering, Thessaloniki, Greece

M. Balczo
Department of Fluid Mechanics, Budapest University of Technology and Economics, Budapest, Hungary

S. Andronopoulos
National Centre for Scientific Research "Demokritos", Institute of Nuclear and Radiological Sciences and Technology, Energy and Safety, Aghia Paraskevi, Greece

P. Armand
Radiological and Chemical Impact Laboratory, French Atomic Energy Commission, Paris, France

K. Jurcakova
Institute of Thermomechanics AS CR, Prague, Czech Republic

D. Steyn and R. Mathur (eds.), *Air Pollution Modeling and its Application XXIII*,
Springer Proceedings in Complexity, DOI 10.1007/978-3-319-04379-1_64,

## 64.1 Introduction

The main aim of COST Action ES1006 (http://www.elizas.eu) is to evaluate and improve the reliability of neighborhood-scale emergency response tools on the basis of a comprehensive, concerted and harmonized cross-national approach. The main topics in the Action are the evaluation of the air dispersion models and their integration in the emergency response systems. A special attention is devoted to the specific needs of operators and stakeholders, who use these tools to respond to accidental or malevolent releases.

In the frame of this research, two first tests have been established in order to evaluate the performance of different modeling methodologies, from the simple parametric models to the most advanced CFD ones, with an application-oriented approach. In this way, not only the physical reliability of the models is considered, but also their applicability in terms of run-time and response speed, simplicity to use and computational costs, for-purpose adaptability.

The test cases refer to wind-tunnel experiments, where the meteorology and dispersion were reproduced for continuous and short-duration releases in an idealised European urban environment called "Michelstadt".

The preliminary results of an intercomparison among the different modeling methodologies, available in the frame of the Action, are briefly presented and discussed for the first test case, addressing the differences and performances through the application-oriented approach outlined above.

## 64.2 The Michelstadt Open Test Case

The "Michelstadt" wind-tunnel experiment [1] was chosen as first test case in the frame of Action, since it was designed to provide observed data for the validation of local scale emergency response models. The measurements were carried out in the WOTAN atmospheric boundary layer wind tunnel at the Environmental Wind Tunnel Laboratory in Hamburg. A 2D Laser Doppler Velocimetry and a fast Flame Ionization Detector were used. The building structure named as 'Michelstadt' is a model that represents an idealized Central-European urban environment. Measurements were collected for five scenarios corresponding to different point source locations. Two wind directions were considered and both continuous and short-term (puff) releases were carried out. Flow and concentration data were made available in a first 'open' test case for the modeling exercise. In a second 'blind' test, currently

M. Milliez
CEREA Teaching and Research Center in Atmospheric Environment – EDF R&D, Chatou, France

All COST ES1006 Members
http://www.cost.eu/domains_actions/essem/Actions/ES1006

http://www.elizas.eu/

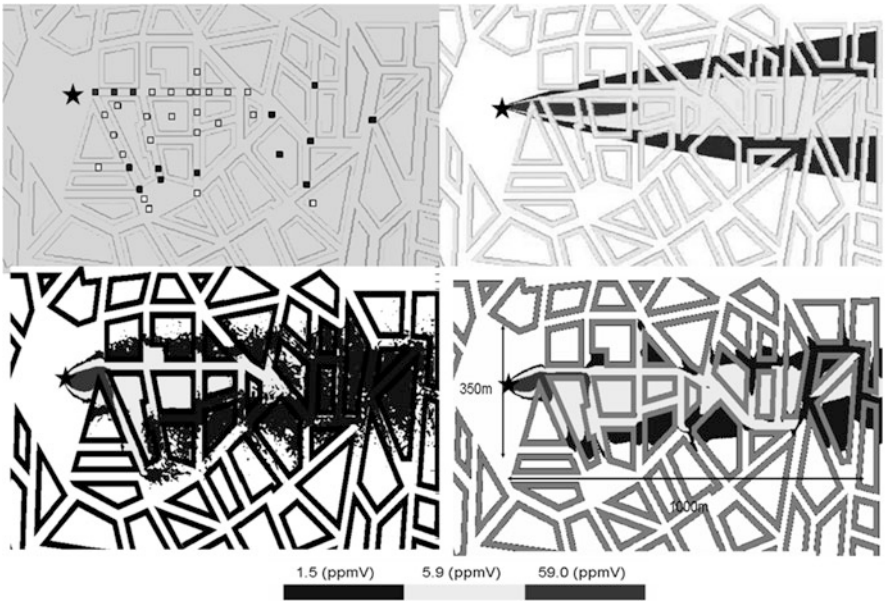


**Fig. 64.1** Sketch of the Michelstadt wind-tunnel experiment (*top left*) and simulation concentration contours for source S2, continuous release: Type 1 (*top right*), Type 2 (*bottom left*) and Type 3 (*bottom right*) models

running, only minimum information on flow data and the emission description are provided to the modelers. In both cases, an inter-comparison among the different modeling approaches is performed using an ad-hoc tool developed in the frame of the Action [2] for elaborating and processing the simulation outputs and comparing the physical measurements with the results of numerical simulations. The final goal of these exercises is to identify the key aspects, such as advantages and limitations of different types of models, and possible problems arising when applying these models in the emergency response frame. In Fig. 64.1 a sketch of the Michelstadt configuration is given for the measurements related to source S2 (top left panel).

## 64.3 The Models and the Simulations: First Results and Discussion

Different types of models, characterized by different level of complexity, have been applied in the test cases. We classified them in three categories, as follows:

Type 1: models not resolving the flow (uniform flow);

**Table 64.1** Types of models applied to simulate Michelstadt test case

| Modeling approach | Number of models | Dispersion modeling method | Computational time |
|---|---|---|---|
| Type 1 | 7 | Gaussian – 2 with building parameterization | 1–5 min |
| Type 2 | 5 | Lagrangian | 2 min – 5 h |
| Type 3 | 10 (6 models) | CFD 8 RANS; 3 LES; 1 RANS-Lagrangian | 2 h – 4 days |

**Table 64.2** FAC2 for the "open" Michelstadt test case, releases from sources S2, S4, S5

| | FAC2 | | |
|---|---|---|---|
| Modeling approach | min | max | average |
| Type 1 | 0.14 | 0.33 | 0.25 |
| Type 2 | 0.25 | 0.46 | 0.40 |
| Type 3 | 0.25 | 0.81 | 0.59 |

Type 2: models resolving the flow between the buildings with simplified equations (diagnostic approach);

Type 3: models resolving the flow between the buildings with full dynamical equations.

In Table 64.1 the three types of models are reported together with some of their main features. A particular attention is dedicated also to the performance of the model in computational time, since the evaluation is conducted for emergency response.

The models were run in their standard configuration and no post-evaluation re-configuration of them was applied. In Fig. 64.1 some exemplificative results are reported for the three types of models used in the S2-source continuous release case.

We notice major differences between models that are able to explicitly account for the presence of buildings with respect to models that do not resolve the obstacles. This aspect is particularly important for correctly describing the pattern of the plume in such complex geometries, the channeling and possible accumulation of the tracer in between the buildings. Of course, more advanced models should be more accurate but they are also more time consuming (Table 64.1).

A statistical analysis was performed computing the standard metrics: as an example, in Table 64.2 we report the factor-of-two (FAC2) computed for S2-source release together with two other sources, S4 and S5 (Fig. 64.2), in order to have a larger set of paired observed-predicted values. When considering the statistics, it is worth taking into account that the number of the applied models differ for the three types (Table 64.1).

Hanna and Chang [3] define FAC2 $\geq$0.30 as one of the acceptance criteria for models in urban applications. In these preliminary results, on average this criterion is satisfied by more advanced models. At present, we are also investigating other specific metrics than the standard ones, which could be more suitable for emergency response applications.

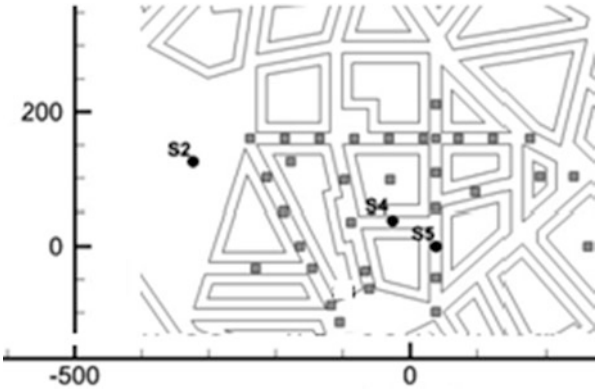


**Fig. 64.2** Zoom on the experimental area including sources S2, S4 and S5

**Acknowledgments** The work presented here is performed in the framework of the COST (European Cooperation in Science and Technology) Programme.

## References

1. Fischer R, Bastigkeit I, Leitl B, Schatzmann M (2010) Generation of spatio-temporally high resolved datasets for the validation of LES-models simulating flow and dispersion phenomena within the lower atmospheric boundary layer. In: Proceedings of the 5th international symposium on Computational Wind Engineering (CWE2010), Chapel Hill, NC, USA
2. Stern M, Milliez M (2013) Developing tools for comparison of physical measurements and results of numerical simulations. Scientific report. COST Action ES1006 – STSM, http://www.elizas.eu/index.php/stsms, COST Office, Brussells, Belgium
3. Hanna S, Chang J (2012) Acceptance criteria for urban dispersion model evaluation. Meteorol Atmos Phys 116:133–146

# Chapter 65
# Development of a Numerical Prediction Model System for the Assessment of the Air Quality in Budapest

**Zita Ferenczi, Krisztina Labancz, and Roland Steib**

**Abstract** Air pollution can severely affect the health of citizens living in urban environment. Monitoring and assessment of air pollution by applying appropriate modeling tools are essential to provide information on air quality to the public. Several air quality forecast and information systems exist in Europe calculating present and predicted concentrations and potential exceedances using a combination of weather forecasting and chemical composition simulations. This paper presents an air quality prediction model system for the area of Budapest. The forecasting modeling system recently consists of a version of the WRF meteorological model and the CHIMERE chemistry transport model. The model system calculates the $PM_{10}$, $NO_2$, $SO_2$ and $O_3$ concentration values for the city area with 1-h temporal resolution. In this work we present the results of the validation of the prediction system. In the evaluation work, the $PM_{10}$, $NO_2$ and $O_3$ data detected by the air quality monitoring network of Budapest, as well as the forecasted air pollutant concentration values of the air quality prediction model system are used.

## 65.1 Introduction

The harmful effect of air pollution on human health [1] have raised a series of concerns in recent years and imposed needs for accurate descriptions of air pollution levels in urban areas. This implies that tools supporting national pollution control and planning need to be developed including public web sites or other media where citizens exposed to the air pollutants can catch urban background concentration data, predicted concentrations or alerts.

Z. Ferenczi (✉) • K. Labancz • R. Steib
Analysis of Atmospheric Environment, Hungarian Meteorological Service, Budapest Kitaibel Pal Utca 1, P.O. Box 39, H-1675 Budapest, Hungary
e-mail: ferenczi.z@met.hu

D. Steyn and R. Mathur (eds.), *Air Pollution Modeling and its Application XXIII*, Springer Proceedings in Complexity, DOI 10.1007/978-3-319-04379-1_65,

For the past years, industrial production and especially transportation have caused serious environmental contamination in Budapest. There are significant differences between the air quality of the downtown and that of the outskirts in Budapest. PM, $O_3$ and $NO_2$ concentrations are often around or above the health threshold values not only in the downtown. The aim of this paper is to present a newly developed system producing enhanced maps of present and predicted concentrations of air pollutants in Budapest. The results have been available for the public on the official web page of the Hungarian Meteorological Service since June 1, 2010. In addition to the in-situ concentrations observed at a station, the web page presents maps of 24 and 48 h predictions for air pollutant distributions as well as time series at the monitoring stations. The forecasting tool is an integrated system of the WRF meteorological and CHIMERE chemical transport models.

## 65.2 Model Overview

### *65.2.1 Meteorological Preprocessor*

CHIMERE chemical model does not contain any meteorological drivers, therefore meteorological data have to be provided in order to perform a simulation. The provided code only contains a meteorological interface, which allows the model to start from standard meteorological variables, and transforms it to CHIMERE inputs. The WRF numerical weather prediction model is operatively run four times per day (00, 06, 12 and 18 UTC) by the Hungarian Meteorological Service (HMS) for nowcasting purposes (forecast for 24 h time period). The 18 UTC WRF run was extended from 24 to 54 h to produce the meteorological variables, which are needed for the 48 h chemical transport model calculations for the area of Budapest. The domain of the operational WRF run covers the Carpathian Basin ($199 \times 149 \times 37$ grid points), but from the results of the 18 UTC WRF run, a smaller domain ($65 \times 50 \times 37$ grid points) was cut out, which covers our air quality modeling area, in order to reduce file size and model runtime.

### *65.2.2 Chemical Transport Model*

The CHIMERE chemistry transport model was adopted for calculating the pollutant concentrations in Budapest [2]. CHIMERE is a multi-scale model, which uses numerical weather prediction data to produce daily forecasts of ozone, aerosols and other pollutants and it runs over a range of spatial scales from the regional to the urban scale. The chemical core of the model is the MELCHIOR2 gas-phase chemical mechanism. A set of boundary conditions from LMDZ-INCA (*IPSL/LSCE)* model is proposed as a default solution which allows tropospheric

simulation below 200 hPa. For aerosols, a set of boundary conditions is proposed based on GOCART (*NASA*) global simulations. For first model runs, emissions are proposed based on the EMEP annual inventory data (on the EMEP grid for the activity sectors).

### *65.2.3 Local Emission Data*

Two types of emissions are handled by the CHIMERE model: anthropogenic and natural (biogenic) emissions. Biogenic and natural emissions are automatically calculated by the model using NASA-GLCF land use data with 1 km × 1 km grid resolution. Annual data of anthropogenic emissions for $NO_x$, $SO_2$, CO, $PM_{10}$, $PM_{2.5}$, $NH_3$, NMVOC and POPs are taken from the EMEP data base (http://www.ceip.at). For making this picture more specific for our purposes, an investigation was started to find emissions data for Budapest. Unfortunately this question proved to be the most difficult task of the whole work. Finally, two official report were made available for us by the local authorities of Budapest. The first is an annual emission inventory for 2008, containing the local industrial and power plant point source data including detailed stack-data, small industrial emission data and estimated domestic emission. The other is a traffic count data base for 2004, containing detailed traffic data for the whole territory of Budapest, made for the noise map of the city. This latter data base is a very useful tool, as there is no continuous traffic counting control in Budapest, except for some targeted campaigns. Thus, road traffic emission values were calculated using the European standard methodology based on road traffic counting data, car type distribution, ratio of heavy vehicles by type of road and fuel characteristics.

## 65.3 Model Results

In Budapest, there is an air quality network with 11 stations, which detects the concentration values of different pollutants in every hour. Using the measured concentration data the Hungarian Meteorological Service developed an information homepage to inform the public about the air quality situation in Budapest. Our forecasting system is the part of this page. The results of the application of the developed dispersion modeling system to predict the air quality in Budapest for 48 h shows that the system operated properly. The quality of the results depends on the quality of the weather forecast [3]. Especially, the $O_3$ forecast are determined by the forecasted temperature and cloudiness, while the most important parameter in case of $PM_{10}$ is the mixing height [4]. When the meteorological forecast is not accurate enough, the predicted concentration fields will rather differ from the measured values. Especially in winter, when episode situations can be formed in Budapest, the accurate prediction of this parameter can determine the success of chemical forecast.

**Table 65.1** Correlation values

| Stations | $O_3$ | $NO_2$ | $PM_{10}$ |
|---|---|---|---|
| Csepel | 0.70 | 0.52 | 0.39 |
| Erzsebet ter | – | 0.66 | 0.49 |
| Gergely utca | 0.71 | 0.69 | 0.45 |
| Gilice ter | 0.72 | 0.50 | 0.31 |
| Honvéd | – | 0.61 | 0.53 |
| Kőrakás park | 0.80 | 0.66 | 0.36 |
| Kosztolányi ter | 0.73 | 0.68 | 0.33 |
| Pesthidegkút | 0.70 | 0.56 | 0.15 |
| Széna ter | 0.73 | 0.64 | 0.35 |
| Teleki ter | 0.77 | 0.67 | 0.49 |
| Tétényi ut | 0.64 | 0.60 | 0.19 |

The other important information concerns the emission data. During the evaluation work we found that there is a lack in the emission input data base calculated for $PM_{10}$ and $SO_2$. The long term transport of these two pollutants plays very important role in formation of the air quality of Budapest. The chemical analysis of aerosol samples collected in Budapest in 2009 shows, that half of the amount of $PM_{10}$ comes from outside of Budapest. These facts are reflected in our results, mainly as the uncertainty in the predicted $PM_{10}$ concentrations, which corresponds to the measured values in one case and there are big differences in the other. In case of big differences, the polluted material comes outside of Budapest.

## 65.4 Validation of the Prediction System

The air quality prediction system has been operating since June 1, 2010, which means, thus there are more than 2-year data sets to evaluate how it is working. In the validation work the $PM_{10}$, $NO_2$ and $O_3$ data detected by the air quality monitoring network of Budapest, as well as the forecasted air pollutant concentration values of the air quality prediction model system are used. Correlation and NMSE (Normalized mean square error) values are determined for the three pollutants and for the grid points, where the air quality monitoring stations are located. The Table 65.1 shows the results of this examination. The values indicate that the best forecast can be expected for the $O_3$ (the correlation values are over 0.7) and the worst for $PM_{10}$ (the correlation values are about 0.4).

## 65.5 Conclusion

A dispersion modeling system was developed by the Hungarian Meteorological Service to predict the air quality in Budapest for 48 h. The core of this system is the CHIMERE chemical transport model. For meteorological input a 54-h WRF output

is used. Beside CHIMERE's built-in emission data base, also own emission data (point sources, traffic count) for Budapest are used during modeling. It was shown that the quality of the results depends on the quality of the weather forecast. It was also demonstrated that there is a lack in the emission input data base calculated for $PM_{10}$ and $SO_2$. Long-term transport of these two pollutants seems to play an important role during concentration calculations. Validation of the system also confirms these statements.

## References

1. Bernard SM, Samet JM, Grambsch A, Ebi KL, Romieu I (2001) The potential impacts of climate variability and change on air pollution-related health effects in the United States, environmental health perspectives. Environ Health Perspect 109:199–209
2. CHIMERE version 2008, Institut Pierre-Simon Laplace (C.N.R.S.), INERIS, LISA (C.N.R.S.)
3. Barmpadimos I, Hueglin C, Keller J, Henne S, Prévôt ASH (2011) Influence of meteorology on PM10 trends and variability in Switzerland from 1991 to 2008. Atmos Chem Phys 11:1813–1835
4. Holst J, Mayer H, Holst T (2008) Effect of meteorological exchange conditions on $PM_{10}$ concentration. Meteorol Z 17(3):273–282

# Chapter 66
# Analysis of the Differences Between Pollution Levels into a New and an Old District of a Big City Using Dispersion Simulations at Microscale

**Gianni Tinarelli, Lorenzo Mauri, Cristina Pozzi, Alessandro Nanni, Andrea Ciaramella, Valentina Puglisi, Tommaso Truppi, and Giuseppe Carlino**

**Abstract** The new residential district 'CityLife' is under construction inside the city of Milan, northern Italy, replacing the old structure of the trade fair. It consists of relatively insulated blocks, surrounded by many gardens and commercial buildings and no car traffic at the surface. The objective of this study is to simulate and compare the pollution level inside this new area with a more common residential district located not so far away. High resolution simulations have been performed inside two domains – having linear dimension of approximately 1 km – using a microscale modeling system, taking directly into account the effects of buildings and street canyons to the atmospheric mean flow and turbulence. Emissions coming from car traffic (around the new district and inside the old one), underground traffic (emerging from ground-level openings in the new district) and heating systems (during winter) have been taken into account. Background values have been estimated from local measurements using a box model and added to the simulated concentration fields in order to produce a complete view of the local pollution levels. Both average levels of pollution at district scale and local behaviours into sub-zones of the two domains where similar activities are supposed to take place are compared showing the potential benefits inside the new district both in absolute terms and in percentage, setting in evidence which portion of the pollution can be reduced by local interventions.

G. Tinarelli (✉) • L. Mauri • C. Pozzi • A. Nanni
Arianet, via Gilino 9, 20128 Milano, Italy
e-mail: g.tinarelli@aria-net.it; l.mauri@aria-net.it; c.pozzi@aria-net.it; a.nanni@aria-net.it

A. Ciaramella • V. Puglisi • T. Truppi
Built Environment and Construction Engineering A.B.C. Department, Politecnico di Milano, via Bonardi 5, 20133 Milano, Italy
e-mail: andrea.ciaramella@polimi.it; valentina.puglisi@polimi.it; tommaso.truppi@polimi.it

G. Carlino
Simularia, via Principe Tommaso 39, 10125 Torino, Italy
e-mail: g.carlino@simularia.it

D. Steyn and R. Mathur (eds.), *Air Pollution Modeling and its Application XXIII*, Springer Proceedings in Complexity, DOI 10.1007/978-3-319-04379-1_66,

## 66.1 Introduction

In the city of Milan (Northern Italy) is under development the new residential district "CityLife", characterized by innovative architectural and urban solutions in term of energy efficiency, local traffic and use of green spaces. This district represents the renovation of the old exhibition complex, located well inside the city of Milan. Within a zone of this type, potentially able to bring benefits to the local air quality, the air pollution due to the rest of the city must be added to the effects generated by local emissions. The aim of the work is to reproduce the levels of air quality in the new district through dispersion simulations at microscale, taking into account local effects at very high resolution. The results of these simulations are then compared with similar results obtained in a reference residential district with more traditional features, in order to verify the possible benefits for the population due to the new district design.

## 66.2 Modeling Setup

To perform the simulations, the MSS [1] modeling system, already tested in an urban context [1, 2], has been used. MSS is the combination of the meteorological Micro-Swift code and the Micro-Spray dispersion model [3], both able to directly take into account the effect of buildings. Micro-Swift is a mass consistent diagnostic 3D wind model, in which the aerodynamic effects due to the buildings are represented by analytical flow zones with a fast-response solution. Micro-Spray is a 3D Lagrangian Particle Dispersion Model taking into account of particle bouncings against obstacles, the effect of both a local and background turbulence and being able to consider different physical and geometrical emissions, such as those coming from traffic or domestic heating. Two urban areas are investigated representing the new CityLife district, (left side of Fig. 66.1) covering $900 \times 900$ m$^2$, and a reference district, in the (right side of the same figure) with an extension of $1{,}100 \times 500$ m$^2$.

Inside these areas, meteorological and dispersion simulations have been performed at 3 m horizontal resolution taking into account the complex structure of 3d obstacles. Two one-day periods representing typical and recurrent conditions in winter and summer have been simulated taking into account a complex set of local emissions (traffic, domestic heating). Ground level concentrations on hourly basis have been locally simulated for species NOx, $NO_2$, CO, $PM_{10}$, Benzene, $PM_{10}$, then background values have been estimated using a box-model and added to produce total concentration levels. Inside the new CityLife district, in the inner part of the first domain, heating systems are not considered as sources of pollutants, due to the presence of zero emission advanced heat pumps, while the only local traffic admitted here are the underground paths to parking spaces. Figure 66.2 shows an example of daily average NOx concentrations generated by the contribution of different local sources inside the domain of the new district.

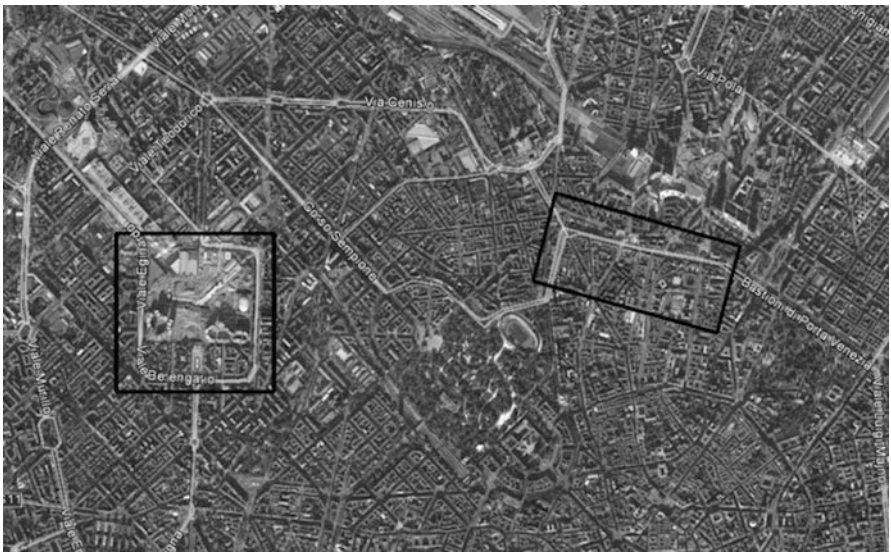


**Fig. 66.1** Position of the two considered domains (*black rectangles*)

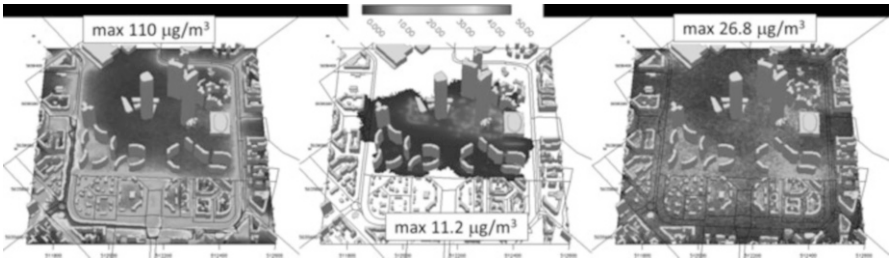


**Fig. 66.2** Ground level daily averaged concentration maps of NOx ($\mu g/m^3$) generated by the traffic around (*left*), internal to the new district (*center*) and domestic heating (*right*) in the winter case, CityLife district domain

## 66.3 Main Results

Total concentration fields inside the two domains for the various species considered have been used to compare a reference and existing situation to the one in the new district, in order to show the local potential benefits of the solutions adopted in this last case. This comparison shows systematic enhancements on the local levels of $NO_2$ at ground, up to 15 % on hourly concentrations during winter and about 40 % during summer. The situation for $PM_{10}$ shows to be less good due to the presence of higher levels of the background contribution for this specie, that prevents the possibility for a more drastic reduction of local concentration levels. In any case,

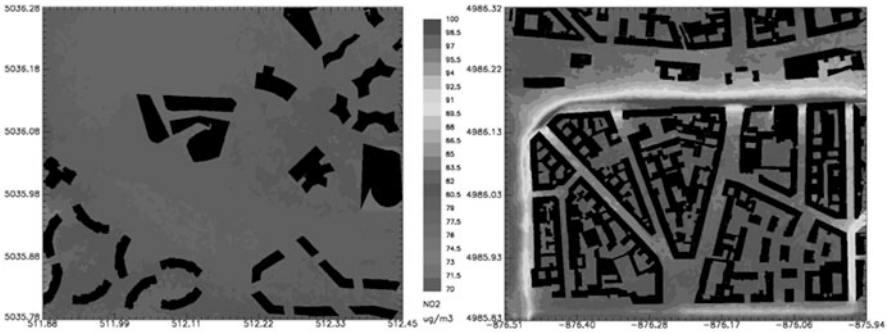


**Fig. 66.3** Ground level concentration daily average fields of $NO_2$ in the winter case ($\mu g/m^3$), details of the CityLife district (*left*) and reference district (*right*)

also for $PM_{10}$ a maximum reduction of the order of 5–6 % during winter and 25 % during summer is visible inside the CityLife district. The absence of traffic at surface level in the new CityLife district determines also local concentration levels lower for Benzene and CO. As an example, the Fig. 66.3 shows daily average concentrations fields for the $NO_2$ specie in the CityLife district and in the reference district. It is evident the impact of the main roads inside the reference district, generating local maximum present also into secondary roads and totally absent inside the CityLife district.

Inside the reference district the small distance among building blocks determines the presence of many urban canyons. This generates a more efficient vertical mixing of the emitted pollutants, leading to larger concentration values at vertical levels corresponding to the higher floors. Simulation results show that inside the new CityLife district, where the distance among building block is maintained larger, concentration levels up to 20 m in vertical remain smaller.

**Acknowledgments** The authors thanks CityLife S.p.A., for their support in supplying the data necessary for the realization of the work.

## References

1. Tinarelli G, Brusasca G, Oldrini O, Anfossi D, Trini Castelli S, Moussafir J (2004) Micro-Swift-Spray (MSS) a new modelling system for the simulation of dispersion at microscale, general description and validation. In: Proceedings of the 27th CCMS-NATO meeting, Banff, Canada, 25–29 Oct 2004
2. Tinarelli G, Piersanti A, Radice P, Clemente M, De Maria R (2009) Microscale modelling simulation for the site characterization of air quality stations in an urban environment. Radiat Prot Dosimetry 137(3–4):294–299
3. Tinarelli G, Mortarini L, Castelli ST, Carlino G, Moussafir J, Olry C, Armand P, Anfossi D (2012) Review and validation of MicroSpray, a Lagrangian particle model of turbulent dispersion. In: Lagrangian modeling of the atmosphere, Geophysical monograph series 200. American Geophysical Union, Washington, DC, pp 311–327. doi:10.1002/9781118704578.fmatter

# Chapter 67
# Water Tank Simulation of a Dense Fluid Release

**L. Mortarini, S. Alessandrini, E. Ferrero, D. Anfossi, and M. Manfrin**

**Abstract** The turbulent velocity field of a dense fluid release has been measured in a water tank experiment carried out in the TURLAB laboratory in Turin (Italy). A vertical density driven current was created releasing a saline solution in a water tank with no mean flow. The experiment reproduces in physical similarity, based on the density Froud number, the release of a dense gas in the atmosphere and the PIV technique has been used to analyse the buoyancy generated velocity field. The high temporal and spatial resolution of the measurements gives a deep insight to the problems of the bouncing of dense gases and of the creation of the outflow velocity at the ground. The experimental findings are used to test and improve an original method for the dispersion of a positively and negatively buoyant plume. The method is based on the idea of Alessandrini and Ferrero (Phys. A 388:1375–1387, 2009) for the treatment of a background substance entrainment into the plume and it consists on the introduction of two fictitious scalars inside the Lagrangian Model SPRAY. The fictitious scalars represent the density and momentum difference between the plume and the environment air that naturally takes into account the interaction between the plume and the environment. As a consequence, no more particles than

L. Mortarini (✉) • D. Anfossi
Institute of Atmospheric Sciences and Climate, CNR, Torino, Italy
e-mail: l.mortarini@isac.cnr.it; d.anfossi@isac.cnr.it

S. Alessandrini
RSE, Milan, Italy
e-mail: stefano.alessandrini@rse-web.it

E. Ferrero
Dipartimento di Scienze e Innovazione Tecnologica, University of Piemonte Orientale, Alessandria, Italy
e-mail: enrico.ferrero@mfn.unipmn.it

M. Manfrin
Department of Physics, University of Torino, Torino, Italy
e-mail: manfrin@to.infn.it

D. Steyn and R. Mathur (eds.), *Air Pollution Modeling and its Application XXIII*,
Springer Proceedings in Complexity, DOI 10.1007/978-3-319-04379-1_67,

those inside the plume are released to simulate the entrainment of the background air temperature. In this way the entrainment is properly simulated and the plume sink is calculated from the local property of the flow. The approach is wholly Lagrangian.

## 67.1 Water Tank Experiment

The laboratory experiments were carried out at the rotating tank laboratory, TURLAB [4]. The facility is composed of a 5 m diameter cylindrical tank, able to reach a maximum rotation speed of 20 revolutions per minute. The data were acquired by a non-intrusive PIV technique, which allows the detection of Eulerian velocity fields. The simulation was based on the Froude number, $Fr = w/\sqrt{g'H}$, where $g' = g\Delta\vartheta/\vartheta$ for the atmosphere and $g' = g\Delta\rho/\rho$ for the tank; $g$ is the gravity acceleration, $w$ is the velocity scale, $H$ is the vertical length scale and $\vartheta$, $\rho$ are the potential temperature and the density respectively. In order to create the density current a reservoir was placed just below the water surface. Then, it was filled with salt water, which, passing through a small hole in the reservoir bottom, develops a vertical density current. It is worth to notice that, since the reservoir was immersed in the tank water, the effects due to the hydrostatic pressure were negligible. The density current propagated throughout the whole water layer up to the tank bottom (Fig. 67.1, top). In Table 67.1 the main parameters of the experiment and the corresponding values for the numerical model are listed.

## 67.2 Plume Rise Model Description

The new Lagrangian plume rise module [3] was introduced in the Lagrangian stochastic particle model SPRAY [2, 5]. In the new module each particle carries two quantities that specify the difference between the temperature and the momentum of the plume air and the environment. To this aim we assign to any $i$-th emitted particle in the time interval $\Delta t$ the "temperature mass" $m_T$, which can be considered a "mass" when the temperature difference is considered a density. Considering the domain divided in fixed regular cubic cells, the air-plume temperature difference for the generic cell, $\Delta T_c$, is $\Delta T_c = \sum_i^M m_{T_i}(t_0)/V_C$, where $M$ is the number of particles in the cell $c$ and $V_c$ is the cell volume. In order to take into account the momentum flux we define the momentum mass $m_{w_i}$, which is assigned to each particle. Also in this case, $m_{w_i}$ has not the dimension of a mass but it can be considered so when the vertical momentum is considered a density. Then the cell vertical velocity $w_c(t_1)$ at the time $t_0$ is computed as $w_c = \sum_i^M m_{w_i}(t_0)/V_C$. The new temperature difference $\Delta T_c(t_1)$ at the time $t_1$ (where $t_1 = t_0 + \Delta t$) is calculated by the equation:

$$\Delta T_c(t_1) = \Delta T_c(t_0) + \Gamma(z_c)\, w_c(t_0)\, \Delta t - 0.0098 w_c(t_0)\, \Delta t \tag{67.1}$$

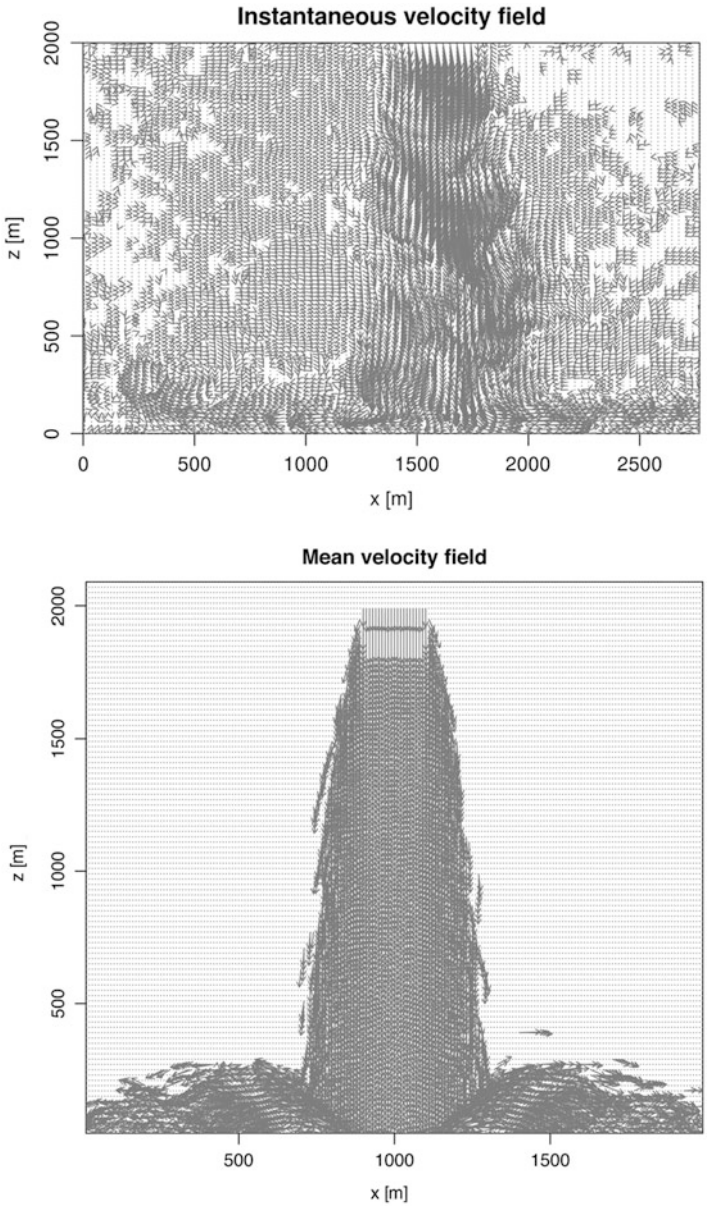


**Fig. 67.1** *Top*, a snapshot of the instantaneous velocity field measured at the TURLAB, the axes are rescaled using the Froude number similarity. *Bottom*, vertical section taken at the middle of the plume of the mean velocity field evaluated by the model

**Table 67.1** Experiment parameters

| Parameter | Experiment | Model |
|---|---|---|
| H(m) | 0.07 | 2,000 |
| W($ms^{-1}$) | 0.05 | 28 |
| $\Delta\theta/\theta$ ($\Delta\rho/\rho$) | 0.003 | 0.033 |
| Fr | 1.1 | 1.1 |

where $z_c$ is the cell height and $\Gamma(z_c)$ is the lapse rate of the ambient air at cell height $z_c$. The second term on the right side updates the temperature difference between the cell and the ambient considering the vertical inhomogeneity of the atmosphere temperature. The third term on the right takes into account the adiabatic expansion due to the plume ascending motion. Clearly, in case of neutral temperature profile, these two terms delete each other. Afterwards, the value of $w_c$ at the time $t_1$ is computed for every cell using the following equation:

$$w_c\left(t_1\right) = w_c\left(t_0\right) + \frac{\Delta T_c\left(t_0\right)}{T_a\left(z_c\right) + \Delta T_c\left(t_0\right)}\, g\, \Delta t - \frac{0.5 \cdot c_D \cdot S \cdot w^2\left(t_0\right) \cdot \rho_a}{\rho_p \cdot V_c} \cdot \Delta t \tag{67.2}$$

where $T_a(z_c)$ is the ambient air temperature at the same cell height $z_c$, $S$ the cell horizontal surface area, $C_D$ the drag coefficient and $\rho_a$ and $\rho_b$ are the ambient air and plume density, respectively. The second term on the right represents the buoyancy vertical acceleration while the last term on the right represents the aerodynamic drag. This Equation simulates the plume vertical ascending velocity variation in time due to the buoyancy acceleration and the aerodynamic drag. Then, the temperature difference and velocity masses at the time $t_1$, $m_{T_i c}\left(t_1\right)$ and $m_{w_i c}\left(t_1\right)$ are computed assuming that the ratios between the values a two consecutive times is equal to the ones of the temperature difference and momentum respectively.

## 67.3 Results

With more than 2,000 instantaneous velocity field measured with a resolution of approximately $70 \times 70$ grid points, the tank experiment provides an extremely accurate dataset for the behavior of the velocity field of a dense gas. The high temporal and spatial resolution measurements offer an insight on the interaction between a buoyant plume and a still environment. Figure 67.1 (bottom) show the averaged mean velocity field evaluated by the model. Far from the ground the qualitative comparison between the data and the model is satisfactory. It must be stressed that this is a peculiar situation for a Lagrangian particle model, the particles, being released in an unperturbed flow, are not moved by the ambient turbulence, but somehow have to produce their own turbulence exchanging momentum with the air. The experimental data are also useful to analyze the vorticity field on the plume boundaries and to study the behavior of the dense gas close to the ground. The model

is able to simulate the donut shaped horizontal dispersion (not shown in Fig. 67.1), nevertheless it is not able to reproduce the data vorticity field close to the ground where the data show the development of a vortex ring that seem to accelerate the dense plume. This vortex ring formation may be due to a friction boundary layer with opposite vorticity encountered by the plume when it approaches the ground.

## References

1. Alessandrini S, Ferrero E (2009) A hybrid Lagrangian–Eulerian particle model for reacting pollutant dispersion in non-homogeneous non-isotropic turbulence. Phys A 388:1375–1387
2. Alessandrini S, Ferrero E (2011) A Lagrangian particle model with chemical reactions: application in real atmosphere. Int J Environ Pollut 47(1–4):97–107
3. Alessandrini S, Ferrero E, Anfossi D (2013) A new Lagrangian method for modelling the buoyant plume rise. Atmos Environ 77:239–249
4. Ferrero E, Genovese R, Longhetto A, Manfrin M, Mortarini L (2008) Experimental study of higher order moments in shear-driven boundary layers with rotation. J Fluid Mech 598:121–139
5. Tinarelli G, Mortarini L, Castelli ST, Carlino G, Moussafir J, Olry C, Armand P, Anfossi D (2012) Review and validation of MicroSpray, a Lagrangian particle model of turbulent dispersion. In: Lagrangian modeling of the atmosphere. American Geophysical Union, Washington, DC, pp 311–327

# Chapter 68
# The Porosity Concept Applied to Urban Canopy Improves the Results of Gaussian Dispersion Modelling of Traffic-Dominated Emissions

**Marko Kaasik, Mihkel Pindus, Tanel Tamm, and Hans Orru**

**Abstract** The Gaussian plume model AEROPOL 5 is applied to estimate the yearly average $NO_2$ concentrations in Tartu, the second largest town of Estonia with about 100,000 inhabitants, for RHINE study. We apply the porosity concept by Genikhovich E, Gracheva I, Filatova E (Modelling of urban air pollution: principles and problems. In: Borrego C, Schayes G (eds) Air pollution modelling and its application, XV. Kluwer, New York, pp 275–283, 2002) in post-processing of modelled ground-level concentrations: the area under buildings is excluded from dispersion volume in each grid cell, thus the concentration is divided to the fraction of porosity, i.e. non-built-up area. It appears that porosity correction substantially enhances the site-wise correlations between model-estimated and measured concentrations, bringing the underestimated levels in particular monitoring sites closer to reality. Moreover, correlations are even higher, when dividing the "raw" modelled concentrations by squared porosities. We suppose that reason of non-linearity is in slowing down the wind between the buildings.

## 68.1 Introduction

The urban canopy is a great challenge for air pollution dispersion modelling. Although micro-scale models for turbulent flows in complex building structures are developed intensely, both high resource demand and lack of high-resolution

M. Kaasik (✉)
Institute of Physics, University of Tartu, Ülikooli 18, 50090 Tartu, Estonia
e-mail: marko.kaasik@ut.ee

M. Pindus • H. Orru
Department of Public Health, University of Tartu, Ülikooli 18, 50090 Tartu, Estonia

T. Tamm
Institute of Ecology and Earth Sciences, University of Tartu, Ülikooli 18, 50090 Tartu, Estonia

D. Steyn and R. Mathur (eds.), *Air Pollution Modeling and its Application XXIII*,
Springer Proceedings in Complexity, DOI 10.1007/978-3-319-04379-1_68,

micrometeorological data are limiting their applications in urban scale. The simple modelling techniques are still widely in use [2].

In this study the Gaussian AEROPOL model (basic features see [3]) is applied to estimate the annual concentrations of nitrogen dioxide in Tartu, the second largest town of Estonia, for RHINE (Respiratory Health in Northern Europe) study. It is evident that in densely built-up areas the plain Gaussian model does not perform well due to multiple obstacles and volume occupied by the buildings. The street canyon approach (e.g. [6]) is not applicable in towns of Estonia, as the building facades are mostly of non-uniform height and include many gaps. In this paper the Gaussian model results are improved, applying the concept of urban canopy as a porous media by Genikhovich et al. [1]. It is evident that indoor air within the buildings is nearly standing still compared to the outdoor air and thus, excluded from the active dispersion of pollutants in fact. As the street emissions mix initially only in a few meters thick layer, the correction based on open air fraction between the buildings for near-street dispersion is justified.

## 68.2 Methods

The $NO_X$ dispersion calculations for Tartu, the second largest town of Estonia (about 100,000 inhabitants) were carried out for each year from 1993 to 2011, relying on (i) statistical data of industrial point sources, (ii) domestic heating emissions according to questionnaire-based studies [4] and (iii) traffic emissions based on annual traffic flow modelling studies ordered by Tartu City Government and emission coefficients of CAR-FMI [5]. It was found that street transport emissions constitute about a half of total emissions and are highly dominating in peak concentrations due to low emission height from main streets. The purpose of the modelling was to quantify the RHINE study-population's exposure to $NO_X$ for later linking with self-reported health symptoms. Main focus of this questionnaire is to determine respiratory complaints [7].

As the emission data exist for $NO_X$ and AEROPOL model does not include chemical transformations, $NO_2$ fractions in $NO_X$ were derived from multi-annual monitoring data from stations in Estonia, as a function of total $NO_X$ concentration – the long-term average $NO_2$ fraction depends strongly on total concentration, from less than 50 % in most polluted urban sites to 90–95 % in background sites.

In post-processing of modelled ground-level concentrations, the porosity concept by Genikhovich et al. [1] was applied to modelled gridded concentrations originating from street emissions: the area under buildings is excluded from dispersion volume in each grid cell, i.e. the concentration is divided to the fraction of porosity, i.e. non-built-up area. The grid step of modelling was 40 m, but the porosity was taken as moving average of current cell and neighbour cells, thus in surrounding 120 by 120 m area. With this resolution, we assume well-spread porosity instead of individual buildings and gaps between them. The typical fractions of built-up area in city center are 0.2–0.5 and in outskirts 0.05–0.2, the building heights 10–20 and up to 10 m respectively.

The computed annual average concentrations were validated against $NO_2$ passive sampling results available since 1997 (2-week measuring campaigns four times a year) and an urban monitoring station since 2007.

## 68.3 Results

The "raw" concentration fields from the AEROPOL model show too sharp transitions from near-street high levels to the urban background, thus fitting not well to the measured concentrations at sampling points. It is found that smoothing the concentrations with 3 by 3 cell moving average improves the fit.

On average for 1997–2011, the fit of modelled to measured concentrations improves significantly after porosity correction (Fig. 68.1, Table 68.1). For none of these years this correction made the fit worse. As the modelled concentrations are slightly underestimated on average, the porosity correction takes them closer

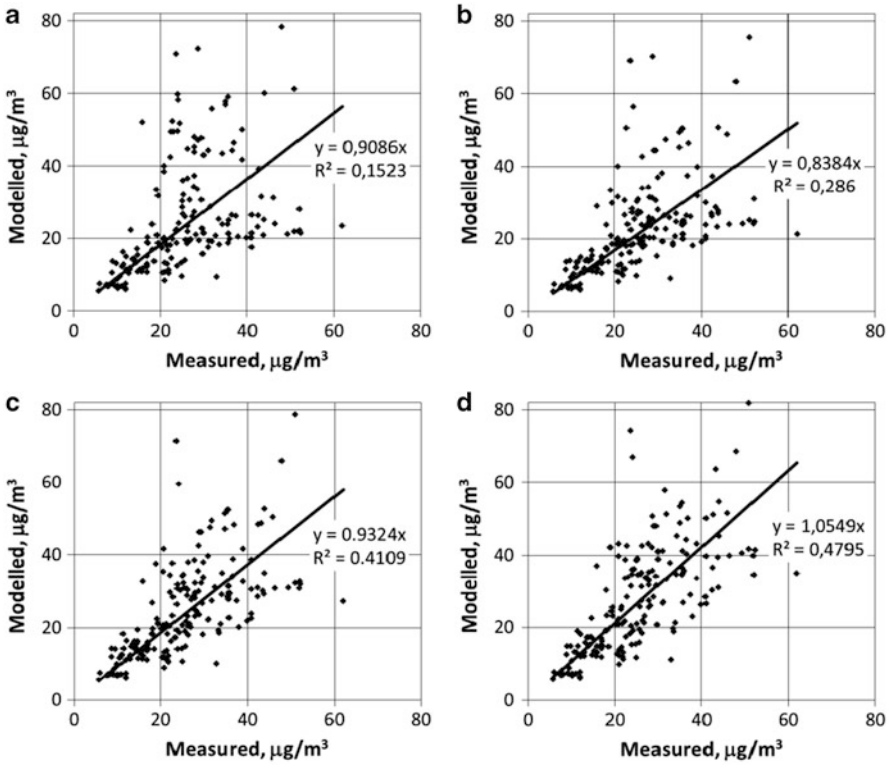


**Fig. 68.1** Fit of modeled to measured concentrations of $NO_2$ ($mg/m^3$) in Tartu based on yearly averages in all measurement sites from 1997 to 2011: (**a**) raw output from AEROPOL, (**b**) smoothed, 3 by 3 cell moving average, (**c**) smoothed and divided by porosity, (**d**) smoothed and divided by squared porosity

**Table 68.1** Fit parameters of modeled vs. measured yearly average concentrations of $NO_2$ in Tartu

| | Initial (smoothed) | | Porosity-corrected | | Porosity square corrected | |
|---|---|---|---|---|---|---|
| | Slope | $R^2$ | Slope | $R^2$ | Slope | $R^2$ |
| Average | 0.86 | 0.42 | 0.95 | 0.54 | 1.08 | 0.62 |
| Std. dev. | 0.16 | 0.16 | 0.17 | 0.13 | 0.20 | 0.13 |

Statistics based on all yearly averages from 1997 to 2011

to the measured ones. Even better fit (higher determination coefficients $R^2$ and correlations) is found when dividing the modelled concentrations by squared porosities. Stronger than linear dependence may occur due to slowing down the air flow between the buildings.

## 68.4 Conclusion

The porosity concept is efficient for correcting the urban concentrations estimated with a Gaussian model and thus, we encourage including it into model code.

**Acknowledgements** This study was funded by FAS grant 2010–0442 and Estonian Research Council grant 8523.

## References

1. Genikhovich E, Gracheva I, Filatova E (2002) Modelling of urban air pollution: principles and problems. In: Borrego C, Schayes G (eds) Air pollution modelling and its application, XV. Kluwer, New York, pp 275–283
2. Hanna S (2014) A 40-year history of a simple urban dispersion model and its evaluation. In: Steyn D, Mathur R (eds) Air pollution modeling and its application XXIII. Springer, Dordrecht
3. Kaasik M, Kimmel V (2004) Validation of the improved AEROPOL model against the Copenhagen data set. Int J Environ Pollut 20(1–6):114–120
4. Kaasik M, Orru H, Tekkel E, Vals P (2007) Situation and tendencies in air quality in a North European medium-sized town. In: Abstracts of the 6th international conference on urban air quality, University of Hertfordshire, Hatfield, 212
5. Karppinen A, Kukkonen J, Elolähde T, Konttinen M, Koskentalo T (2000) A modelling system for predicting urban air pollution, comparison of model predictions with the data of an urban measurement network. Atmos Environ 34:3735–3743
6. Mensink C, Lewyckyj N (2001) A simple model for the assessment of air quality in streets. Int J Veh Des 27(1–4):242–250
7. Toren K, Gislason T, Omenaas E, Jogi R, Forsberg B, Nystrom L, Olin AC, Svanes C, Janson C (2004) A prospective study of asthma incidence and its predictors: the RHINE study. Eur Respir J 24(6):942–946

# Chapter 69
# An Evaluation of the Box Model Estimating Carbon Monoxide Concentration in the City of Caracas, Venezuela

**Arcangelo Sena D'Anna, Luis Díaz Alarcón, Alberto Espinoza Cedeño, and Enrique Chacón Melgarejo**

**Abstract** In 1999, a pilot monitoring program was conducted by PDVSA in order to assess air quality changes in Caracas as part of elimination of leaded gasoline in Venezuela, which started in the year 2000 with the implementation of premium unleaded gasoline and automobiles provided of catalytic converters. Elimination of leaded gasoline was completed in 2005 when its use was banned. This study presents an evaluation of an air quality model performance estimating carbon monoxide concentrations in Caracas from 2000 to 2010 in two scenarios: (i) fixed mixing height and (ii) variable mixing height, which consisted in a quantitative comparison of the box model output with observed data of carbon monoxide concentrations. The box model required information of seasonal behavior of meteorology, specifically wind speed data. In order to estimate carbon monoxide emissions, a traffic model which consider growth of vehicles fleet and employs emission factors associated with fuel quality changes during the study period was used. Results show that the model can estimate carbon monoxide concentrations with an agreement index of 0.52 and 0.57 that are acceptable. Some difference were found between observed and estimated values, mainly during the years 2005 and 2010, related to changes in vertical diffusion and another carbon monoxide source not considered in this model. The box model allows predicting concentrations of carbon monoxide with an NMSE of 0.11 and 0.12 when comparing with observed values for two evaluated scenarios.

A. Sena D'Anna (✉) • L. Díaz Alarcón • A. Espinoza Cedeño • E. Chacón Melgarejo
PDVSA-Intevep. Environment Department, Air Pollution Laboratory and Emission Control Technologies Group, P.O. Box 76343, Caracas 1070-A, Venezuela
e-mail: senaa@pdvsa.com; diazlvx@pdvsa.com; espinozaap@pdvsa.com; chaconen@pdvsa.com

D. Steyn and R. Mathur (eds.), *Air Pollution Modeling and its Application XXIII*, Springer Proceedings in Complexity, DOI 10.1007/978-3-319-04379-1_69,

## 69.1 Introduction

Since 1990, Bolivarian Republic of Venezuela enacted a policy oriented to improve air quality through leaded gasoline elimination. The first step was reducing lead content from 4.7 to 2.8 gPb/l in the year 2000 [1], then in the same year was introduced unleaded gasoline and vehicles with catalytic converter. Finally in 2005 leaded gasoline was banned. Some studies have been developed since 1982 in order to verify reduction of lead concentration in air and human blood lead levels [2–5]. A significant reduction of lead in air since program was started had been evidenced. In 2000, an air quality monitoring program was conduced by PDVSA, who installed an air quality network around of Caracas City, which is located at 10° 30′ 24″ North latitude and 66° 55′ 39″ west longitude and 900 m.a.s.l. This city is inside of a valley of 25 km long (east – west) and 5 km wide (north – south), limited at north by Waraira Repano mountain. Population in Caracas is approximately 5.4 million, and it is mainly influenced by vehicles fleet emissions [6]. Several studies of air quality have been done in Caracas [7–9], however there are not studies using air pollution models. The aim of this work is to study box model performance for carbon monoxide (CO) comparing two sceneries: (i) fixed mixing height and (ii) variable mixing height.

## 69.2 Methods

In this study, CO concentrations for the period 2000–2010 were measured hourly in an air quality station named Sta. Eduvigis, located at the east of the city (10° 30′ 24″ N and 66° 50′ 18″ W) (See Fig. 69.1).

Non-dispersive infrared absorption technique was used to measure CO concentrations. Additionally hourly surface meteorology data (wind speed and direction, temperature and relative humidity) were also recorded. We apply the box model formulation proposed by Jonquera [10], and CO monthly concentrations forecast were compared with CO measured in the same period. The box model consider a spatial region consisting of a box with width Δx, depth Δy and height H. The horizontal axes $x$ follows the wind direction and $y$ the crosswind orientation. Then, the mass balances for a given species which is well mixed in the volume we can be describe as follow:

$$\frac{d}{dt}(C_i) = \frac{q_i}{H} - R_i - \frac{s_i}{H} + \frac{u}{\Delta x}\left(C_i^0 - C_i\right) \tag{69.1}$$

Where $C_i$ is the concentration of species $i$ in the volume, $C_i^0$ is the upwind concentration of species $i$, $u$ is the wind speed and H is the mixing height. $q_i$ and $s_i$ are emission and removal rates per area unit respectively, and $R_i$ is the net rate of chemical transformation for species $i$. Assuming that $\Delta x$, $\Delta y$, H are constant and $R_i$

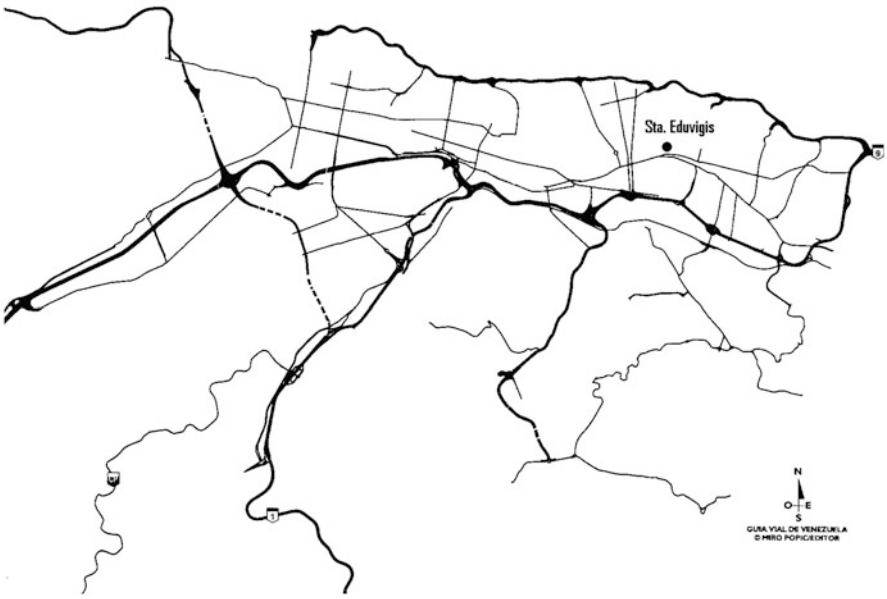


**Fig. 69.1** Study area

is negligible for CO, the analytical solution to forecast the average concentrations $\langle C_i \rangle$ by the box model can be written as follow:

$$\langle C_i \rangle = \left\langle \frac{C_i(0)}{\left[\frac{\upsilon_{d,i}}{H} + \frac{1}{\tau_r}\right] t'} \right\rangle + \left\langle \frac{C_i^0}{1 - \frac{\upsilon_{d,i}\,\Delta x}{Hu}} \right\rangle + \left\langle \frac{q_i}{\upsilon_{d,i} + \frac{uH}{\Delta x}} \right\rangle \tag{69.2}$$

Where $\tau_r$ is the residence time for an air parcel moving across of the city in the average time, $\upsilon_{d,i}$ is deposition velocity (0.006 m/s), $t'$ is the average time (720 h) and $\Delta x$ is 1,000 m.

$$\tau_r = \frac{\Delta x}{u} \tag{69.3}$$

We assume that CO initial concentration $C_i(0)$ is 1.1 ppm and upwind concentration of CO $C_i^0$ is 30 % of emission in Caracas. Emission model proposed by Sena [11] was used to estimate $q_i$, which include an intensive road description and vehicles fleet circulation. We also assume that emission is spatially homogenous and variable in time. Model use emission factors reported by González et al. [12] and Martín et al. [13] which were selected by the model depending of vehicles category (carburettor, fuel injection and fuel injection with catalytic converter), quality of fuel (lead and unleaded gasoline) and were modified depending of speed vehicles endwise of study period. $u$ is month average values calculated from data measured.

We studied two scenarios of H values. First, H was 400 m fixed and second, H was considered as mixing condensation level (MCL), which is an approximation of elevation of the cloud base where temperature lapse rate is dry adiabatic and mixing ratio is constant from the ground to the cloud base. This height was estimated for each month with follow equation [14]:

$$H = -\frac{T - T_d}{\Gamma_a - \Gamma_d} \tag{69.4}$$

Where $T$ is ambient temperature, $T_d$ is dew point temperature and $\Gamma_a$ and $\Gamma_d$ are dry and wet adiabatic rates respectively. $\Gamma_a$ is −9.8 °C/Km and $\Gamma_d$ is −1.8 °C/Km. Performance of the box model was evaluated using the agreement index $d$ recommended by Willmott [15] and the normalized mean square error (NMSE) [16].

## 69.3 Results and Discussion

The box model showed an acceptable agreement index of 0.52 when H was fixed in 400 m (first scenario), and of 0.57 when mixing condensation level was used as H (Second scenario). Statistical errors of the model expressed as normalized mean square error (NMES) were 0.11 and 0.12 for both scenarios respectively, which are acceptable since NMES most be less to 0.5. Figure 69.2 shows CO concentration modeled versus observed data for both scenarios, where some out layer points could be associate another sources of CO different to fleet vehicles, such as fire forest. These out layer points correspond to events occurred between 2005 and 2010,

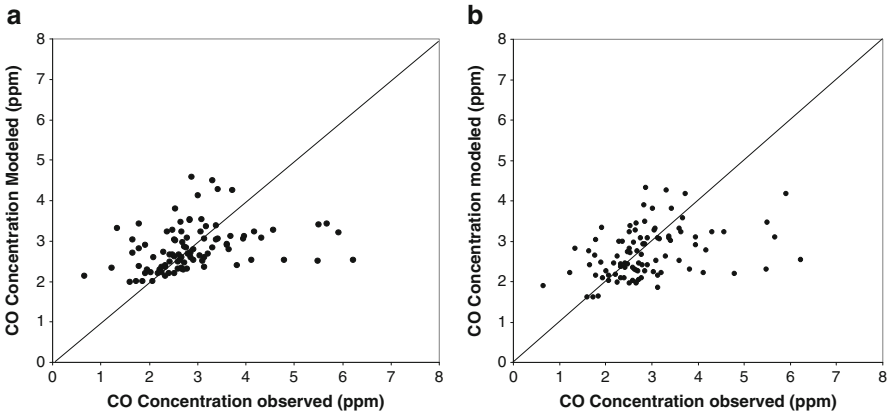


**Fig. 69.2** Comparison CO concentration modeled and observed for two sceneries (**a**) H: 400 m fixed and (**b**) H is free convection height

however in second scenario those out layer points tended adjust when MCL was used, indicating that not all out layer points correspond entirely to fire forest, but also meteorological condition as low vertical diffusion in the boundary layer planetary.

## 69.4 Conclusion

The box model evaluated shows an agreement index and normalized mean square error acceptable for estimating carbon monoxide concentration in Caracas. Moreover, meteorology plays an important role in the pollution model of this tropical region, particularly vertical diffusion. The next model to use must consider vertical diffusion process in order to reduce the uncertainty.

## References

1. ESMAP Eliminación del Plomo en la Gasolina en America Latina y el Caribe. Informe situacional 1996. N°. 194/97EN. 120 p
2. Cedeño A, Arrocha A, Lombardi C (1988) Estudio Comparativo de los niveles de Plomo en sangre y plomo en aire. Informe Técnico. INT-EPTP-00036,87. 42 p
3. Cedeño A, Arrocha A, Lombardi C (1990) Estudio Comparativo de los Niveles de Plomo en Aire y Sangre Parte II. Informe Técnico. INT-0009, 90. 45 p
4. MARNR (1982–1990) Boletines de Calidad del Aire de la Zona Metropolitana del Valle de Caracas. Dirección General de Calidad Ambiental del Ministerio del Ambiente y de los Recursos Naturales Renovables, Caracas, 28 p
5. MINAMB (2007) Informe de Calidad del Aire 2006. Dirección General de Calidad Ambiental del Ministerio del Poder Popular para el Ambiente, Caracas. 17 p
6. Sena D'Anna A (2003) Determinación de los Factores que Intervienen en los Procesos Fotoquímicos en la Atmósfera de Caracas. MSc Thesis, Universidad Central de Venezuela, Caracas-Venezuela, 164 p
7. Guajardo N, Ramírez A, Díaz F, Castillo E, Otero A, Parra J (2010) Concentración de las partículas totales suspendidas en la atmósfera de Caracas. Revista de la Facultad de Ingeniería UCV 25(2):81–91
8. Santana R, Anselmi A, Delgado N, Diaz A, Sena A, Martin P, Perez O (2001) Estudio de Calidad de Aire y Calidad de combustible en el Área Metropolitana de Caracas. Visión Tecnológica 8(2):131–146
9. Sena D'Anna A, Díaz A, Espinoza A, Chacón E, Toro N, Alfonzo Ingrid (2011) Estudio de la calidad del aire en la ciudad de Caracas y Maracaibo durante el año 2011. INT-13792,2011, 46 p
10. Jorquera H (2002) Air quality at Santiago, Chile: a box modeling approach-I. Carbon monoxide, nitrogen oxides and sulfur dioxide. Atmos Environ 36:315–330
11. Sena D'Anna A, Lopez R (2012) Modelo de emisiones atmosféricas del parque automotor en la ciudad de Caracas, Venezuela (Formulación del modelo). INT-13875,2012, 25 p
12. González M, Rodríguez G, De Vita R (1995) Característica del parque automotor y de la utilización de las gasolinas en Venezuela. Visión Tecnológica 1(2):2–12
13. Martin P, Tachon O, Perez O, Medina T, Celta D (1995) "Evaluación de combustibles: Actividad reformulación de Gasolinas. Evaluación de las emisiones de escape de gasolinas oxigenadas y convertidores catalíticos". Reporte técnico INT-03048,95, 30 p

14. Saucier WJ (1995) Principles of meteorological analysis. Dover, Mineola, 438 p
15. Willmott CJ (1981) On the validation of models. Phys Geogr 2(2):184–194
16. Kumar A, Bellman NK, Sud A (1999) Performance o fan industrial source complex model: predicting long-term concentrations in an urban area. Environ Prog 18(2):93–100

# Chapter 70
# Implications of Vegetation on Pollutant Dispersion in an Idealized Urban Neighborhood

**Christof B. Gromke and Bert J.E. Blocken**

**Abstract** Configurations of avenue-trees and a central park in an idealized urban neighborhood and their implications on traffic pollutant concentrations at the pedestrian level were investigated with Computational Fluid Dynamics (CFD). Steady state simulations were performed using a Reynolds Stress Model (RSM) extended with additional terms to represent the effects of vegetation on air flow. The results show that the type of configuration of avenue-trees and/or park has a clearly noticeable effect on the overall pollutant distribution and on the maximum concentration. The central park was found to lead to a general reduction of concentrations in its immediate vicinity and at locations downwind.

## 70.1 Introduction

In the recent years, a number of studies has revealed that trees in urban street canyons cause increased traffic pollutant concentrations by reducing the natural ventilation, see e.g. Gromke and Ruck [7] and references therein. However, these studies were limited to the street canyon scale. To the best of our knowledge, the effects of trees on air quality at the neighborhood scale have not yet been investigated apart from intermediate scale studies for two intersecting street canyons by Buccolieri et al. [4] and Vos et al. [10]. To that end, traffic pollutant dispersion studies for an idealized urban neighborhood with various configurations of avenue-trees and a central park were performed and are presented here.

C.B. Gromke (✉) • B.J.E. Blocken
Building Physics and Services, Eindhoven University of Technology,
P.O. Box 513, 5600 MB Eindhoven, The Netherlands
e-mail: c.b.gromke@tue.nl

D. Steyn and R. Mathur (eds.), *Air Pollution Modeling and its Application XXIII*,
Springer Proceedings in Complexity, DOI 10.1007/978-3-319-04379-1_70,

## 70.2 Setup and Methods

A generic urban neighborhood consisting of $5 \times 5$ building blocks with dimensions of 90 m $\times$ 90 m $\times$ 30 m (L $\times$ W $\times$ H) and streets of 18 m width was investigated (Fig. 70.1). In total, five vegetation configurations differing in the arrangement of avenue-trees, a park and combinations of these, plus the vegetation-free neighborhood were studied (Fig. 70.2). The avenue-trees were positioned horizontally centered in street canyons with crowns of 6 m width and 12 m height, starting 6 m above the street level. The park, consisting also of 12 m high trees starting at 6 m above the ground level, was positioned in the center of the neighborhood replacing an entire building block. A leaf area density (LAD) of 1 $m^2/m^3$ was assigned to both the avenue-trees and the trees in the park. The computational domain size and boundary conditions were made according to recommendations specified in Franke et al. [6] and Tominaga et al. [9]. Based on a grid sensitivity study, cubical cells with 1.5 m edge length were used to discretize the street canyons within the building array. A stretching factor of 1.2 was applied to cells outside the array.

The numerical simulations were performed with the Computational Fluid Dynamics (CFD) code ANSYS FLUENT 12.1.4 [1]. The implemented Reynolds Stress Model (RSM) with standard wall functions for near-wall treatment was employed to solve the steady state Reynolds-averaged Navier Stokes (RANS) equations. At the inlet boundary, vertical profiles for the streamwise mean velocity U, the turbulence kinetic energy k, and the dissipation rate ε according to Richards and Hoxey [8] were imposed with an aerodynamic roughness length $z_0 = 1.0$ m and a friction velocity $u^* = 1.18$ m/s, resulting in an approach flow velocity of $U(H) = 10$ m/s at building height H. A wall roughness of $k_s = 0.01$ m together with a roughness constant $C_s = 0.5$ corresponding to a roughness length $z_0 = 0.0005$ m, see Blocken et al. [3], was assigned to the building surfaces and the streets inside the building array. More boundary conditions are provided in Fig. 70.1. The crowns of the avenue-trees were defined as porous fluid zones in which additional terms accounting for the effects of vegetation on flow and turbulence according to Ayotte et al. [2] were assigned. A passive scalar was released from the entire street area within the building array by specifying a constant flux boundary condition. The dispersion calculations were performed with a turbulent Schmidt number $S_{ct} = 1.0$ based on a comparison with measurements from the database CODASC [5].

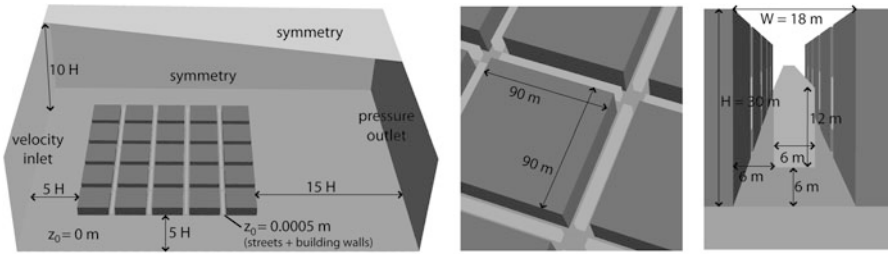


**Fig. 70.1** Computational domain, boundary conditions, and building arrangement with avenue-trees

## 70.3 Results and Discussion

In Fig. 70.2 the normalized pollutant concentrations $c^+ = c\ U(H)/Q$, with the scalar concentration c, the approach wind speed U(H), and the scalar source flux from the street surface Q, at 2 m above ground are shown for the vegetation-free (panel a) and the vegetation configurations as indicated by the insert in the upper right part in each of the panels (b–f).

### *70.3.1 Avenue-Trees in Every Street Canyon (Panel b)*

In comparison to the vegetation-free configuration (panel a), a faster build-up of concentrations in the wind-parallel canyons is observed. Strong increases are present around the intersections D2 and D4. Higher concentrations also occur generally in the wind-perpendicular canyons. However, the trees do not lead everywhere in the neighborhood to increased concentrations. At the downwind side, lower concentrations are found in the wind-parallel canyons G2/4 and I2/4.

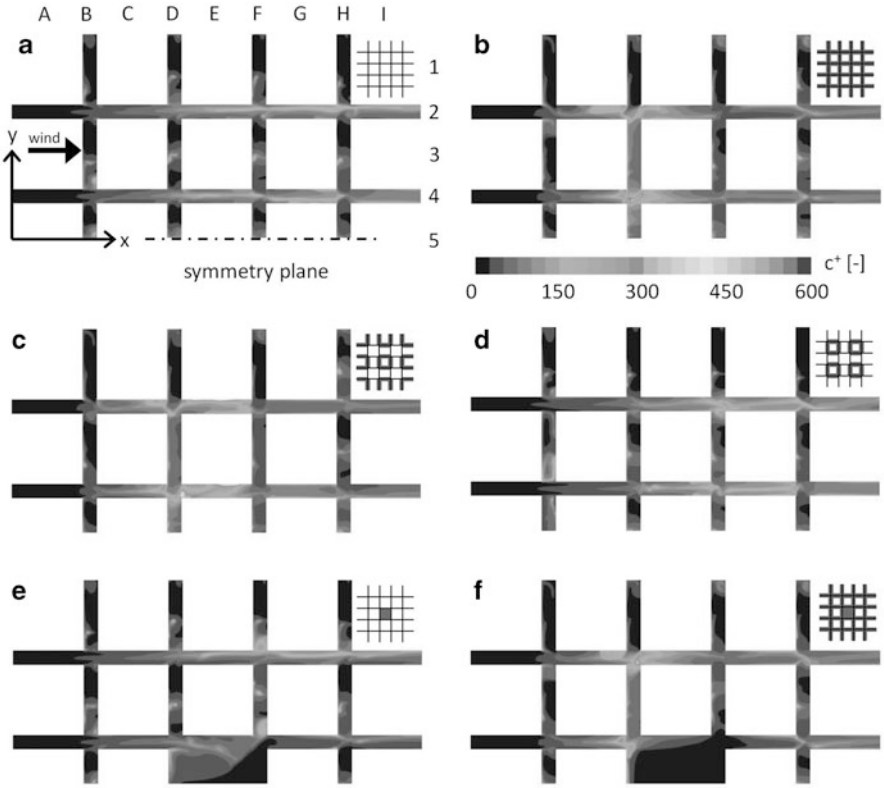


**Fig. 70.2** Normalized pollutant concentrations $c^+$ [−] at 2 m height above street

### *70.3.2 Avenue-Trees in Every Second Street Canyon, Type I (Panel c)*

For this configuration, the highest maximum concentrations are found. In particular in the central wind-parallel street canyons E2/4, increased pollutant concentrations are present. They are also higher than those in the tree-everywhere configuration (panel b).

### *70.3.3 Avenue-Trees in Every Second Street Canyon, Type II (Panel d)*

The maximum pollutant concentrations are clearly lower in comparison to the previous configurations (panel b and c). However, in the downwind located wind-parallel canyons G2/4 and I2/4, and in some wind-perpendicular canyons (F3/5), higher concentrations compared to the tree-everywhere configuration (panel b) are found.

### *70.3.4 Park (Panel e)*

In comparison to the vegetation-free configuration (panel a), the park in the center of the neighborhood results in decreased concentrations at downwind locations in the central wind-parallel street canyons (G4 and I4). Lower concentrations are also present in the street next to the park (E4). Immediately windward of the park, in street D5, however, higher concentrations are observed.

### *70.3.5 Park and Avenue-Trees in Every Street Canyon (Panel f)*

The high concentrations at the intersection D4 which are observed in the tree-everywhere configuration (panel b) are reduced. In comparison to the park-only configuration (panel e), lower pollutant concentrations are found for large areas within the park.

## 70.4 Summary

The results show that different configurations of avenue-trees in urban neighborhoods result in considerably altered traffic pollutant concentrations at the pedestrian level. Reducing the overall number of avenue-trees (or the total vegetation volume)

does neither necessarily lead to lower concentrations in general nor to lower maximum concentrations. A park leads to a general reduction of concentrations in its immediate vicinity and at locations downwind.

**Acknowledgments** This research was supported by a Marie Curie Intra European Fellowship within the 7th European Community Framework Programme.

## References

1. ANSYS Inc (2009) ANSYS FLUENT 12.0 – theory guide. April 2009, p 816
2. Ayotte KW, Finnigan JJ, Raupach MR (1999) A second-order closure for neutrally stratified vegetative canopy flows. Bound-Lay Meteorol 90:89–216
3. Blocken B, Stathopoulos T, Carmeliet J (2007) CFD simulation of the atmospheric boundary layer: wall function problems. Atmos Environ 41:238–252
4. Buccolieri R, Salim SM, Leo LS et al (2011) Analysis of local scale tree-atmosphere interaction on pollutant concentration in idealized street canyons and application to a real urban junction. Atmos Environ 45:1702–1713
5. CODASC (2008) Concentration data of street canyons, Karlsruhe Institute of Technology (KIT). www.codasc.de. Accessed 14 June 2013
6. Franke J, Hellsten A, Schlünzen H et al (2007) Best practice guideline for the CFD simulation of flows in the urban environment. COST action 732. Available via http://www.mi.uni-hamburg.de/fileadmin/files/forschung/techmet/cost/cost_732/pdf/BestPractiseGuideline_1-5-2007-www.pdf. Accessed 9 June 2013
7. Gromke C, Ruck B (2012) Pollutant concentrations in street canyons of different aspect ratio with avenues of trees for various wind directions. Bound-Lay Meteorol 144:41–64
8. Richards PJ, Hoxey RP (1993) Appropriate boundary-conditions for computational wind engineering models using the kappa-epsilon turbulence model. J Wind Eng Ind Aerodyn 46:145–153
9. Tominaga Y, Mochida A, Yoshie R et al (2008) AIJ guidelines for practical applications of CFD to pedestrian wind environment around buildings. J Wind Eng Ind Aerodyn 96:1749–1761
10. Vos PEJ, Maiheu B, Vankerkom J et al (2013) Improving local air quality in cities: to tree or not to tree? Environ Pollut 183:113–122

# Chapter 71
# Dynamic Evaluation of the CMAQv5.0 Modeling System: Assessing the Model's Ability to Simulate Ozone Changes Due to $NO_x$ Emission Reductions

**Kristen M. Foley, Christian Hogrefe, George A. Pouliot, Shawn J. Roselle, Norm Possiel, Heather Simon, and Brian Timin**

**Abstract** Regional air quality models are frequently used for regulatory applications to predict changes in air quality due to changes in emissions or changes in meteorology. Dynamic model evaluation is thus an important step in establishing credibility in the model predicted pollutant response. Beginning in 2003, the U.S. Environmental Protection Agency required substantial reductions in $NO_x$ emissions from power plants in the eastern U.S. which resulted in a decrease in ozone concentrations at monitoring sites in this region. This observable change in air quality has been used previously as a case study for dynamic evaluation of the Community Multiscale Air Quality (CMAQ) modeling system. Evaluation studies of previous CMAQ versions have shown that the model predicted decrease in ozone from 2002 to 2005 is less than the observed ozone change in this region. In this study, summertime simulations of 2002 and 2005 were conducted using the CMAQ version 5.0 modeling system released in 2012 that included several model updates aimed at improving the model predicted response, including updates to important model inputs. "Cross" simulations were conducted to separate the modeled impact of the emissions changes on ozone concentrations from the changes attributable to differences in meteorology across these years. Results show the change in the upper end of the ozone distribution explained by emission reductions is similar

K.M. Foley (✉) • C. Hogrefe • G.A. Pouliot • S.J. Roselle
Atmospheric Modeling and Analysis Division/National Exposure Research Laboratory, United States Environmental Protection Agency (US EPA), Research Triangle Park, NC 27711, USA
e-mail: Foley.Kristen@epa.gov; Hogrefe.Christian@epa.gov; Pouliot.George@epa.gov; Roselle.Shawn@epa.gov

N. Possiel • H. Simon • B. Timin
Air Quality Assessment Division/Office of Air Quality Planning and Standards, United States Environmental Protection Agency (US EPA), Research Triangle Park, NC 27711, USA
e-mail: Possiel.Norm@epa.gov; Simon.Heather@epa.gov; Timin.Brian@epa.gov

D. Steyn and R. Mathur (eds.), *Air Pollution Modeling and its Application XXIII*, Springer Proceedings in Complexity, DOI 10.1007/978-3-319-04379-1_71,

in magnitude to the change in ozone due to changes in meteorology across these years. Overall, the observed ozone decrease in the eastern U.S. continues to be underestimated by the model at both urban and rural monitoring sites.

## 71.1 Introduction

EPA's Nitrogen Oxides State Implementation Plan Call ($NO_x$ SIP Call) rule was implemented in 2003 through early 2004. A $NO_x$ Budget Trading program was established that led to reductions in $NO_x$ emissions from large electrical generating units (EGUs) in 20 states and Washington DC. Emission reductions contributed to a 30 % reduction in observed ozone levels in many parts of the region between the summers of 2002 and 2005 [2]. Continuous emissions monitoring data were available for major units, allowing for very accurate quantification of the emission reduction. These features make this an excellent retrospective case for evaluating the ability of models to predict changes in air quality resulting from changes in emissions, referred to as dynamic evaluation [1]. Here we build upon the dynamic evaluation of the Community Multiscale Air Quality (CMAQ) modeling system documented by Gilliland et al. [2] and Godowitch et al. [3] using this case study to evaluate a new version of the modeling system (CMAQv5.0.1) and utilizing novel "cross" simulations to separately quantify the impact on ozone predictions stemming from (a) changes in emissions and (b) changes in meteorology.

## 71.2 Methods

CMAQv5.0.1 simulations were performed over the continental U.S. for June 1 through September 30th 2002 and 2005 using a grid with 12 km horizontal resolution and 35 vertical layers. Meteorological inputs were based on WRF3.3 with MCIPv4.0. Emissions inputs used SMOKE3.1 with MOVESv2010b for 2002 and 2005 mobile emissions. Emissions inputs included inline NO produced from lightning using year specific data from the National Lightning Detection Network. Boundary conditions were based on 2005 monthly median values from a GEOS-Chem v9-01-02 simulation using v8-02-01 chemistry, GEOS-5 meteorology and ICOADS shipping emissions. Ozone observations from the AQS and CASTNET networks were used to evaluate model predicted daily maximum 8-h average ozone (MDA8 $O_3$), the model metric used for attainment demonstrations. In addition, AQS $NO_2$ monitors are used to diagnose errors in emission inputs.

In addition to the 2002 and 2005 simulations (Sim02e02m, Sim05e05m), two "cross" sensitivity simulations are used to simulate air quality under 2005 emissions with 2002 meteorology (Sim05e02m) and 2002 emissions with 2005 meteorology (Sim02e05m). The processing of emissions from EGUs with available continuous emission monitoring systems (CEM) data for these simulations is based on unit

specific adjustments of the emissions to account for the impact of different meteorological influences in a different year. Summertime 2005 $NO_x$ emissions are generally lower than 2002 emissions, but the temporal fluctuations are different due to differences in electricity demand which is heavily influenced by year-specific meteorology. To estimate 2002 emissions with 2005 meteorological patterns ($EMIS_{02e05m}$) we scale the hourly 2005 CEM emissions ($CEM_{2005}$) based on the ratio of summer total CEM emissions ($S_{Y1}/S_{Y2}$) for a particular EGU unit in 2002 versus 2005:

$$EMIS_{02e05m} = CEM_{2005} \times (S_{2002}/S_{2005}) \tag{71.1}$$

An analogous calculation is made to estimate 2005 emissions with 2002 meteorological patterns.

Mobile emissions for the cross runs are based on MOVES simulations using the designated emissions year and meteorology year (e.g. 2002 emissions with 2005 meteorology). Emissions from nonroad (e.g. construction), industrial point and large marine sectors are based on the emissions year but shifted to match the day-of-the week of the meteorology year. Emissions from fertilizer application, biogenic sources, $NO_x$ from lightning, fires and dust are tied to the meteorological year. All other sectors have the same inventory for all scenarios except modified for the day-of-the-week of the meteorology year.

## 71.3 Results and Discussion

Figure 71.1 shows the 2005–2002 difference in the average of the top ten summer MDA8 ozone values. The model predicts large ozone decreases in NC and VA, but not as large as what is seen in the observations. In addition, the model misses the region of 15–25 ppb observed decreases along the east coast and Ohio River


**Fig. 71.1** 2005–2002 difference in the average of the top ten summer MDA8 ozone values (ppb) at AQS sites (*circles*) and CASTNET sites (*diamonds*)

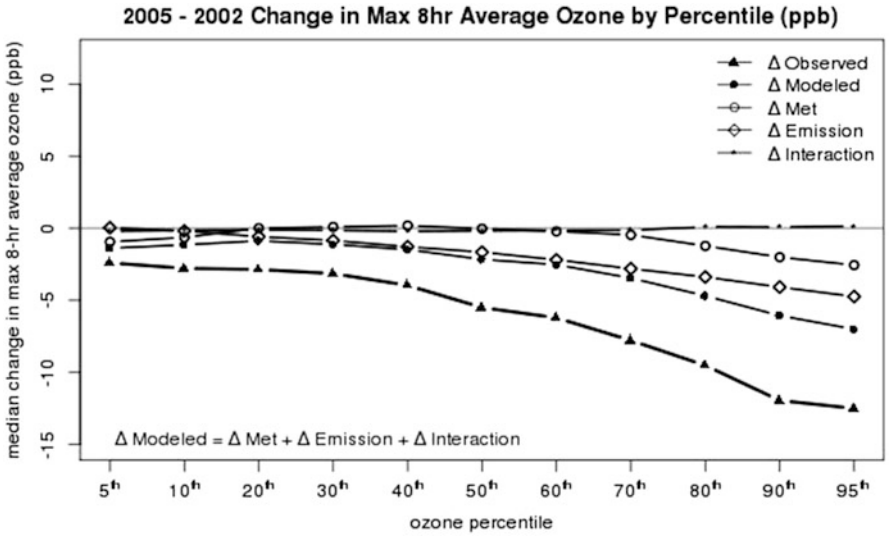


**Fig. 71.2** The median change in ozone across AQS sites within NOx SIP Call states at different percentiles of max 8 h average ozone (ppb) based on the 2005–2002 observations (*filled triangles*), and model simulations: Sim05e05m-Sim02e02m (*filled circles*; total modeled change), Sim05e02m-Sim02e02m (*diamonds*; emissions change) and Sim02e05m-Sim02e02m (*circles*; meteorology change). The remaining interaction term (*stars*) represents the effect of meteorology on ozone chemistry that is not captured by the cross simulations

Valley. In order to diagnose this model error we evaluate the change in $NO_2$ mixing ratios at AQS sites within $NO_x$ SIP call states. Analysis by Godowitch et al. [4] indicates that morning $NO_x$ concentrations are strongly related to ground level $NO_x$ emissions levels. An evaluation of the change in 2005–2002 weekday $NO_2$ mixing ratios showed that the decrease in morning (5–9 am) $NO_x$ levels from 2002 to 2005 is underestimated by the model (observed median decrease of 15 % verses modeled decrease of 6 %), suggesting an underestimation of the decrease in surface $NO_2$ emissions across these years [5, 6].

Figure 71.2 shows the change in modeled and observed ozone at different percentiles (calculated across 122 summer days at each site). For each percentile, the median change across all 444 AQS sites within NOx SIP Call states is plotted. Utilizing the cross simulations, the change in the modeled ozone at each percentile is decomposed into the change due to emissions, the change due to meteorology and the interaction between emissions and meteorology. Changes in the upper end of the ozone distribution are driven by both emissions and meteorology. The change in the lower end of the ozone distribution is driven almost entirely by meteorological changes.

The methodology presented here is able to account for the effect of meteorology on emissions as well as the meteorological impact on air quality through advection and dispersion. As a result we are able to isolate and quantify the impact of

the emission controls across these years. Understanding the specific emissions or meteorological-driven causes of the remaining difference between the observed and modeled change in high summertime ozone levels will require additional diagnostic evaluation. Ongoing work includes decomposing the change in $NO_x$ and CO to compare the meteorology-based changes to what we see in ozone. We also plan to evaluate the predicted change in meteorological parameters (e.g. temperature, wind speed) during "high" and "low" ozone days.

**Acknowledgments** The authors would like to recognize the many contributions of others in the development and evaluation of the model simulations described here: Wyat Appel, Kirk Baker, Alison Eyth, Rob Gilliam, Jim Godowitch, Sharon Philips, Rob Pinder (U.S. EPA), Farhan Akhtar (now at the U.S. State Department), Barron Henderson (now at the University of Florida), Lucille Bender, Ryan Cleary, Allan Beidler and Lara Reynolds (Computer Sciences Corporation).

**Disclaimer:** The United States Environmental Protection Agency through it Office of Research and Development funded and managed the research described here. It has been subjected to the Agency's administrative review and approved for publication.

## References

1. Dennis R, Fox T, Fuentes M, Gilliand A, Hanna S, Hogrefe C, Irwin J, Rao ST, Scheffe R, Schere K, Steyn D, Venkatram A (2010) A framework for evaluating regional-scale numerical photochemical modeling systems. Environ Fluid Mech 10:471–489
2. Gilliland AB, Hogrefe C, Pinder RW, Godowitch JM, Foley KM, Rao ST (2008) Dynamic evaluation of regional air quality models: assessing changes in $O_3$ stemming from changes in emissions and meteorology. Atmos Environ 42:5110–5123
3. Godowitch JM, Gilliland AB, Draxler RR, Rao ST (2008) Modeling assessment of point source $NO_x$ emission reductions on ozone air quality in the eastern United States. Atmos Environ 42:87–100
4. Godowitch JM, Pouliot GA, Rao ST (2010) Assessing changes in modeled and observed urban $NO_x$ concentrations from a dynamic model evaluation perspective. Atmos Environ 44:2894–2901
5. Kang D, Hogrefe C, Foley K, Napelenok S, Marthur R, Rao ST (2013) Application of Kolmogorov-Zurbenko filter for the dynamic evaluation of a regional air quality model. Atmos Environ 80:58–69
6. Zhou W, Cohan DS, Napelenok SL (2013) Reconciling $NO_x$ emissions reductions and ozone trends in the U.S., 2002–2006. Atmos Environ 70:236–244

## Questions and Answers

Q: Are you distinguishing between two effects of meteorology: (a) an advection and dispersion effect, and (b) an emission-related effect, e.g. temperature on evaporative emissions? Do you think we need new terms in order to discriminate clearly between these two effects, e.g. for discussions with policy makers? Do you think such "meteorological normalization" will be important for regulatory modeling in the future?

A: You are exactly correct. When we talk about changes due to meteorology in this paper, this includes both the (a) and (b) effects that you describe. For example, we found a small (±0.5 %) change in state wide total $NO_x$ emissions from mobile sources due to changes in meteorology from 2002 to 2005, which could have a slight impact on the modeled ozone predictions. With an additional set of sensitivity simulations it would be possible to further decompose the meteorological effects into these categories in order to quantify the impact from each effect on the final ozone levels. In this application, we suspect the advection and dispersion effect would dominate the ozone signal, but we agree that this would be interesting to explore. We agree that quantifying the impact of a retrospective emission control by removing the impacts of meteorology during the control period is a very valuable approach for communicating to policy makers the net benefit of expensive control measures.

Q: How many alternative meteorological fields did you use to determine the influence of meteorology on ozone concentration? In which way did you evaluate the meteorological fields?

A: The simulations described here rely on meteorological inputs from WRF3.3 simulations for 2002 and 2005. The WRF simulations are considered the state-of-the-art for air quality applications in terms of the parameterizations and data assimilation methods used. The meteorological fields were evaluated against surface measurements for 2 m temperature, wind speed, wind direction and mixing ratio and the evaluation metrics were found to be similar or better than previous simulations for these time periods. We agree that it would be valuable to repeat these simulations using alternative meteorological inputs to identify if the impacts on ozone are consistent under different scientifically valid input fields.

Q: Given that health effects assessments are sensitive to "average" ozone (the entire distribution), not just the 8-h max statistics, how well did the model capture the change in median ozone levels (both over the whole year and the ozone season)?

A: We looked at a plot similar to Fig. 71.2 based on June–September daily median ozone levels rather than daily maximum 8 h average ozone. As expected, the change in the daily median ozone levels is smaller than the change in the max 8-h metric across all percentiles for both the modeled and observed values. Similar to Fig. 71.2, the difference between the modeled and observed change in the median increases with increasing percentiles. Overall, the model performs slightly better at capturing the change in the median ozone, compared to results for the max 8-h statistic. We have not looked at the change over the entire year but agree that this would be very relevant for health effect assessment applications.

# Chapter 72
# Evaluation of a Chemical Data Assimilation System

**Jeremy D. Silver, Jesper H. Christensen, Michael Kahnert, Lennart Robertson, and Jørgen Brandt**

**Abstract** An ensemble Kalman filter data assimilation system has been coupled to the Danish Eulerian Hemispheric Model (DEHM), a hemispheric-scale, offline, chemistry-transport model. We present an evaluation of the performance of the assimilation system in the framework of an Observing System Simulation Experiment (OSSE). This involves assimilating "pseudo-observations" derived from a reference simulation, and then comparing the assimilation run with the reference run. We focus on nitrogen dioxide and the pseudo-observations are generated to mimic the spatial/temporal pattern of retrievals from the Ozone Monitoring Instrument.

## 72.1 Introduction

Data assimilation is widely used in the geophysical sciences to integrate model and observational data in a statistically consistent framework. In-situ or remotely sensed measurements are often assimilated into chemical transport models to generate historical reanalyses or initial conditions for chemical weather forecasts. The ensemble Kalman filter (EnKF) is a common assimilation technique [5], which is relatively simple to implement, accounts for model non-linearity and dynamically evolves background covariances. An EnKF data assimilation system has been coupled to the Danish Eulerian Hemispheric Model (DEHM), a hemispheric-scale, offline, chemistry-transport model [2, 3].

J.D. Silver (✉) • J.H. Christensen • J. Brandt
Department of Environmental Science, Aarhus University, Aarhus, Denmark
e-mail: jds@dmu.dk; jc@dmu.dk; jbr@dmu.dk

M. Kahnert • L. Robertson
Research Department, Swedish Meteorological and Hydrological Institute, Norrköping, Sweden
e-mail: Michael.Kahnert@smhi.se; Lennart.Robertson@smhi.se

D. Steyn and R. Mathur (eds.), *Air Pollution Modeling and its Application XXIII*,
Springer Proceedings in Complexity, DOI 10.1007/978-3-319-04379-1_72,

To evaluate the performance of the assimilation scheme we conducted an Observing System Simulation Experiment (OSSE). The OSSE framework is often used to assess potential benefits of a new measurement platform, especially if the corresponding physical experiment would be technically difficult or very expensive to conduct (e.g. involving satellites). An OSSE involves two sets of simulations: the first simulation (the "nature" run) is used to generate "pseudo-observations", which are then assimilated into the second simulation (the "test" run). The resulting analysis or forecast from the test run can be compared with the nature run [6].

Here we use the OSSE framework to determine the effectiveness of the chemical data assimilation system, and to assess where in the model field the assimilation is most effective. We focus on satellite retrievals of $NO_2$ tropospheric column concentrations (TCCs) derived from OMI. The estimated sensitivity of the retrieved TCCs are provided by the averaging kernels, which are used in the observation operator in the assimilation system. While concentrations are generally highest at the surface, the retrievals are typically more sensitive to trace gas concentrations in the free troposphere. In particular, it is of interest to assess the extent to which assimilation of total- or tropospheric-column satellite retrievals can yield more accurate surface concentrations.

### *72.1.1 Coupled DEHM-EnKF Systems*

The DEHM domain used a coarse $96 \times 96$ horizontal grid on a polar-stereographic projection at about 150 km × 150 km spacing, with 29 vertical layers using terrain-following σ-coordinates up to 100 hPa. Concentrations of 58 reactive gases and 9 particle classes are modelled. The DEHM was run offline with meteorology from MM5. Three-hourly assimilations were performed with an asynchronous local ensemble transform Kalman filter (see references in [5]), a variant on the EnKF. Additive model error (to maintain ensemble spread) and localisation length-scales were based on climatological background errors [8].

### *72.1.2 Simulations*

Two different nature runs were used: the first (termed NR1) was a "perturbed" DEHM simulation and the second (NR2) was a MOZART-IFS simulation made available by the ECMWF as part of the MACC project [9]. A control simulation (termed CN) was run without assimilation, using the same DEHM setup as with the assimilation. NR1 is more easily comparable with the analysed fields, whereas the differences between the NR2 and CN should be substantial, which is desirable in the OSSE framework. A limited number of species ($NO_x$, CO, $O_3$, HCHO, $CH_4$, $SO_2$, $SO_4^{2-}$) were available for NR2, and at a 6 h temporal

**Table 72.1** Differences between the simulations are given

| Run | Model | NWP | Emissions | Assimilation |
|---|---|---|---|---|
| CN | DEHM | MM5 a | Set a | No |
| NR1 | DEHM | MM5 b | Set b | No |
| NR2 | MOZART | IFS | Set c | Yes[a] |
| AN1 | DEHM | MM5 a | Set a | Yes: $NO_2$ TCCs from NR1 |
| AN2 | DEHM | MM5 a | Set a | Yes: $NO_2$ TCCs from NR2 |

NWP simulation "MM5 a" was run continuously with nudging towards the NCEP reanalysis each 6 h. NWP simulation "MM5 b" was nudged for the first 6 h, then ran freely for 48 h, before storing 12 h of results. Emission "Set a": global anthropogenic – RCP, European anthropogenic – EMEP, biogenic – GEIA, wildfires – GFED, shipping – IAS (see Brandt et al. [2] and references therein for details). Emission "Set b": global anthropogenic – EDGAR, biogenic – GEIA, wildfires – RETRO, shipping – Corbett and Fischbeck [4]. Emission "Set C": see Stein [9]
[a]The MOZART-IFS simulation included assimilation of chemical trace gas retrievals from multiple satellite instruments [9]

resolution. Pseudo-observations derived from NR1 and NR2 were assimilated into the DEHM-EnKF system for the period Jan-Mar 2008, and the analyses are termed AN1 and AN2, respectively. See Table 72.1 for details.

### *72.1.3 Pseudo-observations*

The purpose of using pseudo-observations is so that we know the "true" state of the atmosphere (as embodied by the nature run), in order to assess the results from the assimilation. Pseudo-observations were derived from the two nature runs using the same spatial and temporal pattern as for the Ozone Monitoring Instrument (OMI) aboard the NASA satellite AURA. Averaging kernels specified in the satellite retrievals were used to interpolate from model space to observation space, and Gaussian independent random errors were added with standard deviation proportional to the errors specified in the retrieval product. The observation errors and averaging kernels were obtained from the DOMINO product (v. 2.0.1, [1]).

## 72.2 Results

Figure 72.1 shows the bias in $NO_x$, comparing the analysis with the corresponding nature run. As a benchmark, Fig. 72.1 also shows the comparison between CN and the two nature runs. The relative, rather than absolute, $NO_x$ concentrations are given, since the concentration varies dramatically with altitude and latitude. The differences between the top and bottom rows of Fig. 72.1 (i.e. CN – NR vs. AN – NR) are relatively minor, which is not surprising given the short atmospheric lifetime of $NO_2$. Ignoring the changes to the upper few layers (which are influenced

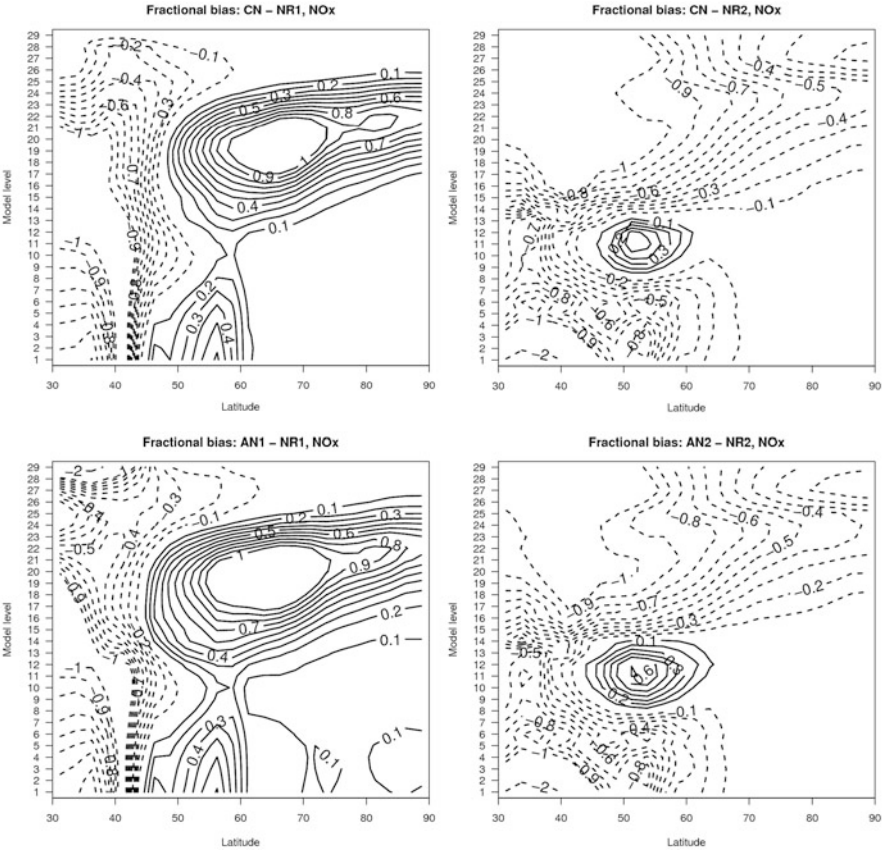


**Fig. 72.1** Mean $NO_x$ fractional bias, averaged over latitude bands for each model layer. *Top-left*: AN1 – NR1, *top-right*: AN2 – NR2, *bottom-left*: CN – NR1, *bottom-right*: CN – NR2. The bias was normalised by the mean concentration in the respective nature-run in the respective model level. *Dashed and solid lines* indicate contours of negative and positive values of the fractional bias, respectively

by strong damping from the upper boundary condition in DEHM), the biggest differences are evident around layer 14, which roughly coincides with the top of the mixed layer.

The biases in AN1 – NR1 tend to be larger than in CN – NR1, since NR1 is still very similar to CN, despite the different meteorology and emissions. The pseudo-observations have noise added to them (to simulate real scatter in the satellite retrievals), and we have included an additive model-error contribution to maintain ensemble spread, which also makes it harder to recover the "truth" (represented by the nature-run). Perhaps of greater interest is the equivalent comparison for NR2, since the underlying models are fundamentally different. The assimilation led to a general increase in $NO_x$ concentrations, with negative biases (which are most common) in AN2 – NR2 slightly smaller than in CN – NR2, and positive biases slightly larger.

## 72.3 Conclusion

We examined the performance of a chemical data assimilation system using the OSSE framework. The potential benefits from assimilation of $NO_2$ are limited in the current framework due to the short atmospheric lifetime of this species, as forcing from chemistry and emissions quickly erases changes to the initial conditions. This problem can be to some extent overcome by simultaneous re-estimation of emission rates [6].

The NR1, a DEHM simulation using different meteorology and emissions, was potentially too similar to the model used in the test runs (i.e. with assimilation), and the biases in the AN1 were greater than those seen in CN. The NR2, a simulation from a fundamentally different CTM, provided an alternative, and perhaps more useful, perspective. The biases (relative to NR2) in AN2 tended to be more positive than in CN, yet overall smaller in absolute value. However the bias patterns in both AN1 and AN2 were very similar to those in CN. This is not surprising, given the short-lived nature of $NO_2$ (leading to short effective correlation length-scales), and that retrievals are available only daily over any given region. We plan to extend this work to incorporate pseudo-observations from other species, including CO, $O_3$ and HCHO.

**Acknowledgments** This work was funded by a program grant from the Danish Council for Technology and Innovation: Effects of climate changes on ecosystems – a global comparative analysis. We are grateful to the ECMWF for making the MACC reanalysis freely available. We acknowledge the free use of the tropospheric $NO_2$ column data from the OMI sensor from www.temis.nl.

## References

1. Boersma KF, Eskes HJ, Veefkind JP, 8 others (2007) Near-real time retrieval of tropospheric $NO_2$ from OMI. Atmos Chem Phys 7:2013–2128
2. Brandt J, Silver JD, Frohn LM, 9 others (2012) An integrated model study for Europe and North America using the Danish Eulerian Hemispheric Model with focus on intercontinental transport of air pollution. Atmos Environ 53:156–176
3. Christensen J (1997) The Danish Eulerian hemispheric model – a three-dimensional air pollution model used for the arctic. Atmos Environ 31:4169–4191
4. Corbett JJ, Fischbeck PS (1997) Emissions from ships. Science 278:823–824
5. Evensen G (2009) Data assimilation: the ensemble Kalman filter, 2nd edn. Springer, Dordrecht
6. Miyazaki K, 5 others (2012) Simultaneous assimilation of satellite $NO_2$, $O_3$, CO, and $HNO_3$ data for the analysis of tropospheric chemical composition and emissions. Atmos Chem Phys 12:9545–9579
7. Sakov P, Evensen G, Bertino L (2010) Asynchronous data assimilation with the EnKF. Tellus A 62(1):24–29
8. Silver JD, 4 others (2013) Ensemble perturbations for chemical data assimilation. In: Steyn D, Builtjes PJH, Timmermans RMA (eds) Air pollution modeling and its application XXII. Springer, Dordrecht
9. Stein O (2009) Model documentation of the MOZART CTM as implemented in the GEMS system. GEMS report. http://gems.ecmwf.int/do/get/PublicDocuments/1531/1172?showfile=true. Accessed 11 June 2013

## Questions and Answers

**Questioner name:** Luca Delle Monache

**Q:** Have you tested the EnKF with more members? Which localisation algorithm have you used?

**A:** So far we have only run the EnKF with 16 members, but we plan to test it with a larger ensemble size in the near future. We ran a local analysis, with separate assimilations for each grid-point, as described by Sakov et al. [7]. This required localisation weights between grid-points and observations, which were based on the linearised observation operator as well as correlations derived from a climatological background error covariance matrix.

**Questioner name:** Pius Lee

**Q:** The array of satellite retrievals you used has characteristic pixel resolutions. Have the satellite data clustered to your rather large 150 km $\times$ 150 km box specifically with respect to the retrieval characteristics of the instrument?

**A:** The footprint of the satellite retrievals is typically much smaller than the model grid-cell. As such, the representativity error is an important component of the total observation error. We have not yet considered the within-pixel clustering behaviour of the different retrievals, other than to estimate the representativity error. Currently the horizontal interpolation accounts only for the pixel centre, rather than the corner-points. Such a refinement is under consideration, however not a priority while working with such coarse horizontal resolution.

**Questioner name:** Dominik Brunner

**Q:** Do you consider the averaging kernels of the satellite data? How do you deal with the issue of biased observations, which can be significant for satellite data?

**A:** The averaging kernels (AKs) are required to define the observation operator. Many satellite retrievals are available without the corresponding AKs, so we were restricted to using only those products where the AKs were available. Currently we do not take account for systematic bias in either the model or the observations, even though that we know that such biases exist. This is clearly a short-coming of the system; however accounting for bias adds an extra level of complexity. Further testing is required before we can take this next step. Without an independent, bias-free data source, it is impossible to bias-correct both the model and the observations, and one must choose to assume that either the model or the observations are bias-free. At present it is unknown whether the model or the observations have bigger biases.

# Chapter 73
# Resolving and Quantifying Ozone Contributions from Boundary Conditions Within Regional Models

**Greg Yarwood, Chris Emery, Kirk Baker, and Pat Dolwick**

**Abstract** In regional model simulations, ozone introduced by boundary conditions (BCs) is important to model performance, model sensitivity and for policy reasons such as transport assessments. Quantitatively tracking the contribution of ozone BCs throughout a regional model is highly desirable. A simple and efficient solution is to add a tracer (O3BC) to the regional model simulation with a source term equal to the ozone BC. However, it is also necessary to model the removal of O3BC by deposition and chemistry. Modeling tracer deposition is relatively straightforward but modeling the photochemical removal of O3BC is complex. We developed a chemical mechanism for the photochemical removal of O3BC that is compact, represents all major removal pathways (i.e., photolysis, reactions with HOx radicals), accounts for important dependencies on NO, and can be implemented as an extension of the main gas-phase chemical mechanism. The method provides great flexibility by permitting O3BC to be factored into components that are then tracked independently. Example components of potential interest are different lateral boundaries segments (north vs. south boundary, etc.), altitude segments (boundary layer vs. free troposphere vs. stratosphere) and geographic origin (e.g., Asia vs. North America vs. Europe). Information about the geographic origin of O3BC can be derived from global model sensitivity simulations. The method is implemented in the CAMx regional model by using an existing model option to add reactive tracers (RTRAC) with complex chemistry. The method is applied and evaluated in simulations for continental North America.

G. Yarwood (✉) • C. Emery
ENVIRON International Corporation, Novato, CA 94998, USA
e-mail: gyarwood@environcorp.com; cemery@environcorp.com

K. Baker • P. Dolwick
Office of Air Quality Planning and Standards, U.S. Environmental Protection Agency, 109 TW Alexander Drive, Research Triangle Park, NC 27711, USA
e-mail: baker.kirk@epa.gov; dolwick.pat@epa.gov

D. Steyn and R. Mathur (eds.), *Air Pollution Modeling and its Application XXIII*, Springer Proceedings in Complexity, DOI 10.1007/978-3-319-04379-1_73,

## 73.1 Introduction

In regional models like the Comprehensive Air quality Model with extensions (CAMx; [3]) ozone introduced by boundary conditions (BCs) is important to model performance, model sensitivity and for policy reasons such as transport assessments. Quantitatively tracking the contribution of ozone BCs throughout a regional model is highly desirable. The CAMx ozone source apportionment technology (OSAT; [1]) probing tool tracks BC contributions to ozone. However, OSAT has limited flexibility in how BC contributions are organized and OSAT tracks ozone contributions from emissions that may not be needed. We have developed and implemented an efficient method for tracking BC ozone contributions using reactive tracers. The new method is flexible because the BC contributions to be tracked are defined using CAMx input files, i.e., specially prepared BC files.

The CAMx reactive tracer (RTRAC) probing tool provides a flexible approach for introducing gas and particulate matter tracers within CAMx simulations [3]. Each RTRAC tracer is influenced by boundary conditions, advection, diffusion, emissions and dry deposition. Gas-phase tracers can also undergo chemical destruction and/or production using either a simpler (RTRAC) or more complex (RTCMC) chemistry interface. The RTRAC Chemical Mechanism Compiler (RTCMC) permits a full chemistry mechanism to be defined through a model input file with no limits on mechanism complexity (within available computer resources). We configured RTCMC to track of ozone from BCs in a manner that is similar to OSAT.

## 73.2 Tracking Photochemical Ozone Destruction

Ozone is destroyed by reactions with NO, $NO_2$, OH, $HO_2$ and alkenes. Some reactions destroy $O_3$ permanently and are straightforward to implement in a scheme to track $O_3$ destruction. Examples are reactions with alkenes (e.g., isoprene) that remove $O_3$ by forming an ozonide that decomposes to products such as aldehydes. Other reactions may initially destroy $O_3$ but form products that subsequently re-form $O_3$. An example is the reaction of $O_3$ with NO which forms $NO_2$ that can then photolyze causing $O_3$ to re-form. In this case, determining whether $O_3$ is permanently destroyed amounts to deciding whether $NO_2$ photolyzes to NO or is converted to another NOy species (e.g., HONO, $NO_3$, $HNO_3$, etc.) by complex chemical reactions. During daylight, $NO_2$ photolysis usually dominates over $NO_2$ conversion to NOy species other than NO. At night, $O_3$ reaction with NO may permanently destroy $O_3$ if the $NO_2$ formed is removed before it can photolyze on the following day. The RTCMC scheme assumes zero net destruction of $O_3$ by reaction with NO and so does not include the $O_3 + NO$ reaction. The reactions of $O_3$ with OH and $HO_2$ are simplified for the RTCMC scheme by assuming that: (1) OH and $HO_2$ inter-convert rapidly and may be treated as a pool ($HOx = OH + HO_2$); (2) At high NO, HOx removal is dominated by $HO_2$ reacting with NO to form $NO_2$ which

```
01 [O3A]              ->  [O1DA]
02 [O1DA]             ->  [O3A]
03 [O1DA]             ->
04 [O3A]  + [OH]      ->  [HOXA]
05 [O3A]  + [HO2]     ->  [HOXA]
06 [HOXA] + [NO]      ->  [O3A]
07 [HOXA] + [HO2]     ->
08 [HOXA] + [HO2]     ->
09 [HOXA] + [MEO2]    ->
10 [HOXA] + [XO2]     ->
11 [HOXA] + [XO2N]    ->
12 [HOXA] + [C2O3]    -> (0.2) [O3A]
13 [HOXA] + [CXO3]    -> (0.2) [O3A]
14 [O3A]  + [ISOP]    ->
15 [O3A]  + [TERP]    ->
```

**Fig. 73.1** Reaction scheme for tracking chemical destruction of an ozone tracer (O3A) with the CAMx RTCMC probing tool. These reactions are implemented to work with the CB05 chemical mechanism

then photolyzes to re-form $O_3$, resulting in zero net $O_3$ destruction, and (3) At low NO, HOx removal is dominated by reactions of $HO_2$ with $HO_2$ and $RO_2$ radicals, resulting in net destruction of one $O_3$.

The RTCMC scheme for tracking chemical destruction of $O_3$ tracers is shown in Fig. 73.1 as implemented for use with CB05. The scheme tracks one BC $O_3$ contribution (O3A) using 15 reactions and 3 RTCMC tracers (i.e., O3A, O1DA and HOXA.) Other chemical species appearing in Fig. 73.1 (i.e., OH, HO2, NO, XO2, XO2N, C2O3, CXO3, ISOP and TERP) are from the CB05 chemical mechanism [4] and their concentrations are provided by CAMx and considered constant within RTCMC. Thus, an RTCMC reaction between O3A and ISOP depletes the RTCMC species O3A but does not change the CB05 species ISOP. CB05 treats the ISOP decay.

## 73.3 Contributions of Tropospheric and Stratospheric Ozone

To illustrate how the RTCMC scheme can be applied we used it to quantify contributions of tropospheric and stratospheric $O_3$ BCs for the continental US (CONUS). The CONUS simulation inputs were for calendar year 2008 with meteorology from WRF, anthropogenic emissions from the 2008 NEI, biogenic emissions from MEGAN and BCs from GEOS-Chem. We classified CAMx layers below ~6 km above ground as tropospheric, layers above ~9 km as stratospheric, and also tracked the contribution from layers between 6 and 9 km. This classification scheme was used for the purpose of demonstrating the method and a more refined classification of BCs into tropospheric vs. stratospheric could be developed.

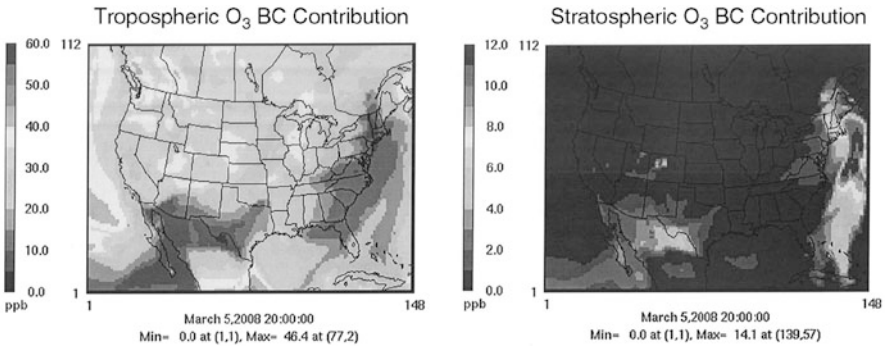


**Fig. 73.2** Ground-level $O_3$ (ppb) from $O_3$ boundary conditions (BCs) in the troposphere (below 6 km above ground) and the stratosphere (above 9 km) on March 5, 2008. The contribution of $O_3$ BCs between 6 and 9 km was also tracked but is omitted for brevity. Note that the *scale bars* have different ranges

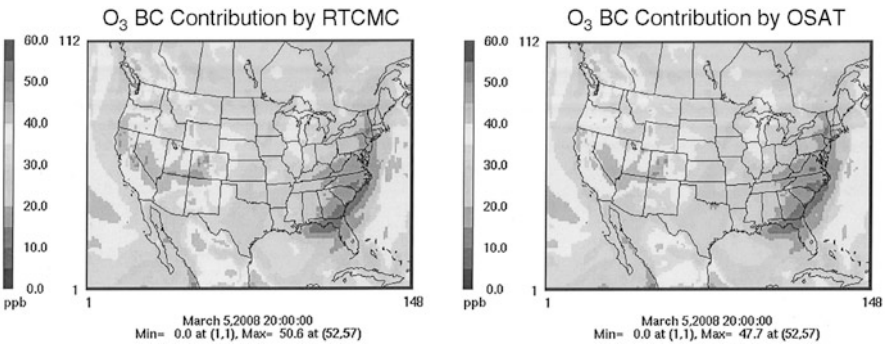


**Fig. 73.3** Boundary condition (BC) contribution to ground-level $O_3$ (ppb) determined by RTCMC and OSAT on March 5, 2008

Contributions to ground-level $O_3$ of BCs classified as troposphere versus stratosphere are shown in Fig. 73.2 for March 5, 2008. Two areas of stratospheric $O_3$ influence are apparent on this day, one over northern Mexico and a second over the North Atlantic Ocean. The areas of high stratospheric $O_3$ influence coincide with areas of low tropospheric influence consistent with air subsiding from near the tropopause to ground level.

We compared the total contribution of BCs to ground level $O_3$ determined by RTCMC and OSAT, as shown in Fig. 73.3. The spatial patterns of BC $O_3$ contribution revealed by both methods are nearly identical.

The RTCMC scheme is computationally efficient. Tracking three $O_3$ BC contributions added 9 tracers and 45 reactions in RTCMC and increased CAMx run time by 10 %.

## 73.4 Summary

We developed and tested a new method for tracking ozone from apportioned BCs within a CAMx simulation by using reactive tracers with the RTCMC probing tool in CAMx. Ozone BC contributions determined by the RTCMC scheme are very similar to those determined by the CAMx OSAT probing tool. The RTCMC scheme is computationally efficient with a 10 % increase in CAMx run time to track 3 ozone BC contributions. The RTCMC scheme provides great flexibility by permitting the ozone BCs to be factored into components that are then tracked independently. Example components of potential interest are different lateral boundaries segments (north vs. south boundary, etc.), altitude segments (boundary layer vs. free troposphere vs. stratosphere) and geographic origin (e.g., Asia vs. North America vs. Europe). Information about the geographic origin of ozone BCs can be derived from global model sensitivity simulations.

**Acknowledgments** This work was supported by the U.S. Environmental Protection Agency under contract EP-S-12-044 work assignment 1–10. The views expressed are those of the authors. Although this work was reviewed by EPA and approved for publication it may not necessarily reflect official Agency policy.

## References

1. Dunker AM, Yarwood G, Ortmann JP, Wilson GM (2002) Comparison of source apportionment and source sensitivity of ozone in a three-dimensional air quality model. Environ Sci Technol 36:2953–2964
2. Emery CA, Jung J, Downey N, Johnson J, Jimenez M, Yarwood G, Morris R (2012) Regional and global modeling estimates of policy relevant background ozone over the United States. Atmos Environ 47:206–217
3. ENVIRON (2013) User's guide to the comprehensive air quality model with extensions, version 6. Available at http://www.camx.com/Files/CAMxUsersGuide_v6-00.pdf
4. Yarwood G, Rao S, Yocke M, Whitten GZ (2005) Updates to the carbon bond mechanism: CB05. Report to the US Environmental Protection Agency RT-04-00675. Available at http://www.camx.com/publ/pdfs/CB05_Final_Report_120805.pdf

## Questions and Answers

### Roger Timmis

**Q**: In the 3-day boundary condition experiment shown in your presentation, is there an explanation for the anomaly (i.e. difference in BC contribution as diagnosed by the RTCMC scheme and OSAT) over the Atlantic Ocean off the Eastern US seaboard? Have you checked whether predicted events with large stratospheric

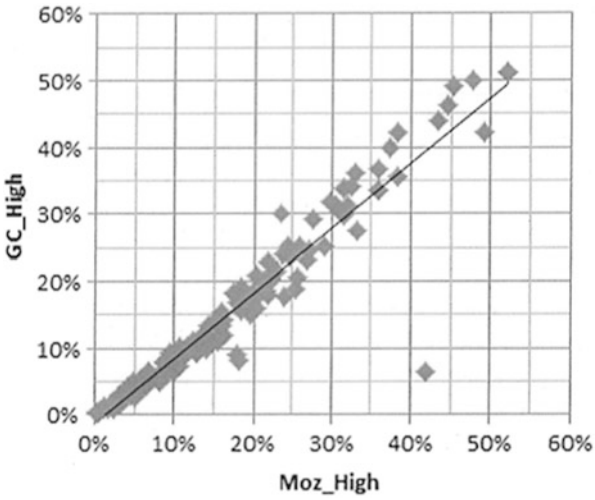


**Fig. 73.4** Percent contribution of modeled daily maximum 8-h ozone concentration at Gothic, CO during April–August 2008 originating from the stratosphere (BCs above 9 km) using the CAMx regional model with BCs from MOZART (Moz_High) or GEOS-Chem (GC_High) (Results courtesy of the Western Regional Air Partnership WestJumpAQMS project)

contributions to ground-level ozone are matched to observed events such as tropospheric folds and cut-off lows?

**A**: Results using the RTCMC scheme and OSAT can differ for two main reasons. First, in areas with sufficient NOx to support net ozone production OSAT diagnoses more rapid ozone destruction than the RTCMC scheme because OSAT can account more completely for ozone destruction chemistry. Second, falling rain can become saturated with ozone limiting further scavenging and OSAT uses saturation with total ozone to limit scavenging of ozone components (e.g., ozone from BCs) whereas the RTCMC scheme considers each ozone component separately with regard to saturation. The three-day experiment showed a stratospheric ozone contribution over the Atlantic which coincided with a deep low-pressure wave and associated frontal system over the eastern US consistent with deep vertical transport from the tropopause to near ground-level. Emery et al. [2] have successfully modeled stratospheric ozone intrusions during tropopause folding events.

**Rohit Mathur**

**Q**: Please clarify the timescale of ozone model results shown for Gothic, CO. Assuming the modeled BC contributions to ground-level ozone are correct, what fraction do they contribute to the observed ozone or the total modeled ozone?

**A**: Daily maximum 8-h average (MDA8) ozone values for April-August 2008 were shown for Gothic, CO, in the central Rocky Mountains. As shown in Fig. 73.4, the percentage of total ozone originating above 9 km (ozone considered to originate from the stratosphere) was up to 52 % using MOZART BCs or 51 % using GEOS-Chem BCs. The average contributions were 15.3 % and 13.7 %, respectively. The outlier in Fig. 73.4 (42 % MOZART and 6 % GEOS-Chem) occurred on July 29, 2008

# Chapter 74
# *E pluribus unum*: KZ Filters and Ensemble Air Quality Modeling

**S. Galmarini, I. Kioutsioukis, and E. Solazzo**

**Abstract** In this study we present a novel approach for improving the air quality predictions using an ensemble of air quality models generated in the context of AQMEII (Air Quality Model Evaluation International Initiative). The development of the forecasting method makes use of modeled and observed time series (either spatially aggregated or relative to single monitoring stations) of ozone concentrations over different areas of Europe and North America. The technique considers the underlying forcing mechanisms on ozone by means of spectrally decomposed previsions. With the use of diverse applications we demonstrate how the approach screens the ensemble members, extracts the best components and generates bias-free forecasts with improved accuracy over the candidate models.

## 74.1 Introduction

Multi-model ensembles (MME) is the practice according to which results obtained from a somehow arbitrary collection of modeling systems and applied to a common case study, are statistically treated in an attempt to capture more effectively the variability of the observational data and to improve the final results In the present study we intend to take a step forward with respect to the ensemble screening and model selection, having as final goal not only the improvement of the ensemble result on hindcast application but also the forecasting capacity of a MME for air quality applications.

S. Galmarini (✉) • I. Kioutsioukis • E. Solazzo
European Commission Joint Research Centre, Institute for Environment and Sustainability, Air and Climate Unit, TP441, 21027 Ispra, Italy
e-mail: dsteyn@eos.ubc.ca

D. Steyn and R. Mathur (eds.), *Air Pollution Modeling and its Application XXIII*, Springer Proceedings in Complexity, DOI 10.1007/978-3-319-04379-1_74,

## 74.2 Methodology

The Kolmogorov–Zurbenko filter was first proposed by Kolmogorov and formalized later by Zurbenko. It is defined as an iteration of a moving average filter applied on a time-series *S(t)*:

$$KZ_{m,p} = R_{i=1}^{p}\left\{J_{k=1}^{W_i}\left[\frac{1}{m}\sum_{j=-\frac{m-1}{2}}^{\frac{m-1}{2}} S(t_i)_{k,j}\right]\right\}\begin{cases} R: iteration \\ J: running\ window \\ W_i = L_i - m + 1 \\ L_i = length\ of\ S(t_i) \end{cases} \tag{74.1}$$

It is a two-parameter filter controlled by the window size (m) and the number of iterations (p). The KZ-f removes high-frequency variations from the data (with respect to the window size) and belongs to the class of low-pass filters (since it filters periods smaller than the selected cut-off period). By modifying the controlling parameters (m, p), different scales of motion can be eliminated and others retained. In particular, by taking the difference between two KZ-f corresponding to different parameters (m, p), a band-pass filter is created.

For the case of ground-level ozone, four separate scales of motion have been defined relevant, detected by means of physical considerations and periodogram analysis. They are namely the intra-day component (ID), the diurnal component (DU), the synoptic component (SY) and the baseline or long-term component (LT). The hourly time series of ozone can therefore be decomposed as:

$$S(t) = ID(t) + DU(t) + SY(t) + LT(t) \tag{74.2}$$

where: $ID(t) = S(t) - KZ_{3,3}$, $DU(t) = KZ_{3,3} - KZ_{13,5}$, $SY(t) = KZ_{13,5} - KZ_{103,5}$ and $LT(t) = KZ_{103,5}$. The total error of the decomposed by Eq. (74.2) time-series is propagated through the spectral components and consists of each component's contribution as well as its interaction with the other components. The magnitude of the covariance terms of the error matrix determines the degree of association of the spectral components derived from the KZ-f.

### *74.2.1 Properties of the Spectral Components*

The spectral components are composed by three signals with zero mean (ID, DU and SY) and one slow varying signal (LT). The ID, DU, and SY signals are zero mean fluctuations about the smoothed time series (LT). In terms of their relative strength, the amplitude of the zero mean signals is highest for the DU component and lowest for the ID component [1].

The explained variance from the single contributions of the four components accounts for roughly 80 % of the total variability. The DU component drives the

ozone variability and accounts for more than half of its variance. In contrast, the ID component explains the least amount of the ozone variability due to the small magnitude of its fluctuations [1].

The decomposed observed and modeled time-series generally reveal similar patterns. Spectral decomposition does not distort the allocation of variance between the components and hence maintains their relative importance. Moreover, this decomposition results at equal amounts of explained by individual components variance [1].

### *74.2.2 The Proposed Ensemble Strategy and the KZ Model*

The methodology we put into place is explained as follow. Equal lengths of the observed and the time series of ozone obtained from all ensemble members are decomposed into four components by the KZ-f. The modelled spectral components are evaluated against the observed ones and the models producing each one of the four best components are identified. Then, future time series (i.e., a time series with the same length as the historic time series that is shifted to include a future horizon) of the identified models are KZ-f decomposed and for each spectral component the respective one is taken. Finally, a new model (*kz* model) is built by adding the respective future components. For the historic period, if the spectral components were independent (i.e., the off-diagonal terms of the covariance matrix would be zero), the *kz* model skill would outperform any other model skill. However, since the components are not independent and in addition, the interest lies in the forecast period (that is, *kz* forecast skill), the idea needs to be evaluated.

The novelty on this approach is that the ensemble result is not anymore a mere statistical treatment of the outcome of model results but it is diagnosed in the fundamental aspects that constitute each member which are then *re-ensembled* to constitute the only model set used for forecast.

## 74.3 Results

The first operational assessment is presented in Fig. 74.1, where all models are directly compared to the observations (EU1, results are similar for the other sub-regions). The scatter diagram shows super-imposition of three clouds pertaining to the comparison with observed concentrations at rural, sub-urban and urban stations. The individual models are compared in the first 13 panels and are followed by *mm (median model)*, *sm (spectral median model)* and *kz*. The improvement of *kz* is evident with respect to all other models. The cloud is tilted upward gaining a good deal of positions even against *mm* and *sm*. The spread of the data appears slightly larger than for *sm* and *mm* because the median aggregation in those models always results in deterioration of their variance. Another reason is related

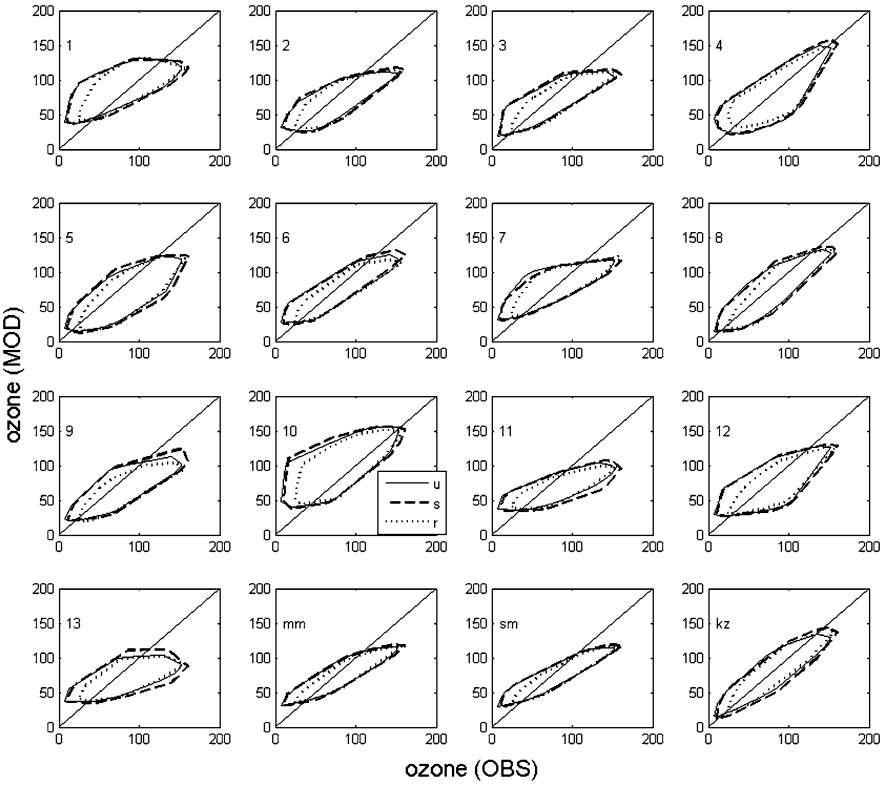


**Fig. 74.1** Convex hull around scatterplot of all examined cases corresponding to the prediction week, for the EU1 sub-domain and all three ozone aggregation types (urban, suburban, rural). Compared to the rest of the models, the cloud of the *kz* model scatter is tilted towards the diagonal

to imperfect selection of the best spectral components. However *kz* model forecasts are homogeneous throughout the range of values. From a purely visual view point the improvement produced by the *kz* model are clear (full details in [1]).

The methodology adopted and applied for ozone has been also tested for the case of Nitrogen Dioxide ($NO_2$) and coarse Particulate Matter ($PM_{10}$). Although this work is ongoing, results (not shown) demonstrate that the presented approach is not bounded by the physical, chemical and dynamical nature of ozone formation and can be easily extended to other pollutants.

The presented approach is adaptive and screens each time the ensemble members to extract the best spectral components on the basis of the most accurate recent representation of the observed state. Its advantages were demonstrated for seven sub regions (four in EU, three in NA) at all aggregation types (urban, suburban, rural) but also at the station level. As the skill of the models varies with sub-region, synoptic conditions and chemical conditions, more sophisticated approaches (utilizing eg synoptic clustering) are expected to further improve the forecast skill.

## Reference

1. Galmarini S, Kioutsioukis I, Solazzo E (2013) E pluribus unum: ensemble air quality predictions. Atmos Chem Phys 13:7153–7182

## Questions and Answers

**Questioner Name:** Luca delle Monache

**Q:** You have clearly shown that with this approach you can improve a deterministic ensemble-based prediction. Can the same approach, or a variation of it, be used to improve probabilistic ensemble-based predictions?

**A:** Assuming that the total number of combinations originating from an ensemble is *ncomb*, the total number of combinations using the specific spectral decomposition is $ncomb^4$. The output uncertainty using this approach is at least as wide as in the non-decomposed version; at the same time, it can achieve lower forecast error. This uncertainty can be narrowed by restricting the variability of certain modes.

**Questioner Name:** Kristen Foley

**Q:** You use a training time period to select which ensemble members to use in your k-z filter approach for forecasting. If you were to also use the observed data in the training period to select from your original ensemble without decomposing into the four components, how would this ensemble perform compared to your proposed approach?

**A:** The comparison between the first order kz decomposed model against the lowest MSE combination of all models constituting the ensemble does not identify a clear winner across sub-regions and aggregations (urban, suburban, rural). However, switching to decompositions of equal order to the lowest MSE combination, the forecast error is always lower in the kz case.

**Questioner Name:** Jeremy Silver

**Q:** The method looks very promising. How much spatial information can it provide? Can it give you forecasts at sites not used in the training set?

**A:** The method has been also applied to station level data and yield similar results with the spatially aggregated test case. In view of its spatial extension for forecasting purposes at blind sites, results are sensitive to the spatial window of influence of the best spectral components. Using too wide one (e.g. whole sub-region) does not provide an improvement over the ensemble mean.

**Questioner Name:** Armin Aulinger

**Q:** Do noisy measurement data make it difficult to select the appropriate "Frankenstein" components from the ensemble? Can physical/chemical reasons for better or worse performing models be detected from the decomposed model results?

**A:** The successful application of the method to the nosier station level data showed that generally the method can deal with noisy measurements. Besides that, the noisiest component (intra-diurnal) is also the least important. In terms of the properties of the best components, practical experience showed that very few models contribute principally to ID & DU (physical parameterizations), more to the LT (background) and almost all to SY (weather uncertainty).

**Questioner Name:** Paul Makar

**Q:** Could the method be modified slightly to be used in a forecasting context? T

**A:** The method can be directly applied to forecasts by replacing the simulations with predictions. The scope of the study was to identify accurate recent representations of the four components, guaranteeing in principle also an appropriate behavior in the future.

# Chapter 75
# Air Quality Model Evaluation Using Gaussian Process Modelling and Empirical Orthogonal Function Decomposition

**Tianji Shi, Douw Steyn, and William J. Welch**

**Abstract** We propose a statistical air quality model that simultaneously performs two major tasks: (1) provides a computationally inexpensive means of modelling and forecasting complex space-time air pollution processes, (2) enables an informative and statistically defensible approach for evaluation of air quality models. Rather than working with raw data, we analyze the spatio-temporal variability of a pollution process by extracting data features using Empirical Orthogonal Function decomposition. Our modelling approach thus avoids the complications of point-to-point comparison, and the statistical model's flexible structure allows for extensive fine-tuning. We develop and demonstrate our approach on observations and CMAQ model output of ozone episodes in the Lower Fraser Valley (LFV) of British Columbia, Canada. We believe the principle and methodology of our statistical analysis is applicable to a wide range of air pollution problems.

## 75.1 Introduction

Air quality model outputs are averaged values on a uniform grid, whereas ozone observations are point measurements at irregularly placed locations. Point-to-point comparisons between model and observation can be uninformative or even misleading since they are governed by different stochastic spatial processes. We propose an alternative model evaluation approach that is implemented in two steps: build statistical models of both model outputs and observations; then compare statistical

T. Shi (✉) • W.J. Welch
Department of Statistics, The University of British Columbia, Vancouver, BC, Canada
e-mail: tshi@stat.ubc.ca; will@stat.ubc.ca

D. Steyn
Department of Earth, Ocean and Atmospheric Sciences, The University of British Columbia, Vancouver, BC, Canada
e-mail: dsteyn@eos.ubc.ca

D. Steyn and R. Mathur (eds.), *Air Pollution Modeling and its Application XXIII*, Springer Proceedings in Complexity, DOI 10.1007/978-3-319-04379-1_75,

model components as a means of evaluating the model against observation. In essence, we are comparing how CMAQ (or air quality models in general) and physical measurements differ or agree in their governing processes. Our statistical model does not process raw data (or model output) directly, rather the data features are extracted via EOF decomposition, and these features are modelled as Gaussian Processes (GPs). GP modelling is used for its proficiencies in emulating computer model outputs [1] and modelling air quality observations [2]. We view this as a "big-picture" way of evaluating CMAQ, or any other process-based model.

## 75.2 General Framework of Our Statistical Model

Suppose $\mathbf{O}$ is a $t \times n$ matrix of ozone data, where $t$ is the number of time points and $n$ the number of locations. By EOF decomposition, we obtain an $n \times n$ EOF matrix $\mathbf{E}$, where each column is an EOF. Multiplying the original data $\mathbf{O}$ by $\mathbf{E}$ we obtain a $t \times n$ Principal Component (PC) matrix, denoted as $\mathbf{C}$ (there are $n$ PC vectors of length $t$). We sort the EOFs and PCs by the criterion "proportion of data variation explained", and use the term "1st EOF" or "1st PC" to describe the data component that explains the most data variation, so on for "2nd EOF", "2nd PC", etc.

Our study shows that each of the lower order EOFs represents identifiable spatial ozone features/patterns, either individually or collectively with other EOFs, whereas lower order PCs describe certain temporal ozone features. We model these features as a GP. This allows the stochastic process vector to follow a multi-variate normal distribution (MVN). We use the generic notation of $\mathbf{Y}$ as a random process vector and $\mathbf{X}$ a matrix of corresponding model covariates.

Our GP model, as a specific instance of a general GP model is:

$$\mathbf{Y}(\mathbf{X}) = \mathbf{f}(\mathbf{X})\boldsymbol{\beta} + \mathbf{Z}, \quad \mathbf{Z} \sim MVN(\mathbf{0}, \sigma^2\mathbf{R}), \tag{75.1}$$

where $\boldsymbol{\beta}$ is a regression coefficient vector. $\mathbf{Z}$ is a zero-mean GP that models $\mathbf{Y}$'s stochastic variation about the mean $\mathbf{f}(\mathbf{X})\boldsymbol{\beta}$. $\mathbf{R}$ is a correlation matrix, and we use a form of correlation function that measures correlation between $Y$ and $Y'$ based on the covariate distance $|x - x'|$. Given $\mathbf{x}_0$, which are covariates at unobserved (or unmodelled) locations and/or future time, we predict $Y(\mathbf{x}_0)$ using a Kriging based equation:

$$\hat{y}(\mathbf{x}_0) = \mathbf{f}(\mathbf{x}_0)\hat{\boldsymbol{\beta}} + \mathbf{r}^{\mathrm{T}}\mathbf{R}^{-1}(\mathbf{Y} - \mathbf{f}(\mathbf{X})\hat{\boldsymbol{\beta}}), \tag{75.2}$$

where $\mathbf{r}$ contains correlations between $Y(\mathbf{x}_0)$ and observed $\mathbf{Y}$ and $\hat{\boldsymbol{\beta}}$ is the generalized least-square estimation. To estimate the parameters within (75.1), we derive a MVN-based "profile likelihood" function and run iterative algorithms to find the likelihood-maximizing parameter estimates.

EOFs and PCs are modelled and predicted by their unique forms of (75.1). To model the ozone process at its original spatio-temporal domain and value scale,

we use the property that $\mathbf{E}$ is an orthogonal matrix. This allows us to reconstruct the original ozone field via equation $\mathbf{O} = \mathbf{C}\mathbf{E}^T = \sum_{j=1}^{n} \mathbf{C}[,j]\mathbf{E}[,j]^{\mathrm{T}}$. $\mathbf{C}[,j]$ and $\mathbf{E}[,j]$ are the $j$-th columns of $\mathbf{C}$ and $\mathbf{E}$. However, it is usually possible to recover a majority of data variation using fewer EOFs and PCs. Hence, we have the approximation equation

$$\mathbf{O} \approx \sum_{j=1}^{p} \mathbf{C}[,j]\mathbf{E}[,j]^{\mathrm{T}}, \quad p \ll \min(t,n). \tag{75.3}$$

In summary, our approach is to first extract essential ozone features/patterns from the data using EOF decomposition, model them as Gaussian Processes, and apply (75.3) to combine these GP models to model a space-time ozone process and make ozone forecasts. Since only individual data features are modelled, we greatly lessen the computational load of dealing with large dimensional data.

## 75.3 Data Analysis

It is important to determine $p$, the number of EOF/PC pairs to use in (75.3). For this purpose, we created a synthetic data set that emulates the spatio-temporal evolution of the ozone field over the LFV. We use (75.3) calculated from one synthetic field to predict another synthetic field. By varying $p$, we found that the predictive quality deteriorates after $p = 3$, signalling that this is the point in which data noise is introduced into prediction, i.e., any EOF/PC of higher order is either noise or contains non-significant information about the ozone pattern.

We implemented our model using CMAQ output for an ozone episode that lasted from 1200 PST on June 23rd to 1000 PST on June 27th, 2006 [3]. The first two *full days* of the episode are used as training data for covariate selection and estimating GP model parameters. The 4th day is used for prediction. Model covariates include: hour of the day, longitude, latitude, elevation, emission rate and lagged concentration of NOx and VOC, wind speed, temperature and boundary layer height.

The covariate information of the 4th day of this ozone episode are inserted into our estimated GP models to make ozone forecasts. Figure 75.1 shows the prediction results for 0100 PST and 1300 PST of June 26th.

## 75.4 Evaluating CMAQ Against Observations

We are implementing and analyzing two feature-based model evaluation techniques:

- Build our feature-based ozone GP models for both CMAQ outputs and observations, and then compare model parameters as a means of evaluating CMAQ

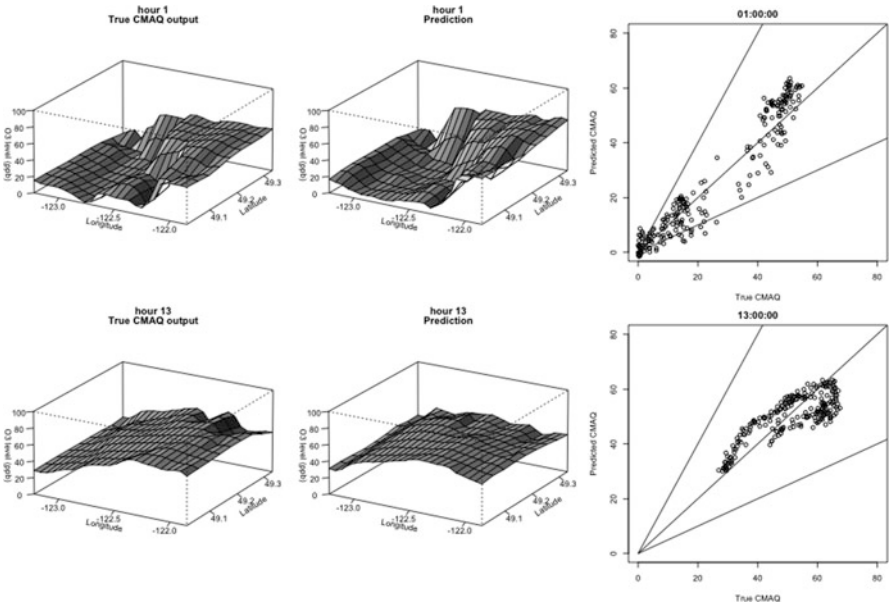


**Fig. 75.1** Comparison plot between the real CMAQ output (*left*) and prediction (*middle*) for the hour 0100 PST (*top*) and 1300 PST (*bottom*) of June 26th, 2006. The *rightmost plot* is the scatter plot of real CMAQ (x-axis) vs. prediction (y-axis), the three lines are: $y = x$, $y = (1/2)x$ and $y = 2x$

against observations. Comparison of model parameters is equivalent to comparing how two different ozone processes respond to chemical precursor emission rate and meteorological conditions. Given the asymptotic normality of estimated parameters, appropriate statistical tests can be designed to assess whether the differences are significant. The differences/similarities can also be visualized by producing univariate or interaction plots over a range of covariate values.

- Independently extract spatial and temporal features from CMAQ output and observations, calculate their differences, and build GP models of the *differences*. By incorporating chemical precursor and meteorological information as covariates, we can statistically assess how various factors influence the "ozone feature discrepancies" between CMAQ output and ozone measurements.

We have demonstrated the development and implementation of GP models for essential features of regional ozone. These statistical models will serve as the basis for CMAQ evaluation. The approach avoids the problems of point-to-point comparison through the use of EOF decomposition, and provides a statistically defensible way of comparing air-quality model output with observations.

## References

1. Sacks J, Welch WJ, Mitchell TJ, Wynn HP (1989) Design and analysis of computer experiments. Stat Sci 4:409–423
2. Gao F, Sacks J, Welch WJ (1996) Predicting urban ozone levels and trends with semiparametric modeling. J Agric Biol Environ Stat 1(4):404–425
3. Steyn DG, Ainslie B, Reuten C, Jackson PL (2013) A retrospective analysis of ozone formation in the Lower Fraser Valley, B.C. Part I: dynamical model evaluation. Atmosphere-Ocean 51(2):153–169

## Questions and Answers

**Questioner Name:** Armin Aulinger

**Q1:** Do predictions of the ozone fields become significantly worse if only the 1st EOF and PC are used in the statistical model?

**A1:** When only the 1st EOF is used, the predicted ozone fields lose the fine spatial variation and definition seen in Fig. 75.1. This could be that the 1st EOF represent spatial ozone mean, and finer spatial variations are captured by the remaining EOFs. However, due to scaling by the 1st PC (temporal ozone mean), the predictions are in similar ranges of values as those in Fig. 75.1.

**Q2:** How should peak values – that could have high leverage on EOFs – be treated?

**A2:** We believe in our model, high peak values do *not* require additional treatment. By design, EOFs model different aspects of peak values' influences. The 1st EOF captures, by the location, the effect of daily high peaks on the spatial mean. High peaks also contribute to high "daily variation" of corresponding locations, and this aspect is modelled by the 2nd EOF. Averaging out high peak values does appear to "lessen" their influences on an ozone process. However, we are modelling *ozone features*, and the nature of our analysis dictates that the focus is not placed on high ozone peak of any particular point in space and time.

**Questioner Name:** K. Heinke Schlunzen

**Q:** How can the EOF/PC method be applied to irregularly distributed observations, without merely imposing a need for kriging?

**A:** The method is applied the same way for irregularly distributed observations. In the $t \times n$ space-time data, the space is simply concatenated into the columns. Each value in an EOF is modelled by its associated locational index, meteorological and chemical covariates. The PCs are temporal features summarized over all locations.

**Questioner Name:** Paul Makar

**Q:** How would you explain or demonstrate the utility of this form of analysis to a member of the general public (who may want to know how well the model is predicting $O_3$, $PM_{2.5}$, etc, at a specific location)?

**A:** We model and analyze *generalized ozone features*. The generalized features give us the "big picture" on the behavior of an ozone process, it is more useful than detailed information at a specific time and space: a temporary spike in afternoon pollution in the downtown is not as harmful, or the information as relevant, as a sustained high concentration over the entire city. That being said, individual ozone features can be used *together* to model and predict ozone level at any specific time and location.

# Chapter 76
# AQMEII Phase 2: Overview and WRF-CMAQ Application Over North America

**Christian Hogrefe, Stefano Galmarini, Shawn Roselle, and Rohit Mathur**

**Abstract** In this study, we provide an overview of the second phase of the Air Quality Model Evaluation International Initiative (AQMEII). Activities in this phase are focused on the application and evaluation of coupled meteorology-chemistry models. Participating modeling systems are being applied for annual simulations over both North America and Europe using common emissions and boundary conditions. We present an overview of these common input datasets. In addition, we discuss some of the planned analysis approaches using WRF-CMAQ simulations performed over North America for both 2006 and 2010.

## 76.1 Introduction

The Air Quality Model Evaluation International Initiative (AQMEII) was launched in 2009 by bringing together scientists from both sides of the Atlantic Ocean [6]. The first phase of AQMEII culminated in the publication of a special issue of Atmospheric Environment [3]. Phase 2 of AQMEII was launched at a workshop in Utrecht, The Netherlands in May 2012 with the goal of applying coupled

C. Hogrefe (✉) • S. Roselle
Atmospheric Modeling and Analysis Division, U.S. Environmental Protection Agency,
Mail Drop E243-04, Research Triangle Park, NC 27711, USA
e-mail: hogrefe.christian@epa.gov; roselle.shawn@epa.gov

S. Galmarini
Institute for Environment and Sustainability, European Commission Joint Research Centre,
Tp441, Ispra 21027, Italy
e-mail: stefano.galmarini@jrc.ec.europa.eu

R. Mathur
Atmospheric Modeling and Analysis Division, United States Environmental Protection Agency,
Research Triangle Park, NC, USA
e-mail: mathur.rohit@epa.gov

D. Steyn and R. Mathur (eds.), *Air Pollution Modeling and its Application XXIII*,
Springer Proceedings in Complexity, DOI 10.1007/978-3-319-04379-1_76,

meteorology-chemistry regional models over Europe and North America and assessing feedbacks among aerosols, clouds, and radiation as called for in Alapaty et al. [1]. As in the first phase of AQMEII, it is expected that the model evaluation approaches suggested by Dennis et al. [2] can provide a common basis for evaluating participating models. Standardized modeling outputs from each modeling group as well as observational data from a number of ground based and upper air networks will be shared on the web-distributed ENSEMBLE system [4], facilitating statistical and ensemble analyses to be performed by each group.

## 76.2 Datasets and Model Overview

A common set of input data was provided to all modeling groups to facilitate the interpretation of model-to-model differences. In particular, concentrations from the global MACC reanalysis fields [5] were provided at three-hourly resolution over North America and Europe to specify boundary conditions for the regional-scale models for both 2006 and 2010. Anthropogenic emissions over North America and Europe were processed and provided by the U.S. Environmental Protection Agency (U.S. EPA) and the Netherlands Organization for Applied Scientific Research (TNO), respectively, for both 2006 and 2010. Over the U.S., anthropogenic emissions of $SO_2$ and $NO_x$ decreased by roughly 35 and 20 %, respectively, largely due to reductions in power plant and mobile source emissions.

It is expected that a total of about 20 annual regional-scale simulations will be performed as part of AQMEII Phase 2, with about fifteen of these simulations performed over Europe and five over North America. Since model results are still becoming available as of the writing of this paper, we only discuss results from simulations performed by the U.S. EPA using the WRF-CMAQ two-way coupled model [7]. Annual WRF-CMAQ simulations at a horizontal grid spacing of 12 km were performed for 2006 and 2010 over the continental U.S. considering direct aerosol feedback effects on shortwave radiation. A sensitivity simulation without feedback effects was performed for July 1–17, 2006.

## 76.3 Discussion

In this section, we discuss the types of analyses to be performed during Phase 2 of AQMEII using the WRF-CMAQ simulations described above as illustrative example. One of the first steps will be to establish the strength of the simulated feedback effects by performing sensitivity simulations. For the period from July 1–17, 2006 when WRF-CMAQ simulations were performed with and without direct feedback effects, results indicated that there was a non-negligible impact of these feedback effects on a number of variables. In particular, when averaged over all daytime hours over all model grid cells with AOD values of at least 0.1, the simulations with direct feedback effects showed lower temperatures (−0.05 K), lower PBL heights (−15 m) and higher surface $PM_{2.5}$ concentrations (+0.16 $\mu g/m^3$). Future

analysis will focus on determining the strength of the direct feedback effect for other models, the time periods and regions when the simulated feedback effects are largest, and the relative strength of direct vs. indirect effects.

Another objective is to compare simulated aerosol and radiation variables against available observations. Based on a comparison of WRF-CMAQ against ground-based AERONET measurements of AOD as well as MODIS satellite AOD retrievals, results indicate that WRF-CMAQ tends to underestimate AOD, especially during summer. In both years, WRF-CMAQ shows an overestimation of total $PM_{2.5}$ during winter and an underestimation during summer at these predominantly rural monitors. While the summertime underestimation of PM mass is consistent with the underestimation of AOD, AOD during wintertime is not overestimated despite an overestimation of $PM_{2.5}$ mass. Future analysis will focus on evaluating $PM_{2.5}$ composition, both at the surface and aloft. In addition, there is a need to study the diurnal cycle of $PM_{2.5}$ mass and components to evaluate whether the models capture the strength and timing of emissions and vertical mixing. To attribute model-to-model differences in AOD to differences in $PM_{2.5}$ composition and distribution vs. differences in aerosol optics calculations, there are plans to employ stand-alone aerosol optics calculation models such as FlexAOD (http://pumpkin.aquila.infn.it/flexaod/) driven by $PM_{2.5}$ concentrations simulated by the different coupled models.

One key consideration when designing the AQMEII Phase 2 activity was to enable dynamic model evaluation as defined in Dennis et al. [2]. To this end, model inputs were prepared for both 2006 and 2010 and groups were encouraged to consider simulating both years. Over North America, such simulations are being performed by at least three models, among them the WRF-CMAQ simulations described above. Results from an analysis of these simulations show a decrease in the observed and modeled concentrations of many gas phase and aerosol concentrations between 2006 and 2010, both during the warm and cold season. In addition, there also is a general decrease in observed and modeled AOD and an increase in simulated clear-sky short wave radiation. For key species such as $O_3$, $NO_x$, and $SO_4$, the percentage reductions in the modeled concentrations tend to be less than the reductions in the observed concentrations (for example, observed May – September $SO_4$ concentrations decreased by roughly 40 % averaged over all rural IMPROVE monitors while modeled concentrations decreased by roughly 35 %), but spatial patterns of changes are captured by the WRF-CMAQ simulations.

While the changes in North American anthropogenic emissions between 2006 and 2010 likely are a major driver for these observed and modeled concentration decreases, other factors need to be considered as well. In particular, there are differences in wildfire emissions that affect simulated changes in aerosol concentrations and radiation effects, changes in hemispheric background concentrations as represented by MACC that influence the regional-scale simulations through lateral boundary conditions, and changes in meteorology that affect pollutant transport, transformation and removal. For example, wintertime average mid-tropospheric $O_3$ concentrations in MACC decreased between 5 and 15 ppb from 2006 to 2010 near the western and northern boundaries of the regional scale simulations. Similarly, an initial analysis of meteorological fields indicates that changes in meteorology likely counteracted some of the effects of reduced anthropogenic emissions on

summertime ozone in parts of the Eastern U.S. and enhanced them in the Western U.S. Future work will be aimed at separating the various effects influencing year-to-year changes in pollutant concentrations and conducting such analyses for other modeling systems besides WRF-CMAQ.

## 76.4 Summary

AQMEII Phase 2 focuses on evaluating and intercomparing online coupled meteorology/chemistry modeling systems. By preparing inputs for 2006 and 2010 and by collecting a large observational dataset, it will be possible to perform operational, diagnostic, dynamic, and probabilistic evaluation of these models [2]. WRF-CMAQ simulations were used to illustrate some of the planned analysis approaches. Through these analyses and a planned journal special issue, it is envisioned that AQMEII Phase 2 will document the state of science in coupled regional-scale modeling and help to determine the value of including feedback effects in different model applications.

**Acknowledgments and Disclaimer** Although this work has been reviewed and approved for publication by the U.S. Environmental Protection Agency, it does not necessarily reflect the views and policies of the agency. We gratefully acknowledge the contribution of various groups to the second Air Quality Model Evaluation International Initiative (AQMEII) activity: U.S. EPA, Environment Canada, Mexican Secretariat of the Environment and Natural Resources (Secretaría de Medio Ambiente y Recursos Naturales-SEMARNAT) and National Institute of Ecology (Instituto Nacional de Ecología-INE) (North American national emissions inventories); TNO (European emissions processing); ECMWF/MACC project & Météo-France/CNRM-GAME (Chemical boundary conditions).

## References

1. Alapaty K et al (2012) New directions: understanding interactions of air quality and climate change at regional scales. Atmos Environ 49:419–421. doi:10.1016/j.atmosenv.2011.12.016
2. Dennis R et al (2010) A framework for evaluating regional-scale numerical photochemical modeling systems. Environ Fluid Mech 10:471–489. doi:10.1007/s10652-009-9163-2
3. Galmarini S, Bianconi R, Appel W, Solazzo E et al (2012a) ENSEMBLE and AMET: two systems and approaches to a harmonised, simplified and efficient assistance to air quality model developments and evaluation. Atmos Environ 53:51–59. doi:10.1016/j.atmosenv.2011.08.076
4. Galmarini S, Rao ST, Steyn DG (2012b) Preface for the AQMEII special issue of Atmospheric Environment, June 2012, http://dx.doi.org/10.1016/j.atmosenv.2012.03.001
5. Inness A et al (2013) The MACC reanalysis: an 8 yr data set of atmospheric composition. Atmos Chem Phys 13:4073–4109. doi:10.5194/acp-13-4073-2013
6. Rao ST, Galmarini S, Puckett K (2011) Air quality model evaluation international initiative (AQMEII). Bull Am Meteorol Soc 92:23–30. doi:10.1175/2010BAMS3069.1
7. Wong DC et al (2012) WRF-CMAQ two-way coupled system with aerosol feedback: software development and preliminary results. Geosci Model Dev 5:299–312. doi:10.5194/gmd-5-299-2012

# Chapter 77
# Modelling UK Air Quality for AQMEII2 with the Online Forecast Model AQUM

**Lucy Davis, Nick Savage, Paul Agnew, Carlos Ordóñez, and Marie Tilbee**

**Abstract** AQUM is an online air quality modelling system which is used to provide the operational Met Office air quality forecast for the UK. The standard model configuration runs at a resolution of 12 km and covers a domain including the UK and part of Western Europe. The model is routinely verified against near-real-time surface pollutant measurements from the UK Automatic Urban and Rural Network (AURN) to provide a continuous evaluation of model performance. We have developed a new configuration of AQUM to run on the AQMEII (Air Quality Modelling Evaluation International Initiative) Phase 2 European domain at a resolution of 22 km, using the prescribed AQMEII emission datasets. This latter dataset contains wildfire emissions which are not included in the standard AQUM emissions. An initial analysis is conducted to compare the emissions over the UK used as input to both models. Model simulations for 2010 from the AQUM standard and AQMEII configurations are compared to AURN surface observations and an analysis of the effect of the differing model domain, resolution and emissions is made. In 2010 Russian wildfires constituted a significant additional source of pollutants in Eastern Europe; we evaluate the impact of these wildfire emissions on UK air quality.

## 77.1 Introduction

AQUM (Air Quality in the Unified Model) is an online air quality modelling system which is used to provide the Met Office air quality forecast for the UK. AQUM is a limited area configuration of the Met Office Unified Model (MetUM), with a standard model domain of 12 km horizontal resolution, covering the UK and nearby European regions (see insert in Fig. 77.1). For further details, see [3].

L. Davis (✉) • N. Savage • P. Agnew • C. Ordóñez • M. Tilbee
UK Met Office, FitzRoy Road, Exeter, Devon EX1 3PB, UK
e-mail: Lucy.Davis@metoffice.gov.uk

D. Steyn and R. Mathur (eds.), *Air Pollution Modeling and its Application XXIII*,
Springer Proceedings in Complexity, DOI 10.1007/978-3-319-04379-1_77,

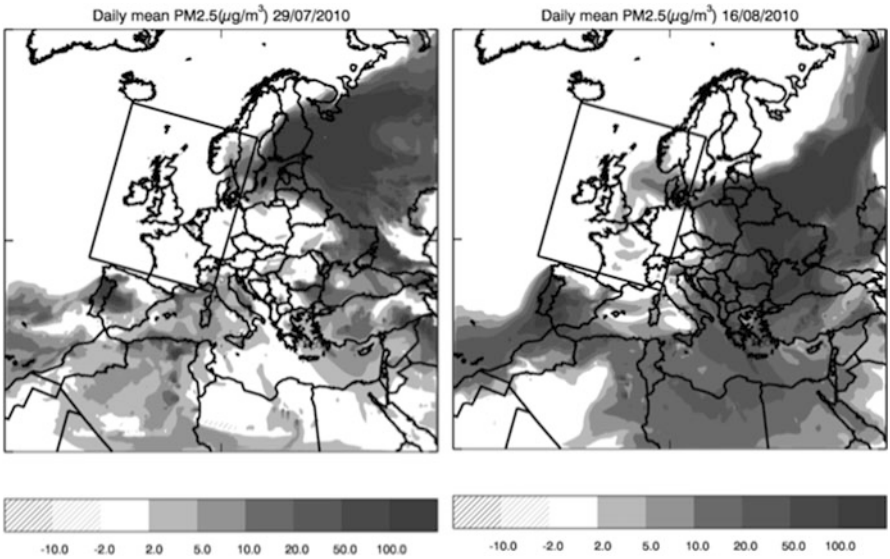


**Fig. 77.1** PM2.5 concentration difference plots for AQMEII-2 run with fire emissions – no fire emissions. On the left is shown a plot which is typical of most of the days, while on the right is a plot for the 16th August 2010 which is the only day the plume reached the UK. Also shown is the outline of the AQUM UK domain

AQMEII (Air Quality Modelling Evaluation International Initiative) Phase 1 was an inter-comparison between North American and European regional air quality models which simulated 2006; results from this can be found in [2]. Phase 2 [1] was launched in May 2012 and is focussing on the interactions of air quality and climate change, through the use of coupled meteorology-atmospheric chemistry models.

AQUM is participating in Phase 2 of AQMEII as part of COST Action ES1004, by simulating 2010 on a 22 km resolution European domain (Fig. 77.1). Lateral boundary conditions (LBCs) for chemical species are taken from the MACC model, while meteorological LBCs are taken from a global model run of the MetUM. An initial control run of 2010 for AQMEII-2 has now been completed, so here we present some preliminary results comparing the AQMEII-2 simulation to a standard AQUM run by verifying against UK surface observations. Some additional runs to aid interpretation of the comparison are also described.

## 77.2 Emissions

Standard emissions for AQUM use a combination of 2010 UK NAEI (National Atmospheric Emissions Inventory) 1 km resolution emissions, ENTEC shipping emissions at 5 km, and EMEP (European Monitoring and Evaluation Programme)

**Table 77.1** Standard AQUM and AQMEII-2 annual emission totals over the UK only

| Species | AQUM total (Gg/year) | AQMEII-2 total (Gg/year) |
|---|---|---|
| S in $SO_2$ | 212 | 213 |
| $NH_3$ | 231 | 232 |
| CO | 2029 | 2171 |
| NOx | 1023 | 1093 |
| Isoprene | 153 | 43 |
| Non-isoprene VOCs | 829 | 745 |
| Black+Organic carbon | 108 | 110 |

emissions at 50 km for the remainder of the European emissions. Isoprene emissions are generated from a vegetation climatology combined with meteorology from 2006.

For the AQMEII-2 simulation, emissions are taken from several completely different sources. Standard anthropogenic emissions for 2009 have been prepared by TNO, at a resolution of 0.125° longitude by 0.0625° latitude. Detailed temporal profiles are also provided which were used to produce a daily-varying gridded dataset with hourly variations then applied within the model. Biogenic emissions of isoprene are also provided by TNO, produced using ECMWF meteorology and the Corine/Phare Land Cover Data. Fire emissions from FMI at 0.1° resolution were downloaded from http://is4fires.fmi.fi, with speciation of these emissions as advised by the AQMEII-2 community.

As the emissions are one of the significant differences between the standard run and the AQMEII-2 simulation, it is worth highlighting the key differences between them. Annual UK totals for both datasets are given in Table 77.1. For most species it can be seen that AQUM and AQMEII-2 emissions are very similar. However, isoprene is three-times higher for AQUM; the seasonal cycle is also different in that the AQUM July total (21.4Gg) is six-times that of AQMEII-2 (3.51Gg), while AQUM winter emissions are lower.

## 77.3 Analysis

Several different model runs have been performed to examine various components of the performance of the AQMEII-2 simulation. All runs are compared to UK rural and urban-background surface observations from the AURN (Automatic Urban and Rural Network, http://uk-air.defra.gov.uk/networks/network-info?view=aurn). Any variations in results between AQUM UK-domain and AQMEII-2 runs should be attributable to two main differences in the set-ups: larger domain and coarser resolution in the AQMEII-2 run; or from using a different set of emissions.

**Table 77.2** AQUM and AQMEII-2 model performance statistics for key air quality species during 2010

| | $O_3$ | | $NO_2$ | | PM10 | | PM2.5 | |
|---|---|---|---|---|---|---|---|---|
| | AQUM | AQMEII | AQUM | AQMEII | AQUM | AQMEII | AQUM | AQMEII |
| Bias | 4.21 | 4.78 | −4.28 | −4.72 | −9.38 | −8.67 | −3.74 | −2.75 |
| RMSE | 21.39 | 21.46 | 17.93 | 18.87 | 15.44 | 16.17 | 11.14 | 12.83 |

Bias and RMSE are given in $\mu gm^{-3}$

### *77.3.1 AQMEII-2 Compared to Standard AQUM Run*

An analysis comparing the results from the AQMEII-2 run to a standard AQUM case-study of 2010 has been conducted to provide an initial evaluation of the AQMEII-2 run. Model bias and error statistics from these runs are given in Table 77.2. It can be seen that in general the AQMEII-2 run has similar characteristics to the standard AQUM run for ozone and $NO_2$, with positive and negative biases respectively, although there are slightly worse results for AQMEII-2, probably due to the coarser resolution. The large negative bias for PM found with AQUM is reduced slightly in magnitude in AQMEII-2. However a substantial level of underprediction remains in the coarse component.

### *77.3.2 Isolating the Impact of Emission Datasets on UK Air Quality*

To examine the impact of the different emission datasets in isolation, two model runs were conducted using the AQUM UK domain at 12 km resolution: one with AQUM standard emissions and one with AQMEII-2 emissions. Model bias and error statistics from these two runs are shown in Table 77.3. The improved ozone bias appears to be due to the reduction in summer isoprene fluxes when using AQMEII-2 emissions – the June-August bias in particular reduces from $18.23 \mu gm^{-3}$ to $12.25\ \mu gm^{-3}$. Although the AQMEII-2 dataset contains similar quantities of PM emissions, there is a small improvement in the PM10 and PM2.5 negative biases, although the coarse bias is still much larger than for PM2.5. This suggests that there are still some significant sources of the coarse component of PM missing from the emissions, such as resuspended traffic particulates and sea salt. It can also be seen that the $NO_2$ bias is improved when using AQMEII-2 emissions. Further investigation has shown that a large component of this improvement derives from the different hourly time profiles used in the two runs – the AQUM profile is based entirely on a traffic cycle, whereas the AQMEII-2 profile is averaged over all source types, resulting in greater emissions in AQMEII-2 overnight. Another component of the $NO_2$ differences is due to spatial changes in emissions: Around the London area

**Table 77.3** AQUM UK domain model performance statistics for key air quality species during 2010, using AQUM and AQMEII-2 emissions

| | $O_3$ | | $NO_2$ | | PM10 | | PM2.5 | |
|---|---|---|---|---|---|---|---|---|
| | AQUM | AQMEII | AQUM | AQMEII | AQUM | AQMEII | AQUM | AQMEII |
| Bias | 4.21 | 0.89 | −4.28 | −1.42 | −9.38 | −8.62 | −3.74 | −2.67 |
| RMSE | 21.39 | 20.26 | 17.93 | 17.92 | 15.44 | 15.24 | 11.14 | 11.58 |

Bias and RMSE are given in $\mu gm^{-3}$

emissions are greater in AQMEII-2, whereas in Scotland they are smaller, leading to corresponding changes in $NO_2$ concentrations. However the large number of AURN $NO_2$ sites in London gives an apparent improvement in the overall bias.

### *77.3.3 Impact of Wildfires on UK Air Quality*

In 2010, there were some very large wildfires in Russia, particularly towards the end of July and into August. Similar wildfires in 2006 have been shown to impact UK air quality [4]. To examine the impact that the 2010 fires may have had on UK air quality, the AQMEII-2 model simulation was run both with and without fire emissions. Contour plots of the difference between the two runs are shown in Fig. 77.1. For the majority of the time the plume from the wildfires is nowhere near the UK; there is only one day when it passes over the UK at low concentrations. Comparison of model results against UK AURN observations show little difference between statistics for all species, for example for ozone the bias with fire emissions is 16.87 $\mu gm^{-3}$, while without fire emissions the bias is 16.82$\mu gm^{-3}$. Hence although there is a significant impact near the source of the fires, there is little or no impact on the UK. A separate analysis of air mass histories for summer 2010 showed that for the duration of the fires the UK experienced predominantly westerly winds, which brought clean Atlantic air to the UK.

## 77.4 Conclusions

An initial comparison of results from the AQMEII-2 simulation using AQUM, with a standard AQUM UK-domain set-up has validated the AQMEII-2 AQUM model configuration for surface air quality prediction in the UK. Model performance was generally similar for ozone and $NO_2$. Although the AQMEII-2 emissions for PM improve the negative bias marginally, a significant negative bias in the coarse component of PM still remains. The much lower isoprene emissions in AQMEII-2 seem to reduce the ozone bias, particularly over the summer period when the isoprene emissions are at their highest. The AQMEII-2 temporal profile for $NO_2$ emissions appears to give improved predictions for this pollutant. Model simulations

with and without wildfire emissions indicate that, unlike in 2006, in 2010 wildfires had no significant impact on UK air quality, due to the prevalence of westerly winds in the UK over the summer.

Overall, the AQMEII-2 simulation shows results similar to the AQUM UK domain giving confidence that the AQMEII-2 inter-comparison will be useful for improving the operational model.

## References

1. Alapaty K, Mathur R, Pleim J, Hogrefe C, Rao ST, Ramaswamy V, Galmarini S, Schaap M, Makar P, Vautard R, Baklanov A, Kallos G, Vogel B, Sokhi R (2012) New directions: understanding interactions of air quality and climate change at regional scales. Atmos Environ 49:419–421. doi:10.1016/j.atmosenv.2011.12.016
2. Galmarini S, Rao ST, Steyn DG (2012) Preface for the AQMEII special issue of atmospheric environment. Atmos Environ 53:1–3. doi:10.1016/j.atmosenv.2012.03.001
3. Savage NH, Agnew P, Davis LS, Ordóñez C, Thorpe R, Johnson CE, O'Connor FM, Dalvi M (2013) Air quality modelling using the Met Office Unified Model (AQUM OS24-26): model description and initial evaluation. Geosci Model Dev 6:353–372. doi:10.5194/gmd-6-353-2013
4. Witham C, Manning A (2007) Impacts of Russian biomass burning on UK air quality. Atmos Environ 41:8075–8090. doi:10.1016/j.atmosenv.2007.06.058

## Questions and Answers

**Questioner Name:** Pius Lee

**Q:** On the slide showing emission difference between AQMEII and AQUM cases, the 'outstanding' along ship track emission implied the AQUM case had very little maritime emission, if it had been accounted for (the plot at least gave such an impression)? Maybe that did not impact the comparison of the two case results (westerly dominant in August?). But maybe not, as MACC derived LBC based on TNO would possibly increase the marine emission into the UK domain. If the maritime emissions was a candidate causing the difference in the case results, it could be more binding than that from the Russian wildfires.

**A:** The differences between the $NO_x$ marine emissions in the two datasets are very small. For AQUM there is a total of 1338Gg/year over the whole UK domain, while for AQMEII the total is marginally less at 1295Gg/year. The differences shown in the plot are mainly spatial differences between the two datasets with slightly different locations of the ship tracks. The similarities of the overall total emissions shows that there should be little impact of ship emissions between the two runs.

**Questioner Name:** Tianfeng Chai

**Q:** Is chemical data assimilation planned in the future?

**A:** There is no full data assimilation prior to the model run planned for the near future. However statistical post-processing to incorporate observations is used in the operational forecast. Note this is not included in any results shown in this paper.

**Questioner Name:** Roger Timmis

**Q:** Your comparison of NOx hourly time profiles appears to compare profiles for two different groups: (a) traffic sources only for AQUM and (b) all sources combined for AQMEII-2. Is this a true 'like-for-like' comparison, or would it be more instructive to compare emission profiles for identical source groups? What hourly profiles does AQUM use for non-traffic sources – like power stations?

**A:** These are like-for-like comparisons, as traditionally AQUM applies the traffic cycle to all gas-phase emissions, including non-traffic sources such as power stations. For the AQMEII-2 project this has been altered to have an average of all source types. Note there is currently development work ongoing to allow different source profiles to be applied to different SNAP sectors.

# Chapter 78
# Model Inter-comparison Study Between NMMB/BSC-CTM and Enviro-HIRLAM On-Line Systems Contributing to the AQMEII-Phase2 Initiative

**Alba Badia, Oriol Jorba, Roman Nuterman, Alexander Baklanov, and Jose María Baldasano**

**Abstract** The Air Quality Model Evaluation International Initiative (AQMEII) Phase-2 aims to inter-compare on-line couple regional-scale models over North America and Europe. Common chemical boundary conditions, emissions, and domain configurations are pre-defined.

In this study, we present the 2010 annual modelling results from two on-line integrated models, NMMB/BSC-CTM and Enviro-HIRLAM, as a contribution to the European domain simulations of AQMEII-Phase2 initiative and COST Action ES1004 EuMetChem. Both models have been configured according to requirements of AQMEII-Phase2 initiative. Model results will be evaluated against ground-based monitoring stations and vertical profiles. The performance and capability of both systems to reproduce surface and vertical structure of relevant reactive gases and aerosols will be discussed.

## 78.1 Introduction

Several on-line coupled meteorology-chemistry regional-scale models have been developed in the last decades. The COST Action ES-1004 "European framework for online integrated air quality and meteorology modelling" (EuMetChem –

A. Badia (✉) • O. Jorba • J.M. Baldasano
Earth Sciences Department, Barcelona Supercomputing Center ¨C Centro Nacional de Supercomputación (BSC-CNS), Barcelona, Spain
e-mail: alba.badia@bsc.es; oriol.jorba@bsc.es; jose.baldasano@bsc.es

R. Nuterman
Niels Bohr Institute, Climate and Geophysics, University of Copenhagen, Copenhagen, Denmark
e-mail: nuterman@gfy.ku.dk

A. Baklanov
Research Department, Danish Meteorological Institute (DMI), Copenhagen, Denmark
e-mail: alb@dmi.dk

D. Steyn and R. Mathur (eds.), *Air Pollution Modeling and its Application XXIII*, Springer Proceedings in Complexity, DOI 10.1007/978-3-319-04379-1_78,

http://eumetchem.info) has reviewed those integrated models developed or applied in Europe. A model intercomparison effort is defined within the Action ES-1004, and is coordinated with the AQMEII-Phase2 international initiative. The main objectives is the intercomparison of on-line models to better understand the impact of feedbacks on both meteorology and chemistry processes when ones solved in an integrated approach.

This contribution will present annual results of two European integrated models, NMMB/BSC-CTM and Enviro-HIRLAM, which participate in the AQMEII-Phase2 initiative. Gas and aerosol simulations are evaluated and compared in a 2010 annual simulation.

## 78.2 Models Description

### *78.2.1 NMMB/BSC-CTM*

The NMMB/BSC Chemical Transport Model (NMMB/BSC-CTM) is a chemical weather prediction system for short-term forecast applications developed at the Barcelona Supercomputing Center (BSC) in collaboration with several research institutions. The meteorological driver is of the system is the Nonhydrostatic Multiscale Model on the B grid (NMMB; [1]) developed at the National Centers for Environmental Prediction (NCEP) for a broad range of spatial and temporal scales.

An aerosol module for the relevant global aerosols (e.g., mineral dust, sea salt, black carbon, organic carbon and sulphate) is under development within the NMMB/BSC-CTM. All mineral dust processes are fully in-lined within NMMB, and an extensive description and evaluation of the dust implementation is presented in Pérez et al. [2]. The sea-salt aerosol module is described and evaluated at global scale in Spada et al. [3]; black carbon, organic carbon and sulphate are currently under development.

The tropospheric gas-phase chemistry has been implemented and evaluated within NMMB/BSC-CTM [4]. The photolysis scheme is based on the Fast-J scheme and has been upgraded with the used CB05 chemical mechanism. The modular structure of the system allows configuring the model with feedbacks among the different processes implemented (e.g., radiation-aerosols-gases, photolysis-gases-aerosols).

### *78.2.2 Enviro-HIRLAM*

The current version of Enviro-HIRLAM [5–7] is based on reference HIRLAM version 7.2. The model's hydrostatic dynamical core was recently improved by

adding a locally mass conserving semi-Lagrangian numerical advection scheme [8] ensuring mass conservation and shape preservation. It improves forecast accuracy and makes it possible to perform longer duration runs.

The Savijarvi radiation scheme has been improved to account explicitly for aerosol radiation interactions. Now, it explicitly treats ten aerosol subtypes (soluble/insoluble nucleation, accumulation and coarse modes of sulfate, soot, sea-salt and mineral dust particles) according to Global Aerosol Data Set (GADS) classification. The short-wave radiative transfer calculations are performed as standard 2-stream calculations for averages of aerosol optical properties weighted over the entire spectrum.

The aerosol activation scheme was also implemented in STRACO condensation-convection scheme. Now, nucleation is dependent on aerosol properties and the ice-phase processes are reformulated in terms of classical nucleation theory. Moreover, the precipitation release is more dependent on cloud droplet effective radius.

The model includes a new tropospheric condensed gas-phase chemistry scheme based on Carbon Bond Mechanism version-Z (CBM-Z) with a fast solver based on radical balances. A sophisticated "pseudomodal" aerosol dynamics module M7 with tropospheric sulphur cycle chemistry has also been implemented. Moreover, several interactive parameterizations of dust, sea-salt and isoprene fluxes as well as sedimentation and dry-/wet-deposition schemes for both aerosols and gases have been added.

## 78.3 AQMEII Phase 2 Description

The Air Quality Model Evaluation International Initiative (AQMEII) aims to evaluate regional scale air quality models and to develop a common evaluation framework across European and North American atmospheric modelling communities. AQMEII Phase-2 focuses on inter-comparison of on-line coupled regional-scale models. Around 20 groups from EU and 4 from NA are participating in the second phase with annual simulations for the years 2006 (NA) or/and 2010 (EU). Common chemical boundary conditions from MOZART-IFS modelling system, anthropogenic emissions from TNO-MACC database, forest fires emission by FMI and domain configuration (30W- 60E, 25N-70N at $0.25 \times 0.25$ horizontal resolution) are pre-defined and provided by AQMEII.

## 78.4 Models Results

Both groups are currently producing the results of the annual simulation of 2010 for the European domain. Enviro-HIRLAM results have not evaluated yet. Thus, in this section, we present preliminary results of the NMMB/BSC-CTM ozone simulations. NMMB/BSC-CTM is configured at regional scale with horizontal resolution of

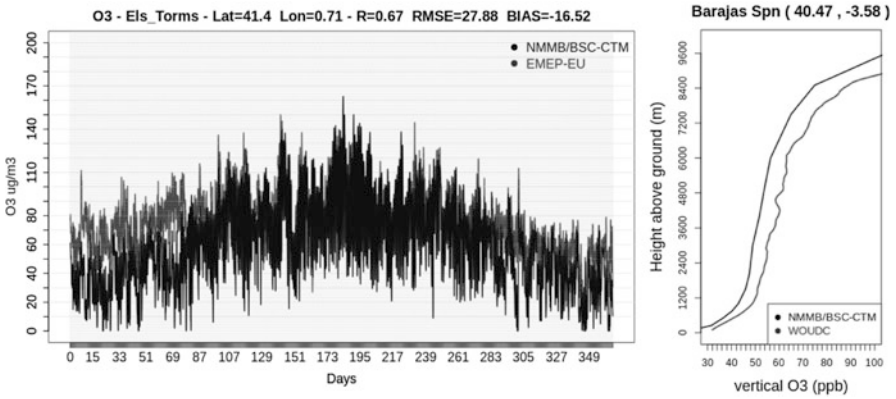


**Fig. 78.1** NMMB/BSC-CTM preliminary model results (*dark lines*) and observations (*grey lines*) of surface O3 (*left*) concentrations at Els Torms, and mean vertical profiles (*right*) at Barajas for the year 2010

$0.2° \times 0.2°$ and 24 vertical layers with the domain top at 50 hPa. Meteorological boundary conditions are taken from NCEP/GFS analysis and biogenic emissions are computed in-lined with the MEGAN model. The model results are preliminary evaluated against ground level observations and ozonesondes. Figure 78.1 (left) shows the annual pattern of surface $O_3$ between the model run and EMEP data at Els Torms station. The model overestimates $O_3$ during January, February, half of March and December, however during the ozone season, it has a good seasonal and daily pattern representation capturing both the maximum and the minimum values of $O_3$. It is important to note that the winter behaviour of $O_3$ is highly influenced by the chemical boundary conditions. Figure 78.1 (right) represents a comparison between annual mean vertical profile of the simulation and the ozonesonde at Barajas station. The model reproduces reasonably well the vertical structure in the troposphere, but a systematic cold bias is observed through the free-troposphere. Better agreement with the ozonesondes is observed within the PBL. The upper layer ozone underestimation is partly attributed to the chemical boundary conditions used in the simulation.

## 78.5 Conclusion

Preliminary results of the NMMB/BSC-CTM ozone show a good agreement at surface layer from April to September. A systematic bias is observed both in the horizontal (winter months) and in the vertical distribution (mainly above 1,500 m a.g.l.) of simulated ozone. This deviation is partly associated to the boundary condition. Enviro-HIRLAM results are currently evaluating. Results and comparisons with the NMMB/BSC-CTM will be presented on the conference for both gases and aerosols.

**Acknowledgments** The authors wish to thank the initiative of AQMEII-Phase2 for providing an automatic evaluation system with a large set of observations, and COST Action ES1004 "European framework for online integrated air quality and meteorology modelling" for supporting a Short Term Scientific Mission of Alba Badia to DMI. BSC acknowledges the support from projects CGL2010/19652 and CSD2007-00050 of the Spanish Ministry of Economy and Competitiveness, and support of the grant SEV-2011-00067 of Severo Ochoa Program, awarded by the Spanish Government. BSC simulations were performed with the Marenostrum Supercomputer at BSC. DMI and NBI/UC acknowledge the support from EU FP7 PEGASOS project (FP7-ENV-2010-265148) and Nordic EnsCLIM project.

## References

1. Janjic ZI, Gall R (2012) Scientific documentation of the NCEP nonhydrostatic multiscale model on the B grid (NMMB). Part 1 dynamics, Technical report, NCAR/TN-489+STR
2. Pérez C, Haustein K, Janjic Z, Jorba O, Huneeus N, Baldasano JM, Black T, Basart S, Nickovic S, Miller RL, Perlwitz JP, Schulz M, Thomson M (2011) Atmospheric dust modeling from meso to global scales with the online NMMB/BSC-dust model – Part 1: model description, annual simulations and evaluation. Atmos Chem Phys 11:13001–13027
3. Spada M, Jorba O, Pérez C, Janjic Z, Baldasano JM (2013) Modeling and evaluation of the global sea-salt aerosol distribution: sensitivity to emission schemes and resolution effects at coastal/orographic sites. Atmos Chem Phys Discuss 13:11597–11657. (in discussion)
4. Jorba O, Dabdub D, Blaszczak-Boxe C, Pérez C, Janjic Z, Baldasano JM, Spada M, Badia A, Gonçalves M (2012) Potential significance of photoexcited NO2 on global air quality with the NMMB/BSC chemical transport model. J Geophys Res 117:D13301
5. Baklanov A, Korsholm U, Mahura A, Petersen C, Gross A (2008) ENVIRO-HIRLAM: on-line coupled modelling of urban meteorology and air pollution. Adv Sci Res 2:41–46
6. Baklanov AA, Korsholm US, Mahura AG, Nuterman RB, Sass BH, Zakey AS (2011) Physical and chemical weather forecasting as a joint problem: two-way interacting integrated modelling. American Meteorological Society 91st Annual Meeting (Seattle, WA, USA; 23–27 Jan 2011), Paper 7.1 (Invited Speaker), AMS2011_paper_7-1_fv.pdf, 2011
7. Korsholm US, Baklanov A, Gross A, Mahura A, Sass BH, Kaas E (2008) Online coupled chemical weather forecasting based on HIRLAM – overview and prospective of Enviro-HIRLAM. HIRLAM Newsl 54:151–168
8. Sørensen B, Kaas E, Korsholm US (2012) A mass conserving and multi-tracer efficient transport scheme in the online integrated Enviro-HIRLAM model. Geosci Model Dev Discuss 5:3733–3769. doi:10.5194/gmdd-5-3733-2012, 2012

## Questions and Answers

**Questioner Name:** Dominik Brunner

**Q:** How did you select stations for validation?

**A:** We selected stations following two criteria: (1) only stations below 1,000 m were selected considering that the model resolution is 20 km and mountain stations would not be well represented by the model, (2) only rural stations from the AQMEII-Phase2 database were selected, again considering the model resolution and its representativeness of background areas.

**Q:** Are you aware of problem of $NO_2$ measurements at rural sites?

**A:** We identified some problems with CO and $SO_2$ observations, but not for $NO_2$. We were not aware of the problem of some sensors measuring $NO_2$ at rural areas, but it is an issue to be considered when evaluating model results.

# Chapter 79
# Can We Explain the Observed Decrease in Secondary Inorganic Aerosol and Its Precursors Between 1990 and 2009 over Europe Using LOTOS-EUROS?

**S. Banzhaf, M. Schaap, R. Kranenburg, A.M.M. Manders, A.J. Segers, A.H.J. Visschedijk, H.A.C. Denier van der Gon, J.J.P. Kuenen, C. Hendriks, E. van Meijgaard, L.H. van Ulft, and P.J.H. Builtjes**

**Abstract** In this study we investigate the ability of the Chemistry Transport Model (CTM) LOTOS-EUROS to explain the observed decrease in secondary inorganic aerosol (SIA) and its precursors between 1990 and 2009 over Europe. The model explicitly accounts for cloud chemistry and aerosol thermodynamics. The results have shown that the model largely captures the observed trends in SIA and its precursors' concentrations while it underestimates the interannual variability. Using a source-apportionment module the amount of SIA formed per unit emission was traced for a number of regions. The results show 20–50 % more efficient $SO_4^{2-}$ formation in 2009 compared to 1990, whereas the change in $NO_3^-$ formation per unit $NO_x$ emission is lower (−10 % to +20 %) for the same time period.

## 79.1 Introduction

SIA forms a substantial fraction of PM, which has adverse impact on public health [3]. Moreover, sulphur and nitrogen deposition fluxes damage ecosystems by eutrophying and acidifying soils and fresh water leading to a decrease in biodiversity [1].

S. Banzhaf (✉)
Institute of Meteorology, Free University Berlin, Berlin, Germany
e-mail: sabine.banzhaf@met-fu-berlin.de

M. Schaap • R. Kranenburg • A.M.M. Manders • A.J. Segers • A.H.J. Visschedijk
H.A.C. Denier van der Gon • J.J.P. Kuenen • C. Hendriks
TNO, Department of Climate, Air and Sustainability, Utrecht, The Netherlands

E. van Meijgaard • L.H. van Ulft
KNMI, De Bilt, The Netherlands

P.J.H. Builtjes
Institute of Meteorology, Free University Berlin, Berlin, Germany

TNO, Delft, The Netherlands

D. Steyn and R. Mathur (eds.), *Air Pollution Modeling and its Application XXIII*,
Springer Proceedings in Complexity, DOI 10.1007/978-3-319-04379-1_79,

In the last two decades emission abatement strategies have been implemented all over Europe targeting the adverse effects of SIA and its precursors on human health and environment (e.g. NEC Directive). The implemented mitigation measures have led to significant emission reductions. However, the responses of the pollutants' concentrations and deposition fluxes to the emission changes are not one to one but show non-linear behaviour Tarrasón et al. [6].

CTMs are used to analyse potential emission reduction strategies and quantify their effectiveness. Modelling the non-linear relationships between gas- and particle-phase i.e. modelling secondary species is still challenging for state of the art CTMs. Thus, analysing the ability of CTMs to capture non-linear responses and interannual variability of the last 20 years is fundamental before the models can be used to analyse future emission strategies.

In this study we compare concentrations of SIA and its precursors of a 20 years LOTOS-EUROS model run to observations to investigate if the model is able to explain the observed decrease in SIA and its precursors between 1990 and 2009 over Europe. Moreover, a source-apportionment module has been applied to trace the amount of SIA formed per unit emission of $SO_2$, $NO_x$ and $NH_3$ for three different regions over Europe.

## 79.2 Methods and Data

### *79.2.1 Observational Data*

Observational data for the years 1990–2009 have been provided by the European measurement networks EMEP (European Monitoring and Evaluation Programme) and AirBase, which is the public air quality database system of the European Environmental Agency. The performed trend analysis and model comparison are based on observed daily averages of SIA and its precursors at rural background stations. The quality criteria for the data included: The time series had to cover at least 75 % of data each year and each time series had to pass a visual inspection after which suspicious data was excluded. Stations with at least 16 years (=80 %) of data were considered.

### *79.2.2 Simulation Description*

#### 79.2.2.1 Model Description LOTOS-EUROS

The off-line 3D chemistry transport model LOTOS-EUROS simulates air pollution concentrations solving the advection–diffusion equation on a regular lat-lon-grid with variable resolution over Europe. LOTOS-EUROS is aimed at the simulation

of air pollution in the lower troposphere and includes a source apportionment module, which enables tracking the origin of the modelled concentrations for different tracers. The model and its source apportionment module are extensively described in Kranenburg et al. [2]. The LOTOS-EUROS model has participated in several international model intercomparison studies addressing ozone (e.g. [4]) and particulate matter (e.g. [5]) and shows comparable performance to other European models.

#### 79.2.2.2 Model Setup

A long-term model run of 20 years (1990–2009) has been performed on a domain covering Europe (35N–70N and 10W–40E). The grid resolution was 0.50° longitude x 0.25° latitude on a rectangular regular latitude-longitude grid. In the vertical, three dynamic layers on top of a surface layer (=25 m) were used. The lowest dynamic layer was the mixing layer, taken from the meteorological input. Lateral boundary conditions were taken from climatological background concentrations. The simulation was forced with a consistent meteorological data set obtained from RACMO2. Emissions were generated using IIASA RAINS/GAINS output. For the source apportionment of SIA we have defined three labels to track 10kt of $SO_2$, $NO_x$ and $NH_3$ emissions from either one of these: (1) The Netherlands and Belgium (NLBE), (2) Czech Republic (CZE) and (3) Romania (ROM).

## 79.3 Results and Discussion

### *79.3.1 Model Evaluation*

Figure 79.1 shows the mean 60 days moving average for $NO_2$ (a) and $TNO_3$ (b) at 57 and 9 stations, respectively, spread over Europe. The model underestimates the concentrations and the interannual variability for $NO_2$ while for $TNO_3$ both features are captured well. Also most nitrate episodes during the considered time period are well reproduced by the model. For sulphate (not shown here) several episodes that have partly already been investigated in former studies (e.g. [5]) are underestimated in their extent or not captured by the model.

### *79.3.2 Observed and Modelled Trends*

Figure 79.2a shows a scatter plot of the absolute observed and modelled trends in $SO_2$ concentrations for 1990–2009 at 51 stations spread over Europe. The significance of the trends has been assessed using the Mann-Kendall test at the 95 %

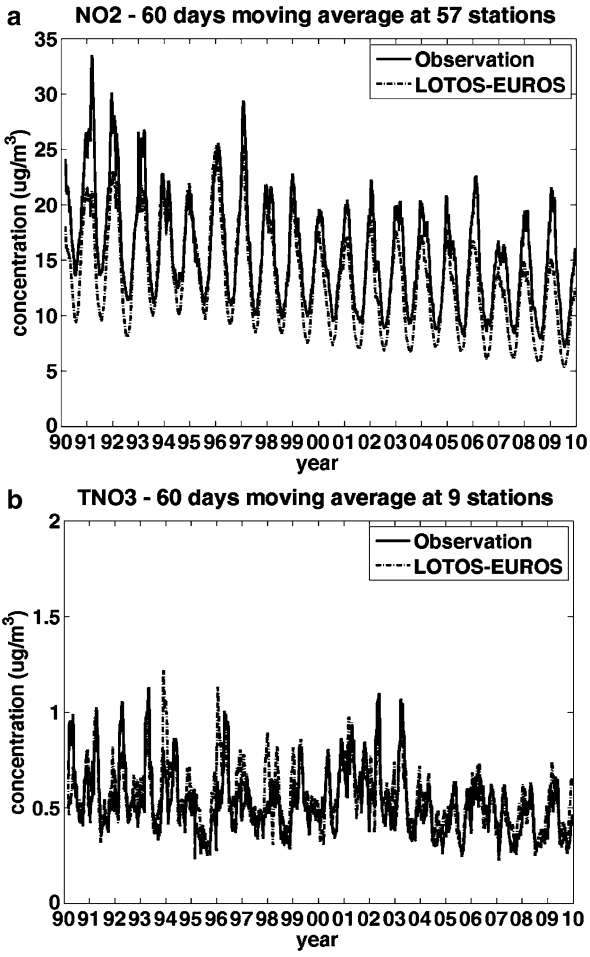


**Fig. 79.1** Mean 60 days moving average for (**a**) NO2 and (**b**) TNO3 at 57 and 9 European rural background stations, respectively

confidence level. The observed trend is negative and significant at all stations. The model results also indicate significant negative trends at all stations. However, the model underestimates the trends at several stations. The significant negative trend in sulphate concentrations (not shown here) is also underestimated by the model at most stations. As Fig. 79.1a, b indicate the model overestimates the absolute negative trend in $NO_2$ concentrations at most stations while the comparatively low trends in $TNO_3$ are captured well by the model. In general, it was found that the model reproduces the observed relative trends better than the absolute trends for all investigated components. In order to analyse the trends in gas to particle conversion and residence time of the involved species 10 kt of $SO_2$, $NO_x$ and $NH_3$ emissions of three labels have been traced using a source apportionment module. Figure 79.2b shows the amount of sulphate (solid lines) formed from 10 kt $SO_2$ emissions relative to the amount formed from 10kt $SO_2$ emissions in 1990 for the different labels for

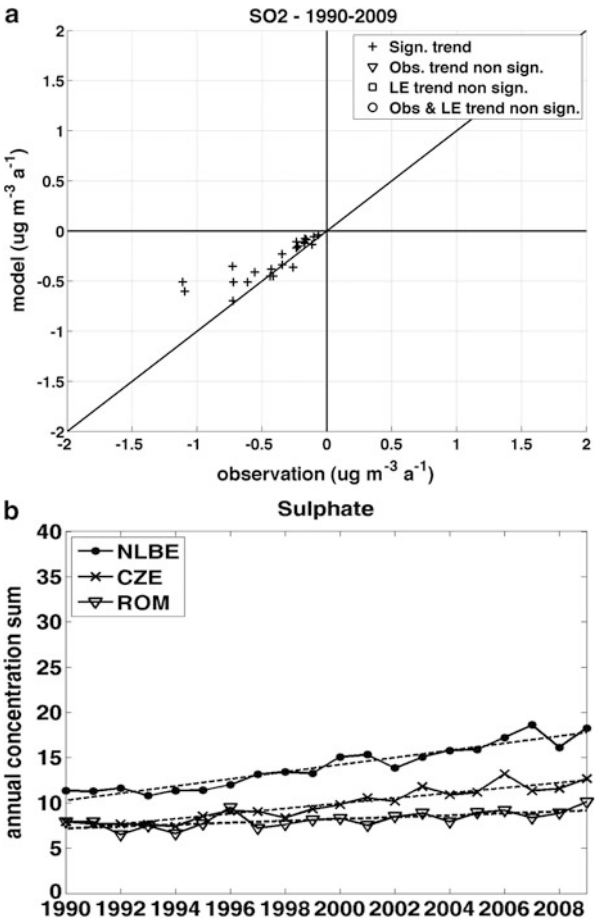


**Fig. 79.2** (**a**) Observed versus modelled trend in $SO_2$ air concentrations in $\mu g\ m^{-3}a^{-1}$ for 1990–2009 and (**b**) amount of sulphate (*solid lines*) formed from 10 kt $SO_2$ emissions relative to the amount formed from 10 kt $SO_2$ emissions in 1990 for the different labels for 1990–2009

1990–2009. A trend line (dashed line) is added for all labels. Following the Mann-Kendall Test at a 95 % confidence level the positive trends are significant for all labels. The results reveal an increase in sulphate formation efficiency by 20–50 % from 1990 to 2009 for all regions. The increase in sulphate formation efficiency is most likely connected to extensive $SO_2$emission reductions over Europe during the considered time period while $NH_3$ emissions have only been slightly reduced or even increased in some regions over Europe. The latter leads to an increased neutralisation of cloud acidity and consequently to an increase in sulphate formation efficiency. The changes in nitrate formation efficiency from 1990 to 2009 (not shown here) are lower than for sulphate. A significant trend has only been found for the label NLBE showing an increase in nitrate formation efficiency by +20 %. The latter may be induced by changes in oxidant levels following the $NO_x$ emission decrease over Europe.

## 79.4 Conclusion

The results of the study have shown that the model captures the observed relative trends in SIA and its precursors' concentrations better than the absolute trends. Applying a source-apportionment module the results have revealed changes in SIA formation efficiency from 1990 to 2009. This non-linear effect seems to also exist in the observations. The latter is induced by shifts in the partitioning between aerosol- and gas-phase and changes in oxidant levels due to changes in the emission regime following emission reductions over Europe.

## References

1. Bobbink R et al (1998) The effects of airborne pollutants on species diversity in natural and semi-natural European vegetation. J Ecol 86:717–738
2. Kranenburg R et al (2012) Source apportionment using LOTOS-EUROS: module description and evaluation. Geosci Model Dev 6:721–733
3. Pope CA (2007) Mortality effects of longer term exposures to fine particulate air pollution: review of recent epidemiological evidence. Inhal Toxicol 19(Suppl 1):33–38
4. Solazzo E et al (2012) Model evaluation and ensemble modelling of surface-level ozone in Europe and North America in the context of AQMEII. Atmos Environ 53:60–74
5. Stern R et al (2008) A model inter-comparison study focussing on episodes with elevated PM10 concentrations. Atmos Environ 42:4567–4588
6. Tarrasón L et al (2003) EMEP status report 1/2003 – Part III: Source-receptor relationships, transboundary acidification, eutrophication and ground level ozone in Europe. Norwegian Meteorological Institute, Oslo

## Questions and Answers

**Questioner Name:** Dominik Brunner

**Q:** Did you look at cloud pH trends in the model to confirm hypothesis?

**A:** We have re-run the model and output cloud pH. The results show an increasing cloud pH from 1990 to 2009 which confirmed our hypothesis.

**Q:** Did you look at trends separately for different regions?

**A:** Unfortunately, the observations that were available for the time period 1990–2009 were not distributed all over Europe. For $SO_2$ and $NO_2$ most of the available stations were located in Central Europe while SIA observations were mostly available at Northern and Eastern European station locations. Hence, based on the observations a regional consideration of the trend analysis was not possible.

However, results have shown that the model satisfactorily simulates the relative trends for the time period 1990–2009. Figure 79.3a, b show the modelled relative trend in sulphate and total nitrate concentrations in (% year$^{-1}$)

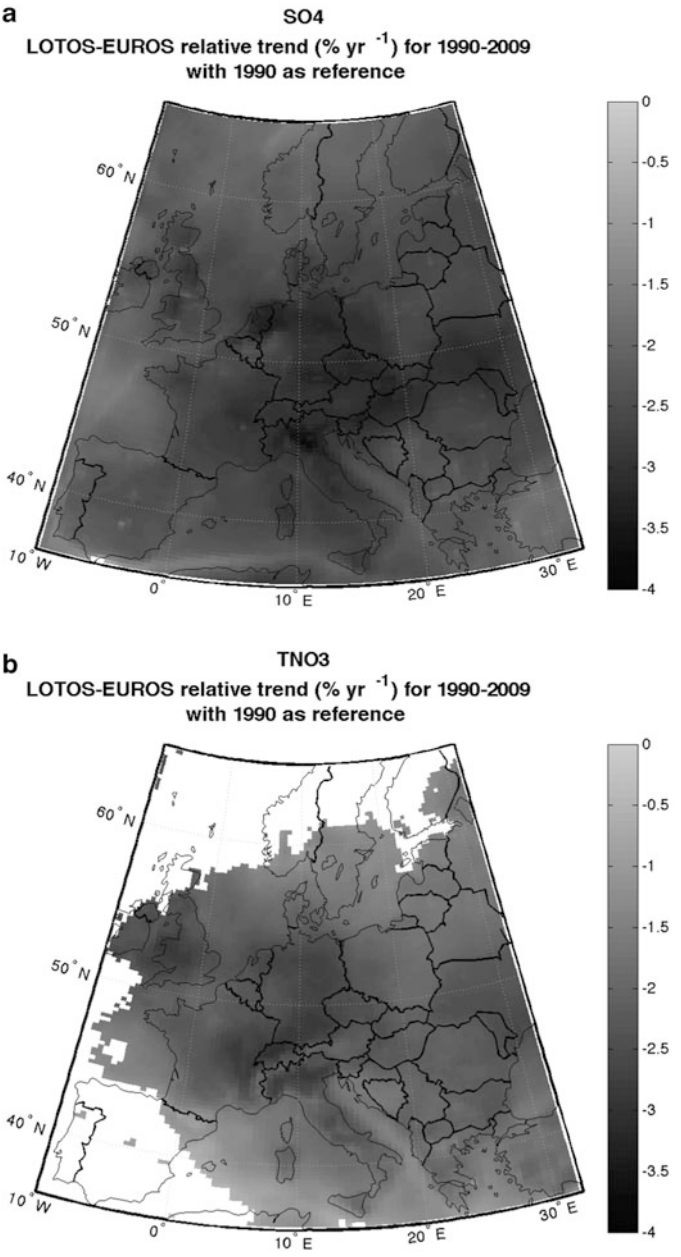


**Fig. 79.3** Relative trends in (**a**) $SO_4$ and (**b**) $TNO_3$ concentrations in (% year$^{-1}$) for 1990–2009 with concentration of 1990 as reference

with concentrations of 1990 as reference for 1990–2009. White areas indicate a non-significant trend. Sulphate concentrations show a significant negative trend all over Europe with largest decreases of up to $-3.8$ % year$^{-1}$over The Netherlands and the Po Valley. For total nitrate the outcome is less distinct. For Northern Europe and Spain the trend in total nitrate concentrations is non-significant. For the rest of Europe Fig. 79.3b indicates a significant negative trend in concentrations of total nitrate. However, the trend is considerably lower than that for sulphate concentrations with the largest decrease of $-3$ % year$^{-1}$ over the Po Valley.

# Chapter 80
# Application and Evaluation of High-Resolution WRF-CMAQ with Simple Urban Parameterization

**Jonathan Pleim, Robert Gilliam, Wyat Appel, James Godowitch, David Wong, George Pouliot, and Limei Ran**

**Abstract** The 2-way coupled WRF-CMAQ meteorology and air quality modeling system is evaluated for high-resolution applications by comparing to a regional air quality field study (DISCOVER-AQ). The model was modified to better account for the effects of urban environments. High-resolution spatial data for fractions of impervious surfaces and tree canopy from the National Land-Cover Database (NLCD) were processed for each grid and used to scale ground heat capacity and to constrain vegetation coverage and characteristics. These simple algorithms along with modified albedo and roughness length in urban areas result in improved simulation of urban heat island and urban boundary layers. The reduced nocturnal stability and enhanced vertical mixing lead to reduced temperature and humidity biases and reduced under-predictions of ozone concentrations in urban areas.

## 80.1 Introduction

A new modeling system for coupled meteorology and air quality composed of the Weather Research and Forecast (WRF) model [1] and the Community Multiscale Air Quality (CMAQ) model [2] has been recently developed and evaluated for regional and mesoscale applications [3]. The 2-way coupled WRF-CMAQ model has several advantages over traditional sequential meteorology and air quality modeling systems including more frequent data transfer of meteorological information (e.g. winds, temperature, and humidity) to the chemical transport model.

J. Pleim (✉) • R. Gilliam • W. Appel • J. Godowitch • D. Wong • G. Pouliot
Atmospheric Modeling and Analysis Division, U.S. EPA, Research Triangle Park, NC 27711, USA
e-mail: pleim.jon@epa.gov

L. Ran
Institute for the Environment, University of North Carolina at Chapel Hill, Chapel Hill, NC 27599, USA

D. Steyn and R. Mathur (eds.), *Air Pollution Modeling and its Application XXIII*, Springer Proceedings in Complexity, DOI 10.1007/978-3-319-04379-1_80,

As model grid resolution increases, the frequency of data transfer should also increase such that meteorological input is updated more frequently than the typical hourly interval. Another advantage of 2-way coupled systems is the possibility of feedback of chemical information to the meteorological processes that can be affected by gaseous or aerosol species. Currently, direct feedback effects of aerosols on shortwave and long wave radiation is implemented in the WRF-CMAQ system while an experimental implementation of effects of aerosols on CCN activation and cloud microphysics is being evaluated.

## 80.2 Urban Parametrization

Meteorological and air quality modeling at high-resolutions in urban areas requires consideration of the specific characteristics of urban environments that affect surface energy and moisture budgets, dynamic wind drag, and mechanical turbulence generation. In recent years, urban surface models with three levels of complexity have been added to WRF [4]: a bulk surface scheme, a single-layer model, and a multi-layer model, all of which are coupled to the Noah Land Surface Model (LSM). However, since the coupled WRF-CMAQ system relies on the Pleim-Xiu LSM (PX LSM) [5] for meteorological surface fluxes as well as chemical air-surface exchange (i.e. dry deposition and bi-directional flux) simple urban parameterizations have been added to the PX LSM that leverage the very high resolution (30 m) impervious surface fraction data that are available as part of the National Land Cover Database (NLCD, http://www.mrlc.gov/nlcd06_data.php) to scale surface heat capacity. In addition, albedo and roughness length for the four NLCD urban related land use categories have been revised to better represent developed areas. The NLCD tree canopy coverage data is also used to better account for the effects of urban trees on evapotranspiration and latent heat flux.

## 80.3 Comparison to Field Studies

A persistent problem in air quality modeling of urban areas is the over-prediction of surface emitted pollutants, such as CO, $NO_X$ and primary PM, and under-prediction of $O_3$ during the morning and evening hours. The precise cause of these persistent errors is not known but a prime suspect is an under-prediction of turbulent mixing in the PBL during these transitional times. The neglect of urban surface effects may contribute to these problems since the urban heat island tends to destabilize the lower boundary layer at night and delay the evening transition to downward sensible heat flux. In addition, urban structures induce mechanical turbulence on wind flow through the building canopy.

The simple urban parameterization for the PX LSM, outlined above, is tested for the DISCOVER-AQ field study in July 2011 by running Base and Urban versions

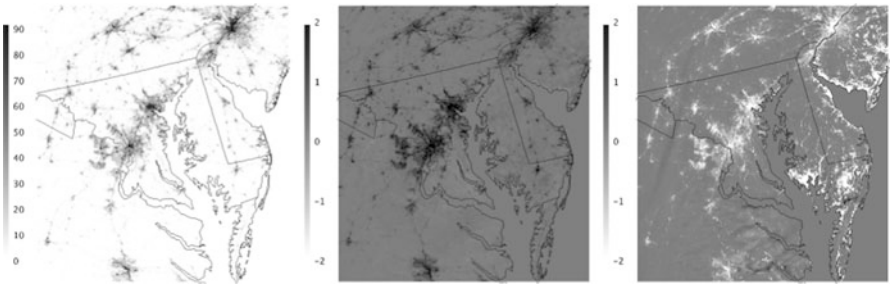


**Fig. 80.1** Impervious surface fraction (*left*), skin temperature difference (Urban – Base) at July 2, 0600 LT (*center*), and July 2, 1100 LT (*right*)

of WRF-CMAQ on 4 and 1 km horizontal resolution grids over the Mid-Atlantic region. Figure 80.1 shows the percentage of impervious surface for every grid cell in the 1 km grid resolution model domain as well as the effects of the urban scheme compared to the base case on skin temperature at two times on July 2, 2011. In urban areas with high fractions of impervious surfaces, the skin temperature is warmer at 6 am LT in the Urban run because of slower nighttime cooling due to greater heat capacity, while the Urban run is cooler at 11 am LT because of slower late morning heating.

The urban modifications reduce average 2-m temperature and mixing ratio biases in and around the urban areas (not shown). Consequently, average hourly ozone mixing ratios are higher in the Urban run, mainly in the evening and overnight, because of the deeper and less stable nocturnal boundary layers in the Urban run that better simulates the Urban Heat Island (UHI) effects (Fig. 80.2, top). Figure 80.2 (bottom) also demonstrates that the higher ozone mixing ratios are in better agreement with observations since average bias is reduced for the Urban run in the urban areas.

## 80.4 Conclusions

A new simple bulk urban parameterization that leverages the highly accurate, high resolution impervious fraction and tree canopy fraction data that are available in the NLCD has been implemented in the PX LSM in the 2-way coupled WRF-CMAQ model system. Model comparisons and evaluation for the DISCOVER-AQ field study show that the Urban scheme improves representation of the UHI effects that lead to reduced biases of 2 m temperature and mixing ratio as well as ozone mixing ratios in urban areas. The effects of the Urban scheme on air quality are most pronounced in the evening when the transition to a stable regime is delayed relative to the Base run resulting in reduced over-predictions of $NO_x$ and reduced under-predictions of $O_3$.

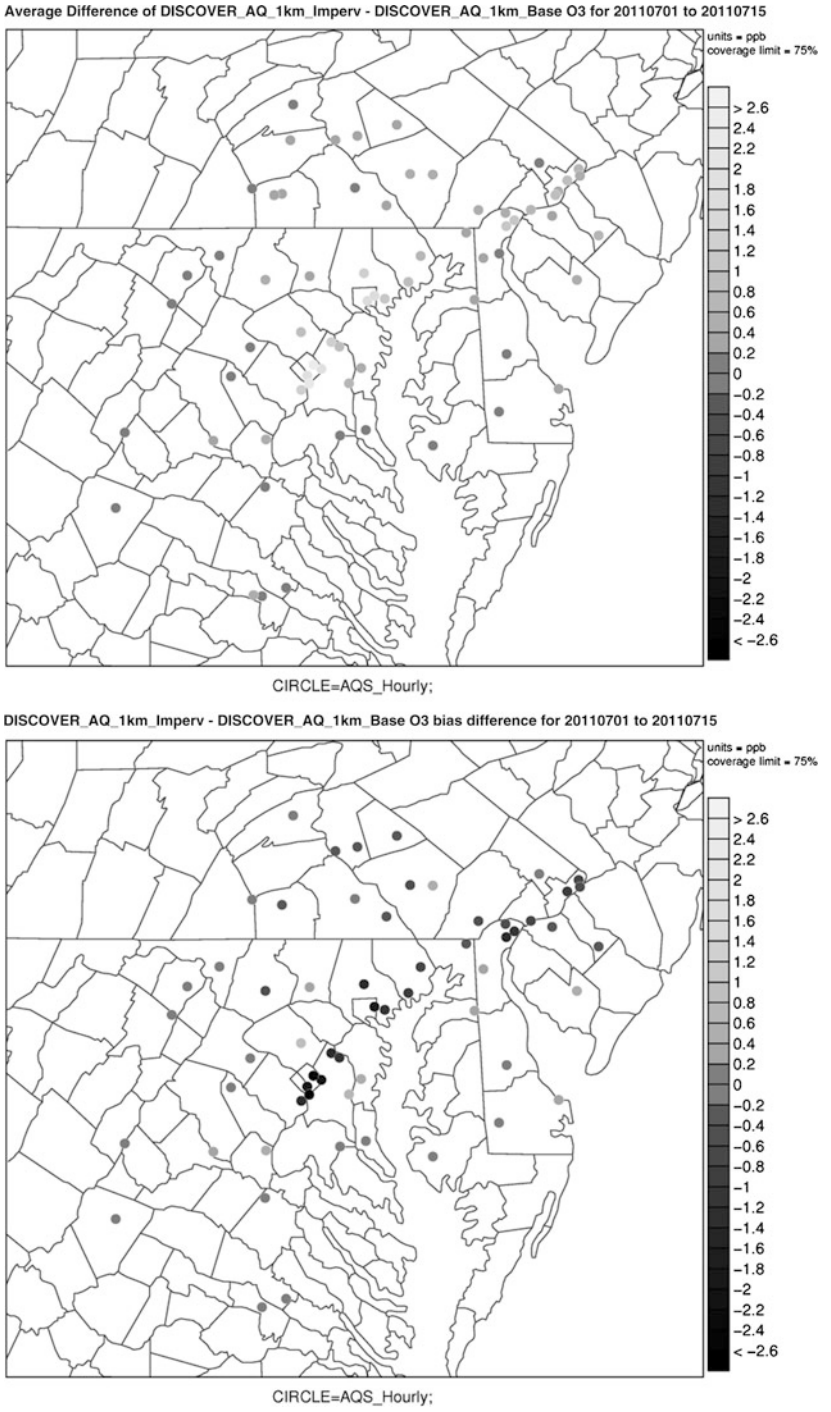


**Fig. 80.2** Hourly ozone difference (Urban – Base) (*top*) and difference in hourly bias (Urban – Base) (*bottom*) averaged over July 1–16, 2011

## References

1. Skamarock WC, Klemp JB, Dudhia J, Gill DO, Barker DM, Duda MG, Huang X-Y, Wang W, Powers JG (2008) A description of the advanced research WRF Version 3, NCAR tech note NCAR/TN 475 STR, 125 pp. Available from: UCAR Communications, P.O. Box 3000, Boulder, CO 80307
2. Byun D, Schere KL (2006) Review of the governing equations, computational algorithms, and other components of the models-3 community multiscale air quality (CMAQ) modeling system. Appl Mech Rev 59:51–77
3. Wong DC, Pleim J, Mathur R, Binkowski F, Otte T, Gilliam R, Pouliot G, Xiu A, Young JO, Kang D (2012) WRF-CMAQ two-way coupled system with aerosol feedback: software development and preliminary results. Geosci Model Dev 5:299–312. doi:10.5194/gmd-5-299-2012
4. Chen F, Miao S, Tewari M, Bao J-W, Kusaka H (2011) A numerical study of interactions between surface forcing and sea breeze circulations and their effects on stagnation in the greater Houston area. J Geophys Res 116:D12105. doi:10.1029/2010JD015533
5. Pleim JE, Xiu A (1995) Development and testing of a surface flux and planetary boundary layer model for application in mesoscale models. J Appl Meteorol 34:16–32

## Questions and Answers

**Questioner name:** Steve Hanna

**Q:** Why did you not want to use the WRF-Urban model developed by Fei Chen and colleagues at NCAR?

**A:** The main reason is that the current WRF-Urban options are tied to the Noah land surface model (LSM) and the TKE PBL schemes. We have been developing and using the Pleim-Xiu LSM and the ACM2 non-local closure PBL scheme, neither of which can be used with the Urban options. We not only use these schemes in WRF but also in the air quality part of the system (CMAQ) for PBL mixing, dry deposition, and bi-directional surface fluxes. We are not certain that the simple urban modifications described here are sufficient and plan to continue development and evaluation including inter-comparison with the WRF-Urban models.

**Questioner name:** Douw Steyn

**Q:** Why iterate only once?

**A:** This question refers to the new iterative technique for data assimilation in the soil temperature and moisture for high-resolution (1–4 km) modeling which was discussed in the presentation but could not be included in this extended abstract due to page limitations. We have tried 2 iterations but saw only minor reductions in error. Thus, in the trade-off between accuracy and run time we don't feel that multiple iterations are worthwhile. However, we will do more testing.

# Chapter 81
# A One Year Evaluation of the CTM CHIMERE Using SURFEX/TEB Within the High Resolution NWP Models ALARO and ALADIN for Belgium

**Andy Delcloo, Rafiq Hamdi, Alex Deckmyn, Hugo De Backer, Gilles Forêt, Piet Termonia, and Herman Van Langenhove**

**Abstract** At the Royal Meteorological Institute of Belgium the chemical transport model (CTM) CHIMERE runs at a spatial resolution of $7 \times 7$ km on a domain, covering Belgium and The Netherlands ($680 \times 680$ km). The CTM is first run on a coarse resolution of 50 km covering Western Europe, using the meteorological fields of ECMWF. The emission database is provided by EMEP. The output of this model run is used as input for the boundary conditions for the coupled high resolution chemical transport model run.

From previous studies, it has been shown that this one-way nested coupling with the limited area NWP models ALADIN and ALARO ($7 \times 7$ km) already improved significantly the modelling of ozone concentrations by improving the physical parameterization, i.e. cloud cover, surface temperature, surface sensible heat flux, surface latent heat flux and relative humidity fields. The emission database used as input for this high resolution model is the TNO/GEMS emission database. In this study, we will also investigate the influence on the modelling of particulate matter when the CTM is coupled to these different high resolution NWP-configurations. We will investigate the air quality model forecast performance for a three day

A. Delcloo (✉) • R. Hamdi • A. Deckmyn • H. De Backer • P. Termonia
Royal Meteorological Institute of Belgium, Brussels, Belgium
e-mail: Andy.Delcloo@meteo.be; Rafiq.Hamdi@meteo.be; Alex.Deckmyn@meteo.be; Hugo.DeBacker@meteo.be; Piet.Termonia@meteo.be

G. Forêt
LaboratoireInteruniversitaire des SystèmesAtmosphériques,
NRS/INSU/IPSL/UPEC/Université, P7, Créteil, France
e-mail: Gilles.Foret@lmd.polytechnique.fr

H. Van Langenhove
Research Group EnVOC, Department of Sustainable Organic Chemistry and Technology,
Faculty of Bioscience Engineering, Ghent University, Ghent, Belgium
e-mail: Herman.Vanlangenhove@ugent.be

D. Steyn and R. Mathur (eds.), *Air Pollution Modeling and its Application XXIII*,
Springer Proceedings in Complexity, DOI 10.1007/978-3-319-04379-1_81,

lead time on a daily basis, covering a one year time period (2008), implementing inline a new land surface scheme (SURFEX) – with and without taking into account The Town Energy Balance (TEB) – on the modelled ozone- and particulate matter concentrations.

## 81.1 Introduction

The chemical transport model CHIMERE [4] has been coupled to the IFS/ECMWF at a coarse resolution of $50 \times 50$ km. The CHIMERE model is able to catch most of the day-to-day variability when verified against observations for Belgium at this coarse resolution, especially for the modelling of ozone concentrations.

Running CHIMERE on this coarse resolution, using a large domain (Europe) helps us understand the contribution of synoptic weather phenomena to pollution events. However, to study the ability of a CTM to capture the day-to-day variability on a local scale, it is necessary to feed the model with high-resolution meteorological data from a NWP-model. The NWP-models we use for our analysis run four times a day in an operational context at our institute; the ALADIN model and its updated version ALARO receive their boundary conditions from ALADIN France, run by Météo France.

Also the performance of the use of the Town Energy Balance (TEB, [3]) single-layer module within the ALARO and ALADIN NWP models in an operational configuration will be verified using the SURFEX module online for a 1 year period. SURFEX is a new externalized (i.e. it can run independently from the ALADIN model) land surface scheme that has recently been coupled with the ALARO version [2]. SURFEX contains four modules, describing the exchanges of water, momentum, and energy on four tiles of surface: sea, lake, vegetation, and urban area. The vegetation tile is considered as a composition of various sub-homogenous entities called patches (forest, meadows, fields . . . ). The emission database used as input for this high resolution model is the TNO/GEMS emission database [5].

## 81.2 Results and Discussion

To validate our results, observational data (PM10 and $O_3$) are used from IRCELINE. Four different versions of our NWP-model are verified: ALADIN and ALARO, applying the SURFEX scheme, further referred as ALD-SFX and ALR-SFX. When the option TEB is activated, the simulations are referred as ALD-SFX-TEB and ALR-SFX-TEB.

The improved physical parameterization scheme of ALARO leads to an improved precipitation-, temperature- and cloud field [1]. A qualitative and quantitative evaluation is made between the one-way nested couplings of CHIMERE with the four different LAM's. Table 81.1 gives an overview of some

**Table 81.1** Correlation, RMSE ($\mu g/m^3$) and bias ($\mu g/m^3$) for the time period 01/01/2008 – 31/12/2008 are shown for some stations for the scenarios ALD-SFX, ALD-SFX-TEB, ALR-SFX, ALR-SFX-TEB for the analysis (D-1)

| | | Dessel | Houtem | Moer-kerke | Destel-bergen | Ukkel | Hasselt |
|---|---|---|---|---|---|---|---|
| | Corr | 0.60 | 0.75 | 0.66 | 0.72 | 0.70 | 0.67 |
| ALD-SFX | Rmse | 10.23 | 9.82 | 12.30 | 11.46 | 12.30 | 10.46 |
| | Bias | 1.98 | −3.89 | −5.76 | −1.90 | 7.17 | 0.07 |
| | Corr | 0.62 | 0.76 | 0.68 | 0.75 | 0.73 | 0.68 |
| ALD-SFX-TEB | Rmse | 9.76 | 9.84 | 12.22 | 11.33 | 10.06 | 10.29 |
| | Bias | 1.17 | −4.33 | −6.17 | −3.30 | 4.55 | −1.01 |
| | Corr | 0.61 | 0.76 | 0.68 | 0.72 | 0.70 | 0.68 |
| ALR-SFX | Rmse | 12.07 | 9.72 | 11.90 | 12.02 | 15.86 | 11.77 |
| | Bias | 5.48 | −1.80 | −4.02 | 0.89 | 10.94 | 3.38 |
| | Corr | 0.62 | 0.77 | 0.70 | 0.75 | 0.74 | 0.68 |
| ALR-SFX-TEB | Rmse | 11.18 | 9.61 | 11.74 | 11.47 | 11.77 | 11.26 |
| | Bias | 4.19 | −2.47 | −4.74 | −1.20 | 7.02 | 1.74 |

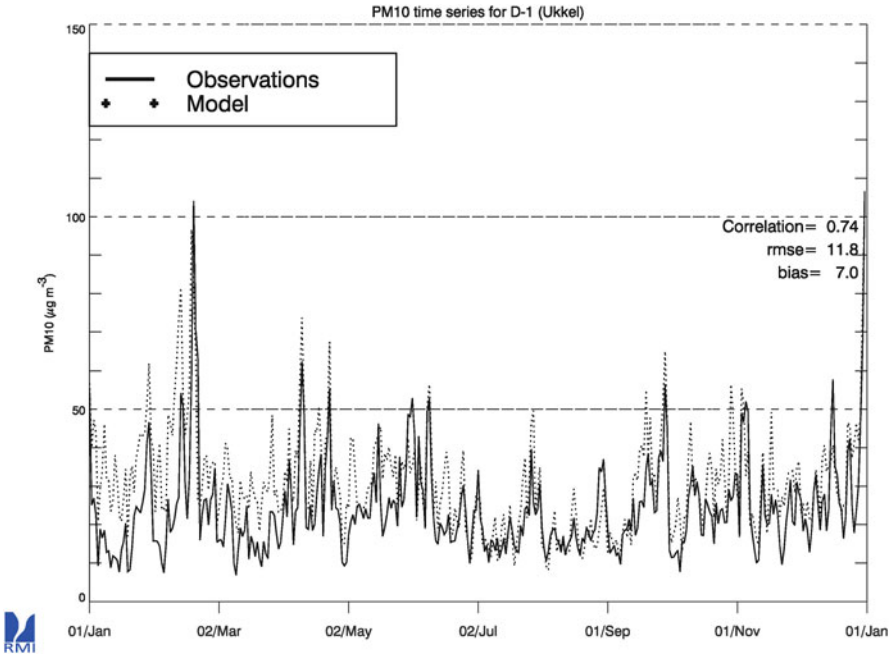


**Fig. 81.1** Time series of observed- and modelled averaged daily particulate matter (PM10) concentrations for the time period 01/01/2008–31/12/2008 for the station of Ukkel (D-1)

general statistics on the modelling of averaged PM10 concentrations for the year 2008 for some specific observation stations and different scenarios. Figure 81.1 shows a time series of modelled- against observed averaged PM10 stations for the station of Ukkel, applying the ALARO-SFX-TEB scenario.

Table 81.1 shows that the updated versions, using TEB reduces the bias in the sub-urban station of Ukkel considerably and improves the modeling of the day-to-day variability of particulate matter. In general, the correlation and RMSE values are better using SURFEX with TEB. During the winter period, there is a more pronounced overestimation of PM10 in the sub-urban station of Ukkel (Fig. 81.1), while for the rural stations an underestimation of particulate matter by the model can be shown during summer time.

For a 2 day lead time, the correlation decreases towards values between 0.59 and 0.71. RMSE and bias obtained from these forecasts are of the same order of magnitude as the values obtained from Table 81.1.

## 81.3 Conclusions

When the CTM was coupled to the updated ALADIN/ALARO NWP-models, using the SURFEX and the TEB scheme, statistics significantly improved for the modelling of particulate matter (PM10) when compared with the results obtained by not using the TEB scheme.

During the winter period, there is a more pronounced overestimation of PM10 in the sub-urban stations present, while for the rural stations, an underestimation of PM10 by the models is more pronounced during summer time.

**Acknowledgments** The authors would like to thank IRCELINE for providing the ozone and PM10 data.

## References

1. Delcloo AW, Deckmyn A, Hamdi R, Van Langenhove H, Foret G, De Backer (2012) Coupling of the CTM CHIMERE to the high resolution LAM ALADIN for Belgium, air pollution modeling and its application XXI, NATO Science tor Peace and Security Series C: Environmental Security, vol 4, Part 2: 315–319. doi:10.1007/978-94-007 -1359-8_54
2. Hamdi R, Degrauwe D, Termonia P (2012) Coupling the Town Energy Balance (TEB) scheme to an operational limited area NWP model: evaluation for a highly urbanized area, Belgium. Weather Forecast 27(2):323–344
3. Masson V (2000) A physically based scheme for the urban energy budget in atmospheric models. Bound Layer Meteorol 94:357–397
4. Vautard R, Beekmann M, Roux J, Gombert D (2001) Validation of a deterministic forecasting system for the ozone concentrations over the Paris area. Atmos Environ 35:2449–2461
5. Visschedijk AJH, Zandveld PYJ, Denier van der Gon HACA (2007) High resolution gridded European database for the EU Integrate Project GEMS, TNO-report 2007-A-R0233/B

# Chapter 82
# Application of Performance Indicators Based on Observation Uncertainty to Evaluate a Europe-Wide Model Simulation at Urban Scale

**Philippe Thunis, Bertrand Bessagnet, Etienne Terrenoire, and Augustin Colette**

**Abstract** In the frame of the European Consortium for Modeling of Air Pollution and Climate Strategies (EC4MACS) the CHIMERE chemistry transport model has been run over Europe for the entire year 2009 with a spatial resolution of 7 km with the aim of assessing the urban impact on daily exceedances of PM and NO2 in European cities. In order to better capture these urban impacts, improvements on urban scale meteorology, vertical resolution and emissions have been implemented. In the current work an evaluation of the model results against the AIRBASE European monitoring network measurements is done using model performance indicators (MPC) based on observation uncertainty.

The MPC used in this approach, constructed on the hypothesis that model results are allowed the same margin of uncertainty as measurements, are developed for four statistical indicators (Root Mean Square Error, Normalized Mean Bias, Normalized Mean Standard Deviation and temporal correlation) to summarize the model-observation errors in terms of phase, amplitude and bias. The utility of this approach is to provide a performance scale to inform the user on the expected value an indicator should reach for a particular modeling application. These indicators are then used to identify the strengths and weaknesses of the model application in terms of geographical areas, cities, pollutants and/or period of the year.

P. Thunis (✉)
European Commission, JRC, Institute for Environment and Sustainability, Air and Climate Unit, Via E. Fermi 2749, 21027 Ispra, VA, Italy
e-mail: philippe.thunis@jrc.ec.europa.eu

B. Bessagnet • E. Terrenoire • A. Colette
Institut National de l'Environnement Industriel et des Risques, INERIS, 60550 Verneuil en Halatte, France
e-mail: bertrand.bessagnet@ineris.fr; etienne.terrenoire@ineris.fr; augustin.colette@ineris.fr

D. Steyn and R. Mathur (eds.), *Air Pollution Modeling and its Application XXIII*, Springer Proceedings in Complexity, DOI 10.1007/978-3-319-04379-1_82,

## 82.1 Introduction

As Chemistry-Transport Models (CTMs) were initially designed to simulate ozone concentrations within the lower troposphere, a coarse horizontal resolution was sufficient to reach this objective. But during the last decade, air quality legislation has focussed more and more on particulate matter (PM) and CTMs were required to refine their resolution to capture the urban signals as high PM concentrations usually occur in urban areas. In this work a fine resolution ($0.0625 \times 0.125°$ i.e. about 7 km) simulation is performed over Europe for the meteorological year 2009 with the CHIMERE CTM [1]. For the evaluation model performance indicators based on the observation uncertainty [2] are used to identify the main strengths and weaknesses of the CHIMERE application in terms of geographical area, pollutant and period of the year. Results are presented here for NO2 and PM10 based on a comparison with the AIRBASE monitoring network measurements.

## 82.2 Methodology

The offline Chemistry Transport Model CHIMERE model is fed with ECMWF meteorological fields. Despite their relatively coarse horizontal resolution (16 km) this meteorological input dataset has been preferred to the higher resolution WRF fields since the latter tends to overestimate significantly the magnitude of the wind fields [3]. Anthropogenic emission fields were derived using a top-down approach over the entire domain extending from 10°W to 30°E in longitude and from 36°N to 62°N in latitude. Boundary conditions were obtained from the monthly mean LMDz-INCA climatology for gaseous species and from the GOCART model for aerosols. Biogenic species are calculated using the MEGAN model while wildfire emissions are issued from GFED3. Some important modifications were made to the code itself and to the input dataset:

- The relatively coarse resolution of the ECMWF meteorological fields prevents a good representation of the urban effects. Based on literature overview wind fields intensities in urban centres have arbitrarily been decreased by a factor two. Similarly the turbulent diffusion coefficients have been decreased within the urban canopy by a factor 2.
- Based on a comparison between bottom-up and top-down approaches on one hand and on expert judgments on the other, anthropogenic emissions in some Eastern country regions have been increased significantly to reflect the larger effective residential heating emissions in these regions.
- In addition new temporal profiles for residential emissions based on a "degree-days" concept have been generated to account for the fact that emissions related to heating would increase during the colder winter days (same total emissions distributed according to temperature).

The evaluation of the model performances is based on a comparison with the AIRBASE monitoring stations which are classified in terms of urban, suburban and rural background. The evaluation is performed by grouping stations around a series of cities (30 city areas). For each of these 30 cities the monitoring stations within a circle of radius 200 km are used for the evaluation. In total about 650 stations are used both for PM10 and NO2.

The evaluation itself is based on performance indicators normalised by the observation uncertainty [2]. The main performance indicator is constructed as the ratio between the model to observed root mean square error and a function of the observation uncertainty. As discussed in Thunis et al. [2], values of this ratio between 0 and 0.5 indicate that, on average, differences between model results and measurements are within the range of their associated uncertainties. Conversely, values larger than 1 indicate statistically significant differences between model and measured values. Based on measurement inter-comparison exercises measurement uncertainties values for NO2 and PM10 are provided [4]. As observation uncertainties generally exhibit much larger relative uncertainties at low concentration levels the required on model performance within the range of concentrations becomes less stringent. In this way the less certain the measurements are the less stringent the model performances requested should be.

For visualization of this indicator the target diagram proposed by [5] has been modified by normalizing all quantities by the observation uncertainty (Fig. 82.1, top and bottom rows). The X and Y axis of the diagram represent the observation normalized centered root mean square error (CRMSE) and bias (BIAS), respectively. The distance from the origin then represents the observation uncertainty normalized root mean square error (RMSE). The green area circle identifies the fulfillment of the performance criteria while the dashed green area represents the zone for which model results are within the observation uncertainty range. The negative and positive sides of the X axis are used to identify observed-model differences which are dominated by amplitude (standard deviation) or phase (correlation), respectively. The negative and positive sides of the Y axis identify negative and positive biases, respectively.

## 82.3 Results

Figure 82.1 provides an overview of the results for PM10 (right) and NO2 (left) where results have been averaged by city areas (each circle represents a city area) and where all station types (urban, suburban and rural) have been included in the analysis. The PM10 target diagram points out an underestimation of the observed levels, especially in Eastern country cities (Prague, Warsaw, Sofia and Krakow) with an error dominated by a lack of amplitude. Despite the increase of domestic emissions in these countries and the new temporal profiles based on degree days, the amplitude of the signal is yet underestimated. For many of the Mediterranean

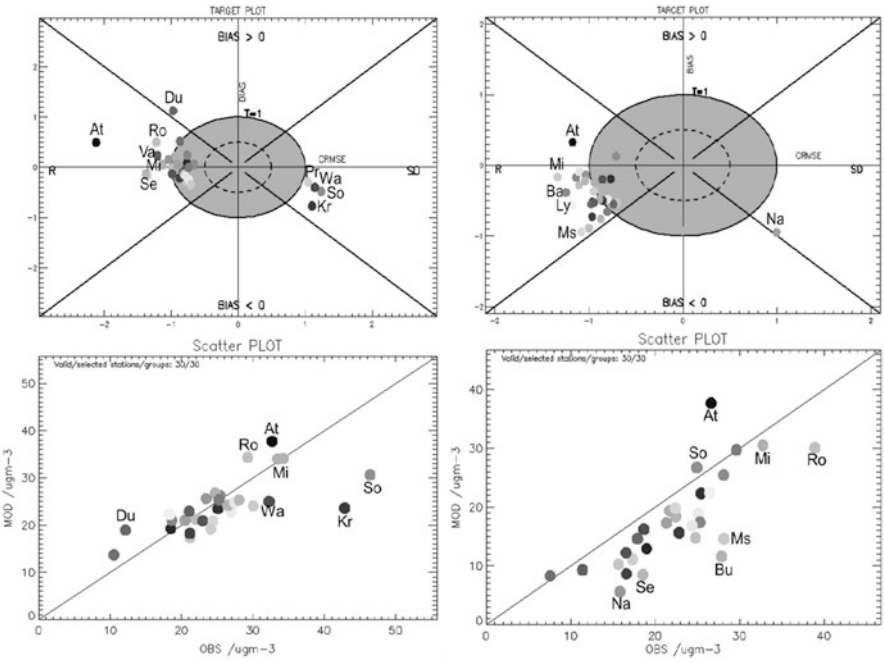


**Fig. 82.1** PM10 – all station types (*left*) and NO2 – urban background stations (*right*) model-observed evaluation. Target diagrams (*top*) and scatter plots (*bottom*) provide information for statistics averaged by city areas. For the Target diagrams, stations statistics are sorted and the 10 % worst ones are eliminated. The *circle* on the plot represents the worst remaining statistic. Acronyms are: Du (Dublin), Ro (Rome), Va (Valencia), At (Athens), Mi (Milan), Wa (Warsaw), Kr (Krakow), So (Sofia), Na (Napoli), Ms (Marseille), Se (Sevilla), Pr (Prague). For more information on target diagrams, refer to text

cities (e.g. Rome, Valencia, Milan, Sevilla, Athens) the model results show a lack of temporal correlation which might be caused by to the difficulty to adequately capture the local scale effects (e.g. sea-breezes) with the 16 km meteorology. The scatter plot (bottom) provides some information on the absolute concentrations and confirms the Eastern Europe underestimation while other city areas do not show significant biases.

For NO2 model concentrations exhibit a significant underestimation at almost all cities. According to the Target diagram, the error is dominated by a lack of temporal correlation. The general underestimation could be explained by the fact that NOx emissions generally occur at street level, scale which cannot be sufficiently captured with the current spatial resolution. The lack of temporal correlation might be due to a lack of sufficiently accurate temporal emission profiles for the NOx traffic emissions, as these are emissions that are directly linked to the observed NO2 concentrations.

## 82.4 Conclusion

CTMs are currently able to simulate air quality over large domains with a refined resolution. This allows assessing model performances with respect to PM10 and NO2 in urban areas in different geographical areas in the frame of a single simulation. In this work the CHIMERE CTM has been run over the entire European territory with a spatial resolution of about 7 km. To better capture urban scale effects some improvements have been made to the model itself (e.g. urban sub-scale paramerisations) but also to some input datasets (e.g. emissions). Model performances have been evaluated around 30 European city areas against the AIRBASE measurements. To perform this evaluation model performance criteria based on observation uncertainty have been used.

Despite corrections made to the PM anthropogenic emissions in some eastern country areas (increase of overall emitted totals, degree days corrections) CHIMERE still underestimates the observed concentration levels. Although the timing of the peaks is quite well reproduced the peaks amplitude is underestimated. Problems also arise from some Mediterranean areas where the model faces difficulties in reproducing the temporal variations of the concentrations. For NO2 the concentration levels are generally underestimated and show a lack of temporal correlation probably due to a lack of sufficiently accurate temporal emission profiles for the NOx traffic emissions.

The proposed evaluation methodology has proved its usefulness to screen model performances. The same methodology can then be used to check the model behaviour in more details (seasonal variations, station details). Further work will also be done to relate model performances in terms of meteorological and air quality fields.

## References

1. Bessagnet B, Menut L, Curci G, Hodzic A, Guillaume B, Liousse C, Moukhtar S, Pun B, Seigneur C, Schulz M (2009) Regional modeling of carbonaceous aerosols over Europe – focus on secondary organic aerosols. J Atmos Chem 61:175–202
2. Thunis P, Pederzoli A, Pernigotti D (2012) Performance criteria to evaluate air quality modeling applications. Atmos Environ 59:476–482
3. Miglietta M, Thunis P, Georgieva E, Pederzoli A, Bessagnet B, TErrenoire E, Colette A (2012) Evaluation of WRF model performance in different European regions with the DELTA-FAIRMODE evaluation tool. Int J Environ Pollut 50(1/2/3/4):83–97
4. Pernigotti D, Thunis P, Gerboles M, Belis C (2013) Model quality objectives based on measurement uncertainty. Part II: NO2 and PM10. Atmos Environ 79:869–878
5. Jolliff JK, Kindle JC, Shulman I, Penta B, Friedrichs MAM, Helber R, Arnone RA (2009) Summary diagrams for coupled hydrodynamic-ecosystem model skill assessment. J Mar Syst 76:64e82

## Questions and Answers

Q: What is the reason for selecting a 200 km radius around the cities?

A: Two different radiuses around cities have been considered in this work: the first one of 30 km corresponding approximately to the area covered by a $50 \times 50$ km regional scale model grid cell. But to capture rural background stations away from the city centers, a second radius of 200 km, selected arbitrarily has been used.

Q: Do the newly introduced performance indicators imply that we assume Gaussian distributions of measurements errors, model errors, differences?

A: Yes. From an experimental point of view this assumption is quite reasonable. From a modeling point of view, this is more difficult to assess but the central limit theorem can be used to justify this assumption. In fact, any variable Y that is a combination of Xi (even without normal distributions) can be approximated by a normal distribution because of the Central Limit Theorem provided that the Xi are independent and that the variance of Y is much larger than the variance of any single component from a non-normally distributed Xi. Therefore, it can be assumed that the distribution of individual observations and modeled values is approximately normal.

Q: Your measurement uncertainty is based on measurement error, estimated by the variability of measurements from co-located instruments. Have you considered the issue of spatial representativeness of your monitoring sites. In many cases we would expect the point measurements to be more reliable than a volume average which is what the model predicts. In this case you may have created a performance criteria that is unrealistically strict in terms of identifying "good" or "acceptable" model performance.

A: It is indeed important to consider spatial representativeness and the presented approach could include these impacts whenever realistic estimates for this spatial representativeness are available (work in progress). The performance criteria are not however unrealistically stringent as they are based on an estimate based on the maximum observation uncertainty. The resulting performance criteria in terms of bias and/or correlation are also very close to those proposed in other studies. One possible evolution will be to substitute the maximum by an average measurement uncertainty together with an estimate of the spatial representativeness so that the performance criteria become more station specific.

# Chapter 83
# Multi-model Ensembles: How Many Models Do We Need?

**Efisio Solazzo and Stefano Galmarini**

**Abstract** We explicitly address the fundamental issue of member diversity in multi-model ensembles. Common biases and redundancy are the two issues directly deriving from lack of independence, undermining the significance of a multi-model ensemble, and are the subject of this study. These two issues are analysed in detail using the AQMEII ensemble of AQ model results for four air pollutants in two European regions. We show that models share large portions of bias and variance, extending well beyond those induced by common inputs. We propose and discuss methods of member selection and rate the ensemble performance they produce. We conclude that, although independence of outputs may not always guarantee enhancement of scores (but this depends upon the skill being investigated) we discourage selecting the members of the ensemble simply on the basis of scores, that is, independence and skills need to be considered in separation.

## 83.1 Introduction

The last two decades have witnessed the rise of multi-model-result consultation, often referred to as multi-model (MM) ensemble analysis, in several geophysical modelling contexts. The fundamental advantage of MM ensemble versus single model realizations is the error of the convex-combined MM ensemble guaranteed to be less than the average error of the individuals. This result tells that in a context were we have no criteria for identifying the best members (in forecasting applications, for example), the ensemble mean is possibly the best option as it is better, on average, than any method selecting individual members randomly. It cannot be excluded however that there are individual models outperforming the

E. Solazzo • S. Galmarini (✉)
European Commission, Joint Research Centre, Institute for Environment and Sustainability, Ispra, Italy
e-mail: stefano.galmarini@jrc.ec.europa.eu

D. Steyn and R. Mathur (eds.), *Air Pollution Modeling and its Application XXIII*, Springer Proceedings in Complexity, DOI 10.1007/978-3-319-04379-1_83,

ensemble mean or the existence of subset of members whose mean has lower error than the full ensemble mean. The main strengths of the MM ensemble approach over single model realization are: (a) mutual cancelation of errors and enhancement of skill scores; (b) sampling wider range of uncertainty, and (c) confidence boost when many models agree.

An assumption often given for granted is that different models produce independent results, i.e. that all models are characterized by independent error components. *Independence* of models is rigorously defined as the property of the combined error probability distribution function (PDF) of any two models to be expressed in terms of each individual error PDF. The requirement of error independence is seldom achieved in MM ensemble practice and is difficult to prove. Models sharing large commonalities in the internal modules and/or inputs (meteorology, emission, boundary conditions) are bound to share the biases introduced by these commonalities. The net result are *(i)* an ensemble biased towards the artificious consensus determined by the shared bias, and *(ii)* a reduced degree of variability, leading to overconfident ensembles. For these reasons in this paper we analyse various techniques available to address the following issues:

1. Determine the ensemble redundancy: i.e. the minimum set of members that explains the variance of the observations and maximise the accuracy;
2. Reduce the ensemble redundancy. If many redundant models are combined together, there would be loss of valuable information due to dependant biases.

For our analysis we investigate the correlation between errors produced by air quality (AQ) models run by twelve groups in the context of the Air Quality Modeling Evaluation International Initiative (AQMEII) [1]. We use hourly time series for the months of June July August (JJA) of the year 2006 of the gaseous species of $O_3$, CO, $NO_2$, $SO_2$ and apply the analysis to two regions of Europe, one including the UK, France, northern Spain and Belgium and the other including continental Europe (Germany, Poland, Austria, and Czech Republic) (see [2] for detail).

## 83.2 Effective Number of Models

We calculate the number of effective models sufficient to reproduce the variability of the full ensemble (the MM ensemble generated with all available members) as:

$$M_{eff} = \frac{\left(\sum_{k=1}^{N} \lambda_k\right)^2}{\sum_{k=1}^{N} \lambda_k^2} \tag{83.1}$$

with λ eigenvalue of the $corr(d_i,d_j)$ matrix, the matrix of the Pearson linear correlation coefficient between any pair $d_i$, $d_j$ ($i,j = 1,\ldots,N$) ($N$ is the number of available models). $d$ is a metric defined as:

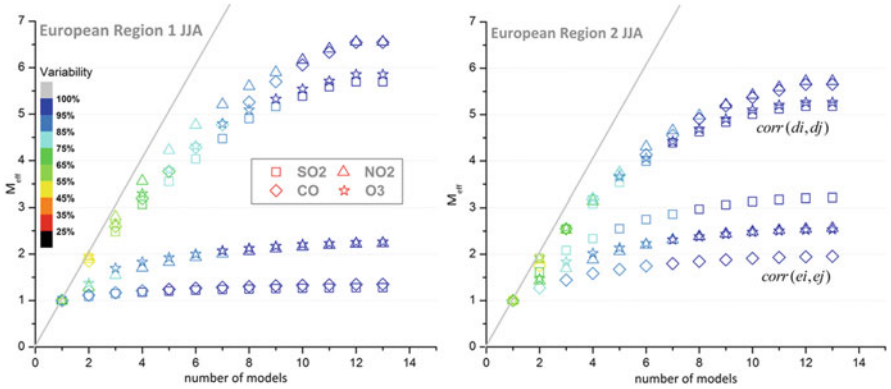


**Fig. 83.1** $M_{eff}$ (from Eq. 83.1) as function of the number of models for EU region 1 and region 2. The two sets of curves have been generated from the corr(*di,dj*) (*top curves*) and the corr (*ei,ej*) (*lower curves*) matrixes

$$\boldsymbol{d}_{\boldsymbol{m}} = \boldsymbol{e}_{\boldsymbol{m}} - R \cdot MME \tag{83.2}$$

where the index $m$ identifies the model, MME is the multi model error (the average over all $e_m$, the individual model's error) and $R$ is the Pearson correlation coefficient between the error of model $m$ and the MME. The removal of MME in Eq. (83.2) makes model errors more dissimilar and uncovers "hidden" trends that are outweighed by overarching commonalities. Indeed the scope of the metric $d_m$ is to establish similarities among models beyond the dominating ones induced by shared inputs and/or common parameterisations.

By applying Eq. (83.1) to the AQMEII datasets of model errors (corr$(d_i,d_j)$) we find that $M_{eff}$ is in the range 5–6.5 out of 13 available models. Figure 83.1 reports $M_{eff}$ as a dependent variable of $N$, the number of models for the four pollutants and the two European regions. The concavity of the curves over $N$ indicates that the addition of more models to the ensemble is not compensated by a linear increase in the overall information. This is a straight consequence of commonalities among members: chances that a new member shares features with an existing one increases as the ensemble size does. This would not happen in the case of independent models.

## 83.3 Reduced MM Ensemble

We apply two methods for optimal selection of members out of the full ensemble. The first is a heuristic method based on the optimisation of skill, while the second is based on minimizing the redundancy among members.

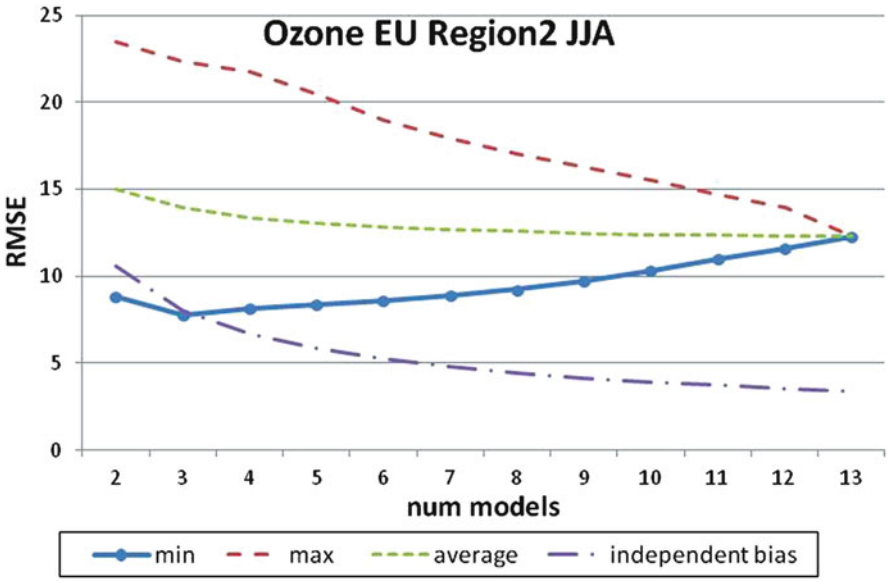


**Fig. 83.2** *Curves* of maximum, mean and minimum RMSE for ozone in EU region 2. The *curves* are obtained by calculating the mean of randomly sampled subsets of models

### *83.3.1 Reduced Ensemble of Optimal Accuracy*

Figure 83.2 shows the curves of maximum, mean and minimum root mean square error (RMSE) for ozone in EU region 2 obtained by calculating the mean of randomly sampled subsets of models. The curve of minimum reveals that exists a subset of three models whose ensemble mean is predicts a RMSE ∼37 % smaller than the full ensemble mean. This is an indication of the deterioration of the skills of the ensemble when more redundant members are combined depending on the fact that the contributions are not independent, model differences are not random and they do not cancel out.

### *83.3.2 Reduced Ensemble of Maximum Diversity*

In this section we explore the associativity among the members of the ensemble and their errors through a clustering analysis with the scope of unveiling and discard overarching commonalities. Detail of the clustering method can be found in Solazzo et al. [2]. A typical output of clustering analysis is a dendrogram, where redundant models are grouped together and the level of similarity among groups is reported based on the distance between the elements of the input matrix. The most

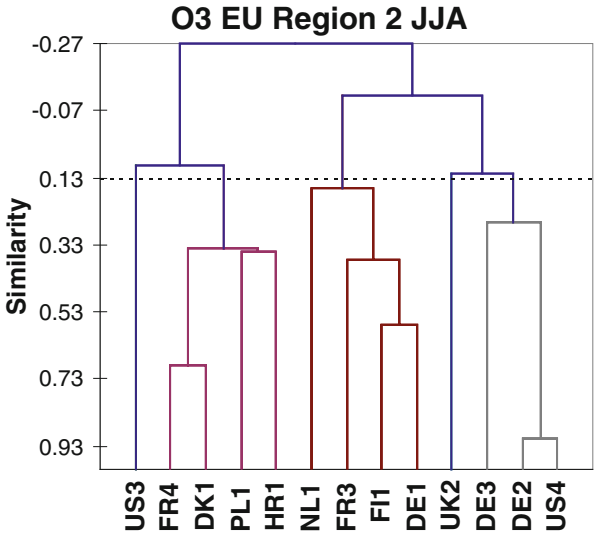


**Fig. 83.3** Hierarchical clustering of *corr(di,dj)*. The *dotted horizontal line* defines the level of similarity

representative model, one for each cluster, is then selected to generate a reduced or ensemble of diverse members. A fundamental challenge of clustering is the high sensitivity to the options controlling the underlying algorithms. In particular, the cut-off (the threshold similarity above which clusters are to be considered disjointed) determines the dimension of the sub-space of non-redundant models and is decided by visual inspection of the dendrogram. The common practice suggests cutting the dendrogram at the height where the distance from the next clustered groups is relatively large, and the retained number of clusters is small compared to the original number of models. Members of the ensemble generated with a higher threshold are more distant and therefore more independent. Looking at the dendrogram for ozone for example (Fig. 83.3), the two main branches at the top further split into two more at a relatively low similarity level, suggesting a plausible way to proceed. At a $\sim$10–15 % similarity level five clusters are detected for all species in both regions.

## 83.4 Conclusion

In this study we explain the risks of combining models sharing high correlated bias into ensembles and apply methods to determine the actual number of models needed to cover the observed variability. Results for the ensemble of AQ models of AQMEII and several species demonstrate that the ensemble is indeed redundant and that there exists subsets of members outscoring the full ensemble. Such subsets have been

identified by maximising the accuracy (minimising the error) and the diversity of the ensemble members via clustering method. Both methods proved successful in determining the size of optimal subsets and in selecting members for creating skilful reduced ensembles.

## References

1. Rao ST, Galmarini S, Puckett S (2011) Air quality model evaluation international initiative (AQMEII). Bull Am Meteorol Soc 92:23–30
2. Solazzo E, Riccio A, Kioutsioukis I, Galmarini S (2013) Pauci ex tanto numero: reducing redundancy in multi-model ensembles. Atmos Chem Phys 13:8315–8333

# Chapter 84
# Diagnostic Evaluation of NOx Emission Upgrade on Air Quality Forecast

**Li Pan, Daniel Tong, Pius Lee, Hyuncheol Kim, Tianfeng Chai, and Charles Ding**

**Abstract** The U. S. National Air Quality Forecasting Capability (NAQFC) provides air quality forecast for the nation by disseminating numerical model predicted surface concentration of O3 and PM2.5 to the public. However, the fidelity of NAQFC is dependent on the accuracies of the emission projection factors employed to estimate the various emissions. This study focuses on comparing variability of surface NOx and O3 concentrations for two emission modeling scenarios for July of 2011: the Base Case and a New Emission Case. The Base Case used the U.S. EPA 2005 National Emission Inventory (NEI2005), its projection procedures adhered to a standard practice used by NAQFC since its inception in 2003. The New Emission Case adopted a scaling procedure based on more recent EPA data demonstrated a significant reduction of the mobile source's share of NOx emission among the major contributors. It reduced from 33.6 % in the Base Case to 25.2 % in the New Emission Case. This is even more significant if one takes into account the large increase in vehicle miles traveled since 2005. The NOx SIP Call had achieved significant reduction of NOx emission from power plants, but still lagged behind that achieved by the reduction in the on-road vehicular (mobile) exhausts. Geographically population change trends in the last decade do not necessarily translates into proportional changes in NOx emission.

L. Pan (✉) • D. Tong • H. Kim • T. Chai
Air Resources Lab., NOAA, NOAA Center for Weather and Climate Prediction, College Park, MD, USA

Cooperative Institute for Climate and Satellite, University of Maryland, College Park, MD, USA
e-mail: Li.Pan@noaa.gov; Daniel.Tong@noaa.gov; Hyun.Kim@noaa.gov; Tianfeng.Chai@noaa.gov

P. Lee • C. Ding
Air Resources Lab., NOAA, NOAA Center for Weather and Climate Prediction, College Park, MD, USA
e-mail: Pius.Lee@noaa.gov; charlesding95@gmail.com

D. Steyn and R. Mathur (eds.), *Air Pollution Modeling and its Application XXIII*, Springer Proceedings in Complexity, DOI 10.1007/978-3-319-04379-1_84,

## 84.1 Introduction

The U. S. National Air Quality Forecasting Capability (NAQFC) is developed and maintained by NOAA to provide numerical guidance for local health and air quality managers across the nation. At present NAQFC is providing gridded 48 h numerical forecast over all 50 states of the country for surface ozone (O3) and atmospheric particulate matter smaller than 2.5 μm in diameter (PM2.5) concentrations, operationally and experimentally respectively [4, 6]. NAQFC employs an off-line coupling of the NOAA National Weather Service Weather Research and Forecasting Non-hydrostatic Mesoscale Model (WRF-NMM) [5] and the U.S. EPA Community Multiscale Air Quality (CMAQ) modeling system [2]. The forecasting performance of NAQFC strongly relies on emission inputs. The emission modeling for future years in NAQFC is basically a tabulation of observed trends of change of emission rates lumped as emission factors organized sector by sector.

Nitrogen oxides (NOx = NO + NO2) is an important precursor to ozone production as well as a potential source contributing to atmospheric aerosol formation. Based on the U. S. EPA 2005 National Emission Inventory (NEI2005), it states that in the U. S. 32 % of NOx emission is from on-road mobile source, 30 % from off-road sources such as ships, aircrafts and locomotives, and 27 % from Electric Generating Unit (EGU) [8], respectively. Although vehicular fuel consumption across the nation has continually gone up; NOx from vehicle emission including on-road and off-road sources has been decreasing since 2007. This is mainly due to the drastic reduction in vehicular NOx emission [1]. NOx emission from power plant has also decreased since the implementation of the so-called "NOx SIP Call" cap and trade program between 2003 and 2008 (http://www.epa.gov/airmarkets/progsregs/nox/sip.html). Consequently, the application of 2005 NOx inventory in NAQFC results in overestimation of NOx emission flux and systematically causes the ozone and PM2.5 forecast biased high most of the time [4].

In this study, we focus on comparing variability of surface NOx and O3 concentrations for two emission scenarios in July of 2011 (Table 84.1): the Base Case and a New Emission Case. Base Case adheres largely to a standard procedure used by NAQFC [7]. The New Emission Case is further discussed in the next section. Model results were verified against the U. S. EPA AIRNow ground-based observations network (http://airnow.gov/). We aim to answering whether or not the new emission scenario captures: (a) observed NOx emission changes; and (b) if (a) is substantiated then would NAQFC forecasts for NOx and O3 be improved by the new emission modeling. These answers imply merits or deficiencies of the new emission projection procedure.

**Table 84.1** Emission projections for the sensitivity cases performed for July 2011

| Source | | Base case | New emission case |
|---|---|---|---|
| Mobile | | 2005 MOVES | 2005 MOBILE6 + 05 to 12 projections |
| Point sources | | NEI05v1 | 2010 CEM + DOE Annual Energy Outlook (AEO) |
| Area source | Non road | NEI05v1 | Cross-state Air Rule Projection (CSAPR) |
| | Other sectors | NEI05v1 | NEI05v1 |
| Biogenic emission | | BEIS3.13 (CMAQ4.7.1 inline) | BEIS3.13 (CMAQ4.7.1 inline) |
| Canadian emissions | | 2001 EI | 2006 EI |

## 84.2 Emission Modelling for $\text{Case}_{\text{new-emission}}$

Table 84.1 illustrates the differences of NOx emission inventory used in the two simulations over the CONterminous U. S (CONUS). The emission projection from 2005 to 2012 in the CSAPR is used to scale the NEI2005 into the forecasting year. The CSAPR projection for mobile sources is derived from using MOtor Vehicle Emission Simulator (MOVES) version 2010 run for National Mobile Inventory Model (NMIM) 2012 estimates. Aggregated state-level data from the CSAPR run are used in the subsequent emission projection. The projected 2012 scenario represents the best estimate for the future year without implementation of Electricity Generating Unit (EGU) remedy controls [3].

## 84.3 Model Results and Discussion

### *84.3.1 $NO_x$ Emission Changes*

The New Emission Case demonstrated a significant reduction in the mobile source's share of NOx emission among the three major contributors: area, mobile and point sources. It reduced from 33.6 % in the Base Case to 25.2 % in the New Emission Case. This is even more significant considering the large increase in vehicle miles traveled since 2005. The NOx SIP Call achieved significant reduction of NOx emission from power plants, but dwarfed by the reduction in the on-road vehicular (mobile) exhausts. In terms of geographical distribution of the NOx emission reduction, it exhibited regionally specific trends: largest reduction is in Upper Middle (20.6 %) followed by Pacific Coast (18.8 %), South East (17.0 %),

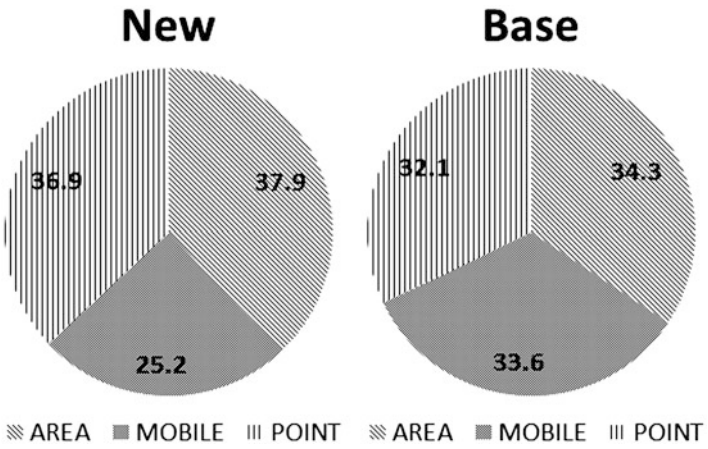


**Fig. 84.1** Contribution of NOx emission (*left*) Base Case and (*right*) New Emission Case (See Table 84.1)

North East (16.3 %), Rocky Mountain (15.9 %) and Lower Middle (11.2 %) (see Figs. 84.1 and 84.2). The change in NOx emission is not sensitively to population change. Consulting the national census trend-tracker of population growth since 1990 (Fig. 84.3); NOx emission change has a weak correlation with population change.

Figure 84.4 is the percent of $NO_x$ concentration decrease in measurement by USEPA in ten metropolitan areas (including Atlanta, Boston, Chicago, Dallas, Houston, Los Angeles, Miami, New York, Philadelphia and Washington DC) in July from 2005 to 2011. All cities reported a decrease in $NO_x$ measurements during July from 2005 to 2011, but trends vary with city: Boston and Chicago had by far the smallest decrease in July $NO_x$ and New York reported a 60 % decrease in July $NO_x$, while Atlanta, Dallas, Los Angeles, Miami, and Washington DC reported a 45–50 % decrease. The $NO_x$ emission reduction (Fig. 84.3.) is supported by $NO_x$ ground station measurements (Fig. 84.4.) and the magnitude of reduction is within the range of suggested by measurements.

### *84.3.2 NOx and O3 Prediction Improvements*

Figure 84.5 shows CMAQ simulated $NO_x$ (left panel) and $O_3$ (right panel) biases in Base and New Cases over CONUS and in six predefined regions. Overall, accompanying $NO_x$ emission reduction, $NO_x$ and $O_3$ biases over CONUS were improved. As specific to regions, positive biases for $NO_x$ in South East, Pacific coast

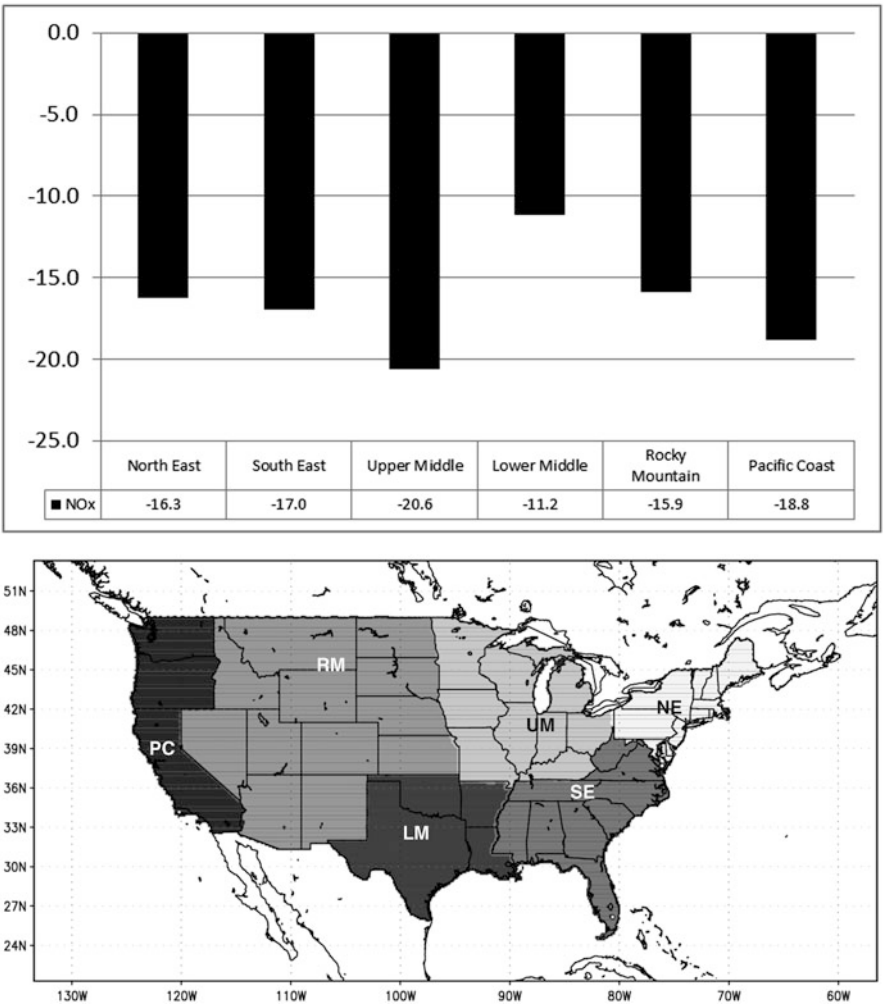


**Fig. 84.2** Regional percentage change of NOx emission by the New Emission Case w.r.t. Base Case. The inset on the right shows the six referenced regions

and Lower Middle $NO_x$ were reduced; positive biases in Upper middle changed to negative bias while in North East and Rock Mountain the already negative biases were aggravated suggesting $NO_x$ emission reduction in those regions were more than reality. For $O_3$, positive biases in all six predefined regions were reduced. However, in South East, Upper Middle and Lower Middle $O_3$ biases in daytime monthly averaged model prediction were still greater than 5 ppbv in July 2011.

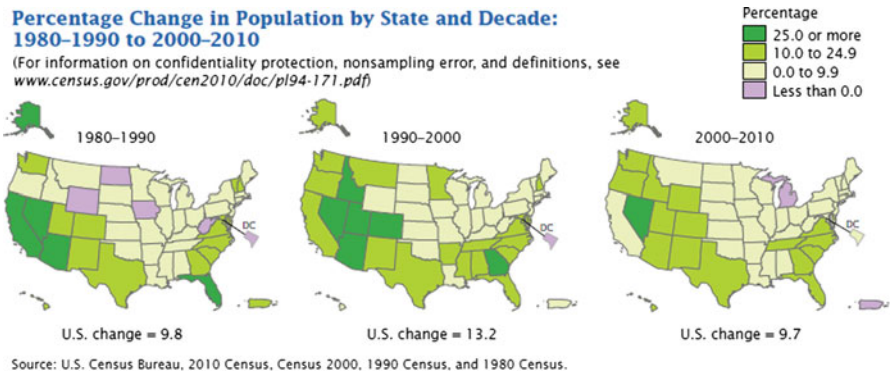


**Fig. 84.3** Percentage population change for the last two decades as reported by the U.S. Census Bureau

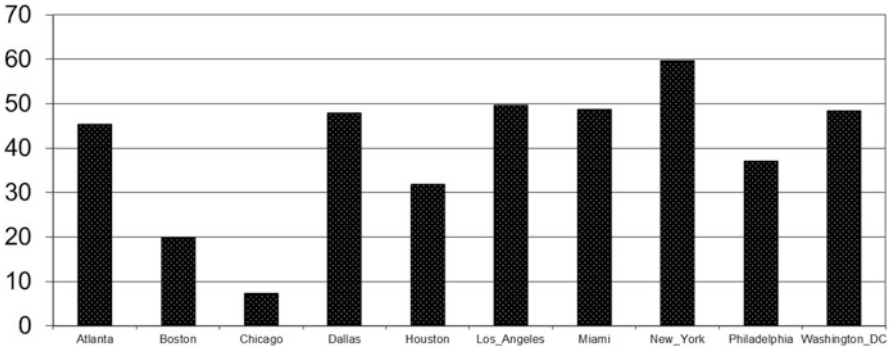


**Fig. 84.4** Measured NOx concentration % decrease in ten large metropolitans in July from 2005 to 2011

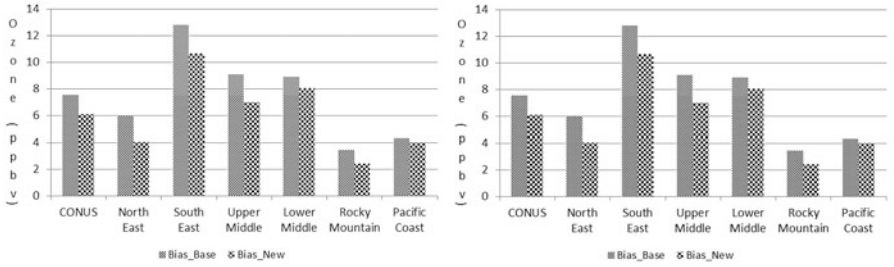


**Fig. 84.5** $NO_x$ (*left*) and $O_3$ (*right*) biases in Base and New Case over CONUS and the six regions (See Fig. 84.2)

## References

1. Bishop GA, Stedman DH (2008) A decade of on-road emissions measurements. Environ Sci Technol 42(5):1651–1656
2. Byun D, Schere KL (2006) Review of the governing equations, computational algorithms, and other components of the models-3 Community Multiscale Air Quality (CMAQ) modeling system. Appl Mech Rev 59(1–6):51–77
3. EPA, Technical Support Document (TSD) for the final Transport Rule. Docket ID No. EPA-HQ-OAR-2009-0491. Accessed online 18 Nov 2012 at http://www.epa.gov/airtransport/pdfs/EmissionsInventory.pdf
4. Gorline JL, Lee P (2009) Performance evaluation of NOAA-EPA developmental aerosol forecasts. Environ Fluid Mech 9(1):109–120
5. Janjic ZI (2003) A nonhydrostatic model based on a new approach. Meteorog Atmos Phys 82(1–4):271–285
6. Kang DW, Mathur R, Rao ST (2010) Real-time bias-adjusted O-3 and PM2.5 air quality index forecasts and their performance evaluations over the continental United States. Atmos Environ 44(18):2203–2212
7. Otte TL, Pouliot G, Pleim JE, Young JO, Schere KL, Wong DC, Lee PCS, Tsidulko M, McQueen JT, Davidson P, Mathur R, Chuang HY, DiMego G, Seaman NL (2005) Linking the Eta model with the Community Multiscale Air Quality (CMAQ) modeling system to build a national air quality forecasting system. Weather Forecast 20(3):367–384
8. Reis S, Pinder RW, Zhang M, Lijie G, Sutton MA (2009) Reactive nitrogen in atmospheric emission inventories. Atmos Chem Phys 9(19):7657–7677

## Questions and Answers

**Questioner Name:** Amir Hakami

**Q:** Did the scaling factor that applied to $NO_2$ also apply to VOCs?

**A:** No. Since this study is focus on summer time. VOC present in July is largely due to biogenic emission sources. They dominate over the anthropogenic components in summer time and do not show much seasonal changes across the years in the time scale of a few years to a decade. On the other hand, the NOx scaling factor is mainly based on the adjustment of anthropogenic sources.

# Chapter 85
# Presentation and Validation of a New Building Downwash Model

**Wouter Lefebvre, Guido Cosemans, Stijn Janssen, and Clemens Mensink**

**Abstract** Olesen et al. (Bound Layer Meteorol 131(1):73–83, 2009) have shown that current building downwash parameterizations, which are essential in the vicinity of build up areas, perform poorly at very short distances. Therefore, a new building downwash model has been developed based on the Thompson-wind tunnel dataset. The model consists of the Gaussian transport and diffusion equation, in which the variables xR (distance source-receptor) and Hs (stack height) have been replaced with functions that define a receptor dependent virtual origin. The virtual source functions account for the impact of building downwash (1) by changing the height of the plume to account for the vertical displacement of the plume and the extra turbulence around the building, (2) by using an upwind displacement of the plume origin to simulate the impact of the wind-upward displacement of the plume and (3) by accounting for the entrainment of clean air into the plume by increasing the distance between the virtual source and the receptor point. The model results are compared to the several measurement time series in Flanders, Belgium, at industrial locations where building downwash plays an important role. We have shown an increased modeling ability in all cases: for instance, biases ranging from −4 to −33 ng/m$^3$ (−46 to −77 %) improve to values ranging from 1.3 to −7.5 ng/m$^3$ (−29 to +14 %) and $R^2$ values improve dramatically (up to 0.83 from 0.65 in cases with a strong building downwash effect).

W. Lefebvre (✉) • G. Cosemans • S. Janssen • C. Mensink
VITO, Boeretang 200, 2400 Mol, Belgium
e-mail: Wouter.lefebvre@vito.be; guido.cosemans@vito.be; stijn.janssen@vito.be; Clemens.mensink@vito.be

D. Steyn and R. Mathur (eds.), *Air Pollution Modeling and its Application XXIII*,
Springer Proceedings in Complexity, DOI 10.1007/978-3-319-04379-1_85,

## 85.1 Introduction

Olesen et al. [4] have shown that the state of the art of gaussian plume modelling at short distances from the building is disappointing, due to an inaccurate description of building downwash effects. They compared two major existing building downwash plume models and one computational fluid dynamics (CFD) model with the measurements of the Thompson wind tunnel dataset [5, 6]. The CFD model shows reasonable correspondence to the measurements. However, the two plume models fail to reproduce some of the major characteristics such as the order of magnitude of the ground-level concentrations close to the building.

Therefore, in Cosemans et al. [2], further denoted as CLM12, a new parameterization for building downwash in plume models has been developed on the basis of the Thompson [5, 6] dataset. The CLM12 parameterization reproduces the following major effects of building downwash by functions to quantify the following phenomena:

- Plume material, following the streamlines, is lowered towards the ground by $\Delta H$ over a distance $x_{FPH}$, where $x_{FPH}$ is approximately the distance downwind the building where the maximum ground-level concentration is found;
- The increased turbulence caused by the building causes an upwind displacement ($\Delta x_{DISP}$) of the plume origin;
- Clean air gets mixed into the plume more rapidly than in absence of a building, which is reproduced by an increase of the virtual source origin value till a distance roughly equal to $2*x_{FPH}$;
- Finally, building downwash has an important effect on the plume rise.
- It has been shown in CLM12 that this parameterization reproduces the Thompson dataset well.

## 85.2 Model and Measurements

The Immission Frequency Distribution Model (IFDM) is a bi-Gaussian plume model, used in Belgium since 1972 for impact assessment of complex configurations of industrial, residential, traffic and agricultural pollutant sources on a local scale. The Gaussian dispersion parameters depend on the Bulk Richardson number measured along a 120 m high meteorological tower located at the nuclear energy research site at Mol [1]. More information on the IFDM model can be found in the European Model Database (http://air-climate.eionet.europa.eu/databases/MDS/index_html), which includes an extensive set of references regarding the validation of this model.

The parameterization proposed by CLM12 is based on single stack-single building configurations (almost 400 in total, all having the wind direction frontal to a building face) and the buildings having four different height/width/length ratios. The features additional to the CLM12 parameterization needed for arbitrary

building-stack configurations as found in the real world are a series of interpolations and adaptations to make the step between the a selected set of wind-tunnel data and all possible real-life situations, concerning building height, different building types, non-frontal winds, multiple buildings, wind speed dependency and changes in the plume width.

Ground-level concentrations of As, measured near an industry plant located in flat terrain that emits small amounts of Arsenic (As) is used to evaluate the model. Four measurement locations are operated by the Flemish Environmental Agency (VMM) and provide daily concentrations of As in PM10 for the period 2010–2011. The locations are indicated by the codes HB23, HB17, HB18 and HB01. The measurements (daily resolution) were delivered in integers in ng/m$^3$. Measured and modeled concentrations of 0 ng/m$^3$ are converted to 0.5 ng/m$^3$ in order to take into account the detection limit.

## 85.3 Evaluation of the Model

Two simulations have been performed. The first one has no building downwash (var_nobd), while the second one takes into account building downwash (var_bd). Both simulations have variable emissions, created by scaling the emissions of some of the sources with the results of the Pourbaix-measurement in the recirculation loop of these sources, so that the average emission is kept constant. Of course, this does not account for the possible intersource variability, nor is it a perfect measure of the source variability.

Looking at the annual mean characteristics, we see again a marked improvement between the model without and with building downwash module (Table 85.1). Furthermore, the results show the ability to reproduce some of the high peaks in the measurements (Fig. 85.1), especially those in the beginning of February 2011. This difference is mainly observed for the measurement locations which are most

**Table 85.1** Yearly averaged measurement and model values (in ng/m$^3$) for the different measurement locations and model scenarios with time-varying sources. In bold: |bias| >50 % of the measurements. Underlined: |bias| <30 % of the measurements

| Monitoring site | Year | Number of measurements | Period average concentration (ng/m$^3$) | | |
|---|---|---|---|---|---|
| | | | Measured | Var_nobd | Var_bd |
| HB01 | 2010 | 358 | 16 | **6.6** | 11.9 |
| | 2011 | 364 | 14 | 7.5 | 13.4 |
| HB17 | 2010 | 349 | 29 | **10.1** | 16.3 |
| | 2011 | 357 | 23 | 13.0 | 20.7 |
| HB18 | 2010 | 364 | 9.6 | **4.6** | 10.2 |
| | 2011 | 348 | 8.8 | 5.4 | 10.8 |
| HB23 | 2010 | 364 | 44 | **8.7** | 40.3 |
| | 2011 | 357 | 41 | **11.0** | 37.0 |

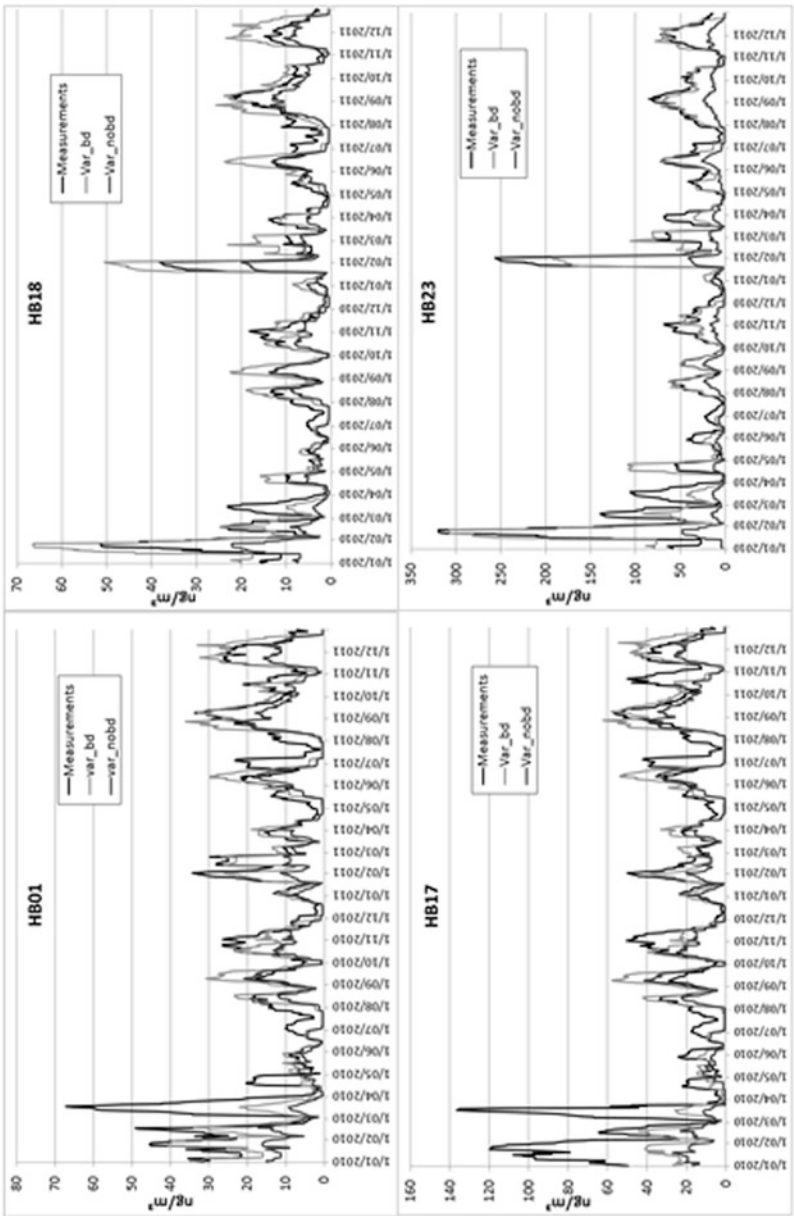


**Fig. 85.1** 14-day-average measurements and modelling (in ng/m$^3$) at the four measurement locations for the two scenarios with variable emissions. Building downwash: *brightest lines*. No building downwash: *darkest lines*; Measurements: *darkest lines*

influenced by the sources known to be strongly affected by building downwash (respectively HB23, HB18 and to a lesser degree HB01, Table 85.1). In HB18, the modelled Var-bd average is higher than is measured, in the other sites the modelled value is lower than measured, leaving 'room' for the impact of still unquantified emissions.

## 85.4 Conclusion

In this paper, several points concerning building downwash have been shown. First of all, the strong influence of building downwash on measurement sites close to the sources has been demonstrated. Secondly, the inclusion of a building downwash parameterization into a plume model has been established, explaining the choices that have been made. These choices can serve as a guide to other modelling groups wishing to include the same parameterization in their plume models. Thirdly, it has been shown that the building downwash parameterization improves the accuracy of the model in simulating cases affected by building downwash. Furthermore, it has been demonstrated that the model is capable of predicting at a sufficient accuracy the annual mean concentrations, so that estimations can be made if the European norms will be met. Finally, inclusion of more detailed emission data has revealed that the model is also capable of explaining the outliers which have been measured in the recent past. Therefore, the model can also be used in order to assess in detail the exposure of the population to the emitted pollutants. More information and a more thorough validation can be found in Lefebvre et al. [3].

## References

1. Bultynck H, Malet LM (1972) Evaluation of atmospheric dilution factors for effluents diffused from an elevated continuous point source. Tellus XXIV(5):465–471
2. Cosemans G, Lefebvre W, Mensink C (2012) Calculation scheme for a Gaussian parameterization of the Thompson 1991 wind tunnel building downwash dataset. Atmos Environ 59:355–365. doi:10.1016/j.atmosenv.2012.05.17
3. Lefebvre W, Cosemans G, Kegels J (2013) Comparison of the IFDM building downwash model predictions with field data. Atmos Environ 75:32–42. doi:10.1016/j.atmosenv.2013.04.022
4. Olesen HR, Berkowicz R, Ketzel M, Løfstrøm P (2009) Validation of OML, AERMOD/PRIME and MISKAM using the Thompson wind-tunnel dataset for simple stack-building configurations. Bound Layer Meteorol 131(1):73–83
5. Thompson RS (1991) Data report. Project: building amplification factors. US EPA
6. Thompson RS (1993) Building amplification factors for sources near buildings – a wind-tunnel study. Atmos Environ Part A Gen Top 27:2313–2325

# Chapter 86
# Boundary-Layer and Air Quality Study at "Station Nord" in Greenland

**Ekaterina Batchvarova, Sven-Erik Gryning, Henrik Skov, Lise Lotte Sørensen, Hristina Kirova, and Christoph Münkel**

**Abstract** Knowledge on the forcing mechanisms (meteorological and chemical) that come into play in the Arctic environment is highly uncertain. We analyse data from measurements and mesoscale meteorological modelling for periods in summer 2011 and winter 2011/2012 to elucidate the boundary-layer features at Station Nord situated in Northern Greenland (81.6 N, 16.7 W). A major challenge for modelling is to connect local-scale observations with larger scales modelling of the atmosphere. In particular, in summer, bare soil in the vicinity of the station may not be present in the global boundary and surface conditions. Thus, in summer the deviations of modeled from measured values of temperature and humidity near the surface are larger compared to winter. We found that the underestimation of temperature near the ground is larger at clear sky compared to cloudy conditions; and the underestimation reached up to height 1-1, 5 km at clear sky and up to the first 100 m for the cloudy days. The measured wind speed profiles showed high

E. Batchvarova (✉)
National Institute of Meteorology and Hydrology, Bulgarian Academy of sciences, Blvd Tzarigradsko chaussee 66, 1784 Sofia, Bulgaria

DTU Wind Energy, Technical University of Denmark, Risø campus, 4000 Roskilde, Denmark
e-mail: Ekaterina.Batchvarova@meteo.bg

H. Kirova
National Institute of Meteorology and Hydrology, Bulgarian Academy of sciences, Blvd Tzarigradsko chaussee 66, 1784 Sofia, Bulgaria

S.-E. Gryning
DTU Wind Energy, Technical University of Denmark, Risø campus, 4000 Roskilde, Denmark
e-mail: sveg@dtu.dk

H. Skov • L.L. Sørensen
Environmental Institute, Aarhus University, 4000 Roskilde, Denmark

C. Münkel
Weather Instruments, 22607 Hamburg, Germany

D. Steyn and R. Mathur (eds.), *Air Pollution Modeling and its Application XXIII*, Springer Proceedings in Complexity, DOI 10.1007/978-3-319-04379-1_86,

variability, while the modeled were smoothed. During summer the modeled wind speed was close to or larger than the measured without clear indication for the role of clouds. In winter, the over-estimation of wind speed was more pronounced.

## 86.1 CRAICC Network

CRAICC (Cryosphere-atmosphere interactions in a changing Arctic climate) is part of the Top-level Research Initiative (TRI), the largest joint Nordic research and innovation initiative to date, aiming to strengthen research and innovation regarding climate change issues in the Nordic Region.

## 86.2 Observational Site and Measurements Campaigns

Station Nord in Greenland (81.6N; 16.7W) serves as a Greenlandic background station for air pollution as part of the Danish/Greenlandic contribution to Arctic Monitoring and Assessment Program (AMAP), Fig. 86.1 (In warm summer conditions, the surface may be snow free, but the waters are normally always frozen). Parallel, extensive meteorological measurements programme was organized, including cloud base height measurements using a CL51 Vaisala ceilometer, Fig. 86.2 (left panel). Radiosoundings were performed during a 10-day periods in summer 2011 and winter 2012 using a MODEM system, Fig. 86.2.

One of the main results from the feasibility measurements at Station Nord was that the ceilometer used is a robust instrument that can stand the harsh Arctic conditions and that the aerosol backscatter signal allows to study the aerosol distribution in the area during the year, Fig. 86.3. The ceilometer measurements are performed continuously from July 2011 until April 2013. Two radio soundings campaigns have been carried out, one from 28 July to 5 August 2011 and the second for 3 weeks in March 2012. Simultaneously, Aarhus University is measuring gas and aerosol concentrations, Fenger et al. [1]. Concentrations reach 0.6 ppb for NOx and a constant level of ozone at about 20 and 30 ppbv in the two campaign periods respectively.

**Fig. 86.1** Station Nord location and view in July/August 2011

**Fig. 86.2** Ceilometer and the 10 m mast for flux measurements (*left*), air quality measurements (*middle*) and releasing radio sonde, (*right panel*)

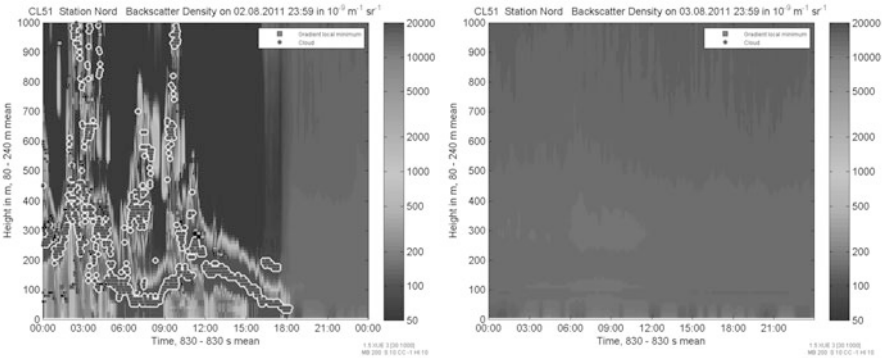


**Fig. 86.3** Ceilometer measurements on 2 and 3 August 2011 covering cloudy (*left*) and clear sky (*right panel*) periods. Radiosoundings were performed at 6, 12, 18 and 24 GMT

| Process | WRF parameter |
|---|---|
| Mycrophysics | 8 (D3) = Thompson graupel;<br>4 (D1&D2)=WSM 5-class |
| Longwave radiation | 1 = RRTM |
| Shortwave radiation | 2 = Goddard |
| Surface layer | 2 = Eta similarity |
| Land surface | Noah LSM |
| ABL | 2 = Mellor-Yamada-Janjic |
| Cumulus parametrization | 5 = New Grell scheme (D1&D2) |

**Fig. 86.4** Model domains and physics options used

## 86.3 Mesoscale Modeling Results

Mesoscale modelling was performed with the Weather Research Forecasting model (with ARW core) WRF, v.3.3.1 [2]. The domain and physics used for the simulations are shown in Fig. 86.4. WRF was initialized with the US National Center for

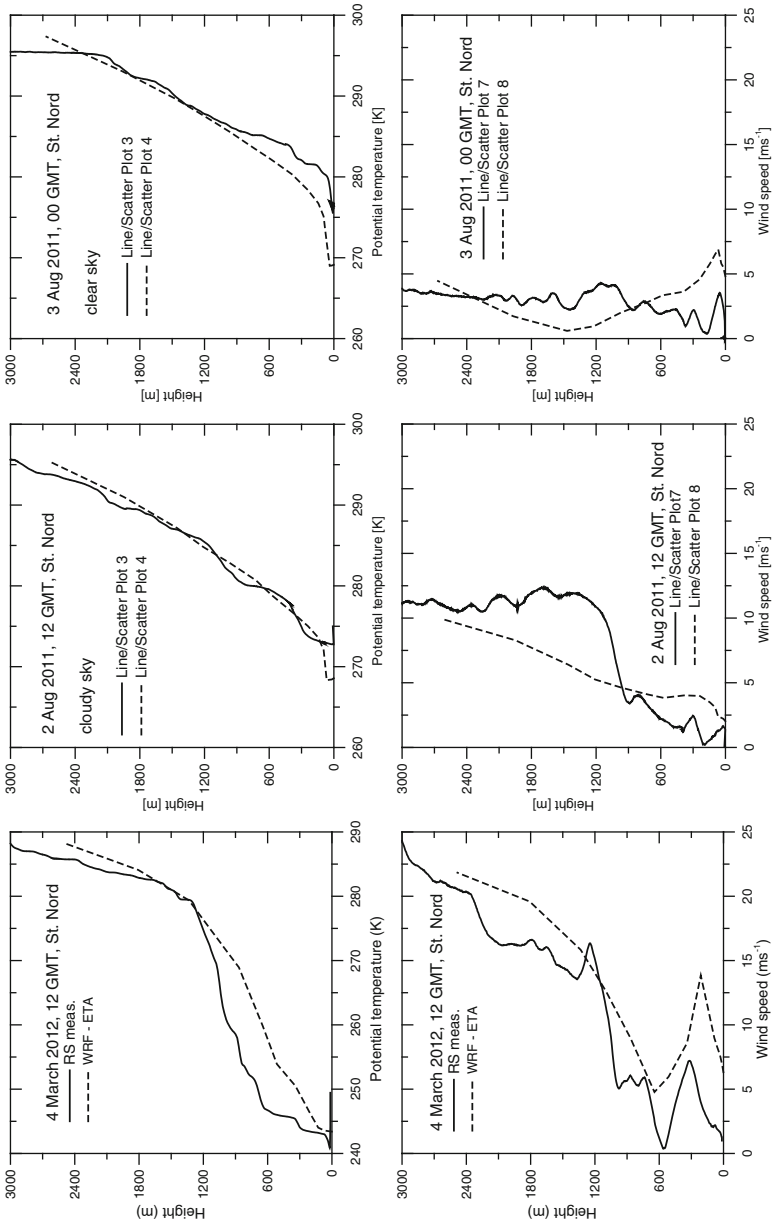


**Fig. 86.5** Comparison of modeled and measured profiles

Environmental Prediction Global Analyses data (FNL), with space resolution $1 \times 1°$ and time resolution of 6 h. WRF was run with two-way nesting on 3 domains with horizontal grid resolution 36, 12, and 4 km, on 26 vertical levels up to 50 hPa (13 of them are below 2,000 m). Land use categories of USGS 24-category data were used. The snow free surroundings of the Station Nord in summer are likely not accounted for in the surface conditions and poorly resolved with resolution of 4 km. The model temperature near the ground is lower in summer with bigger difference at clear sky compared to cloudy conditions; and is closer to measurements in winter. The temperature under estimation reaches height of 1-1, 5 km in clear skies and only the first 100 m for the cloudy days, Fig. 86.5 (middle and right upper panels). The measured wind speed profiles show high variability, while the modeled are smooth; without clear indication for the role of clouds. Larger discrepancies were found in winter, compared to summer, Fig. 86.5 (lower panels).

**Acknowledgments** The study is part of the Nordic Centre of Excellence CRAICC – TRI-NCoE and related to COST ES1004. The Danish Environmental Protection Agency with means from the Dancea funds for environmental support to the Arctic Region (Grant no M 112 00270). The findings and conclusions presented here do not necessarily reflect the views of the Agency. Thanks are given to Søren Lund and Bjarne Jensen for maintaining instruments and performing radio soundings. The Royal Danish Air Force is gratefully acknowledged for providing transport to Station Nord and the authors wish in particular to thank the staff at Station Nord for excellent support during sampling.

## References

1. Fenger M, Sørensen LL, Kristensen K, Jensen B, Nguyen QT, Nøjgaard JK, Massling A, Skov H, . Becker T, Glasius M (2013) Sources of anions in aerosols in northeast Greenland during late winter. Atmos Chem Phys 13:1569–1578. www.atmos-chem-phys.net/13/1569/2013/doi:10.5194/acp-13-1569-2013
2. Skamarock WC, Klemp JB, Dudhia J, Gill DO, Barker DM, Duda MG, Huang XY, Wang W, Powers JG (2008) A description of the Advanced Research. WRF version 3. NCAR/TN–475 + STR, NCAR Technical note, Mesoscale and Microscale Meteorology Division, National Center for Atmospheric Research, Boulder, CO, USA, 113 pp

# Chapter 87
# Evaluation of Mesoscale Model Profiles Against Consecutive Radiosounding Data During the Sofia 2003 Experiment

**Hristina Kirova, Ekaterina Batchvarova, and Valeri Nikolov**

**Abstract** Sofia is 1.5 million citizens city situated in a mountain valley and thus characterised with complex structure of the planetary boundary layer (PBL) caused by both terrain and urban features. Stagnant stable conditions lead to fogs and smog in winter, and dry climate leads to high PM concentrations in summer albeit the deep PBL. In this study we evaluated the dynamics given by two configurations of the Weather Research Forecasting (WRF) model against data from consecutive high vertical resolution radiosoundings during 5 days in Sofia under early autumn convective conditions in PBL (Sofia Experiment 2003). Statistical comparisons between modelled and measured parameters showed that WRF simulated relative humidity, temperature and wind direction better in the transition than in the afternoon hours, while the wind speed was insignificantly better simulated in the afternoons. We found that WRF with Mellor-Yamada-Janjic PBL scheme simulated relatively well the vertical profiles of all analysed parameters, except for wind direction which was poorly resolved in the lowest 1,000 m above ground.

## 87.1 Sofia Experiment 2003 and Modelling Configuration

The "Sofia Experiment 2003" field campaign was carried out in Sofia in September and October 2003 [1]. The sondes were launched at NIMH in "Mladost" district in south-east part of the city. For westerly and northerly flows the measurements represent urban conditions, while for southerly and easterly flows – suburban and rural conditions. Thirty five soundings were performed from September 27 to October 03. This period covered days of well-developed convective boundary layer. The soundings were performed with 2 h temporal resolution starting at 7 a.m. and

H. Kirova (✉) • E. Batchvarova • V. Nikolov
National Institute of Meteorology and Hydrology, Bulgarian Academy of Sciences,
66 Tsarigradsko Shose Blvd, 1784 Sofia, Bulgaria
e-mail: Hristina.Kirova@meteo.bg; Ekaterina.Batchvarova@meteo.bg; Valeri.Nikolov@meteo.bg

D. Steyn and R. Mathur (eds.), *Air Pollution Modeling and its Application XXIII*,
Springer Proceedings in Complexity, DOI 10.1007/978-3-319-04379-1_87,

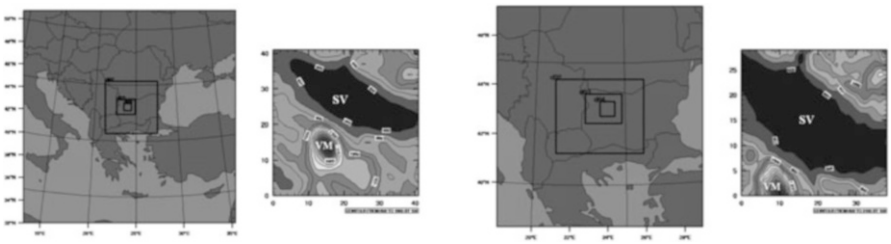


**Fig. 87.1** Domain configuration and terrain features of domain 4 (*left panel* WRF1, *right* – WRF2)

**Table 87.1** Domain configuration

| | WRF1 | WRF2 |
|---|---|---|
| Grid resolution | 36, 12, 4, 1.33 km | 32.4, 10.8, 3.6, 1.2 km |
| Number of gr. points | 58 × 58, 43 × 43, 37 × 34, 43 × 43 | 29 × 31, 37 × 31, 40 × 34, 40 × 31 |
| Vertical levels | 26 going up to 50 hPa | 38 going up to 50 hPa |
| Lambert conformal conic map project (true coordinates 30N, 60E) | Central point: 42N and 24E | Central point: 42.6537N and 23.383E |
| Land use data | USGS 24-category | USGS 24-category |

**Table 87.2** Physical options for WRF1 and WRF2

| | WRF1 | WRF2 |
|---|---|---|
| Microphysics | 8 (D3&D4) = Thompson graupel<br>4 (D1&D2) = WSM 5-class | 7 = Goddard |
| Longwave radiation | 1 = RRTM | 1 = RRTM |
| Shortwave radiation | 2 = Goddard | 1 = Dudhia(D1, D2, D3)<br>2 = Goddard (D4) |
| Surface layer | 2 = Eta similarity | 2 = Eta similarity |
| Land surface | Noah LSM | 1 = 5-layer thermal diffusion |
| ABL | 2 = Mellor-Yamada-Janjic | 2 = Mellor-Yamada-Janjic |
| Urban physics | Off | 1 = single-layer UCM (D3&D4) |
| Cumulus parameterisation | 5 = New Grell scheme (D1&D2) | 1 = Kain-Fritsch scheme (for all domains) |

ending at 7 p.m. local time and twice increased vertical resolution compared to standard, as the ascend velocity was kept 3–4 $ms^{-1}$.

Numerical simulations were performed with the Weather Research and Forecasting (WRF) model with ARW core, 3.3.1 [2]. Two configurations denoted as WRF1 and WRF2 were used, both initialized with the US National Center for Environmental Prediction Final Analyses (FNL) with 1 × 1° spatial and 6 h temporal resolution. In both configurations 4 two-way nested domains (Fig. 87.1) were created with land use categories USGS – 24 category data. In WRF1 Sofia Valley (SV) and the Vitosha mountain (VM) fell entirely in the innermost domain (Fig. 87.1, left), while in WRF2 mainly the city is encompassed (Fig. 87.1, right). Details on domain configurations are listed in Table 87.1. Physics is summarized in Table 87.2.

## 87.2 Analyses and Results

Figure 87.2 illustrates direct comparisons between measured and modeled profiles of potential temperature at 15 LST. Considerable difference is noted between WRF1 and WRF2 simulations although the set up options are close. For wind speed (not shown here) the differences are smaller.

Statistical comparisons between modeled and measured parameters are shown in Table 87.3. Data from all 35 radio soundings compared to all model levels within 8,000 m are used in the analysis, forming a set about 700 pairs. WRF1 performs slightly better in the transition hours (TH) – which covered data/model output at 07, 09 and 19 LST than in the afternoon hours (AH) – 11, 13, 15, 17 LST, except for wind speed. WRF2 results for temperature and wind speed are closer to measurements in the afternoon compared to transition hours.

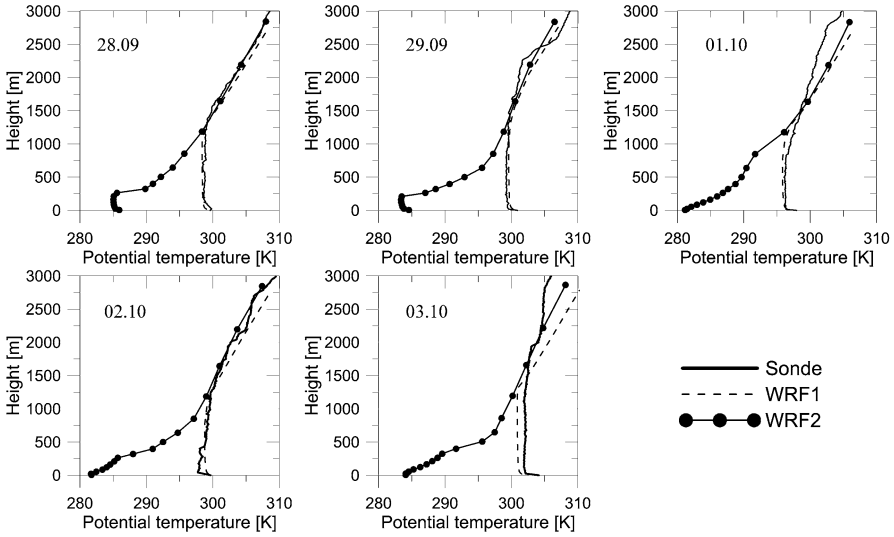


**Fig. 87.2** Potential temperature vertical profiles from model compared to radiosoundings at 15 LST

**Table 87.3** Values of coefficient of determination in transition and afternoon hours

| | Coefficient of determination, R-squared (R) | | | |
|---|---|---|---|---|
| | WRF1 | | WRF2 | |
| | Transition hours | Afternoon hours | Transition hours | Afternoon hours |
| Relative humidity (RH) | 0.676919 | 0.674078 | 0.608968 | 0.451179 |
| Potential temperature (Theta) | 0.988321 | 0.987029 | 0.942279 | 0.956123 |
| Temperature (Temp) | 0.993557 | 0.992711 | 0.94959 | 0.959776 |
| Wind speed (Wsp) | 0.782512 | 0.828081 | 0.874124 | 0.939289 |
| Wind direction (Wdir) | 0.240608 | 0.16046 | 0.187802 | 0.149359 |

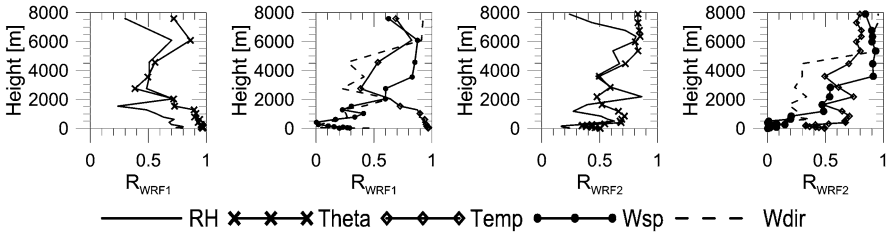


**Fig. 87.3** Coefficient of determination profiles ($R_{WRF1}$, $R_{WRF2}$) at specific WRF modelling level averaged for all radiosoundings

Regarding potential temperature profiles, R values for WRF1 are close to 1 near the ground, decrease by 20 % up to 1,500 m, and decrease faster higher up (Fig. 87.3). R for RH starts at 0.8 near ground and decreases similarly higher up. R for wind speed and direction is small near the ground and increases with height reaching about 0.8 above 3,000 m. R values for all parameters calculated with WRF2 are smaller near the ground similar higher up compared to WRF1. At height of about 2,000 m ag the R for all parameters exhibits changes, which might be associated with the influence of the Vitosha mountain (the height of which is 2,290 m).

## 87.3 Concluding Remarks

In this study, two WRF simulations were evaluated against consecutive radio sounding data showing the development of PBL in convective conditions in complex terrain. Good agreement was found for temperature and wind speed, worse for relative humidity and poor for wind direction based on overall statistics. The WRF1 simulation gave satisfactory result for vertical profiles of temperature, potential temperature and relative humidity. The wind speed was reasonably resolved above 1,500 m and the wind direction was poorly reproduced in the lowest 1,000 m pointing inability of the model to reconstruct always the complex structure of profiles influenced by a complex terrain, urban conditions and synoptic forcing.

**Acknowledgments** The study is related to the collaboration within COST ES1004 Action and the Nordic Centre of Excellence programme CRAICC.

## References

1. Batchvarova E, Gryning S-E, Rotach MW, Christen A (2006) Comparison of modelled aggregated turbulent fluxes and measured turbulent fluxes at different heights in an urban area. In: Borrego C, Norman A (eds) Air pollution model and its application, vol XVII, pp 363–370
2. Skamarock W, Klemp JB, Dudhia J, Gill DO, Barker DM, Duda MG, Huang XY, Wang W, Powers JG (2008) A description of advanced research WRF Version 3. http://www.mmm.ucar.edu/wrf/users/docs

# Chapter 88
# The Use of a Mesoscale Modeling System Together with Surface and Upper Observational Data to Estimate Hourly Benzene Impacts in a Mountainous Coastal Area

**V. Valdenebro, E. Sáez de Cámara, G. Gangoiti, L. Alonso, J.A. García, J.L. Ilardia, N. González, and E. Arraibi**

**Abstract** An application of the CALPUFF modeling system in the near-field in an area of very-complex topography is presented. Different configurations for both the meteorological and the dispersion simulations were tested. The RAMS high-resolution (1 km) output as well as the data from a network of surface stations and the high-resolution data from a wind profiler radar (WPR) located in the area were available for assimilation and validation purposes. The 250 m resolution three-dimensional CALMET meteorological fields, after being validated against surface and upper air data, were fed into CALPUFF to simulate the potential impacts of the emissions of a coke factory over a nearby urban area. Benzene was used as a tracer of the emitted pollutants. The results of the dispersion simulations were compared against the available hourly benzene records. Our results showed that, no matter the selected synoptic forcing for RAMS (NCEP/ECMWF), the assimilation of meteorological data into CALMET is necessary for a correct representation of the wind flows in the area, and as a consequence, for a correct representation of the actual benzene impacts.

## 88.1 Introduction and Method

The impacts of the benzene emissions from an old coke factory in the nearby urban area of Zorroza (northern Spain) during two periods of 10 days under anticyclonic conditions were analyzed using the mesometeorological model RAMS and the

V. Valdenebro (✉) • E. Sáez de Cámara • G. Gangoiti • L. Alonso • J.A. García
J.L. Ilardia • N. González • E. Arraibi
School of Engineering, University of the Basque Country UPV/EHU,
Alameda de Urquijo s/n, 48 013 Bilbao, Spain
e-mail: veronica.valdenebro@ehu.es; estibaliz.saezdecamara@ehu.es; g.gangoiti@ehu.es; lucio.alonso@ehu.es; joseantonio.garcia@ehu.es; juanluis.ilardia@ehu.es; negopodo@gmail.com; esti_arraibi@hotmail.com

D. Steyn and R. Mathur (eds.), *Air Pollution Modeling and its Application XXIII*,
Springer Proceedings in Complexity, DOI 10.1007/978-3-319-04379-1_88,

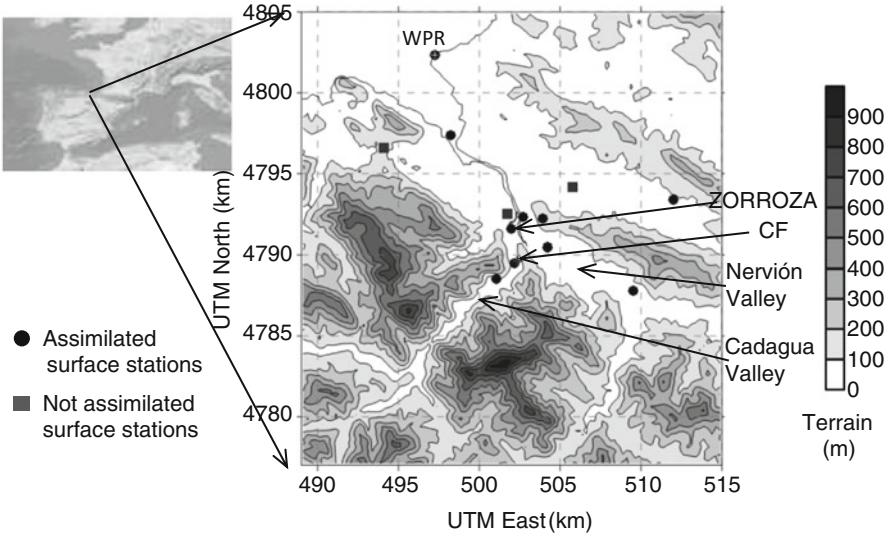


**Fig. 88.1** Study area. The locations of the meteorological and air quality networks stations and the WPR are shown. Zorroza and the coke factory (CF) have also been marked

CALPUFF non-steady-state modeling system. The complex topography of the region (a mountainous region near the coast) strongly influences the air flows in the area, causing important daily cycles/changes in stability and wind almost every day, which directly affects the dispersion of pollutants. These characteristics make it inappropriate to use steady-state Gaussian plume models for air quality studies in the region, specially under the "stagnation or re-entry cycles" dispersion pattern [1]. The study area (Fig. 88.1), the available data and the local flows, as well as the meteorology during both analyzed periods, the RAMS and CALMET computational grids and the emission scenarios were described in detail by Valdenebro et al. [2], who performed a first analysis of the need to assimilate surface data into CALMET to reproduce the main flows in the area.

Now, two different RAMS simulations were performed for each period, corresponding to the two different databases used for initialization and nudging (NCEP Reanalysis-II data and ECMWF Era-Interim data). For each RAMS run, the resulting 1 km horizontal resolution fields, after being validated as described by Valdenebro et al. [2], were adjusted to the finner CALMET 250 m resolution topography. Surface data as well as the high-resolution data from a WPR located in the area were assimilated into CALMET. The effect of such assimilation on the simulated wind fields and benzene levels was studied. Several configurations were tested, with the final goal of setting up a methodology for dispersion studies in the region.

## 88.2 Results

Better RAMS results, both at surface and upper levels, were found when using ECMWF forcing. For any RAMS configuration the assimilation of surface data into CALMET was key to reproducing the main flows in the area at surface level and, consequently, to reproducing the daily cycle of pollutants impacts in Zorroza (Fig. 88.2). These cycles could be quite well captured by the modeling system when surface data were assimilated into the model; this assimilation would finally overcome the differences due to different RAMS initializations. In all cases the actual levels of benzene concentrations were underestimated, probably due to an underestimation of the registered benzene emissions, which were inferred from the annual data of the 2009' Spanish E-PRTR Register.

No upper air meteorological data were available to perform an independent validation of the assimilation of the WPR data into CALMET. However, we found a positive impact on the simulated benzene levels (days 19, 20 and 22 on Fig. 88.2), which could be interpreted as a better simulation of the transport over the Cadagua Valley (far from the WPR). Figures 88.3 and 88.4 show the improvement in the simulated wind on the vertical of the site of the WPR.

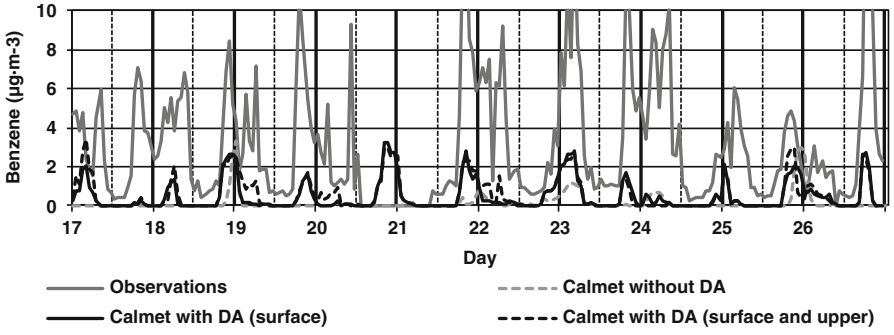


**Fig. 88.2** Observed and simulated benzene concentrations at the Zorroza station (surface emission scenario) for the 2010 period (ECMWF synoptic forcing). Results obtained without and with meteorological data assimilation (DA) into CALMET are shown

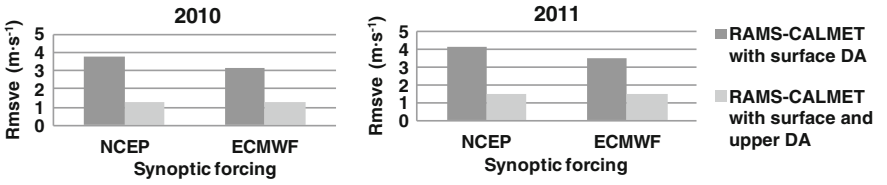


**Fig. 88.3** Comparison of the simulated and observed wind on the vertical of the location of the WPR for both periods. The root mean square vectorial error (RMSVE) is shown for RAMS-CALMET with surface DA and RAMS-CALMET with surface and upper DA simulations

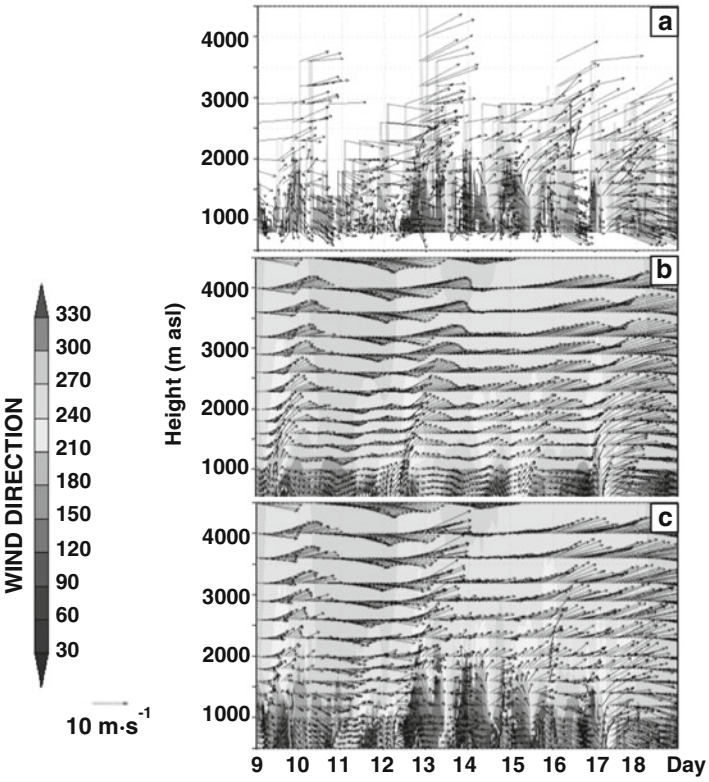


**Fig. 88.4** Time sequence of wind on the vertical of the site of the WPR for the June 2011 period: (**a**) observed (represented every 2 h), (**b**) and (**c**) simulated by CALMET without and with assimilation of the WPR data, respectively. NCEP synoptic forcing

**Acknowledgements** To the Basque Government for providing data. This work has been financed by the Consolider-Ingenio 2010 Program (GRACCIE project CSD2007-00067) of the Spanish Ministry of Education and Science, the Viceconsejería de Medio Ambiente of the Basque Government and the University of the Basque Country (Funding Agency: UPV/EHU, Grant Number: UFI11/47).

## References

1. Millán MM, Otamendi E, Alonso L, Ureta I (1987) Experimental characterization of atmospheric diffusion in complex terrain with land-sea interactions. J Air Pollut Control Assoc 37:807–811
2. Valdenebro V, Sáez de Cámara E, Gangoiti G, Alonso L, García JA, Ilardia JL, González N (2013) Evaluations of benzene impacts of a coke plant in a complex-topography urban area with the RAMS-CALMET-CALPUFF modelling system. In: Longhurst JWS, Brebbia CA (eds) Air Pollution 2013. 21st international conference on modelling, monitoring and management of air pollution, Siena, June 2013. WIT Transactions on Ecology and the Environment, vol 174. WIT Press, Southampton, pp 39–51

# Chapter 89
# A Sensitivity Analysis of the WRF Model to Shortwave Radiation Schemes for Air Quality Purposes and Evaluation with Observational Data

**Kinga Wałaszek, Maciej Kryza, and Małgorzata Werner**

**Abstract** Shortwave radiation is a key meteorological component influencing formation and destruction of many atmospheric pollutants, most of all tropospheric ozone. It is the main driver of photochemical reactions, affects surface temperature and enhances biogenic VOC production. Because uncertainties in meteorological fields provided by meteorological models highly affect chemical transport model simulations, accurate information on spatial and temporal variability of shortwave radiation is needed for reliable air quality modeling. The main aim of this study is to assess the meteorological model performance in representing observational data. In this study, the Weather Research and Forecasting (WRF) model is applied to the area of Lower Silesia, Poland, in order to test three shortwave radiation schemes: Goddard, RRTMG and GFDL scheme. The test period is a high ozone episode of 17.06-04.07.2008. Simulations were run with different shortwave radiation options, while all other physics parameterizations remained constant. The results were then evaluated based on radiation measurements conducted in the Observatory of the Department of Climatology and Atmosphere Protection in Wroclaw, Poland. There are some discrepancies between the employed parameterizations both in terms of quality of the results and computational costs but in general, all schemes applied show reasonable consistency with observations.

## 89.1 Introduction

Shortwave radiation is known to have significant impact not only on the Earth's energy budget, but also on the intensity of various chemical and physical processes taking place in the troposphere. It has a particularly large effect on regional and

K. Wałaszek (✉) • M. Kryza • M. Werner
Department of Climatology and Atmosphere Protection, University of Wroclaw, Wroclaw, Poland
e-mail: kinga.walaszek@uni.wroc.pl; maciel.kryza@uni.wroc.pl; malgorzata.werner@uni.wroc.pl

D. Steyn and R. Mathur (eds.), *Air Pollution Modeling and its Application XXIII*, Springer Proceedings in Complexity, DOI 10.1007/978-3-319-04379-1_89,

urban air quality because of its role in photochemical reactions of $O_3$, $NO_x$, VOCs, and other constituents of photochemical smog. Irradiation data in meteorological models influence many other physical parameterizations related to energy fluxes and atmospheric motion [7]. In chemical transport models, radiation data from meteorological model is vital input information [4], especially in systems with meteorology coupled with chemistry, such as the Weather Research and Forecasting model (WRF; [8]) with WRF-Chem [3]. Therefore, accurate estimation of radiation fluxes by a meteorological model is essential for air quality simulations.

In this study, the WRF model is applied for the area of Lower Silesia in SW Poland to verify three shortwave radiation schemes for a high ozone episode. The results are then compared to observational data derived from University of Wroclaw Meteorological Observatory in Wroclaw, Poland.

## 89.2 Data and Methods

In this study, the WRF v3.4 is used with three one-way nested domains. The study area is the Lower Silesian district, located in the south-western part of Poland, lying within the innermost nested domain (2km x 2km grid; [6]). The simulations were conducted for a test period of June 17th to July 4th, 2008, when high concentrations of tropospheric ozone were recorded. Three simulations were performed, each one with a different shortwave radiation scheme: Goddard, RRTMG, and GFDL. The Goddard scheme [1], which has 11 spectral bands and several ozone profiles, is required to account for radiative feedback of aerosols with WRF-Chem. RRTMG [5], designed for climate models, is used by many institutions for operational forecasts. It includes 16 spectral bands and accounts for random cloud overlap. GFDL scheme [2], which is Eta model operational scheme, includes cloud effects and ozone profiles from climatology. Other model physics options used are Goddard microphysics, Kain-Fritsch cumulus parameterization, Unified Noah land-surface model, YSU PBL scheme and RRTM for longwave radiation. The results are compared against 10-min total solar irradiation measurements conducted in meteorological observatory at University of Wroclaw, Department of Climatology and Atmosphere Protection, aggregated to the model's temporal resolution of 1 h.

## 89.3 Results and Discussion

The results are organized as follows: first, model performance with different shortwave radiation parameterizations using several error statistics: mean bias (MB), root mean square error (RMSE), mean absolute error (MAE), and index of agreement (IOA; [9, 10]) is compared. Afterwards, temporal variability of modelled and measured total irradiation is analyzed.

**Table 89.1** Error statistics values for the selected WRF shortwave radiation options

| Shortwave radiation scheme | MB | MAE | RMSE | IOA |
|---|---|---|---|---|
| Goddard | 74.62 | 94.59 | 161.71 | 0.94 |
| RRTMG | 62.04 | 88.15 | 151.21 | 0.95 |
| GFDL | 76.89 | 96.96 | 163.73 | 0.94 |

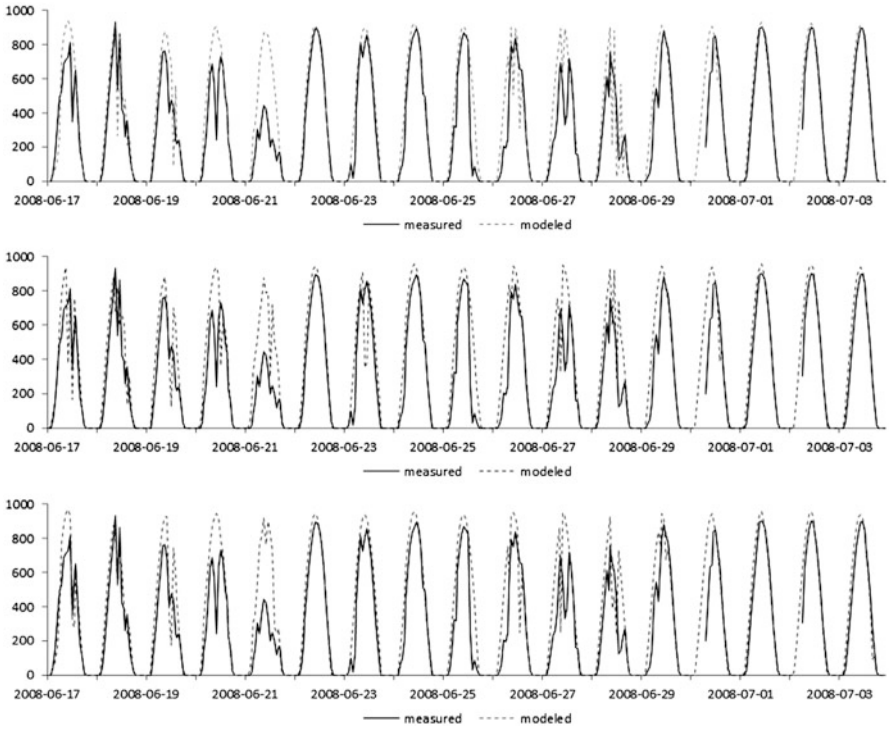


**Fig. 89.1** Modelled vs. measured temporal variation of total solar irradiation. From the top: Goddard, RRTMG, and GFDL scheme

Error statistics calculated for the three analyzed simulations are presented in Table 89.1. All three simulations have very high index of agreement. However, RMSE values are also large, which suggest a few large errors, possibly for cloudy conditions (see below). All predictions have a tendency to overestimate measured radiation values, with RRTMG scheme having the lowest bias. All error statistics analyzed show substantially better performance of the RRTMG scheme.

In terms of temporal variability, it is generally well predicted, with slight overestimation of daily maxima (Fig. 89.1). However, during days with clouds present (e.g. June 21st) the decrease in total solar irradiation is poorly represented, which may be a result of either inadequate estimation of cloud cover fraction

or inaccurate parameterization of their influence on the downward radiation flux. However, for the selected period, the number of cloudy days was too low to draw general conclusions.

## 89.4 Conclusions

In this paper, the Weather Research and Forecasting model results of downward shortwave radiation flux for three radiation options were evaluated. Main conclusions drawn from this study are as follows:

- All three simulations are in relatively good agreement with measurements for clear-sky conditions, but perform worse when clouds are present, which may be connected with model's estimation of cloud fraction or algorithms determining the influence of cloud cover on deflection and diffusion of sunlight;
- The cloudy sky overestimations are also probably the source of high RMSE values for all simulations;
- There is a clear dominance of the RRTMG scheme, which presents the lowest bias and highest agreement with observational data, whereas the other schemes provide comparable performance.

**Acknowledgments** Calculations have been carried out in the Wrocław Centre for Networking and Supercomputing (http://www.wcss.wroc.pl), Grant No. 170. This work was supported by the Polish National Science Centre, grant no 2011/03/B/ST10/06226.

## References

1. Chou M, Suarez M (1994) An efficient thermal infrared radiation parameterization for use in general circulation models. NASA Tech Memo. doi: 10.1.1.26.4850
2. Fels SB, Schwarzkopf MD (1981) An efficient, accurate algorithm for calculating CO2 15 μm band cooling rates. J Geophys Res 86(C2):1205–1232. doi:10.1029/JC086iC02p01205
3. Grell G, Peckham S, Schmitz R (2005) Fully coupled "online" chemistry within the WRF model. Atmos Environ 39:6957–6975. doi:10.1016/j.atmosenv.2005.04.027
4. Iacono M, Nehrkorn T (2010) Assessment of radiation options in the advanced research WRF weather forecast model. In: Proceedings, 1st atmospheric system research science team meeting. Office of Science, U.S. Department of Energy, Bethesda, MD, pp 3–6
5. Iacono MJ et al (2008) Radiative forcing by long-lived greenhouse gases: calculations with the AER radiative transfer models. J Geophys Res Atmos 113(D13):D13103. doi:10.1029/2008JD009944
6. Kryza M et al (2012) Modelling meteorological conditions for the episode (December 2009) of measured high PM10 air concentrations in SW Poland – application of the WRF model. Int J Environ Pollut 50(1/2/3/4):41–52. doi:10.1504/IJEP.2012.051179
7. Lacis A, Hansen J (1974) A parameterization for the absorption of solar radiation in the earth's atmosphere. J Atmos Sci 31:118–133. doi:10.1175/1520-0469

8. Skamarock W, Klemp J (2008) A time-split nonhydrostatic atmospheric model for weather research and forecasting applications. J Comput Phys 227:3465–3485. doi:10.1016/j/jcp2007.01.037
9. Willmott CJ (1981) On the validation of models. Phys Geogr 2(2):184–194. doi:10.1080/02723646.1981.10642213
10. Willmott C, Matsuura K (2005) Advantages of the mean absolute error (MAE) over the root mean square error (RMSE) in assessing average model performance. Clim Res 30:79–82

# Chapter 90
# Comparing WRF PBL Schemes with Experimental Data over Northern Italy

**A. Balzarini, F. Angelini, L. Ferrero, M. Moscatelli, G. Pirovano, G.M. Riva, A. Toppetti, and E. Bolzacchini**

**Abstract** A sensitivity test has been carried out for five PBL schemes using the WRF meteorological model over Italy for February 2008. The model has been applied over the polluted area of the Po Valley with a grid resolution of 5 km. Model results have been compared to surface measurements as well as vertical profiles by balloon soundings, meteorological balloons and Lidar measurements. Results show a good agreement between simulations and observations for mixing ratio, while model reveals higher bias in reconstructing temperature, wind speed and planetary boundary layer height. The best performances in reconstructing PBL height are highlighted for YSU scheme, while other ground meteorological fields are better reproduced by ACM2 parameterization.

## 90.1 Introduction

Planetary Boundary Layer (PBL) plays a key role in determining ground concentrations of pollutants, especially in densely populated areas characterized by weak circulation conditions, such as the Po Valley [1]. Nevertheless, the determination of PBL height remains one of the most uncertain parameters in modeling estimation,

A. Balzarini (✉) • G. Pirovano • G.M. Riva • A. Toppetti
Sustainable Development and Energy Sources Department, Ricerca sul Sistema Energetico (RSE S.p.A.), via Rubattino 54, Milan, Italy
e-mail: alessandra.balzarini@rse-web.it

F. Angelini
ENEA/UTAPRAD-DIM, via Enrico Fermi, 45, 00044 Frascati, Italy

L. Ferrero • M. Moscatelli • E. Bolzacchini
POLARIS Research Center, Department of Earth and Environmental Sciences, University of Milano-Bicocca, Piazza della Scienza 1, Milan, Italy

D. Steyn and R. Mathur (eds.), *Air Pollution Modeling and its Application XXIII*, Springer Proceedings in Complexity, DOI 10.1007/978-3-319-04379-1_90,

strongly affecting the reconstruction of dispersion processes and, thus, ground concentrations [2]. In this study a sensitivity test has been performed on PBL by comparing experimental data and different model simulations in order to assess the skill of the WRF meteorological model in reproducing its structure and evolution in the critical area of the Po Valley (Italy).

## 90.2 Modeling and Experimental Set Up

Five PBL schemes have been selected and compared to ground observations, particle vertical profiles by balloon soundings, meteorological balloons and Lidar measurements (Table 90.1).

Particle vertical profiles were collected in the metropolitan area of Milan by means of a tethered balloon equipped with an optical particle counter (Grimm 1.108) and a meteorological station as well as by an automated Lidar (LD-40 ceilometer). The PBL height was derived in both cases using a gradient method [8, 9]. Additionally, meteorological soundings of Milano Linate airport were considered, too. The availability of this set of highly specialized experimental data represented an unprecedented opportunity for model evaluation over Northern Italy.

WRF has been applied for February 2008 over three nested domains, with the last one focused on the Po Valley area with a spatial resolution of 5 km. The model employs the RRTM longwave radiation scheme and the Goddard shortwave radiation scheme, the Noah land surface model, the Morrison double moment microphysics scheme and the Grell 3D ensemble cumulus.

Initial and boundary conditions were obtained from the ECMWF analysis fields. Only the 5 km domain was compared to observations.

**Table 90.1** PBL schemes used in the analysis

| PBL scheme | Unstable PBL | Entrainment treatment | PBL Top | Surface layer scheme |
|---|---|---|---|---|
| YSU – Yonsei University PBL [3] | Parabolic K profile | Explicit term | From critical bulk *Ri* | MM5 similarity theory |
| MYJ – Mellor Yamada Janjic PBL [4] | K from prognostic TKE | Part of PBL mixing | From TKE | Eta similarity theory |
| ACM2- Asymmetrical Convective Model version 2 [5] | Non-local mixing up, local-K mixing down | Part of PBL mixing | From critical bulk *Ri* | MM5 similarity theory |
| UW – University of Washington Moist Turbulence Model [6] | K from diagnostic TKE | Explicit term | From critical bulk *Ri* | Eta similarity theory |
| MRF – Medium Range Forecast Model [7] | Parabolic K profile | Part of PBL mixing | From critical bulk *Ri* | MM5 similarity theory |

## 90.3 Results and Discussion

Model results were compared against a set of ground meteorological stations as well as vertical profiles by balloon soundings and ceilometer data.

Table 90.2 shows statistical indices for temperature, mixing ratio and wind speed in a set of ground meteorological sites.

All the simulations reveal a similar behavior. However, the best performances in terms of bias and anomaly correlation are reported for ACM2.

The mixing ratio is well reproduced by all schemes, while temperature and wind speed show higher BIAS.

As an example, the PBL hourly evolution for February 11th is reported in Fig. 90.1. As it can be seen from this figure, there are substantial differences between

**Table 90.2** BIAS, Root Mean Square Error (RMSE) and Anomaly Correlation (AC) indexes of temperature, mixing ratio and wind speed for five PBL schemes in the Po Valley stations. The best performances are in bold

| | ACM2 | MRF | MYJ | UW | YSU |
|---|---|---|---|---|---|
| Temperature (K) | | | | | |
| BIAS | **0.617** | 0.870 | 0.876 | 0.911 | 0.776 |
| RMSE | 3.467 | 3.648 | **3.285** | 3.360 | 3.447 |
| AC | **0.832** | 0.822 | 0.830 | 0.828 | **0.832** |
| Mixing ratio (g/kg) | | | | | |
| BIAS | 0.041 | **−0.026** | 0.278 | 0.265 | 0.122 |
| RMSE | **0.811** | 0.848 | 0.966 | 0.933 | 0.832 |
| AC | **0.852** | 0.842 | 0.799 | 0.810 | 0.847 |
| Wind speed (m/s) | | | | | |
| BIAS | **0.354** | 0.381 | 0.776 | 0.768 | 0.457 |
| RMSE | 2.916 | 2.921 | 2.870 | **2.905** | 2.935 |
| AC | 0.465 | 0.460 | 0.501 | **0.490** | 0.464 |

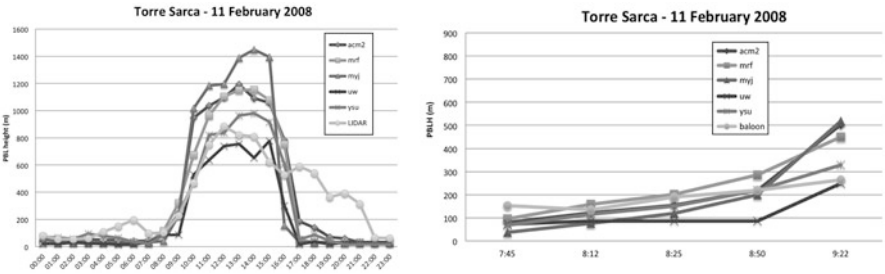


**Fig. 90.1** Comparison between five PBL schemes and LIDAR data (*left*) and balloon soundings (*right*) for February 2008, 11th

the five parameterizations. YSU and UW schemes give lower values than MYJ, MRF and ACM2. In particular, ACM2 and MYJ schemes show the most pronounced hourly cycle.

In the early hours of the day there is closer agreement between models and among these and both Lidar and balloon observations. Deviation between simulated and observed grows with time. Indeed, the daytime development of PBL appears to be too fast in all simulations. Largest overestimation exists for MRF, MYJ and ACM2. The best performances in reconstructing the PBL height can be shown in the YSU scheme in both Lidar and balloon comparisons. Moreover all schemes show a too rapid decrease of PBL that collapses to the night-time value by 5 PM, while Lidar data seem to show a smoother profile.

However, the problem of the afternoon turbulence and PBL decay is still under investigation. When the solar forcing decreases, the atmosphere reaches a neutral temperature lapse rate. Under these conditions, the lower atmosphere still experiences turbulence, but its actual mixing capability is strongly reduced. Aerosols lifted during strong convection keep aloft, but new aerosols produced at ground start accumulating in the surface layer. The effect of the smooth decay observed in Lidar data (Fig. 90.1) is due to the aerosol falling down after the slackening of solar forcing, although the thermodynamical situation indicates that turbulence is very low. As a consequence the comparison between models and observations in this period becomes particularly hard.

## 90.4 Conclusions

The WRF model has been applied over the Po Valley area and compared against measurement stations, vertical profiles by balloon soundings and Lidar data in order to assess the skill of the meteorological model in reproducing PBL structure and evolution. Five PBL schemes have been tested for a 5 km simulation.

Vertical profiles of aerosol distribution and Lidar measurements were collected in the area of Milan together with surface temperature, mixing ratio and wind speed of different meteorological sites.

Results show a good agreement between simulations and observations for mixing ratio, while model reveals higher bias in reconstructing temperature, wind speed and planetary boundary layer height. The best performances in reconstructing PBL height are highlighted for YSU scheme, while other meteorological fields are better reproduced by ACM2 parameterization. However, the afternoon transition still represents a hard test bed for models and techniques aimed to the determination of the PBL height.

**Acknowledgments** RSE contribution to this work has been financed by the Research Fund for the Italian Electrical System under the Contract Agreement between RSE S.p.A. and the Ministry of Economic Development – General Directorate for Nuclear Energy, Renewable Energy and Energy Efficiency in compliance with the Decree of March 8, 2006.

## References

1. Marcazzan GM, Vaccaro S, Valli G, Vecchi R (2001) Characterisation of PM10 and PM2.5 Particulate matter in the ambient air of Milan (Italy). Atmos Environ 35:4639–4650
2. Minesis C, Zhang Y (2010) An examination of sensitivity of WRF/Chem predictions to physical parameterizations, horizontal grid spacing, and nesting options. Atmos Res 97:315–334
3. Hong S-Y, Noh Y, Dudhia J (2006) A New vertical diffusion package with an explicit treatment of entrainment processes. Mon Weather Rev 134:2318–2341
4. Janjic ZI (1994) The step-mountain Eta coordinate model: further developments of the convection, viscous sublayer, and turbulence closure schemes. Mon Weather Rev 122:927–945
5. Pleim JE (2007) A combined local and nonlocal closure model for the atmospheric boundary layer. Part I: model description and testing. J Appl Meteorol Climatol 46:1383–1395. doi:10.1175/JAM2539.1
6. Bretherton CS, Park S (2009) A New moisture parameterization in the community atmosphere model. J Clim 22:3422–3448. doi:10.1175/2008JCLI2556.1
7. Hong S-Y, Pan H-L (1996) Nonlocal boundary layer vertical diffusion in a medium-range forecast model. Mon Weather Rev 124:2322–2339
8. Ferrero L, Perrone MG, Petraccone S, Sangiorgi G, Ferrini BS, Lo Porto C, Lazzati Z, Cocchi D, Bruno F, Greco F, Riccio A, Bolzacchini E (2010) Vertically-resolved particle size distribution within and above the mixing layer over the Milan metropolitan area. Atmos Chem Phys 10:3915–3932
9. Angelini F, Barnaba F, Landi TC, Caporaso L, Gobbi GP (2009) Study of atmospheric aerosols and mixing layer by LIDAR. Radiat Prot Dosim 137(3–4):275–279. doi:10.1093/rpd/ncp219

# Chapter 91
# Surface Ozone Variability in Synoptic Pattern Perspectives

**Hyun Cheol Kim, Heesu Choi, Fantine Ngan, and Pius Lee**

**Abstract** Synoptic weather pattern plays an important role in regional air quality. It influences strongly the daily maximum surface level ozone concentrations. We utilize Spatial Synoptic Classification methodology, surface ozone simulations from the NOAA National Air Quality Forecast Capability and observations from the US EPA Air Quality System, to investigate the behavior of surface ozone and air quality model's performance in different synoptic weather patterns. This study was conducted for the following six air quality air-shed regions: California (CA), Michigan Lake (MI), Ohio River Valley (OV), Northeastern (NE), Southeastern (SE), and Texas (TX), during the ozone season (May to September) in years 2009–2011. Based on air mass' thermal characteristics and origins, the SSC methodology provides six types of air mass classifications: Dry Polar (DP), Dry Moderate (DM), Dry Tropical (DT), Moisture Polar (MP), Moisture Moderate (MM), and Moisture Tropical (MT). Results show distinct behaviors of ozone's magnitude and model's performance among the various air mass types, implying the impact of synoptic weather patterns to regional air quality, and NAQFC's success in reproducing these patterns. The MT and DT air mass types are the most important types conducive to high surface ozone episodes throughout their occurrence frequency and high

H.C. Kim (✉) • F. Ngan
Air Resources Laboratory, NOAA, College Park, MD, USA

Cooperative Institute for Climate and Satellites, University of Maryland, College Park, MD, USA
e-mail: hyun.kim@noaa.gov; fantine.ngan@noaa.gov

H. Choi
Air Resources Laboratory, NOAA, College Park, MD, USA

Environmental Science and Ecological Engineering, Korea University, Seoul, South Korea
e-mail: miso-hun@korea.ac.kr

P. Lee
Air Resources Laboratory, NOAA, College Park, MD, USA
e-mail: Pius.Lee@noaa.gov

D. Steyn and R. Mathur (eds.), *Air Pollution Modeling and its Application XXIII*,
Springer Proceedings in Complexity, DOI 10.1007/978-3-319-04379-1_91,

ozone production efficiency, respectively. The MT air mass also shows highest in both mean bias and root mean square error, implying the high uncertainty in model performance due to cloudy or unstable atmospheric conditions.

## 91.1 Introduction

Understanding the relationship between synoptic weather pattern and regional air quality is important to estimate the contribution of meteorology in air pollution event occurrences. Change of synoptic weather pattern often accompanies dramatic change of air mass' characteristics, especially in temperature, relative humidity, and wind fields. These three state variables among others govern the advection, dilution, photolysis, and removal processes of air pollutants. For instance, temperature affects rates of chemical reactions and yields of biogenic emissions, and relative humidity, associated with cloud fraction, is an indicator of surface radiances that affect photolysis rate. Wind speed and directions are both important in diluting or accumulating pollutants and their precursors, as well as in mixing and transporting them under meteorological phenomena of various temporal and spatial length scales.

There have been numerous studies to use the classification of meteorological fields to investigate the impact of meteorology on air quality. The principal component analysis is one of the two popular approaches that examines the association of individual weather variable's pattern to pollution level [1]. On the other hand, the weather typing approach uses analyses based on characteristics of varying air mass types. The Spatial Synoptic Classification (SSC; [2], http://sheridan.geog.kent.edu/ssc.html) provides daily synoptic weather classification, and is widely used for numerous studies, such as ozone-related morbidity, urban heat island, snow trends, and air quality studies [3, 4].

The goal of this study is to investigate the relationship between synoptic weather patterns and surface ozone concentration. We focus on the following questions: (1) what weather type is the most dominant contributor to high ozone episodes in terms of "frequency", (2) what weather type is the most effective contributor to high ozone episodes in terms of "ozone production efficiency", and (3) if there is specific air mass type skews NAQFC's performance. The further application of this study is to improve regional air quality models such as NAQFC in anticipation of climate change.

## 91.2 Data and Methodology

The SSC utilizes multiple meteorological variables, such as temperature, dew point depression, mean cloud cover, mean sea level pressure, diurnal temperature range, and diurnal dew point range, to classify the regional weather types into six categories: Dry Polar (DP), Dry Moderate (DM), Dry Tropical (DT), Moisture Polar (MP), Moisture Moderate (MM), and Moisture Tropical (MT). In addition,

Transition (Ts) is defined as a day in which a frontal passage occurred and thus cannot be classified into a single air mass type. We also adopt NAQFC, a joint effort between NOAA and the U.S. EPA, as our tool to provide advance notice for future air pollution events [5]. It couples the Weather Forecasting and Research (WRF) non-hydrostatic mesoscale model (NMM) [6], and the Community Multi-scale Air Quality (CMAQ) modeling system [7]. CMAQ uses aerosol module version 4 (AERO-4) and Carbon Bond version CB05 gas-phase chemical mechanism. Hourly surface ozone concentrations are obtained from the EPA Technology Transfer Network (TTN) Air Quality System (AQS). Locations of around 1,100 surface ozone measurement sites are compared with collocating meteorological monitoring sites that contributed to the SSC data set to determine the daily condition of SSC weather types.

## 91.3 Results and Discussion

According to Byun et al. [8], we have defined six air quality air-shed regions as California (CA), Michigan Lake (MI), Northeast (NE), Ohio River Valley (OV), Southeast (SE), and Texas (TX). Figure 91.1 shows locations of the six air-sheds and SSC sites, and Table 91.1 shows the occurrence frequency of SSC weather types in six regions during the study period. DM and MT weather types are the two dominant types in most of regions, except California and Texas. Figure 91.2a, c show occurrence frequency distributions of daily maximum 8-h zone in NE region for

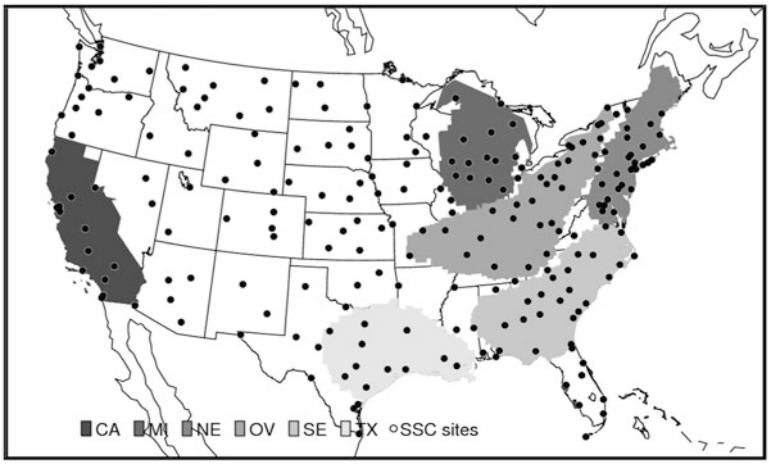


**Fig. 91.1** Geographical definition of six air quality air-sheds, California (CA), Michigan Lake (MI), North East (NE), Ohio Valley (OV), South East (SE), and Texas (TX), and locations of SSC sites (*black circles*). The filled *black circles* depict locations of the monitoring sites contributing to SSC data set

**Table 91.1** Occurrence frequencies of SSC weather types in six air quality air-shed regions

| | CA | MI | NE | OV | SE | TX |
|---|---|---|---|---|---|---|
| DM | 39.4 % | 31.0 % | 26.7 % | 25.9 % | 18.2 % | 10.2 % |
| DP | 4.1 % | 10.8 % | 6.0 % | 7.1 % | 1.6 % | 0.7 % |
| DT | 19.6 % | 3.2 % | 7.0 % | 4.5 % | 11.4 % | 23.8 % |
| MM | 13.7 % | 16.6 % | 20.9 % | 20.3 % | 13.1 % | 8.2 % |
| MP | 13.4 % | 8.1 % | 4.1 % | 4.4 % | 0.9 % | 0.3 % |
| MT | 3.1 % | 22.5 % | 28.6 % | 30.6 % | 49.4 % | 51.4 % |
| Ts | 6.7 % | 7.7 % | 6.7 % | 7.1 % | 5.4 % | 5.5 % |

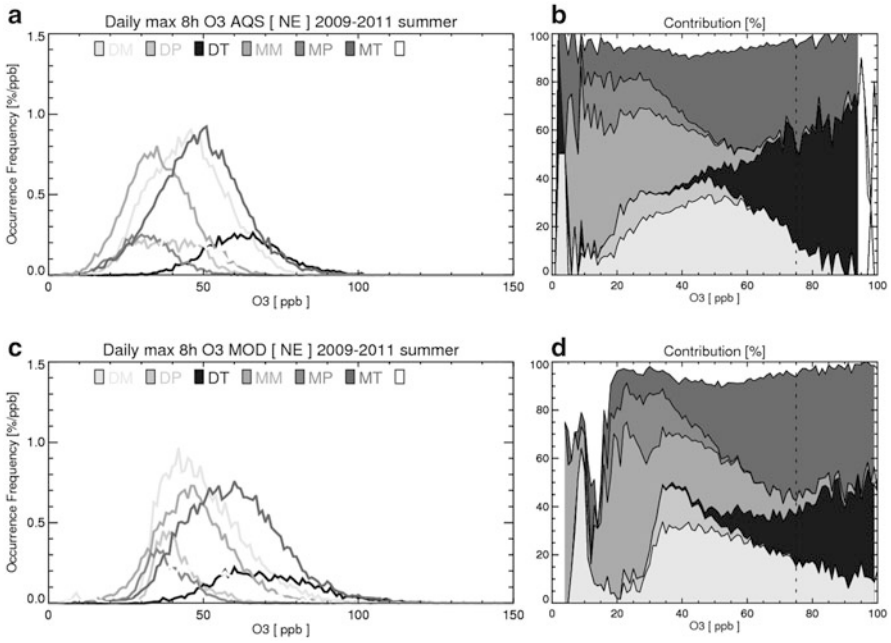


**Fig. 91.2** Occurrence frequency distributions (**a** & **c**) and contribution percentages (**b** & **d**) of daily max 8 h ozone in six SSC air mass types in northeastern US region from AQS surface observations (*upper*) and from NAQFC model (*lower*)

varying SSC types from AQS measurements and from NAQFC model simulations. Contributing percentages of SSC weather type for each ozone level are also shown in Fig. 91.2b, d. It is clear that MM, MP, and DP SSC types are associated with lower level ozone concentrations while ozone exceedance, defined as exceeding the U.S. EPA daily maximum 8-h averaged ozone concentration of 75-ppb, mostly happened during MT and DT SSC weather types. These patterns are generally well reproduced by NAQFC. Table 91.2 shows mean bias and RMSE of daily max 8-h ozone for each SSC weather types and air-shed regions. In most regions, moist SSC types (MM, MP, and MT) have higher mean bias and RMSE, implying model's performance

**Table 91.2** Mean bias (left) and RMSE (right) of daily max 8 h ozone for each SSC weather types and air-shed regions (unit:ppb)

| | Mean bias | | | | | | RMSE | | | | | |
|---|---|---|---|---|---|---|---|---|---|---|---|---|
| | CA | MI | NE | OV | SE | TX | CA | MI | NE | OV | SE | TX |
| DM | 3.98 | 4.18 | 5.08 | 4.88 | 9.75 | 2.35 | 14.59 | 11.02 | 11.24 | 11.49 | 14.15 | 14.97 |
| DP | 0.77 | 3.60 | 4.28 | 4.44 | 5.66 | 1.60 | 10.33 | 10.56 | 9.41 | 10.41 | 9.24 | 7.13 |
| DT | 3.98 | 4.43 | 6.78 | 5.96 | 11.30 | 10.53 | 15.15 | 13.00 | 12.86 | 11.18 | 14.36 | 16.70 |
| MM | 6.73 | 9.70 | 11.27 | 9.09 | 15.37 | 8.99 | 15.57 | 13.48 | 14.99 | 14.45 | 17.68 | 15.76 |
| MP | 7.53 | 7.75 | 6.72 | 9.70 | 14.70 | 4.99 | 14.51 | 12.12 | 10.70 | 12.86 | 16.69 | 9.02 |
| MT | 5.80 | 10.29 | 10.80 | 5.74 | 14.40 | 11.40 | 17.00 | 14.64 | 14.81 | 14.24 | 16.93 | 16.28 |

**Table 91.3** Contribution percentages of three SSC weather types to over-75 ppb ozone episodes (left), and Percentages of high ozone (over 75 ppb) episodes in three SSC weather types (right)

| | Contribution (a) | | | | | | Frequency (b) | | | | | |
|---|---|---|---|---|---|---|---|---|---|---|---|---|
| | CA | MI | NE | OV | SE | TX | CA | MI | NE | OV | SE | TX |
| DT | 56 % | 22 % | 50 % | 24 % | 46 % | 57 % | 16.7 % | 6.6 % | 16.7 % | 6.9 % | 4.5 % | 9.4 % |
| MT | 3 % | 58 % | 37 % | 46 % | 6 % | 18 % | 10 % | 2.4 % | 3.2 % | 2.0 % | 0.6 % | 1.0 % |
| DM | 29 % | 18 % | 9 % | 25 % | 25 % | 17 % | 6.1 % | 0.7 % | 0.8 % | 1.4 % | 1.8 % | 5.7 % |

is clearly sensitive to the regions associated with cloudy or unstable atmospheric conditions. Table 91.3a shows percentages of SSC weather types that contributed to frequent ozone exceedances. In CA, NE, SE and TX regions, DT weather type is responsible for almost half of the ozone exceedances while MT type is a top contributor in MI and OV regions. Table 91.3b shows chances of ozone exceedance for each of the SSC weather types. For CA, the chance of ozone exceedance is 16.7 % during DT weather type, which is significantly higher than other weather types, such as MT (10 %) and DM (6.1 %). DT weather type is most efficient type in high ozone production in all regions.

## 91.4 Conclusive Remark

We utilized the SSC synoptic weather classification data to investigate the relationship between meteorology and surface ozone concentration, in six air quality air-shed regions. Analyses on daily maximum 8–hour ozone showed that MT and DT weather types are the two mostly contributing air masses associated with high ozone concentration episodes, in terms of occurrence frequency and ozone production efficiency, implying the association of air mass' thermal characteristics in the formation of high ozone concentrations. MT is also associated with the worst NAQFC model performance, showing highest mean bias and RMSE. DT shows highest correlation with high ozone episodes, implying that any change of DT weather type's occurrence in an anticipated climate change scenario may direct the pursuit of future regional air quality development for all regions.

## References

1. Ngan F, Byun DW (2011) Classification of weather patterns and associated trajectory analysis of high ozone episodes in Houston during the 2005/2006 TexAQS-II. J Appl Meteorol Climatol 50:485–499
2. Sheridan SC (2002) The redevelopment of a weather-type classification scheme for North America. Int J Climatol 22:51–68
3. Hu Y, Chang ME, Russell AG, Odman MT (2010) Using synoptic classification to evaluate an operational air quality forecasting system in Atlanta. Atmos Pollut Res 1:280–287
4. Lee CC, Ballinger TJ, Domino NA (2012) Utilizing map pattern classification and surface weather typing to relate climate to the air quality index in Cleveland. Ohio Atmos Environ 63:50–59
5. Chai T, Kim HC, Lee P, Tong D, Pan L, Tang Y, Huang J, McQueen J, Tsidulko M, Stajner I (2013) Evaluation of the United States national air quality forecast capability experimental real-time predictions in 2010 using air quality system ozone and NO2 measurements. Geosci Model Dev Discuss 6:2609–2654
6. Janjic ZI (2003) A nonhydrostatic model based on a new approach. Meteorog Atmos Phys 82:271–285
7. Byun DW, Schere KL (2006) Review of the governing equations, computational algorithms, and other components of the Models-3 Community Multiscale Air Quality (CMAQ) modeling system. Appl Mech Rev 59:51e77
8. Byun DW, Coauthors (2011) Utilizing conceptual models of summer high ozone events and mid-latitude cyclones to improve air quality forecasting. The 91th AMS annual meeting, Seattle, WA, USA

# Chapter 92
# WRF-Chem Model Sensitivity Analysis to Chemical Mechanism Choice

**A. Balzarini, L. Honzak, G. Pirovano, G.M. Riva, and R. Zabkar**

**Abstract** A comparison between two WRF-Chem simulations has been performed in the framework of the AQMEII modeling initiative for the calendar year 2010. Model configurations shared the same physics options, but different chemical parameterizations were selected. The first run adopted RADM2-MADE/SORGAM chemical mechanisms, whereas the second one employed the CBMZ-MOSAIC chemical option. Comparisons between two simulations show that CMBZ is higher than RADM2 for gas concentrations. On the contrary, MADE-SORGAM reproduces higher aerosol values than MOSAIC, especially over land. The same behaviour is observed in comparison against ground – based measurements. Both simulations underestimate observed values of NOx and PM2.5.

## 92.1 Introduction

Online-coupled meteorology and chemistry models are becoming more and more popular in air quality modeling applications as they allow achieving a significant reduction of inconsistency between meteorological and chemical processes as well as taking into account the influence of feedback effects, mainly related to aerosol load [1]. Nevertheless, an accurate simulation of feedback effects requires a reliable

A. Balzarini (✉) • G. Pirovano • G.M. Riva
Sustainable Development and Energy Sources Department, Ricerca sul Sistema Energetico (RSE S.p.A.), via Rubattino 54, Milan, Italy
e-mail: alessandra.balzarini@rse-web.it

L. Honzak
Center of Excellence "SPACE-SI", Aškerčeva 12, Ljubljana, Slovenia

R. Zabkar
Center of Excellence "SPACE-SI", Aškerčeva 12, Ljubljana, Slovenia

Faculty of Mathematics and Physics, University of Ljubljana, Jadranska 19, Ljubljana, Slovenia

D. Steyn and R. Mathur (eds.), *Air Pollution Modeling and its Application XXIII*, Springer Proceedings in Complexity, DOI 10.1007/978-3-319-04379-1_92,

reconstruction of the main processes driving the fate of the atmospheric aerosol. However, even recent air quality modeling studies highlight significant difficulties in correctly reproducing aerosol processes [2]. Among others, a key role is played by chemical mechanisms affecting both aerosol processes as well as the evolution of gas phase precursors.

To this aim, a sensitivity analysis of the WRF-Chem model to the chemical mechanism choice has been performed in the framework of the AQMEII modeling initiative (http://aqmeii.jrc.ec.europa.eu/) for the calendar year 2010.

## 92.2 Model Set Up

WRF-Chem model has been applied over Europe for the whole year 2010, adopting a horizontal resolution of 23 km. The model has been driven by the input data set provided in the framework of the exercise, including the TNO-MACC anthropogenic and FMI biomass burning emission inventory, and by archived ECMWF meteorological fields. Chemical boundary conditions has also been provided by MACC.

Model configurations shared the same physical parameterizations, namely: YSU PBL scheme [3], Noah LSM [4], Morrison microphysics [5], RRTMG radiation schemes [6], and G3 cumulus scheme [7]. As for chemistry, the first run adopted RADM2 gas phase mechanism [8] and MADE-SORGAM aerosol module [9, 10], whereas CBM-Z [11] and MOSAIC [12] modules were selected for the second run.

## 92.3 Results

As an example, Fig. 92.1 shows NOx monthly mean results in January 2010 for both chemical mechanisms. NOx concentrations follow the same general pattern in the two model applications, but CBMZ simulates higher values in Northern and Eastern Europe.

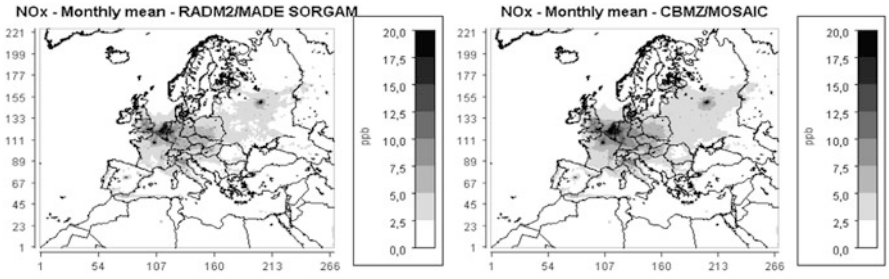


**Fig. 92.1** Monthly mean of NOx concentrations in January 2010 for RADM2/MADE-SORGAM (*left*) and CBMZ/MOSAIC (*right*)

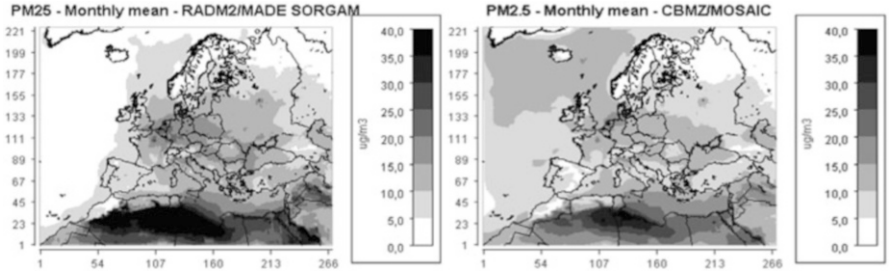


**Fig. 92.2** Monthly mean of PM2.5 concentrations in January 2010 for RADM2/MADE-SORGAM (*left*) and CBMZ/MOSAIC (*right*)

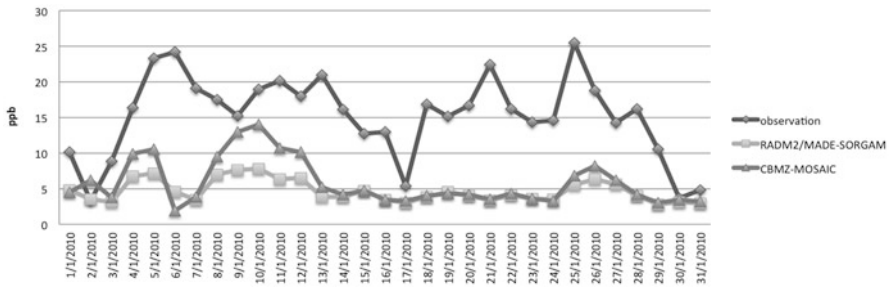


**Fig. 92.3** Time series of daily NOx concentrations at CH0002R station (Switzerland) for January 2010

The same results can be seen in Fig. 92.2 for PM2.5 monthly mean concentrations. MADE-SORGAM reproduces higher concentrations over the land, especially in North Africa and Central Europe regions. On the contrary, MOSAIC is higher over the Atlantic Ocean and the Mediterranean Sea.

A thorough comparison of model performance have been performed against ground level observed data including both criteria pollutants collected at around 500 Airbase sites as well as PM composition data provided by EMEP network. For instance, Figs. 92.3 and 92.4 show time series of NOx and PM2.5 at CH0002R Airbase station (Switzerland) for January 2010.

Simulations underestimate both NOx and PM10 daily mean, however CBMZ generally performs better than RADM2 in reconstructing NOx concentrations. On the contrary, MADE-SORGAM is closer to the PM2.5 observed trend.

## 92.4 Conclusions

A comparison between two WRF-Chem simulations has been performed in the framework of the AQMEII modeling initiative for the calendar year 2010. Model configurations shared the same physics options, but different chemical

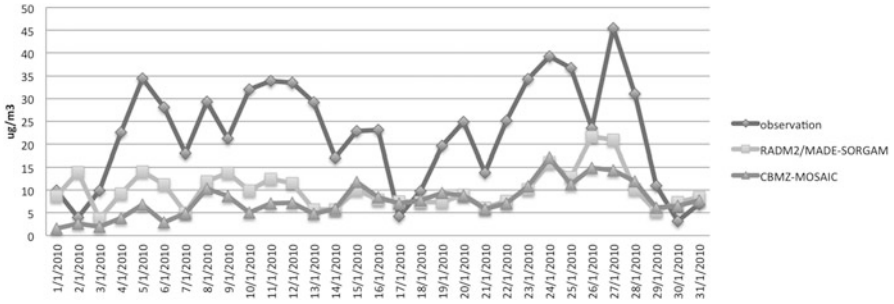


**Fig. 92.4** Time series of daily PM2.5 concentrations at CH0002R station (Switzerland) for January 2010

parameterizations were selected. The first run adopted RADM2/MADE-SORGAM chemical mechanisms, whereas the second one employed the CBMZ/MOSAIC chemical option.

Comparisons between two simulations show that CMBZ is higher than RADM2 for gas concentrations. On the contrary, MADE-SORGAM reproduces higher values than MOSAIC, especially over land.

The same behaviour is observed in comparing against ground – based measurements. In particular, simulations underestimate observed values of NOx and PM2.5.

**Acknowledgments** RSE contribution to this work has been financed by the Research Fund for the Italian Electrical System under the Contract Agreement between RSE S.p.A. and the Ministry of Economic Development – General Directorate for Nuclear Energy, Renewable Energy and Energy Efficiency in compliance with the Decree of March 8, 2006. The Centre of Excellence for Space Sciences and Technologies SPACE-SI is an operation partly financed by the European Union, European Regional Development Fund and Republic of Slovenia, Ministry of Higher Education, Science, Sport and Culture.

## References

1. Zhang Y, Wen X-Y, Jang CJ (2010) Simulating chemistry – aerosol – cloud – radiation – climate feedbacks over the continental U.S. Using the online-coupled weather research forecasting model with chemistry (WRF/Chem). Atmos Environ 44:3568–3582. doi:10.1016/j.atmosenv.2010.05.056
2. Solazzo E et al (2012) Operational model evaluation for particulate matter in Europe and North America in the context of AQMEII. Atmos Environ 53:75–92. doi:10.1016/j.atmosenv.2012.02.045
3. Hong S-Y, Noh Y, Dudhia J (2006) A new vertical diffusion package with an explicit treatment of entrainment processes. Mon Weather Rev 134:2318–2341
4. Chen F, Dudhia J (2001) Coupling an advanced land surface–hydrology model with the Penn state–NCAR MM5 modeling system. Part I: model implementation and sensitivity. Mon Weather Rev 129:569–585

5. Morrison H, Thompson G, Tatarskii V (2009) Impact of cloud micrpohysics on the development of trailing stratiform precipitation in a simulated squall line: comparison of one- and two-moment schemes. Mon Weather Rev 137:991–1007. doi:10.1175/2008MWR2556.1
6. Iacono MJ, Delamere JS, Mlawer EJ, Shephard MW, Clough SA, Collins WD (2008) Radiative forcing by long-lived greenhouse gases: calculations with the AER radiative transfer models. J Geophys Res 113, D13103. doi:10.1029/2008JD009944
7. Grell GA, Devenyi D (2002) A generalized approach to parameterizing convection combining ensemble and data assimilation techniques. Geophys Res Lett 29(14):1693
8. Stockwell WR, Middleton P, Chang JS, Tang X (1990) The second generation regional acid deposition model chemical mechanism for regional air quality modeling. J Geophys Res 95:16343–16367
9. Ackermann IJ, Hass H, Memmesheimer M, Ebel A, Binkowski FS, Shankar U (1998) Modal aerosol dynamics model for Europe: development and first applications. Atmos Environ 32(17):2981–2999
10. Schell B, Ackermann IJ, Hass H, Binkowski FS, Ebel A (2001) Modeling the formation of secondary organic aerosol within a comprehensive air quality model system. J Geophys Res 106:28275–28293
11. Zaveri RA, Peters LK (1999) A new lumped structure photochemical mechanism for large-scale applications. J Geophys Res 104(D23):30,387–30,415
12. Zaveri R, Easter RC, Fast JD, Peters LK (2008) Model for Simulating Aerosol Interactions and Chemistry (MOSAIC). J Geophys Res 113, D13204. doi:10.1029/2007JD008782

# Chapter 93
# Assimilation of Satellite Oceanic and Atmospheric Products to Improve Emission Forecasting

**Daniel Q. Tong, Hang Lei, Li Pan, Tianfeng Chai, Hyuncheol Kim, Pius Lee, Rick Saylor, Menghua Wang, and Shobha Kondragunta**

**Abstract** Satellite data presents an unprecedented opportunity to improve emission inventories at a near-real-time pace. Here we demonstrate how to utilize satellite oceanic and atmospheric products to improve emission forecasting. First, we present the development and validation of a global high resolution marine isoprene emission product. Isoprene emission is calculated from NOAA global weather forecasting

D.Q. Tong (✉)
NOAA Air Resources Laboratory, College Park, MD, USA

George Mason University, Fairfax, VA, USA

Cooperative Institute of Climate and Satellite, University of Maryland, College Park, MD, USA
e-mail: Daniel.Tong@noaa.gov

H. Lei
NOAA Air Resources Laboratory, College Park, MD, USA

Center for Spatial Information Science and Systems, George Mason University, Fairfax, VA, USA
e-mail: Hang.Lei@noaa.gov

L. Pan • T. Chai • H. Kim
NOAA Air Resources Laboratory, College Park, MD, USA

Cooperative Institute of Climate and Satellite, University of Maryland, College Park, MD, USA
e-mail: Li.Pan@noaa.gov; Tianfeng.Chai@noaa.gov; hyun.kim@noaa.gov

P. Lee
NOAA Air Resources Laboratory, College Park, MD, USA
e-mail: pius.lee@noaa.gov

R. Saylor
Atmospheric Turbulence and Diffusion Division, NOAA Air Resources Laboratory, College Park, MD, USA
e-mail: rick.saylor@noaa.gov

M. Wang • R. Kondragunta
NOAA National Environmental Satellite, Data, and Information Services, College Park, MD, USA
e-mail: Menghua.Wang@noaa.gov; shobha.kondragunta@noaa.gov

D. Steyn and R. Mathur (eds.), *Air Pollution Modeling and its Application XXIII*,
Springer Proceedings in Complexity, DOI 10.1007/978-3-319-04379-1_93,

data and Chlorophyll-a and light attenuation rate at 490 nm (K490) data derived from the Moderate Resolution Imaging Spectrometer (MODIS) aboard Aqua. The emission product is validated with isoprene measurements from field campaigns. In the second case, nitrogen dioxide ($NO_2$) data from the EPA Air Quality System (AQS) and the Ozone Monitoring Instrument (OMI) are used to examine the long-term trends in nitrogen oxides ($NO_x$) emissions for the NOAA National Air Quality Forecasting Capability (NAQFC). Comparing of summertime $NO_x$ data from OMI, NAQFC and AQS over New York between 2005 and 2011 shows a similar reduction level from all datasets (33 % reduction from 2005 to 2011), but OMI and AQS agree better while NAQFC emission inventories fail to catch the gradual progression of emission reduction. These case studies, in addressing various aspects of emission uncertainty, collectively demonstrate that satellite remote sensing can play an important role in improving emission forecasting and, hopefully, air quality predictions.

## 93.1 Introduction

Emission data are a key input to air quality forecasting, or chemical weather forecasting, an important air quality application to predict the chemical status and trend of the ambient air. Regardless of many recent improvements (e.g., Granier et al. 2011), emission modeling remains challenging due to the complexity of the problem and the inherent limitations of the current approaches used to compile emission inventories. In light of these inherent limitations, it has been proposed that near-real-time (NRT) data can be used to improve the accuracy of emission data [1, 2]. While in-situ measurements, such as the Continuous Emission Monitoring (CEMs) data, are being used to update annual power plant emissions routinely, various satellite products also present unprecedented opportunities for emission modelers to quantify unknown emissions or update existing inventories more rapidly. To demonstrate how satellite products can be used in emission modeling, we present here two case studies that utilize satellite atmospheric, land and ocean data to: (1) estimate global marine isoprene emissions from phytoplankton; and (2) verify emission updates of nitrogen oxides ($NO_x$).

## 93.2 Methodology

### *93.2.1 Global Marine Isoprene Emission*

The emission rate (vertical flux) of marine isoprene ($E_{iso}$) is calculated from the mass transfer between the gas-water interface [3]:

$$\mathrm{Eiso} = \mathrm{S}^{*}\mathrm{H}_{\max}{}^{*}\,[Chl-a]^{*}\,\mathrm{f}_{\mathrm{iso}}{}^{*}\int_{0}^{\mathrm{H}_{\max}} \mathrm{p}\;\mathrm{dh} \tag{93.1}$$

where S is the surface area of the grid box ($m^2$), $H_{max}$ is the height of the euphotic zone (m), [Chl-a] is the concentration of chlorophyll-a (mg $m^{-3}$), $f_{iso}$ is the fraction of the produced isoprene that is emitted into the atmosphere, p is the normalized isoprene production rate (μmole isoprene (gram chlorophyll-a)$^{-1}$ $h^{-1}$), and h is the downward distance from the ocean surface (m). The height of the euphotic zone is defined as the depth of the seawater column in which isoprene production can occur. It is calculated using the Beer-Lambert's Law [3]. Hourly values of surface irradiance $I_0$ are obtained from the NOAA Global Forecasting System (GFS). The diffuse attenuation coefficient $K_{490}$ is provided by MODIS using an empirical algorithm [4], which has been improved recently by Wang et al. [5] for both open oceans and coastal regions.

### *93.2.2 OMI Observation of $NO_x$ Trend over Metropolitan Areas*

Timely update of $NO_x$ NEIs is often difficult through the conventional emission approach because it is very time consuming to compile NEIs. To understand the effect of time lag on emission updates, we compare 5-year $NO_x$ trends from three independent data sources: OMI data, NAQFC emissions, and AQS data. The AQS data have been used as a surrogate to urban emissions since the morning rush-hour concentrations are predominantly influenced by emission loadings from heavy commuter traffic [6]. Therefore, all three data sources provide independent information of emission changes that could be intercomparable during a fixed time period. Ground $NO_x$ measurements are obtained from the EPA Air Quality System monitoring network. The model emissions data are extracted from the operational NAQFC simulations.

## 93.3 Results

### *93.3.1 Global Marine Isoprene Distribution*

Using the isoprene emission scheme, we estimate global hourly emission rate of isoprene emitted by phytoplankton in 2011 based on MODIS ocean color data and meteorology from NOAA GFS final reanalysis dataset. Figure 93.1 shows the spatial patterns for the marine isoprene emission in January, April, July, and October. It is noted that the marine isoprene emissions are sensitive to seasonal change. Similarly, there is a belt region of marine isoprene production along the southern and northern high latitudes. Overall, the estimated marine isoprene emissions captures the spatial and temporal features of marine biogeochemical cycles that are reported in previous studies [7, 8].

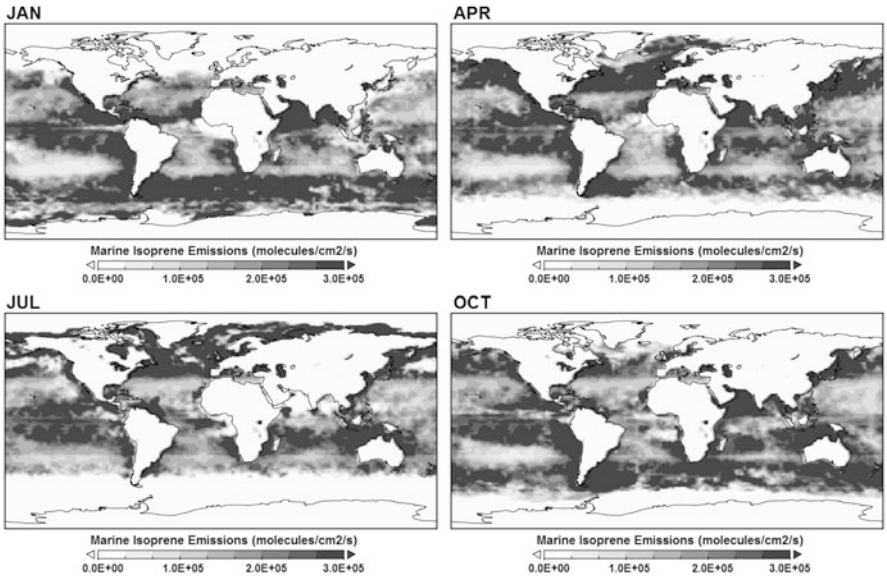


**Fig. 93.1** The spatial distribution of MODIS estimated isoprene emission products over ocean in January, April, July, and October

### *93.3.2 Validation of Marine Isoprene Emission Product*

Data validation is essential for assuring the quality of the proposed product. Figure 93.2 shows that the marine isoprene emission fluxes retrieved from satellite ocean color data basically capture the level of emission from the ocean. Although the flux values from satellite products are generally higher than from in-situ measurements, the difference is still in uncertainty range. The standard deviation is around 0.57, which indicates a good confidence of the comparison. The flux was calculated based on the assumption that isoprene concentrations in the marine air were zero. Therefore, the calculated values represent upper limits of marine isoprene emissions. In general, the satellite retrieved fluxes shows good agreement with field measurements.

### *93.3.3 Intercomparison of OMI, AQS and NAQFC $NO_x$ Emission Trend*

The emission data in NAQFC have been updated each year to keep up with the evolution of the emission trend, but such updates are often hindered by the availability of updated emission inventories and other relevant data. While the new emissions, when implemented in the NAQFC system, have considerably improve

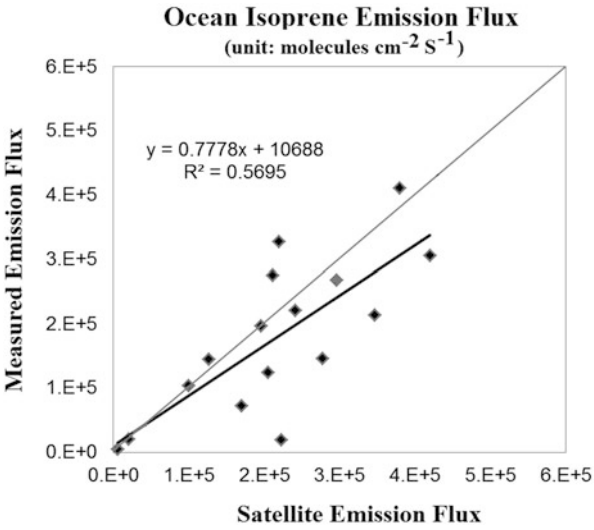


**Fig. 93.2** Comparison of MODIS-based products with field measurements (y-axis)

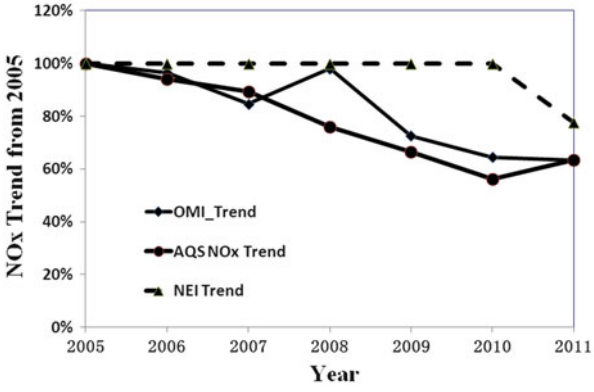


**Fig. 93.3** Intercomparison of summertime (July) $NO_x$ trends from NAQFC emission inventories, EPA AQS ground monitors and OMI $NO_2$ observations in New York City

forecasting performance, such emission updates have never been validated with independent data sources. We provide here some initial results of the three-member comparison of summertime $NO_x$ trend from 2005 to 2011 over the New York City (NYC) metropolitan area (Fig. 93.3). During this period, all three data sources show a similar reduction level over NYC, with the 2011 level being 33–34 % lower than that in 2005. Among the three, OMI and AQS agree better while NAQFC emission inventories fail to catch the gradual progression of emission reduction, although the latest update has caught up with the observed trends. The Intercomparison over NYC here has reinforced the results of prior forecasting evaluations, suggesting the CSAPR projects have captured the emission trends. The consistent trends in OMI $NO_2$ columns with trends in AQS $NO_2$ observations and $NO_x$ emissions inventory confirm the ability and application of OMI $NO_2$ retrievals for providing independent information on emission changes.

## 93.4 Conclusion

Satellite data presents an unprecedented opportunity to improve emission inventories at a near-real-time pace. We demonstrate here with two case studies how to utilize satellite oceanic and atmospheric products to improve and validate the estimation of global marine isoprene emission, and NOx emissions over the United States. By addressing various aspects of emission uncertainty, these works collectively demonstrate that satellite remote sensing can play an important role in future emission modeling works.

## References

1. Tong DQ, Lee P, Saylor RD (2012) New direction: the need to develop process-based emission forecasting models. Atmos Environ 47:560–561
2. Streets DG, Carmichael GR, de Foy B, Dickerson RR, Duncan BN, Edwards DP, Haynes JA, Henze DK, Houyoux MR, Jacob DJ, Krotkov NA, Lamsal LN, Liu Y, Lu Z, Martin RV, Pfister GG, Pinder RW, Wecht KJ (2013) Emissions estimation from satellite retrievals: a review of current capability. Atmos Environ 77:1011–1042
3. Gantt B, Meskhidze N, Kamykowski D (2009) A new physically-based quantification of marine isoprene and primary organic aerosol emissions. Atmos Chem Phys 9:4915–4927
4. Mueller JL (2000) SeaWiFS algorithm for the diffuse attenuation coefficient, K(490), using water-leaving radiances at 490 and 555 nm, SeaWiFS Postlaunch technical report series, 24–27 pp, NASA Goddard Space Flight Center, Greenbelt, Maryland
5. Wang M, Son S, Harding J LW (2009) Retrieval of diffuse attenuation coefficient in the Chesapeake Bay and turbid ocean regions for satellite ocean color applications. J Geophys Res 114, C10011. doi:10.1029/2009JC005286
6. Godowitch J, Pouliot G, Rao ST (2010) Assessing multi-year changes in modeled and observed NOx concentrations from a dynamic evaluation perspective. Atmos Environ 44:2894–2901
7. Mann KH, Lazier JRN (2006) Dynamics of marine ecosystems: biological-physical interactions in the oceans. Blackwell, Oxford. ISBN 1-4051-1118-6
8. Winder M, Cloern JE (2010) The annual cycles of phytoplankton biomass. Philos Trans R Soc B 365:3215–3226. doi:10.1098/rstb.2010.0125
9. Granier C, Bessagnet B, Bond T, D'Angiola A, van der Gon HG, Frost G, Heil A, Kainuma M, Kaiser J, Kinne S et al (2011) Evolution of anthropogenic and biomass burning emissions at global and regional scales during the 1980–2010 period. Clim Change. doi:10.1007/s10584-011-0154-1

## Questions and Answers

**Questioner Name:** Pavel Kishcha, Tel-Aviv U

**Q:** While comparing modeled AOD (with D.A.) with MODIS AOD, you found some discrepancy. Could this discrepancy be explained by the fact that MODIS crosses the CONUS twice a day, and other times the modeled AOD are based only on predicted aerosol concentrations? Also one should take into account

that the comparison was between a 24 h averaged modeled AOD with 2 snap shots of MODIS AOD?

**A:** Yes. We understood the time-averaging of the passes by Aqua and Terra into one single obs ingestion time at around 19:30Z caused some discrepancy. The treatment presented here represents a first step in chemical data assimilation for NAQFC. Tianfeng Chai talks after this talk will cover some aspect of a more frequent data-ingest in synchronization with the actual observation time. The other issue about running the model 24 h in forward mode without constraint is again related to the first issue that we are just starting to build a chemical data assimilation system that would gradually increase its observational ingestion frequency and timing representativeness.

**Questioner Name:** Heinke Schluenzen, U. Hamburg

**Q:** Can you determine emission rates dependent on the different kinds of plants (e.g. Oak species)? Further, is it possible to determine from satellite measurements the kind of organic emission and what amount of emissions (e.g. for isoprene)? Can an AQ forecast be reliably based on such a satellite-data based emission estimation or what is the measurement uncertainty?

**A:** Concerning species-specific emission speciation and rates, we were not as sophisticated as we could be. The BELD3 data does have tree species information and can be exploited to include tree-species specific rate and chemistry characterization. Your second question is very interesting. We have published a New Direction articles at Atmospheric Environment [1] to advocate a more dynamic emission modeling system to support air quality forecast by ingesting more near real time data such as satellite observations. The benefits are twofold: to update emission more rapidly and to look into emission uncertainty in data sources and emission algorithms. While our talk here only considers ocean phytoplankton emitted isoprene, which cannot be estimated from the traditional inventory-based approach, we believe this general methodology can be more widely applied to other emission sources.

# Chapter 94
# Assimilation and Forecasting Fine Aerosols Over North America in Summer 2012

**Mariusz Pagowski and Georg A. Grell**

**Abstract** In a study, we examine impact of assimilation in-situ measurements on the prediction of fine aerosol concentrations over North America in the summer of 2012. We use an online meteorology-chemistry model WRF-Chem and an assimilation system which includes the Gridpoint Statistical Intepolation (GSI) and an Ensemble Kalman Filter. We note large initial benefit of data assimilation and relatively quick deterioration of forecast verification scores with time. Causes for such deterioration include deficiencies of the initial state resulting from the lack of observations of the individual aerosol species and their vertical distribution, weaknesses of chemical and physical parameterizations and errors in emission sources.

Studies on environmental damage show that chronic exposure to particulates with diameters smaller than 2.5 μm (hereafter, particulate matter 2.5, or $PM_{2.5}$) is the single most critical factor affecting human mortality due to air pollution [4, 6]. Despite such importance, even forecasts of aggregated aerosols (such as $PM_{2.5}$ which includes particles of multiple chemical species and sizes) have poor skill that is routinely beaten by persistence (e.g. [3]).

Data assimilation has been an essential part of weather forecasting in all major meteorological centres and is also becoming more widespread in air quality applications. In meteorology, data assimilation has been traditionally applied to improve initial conditions. In air quality, inverse methods of data assimilation are also used to improve estimation of emission sources known to have large impact on the results and to contain significant errors. This manuscript is a continuation of our

M. Pagowski (✉) • G.A. Grell
Global Systems Division, NOAA Earth System Research Laboratory (ESRL), Boulder, CO, USA
e-mail: Mariusz.Pagowski@noaa.gov

D. Steyn and R. Mathur (eds.), *Air Pollution Modeling and its Application XXIII*,
Springer Proceedings in Complexity, DOI 10.1007/978-3-319-04379-1_94,

earlier work that demonstrated an advantage of EnKF over 3D-VAR assimilation for aerosol forecasting [5]. We refer the reader to a comprehensive review of the current status of data assimilation for air quality forecasting by Zhang et al. [8].

In the manuscript, we demonstrate an application of an Ensemble Kalman Filter (EnKF, [7]) to assimilate surface $PM_{2.5}$ observations with the WRF-Chem model [2] over the coterminous USA and southern Canada. The modeling period began on 30 May 2012, ended on 30 June 2012, and included a 5-day spin-up.

Surface $PM_{2.5}$ concentrations used in the assimilation are available through the US Environmental Protection Agency (EPA) AIRNow (http://www.airnow.gov/) Data Exchange program. This program provides hourly-averaged $PM_{2.5}$ concentrations at over 650 locations in the Unites States and Canada. Measurement error of Tapered Element Oscillating Microbalance (TEOM) instruments is calculated as $1.5\,\mu g\,m^{-3}$ plus an inaccuracy of 0.75 % in the species mass measurement. Standard meteorological upper air and surface observations were also assimilated.

Grid resolution of the simulations was set to 60 km. Initial and lateral boundary conditions for meteorology were obtained from the global GFS ensemble from National Centers of Environmental Prediction. The length of ensemble forecasts limited the extent of our forecasts to 9 h. Lateral boundary conditions for chemical species were obtained from a deterministic global model MOZART simulation. Emissions of $PM_{2.5}$ precursors are based on the U.S. EPA 1999 National Emissions Inventory (version 3) with updates of major electrical generating facilities to the observed July 2004 emissions from the Continuous Emissions Monitoring Network. Pollution by forest fires was derived from the Fire emission INventory from NCAR (FINN). Because of computational constraints imposed by ensemble simulations a simple and efficient aerosol module GOCART [1] was employed.

The 6-h assimilation cycle at 00z, 06z, 12z, and 18z used a 1-h assimilation window for $PM_{2.5}$ and a 3-h assimilation window for meteorological observations.

Impact of the assimilation is illustrated by comparison of free running forecasts (NoDA) that included assimilation of meteorological observations only and forecasts with the assimilation of AIRNow $PM_{2.5}$ and meteorological observations (EnKF). Verification statistics presented below were calculated over the period starting 00Z June 04 and ending 00Z July 01, 2012.

In Fig. 94.1, bias and temporal correlation of forecasts interpolated to AIRNow locations are shown for NoDA and EnKF experiments. In calculating these verification statistics, all available forecasts were matched with corresponding observations. Overall, the assimilation reduced the magnitude of negative model bias and improved temporal correlation. However, it is apparent that performance of the model and assimilation is markedly better over the eastern part of the continent. Deficient fire inventory and application of GOCART aerosol module, which lacks parameterization of production of nitrate and organic aerosols, contributed to the weaknesses of the simulations.

In Fig. 94.2, time series of bias and spatial correlation of forecasts are shown. A large positive impact of assimilation is evident but forecast quality deteriorates quickly. Causes for such deterioration include deficiencies of the initial state resulting from the lack of observations of the individual aerosol species and

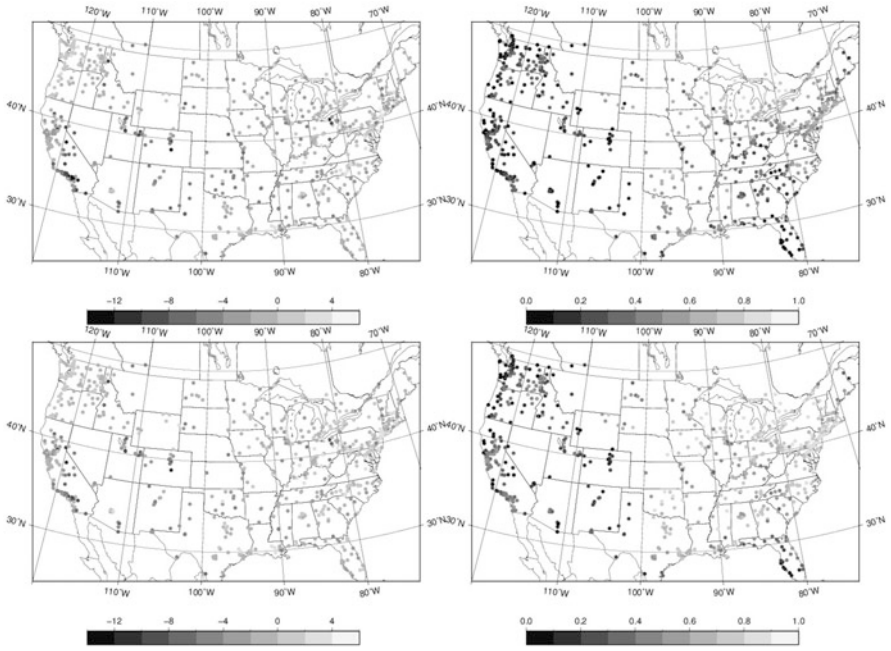

**Fig. 94.1** Bias (*top*) and temporal correlation (*bottom*) of forecasts for NoDA (*left*) and EnKF (*right*) experiments against AIRnow observations. *Black dots* denote negative correlations

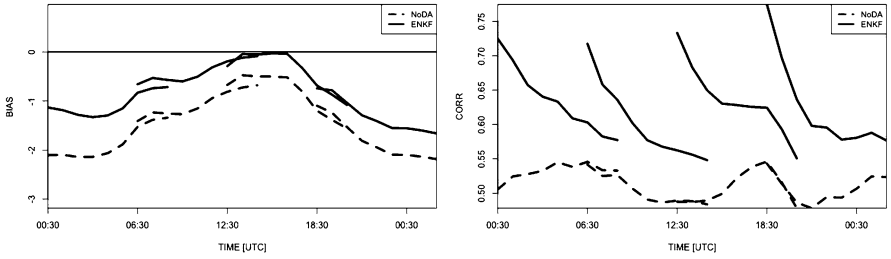


**Fig. 94.2** Bias (*left*) and spatial correlation (*right*) of $PM_{2.5}$ forecasts for experiments NoDA (*black*) and EnKF (*red*) against AIRnow observations. *Black vertical lines* are plotted at assimilation times

their vertical distribution, and errors due to inaccuracies in chemical and physical parameterizations and inaccuracies of emission sources.

Investigation is on-going if more sophisticated parameterizations of aerosol chemistry can maintain the quality of forecasts for a longer period. Short of improving model and emissions, parameterization of model errors within the ensemble and post-processing of forecasts might provide an avenue for better aerosol prediction.

## References

1. Chin M, Rood RB, Lin S-J, Muller J-F, Thompson AM (2000) Atmospheric sulfur cycle simulated in the global model GOCART: model description and global properties. J Geophys Res 105:24671–24687. doi:10.1029/2000JD900384
2. Grell GA, Peckham SE, Schmitz R, McKeen SA, Frost GJ, Skamarock W, Eder B (2005) Fully-coupled online chemistry within the WRF model. Atmos Environ 39:6957–6975. doi:10.1016/j.atmosenv.2005.04.027
3. McKeen SA et al (2009) An evaluation of real-time air quality forecasts and their urban emissions over Eastern Texas during the summer of 2006 TexAQS field study. J Geophys Res 114. doi:10.1029/2006JD011697
4. Muller NZ, Mendelsohn R, Nordhaus W (2011) Environmental accounting for pollution in the United States economy: dataset. Am Econ Rev http://www.aeaweb.org/articles.php?doi=10.1257/aer.101.5.1649
5. Pagowski M, Grell GA (2012) Experiments with the assimilation of fine aerosols using an Ensemble Kalman Filter. J Geophys Res 117, D21302. doi:10.1029/2012JD018333
6. United States Environmental Protection Agency (1999) The benefits and costs of the Clean Air Act: 1990–2010: EPA report to congress. EPA 410-R-99-001. Environmental Protection Agency, Office of Air and Radiation, Office of Policy, Washington, DC, November
7. Whitaker JS, Hamill TM (2002) Ensemble data assimilation without perturbed observations. Mon Weather Rev 130:1913–1924
8. Zhang Y, Bocquet M, Mallet V, Seigneur C, Baklanov A (2012) Real-time air quality forecasting, part II: state of the science, current research needs, and future prospects. Atmos Environ. doi:10.1016/j.atmosenv.2012.02.041

# Chapter 95
# Evaluating the Vertical Distribution of Ozone and Its Relationship to Pollution Events in Air Quality Models Using Satellite Data

**Jessica L. Neu, Gregory Osterman, Annmarie Eldering, Rob Pinder, Jeff McQueen, and Youhua Tang**

**Abstract** Most regional scale models that are used for air quality forecasts and ozone source attribution do not adequately capture the distribution of ozone in the mid- and upper troposphere, but it is unclear how this shortcoming relates to their ability to simulate surface ozone. We combine ozone profile data from the NASA Earth Observing System (EOS) Tropospheric Emission Spectrometer (TES) and a new joint product from TES and the Ozone Monitoring Instrument along with ozonesonde measurements and EPA AirNow ground station ozone data to examine air quality events during August 2006 in the Community Multi-Scale Air Quality (CMAQ) and National Air Quality Forecast Capability (NAQFC) models. We present both aggregated statistics and case-study analyses with the goal of assessing the relationship between the models' ability to reproduce surface air quality events and their ability to capture the vertical distribution of ozone. We find that the models lack the mid-tropospheric ozone variability seen in TES and the ozonesonde data, and discuss future work to determine the conditions under which this variability appears to be important for surface air quality.

J.L. Neu (✉) • G. Osterman • A. Eldering
Earth Atmospheric Science Division, NASA Jet Propulsion Laboratory/Caltech, Pasadena, CA 91109, USA
e-mail: jessica.l.neu@jpl.nasa.gov; gregory.b.osterman@jpl.nasa.gov; annmarie.eldering@jpl.nasa.gov

R. Pinder
Atmospheric Modeling and Analysis Division, Environmental Protection Agency, Research Triangle Park, NC 27711, USA
e-mail: pinder.rob@epa.gov

J. McQueen • Y. Tang
NOAA Center for Weather and Climate Prediction, National Oceanic and Atmospheric Administration/National Weather Service/National Center for Environmental Prediction, Camp Springs, MD 20748, USA
e-mail: jeff.mcqueen@noaa.gov; youhua.tang@noaa.gov

D. Steyn and R. Mathur (eds.), *Air Pollution Modeling and its Application XXIII*, Springer Proceedings in Complexity, DOI 10.1007/978-3-319-04379-1_95,

## 95.1 Introduction

Ozone is a pollutant that is harmful to both human and plant health (e.g. [2, 7]). Ozone produced and transported in the free troposphere can have a significant impact on surface air quality, contributing as much as 20–45 ppb to surface ozone (e.g. [1, 8]). Exchange between the free troposphere and the surface takes place via large-scale subsidence or small-scale mixing and entrainment into the planetary boundary layer. While this exchange can take place at any time, it is especially prevalent as the boundary layer breaks up in the morning. When this morning mixing occurs, nocturnal ozone, which can be transported long distances above the surface inversion layer without chemical destruction or deposition, mixes down to the surface and can rapidly increase ozone concentrations at a rate that rivals chemical ozone production (e.g. [5]).

Evaluation of the spatial distribution of ozone from models such as CMAQ (Community Multi-scale Air Quality modeling system) is usually based on comparison to in situ measurements of surface ozone from the AQS network. However, surface monitor data by itself provides limited information for resolving regional discrepancies between models and data. Ozonesondes have also been used for evaluation of lower and middle tropospheric ozone in regional models, with an emphasis on the boundary layer [4]. The past few years have seen an increase in the use of satellite data in regional modeling, either to help generate or supplement ozone boundary conditions or to constrain or assess modeled aerosols or $NO_2$. In this work, we utilize satellite observations of tropospheric ozone profiles from the NASA Tropospheric Emission Spectrometer (TES) and from a combined TES/OMI (Ozone Monitoring Instrument) data product. TES can provide nighttime observations while the TES/OMI data provide improved sensitivity in the lower troposphere [3] relative to TES. By combining the satellite data measurements with those from sondes and the surface network, we can evaluate how well models such as CMAQ represent the vertical and spatial structure of ozone in the free troposphere, with the goal of gaining a better understanding of how ozone in the free troposphere relates to surface ozone events. Here we utilize model results from two different versions of CMAQ; one is the NOAA/NWS National Air Quality forecast product and the second is the EPA version of CMAQ v4.7.1. Our preliminary results focus on the EPA CMAQ simulations over the continental United States during August 2006.

## 95.2 Comparison of Modeled and Measured Ozone

Measurements from ozonesondes, TES and TES/OMI all have different vertical sensitivities and spatial coverage. Ozonesondes provide vertical resolution of ~100 m but very sparse spatial and temporal sampling. The intensive INTEX Ozonesonde Network Study 2006 (IONS-06) campaign took place in August of 2006; even so there are only 383 sonde profiles from ~20 locations throughout

the continental U.S. for the entire month. In contrast, there are more than 10 times as many TES profiles over the continental U.S. during August 2006, but TES measurements have coarse vertical resolution of 6–7 km with maximum sensitivity at ~600 hPa. TES/OMI measurements are made by combining radiances from the two instruments and provide higher vertical resolution than TES alone (~5.5 km) as well as greater sensitivity to the lowest 2–3 km of the atmosphere [3]. However, TES/OMI measurements require coincident sampling of the two instruments and cloud fractions <30 %, resulting in ~1/2 as many profiles as TES for this study.

There are ~30 matches between sonde, TES, and TES/OMI profiles within 250 km and ±1 h in our dataset. By comparing the different measurements at these coincident times and locations, we can understand the differences between the datasets and what they tell us about model performance. We find that TES agrees very well with sondes in the mid-troposphere, with a mean bias of only a few percent, which is lower than the reported northern hemisphere mean bias of 10–20 % [6] The TES/OMI measurements have a higher mid-troposphere bias, but match the sondes within 10 % in the lowest 3 km of the atmosphere, with a correlation coefficient of ~0.5. Comparison to model profiles for the same times and locations shows that the tropopause is too low in the EPA CMAQ model, resulting in a mean high bias of ~50 % relative to sondes from 10–15 km. Near-surface ozone is also biased high by ~25 % in the model. Comparison to the satellite measurements reveals the same high bias in near-surface ozone (using TES/OMI), but the agreement between the model and the satellite measurements is much better than that between the model and sondes in the 10–15 km region, despite the good agreement between the satellite measurements and sondes there. The reason for this discrepancy is that the application of the satellite observational operator (averaging kernel + constraint) to the model profiles tends to shift the model tropopause upward, in better agreement with the measurements.

In addition to these "matched" profiles with coincident sonde and satellite measurements, we compare the model to sondes, TES, and TES/OMI, as well as to ground-based data for all of the available measurements for the August 2006 period. We also perform conditional sampling by time, latitude, longitude, and ozone abundance. We find, in good agreement with the smaller matched profile dataset, that the model is biased low relative to sondes and TES/OMI for ozone <100 ppb. For ozone >100 ppb, CMAQ is biased high relative to the sondes, but compares well to TES and TES/OMI when the observational operator is used. The model generally performs better near the middle of the model domain, well away from the influence of the boundary conditions. The model bias relative to both TES and TES/OMI differs for clean and polluted scenes, while the bias relative to the sondes does not show any such difference. This may reflect differences in the sensitivity of the satellite measurements under these different conditions or a sampling bias for the sondes.

We also examine case studies, with a preliminary focus on events where nocturnal ozone may play an important role in air quality. One such event occurred on August 9, 2006 (Fig. 95.1). TES passed over the Midwestern U.S. at 1:30 AM and

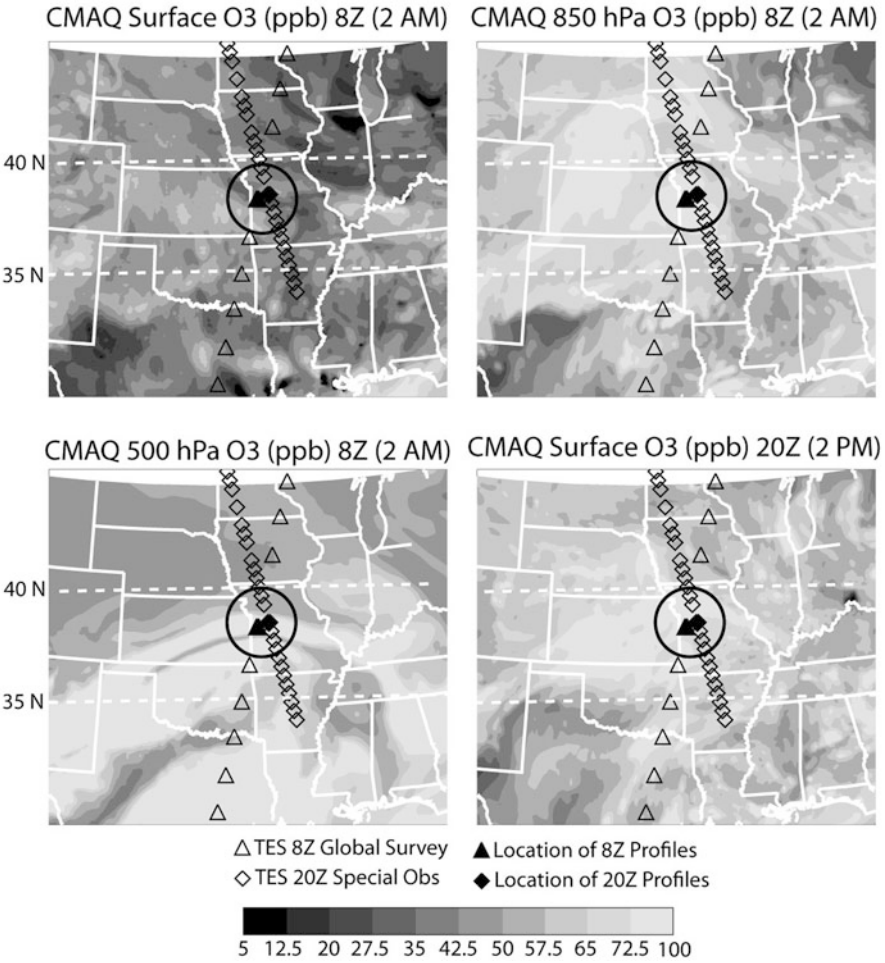


**Fig. 95.1** Maps of ozone on Aug 9, 2006 from CMAQ at 2:00 AM at the surface (*upper left*), 850 hPa (*upper right*), 500 hPa (*lower left*) and a 2:00 PM at the surface (*lower right*). *Black triangles* show the TES Global Survey measurements at 1:30 AM, *black diamonds* show TES special observations at 1:30 PM. *Filled symbols* indicate the location of the profiles discussed in the text

observed elevated ozone (∼85 ppb) at 500 hPa in western Missouri. Twelve hours later, TES observed elevated near-surface ozone (∼90 ppb) at the same location, in good agreement with nearby surface measurements. CMAQ shows a large region of elevated nocturnal ozone at 500 hPa, in good agreement with TES, as well as a second layer at 850 hPa, where TES is not sensitive. In the afternoon, CMAQ shows elevated surface ozone in western Missouri, but the modeled ozone is low (∼80 ppb) relative to TES and the ground-based measurements.

## 95.3 Conclusion

By comparing CMAQ ozone to measurements from multiple data sources, including ozonesondes, satellite measurements, and ground-based data on both a statistical and case study basis, we hope to gain insight into the relationship between mid-tropospheric ozone and surface ozone with the goal of improving ozone forecasting and source attribution. We find thus far that the median CMAQ near-surface ozone is well-simulated, but there is a large spread in the model-measurement difference. We also find that the model tropopause is generally too low, resulting in a high bias of 10–50 % for ozone above 5 km.

Our future work will focus on identifying the conditions under which properly simulating mid-tropospheric ozone is important for capturing surface air quality events. This will include analysis of time-lagged correlations between surface an mid-tropospheric ozone, conditional sampling to determine regions and conditions where mid-tropospheric ozone plays an important role in air quality, and further identification and analysis of case studies to examine the mechanisms by which mid-tropospheric ozone impacts the surface.

**Acknowledgments** The research described in this abstract was carried out at the Jet Propulsion Laboratory, California Institute of Technology, under a contract with the National Aeronautics and Space Administration. The JPL authors' copyright for this publication is held by the California Institute of Technology. Government Sponsorship acknowledged.

## References

1. Fiore AM, Jacob DJ, Bey I, Yantosca RM, Field BD, Fusco AC, Wilkinson JG (2002) Background ozone over the United States in summer: origin, trend, and contribution to pollution episodes. J Geophys Res 107(D15):4275. doi:10.1029/2001JD000982
2. Fishman J, Creilson JK, Parker PA, Ainsworth EA, Vining GG, Szarka J, Booker FL, Xu X (2010) An investigation of widespread ozone damage to the soybean crop in the upper Midwest determined from ground-based and satellite measurements. Atmos Environ 44:2248–2256
3. Fu D, Worden JR, Liu X, Kulawik SS, Bowman KW, Natraj V (2013) Characterization of ozone profiles derived from aura TES and OMI radiances. Atmos Chem Phys 13:3445–3462. doi:10.5194/acp-13-3445-2013
4. Herwehe J, Otte T, Mathur R, Rao ST (2011) Diagnostic analysis of ozone concentrations simulated by two regional-scale air quality models. Atmos Environ 45:5957–5969
5. Kuang S et al (2011) Nocturnal ozone enhancement in the lower troposphere observed by lidar. Atmos Environ 45:6078–6084
6. Nassar R et al (2008) Validation of Tropospheric Emission Spectrometer (TES) nadir ozone profiles using ozonesonde measurements. J Geophys Res 113:D15S17. doi:10.1029/2007JD008819
7. National Research Council (NRC) (2008) Estimating mortality risk reduction and economic benefits from controlling ozone air pollution. Committee on estimating mortality risk reduction benefits from decreasing tropospheric ozone exposure. The National Academy Press, Washington, DC
8. Vingarzan R (2004) A review of surface ozone background levels and trends. Atmos Environ 38:3431–3442

## Questions and Answers

**Questioner Name:** Andy Delcloo

**Q:** How many degrees of freedom do both products, TES and TES/OMI, have? How many layers are produced in both profile products?

**A:** The TES and TES/OMI retrievals are described in detail in Fu et al. [3]. The degrees of freedom for signal (DOFS) for both TES and TES/OMI vary with thermal contrast, clouds, ozone abundance, temperature, and water vapor, but typically TES provides 1.6 DOFS in the troposphere with 0.2 DOFS in the surface-700 hPa layer, and TES/OMI provides 2 DOFS in the troposphere, with 0.4 DOFS in the surface-700 hPa layer. The radiative transfer calculation in the forward model uses a 66-layer fixed pressure grid for both TES and TES/OMI.

# Chapter 96
# Building and Testing Atmospheric Chemistry Reanalysis Modeling System

**Tianfeng Chai, Pius Lee, Li Pan, Hyuncheol Kim, and Daniel Tong**

**Abstract** This study is a first step towards building an atmospheric chemistry reanalysis modeling system. We aim to provide the air quality science community with three-dimensional (3D) reanalysis atmospheric chemical fields over the conterminous U.S. (CONUS). This initial 3D gridded reanalysis product is available at 12 km horizontal grid spacing with 22 uneven vertical levels extending from surface to 100 hPa. The principal components of the modeling system are the Weather Research and Forecasting meteorological model, a chemical data assimilation model based on an optimal interpolation scheme, and the U.S. EPA Community Multi-scale Air Quality modeling system (CMAQ). Only the Moderate Resolution Imaging Spectro-radiometer (MODIS) Aerosol Optical Depth observations are assimilated as we focus on the aerosol reanalysis at this early stage. CMAQ predictions before and after the assimilation are evaluated against the AIRNow surface PM2.5 (Particulate Matter smaller than 2.5 μm in diameter) measurements. Based on the preliminary results, the future directions to improve the chemistry reanalysis modeling system are discussed.

T. Chai (✉)
Air Resources Laboratory, NOAA, NOAA Center for Weather and Climate Prediction, Cooperative Institute for Climate and Satellites, University of Maryland, 5830 University Research Court, College Park, MD 20740, USA
e-mail: Tianfeng.Chai@noaa.gov

P. Lee
Air Resources Laboratory, NOAA, NOAA Center for Weather and Climate Prediction, 5830 University Research Ct, College Park, MD 20740, USA
e-mail: Pius.Lee@noaa.gov

L. Pan • H. Kim • D. Tong
Air Resources Laboratory, NOAA, Cooperative Institute for Climate and Satellites, University of Maryland, College Park, MD, USA
e-mail: Li.Pan@noaa.gov; Hyun.Kim@noaa.gov; Daniel.Tong@noaa.gov

D. Steyn and R. Mathur (eds.), *Air Pollution Modeling and its Application XXIII*, Springer Proceedings in Complexity, DOI 10.1007/978-3-319-04379-1_96,

## 96.1 Introduction

The National Centers for Environmental Prediction (NCEP) and the National Center for Atmospheric Research (NCAR) reanalysis products [4] have been widely used since their introduction. There is a similar need to develop a gridded data set that best represents the atmospheric chemistry for air quality, climate, epidemiology, and many other fields in their research and policy related studies. Ozone and PM2.5 forecasts for the U.S. have been operationally and experimentally generated using the Community Multi-scale Air Quality (CMAQ) Modeling System [1] under the National Air Quality Forecast Capability (NAQFC) program by the National Oceanic and Atmospheric Administration (NOAA) for the conterminous Unites States (CONUS) since 2006 [3]. While NAQFC is capable of providing useful air quality forecasts, the accuracy of the products is limited substantially by the lack of a real-time emission modeling or constraints provided through chemical data assimilation implementation.

At an initial stage, the Moderate Resolution Imaging Spectro-radiometer (MODIS) Aerosol Optical Depth observations are assimilated into the 3-Dimensional CMAQ model system that is derived from the NAQFC developmental system. July 2011 is chosen as a test period to coincide with the Deriving Information on Surface conditions from Column and Vertically Resolved Observations Relevant to Air Quality (DISCOVER-AQ) field experiment (www.nasa.gov/mission_pages/discover-aq). This choice facilitates the use of DISCOVER-AQ measurements in the future testing and development of the atmospheric chemistry reanalysis modeling system. Different assimilation strategies for the atmospheric chemistry reanalysis will be investigated utilizing the DISCOVER-AQ measurements. 3-D gridded atmospheric chemistry reanalysis fields covering the contiguous Unites States are generated in this preliminary test. AIRNow surface PM2.5 (Particulate Matter smaller than 2.5 μm in diameter) measurements are used as independent observations to evaluate the preliminary reanalysis products which have not assimilated the AIRNow observations.

## 96.2 Method

The optimal interpolation (OI) data assimilation scheme is used to assimilate observations into CMAQ chemical transport model (CTM). Analysis solution is obtained by directly solving Eq. (96.1),

$$X^a = X^b + BH^T \left(HBH^T + O\right)^{-1} (Y - HX), \tag{96.1}$$

where X and Y are state and observation vectors, respectively. B and O are background and observation error covariance matrices. B is calculated using

Hollingsworth-Lönnberg method following Chai et al. [2]. H is linearized observational operator. Superscripts a and b indicate analysis and background states. Observations beyond background error correlation length scale have no effect in the analysis.

Daily MODIS AOD products are archived and utilized to generate gridded observations. We used both Terra and Aqua products (MOD04 and MYD04 collection 051), which overpass equator at around 10:30 am and 1:30 pm local time, respectively, with $10 \times 10$ km horizontal resolution. Total AOD was read from 'Optical_Depth_Land_And_Ocean', and then re-gridded into the target domain. MODIS AOD pixels are binned into the target domain cells, and pixel statistics (e.g. pixel counts, average and standard deviation) are calculated for all grid cells. Fine mode AOD observations are separated by applying the fine mode fraction parameters ('Optical_Depth_Ratio_Small_Land_And_Ocean').

In the current study, the daily data injection takes place at 17Z for Terra and 20Z for Aqua. The analysis $X^a$ over background $X^b$ at each grid column is used to scale aerosol related parameters at all levels.

## 96.3 Results

Three test cases are performed with different MODIS AOD assimilation setups, as listed in Table 96.1. They start at 12Z on July 1, 2011 with identical initial conditions. The subsequent runs assimilate AOD observations every day and continue to run until 17Z on July 12, 2011. All three cases show that by assimilating AOD observations of the previous day(s), the AOD predictions for the next day improve over the base case, reflected by AOD biases and root-mean-square errors.

Hourly AIRNow PM2.5 observations are also used to evaluate the MODIS AOD assimilation tests. Figure 96.1 shows PM2.5 predictions with AOD assimilations better match AIRNow observations. Total AOD assimilation has a better performance than fine mode AOD assimilation. Assimilating both Terra and Aqua observations everyday achieve the best results.

**Table 96.1** Description of three preliminary CMAQ CONUS reanalysis test cases

| Cases | MODIS AOD assimilation setup for Terra and Aqua observations |
|---|---|
| C1 | Terra fine-mode AOD assimilated at 17Z, Aqua AOD not assimilated |
| C2 | Terra total AOD assimilated at 17Z, Aqua AOD not assimilated |
| C3 | Terra total AOD assimilated at 17Z, Aqua total AOD assimilated at 20Z |

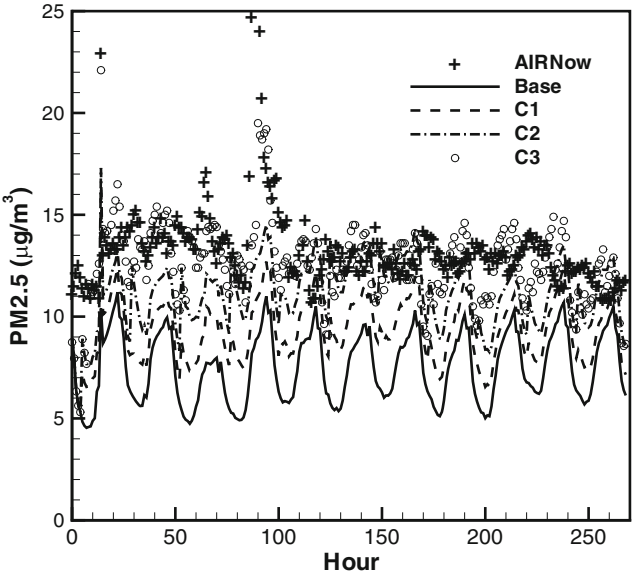


**Fig. 96.1** Time series of mean observed and predicted PM2.5 for base case (without assimilating any observations) and three test cases listed in Table 96.1. Hours are counted from 12Z on July 1, 2011

## 96.4 Summary and Discussion

A prototype chemical reanalysis system has been built. Preliminary tests show that MODIS AOD assimilation is able to improve AOD forecasts. In addition, the model predictions of surface PM2.5 are significantly better than the base case for all three assimilation cases. It is also found that assimilating both Terra and Aqua total AOD achieves the best performance when measured against the AIRNow observations over CONUS. Assimilation of both AIRNow surface measurement and MODIS AOD are being tested. Utilization of DISCOVER-AQ aerosol speciation information and vertical profiles in chemical data assimilation will be explored.

## References

1. Byun D, Schere KL (2006) Review of the governing equations, computational algorithms, and other components of the models-3 community multiscale air quality (CMAQ) modeling system. Appl Mech Rev 59(56):51–77
2. Chai T, Carmichael GR, Tang Y, Sandu A, Hardesty M, Pilewskie P, Whitlow S, Browell EV, Avery MA, Nédélec P, Merrill JT, Thompson AM, Williams E (2007) Four-dimensional data assimilation experiments with International Consortium for Atmospheric Research on Transport and Transformation ozone measurements. J Geophys Res 112(D12S15). doi:10.1029/2006JD007763

3. Eder B, Kang D, Mathur R, Pleim J, Yu S, Otte T, Pouliot G (2009) A performance evaluation of the National Air Quality Forecast Capability for the summer of 2007. Atmos Environ 43:2312–2320
4. Kalnay E, Kanamitsu M, Kistler R, Collins W, Deaven D, Gandin L, Iredell M, Saha S, White G, Woollen J, Zhu Y, Chelliah M, Ebisuzaki W, Higgins W, Janowiak J, Mo K, Ropelewski C, Wang J, Leetmaa A, Reynolds R, Jenne R, Joseph D (1996) The NCEP/NCAR 40-year reanalysis project. Bull Am Meteorol Soc 77(3):437–471
5. Pagowski M, Grell GA, McKeen SA, Peckham SE, Devenyi D (2010) Three-dimensional variational data assimilation of ozone and fine particulate matter observations: some results using the Weather Research and Forecasting – Chemistry model and Grid-point Statistical Interpolation. Q J R Meteorol Soc 136(653):2013–2024

## Questions and Answers

**Questioner Name**: Paul A. Makar, Environment Canada, Canada

**Q**: With regards to the discrepancy between observed AOD and PM2.5, on the west coast, are there different averaging kernels used for marine vs. continental aerosols? I am wondering whether the bias on the west coast is due to a poor choice of averaging kernel in the satellite retrieval algorithm for marine conditions (west coast having on-shore winds).

**A**: The current MODIS AOD retrieval algorithms differentiate between land and ocean. It is likely that the satellite retrieval algorithm contributes to the discrepancy between observed AOD and PM2.5 on the west coast. While AOD is a column integrated optical quantity and PM2.5 here is mass based quantity measured at ground level, there is no simple relationship between AOD and surface PM2.5. The causes of poor correlation between AOD and surface PM2.5 on the west coast need to be further investigated.

**Questioner Name**: Pavel Kishcha, Tel-Aviv University, Israel

**Q**: For PM2.5 predictions you used two kinds of data assimilation: (a) using MODIS AOD only, and (b) MODIS AOD and PM2.5 measurements. Did you try to use only PM2.5 measurements for data assimilation? Maybe it is enough, even without MODIS, as MODIS AOD could bring some bias depending on surface properties/reflection, could contamination, etc.

**A**: Pagowski et al. [5] assimilated AIRNow PM2.5 measurements using Grid-point Statistical Interpolation with the similar CMAQ modeling system. Their results show positive effect after the 3D-Var data insertion, but the effect of assimilation disappears pretty quickly. Our results show that the benefit of MODIS AOD assimilation lasts more than 24 h thanks to a better coverage in space of the MODIS AOD data.

# Chapter 97
# Intensive Campaigns Supported by Air Quality Forecasting Capability to Identify Chemical and Atmospheric Regimes Susceptible to Standard Violations

**Pius Lee, Li Pan, Hyuncheol Kim, and Daniel Tong**

**Abstract** The U.S. National Aeronautics and Space Administration (NASA) has started a series of regional scale multiple platform field measurement intensives between 2011 and 2014. These measurement campaigns are collectively called the Deriving Information on Surface Conditions from Column and Vertically Resolved Observations Relevant to Air Quality (DISCOVER-AQ) project. The emphasis of spatial collocation of multiple space-, air- and ground-based measurements facilitate the characterization of the vertical distribution of various air pollutants. During the January 16 to February 8, 2013 DISCOVER-AQ campaign over the San Joaquin Valley (SJV), California, one of the frontier science questions addressed concerned the frequent wintertime Particulate Matter (PM) standard violation over SJV and its vicinities. This study represents our contribution of real-time air quality forecasting to support flight-planning during the campaign as well as post analysis and model evaluation for some of the air pollutants. Two sets of real-time forecasts based on a coupled National Center for Environmental Prediction (NCEP) North American Model (NAM) and the U.S. EPA Community Multi-scale Air Quality Model (CMAQ) are included in the study: (1) a 12 km horizontal resolution domain over the Conterminous U.S., and (2) a 4 km resolution domain over the SJV

P. Lee (✉)
Air Resources Lab., NOAA, NOAA Center for Weather and Climate Prediction, College Park, MD, USA
e-mail: pius.lee@noaa.gov

L. Pan • H. Kim • D. Tong
Air Resources Lab., NOAA, NOAA Center for Weather and Climate Prediction, College Park, MD, USA

Cooperative Institute for Climate and Satellite, University of Maryland, College Park, MD, USA

D. Steyn and R. Mathur (eds.), *Air Pollution Modeling and its Application XXIII*, Springer Proceedings in Complexity, DOI 10.1007/978-3-319-04379-1_97,

and its adjacent areas nested-in from (1) as its parent. During the campaign there were several episodes of high surface PM concentration in the lowest hundreds of meters over SJV. We performed post-analyses of meteorological parameters such as the planetary boundary height and of chemical characteristics such as verification of modeled concentration of PM components at surface levels. Comparisons of the performance of the two forecasts will shed insight on horizontal resolution requirement to capture the meteorology and chemistry characteristics in SJV air quality modeling. These analyses will aid policy and regulatory relevant decisions as well as assist in improving the model for future applications.

## 97.1 Introduction

With the possible imminent implementation of the U.S. Environment Protection Agency (EPA) Cross State Pollution Rule and tighter environmental standards for surface $O_3$ and Particulate Matter (PM) concentrations, it is important to improve air quality forecast with accurate predictions of fine feature characteristics and background pollutant concentration due to inter-boundary transports. On the other hand, coordinated air quality and meteorological measurement intensives with space- and- air-borne and- surface-based platforms to quantify specific geographical, emission and meteorological conditions for frequent elevated levels of surface pollutant concentrations shed insight into science questions applicable to the specific locales, seasons and beyond. The NASA funded multiple years and multiple campaigns endeavor is such a measurement effort dubbed: Deriving Information on Surface Conditions from Column and Vertically Resolved Observations Relevant to Air Quality (DISCOVER-AQ) (http://www-air.larc.nasa.gov/missions/discover-aq/discover-aq.html). This study focuses on the 2013 San Joaquin Valley (SJV), CA winter campaign. SJV during winter is known for frequent occurrence of prolonged coverage of thick fogs and extremely low Planetary Boundary Layer (PBL) heights. In the SJV, the rather complex terrain of Sierra Nevada and Coastal Range induce flows and strong inversions are primarily responsible for the local pollutant buildups. Even without the so-called Tule fog the frequently occurring regional haze in SJV causes low visibility conditions. It has been speculated that emission due to agricultural tilling and fertilization, the rather efficient production of organic aerosols, stagnant air flows, and the frequent formation of strong low level inversions cause large loadings of atmospheric aerosols in the lowest several tens to a couple hundred of meters. This study attempts to investigate contribution of these factors to the surface concentration of PM equal to or less than 2.5 μm in diameter. Section 97.2 introduces configuration of the fine resolution air quality forecasting model used to generate real time simulation and post analysis for the SJV DISCOVER-AQ campaign. It is followed by Sections for discussion of result and conclusions.

## 97.2 Model Configuration

A limited-area, fine resolution AQ forecasting system has been constructed through the off-line coupling of an operational meteorological forecasting model and a Chemical Transport Model (CTM). The limited-area domain is the child domain of a two-tier nested domain. The parent domain covers CONUS (Fig. 97.1) with a 12 km horizontal grid resolution. The child domain of 4 km horizontal resolution lies strictly within the parent domain with each of its perimeters coinciding with an interior grid mesh-line of the parent domain. The NOAA National Centers for Environmental Prediction (NCEP) North American Meso-scale Model (NAM) provides meteorological fields for both the parent and child domains. The Community Multiscale Air Quality Model (CMAQ) is the CTM used in the system to forecast concentration fields for atmospheric trace species for both the parent and child domains [3]. Extensive literature is available describing and evaluating the NAM model [6, 7]. Identical physical and chemical package options were selected for both the parent and the child domains for CMAQ simulations. Equation 97.1 represents the species continuity equation in a generalized curvilinear co-ordinate system which CMAQ solves [3].

$$\frac{\partial\left(\phi_i J_s\right)}{\partial t} + m^2 \nabla_s \cdot \left(\frac{\phi_i J_s \widehat{V}_s}{m^2}\right) + \frac{\partial\left(\phi_i J_s \widehat{v}^3\right)}{\partial s} = J_s Q_{\phi_i} \tag{97.1}$$


**Fig. 97.1** Parent and nested domain were both used to produce air quality forecast to support DISCOVER-AQ campaign over SJV from Jan 16 to Feb 8, 2013 whose horizontal grid is: 12 km over CONUS and (inset) 4 km over SJV, respectively

Where $\phi_i$ is the concentration of ith advected species. For the model top and bottom layer a zero flux boundary condition, and a flux boundary condition including treatment for dry deposition processes has been prescribed, respectively (*Section* 7.2.2.3 [2]).

At the lateral boundaries, a zero-flux divergence outflow condition is imposed [3]. For the inflow condition, concentrations prescribed by externally derived values are specified as follows: Chemical lateral boundary conditions (LBC) adopted from a species mapping methodology introduced by Tang et al. [10] was followed. A selected set of chemical fields derived from the GEOS-CHEM global model simulation with assimilated meteorology for winter 2006 was employed in accordance with procedures described by Bey et al. [1]. Hourly output from NOAA operational Hybrid Single-Particle Lagrangian Integrated Trajectory (HYSPLIT) based Smoke Forecasting System (SFS) [8] covering Northwards of the Equator and from 50°W westwards to 180°W is used to derive dynamic LBC basing on its $PM_{2.5}$ output for the parent domain CMAQ [9]. We used a $PM_{2.5}$ to CO ratio of $0.08 \pm 0.03$ recommended by Janhäll et al. [5] to estimate CO at the LBC for the parent domain. For the CMAQ wild fire related species of $NO_x$, VOC, $NH_3$, $SO_2$, we obtain their concentrations at the LBC by multiplying CO concentration there with a recommended species mapping factor by Hsu and Divita [4].

## 97.3 Model Results

The SJV campaign consisted many coordinated surface and air-borne measurements took place in 24 days between January 16 and February 8, 2013 where 10 flight days were unevenly spaced throughout those days. There were at least a couple of high mass loading of atmospheric aerosol events measured. They were both episodes due to stagnant conditions with rather shallow PBL heights. The measurement data are not quality assured and has not been publically released yet, therefore we are focusing more in forecast difference and verifications conducted against the AIRNow monitor network in the area. These results will be more thorough presented in the conference as there seemed to be an under-estimation of NOx emissions in the fine resolution domain simulation (Fig. 97.2).

## 97.4 Discussion and Conclusion

Two air quality forecasts were conducted to support NASA's DISCOVER-AQ field intensive carried out over SJV between Jan 16 and Feb 8 2013. Both sets of real-time forecasts were based on the off-line coupling of NCEP's NAM and U.S. EPA's CMAQ version 4.7.1. Their difference is primary in horizontal grid resolution: (1) a 12 km horizontal resolution domain over the CONUS; and (2) a 4 km resolution domain over the SJV and its adjacent area nested-in from the 12 km CONUS

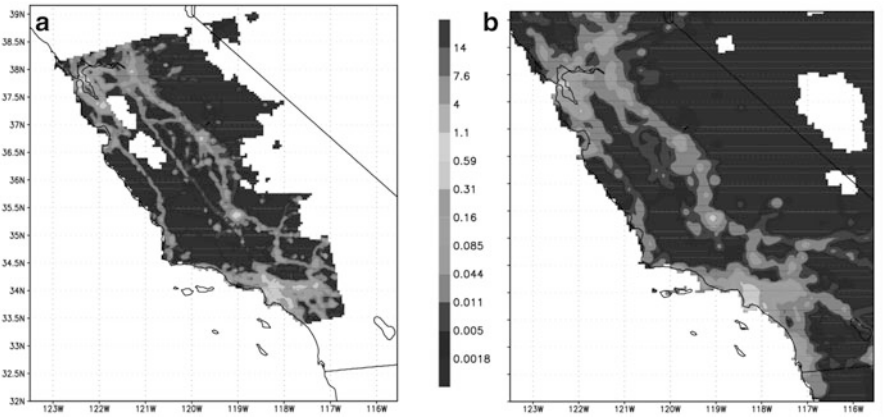


**Fig. 97.2** Surface flux of NOx emission in (mole s-2 km-2) for (**a**) 4 km domain of the inner-nest over SJV, and (**b**) 12 km of the parent domain over CONUS

simulation. During the campaign there were several episodes of high surface PM concentration in the lowest hundreds of meters over SJV. Post-analyses of 4 km resolution simulation were conducted due to deficiencies in emission modeling. With these rerun results, meteorological parameters such as the planetary boundary height and of chemical characteristics such as verification of modeled concentration of PM components at surface levels were compared between the two forecasts. Retrospective rerun of the 4 km results did show improvement in capturing finer scaler features of local flows over that by the 12 km run. Insight on horizontal resolution requirement to capture the meteorology and chemical characteristics in SJV air quality modeling were drawn. These analyses will aid policy and regulatory relevant decisions as well as assist in improving the model for future applications.

## References

1. Bey I, Jacob DJ, Yantosca RM, Logan JA, Field BD, Fiore AM, Li Q, Liu HY, Mickley LJ, Schultz MG (2001) Global modeling of tropospheric chemistry with assimilated meteorology: model description and evaluation. J Geophys Res 106(D19):23073–23095
2. Byun DW, Ching JKS (eds) (1999) Science algorithms of the EPA Models-3 Community Multiscale Air Quality (CMAQ) modeling system. EPA-600/R-99/030, Office of Research and Development, U.S. Environmental Protection Agency, Washington, DC. Available from U.S. EPA, ORD, Washington, DC, 20460
3. Byun D, Schere KL (2006) Review of the governing equations, computational algorithms, and other components of the models-3 Community Multiscale Air Quality (CMAQ) Modeling System. Appl Mech Rev 59:51–77
4. Hsu Y, Divita F Jr (2011) SPECIATE 4.3: addendum to SPECIATE4.2: speciation data base development documentation, technical report EPA/600/R-11/121. U.S. EPA, Research Triangle Park, NC

5. Janhäll S, Andreae MO, Pöschl U (2010) Biomass burning aerosol emissions from vegetation fires: particle number and mass emission factors and size distributions. Atmos Chem Phys 10:1427–1439. www.atmos-chem-phys.net/10/1427/2010/
6. Janjic ZI (2003) A nonhydrostatic model based on a new approach. Meteorol Atmos Phys 82:271–285. doi:10.1007/s00703-001-0587-6
7. Janjic Z, Gall R (2012) Scientific documentation of the NCEP Nonhydrostatic Multiscale Model on B grid (NMMB). Part 1 Dynamics. NCAR technical note NCAR/TN-489+STR, 80 pp. http://nldr.library.ucar.edu/collections/technotes/asset-000-000-000-857.pdf
8. Rolph GD, Draxler RR, Stein AF, Taylor A, Ruminski MG, Kondragunta S, Zeng J, Huang HC, Manikin G, McQueen JF, Davidson PM (2009) Description and verification of the NOAA smoke forecasting system: the 2007 fire season. Weather Forecast 24:361–378
9. Stein AF, Mathur R, Draxler RR (2006) Using combined Lagrangian and Eulerian modeling approaches to improve particulate matter estimations in the Eastern US. Preprint: 5th Annual CMAS Conference, Chapel Hill, NC, October 16–18 2006
10. Tang Y, Lee P, Tsidulko M, Huang HC, McQueen J, DiMego G, Emmons L, Pierce B, Lin HM, Kang D, Tong D, Yu S, Mathur R, Pleim J, Otte T, Pouliot G, Young J, Schere K, Davidson P (2008) The impact of lateral boundary conditions on CMAQ predictions over the continental US: a sensitivity study compared to ozonesonde data. Environ Fluid Mech 9:43–58. doi:10.1007/s10652-008-9092-5

# Chapter 98
# Modeling of Air Pollution over the Ganges Basin and North-West Bay of Bengal in the Early Post-monsoon Season Using the NASA GEOS-5 Model

**Pavel Kishcha, Arlindo M. da Silva, Boris Starobinets, and Pinhas Alpert**

**Abstract** The NASA GEOS-5 model was used to extend the MERRA reanalysis with five atmospheric aerosol components (sulfates, organic carbon, black carbon, desert dust, and sea-salt). The obtained eight-year (2002–2009) MERRA-driven aerosol reanalysis (MERRAero) dataset was applied to the study of aerosol optical thickness (AOT) trends over the Ganges basin and north-west Bay of Bengal (BoB) in the early post-monsoon season. In October, in the absence of aerosol sources in north-west Bay of Bengal (BoB), MERRAero showed increasing AOT trends over north-west BoB exceeding those over the east of the Ganges basin. Various aerosol components showed strong increasing AOT trends over north-west BoB. Our analysis showed that the AOT trends over north-west BoB were reproduced by GEOS-5, not because of MODIS AOT assimilation, but because of the model capability of reproducing meteorological factors contributing to AOT trends. The following factors contributed to the increasing AOT trend over the area in question in October: an increasing number of days when prevailing winds blew from land to sea, resulting in a drier environment and an increase in air pollution over north-west BoB; wind convergence was observed over north-west BoB causing the accumulation of aerosol particles over that region, when prevailing winds blew from land to sea.

P. Kishcha (✉) • B. Starobinets • P. Alpert
Department of Geophysical, Atmospheric, and Planetary Sciences, Tel-Aviv University, Tel-Aviv, Israel
e-mail: pavel@cyclone.tau.ac.il

A.M. da Silva
Global Modeling and Assimilation Office, NASA/GSFC, Greenbelt, MD, USA

D. Steyn and R. Mathur (eds.), *Air Pollution Modeling and its Application XXIII*, Springer Proceedings in Complexity, DOI 10.1007/978-3-319-04379-1_98,

## 98.1 Introduction

The Ganges basin is characterized by a significant population growth accompanied by developing industry and increasing transportation. This has resulted in increased anthropogenic emissions and declining air quality. The early post-monsoon season over the study region is characterized by aerosol transport from the Ganges basin to north-west BoB by prevailing winds; and still significant rainfall of over 150 mm/month over the east of the Ganges basin and north-west BoB. It would be reasonable to consider that AOT trends over sea areas in BoB were created by changes in aerosol sources on the land in the Indian subcontinent. In our previous study [3], we found that it was not always the case. Specifically, we found that, in October, MODIS showed strong increasing aerosol optical thickness (AOT) trends over north-west Bay of Bengal (BoB) in the absence of AOT trends over the east of the Indian subcontinent. It was interesting to determine whether existing aerosol data-assimilated systems were capable of reproducing the aforementioned observed AOT trends over north-west BoB. The NASA Goddard Earth Observing System (GEOS-5) was used to extend the NASA Modern Era-Retrospective Analysis for Research and Applications (MERRA) reanalysis by adding five atmospheric aerosol components (sulfates, organic carbon, black carbon, desert dust, and sea-salt). The obtained eight-year (2002–2009) assimilated aerosol dataset (so-called MERRAero) was applied to the study of AOT and its trends over the Ganges basin and north-west Bay of Bengal (BoB) in the post-monsoon season. Using an assimilated aerosol dataset over north-west BoB provided us with an opportunity to estimate the contribution of different aerosol components to AOT and its trends.

## 98.2 GEOS-5 and the MERRA Aerosol Reanalysis (MERRAERO)

GEOS-5 is the latest version of the NASA Global Modeling and Assimilation Office (GMAO) Earth system model. GEOS-5 contains components for atmospheric circulation and composition (including atmospheric data assimilation), ocean circulation and biogeochemistry, and land surface processes. GEOS-5 includes a module representing atmospheric aerosols [2]. This aerosol module is based on a version of the Goddard Chemistry, Aerosol, Radiation, and Transport (GOCART) model [1]. GOCART treats the sources, sinks, and chemistry of dust; sulfate; sea salt; and black and organic carbon aerosols. Aerosol species are assumed to be external mixtures. Total mass of sulfate and carbonaceous aerosols are tracked, while for dust and sea salt the particle size distribution is explicitly resolved across five non-interacting size bins for each. Both dust and sea salt have wind-speed dependent emission functions, while sulfate and carbonaceous species have emissions principally from

fossil fuel combustion, biomass burning, and bio-fuel consumption, with additional biogenic sources of organic carbon. Sulfate has additional chemical production from oxidation of $SO_2$ and dimethylsulfide (DMS), as well as a database of volcanic $SO_2$ emissions and injection heights. GEOS-5 also includes assimilation of AOT observations from the MODIS sensor on both Terra and Aqua satellites.

## 98.3 Method

We analyzed long-term variations of AOT over seven zones, each $3 \times 3°$, located in the Ganges basin and north-west BoB (Fig. 98.1). As mentioned, in the post-monsoon period, prevailing winds blow along the Ganges basin. The specified zones in the Ganges basin provide us with an opportunity for analyzing air pollution trends produced by local sources and aerosol transport. Figure 98.1a shows the spatial distribution of eight-year mean MERRAero AOT over the region under consideration in October, together with the location of zones $3° \times 3°$ in the Indian subcontinent (zone 1 to zone 5) and in the Bay of Bengal (zones 6 and 7). MERRAero monthly AOT data are available from the year 2002. To analyze AOT and its trends over the Indian subcontinent and north-west BoB, we used monthly MERRAero AOT data with horizontal resolution of approximately 50 km, during the eight-year period 2002–2009.

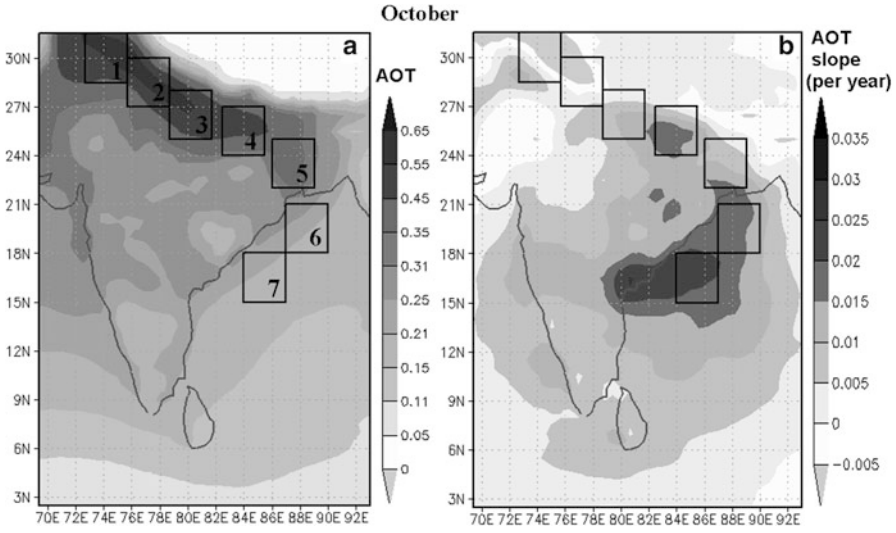


**Fig. 98.1** Spatial distributions of (**a**) the eight year (2002–2009) mean MERRAero AOT and (**b**) its trends (characterized by AOT slopes) in October. The AOT trend values correspond to the slope of the linear regression (From Kishcha et al. [4])

## 98.4 Results and Discussion

In accordance with space distribution of eight-year mean AOT in the early post-monsoon season (October), MERRAero showed high AOT values over the Ganges basin with a maximum over the north-west part of the Ganges basin (Fig. 98.1a). Therefore, MERRAero data were able to reproduce the main structure of aerosol distribution over the Ganges basin. The Ganges basin is the most polluted part of the Indian subcontinent, where highly-populated areas and main industrial centers are located. The MERRAero AOT data set allowed us to determine aerosol species responsible for the AOT maximum over the north-west of the Ganges basin, which are both natural aerosols (dust particles) and anthropogenic aerosols (carbon aerosols from bio-mass burning and sulfates). In accordance with MERRAero data, most of dust particles fell out due to gravitational settling and wet deposition during dust transport from the north-west to the east of the Ganges basin. As a result, over the east of the Ganges basin and north-west BoB in the early post-monsoon season, aerosols were dominated by anthropogenic air pollution, such as sulfates and carbon aerosols. Our analysis showed that sea-salt aerosols did not contribute to the increasing AOT trends over north-west BoB: no sea-salt AOT trend was observed in year-to-year variations during the study period. Taking into account that anthropogenic aerosols are effective cloud condensation nuclei (CCN), these aerosols could influence the strength of typhoons crossing BoB in the early post-monsoon season.

Space distributions of MERRAero AOT trends during the eight-year (2002–2009) study period showed strong increasing AOT trends over north-west BoB exceeding those over the Ganges basin (Fig. 98.1b). This was despite the fact that sources of anthropogenic pollution are located over the Ganges basin and aerosol transport from the Indian subcontinent to north-west BoB is carried out by prevailing winds. Various aerosol components showed strong increasing AOT trends over north-west BoB. Therefore, using MERRAero AOT, we obtained similar results with respect to AOT trends over north-west BoB, as in our previous study based on MODIS data [3].

There could be several factors contributing to the increasing AOT trends over north-west BoB. First, there were changes in the atmospheric circulation over north-west BoB in October during the eight-year study period. During the second 4-year period (2006–2009), prevailing winds blowing mainly from land to sea resulted in a drier environment and less precipitation over the east of the Ganges basin and north-west BoB than during the first 4-year period (2002–2005). This caused less wet removal of air pollution in the second 4-year period than in the first 4-year period. Second, our analysis showed that, during the 8-year study period, there was an increasing number of days (Np, in percentage form) in each October when prevailing winds blew from land to sea. This suggests some increasing trends in the transport of anthropogenic air pollution from their sources in the east of the Ganges basin to north-west BoB. Third, for Octobers when $Np > 50$ %, wind convergence was observed over north-west BoB causing the accumulation of aerosol particles over that region, in line with our previous study [3]. All the three factors contributed to the increasing AOT trend over north-west BoB in the early post-monsoon season.

We estimated the NASA GEOS-5 model performance over the study area analyzing model AOT increments. These AOT increments are the field differences between MODIS AOT and modeled AOT. AOT increments include a complex combination of all model errors in AOT simulations over each specific location. To analyze AOT increments, 3-h MERRAero AOT data were used. These 3-h data allowed us to distinguish between 3-h periods with and without MODIS AOT assimilation. A comparison was conducted between spatial distributions of eight-year (2002–2009) AOT trends at 6 UT with and without AOT assimilation. Here, the modeled AOT without MODIS assimilation was obtained as the field difference between MODIS AOT and AOT increments at 6 UT. Similar AOT trends were obtained using MERRAero AOT with and without MODIS AOT assimilation. This is evidence that the increasing AOT trends over north-west BoB were reproduced by the model not because MODIS AOT assimilation provided us with an opportunity to correct the uncertainty in aerosol emissions, but because the model was capable of reproducing changes in meteorological factors contributing to the AOT trends.

**Acknowledgements** This study was made with support from and in cooperation with the international Virtual Institute DESERVE (Dead Sea Research Venue), funded by the German Helmholtz Association.

## References

1. Chin M, Ginoux P, Kinne S, Torres O, Holben B, Duncan BN, Martin RV, Logan J, Higurashi A, Nakajima T (2002) Tropospheric aerosol optical thickness from the GOCART model and comparisons with satellite and sun photometer measurements. J Atmos Phys 59:461–483
2. Colarco P, da Silva A, Chin M, Diehl T (2010) Online simulations of global aerosol distributions in the NASA GEOS-4 model and comparisons to satellite and ground-based aerosol optical depth. J Geophys Res 115:D14207. doi:10.1029/2009JD012820
3. Kishcha P, Starobinets B, Long CN, Alpert P (2012) Unexpected increasing AOT trends over north-west Bay of Bengal in the early post-monsoon season". J Geophys Res 117:D23208. doi:10.1029/2012JD018726
4. Kishcha P, da Silva A, Starobinets B, Alpert P (2014) Air pollution over the Ganges basin and north-west Bay of Bengal in the early post-monsoon season based on NASA MERRAero data. J Geophys Res 119. doi:10.1002/2013JD020328

## Questions and Answers

**Questioner Name:** Antony Dore

**Q**: You mentioned a decrease in wet removal over the Bay of Bengal. Could this be caused by an increase in particle and cloud droplet numbers forming clouds with a smaller droplet size, which are less likely to grew to raindrop size? If so, has a decrease in rainfall been observed in the region?

**A:** In the early post-monsoon season (October), there are days when winds blow from land to sea. This is accompanied by a decrease in aerosol wet removal over north-west BoB. On the other hand, there are also days when winds blow from sea to land. In these days, aerosol wet removal increases. In our previous study [3], we analyzed long-term changes in accumulated rainfall over north-west BoB in October during the 10-year (2000–2009) period using TRMM rainfall data. No decreasing trend in accumulated rainfall was found.

**Questioner Name:** Roger Timmis

**Q**: Can the change in atmospheric circulation over north-west BoB in the early post-monsoon season between the first and second 4-year study periods be related to the phase of the El Nino South Oscillation (ENSO) cycle?

**A:** There could be different factors causing the change in atmospheric circulation over north-west BoB in the early post-monsoon season, such as monsoon variability, ENSO cycle, etc. To identify the causal factors, further research is needed using a much longer time record of wind data than the eight-year period selected for analysis in the current study.

# Chapter 99
# The Impact of a Wildland Fire on Air Pollution Concentrations Using WRF/Chem/Fire: An Application over Murcia (Spain)

**Roberto San José, Juan Luis Pérez, R.M. González, J. Pecci, and M. Palacios**

**Abstract** In this contribution we will show the impact on air pollution concentration of a Fire developed in the Surrounding area of Murcia (Spain). The impact on air pollution concentrations has been done using the WRF/Chem model developed by NCAR (US) and the Fire model implemented into WRF in on-line mode. The fire spread has been considered in on-line mode to change the use of the different land use grid cells as the fire spreads. This process changes the land use and affects substantially to the Fuel Moisture Content (FMC) modifying the surface turbulent energy balance and the pollution dispersion consequently. A new fuel moisture content model has been developed. The new module allows each time step to calculate the fuel moisture content of the dead fuels (1 h, 10 h, and 100 h) and live fuels. Two simulations have been performed over the Murcia area on September, 7th, 2010 with 9 h of fire starting at 19:09 over an area of 7 km × 7 km: (a) with a fire of 9 h simulation we run the WRF/Chem with 200 m spatial resolution over the fire domain in on-line mode with FIRE model. Emissions from fire have been accounted on; and (b) the same simulation than in case (a) but without fire (no emissions and no changes in the land use).

R. San José (✉) • J.L. Pérez
Environmental Software and Modelling Group, Technical University of Madrid (UPM), Boadilla del Monte, Madrid 28660, Spain
e-mail: roberto@fi.upm.es

R.M. González
Faculty of Physics, UCMCiudad Universitaria, 28040 Madrid, Spain

J. Pecci • M. Palacios
Space Unit. Earth Observation Directorate, INDRA SISTEMAS S.A., c/Mar Egeo, 4, Polígono Industrial, 1, 28830 San Fernando de Henares, Madrid, Spain

D. Steyn and R. Mathur (eds.), *Air Pollution Modeling and its Application XXIII*, Springer Proceedings in Complexity, DOI 10.1007/978-3-319-04379-1_99,

## 99.1 Introduction

Forest fires are problem in most of the south European countries. Spain is plagued by forest and brush fires every summer, when extremely dry weather sets in along with high temperatures. The adverse effects of smoke on air quality and visibility are very important.

In this paper, we describe a simulation of a real case with forecasting of the smoke emissions, dispersion, and their effect on the air quality. In order to estimate smoke spread and its effects on air quality, first one has to assess the amount of the fuel burnt, and convert it into emission fluxes of the particular chemical species. In the next step, the vertical distribution of the smoke in the atmosphere has to be estimated, based on the fire intensity and meteorological conditions. In the last step, the chemical processes associated with smoke dispersion in the atmosphere has to be taken into account in order to assess the smoke impact on the air quality.

## 99.2 System Description

The core of the system is the WRF-Fire model [2], which is a two-way coupled fire atmosphere model based on WRF [1]. It provides forecast of the fire spread based on the local meteorological conditions, taking into account the feedback between the fire and the atmosphere. The fire model is also coupled with WRF-Chem [3], so the smoke emitted from the fire is added at the location of the simulated fire and them is transported within the atmosphere, and undergoes chemical reactions resolved by WRF-Chem. Coupling with WRF-Chem is implemented by inserting the smoke intensity and air pollution emissions in the WRF-Chem arrays at the ground layer. The amount of the chemical species released into the atmosphere is computed from the amount of fuel burned directly by emissions, table (g/kg fuel or mol/kg fuel for each of the 13 Anderson's fuel categories used). RADM2 chemical mechanism is used. Emissions are computed at the fire resolution (in this experiment 20 m) and the averaged to the atmospheric/chemistry resolution (200 m).

A new Fuel Moisture Content (FMC) model has been developed and integrated into the WRF-Chem-Fire system. Our FMC calculations for fine dead fuel (1 h dead fuel) is based on (Eq. 99.1) [4] and (Eq. 99.2) [5] to take into account the effects of condensation.

$$m = \frac{97.9 + 4.06H}{T + 6} - 0.00854H_{surf} + \frac{3000}{C} - 30 \tag{99.1}$$

H and $H_{surf}$ are the air humidity at 1.5 m and surface levels, T is the temperature at 1.5 m and C is the degree of curing (%) and is considered as 100 % for the calculation of dead FMC.

$$\Delta m = \frac{100}{W} \int_{\Delta t} \frac{G - N}{L + C_p \left(T - T_{surf}\right) / \left(Q - Q_{surf}\right)} dt \tag{99.2}$$

where W is the surface fuel mass, G is the soil heat flux, N is the ne all-wave radiation flux, L is the latent heat of vaporization or sublimation, Cp is the specific heat of air at constant pressure, T and $T_{surf}$ are the temperature at 1.5 m and surface levels and Q y $Q_{surf}$ are the specific humilities at 1.5 m and surface levels respectively.

In case of not fine dead fuel, as 10 and 100 h dead fuel, we have implemented into WRF-Fire the Nelson model [6] modified to make operational [7]. Live FMC is calculated following the correlation between vegetation greenness and its moisture content, consequently the Normalized Difference Vegetation Index (NDVI) can be used in estimating live FMC. Live FMC estimations can be improved by including the Land Surface Temperature (LST), because LST would be expected to increase in drier plants on account of reduced evapotranspiration. Specifically the ratio NDVI/LST was found to be very useful [8].

## 99.3 Results and Conclusion

A preliminary model results of a real case of forest fire in the territory of Murcia (Spain). The fire ignited in a region of Murcia (Spain) on September 07, 2010 19:09. The final burned area is 7Km by 1 Km after 9 h.

In the (Fig. 99.1) we can see the fire emissions air quality impact in case of NO2 and PM2.5. We have run two simulations, first without fire emissions, called OFF and the second with fire emissions, named ON. The temporal average concentrations differences show very important impacts up to 270 % for NO2 and 300 % for PM2.5. In case of NO2 we can see a hot spot and for the PM2.5 the impacts are distributed over the burned area. This figure shows very complex fire and smoke emission pattern.

We have presented a real simulation with the system WRF-Fire-Chem with a coupled of atmosphere-fire model WRF-Fire into the atmospheric chemistry and transport model WRF-Chem and a new Fuel Moisture Content model. We showed results from the very first numerical simulations performed of a real case to demonstrate that the system allows simulation the fire spread, smoke emissions and dispersion, as well as smoke chemical transformations. The system can provide also smoke and air quality forecasts allowing for an estimation of comprehensive effect of prescribed burns. The system can be used to study the complex interactions between the fire and the atmosphere, including radiative and microphysical effects of the aerosols ingested into the atmosphere by fire plumes.

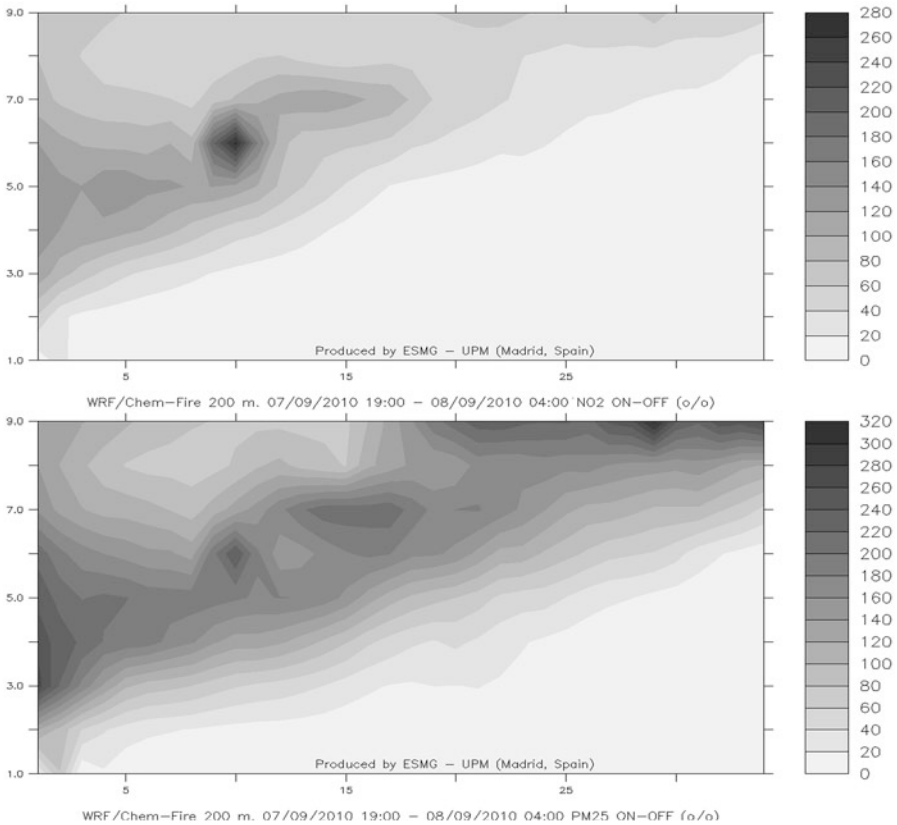


**Fig. 99.1** Average concentration differences (%) ON(fire) – OFF (fire) for NO2 (*upper*) and PM2.5 (*bottom*)

**Acknowledgments** Authors thankfully acknowledge the computer resources, technical expertise and assistance provided by the Centro de Supercomputación y Visualización de Madrid (CeSVIMa) and the Spanish Supercomputing Network (BSC) Centro para el Desarrollo Tecnológico Industrial (CDTI) and Indra Sistemas for supporting the project PROMETO. The authors thankfully acknowledge the forest fire reports and assistance provided by the Autonomous Community of Region of Murcia.

## References

1. Skamarock WC, Klemp JB, Dudhia J, Gill DO, Barker DM, Wang W, Powers JG (2005) A description of the advanced research WRF version 2. National Center for Atmospheric Research, Technical note, NCAR/TN-468þSTR, Boulder, CO
2. Mandel J, Beezley JD, Kochanski AK (2012) Coupled atmosphere-wildland fire modeling with WRF 3.3 and SFIRE 2011. Geosci Model Dev (GMD) 4:591–610. doi:10.5194/gmd-4-591-2011

3. Grell GA, Peckham SE, Schmitz R, McKeen SA, Frost G, Skamarock WC, Eder B (2005) Fully coupled 'online' chemistry in the WRF model. Atmos Environ 39:6957–6976
4. Noble IR, Bary GAV, Gill AM (1980) Mc Arthur's fire-danger meters expressed as equations. Aust J Ecol 5:201–203
5. Viney NR, Hatton TJ (1990) Modelling the effect of condensation on the moisture content of forest litter. Agric For Meteorol 51:51–62
6. Nelson RM Jr (2000) Prediction of diurnal change in 1-h fuel stick moisture content. Canad J For Res 30:1071–1087
7. Andrews PL, Bevins CD, Seli RC (2008) BehavePlus fire modeling system, version 4.0: user's guide. General technical report. RMRS-GTR-106WWW revised. USDA Forest Service, Rocky Mountain Research Station, Fort Collins, CO, 116p
8. Dasgupta S, Qu JJ, Xianjun Hao (2005) Evaluating remotely sensed live fuel moisture estimations for fire behavior predictions. EastFIRE conference 2005

## Questions and Answers

**Questioner Name:** Heinke Schluenzen

**Q:** Did you change the surface cover class after the fire went over it?

**A:** The WRF/Fire-chem version we used in this work does not implement that change on the land use when the grid cell has been burnt. The main limitation to implement the dynamical update of the soil grid cells is due to the differences in spatial resolution between the meteorological grid cell and the fire grid cell. The fire grid cell is ten times higher. We are using 20 me spatial resolution for the fire simulation (Fire) and the WRF/chem model is applied with 200 m spatial resolution, so the change in the grid cells should be applied over the meteorological grid cells. However, there is transfer of information between the Fire (20 m) fluxes and emissions to the WRF/chem model (200 m) because these variables allow performing aggregation operations from the fire grid cells (20 m). We are working on a new version which will change the soil type in the meteorological model (200 m) based on the proportion (or percentage) of the burnt meteorological grid cell by the fire model.

# Chapter 100
# Assimilation of PM Ground Measurements: Looking for Optimal Settings for the PM Forecasts

**Arjo Segers, Astrid Manders, Renske Timmermans, and Martijn Schaap**

**Abstract** PM10 forecasts for Europe and the Netherlands are part of the daily LOTOS-EUROS products, next to ozone forecasts. So far, ozone ground observations and OMI $NO_2$ column observations were assimilated in the forecasting system, using an Ensemble Kalman filter. Previous studies have shown that assimilation of daily PM10 ground observations improve the PM forecasts. Ideally, ozone, $NO_2$, AOD and PM10 can be assimilated within one analysis. If we want to combine ozone and PM assimilation in one system, assimilation of hourly PM observations is needed and the model system was extended by assimilation of PM10 and PM2.5 ground observations.

We have investigated optimal settings of the system, taking several aspects into account. First of all, a complication with regard to ozone and $NO_2$ is that LOTOS-EUROS underestimates the PM concentration. This was previously accounted for by a bias correction, but can more elegantly be solved by introducing a new species of unknown composition which is allowed to vary independently. Secondly, hourly PM observations can have relatively large errors and are sometimes influenced by very local conditions. Therefore, sensitivity experiments were done to investigate the sensitivity to and optimal settings for the correlation length between stations, error constraints on observations, noise factors on the emissions and correlation timescales. We present the lessons learnt and the current performance of the system.

A. Segers (✉) • A. Manders • R. Timmermans • M. Schaap
Department of Climate, Air and Sustainability, TNO, P.O. Box 80015,
3508 Utrecht, TA, The Netherlands
e-mail: arjo.segers@tno.nl; renske.timmermans@tno.nl

D. Steyn and R. Mathur (eds.), *Air Pollution Modeling and its Application XXIII*,
Springer Proceedings in Complexity, DOI 10.1007/978-3-319-04379-1_100,

## 100.1 Introduction

In Manders et al. [1] it was demonstrated that a particulate matter (PM) forecasting service in the Netherlands based on the LOTOS-EUROS chemistry transport model (CTM) performed better regarding timing of events than the statistical model which was used up to then by the user RIVM. As many other CTMs the PM10 concentrations are underestimated by LOTOS-EUROS. Within this study we work on the optimization of the data assimilation system with the goal to improve the particulate matter forecasts to satisfy the information needs in the Netherlands. In previous studies it has been shown that data assimilation of daily PM observations in the LOTOS-EUROS model does improve the analysed PM fields when comparing to an independent set of ground-based observations. The data assimilation of PM has however not yet been included in the operational forecasts for the Netherlands and Europe where currently only data assimilation of ground based ozone observations is performed. Ideally within the operational forecast system the PM observations are simultaneously assimilated with the ozone observations within one analysis. For this we will ideally need the assimilation of hourly instead of daily observations of PM10. The assimilation of hourly PM observations from ground stations has proven to be complicated. First tests did not show a large improvement. Possible reasons could be the large variability within the PM observations, an overestimation of the observation errors or an underestimation of the model errors. Within this study we investigate the optimal settings of the data assimilation system to improve the assimilation of the hourly PM observations and we introduce a new approach by replacing the previously used bias correction with an unknown PM source in the model. We will present the results from a number of sensitivity experiments and the new approach within the next section.

## 100.2 Results

Several tests were performed and the model assimilation settings (representation error of observations, correlation length, temporal correlation scale, noise on model emissions) have been re-evaluated. Especially the representation error of the observations proved to be a leading factor in the performance of the assimilation (see Fig. 100.1). To overcome the large temporal variability on the hourly PM observations, tests with assimilating a 6 h running mean were also performed.

Although all the above mentioned tests did improve the PM forecasts to a certain extent, it did not lead to the desired level of performance, unless unrealistic settings were chosen (such as decreasing the representation error to 5 %). For this reason a new approach was chosen. In the new approach the bias correction applied to the modeled PM concentrations is replaced by an unspecified PM (UPM) source which can be adjusted through the assimilation of the PM observations. We have applied the new approach for the period of January 2010 where large PM concentrations

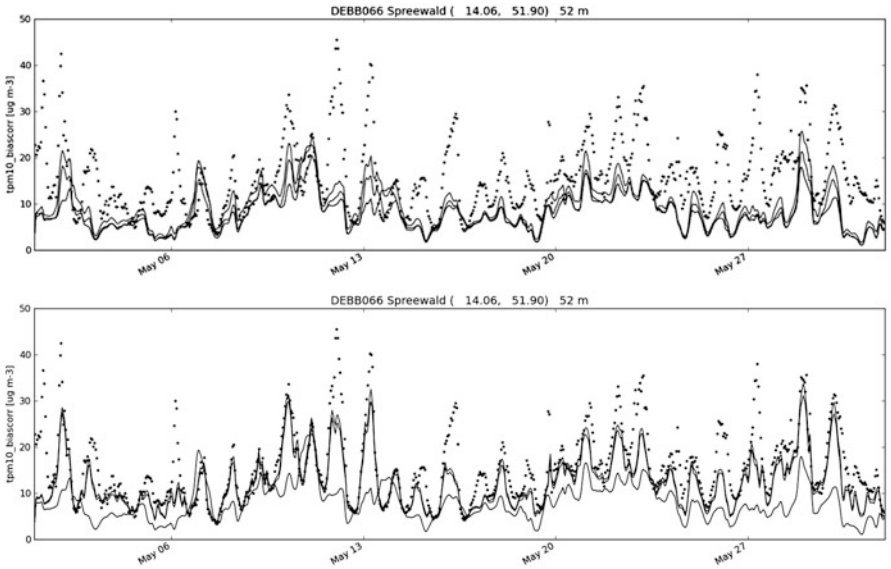


**Fig. 100.1** PM10 time series at the German station Spreewald near Berlin for 1–31 May 2010 from base run (*black*), assimilation run (*grey*) and observations (*dots*). Upper plot using standard settings (representation error 20 %), lower plot with using representation error of 5 %

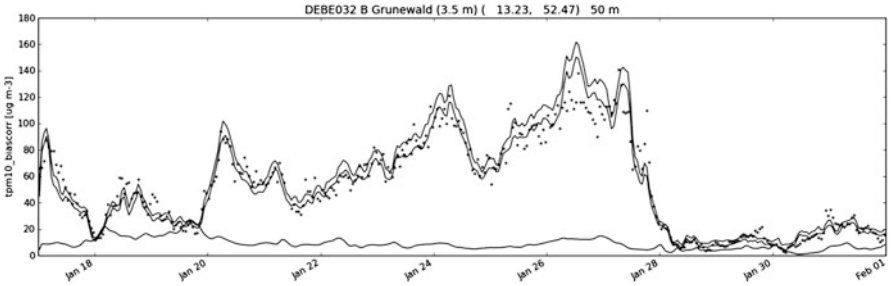


**Fig. 100.2** PM10 time series at the German station Grunewald for 1–31 January 2010 from base run (*black*), assimilation run (*grey*) and observations (*dots*)

were measured over central Europe but not simulated by our model. There is an indication that the high concentrations were due to stagnation in combination with a very low boundary layer.

The new approach leads to simulated PM10 concentrations that are in very close agreement with the observations (see Fig. 100.2).

The question is whether these improved analysed fields do improve our 3 day forecasts of PM10 as this is the aim of this study. For this reason a strategy was implemented to inherit model parameters obtained through the assimilation into the forecast. In this strategy the daily mean values of the UPM source for the day before

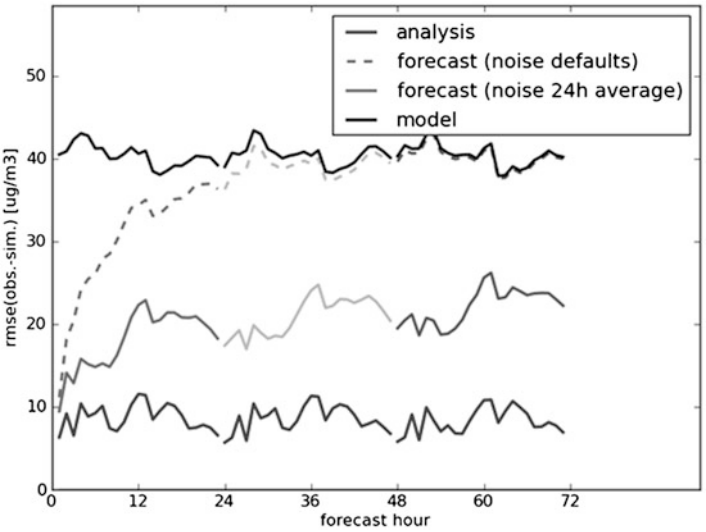


**Fig. 100.3** RMSE between simulated and observed PM10 concentrations from the LOTOS-EUROS model (before (*black* (*top line*)), after assimilation (*dark grey line* (*lowest line*)) and for the forecasts with (*solid line* with three shades of *grey*) and without the inheritance (*dashed line*)

are progressed into the 3-day forecasts. The results show a strong improvement in the exceedance forecasts even for forecast day 3. Without the inheritance, the forecast performance quickly deteriorates when going to 1, 2 and 3 day forecasts (see Fig. 100.3).

## 100.3 Conclusion

We have implemented a new approach for the data assimilation of hourly PM observations into the LOTOS-EUROS model which substantially improves the analysed and forecasted PM10 fields. By including an unspecified PM source which can be adapted through the assimilation of the ground based PM observations, the model results show a much better agreement with the ground based observations. The approach still needs to be tested over longer time periods and larger areas. We would like to note that the approach is quite brute with the sole aim to improve our forecasts without being restricted by current knowledge on emissions, e.g. the unspecified PM source is allowed to have emissions in regions where in reality there might not be any sources. Investigation of the resulting unspecified PM source strengths after assimilation could however provide us hints on missing sources or erroneous source strengths.

**Acknowledgments** The work described here was carried out with support of the European Commission, within the FP7 project PASODOBLE.

## Reference

1. Manders AMM, Schaap M, Hoogerbrugge R (2009) Testing the capability of the chemistry transport model LOTOS-EUROS to forecast PM10 levels in the Netherlands. Atmos Environ 43:4050–4059

# Chapter 101
# Spatial and Temporal Extension of a Novel Hybrid Source Apportionment Model

**Cesunica Ivey, Heather Holmes, Yongtao Hu, James A. Mulholland, and Armistead G. Russell**

**Abstract** Exposure assessment and development of control strategies are limited by the air pollutants measured and the spatial and temporal resolution of the observations. Air quality modeling can provide more comprehensive estimates of the temporal and spatial variation of pollutant concentrations, however with significant uncertainties. Source apportionment, which can be conducted as part of the air quality modeling, provides estimates of the impacts of sources on the mixtures of pollutants and contains surrogate estimates for pollutants that are not measured. This study details results using a novel spatiotemporal hybrid source apportionment method employed with interpolation techniques to quantify the impact of 33 $PM_{2.5}$ source categories. The hybrid model, which aims to reduce estimating uncertainties, adjusts original source impact estimates from a chemical transport model at monitoring sites to closely reflect observed ambient concentrations of measured $PM_{2.5}$ species. Daily source impacts are calculated for the contiguous U.S. Two interpolation methods are used to generate the data needed for spatiotemporal hybrid source apportionment. Hybrid adjustment factors are spatially interpolated using kriging, and daily observations are calculated by temporally interpolating available monitoring data. Methods are evaluated by comparing daily simulated concentrations—generated by reconstruction of source impact results—to observed species concentrations from monitors independent of model development. Results also elucidate U.S. regions with relatively higher impacts from specific sources. Monitoring data in this study originated from the Chemical Speciation Network (CSN), EPA-funded supersites, and the Southeastern Aerosol Research Characterization (SEARCH) Network. Results are to be used in health impact assessments.

C. Ivey (✉) • H. Holmes • Y. Hu • J.A. Mulholland • A.G. Russell
School of Civil and Environmental Engineering, Georgia Institute of Technology, Atlanta, GA, USA
e-mail: civey3@gatech.edu

D. Steyn and R. Mathur (eds.), *Air Pollution Modeling and its Application XXIII*, Springer Proceedings in Complexity, DOI 10.1007/978-3-319-04379-1_101,

## 101.1 Introduction

Two types of models are commonly used for source apportionment (e.g. determining impacts of sources on ambient concentrations): receptor models (RM) and chemical transport models (CTM). RMs are statistical models that use observed concentrations and source profiles to determine source impacts. CTMs are source-oriented models that determine impacts by simulating the formation, fate, and transport of pollutants in the atmosphere. Inherent in both approaches are uncertainties and limitations. RMs do not incorporate complex physical and chemical processes into results and are limited by the number of sources that can be resolved. CTMs do not make use of observations and have uncertainties associated with model inputs and modeled processes. This work builds from a previous study on integrating both methods to strengthen source apportionment estimates. This hybrid approach adjusts CTM source impacts to better reflect observations using constrained nonlinear-optimization with effective variance weighting [1]. This work details the application of the hybrid approach along with spatial and temporal interpolation methods to provide daily spatial hybrid source impacts for CONUS for the month of January 2004 (first and last 3 days omitted). The results are beneficial to trans-disciplinary studies that require spatially and temporally dense air quality data (e.g. epidemiological studies that correlate pollutant concentrations and health outcomes) [2, 3].

## 101.2 Methods

Generating daily, hybrid-kriging source impact spatial fields involves five steps: (1) calculating initial source impact estimates at 36-km resolution for CONUS using CMAQ-DDM3D, (2) generating daily sets of speciated data at monitoring sites over CONUS by temporally interpolating measured concentrations, (3) applying the hybrid source apportionment model for each monitor on each day, (4) spatially interpolating daily sets of hybrid adjustment factors, and (5) finally adjusting original spatial fields of source impacts by applying spatial fields of adjustment factors. Details for each step are discussed below.

The CMAQ-DDM3D model [4] was used to determine source impacts for 41 $PM_{2.5}$ species including total mass at a 36-km resolution. The model apportioned mass to 33 unique source categories, including on- and off-road gasoline and diesel sources, seven biomass burning sources, sea salt, and sources impacted by secondary processes (e.g. biogenic and livestock sources). The hybrid model requires observation data for the monitor and day being analyzed. Observation data from the Chemical Speciation Network (CSN) were used for hybrid-model development. However, CSN data are limited temporally, reporting every 3 or 6 days, hence temporal interpolation is required to generate daily data. Only monitors with speciated data as well as daily Federal Reference Method (FRM) measurements for total mass were used for the temporal interpolation, totaling 55 monitors. Note that

concentrations on non-interpolated days were used from all available monitors for hybrid analysis, regardless of daily FRM availability. Observation uncertainties associated with each species concentration are also interpolated using a propagation of error approach. The hybrid method is then applied using interpolated observations for all monitors and for each day in Jan 2004, generating 33 adjustment factors (R's) for each monitor and for each day (Eq. 101.1).

$$X^2 = \sum_{i=1}^{N} \left[ \frac{\left[ \left( c_i^{obs} - c_i^{sim} \right) - \sum_{j=1}^{J} SA_{i,j}^{base} \left( R_j - 1 \right) \right]^2}{{\sigma_{obs}}^2 + {\sigma_{sp}}^2} \right] + \Gamma \sum_{j=1}^{J} \frac{ln\left(R_j\right)^2}{{\sigma_{\ln\left(R_j\right)}}^2} \tag{101.1}$$

In Eq. 101.1, $c_i^{obs}$ and $c_i^{sim}$ are observed and CMAQ-simulated species (i) concentrations, respectively, $SA_{i,j}^{base}$ are original CMAQ estimates of source j's impact one species i's concentration, R is the adjustment factor for each source (j), and σ are uncertainties in measurements ($\sigma_{obs}$), CMAQ-simulated concentrations ($\sigma_{SP}$), and emissions estimates ($\sigma_{\ln(rj)}$). Equation 101.1 is optimized to find the R's that minimize differences in observed concentration and simulated source impacts. Each daily set of R's are spatially interpolated to generate spatial fields of adjustment factors at 36-km resolution. The spatial fields of adjustment factors are then applied to the original CMAQ source impact fields (grid-cell by grid-cell multiplication) to produce hybrid-kriging spatial fields for Jan 2004. Additional data from the Jefferson Street monitor (Atlanta, GA) of the Southeastern Aerosol Research and Characterization (SEARCH) Network were used to evaluate the hybrid spatiotemporal results [5].

## 101.3 Results

Daily hybrid-kriging spatial fields of source impacts were generated for 33 sources for the month of January 2004 (Fig. 101.1). Source impact fields with significant adjustments include biomass burning (agricultural burning, lawn waste burning, open fires, prescribed burning, wildfires, wood fuel burning, and woodstoves) and dust impact fields. On average for Jan. 2004, for CMAQ-simulated biomass burning spatial fields were reduced by a factor of 2.7. CMAQ-simulated dust spatial fields were reduced by a factor of 5.0. Source impact fields saw fewer changes for stationary diesel sources, non-road sources, and sea salt.

Hybrid-kriging was evaluated with an independent data set by comparing reconstructed concentrations to observations at the Jefferson Street monitor in Atlanta, GA, which reported daily speciated data for January 2004 (Fig. 101.2). The reconstructed, hybrid concentrations show a similar trend as the observations for total $PM_{2.5}$. Initially over-simulated by CMAQ, potassium, silicon, and calcium

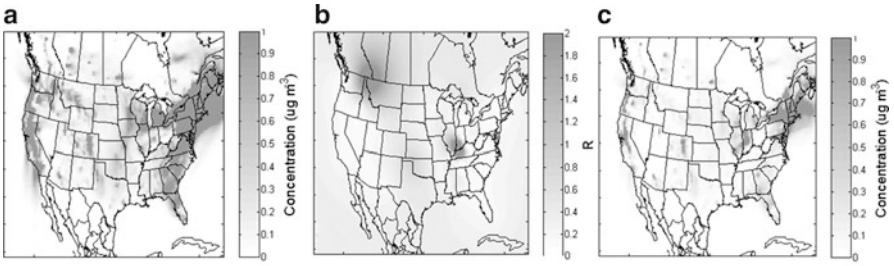


**Fig. 101.1** Hybrid adjustment of 36-km CMAQ woodstove PM2.5source impacts on Jan 4, 2004. (**a**) Original CMAQ simulations. (**b**) Spatial field of kriged hybrid adjustment factors (Rwoodstove). (**c**) Hybrid-kriging source impacts

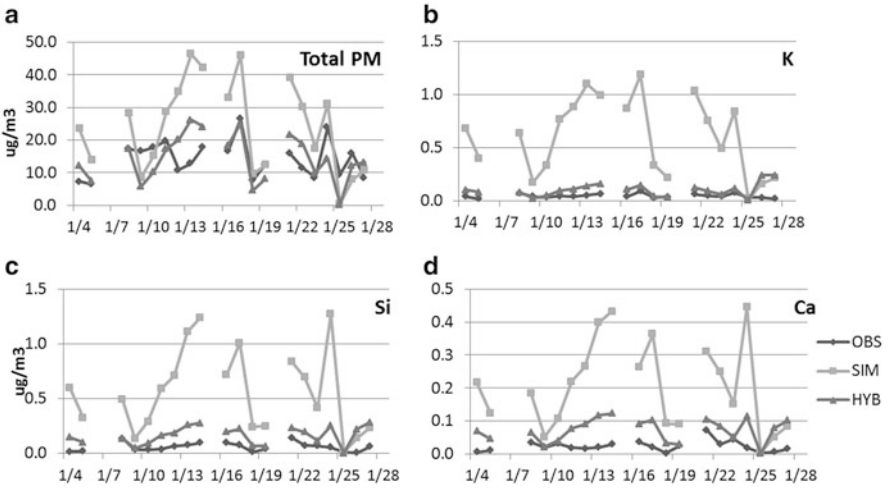


**Fig. 101.2** Comparison of observed, CMAQ, and hybrid-kriging concentrations at the Jefferson Street monitor in Atlanta, GA. (**a**) Total PM2.5, (**b**) potassium (K), (**c**) silicon (Si), and (**d**) calcium (Ca)

concentrations were reduced by hybrid adjustment and became more aligned with observations. Potassium is a tracer for biomass burning, and silicon and calcium are tracers for dust. Reducing the impact of these sources greatly improved CMAQ simulations of the tracer species. The monthly average for potassium was reduced from 0.57 to 0.16 $\mu g/m^3$, which is closer to the average observation of 0.06 $\mu g/m^3$. The monthly average for silicon was reduced from 0.60 to 0.10 $\mu g/m^3$ (average observation 0.04 $\mu g/m^3$). The monthly average for calcium was reduced from 0.21 to 0.07 $\mu g/m^3$ (average observation 0.02 $\mu g/m^3$). Traditionally, biomass burning and dust emissions estimates have a high uncertainty [6, 7]. The hybrid source apportionment method takes into account emissions uncertainties, as well

as observations, to improve source impact estimates. The spatial and temporal extensions of the hybrid-kriging method provide improved daily, spatially dense source impacts for used in health studies.

**Acknowledgments** This work was made possible in part by USEPA STAR grants R833626, R833866, R834799 and RD83479901 and by NASA project SV6-76007 under grant NNG04GE15G. Its contents are solely the responsibility of the grantee and do not necessarily represent the official views of the USEPA and NASA. Further, neither USEPA nor NASA endorses the purchase of any commercial products or services mentioned in the publication. We also acknowledge the Southern Company for their support and thank Eric Edgerton of ARA, Inc. for access to the SEARCH data.

## References

1. Watson JG, Cooper JA, Huntzicker JJ (1984) The effective variance weighting for least-squares calculations applied to the mass balance receptor model. Atmos Environ 18(7):1347–1355
2. Thurston G et al (2005) Results and implications of the workshop on the source apportionment of PM health effects. Epidemiology 16(5):S134–S135
3. Darrow LA et al (2011) "Ambient Air pollution and birth weight in full-term infants in Atlanta", 1994-2004. Environ Health Perspect 119(5):731–737
4. Napelenok SL et al (2006) Decoupled direct 3D sensitivity analysis for particulate matter (DDM-3D/PM). Atmos Environ 40(32):6112–6121
5. Hansen DA et al (2003) The southeastern aerosol research and characterization study: 1-overview. J Air Waste Manage Assoc 53(12):1460–1471
6. Choi YJ, Fernando HJS (2008) Implementation of a windblown dust parameterization into MODELS-3/CMAQ: application to episodic PM events in the US/Mexico border. Atmos Environ 42(24):6039–6046
7. Tian D et al (2009) Assessment of biomass burning emissions and their impacts on urban and regional PM2.5: a Georgia case study. Environ Sci Technol 43(2):299–305

# Chapter 102
# Application of Data Assimilation to the UK Air Quality Forecast

**Andrea Fraser, John Abbott, and Rebecca Rose**

**Abstract** An operational air quality forecasting model based on the Weather Research and Forecasting (WRF) model and the Community Multiscalar Air Quality (CMAQ) model is used to produce a three day forecast for $O_3$, $NO_2$, $SO_2$, $PM_{10}$ and $PM_{2.5}$ and weather in the UK. In 2012 $PM_{2.5}$ was added to the UK air quality forecast. When compared to observations the forecast tends to underestimate the PM2.5 concentration. This study reviews the potential to improve the forecast by assimilation of measurement data for $O_3$, $NO_2$ and particulate matter from the UK's Automated Urban and Rural Monitoring Network (AURN) into the CMAQ daily forecast using a bias correction factors estimated by means of the Kalman filter (KF) approach.

Moderate particulate pollution events in mid-February and a high $PM_{2.5}$ pollution event between 5th and 8th March 2013 provided a good test case for evaluating the basic Kalman filter (KF) methodology. This improved the forecasts of daily mean and daily maximum 1-h concentrations of particulate matter $PM_{2.5}$ and ozone. It effectively eliminates the mean bias between the predictions and the measured concentrations and in most cases reduces the standard deviation of the bias. Using the basic algorithm on the more demanding task of predicting hourly average concentrations reduces the mean bias between the predictions and the measurement, but in many cases in this study it increased the scatter. More tuning to the Kalman gain factor is required before the hourly correction is recommended for application to UK forecasts.

A. Fraser (✉) • J. Abbott • R. Rose
Air Quality & Environment, Ricardo-AEA, Fermi Avenue, Harwell IBC, Oxon OX11 0QR, UK
e-mail: Andrea.Fraser@ricardo-aea.com

D. Steyn and R. Mathur (eds.), *Air Pollution Modeling and its Application XXIII*,
Springer Proceedings in Complexity, DOI 10.1007/978-3-319-04379-1_102,

## 102.1 Introduction

An operational air quality forecasting model based on the Advanced Re-search – Weather Research and Forecasting (WRF) model and the Community Multiscalar Air Quality (CMAQ) model is used to produce a 3 day forecast for $O_3$, $NO_2$, $SO_2$, $PM_{10}$ and $PM_{2.5}$ and weather in the UK. These along with data from a number of different sources are used by Ricardo-AEA to produce the UK operational Air Quality forecast for the UK Department for Environment, Food and Rural Affairs (Defra) and the Devolved Authorities (DA). Data assimilation can be used to improve forecast performance. Four-dimensional variational data assimilation (4DVAR) and Ensemble Kalman Filtering (EnKF) are potentially very powerful techniques; they are also highly computation-intensive, requiring either the implementation of a model adjoint, or the simultaneous integration of several tens of model ensemble members. In recent years, simpler bias adjustment techniques have emerged, in which the bias correction factors are estimated by means of the Kalman filter (KF) approach. These techniques are applied in post-processing (i.e., off-line) mode rather than as a part of the initialization of the deterministic forecast, and they are characterized by a very low computational cost.

In 2012 particulate matter of less than 2.5 μm in diameter ($PM_{2.5}$) was added to the UK air quality forecast. When compared to observations the WRF-CMAQ forecast tends to underestimate the PM2.5 concentration. This makes it difficult to predict pollution events. Moderate particulate pollution events in mid-February and a high $PM_{2.5}$ pollution event between 5th and 8th March 2013 provided a good test case for evaluating the basic Kalman filter (KF) methodology.

## 102.2 Method

This study look at the potential to improve the UK forecast by assimilation of measurement data for $O_3$, $NO_2$ and particulate matter from the UK's Automated Urban and Rural Monitoring Network (AURN) into the WRF-CMAQ daily forecast.

Basic Kalman filter bias adjustment was applied to measured and modelled ozone, $PM_{2.5}$, $PM_{10}$ and $NO_2$ concentrations. It was applied separately and individually at monitoring sites throughout the UK. For each monitoring site, the hourly or daily mean and max concentrations were calculated. The observed bias, y, was then calculated as the difference between the modelled and measured concentrations.

The basic Kalman filter (Eq. 102.1) calculates an estimate of the underlying bias, $x_k$ for day k from the measured and modelled concentrations where $k_g$ is an "optimum" gain factor in the range 0–1.

$$x_k = x_{k-1} + k_{gk}\,(y_{k-1} - x_{k-1}) \tag{102.1}$$

The code used by the US EPA and implemented into its ozone and particulate matter forecasts [1] was adapted for the UK to make the code compatible with UK observation data and with our data handling systems, which are based on the R statistical package.

## 102.3 Main Findings

When testing the FK methods described by [1] with hourly data for 2012 it was observed that use of a Kalman filter reduced bias in the forecast data. However, in the majority of cases, it does this at the expense of increased scatter (i.e. increases likelihood of disagreement) between the bias corrected forecast data and the observed pollutant concentrations. Table 102.1 shows the effect of using the KF and logKF at three sample monitoring sites in 2012, on hourly data at three monitoring sites for $O_3$, $PM_{10}$ and $NO_2$.

The $PM_{2.5}$ air quality index (AQI) is based on a 24 h average rather than an hourly average and so the Kalman filter method was investigated with daily average and daily maximum concentrations. Table 102.2 shows that the basic Kalman filter

**Table 102.1** The mean bias and standard deviation (Std. Dev.) of the residual between the predicted and measured concentrations of $O_3$, $PM_{10}$ and $NO_2$ for 2012 are provided before and after adjustment by the Kalman filter

| Site | Species | | No Kalman filter, $\mu g\ m^{-3}$ | With Kalman filter, $\mu g\ m^{-3}$ | With Log Kalman filter, $\mu g\ m^{-3}$ |
|---|---|---|---|---|---|
| Harwell (Rural) | $O_3$ | Mean bias | 1.88 | 0.09 | 0.12 |
| | | Std. dev. | 14.73 | 15.13 | 15.51 |
| | $PM_{10}$ | Mean bias | 5.15 | 0.08 | −2.79 |
| | | Std. dev. | 8.60 | 9.03 | 13.37 |
| | $NO_2$ | Mean bias | −11.85 | −4.30 | 1.33 |
| | | Std. dev. | 11.98 | 10.87 | 9.58 |
| North Kensington (Urban background) | $O_3$ | Mean bias | −7.29 | −0.94 | −3.30 |
| | | Std. dev. | 16.81 | 16.55 | 31.02 |
| | $PM_{10}$ | Mean bias | 8.04 | 0.51 | −0.94 |
| | | Std. dev. | 10.99 | 11.60 | 16.55 |
| | $NO_2$ | Mean bias | 2.91 | 0.08 | −0.09 |
| | | Std. dev. | 15.94 | 15.98 | 17.19 |
| Aberdeen (Urban) | $O_3$ | Mean bias | −14.08 | −0.18 | 4.25 |
| | | Std. dev. | 17.37 | 18.04 | 19.34 |
| | $PM_{10}$ | Mean bias | 4.87 | 0.16 | 0.18 |
| | | Std. dev. | 8.00 | 9.01 | 8.41 |
| | $NO_2$ | Mean bias | 6.40 | 0.17 | 1.39 |
| | | Std. dev. | 14.29 | 14.55 | 15.30 |

**Table 102.2** The mean bias and standard deviation (Std. Dev.) of the residual between the predicted and measured concentrations of $PM_{2.5}$ are provided before and after adjustment by the Kalman filter

| Site type | | Residual statistics | No Kalman filter, $\mu g\ m^{-3}$ | With Kalman filter, $\mu g\ m^{-3}$ |
|---|---|---|---|---|
| Urban background | Daily average | Mean bias | 8.49 | 0.01 |
| | | Std. dev. | 6.91 | 6.35 |
| | Daily maximum | Mean bias | 16.04 | 0.15 |
| | | Std. dev. | 13.94 | 8.28 |
| Urban | Daily average | Mean bias | 10.88 | 0.06 |
| | | Std. dev. | 8.16 | 7.64 |
| | Daily maximum | Mean bias | 18.37 | 0.13 |
| | | Std. dev. | 13.12 | 8.03 |
| Rural | Daily average | Mean bias | 9.27 | 0.04 |
| | | Std. dev. | 8.19 | 7.32 |
| | Daily maximum | Mean bias | 16.72 | 0.05 |
| | | Std. dev. | 14.60 | 8.73 |

algorithm substantially improves forecasts of daily mean and daily maximum 1-h concentrations of particulate matter $PM_{2.5}$. It effectively eliminates the mean bias between the predictions and the measured concentrations and in most cases reduces the standard deviation of the bias.

Using Birmingham Tyburn monitoring site as an example Fig. 102.1 shows that during this period the unadjusted predictions underestimate the observed concentrations in $PM_{2.5}$, but tend to rise and fall with the same time dependence. Adjustment of the predictions with the Kalman filter improves the agreement between predictions and observations. During this period the predictions (without filtering) never forecast outside of the low category during the pollution event while predictions which have been adjusted by the Kalman filter typically do not under-predict a maximum by more than one category. This is an improvement compared to the raw, unfiltered predictions.

Use of the basic Kalman filter algorithm improves forecasts of daily mean and daily maximum 1-h concentrations of particulate matter $PM_{2.5}$ and ozone. It effectively eliminates the mean bias between the predictions and the measured concentrations and in most cases reduces the standard deviation of the bias. Using the basic algorithm on the more demanding task of predicting hourly average concentrations reduces the mean bias between the predictions and the measurement, but in many cases in this study it increased the scatter. More tuning to the Kalman gain factor is required before the hourly correction is recommended for application to UK forecasts.

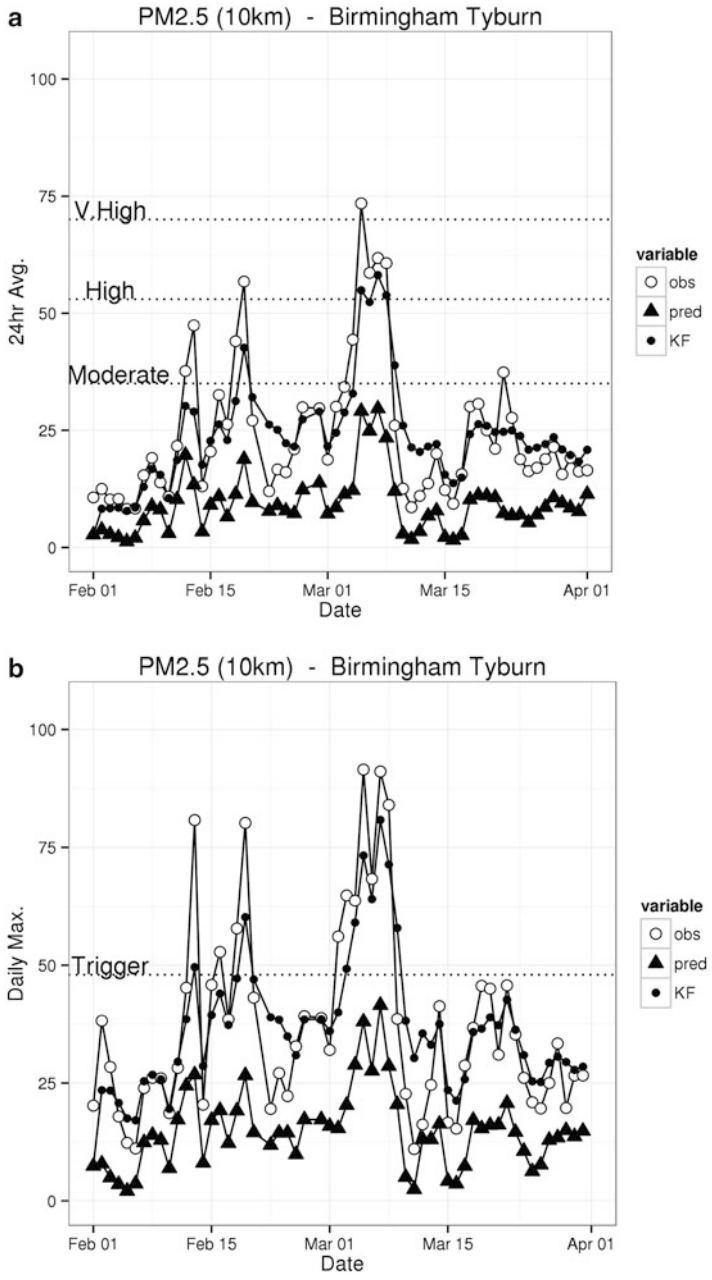


**Fig. 102.1** Time series plots showing the observed (obs) for the (**a**) daily average and (**b**) daily maximum PM2.5 concentrations at Birmingham Tyburn between 1st February and 31st March 2013 along with the WRF-CMAQ predicted concentrations before (pred) and after (KF) application of the Kalman Filter

**Acknowledgments** This work was supported by the UK Department for Environment, Food and Rural Affairs.

## Reference

1. Kang DR, Mathur R, Rao ST (2010) Real-time bias-adjusted O3 and PM2.5 air quality index forecasts and their performance evaluations over the continental United States. Atmos Environ 44(18):2203–2212

# Chapter 103
# Improvements to the Regional Deterministic Air Quality Analysis System for Ozone and PM2.5 at the Surface at the Canadian Meteorological Center

**Yulia Zaitseva, Alain Robichaud, Richard Menard, David Anselmo, Gilles Verner, Lorraine Veillette, Christophe Malek, and Isabelle Provost**

**Abstract** In February 2013, in collaboration with the Air Quality Research Division, the Canadian Meteorological Centre (CMC) implemented into operations a new surface analysis for air quality species (ozone and PM2.5). The Regional Deterministic Air Quality Analysis (RDAQA) generates analyses every hour using the operational GEM-MACH Regional Air Quality Deterministic Prediction System (48 h forecasts on a domain with 10-km horizontal grid spacing and 80-vertical levels) to provide the trial fields. Surface observations are from Canadian regional data providers and the US EPA/AIRNow Program. An optimal interpolation scheme adapted to air quality is used to blend model and observations. A verification of the RDAQA shows major reductions in the error variance and bias of the analysis with respect to the model forecasts as compared to observations.

## 103.1 Introduction

The Regional Deterministic Air Quality Analysis System (RDAQA) is a fundamental first step towards full-scale chemical data assimilation. The high value of the objective analysis products has become well known over the past several years

Y. Zaitseva (✉) • G. Verner • L. Veillette • C. Malek • I. Provost
Data Assimilation and Quality Control Section, Environment Canada CMC, Montreal, Canada
e-mail: yulia.zaitseva@ec.gc.ca; gilles.verner@ec.gc.ca; lorraine.veillette@ec.gc.ca; christophe.malek@ec.gc.ca; isabelle.provost@ec.gc.ca

A. Robichaud • R. Menard
Air Quality Research Division, Atmospheric Science Technology Directorate (ASTD), Environment Canada, Montreal, Canada
e-mail: alain.robichaud@ec.gc.ca; richard.menard@ec.gc.ca

D. Anselmo
Air Quality Modeling Applications Section, Environment Canada CMC, Montreal, Canada
e-mail: david.anselmo@ec.gc.ca

D. Steyn and R. Mathur (eds.), *Air Pollution Modeling and its Application XXIII*, Springer Proceedings in Complexity, DOI 10.1007/978-3-319-04379-1_103,

and regional weather and air quality forecasters have expressed a strong interest in having full support for these products.

In 2003, a first version of objective analysis for surface pollutants was produced at the CMC on an experimental basis using the air quality model CHRONOS [1] together with a scheme of optimal interpolation [2].

The RDAQA is currently running in an "off-line" mode meaning that the resulting analyses do not serve as input for the model in the subsequent integration. The future of the RDAQA is to provide the initial fields necessary to establish an assimilation system for the air quality forecasts. In this note, we will briefly discuss the methodology, air quality data processing, evaluation statistics and applications of the RDAQA.

## 103.2 Methodology and Evaluation

Our Objective analysis (OA) scheme is based on the optimal interpolation (OI) scheme adapted to air quality. It uses a linear combination of the background field and observations and optimized by minimizing the error variance using stationary error statistics. A more complete description of the methodology can be found elsewhere [2, 3]. The RDAQA system ingests surface observations of ozone and PM2.5 from the Canadian provincial and municipal air quality monitoring networks, the Canadian air and precipitation monitoring network and U.S. EPA/AIRNow program (see Fig. 103.1 as an example of surface ozone observations). The observations are acquired in real-time and are subsequently passed through a series of quality control tests including: checks for exceedances of maximum and minimum concentration values, dubious jump detection and a background check of observed-minus-forecast values.

The background field is provided by the operational regional air quality forecast model. The optimal interpolation scheme uses an exponential decaying function of distance and the statistics are obtained from a modified version of the Hollingsworth-Lönnberg method [4]. Estimates of error statistics are computed by using a First Order Autoregressive Model for each hour, pollutant and surface station for the four seasons and for every hour. A bias corrections are also applied to the PM2.5 observations to improve performance. Analyses of ozone and PM2.5 are currently generated operationally while analyses of nitrogen dioxide ($NO_2$) are running in experimental mode.

### *103.2.1 Air Quality Surface Observation Processing*

The operational run task sequencer (MAESTRO) was used to create a modular suite for the RDAQA as part of the larger ensemble of operational suites currently running at the CMC. Each module represents a particular process in the RDAQA

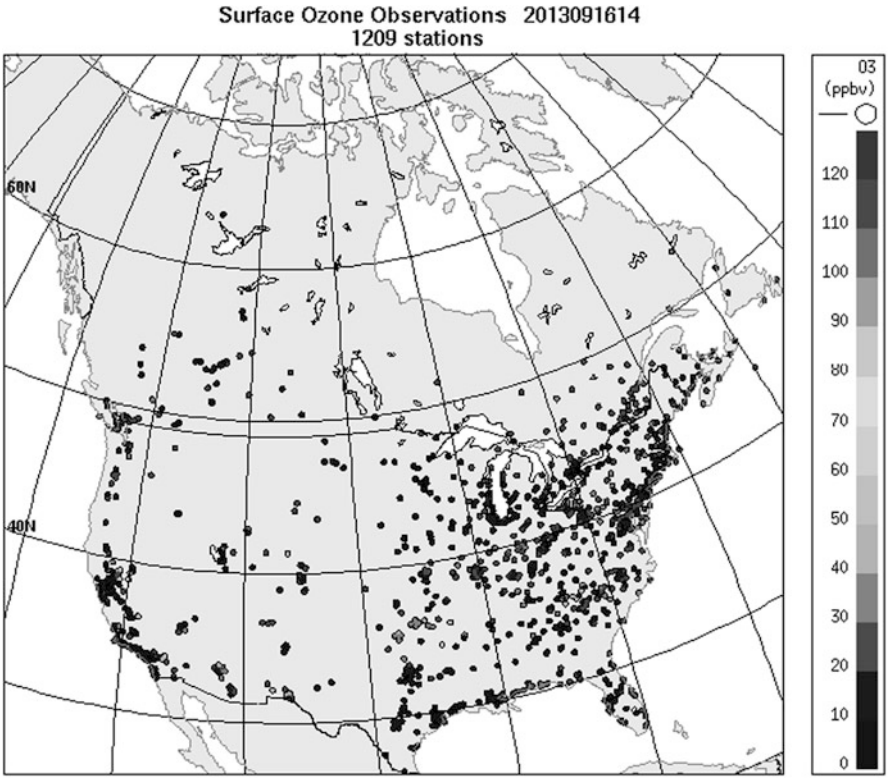


**Fig. 103.1** Distribution map of surface ozone observations for September 16 2013 at 14Z

system for supporting and developing the air quality database (in SQLite format) for the observations and the gridded data files containing the trial fields, analyses and increments.

The air quality data processing includes different stages of file evolution: rawdata → dbase → cutoff → derisfc → bgcksfc → postsfc. A "dbase" 6 h SQLite file contains two tables (header and data) with real-time reports of air quality surface data for nine species (O3, NO, NO2, PM2.5, PM10, SO2, H2S, TRS, CO). The data processing system also includes two cut-off files for each valid hour of the analysis. Two analyses are generated for every analysis hour (24 h per day). The "early analysis" is generated approximately 1 h after the analysis hour and exploits close to 98 and 80 % of the Canadian and U.S. observations, respectively. The "late analysis" is generated approximately 2 h after the analysis hour and it ingests close to 99 and 95 % of the Canadian and U.S. observations, respectively. The "derisfc", "bgcksfc", "postsfc" SQLite files are produce hourly. Various flags, indicating the quality and validity of the observations, have been added to the database as well as processed quantities, such as observation minus first-guess values (O-P), observation minus analyses values (O-A), observation errors, first-guess errors and correlation length.

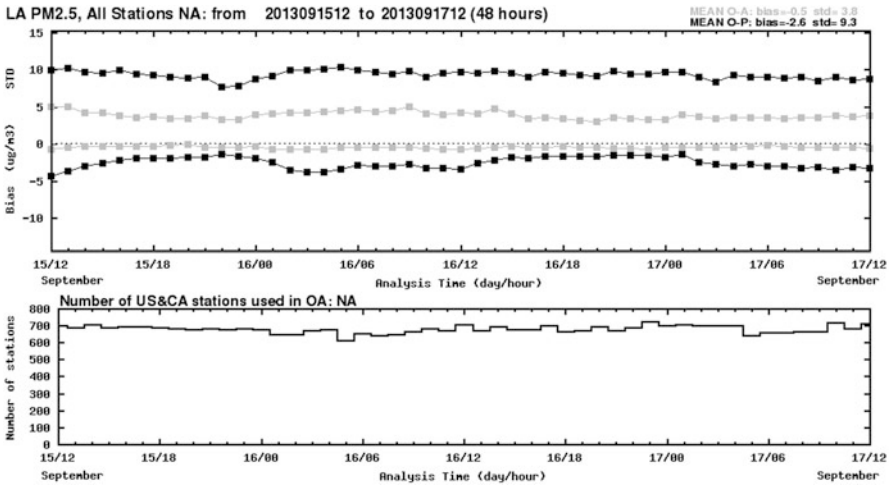


**Fig. 103.2** Example of daily monitoring covering a 48 h period for PM2.5 over North America

### *103.2.2 Monitoring and Verification Results*

Monitoring procedures include the examination of the O-P (Observation minus Prediction) and O-A (Observation minus Analysis) statistics for surface pollutants on a day-to-day basis and in terms of monthly means. Figure 103.2 shows an example of the daily monitoring of PM2.5 for the RDAQA available in real-time for the region of North America. The verification scores of mean bias for O-P (black, lower curve) and O-A (gray, lower curve) and standard deviation for O-P (black, upper curve) and O-A (gray, upper curve) appear as a function of hour. As well the number of stations assimilated is plotted in the bottom panel.

Two types of verification scores have been computed: internal and external. The internal verification means that the analysis is created using all the observations, whereas, in the case of external verification (or cross-validation) independent data that is not seen by the analysis is used to verify the final product. The results indicate that the analysis provides a substantial reduction in standard deviation as well as reducing the bias to near zero for all analysis hours. A separate categorical score called the frequency correct within a factor of 2 (FC2) shows that the analysis is more reliable than the model output for all hours of the day. Figure 103.3 shows an example of the final product from the RDAQA system for ozone. The product contains four images: model trial field (upper left), objective analysis (upper right), analysis increments (or correction to the model; lower left) and observations (lower right) used in the analysis.

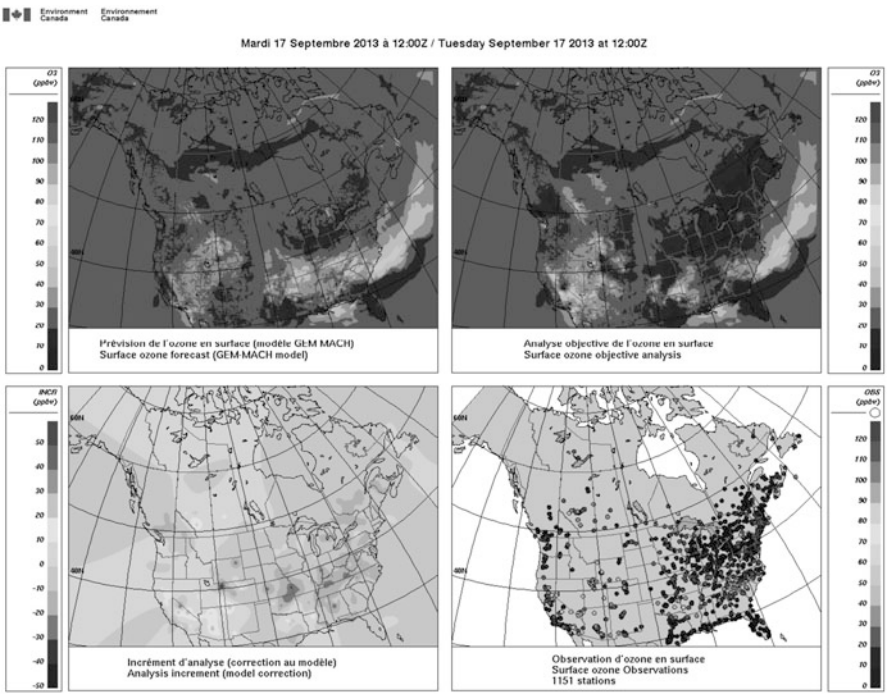


**Fig. 103.3** Example of the final product from the RDAQA system for ozone

## 103.3 Conclusions and Future Work

The RDAQA is a novel product that fills a gap as far as surface pollutant analyses are concerned. The information about and access to the final products are available on an internal Environment Canada website which is used daily by operational air quality forecasters. The daily and monthly monitoring products, as well as cross-validation tests show that with an improved version of the air quality forecast model and upgraded error statistics both show that the error variance is reduced in a very significant way and the O-A bias is practically reduced to zero in the analyses, whereas the forecast bias (O-P) could be important. The future development of this project includes using the analysis to initialize the GEM-MACH model, as well as adding other species to the RDAQA system.

## References

1. Pudykiewicz J, Kallaur A, Smolarkiewicz PK (1997) Semi-Lagrangian modeling of tropospheric ozone. Tellus 49B:231–248
2. Menard R, Robichaud A (2005) The chemistry-forecast system at the Meteorological Service of Canada. In: ECMWF Seminar proceedings on Global Earth-System Monitoring, Reading, UK, pp 297–308

3. Robichaud A, Ménard R (2013) Multi-year objective analyses of warm season ground-level ozone and $PM_{2.5}$ over North America using real-time observations and Canadian operational air quality models. Atmos Chem Phys Discuss 13:13967–14035
4. Hollingsworth A, Lönnberg P (1986) The statistical structure of short-range forecast errors as determined from radiosonde data. Part I Wind Field Tellus 38A:111–113

# Chapter 104
# Current and Future Developments in Numerical Air Quality Forecasting in Canada

**S. Ménard, S. Gravel, M.D. Moran, H. Landry, A. Kallaur, R. Pavlovic, P.A. Makar, C. Stroud, W. Gong, J. Chen, D. Anselmo, and S. Cousineau**

**Abstract** Environment Canada produces twice-daily, 48-h operational air quality (AQ) forecasts for a domain covering North America. At the core of the forecast system is the GEM-MACH model, an on-line coupled meteorology and chemistry model that includes a representation of gas-phase, aqueous-phase, and heterogeneous chemistry and a number of particulate matter (PM) processes. In this paper, a brief description of the recent changes to the Canadian National AQ Forecasting System is given, followed by a discussion of future development plans. The objective for the next version of the system is to deliver improved AQ forecasts by improving initial and boundary conditions and representations of emissions and processes.

## 104.1 Recent Changes to the Canadian National AQ Forecasting System

Since 2009 the Environment Canada (EC) operational air quality forecast model GEM-MACH has been run twice daily at the Canadian Meteorological Centre to produce 48-h forecasts for a domain covering North America (Fig. 104.1). GEM-MACH is an on-line limited-area chemical transport model embedded in GEM, EC's multi-scale operational numerical weather model [1–3]. GEM-MACH's forecasts of ground-level ozone ($O_3$), particulate matter ($PM_{2.5}$ fraction), and

S. Ménard (✉) • H. Landry • R. Pavlovic • J. Chen • D. Anselmo • S. Cousineau
Air Quality Modeling Applications Section, Environment Canada, Montreal, QC, Canada
e-mail: Sylvain.Menard@ec.gc.ca

S. Gravel • A. Kallaur
Air Quality Research Division, Environment Canada, Montreal, QC, Canada

M.D. Moran • P.A. Makar • C. Stroud • W. Gong
Air Quality Research Division, Environment Canada, Toronto, ON, Canada

D. Steyn and R. Mathur (eds.), *Air Pollution Modeling and its Application XXIII*,
Springer Proceedings in Complexity, DOI 10.1007/978-3-319-04379-1_104,

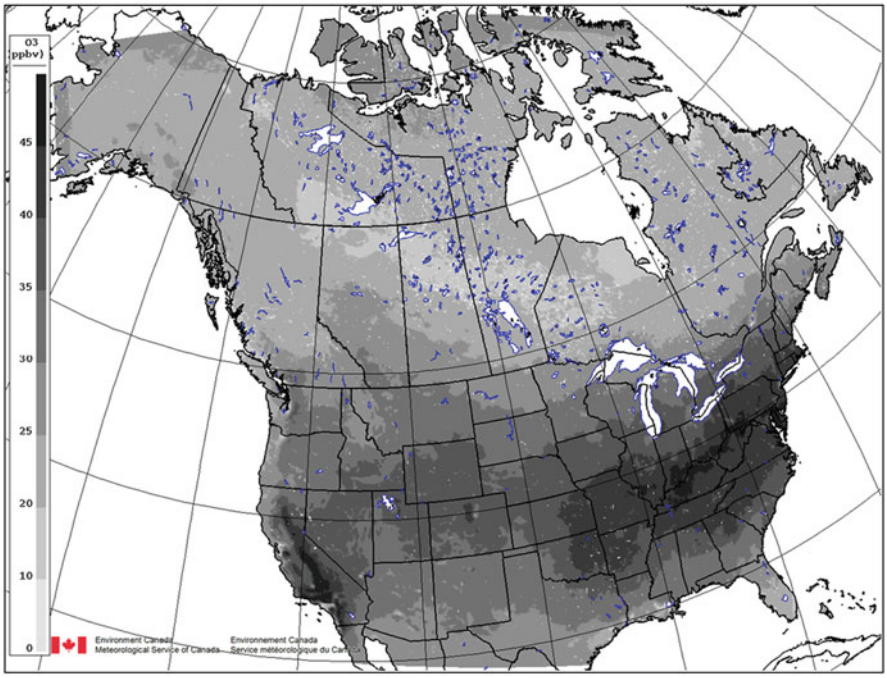


**Fig. 104.1** GEM-MACH modelling domain with the mean hourly predicted ground-level ozone field (ppbv) for the period from July 9 to August 14, 2012

nitrogen dioxide ($NO_2$) are disseminated to the Canadian public through an Air Quality Health Index (AQHI) (Eq. 104.1) developed by Health Canada and numerous partners [4]:

$$\mathrm{AQHI} = (10/10.4)^{*}100^{*}\left[\left(\exp\left(0.000871^{*}\mathrm{NO_2}\right)-1\right) + \left(\exp\left(0.000537^{*}\mathrm{O_3}\right)-1\right)+\left(\exp\left(0.000487^{*}\mathrm{PM_{2.5}}\right)-1\right)\right] \quad (104.1)$$

Improvements in the ability to forecast any of the three components of the AQHI benefit Canadians.

On October 3, 2012 an improved version of GEM-MACH became operational [5]. This version included a reduction of the horizontal grid spacing from 15 to 10 km (while leaving the horizontal extent of the domain virtually unchanged) and an increase in the number of vertical levels from 58 to 80. The latter change improves forecast accuracy and numerical robustness near the model lid (0.1 hPa). The initial and boundary conditions for the meteorology were also improved. The hourly boundary conditions for the system are now provided by the recently implemented operational regional 10-km configuration of GEM, which replaced a 15-km configuration, and the initial conditions for the meteorology are from a 4D-VAR instead of a 3D-VAR analysis cycle. As in previous versions of GEM-MACH,

average vertical profiles based on measurements are used for chemical boundary conditions. In particular, the seasonal averaged ozone profiles for North America were derived from a global ozone climatology [6]. The anthropogenic emissions are unchanged but have been interpolated conservatively from 15 to 10 km. The emissions input files are based on the 2006 Canadian national emissions inventory, a 2012 projected U.S. national emissions inventory, and the 1999 Mexican emissions inventory. A statistical evaluation of the new 10-km version of GEM-MACH showed that it outperformed the previous 15-km version for $O_3$, $PM_{2.5}$ and $NO_2$ forecasts during winter and summer 2011 and 2012 [7].

## 104.2 Future Development Plans for the Canadian National AQ Forecasting System

In the past year, several of the numerical weather prediction systems of EC have migrated to a new version of the GEM model. This version includes a new staggered vertical discretization [8], and supports a new kind of overset grid, named the *Yin-Yang grid*, for spherical geometry ([9]; see Fig. 104.2). Development of the next operational air quality forecast model platform centers on the adoption of this new version of GEM. In addition to the improved dynamics provided by the new GEM, the next version of GEM-MACH will make use of the ability of the new GEM to pilot a limited-area model at the lid as well as at the lateral boundaries. Using this feature, the GEM-MACH lid will be lowered from its current level of 0.1 hPa to approximately 35 hPa. This is particularly desirable since GEM-MACH does not yet include stratospheric chemistry. It will also provide the added benefit of reducing computing time.

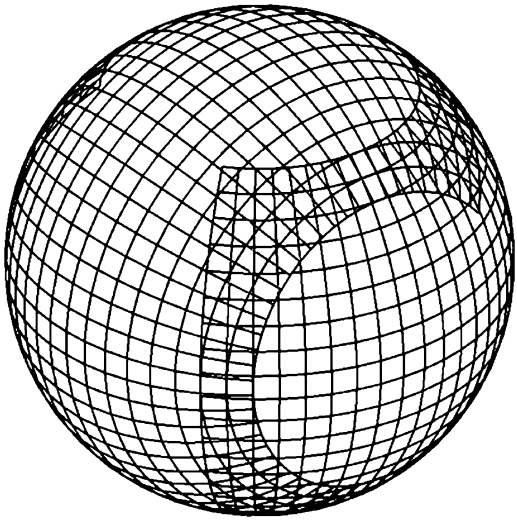

**Fig. 104.2** Yin-Yang double rotated latitude-longitude grid system over the globe

Planned development also includes revising the chemical climatology used to provide lateral boundary conditions. Experiments are in progress to examine the impact of replacing the current climatology by seasonally-averaged states obtained from a 1-year simulation of a global configuration of GEM-MACH. Work is also underway to improve the emissions data set used by GEM-MACH. The current 2006 Canadian national emissions inventory should be replaced by the 2010 emissions inventory, and new or improved spatial surrogates and temporal profiles are being developed for emissions allocation across the continent. Another improvement concerns wildfire emissions. Currently, wildfire emissions are not taken into account in the operational GEM-MACH model. This can lead to severe under-predictions of $PM_{2.5}$ when such events occur. An experimental version of GEM-MACH that includes wildfires was run for the 2012 fire season [10], and will be further tested in 2013. This experimental project, which is being done in collaboration with the Canadian Forest Service and the U.S. Forest Service/STI Inc., has shown the importance of these emissions and also the need to improve the algorithm used to estimate their plume rise.

In response to users' requests, extending the forecast period beyond 48 h will also be considered. To achieve this goal, GEM-MACH will need to use meteorological initial and boundary conditions from the EC medium-range global weather forecasting system rather than the short-range regional weather forecasting system. This change may also require increasing the horizontal coverage of the GEM-MACH domain.

A series of steps is also being examined to improve the chemical initial conditions used by GEM-MACH. Currently, for chemical constituents GEM-MACH is in perpetual forecast mode, where the 12-h chemical forecast from a previous integration is used to initialize the next forecast. In the short term, use of the current operational surface objective analyses (OA) for $O_3$, $PM_{2.5}$, and (soon) $NO_2$ produced at 00 and 12 UTC to initialize the model will be examined. The OA uses an optimal interpolation technique to blend near-real-time surface measurements from Canadian and U.S. AQ networks with the trial field provided by GEM-MACH [5]. The long-term objective, though, is to have a regional variational assimilation system in place by 2017.

## 104.3 Summary

The Canadian National AQ Forecasting System is continuing to evolve and improve. Two new operational versions were implemented at the Canadian Meteorological Centre in October 2012 and February 2013, and work is underway on the next version as well as on some longer-term developments. Improvements have been made or are being made to a number of model aspects, including horizontal and vertical grid discretization, meteorological and chemical initialization, chemical lateral and upper boundary conditions, model process representations, emissions inventories and emissions processing, and real-time wildfire emissions.

## References


1. Anselmo D, Moran MD, Ménard S, Bouchet V, Makar P, Gong W, Kallaur A, Beaulieu P-A, Landry H, Stroud C, Huang P, Gong S, Talbot D (2010) A new Canadian air quality forecast model: GEM-MACH15. In: Proceedings of the 12th AMS conference on atmosphere chemical, 17–21 Jan, Atlanta, GA, American Meteorological Society, Boston, MA, 6 pp. See http://ams.confex.com/ams/pdfpapers/165388.pdf
2. Moran MD, Ménard S, Talbot D, Huang P, Makar PA, Gong W, Landry H, Gravel S, Gong S, Crevier L-P, Kallaur A, Sassi M (2010) Particulate-matter forecasting with GEM-MACH15, a new Canadian air-quality forecast model. In: Steyn DG, Rao ST (eds) Air pollution modelling and its application XX. Springer, Dordrecht, pp 289–292
3. Moran MD, Chen J, Ménard S, Pavlovic R, Landry H, Beaulieu P-A, Gilbert S, Makar PA, Gong W, Stroud C, Kallaur A, Robichaud A, Gong S, Anselmo D (2011) Two years of operational AQ forecasting with GEM-MACH15: a look back and a look ahead. In: Proceedings of the 10th CMAS conference, 24–26 Oct, Chapel Hill, North Carolina, 7 pp. See http://www.cmascenter.org/conference/2011/abstracts/moran_two_years_2011.pdf.
4. Stieb DM, Burnett RT, Smith-Doiron M, Brion O, Hyun Shin H, Economou V (2008) A new multipollutant, no-threshold air quality health index based on short-term associations observed in daily time-series analyses. J Air Waste Manage Assoc 58:435–450
5. Moran MD, Ménard S, Pavlovic R, Anselmo D, Antonopoulos S, Makar PA, Gong W, Gravel S, Stroud C, Zhang J, Zheng Q, Robichaud A, Landry H, Beaulieu PA, Gilbert S, Chen J, Kallaur A (2012) Recent advances in Canada's National Operational AQ Forecasting System. In: Proceedings of 32nd NATO/SPS ITM on air pollution modelling and its application, 7–11 May 2012, Utrecht, The Netherlands
6. Logan JA (1999) An analysis of ozonesonde data for the troposphere: recommendations for testing 3-D models and development of a gridded climatology for tropospheric ozone. J Geophys Res 104(D13):16115–16149
7. Moran MD, Ménard S, Gravel S, Pavlovic R, Anselmo D (2013) RAQDPS Versions 1.5.0 and 1.5.1: upgrades to the CMC Operational Regional Air Quality Deterministic Prediction System Released in October 2012 and February 2013. Environment Canada internal publication, 29 pp. See http://collaboration.cmc.ec.gc.ca/cmc/cmoi/product_guide/docs/lib/op_systems/doc_opchanges/technote_raqdps_20130226_e.pdf
8. Girard C, Plante A, Gravel S, Qaddouri A, Chamberland S, Spacek L, Lee V, Desgagné M (2010) GEM4.1: a non-hydrostatic atmospheric model (Euler equations). Environment Canada internal publication, 59 pp. See http://collaboration.cmc.ec.gc.ca/science/rpn/publications/pdf/GEM4.1.pdf
9. Qaddouri A, Lee V (2011) The Canadian global environmental multiscale model on the Yin-Yang grid system. Quart J R Meteorol Soc 137:1913–1926
10. Chen J, Pavlovic R, Pankratz A, Anderson K (2012) Evaluation of wildfire emissions in the Canadian GEM-MACH air quality forecast system. In: 20th Emissions Inventory Conference, 13–16 Aug, Tampa, Florida. See http://www.epa.gov/ttnchie1/conference/ei20/poster/jchen.pdf

# Index




D. Steyn and R. Mathur (eds.), *Air Pollution Modeling and its Application XXIII*,
Springer Proceedings in Complexity, DOI 10.1007/978-3-319-04379-1,